[redacted]

ISSN 0386-5878
Technical Memorandum
of PWRI No.3797

PROCEEDINGS OF THE SECOND U.S.-JAPAN WORKSHOP ON ADVANCED RESEARCH ON EARTHQUAKE ENGINEERING FOR DAMS

May 1999

Dam department
Public Works Research Institute
Ministry of construction
Japanese Government

1, Asahi, Tukuba-shi, Ibaraki-ken, 305 Japan

Copyright © (2001) by P.W.R.I.

All rights reserved. No part of this book may be reproduced by any means, nor transmitted, nor translated into a machine language without the written permission of the Director General of P.W.R.I.

この報告書は、土木研究所長の承認を得て刊行したものである。したがって、本報告書の全部又は一部の転載、複製は、土木研究所長の文書による承認を得ずしてこれを行ってはならない。

建設省は、平成１３年１月６日付けで国土交通省に再編

Technical Memorandum
of PWRI No.3797

PROCEEDINGS OF THE SECOND U.S.-JAPAN WORKSHOP ON ADVANCED RESEARCH ON EARTHQUAKE ENGINEERING FOR DAMS

Edited by

Yoshikazu YAMAGUCHI, Dr. Eng.
Japan-side Chairman
Task Committee (D) on Earthquake Engineering for Dams Panel on Wind and Seismic Effects
u.s.-JAPAN Cooperative Program in Natural Resources (UJNR)

Synopsis:

This publication contains the papers for keynote lectures and oral session presentations at Secons u.s.-Japan Workshop on Advanced Research on Earthquake Engineering for Dams held in Tokyo, Japan from May 7 through May 8, 1999. In addition to three keynote talks, twenty-three papers were presented orally by U.S.-side and Japan-side participants at the two-day worksshop. The workshop provided a valuable forum to exchange technical information on earthquake engineering for dams in both countries.

Key words: Earthquake Engineering, Concrete Dam, Embankment Dam, UJNR

Contents

page

Preface 1

Photographs 2

Agenda 3

Resolutions of the Second U.S.-Japan Workshop on Advanced Research on Earthquake Engineering for Dams 7

Summary of the Second U.S.-Japan Workshop on Advanced Research on Earthquake Engineering for Dams 8

List of Speakers

U.S.-Side 9

Japan-Side 21

Keynote Lectures

Present States of Construction and Maintenance of Dams in Japan (Tsuneo UESAKA) 37

Status of Construction and Safety of Dams in the United States (Robert L. HALL) 59

On the Behavior of Large Dams near the Epicenter During Earthquakes in Japan(Choshiro TAMURA) 69

Technical Session 1 (Concrete Dam (1))

Vibration Tests and Earthquake Response Observation of Concrete Dams (Hiroo SHIOJIRI, Minoru UEDA and Yukihiro TOYODA) 79

Field Measurements of Dynamic Interactions at Longyangxia Dam (Yusof GHANAAT) 93

Influence of the 1995 Hyogoken-Nambu Earthquake on Hitokura Dam Foundation Rock (Kentaro KIDO and Tomonobu SUGIURA) 107

Experimental Study on Dynamic Tensile Strength of Concrete using Splitting Tensile Tests (Takashi SASAKI, Isao NAGAYAMA, Masahiro HATANO and Yuji KANEKO) 121

Technical Session 2 (Embankment Dams (1))

Hydraulic Fracturing in Fill-type Dams during Earthquake (Yoshio OHNE, Kunitomo NARITA, Yoshio NAKAMURA and Yuji MURASE) 131

Influence of Confining Stress on Liquefaction Resistance (Richard S. OLSEN) 157

Deformation Characteristics of Coarse-grained Materials in Cyclic and Monotonic Loading Triaxial Tests (Yoshikazu YAMAGUCHI, Tsuneo UESAKA, Hitoshi YOSHIDA, Tomoya IWASHITA and Jun MATSUURA) 159

Technical Session 3 (Embankment Dams (2))

Penetration Testing of Liquefied Gravels at Seward, Alaska (Joseph P. KOESTER) 171

Dynamic Deformation and Strength Properties of Rockfill Materials (Naruo YASUDA and Norihisa MATSUMOTO) 187

Seismic Stability and Deformations of Embankment Dams (Gonzalo CASTRO) 209

Factor Analysis of Damage to Small Earth Dams due to the 1995 Hyogoken-Nambu Earthquake (Hitoshi YOSHIDA, Tsuneo UESAKA, Tomoya IWASHITA, Jun MATSUURA and Norihisa MATSUMOTO) 215

Technical Session 4 (Concrete Dams (2))

Seismic Response of Gravity Dams in Near Field During the 1995 Hyogoken-Nanbu Earthquake (Tatsuo OHMACHI, A. JALALI and H. KAWANA) 231

Nonlinear Seismic Response of Concrete Gravity Dams (Enrique E. MATHEU) 247

Proposal of Modified Seismic Coefficient Method for Concrete Gravity Dams (Isao NAGAYAMA and Takashi SASAKI) 255

Effect of Foundation and Reservoir Parameters on Dynamic Results for Arch Dams Using EACD-3D-96 (Richard L. MUNOZ) 265

Technical Session 5 (Embankment Dams (3))

Dynamic Centrifuge Tests on Flow Failure of Fills and Infinite Slopes (Osamu MATSUO, Yukiko SAITO and Tetsuya SASAKI) 281

Evaluation of Motions Recorded at and within Embankment Dams during Earthquakes (Izzat M. IDRISS) 309

Seismic Analysis and Safety Evaluation of Embankment Dams (Gilles BUREAU) 311

Seismic Response of an Earth Dam with Liquefiable Foundation (Michael K. SHARP) 329

Technical Session 6 (Concrete Dams (3))

An Investigation on the Radiation Damping of Dam-foundation System (Yoshiaki ARIGA, Zengyan CAO, Masatoshi YOSHIDA and Hiroyuki WATANABE) 337

A 3-D FE-BE Method for Dynamic Response Analysis of Dam-Foundation-Reservoir Systems (Shojiro KATAOKA) 347

Building a Database of Observational Evidence for Large Structures (Ziyad H. DURON) 355

The Estimation on Dynamic Behavior of Arch Dam Modeling Non-linear Properties of Contraction Joints during Earthquake (Tatsuo NISHIUCHI and Yukihiro TOYODA) 367

Preface

The creation of the Task Committee D, "Earthquake Engineering for Dams", was approved at the 25th Joint Meeting of the Panel on Wind and Seismic Effects, the U.S.-Japan Cooperative Program in Natural Resources (UJNR) held in Tsukuba, Japan from May 17 through May 20, 1993. From the beginning, the Task Committee D was eager to sponsor a workshop on earthquake engineering for dams. The First U.S.-Japan Workshop on Advanced Research on Earthquake Engineering for Dams was held with great success under the sponsorship of the U.S. Army Engineer Waterways Experiment Station (WES) and the Public Works Research Institute of Japan (PWRI) under the auspices of the Task Committee D in Vicksburg, Mississippi, U.S.A., 12-14 November 1996.

The Second Workshop was held in Tokyo, Japan, 7-8 May 1999. In order to efficiently use the workshop as a productive vehicle for the wider technology transfer and enhance exchanges among scientists, engineers and specialists, the Japan Society for Dam Engineers (JSDE) agreed to co-sponsor the workshop. The workshop provided a valuable forum to exchange technical information on earthquake engineering for dams in both countries.

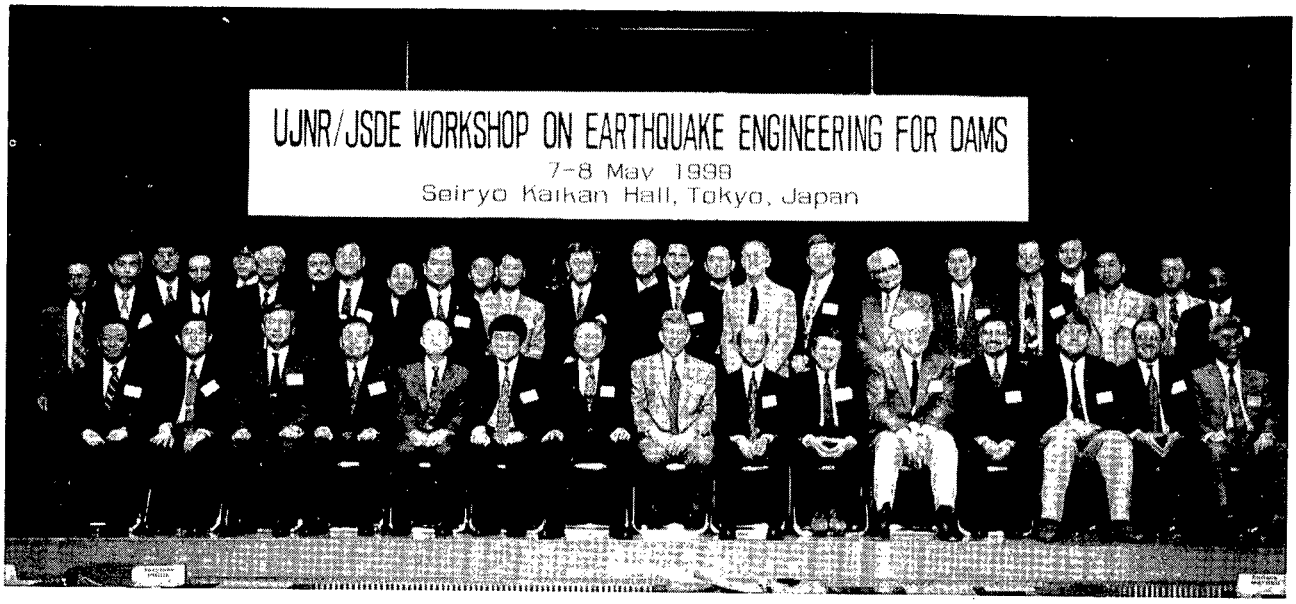
At the time of the Second Workshop, Mr. Hioshi YOSHIDA (PWRI) and Dr. Robert L. HALL (WES) were the Japan-side and U.S.-side chairs of the Task Committee D respectively.

The Task Committee D extends its grateful appreciation for the significant contributions made by speakers, authors and session moderators. We acknowledge the strong support from PWRI and JSDE staff for workshop planning and conduct.

Finally, we expressed thanks to Mr. Takashi SASAKI and Mr. Daisuke HIRAYAMA (PWRI), and Dr. Enrique E. MATHEU (Virginia Polytechnic Institute & State University at the time of the workshop and Louisiana State University at present) who made heavy works to complete the proceedings.

Yoshikazu YAMAGUCHI, Dr. Eng
Japan-side Chairman of the Task Committee D
UJNR Panel on Wind and Seismic Effects
Head of Fill Dam Division, PWRI

Photographs



U.S.-side and Japan-side Attendance
The Second U.S.-Japan Workshop on
Advanced Research on Earthquake Engineering for Dams



Technical Visit to Otaki Dam Construction Site

Agenda

TECHNICAL PROGRAM

May 7, 1999

9:00 **Registration**

9:30-9:55 **Opening Ceremony**

Chairperson - Hitoshi YOSHIDA (PWRI, Japan-side Chairman of UJNR T/C (D))

Welcome Addresses:

Yasutake INOUE (Japan-side Chairman of UJNR Panel on Wind and Seismic Effects, PWRI)

Yusof GHANAAT (QUEST Structure)

Hiroji NAKAGAWA (President of JSDE, Professor Emeritus of Kyoto University, Professor of Ritsumeikan University,)

9:55-10:00 *Break*

10:00-10:25 **Keynote Lecture 1**

Chairperson - Hitoshi YOSHIDA (PWRI, Japan-side Chairman of UJNR T/C (D))

" *Present States of Construction and Maintenance of Dams in Japan* "

Tsuneo UESAKA (PWRI)

10:25-10:40 *Coffee Break*

10:40-11:05 **Keynote Lecture 2**

Chairperson – Enrique E. MATHEU (Virginia Tech)

" *Status of Construction and Safety of Dams in the United States* "

Robert L. HALL (USAEWES, U.S.-side Chairman of UJNR T/C (D))

11:05-11:30 **Keynote Lecture 3**

Chairperson - Hitoshi YOSHIDA (PWRI)

" *On the Behavior of Large Dams near the Epicenter during Earthquakes in Japan* "

Choshiro TAMURA (Professor Emeritus of University of Tokyo, Professor of Nihon University)

11:30-11:40 **Group Photograph on the stage of the hall**

11:40-13:00 **Lunch**

13:00-14:40 **Technical Session 1 (Concrete Dams (1))**

Chairperson - Isao NAGAYAMA (PWRI)

13:00-13:15 " *Vibration Tests and Earthquake Response Observation of Concrete Dams* "

Hiroo SHIOJIRI (Nihon University), Minoru UEDA(Chubu Electric Power Co.Ltd.) and Yukihiro TOYODA (Central Research Institute of Electric Power Industry)

13:15-13:30 " *Field Measurements of Dynamic Interaction at Longyangxia Dam* "

Yusof GHANAAT (QUEST Structures)

13:30-13:45 " *Influence of the 1995 Hyogoken-Nambu Earthquake on Hitokura Dam Foundation Rock* "

Kentaro KIDO and Tomonobu SUGIURA (Water Resources Development Public Corporation)

13:45-14:00 *" Experimental Study on Dynamic Tensile Strength of Concrete using Splitting Tensile Tests "*

Takashi SASAKI, Isao NAGAYAMA, Masahiro HATANO and Yuji KANEKO (PWRI)

14:00-14:40 Discussion

14:40-15:10 *Coffee Break*

15:10-16:30 **Technical Session 2 (Embankment Dams (1))**

Chairperson – Joseph P. KOESTER (USAEWES)

15:10-15:25 *" Hydraulic Fracturing in Fill-type Dams during Earthquake "*

Yoshio OHNE, Kunitomo NARITA, (Aichi Institute of Technology), Yoshio NAKAMURA (AICO Consulting Co. Ltd.) and Yuji MURASE (DAIME Eng. Service Co. Ltd.)

15:25-15:40 *" Influence of Confining Stress on Liquefaction Resistance"*

Richard S. OLSEN (USAEWES)

15:40-16:55 *"Deformation Characteristics of Coarse-grained Materials in Cyclic and Monotonic Loading Triaxial Tests "*

Yoshikazu YAMAGUCHI, Tsuneo UESAKA, Hitoshi YOSHIDA, Tomoya IWASHITA and Jun MATSUURA (PWRI)

16:55-16:30 Discussion

16:30-17:00 *Adjourn*

17:00-19:00 **Welcome Party at Restaurant (4F)**

Master of Ceremonies - Yoshikazu YAMAGUCHI (PWRI)

Welcome Addresses:

--- At the beginning of the party

Yasutake INOUE (Japan-side Chairman of UJNR Panel on Wind and Seismic Effects, PWRI)

Enrique E. MATHEU (Virginia Tech)

Takashi TOYODA (Japan Institute of Construction Engineering)

--- At the end of the party

Tadahiko SAKAMOTO (UJNR Honorary Member, Japan Dam Engineering Center)

May 8, 1999

9:00-10:20 **Technical Session 3 (Embankment Dams (2))**

Chairperson – Michael K. SHARP (USAEWES)

9:00- 9:15 *" Penetration Testing of Liquefied Gravels at Seward, Alaska "*

Joseph P. KOESTER (USAEWES)

9:15- 9:30 *" Dynamic Deformation and Strength Properties of Rockfill Materials "*

Naruo YASUDA (Ministry of Construction) and Norihisa MATSUMOTO (Japan Dam Engineering Center)

9:30- 9:45 *" Seismic Stability and Deformations of Embankment Dams "*

Gonzalo CASTRO (GEI Consultants)

9:45-10:00 " *Factor Analysis of Damage to Small Earth Dams due to the 1995 Hyogoken-Nambu Earthquake* "

Hitoshi YOSHIDA, Tsuneo UESAKA, Tomoya IWASHITA and Jun MATSUURA (PWRI)

Norihisa MATSUMOTO (Japan Dam Engineering Center)

10:00-10:20 Discussion

10:20-10:50 *Coffee Break*

10:50-12:10 **Technical Session 4 (Concrete Dams (2))**

Chairperson – Yusof GHANAAT (QUEST Structures)

10:50-11:05 " *Seismic Response of Gravity Dams in Near Field during the 1995 Hyogoken-Nanbu Earthquake* "

Tatsuo OHMACHI, A. JALALI and H. KAWANA (Tokyo Institute of Technology)

11:05-11:20 " *Nonlinear Seismic Response of Concrete Gravity Dams* "

Enrique E. MATHEU (Virginia Tech)

11:20-11:35 " *Proposal of Modified Seismic Coefficient Method for Concrete Gravity Dams* "

Isao NAGAYAMA and Takashi SASAKI (PWRI)

11:35-11:50 " *Effect of Foundation and Reservoir Parameters on Dynamic Results for Arch Dams Using EACD-3D-96* "

Richard L. MUNOZ (Bureau of Reclamation)

11:50-12:10 Discussion

12:10-13:40 **Lunch**

13:40-15:00 **Technical Session 5 (Embankment Dams (3))**

Chairperson - Norihisa MATSUMOTO (Japan Dam Engineering Center)

13:40-13:55 " *Dynamic Centrifuge Tests on Flow Failure of Fills and Infinite Slopes* "

Osamu MATSUO, Yukiko SAITO and Tetsuya SASAKI (PWRI)

13:55-14:10 " *Evaluation of Motions Recorded at and within Embankment Dams during Earthquakes* "

Izzat M. IDRISS (University of California - Davis)

14:10-14:25 " *Seismic Analysis and Safety Evaluation of Embankment Dams* "

Gilles BUREAU (URS Greiner Woodward Clyde)

14:25-14:40 " *Seismic Response of an Earth Dam with Liquefiable Foundation* "

Michael K. SHARP (USAEWES)

14:40-15:00 Discussion

15:00-15:30 *Coffee Break*

15:30-17:10 **Technical Session 6 (Concrete Dams (3))**

Chairperson – Enrique E. MATHEU (Virginia Tech)

15:30-15:45 " *An Investigation on the Radiation Damping of Dam-Foundation System* "

Yoshiaki ARIGA (Electric Power Development Co., Ltd.), Zengyan CAO, Masatoshi YOSHIDA (Kaihatsu Computing Service Center Ltd.), and Hiroyuki WATANABE (Saitama University)

15:45-16:00 "*A 3-D FE-BE Method for Dynamic Response Analysis of Dam-Foundation-Reservoir Systems*"

Shojiro KATAOKA (PWRI)

16:00-16:15 " *Building a Database of Observational Evidence for Large Structures* "

Ziyad H. DURON (Harvey Mudd College)

16:15-16:30 " *The Estimation on Dynamic Behavior of Arch Dam Modeling Non-linear Properties of Contraction Joints During Earthquake* "

Tatsuo NISHIUCHI and Yukihiro TOYODA (Central Research Institute of Electric Power Industry)

16:30-17:10 Discussion

17:10-17:25 *Short Break*

17:25-18:00 **Closing Ceremony**

Chairperson - Hitoshi YOSHIDA (PWRI)

UJNR T/C (D) Resolutions by Robert L. HALL (USAEWES) & Hitoshi YOSHIDA (PWRI)

Closing Addresses:

Izzat M. IDRISS (University of California - Davis)

Yoshio OHNE (Vice-president of JSDE, Professor of Aichi Institute of Technology)

Resolutions of the Second U.S.-Japan Workshop on Advanced Research on Earthquake Engineering for Dams

Seiryo Kaikan Hall

Tokyo, JAPAN

May 7-8, 1999

The Second U.S.-Japan Workshop on Advanced Research on Earthquake Engineering for Dams was held under the sponsorship of the U.S. Army Engineer Waterways Experiment Station and the Public Works Research Institute of Japan under the auspices of Task Committee D, "Earthquake Engineering for Dams", the UJNR Panel on Wind and Seismic Effects at the Seiryo Kaikan Hall, Tokyo, Japan on May 7-8, 1999.

In order to efficiently use the Workshop as a productive vehicle for the wider technology transfer and enhance to the exchange among scientists, engineers and specialists, the Japan Society for Dam Engineers (JSDE) agreed to co-sponsor this Workshop. This joint workshop was named "UJNR / JSDE Workshop on Earthquake Engineering for Dams".

The workshop provided a valuable forum to exchange technical information of earthquake engineering for dams in both countries. The workshop was attended by 13 U.S. participants (including two spouses) and 110 Japanese participants.

The following resolutions were adopted by the workshop participants:

1. The workshop identified, without priority order, the following topics relevant to dam earthquake engineering for the further cooperative research program:
   a. Methods of analysis for seismic design of dams including outlet works;
   b. Dynamic characteristics of dam construction materials and site conditions;
   c. Analysis of observed behavior of dams and outlet works during an earthquake.

2. The workshop recognizes the importance of continued exchange of research personnel, technical information, research data and use of available research facilities in both countries.

3. The scope of the workshop should be expanded to all aspects of analysis for dam design, evaluation, maintenance and safety.

4. It is very important to develop other means for the future technology transfer, such as seeking other engineering societies with similar interests.

5. In view of the importance of cooperative research programs on earthquake engineering for dams, it is recommended to hold the third Workshop in about two years in USA. The location and time of the workshop will be determined through correspondence between the chairs of Task Committee D of the UJNR Panel on Wind and Seismic Effects.

Summary of the Second U.S.-Japan Workshop on Advanced Research on Earthquake Engineering for Dams

The Second U.S.-Japan Workshop on Advanced Research on Earthquake Engineering for Dams, sponsored by the Public Works Research Institute of Japan (PWRI) and the U.S. Army Corps of Engineers Waterways Experiment Station (WES), was held under the auspices of the Task Committee D, "Earthquake Engineering for Dams", the UJNR Panel on Wind and Seismic Effects at the Seiryo Kaikan Hall, Tokyo, Japan on May 7-8, 1999.

In order to efficiently use the workshop as a productive vehicle for the wider technology transfer and enhance exchanges among scientists, engineers and specialists, the Japan Society for Dam Engineers (JSDE) agreed to co-sponsor this workshop. This forum was called the UJNR / JSDE Workshop on Earthquake Engineering for Dams, but was still the Second Workshop for the members of Task Committee D of the UJNR Panel on Wind and Seismic Effects. In addition, the workshop was supported by the Japan Institute of Construction Engineering (JICE) and the Japan Dam Engineering Center (JDEC).

The workshop provided a valuable forum to exchange technical information on earthquake engineering for dams in both countries. The workshop was attended by 13 U.S. participants (including two spouses) and 110 Japanese participants. The U.S. delegation was led by Dr. Robert L. HALL from the WES.

The two-day workshop was convened by Mr. Hitoshi YOSHIDA (PWRI) and Dr. Robert L. HALL (WES), who were the Japan-side and U.S.-side chairs of the Task Committee D respectively, started with the opening addresses by Mr. Yasutake INOUE, the Director-General of the PWRI / the Japan-side Chairman of the UJNR Panel on Wind and Seismic Effects, Dr. Yusof GHANAAT, the Principal of QUEST Structures, and Dr. Hiroji NAKAGAWA, Professor Emeritus of Kyoto University / the President of the JSDE, which were followed by three keynote lectures. We were fortunate to have three distinguished speakers, Mr. Tsuneo UESAKA, the Director of the Dam Department of the PWRI, Dr. Robert L. HALL, the WES, and Professor Choshiro TAMURA, Professor Emeritus of University of Tokyo. In addition, technical presentations and active discussions were made in six sessions. That covered a wide range of dam earthquake engineering, such as site characterization, dynamic analysis & seismic stability evaluation of concrete / embankment dams, laboratory tests to identify physical properties of construction materials for concrete / embankment dams, vibration tests with shaking table or centrifuge, vibration tests of existing dams, behavior of existing dams during earthquakes, and repair and reinforcement of existing dams.

In addition to the technical program, the participants enjoyed Tokyo hospitality, such as shopping and sightseeing on May 9, 1999. Following the workshop, some U.S.-side participants accompanied by PWRI and JDEC staffs, moved from Tokyo to the Kinki District for sightseeing in Kyoto and technical visit to the Otaki Dam construction site in Nara on May 10-11, 1999. The Otaki Dam is a concrete gravity dam with a height of 100 m and is now under construction by the Kiniki Regional Construction Bureau, the Ministry of Construction of Japan.

We truly enjoyed a successful workshop and the after-hours activities.

List of Speakers

U.S.-Side

GONZALO CASTRO

Date of Birth: August 3, 1938

Birthplace: Santiago, Chile



Education: B.S., Civil Engineering,
Catholic University of Chile, 1961.
M.S., Engineering with concentration in Soil Mechanics,
George Washington University, 1963.
Ph.D., Engineering with concentration in Soil Mechanics,
Harvard University, 1969.

Position: Principal, GEI Consultants Inc
Winchester, Massachusetts (USA)

Dr. Castro is a registered professional engineer in the fields of soil and rock mechanics specializing in soil dynamics, vibrations due to blasting and machine foundations, earthquake engineering, and liquefaction. He is a principal at GEI and has directed numerous geotechnical engineering projects involving evaluation of vibration and earthquake effects in soils.

Dr. Castro has conducted extensive research on dynamic soil properties and the effects of ground vibrations on soils and foundations. His Ph.D. research topic at Harvard was the phenomenon of liquefaction of sands. While at Harvard, he was involved in several projects including the foundations for a 1,200-foot-high stack; seismic stability analysis for Tarbela Dam, Pakistan; San Juan River Dam, Colombia; and Arrow Dam and the Burrard Inlet crossing in British Columbia, Canada.

Dr. Castro has been a consultant on the earthquake stability of dams including tailing dams, in the United States and several foreign countries. He has provided consultant services on the seismic stability of dams to the U.S. Corps of Engineers, U.S. Bureau of Reclamation, U.S. Soil Conservation Service, Nuclear Regulatory Commission, and several utilities. He was a member of the Seismic Advisory Committee for determining Building Code Standards in Massachusetts, the Soil Dynamics and Publication Committees of the Geotechnical Division of ASCE and of the Earthquake and Tailings Dams Committees of the U.S. Committee on Large Dams. He has been the recipient of three National Science Foundation grants for research on the subject of the behavior of soils under cyclic loading.

Dr. Castro has presented many lectures on the subject of earthquake effects on soils, has published numerous papers on the same subject, and has been a panel member at several United States and international conferences on geotechnical earthquake engineering. He has been an invited lecturer on soil properties, particularly under earthquake and vibration loading, at many universities, professional societies, workshops and conferences in the U.S. and abroad.

GILLES BUREAU

Date of Birth: February 8, 1946

Birthplace: Nantes, France

Education: Ingenieur Civil des Mines,
Ecole Nationale Superieure des Mines, 1968.
M.Sc. in Geotechnical Engineering,
University of California at Berkeley, 1971.

Position: Senior Consultant
URS Greiner Woodward Clyde
Oakland, California 94607 (USA)

Gilles Bureau is a Senior Consultant with URS Greiner Woodward Clyde in Oakland, California. Previous employers include: International Engineering Company, San Francisco, California; EDS Nuclear, Paris, France; Civil Systems Inc., San Leandro, California; and Dames & Moore, San Francisco, California.

He has directed numerous seismic safety evaluations of embankment and concrete dams, large intake/outlet towers, water distribution systems, and other major industrial facilities. Many of these studies included development of seismic criteria, finite element, or finite difference analysis, including nonlinear structural response analysis, deformation and/or liquefaction analyses.

His dam safety evaluations have involved over 18 existing concrete dams, 30 embankment dams, and 24 intake/outlet systems with concrete spillways, large towers, outlet tunnels and outlet pipes. Key projects were: Los Leones, Chile (650-feet high embankment), Cherry Valley, California (350-feet rockfill), Hidden, California (184-feet embankment), Pardee, California (345-feet concrete), Lower Crystal Springs, California (140-feet concrete) and Bull Run No. 1, Oregon (200-feet concrete).

He is a member of: the United States Committee on Large Dams (USCOLD), where he acts as Vice-Chairman of the Committee on Earthquakes and Member of the Committee on Methods of Numerical Analysis of Dams; the Association of State Dam Safety Official (ASDSO); the Earthquake Engineering Research Institute (EERI) and the Seismological Society of America (SSA). He is registered as a Civil Engineer and as a Geotechnical Engineer in California, and as a Mining Engineer in France.

ZIYAD H. DURON

Date of Birth: December 29, 1959

Birthplace: Nuremberg, Germany.

Education: B.Sc. in Engineering,
Harvey Mudd College, 1981.
M.Sc. in Civil Engineering,
Massachusetts Institute of Technology, 1983.
Ph.D. in Civil Engineering,
California Institute of Technology, 1987.

Position: Professor of Engineering,
Harvey Mudd College
Claremont, California 91711 (USA)

Professor Duron's areas of expertise include the dynamic testing and response analysis of large civil structures with an emphasis in earthquake engineering. At Harvey Mudd College, Prof. Duron has an endowed research program in Civil Engineering which has focused on the short and long term health monitoring of structures, the development of diagnostic test procedures suitable for detection of changes in structural integrity (damage detection) for bridges and dams, and in the development of a database containing observational evidence of dynamic behavior of large structures. Under his direction, the research group at Harvey Mudd College has actively pursued development of test procedures and instrumentation suitable for testing of large structures including dams, bridges, tunnels, buildings, and launch vehicles. For dams, contributions have included the development of hydrophone instrumentation arrays for the gathering of hydrodynamic pressure response in reservoirs leading to improved understanding of reservoir boundary absorption characteristics and the effect on dam response. Prof. Duron is currently completing analysis of a large reinforced concrete multiple arch dam in California and has helped developed new strategies for evaluating such complex structures under modern seismic requirements. Prof. Duron has also been associated with The Aerospace Corporation since 1988, a company responsible for the engineering support of the U.S. Space Vehicle Launch program under the direction of the U.S. Air Force where he is a Member of The Technical Staff in the Structural Dynamics Group.

YUSOF GHANAAT

Date of Birth: April 13, 1950

Birthplace: Iran



Education: Ph.D., Civil Engineering (Structural),
University of California, Berkeley, 1979.
M.Sc., Civil Engineering (Structural),
University of California, Berkeley, 1976.
B.Sc., Mechanical Engineering,
Arya Mehr University of Technology, Iran, 1972.

Position: Principal, QUEST Structures,
3 Altarinda Road, Suite 203,
Orinda, California 94563 (USA)

Dr. Ghanaat's experience covers more than 20 years in design and analysis and earthquake engineering applications in structural and civil engineering projects. He has served as a consultant on earthquake engineering and structural dynamic analysis, criteria development, earthquake input specification, computer program development and applications, and special problems in design and analysis of dams, navigation locks, intake towers, storage tanks, underground facilities, tunnels, flow-induced gate vibration, and fluid-structure and soil-pile-structure interaction problems. Dr. Ghanaat has published more than 20 journal articles, conference-proceeding papers, and technical reports. Some of Dr. Ghanaat's experience related to concrete dams includes the following: Principal investigator for the NSF-funded US-China co-operative research on experimental study of Longyangxia, and Dongjiang Dams in China. Principal investigator for measurements of reservoir-bottom reflection coefficients at Monticello, Pine Flat, Hoover, Glen Canyon, Morrow Point, Crystal, and Folsom Dams funded by US Army Corps of Engineers and Bureau of reclamation. Project consultant to Earthquake Engineering Research Center at University of California, Berkeley, on the NSF-funded study of Xian Hong Dian and Quan Shui Dams in China and Monticello Dam in CA. Serving on a Consultant Review Board for several Bureau of Reclamation's arch dams. Technical advisor providing specialist consultation on safety evaluation of arch dams to Electric Corporation of New Zealand. Served on a Review Board of Consultants for two Sacramento Municipal District's arch dams. Developed Arch Dams Section of the Federal Energy Regulatory Commission's "*Engineering Guidelines for the Evaluation of Hydropower Projects*." Structural review and consultation on design and analysis of Portugues Arch Dam, Puerto Rico. Investigation of nonlinear earthquake joint opening for Portugues Arch Dam, Puerto Rico. Structural review services for Florence Lake, Agnew Lake, Gem Lake, Balch Diversion and Balch Afterbay Dams, California. Dam safety studies for Bear Valley, Bowman, Combie, McKay's Point, Ralston Afterbay, and Searsville Dams in California, Daniel Johnson in Canada, Broadwater in Montana, Walters in North Carolina, Portugues in Puerto Rico and Karapiro in New Zealand. Dr. Ghanaat is a member of the American Concrete Institute, Association of State Dam Safety Officials, Earthquake Engineering Research Institute, Seismological Society of America, Structural Engineers Association of Northern California, United States Committee on Large Dams.

ROBERT L. HALL



Date of Birth: June 27, 1949

Birthplace: Decatur, Illinois (USA)

Education: B.S. Civil Engineering,
Auburn University, 1971.
M.S. Civil Engineering,
Mississippi State University, 1978.
Ph.D. Civil Engineering,
Oklahoma State University, 1985.

Position: Supervisory Research Structural Engineer
Structural Mechanics Division, Structures Laboratory
U.S. Army Engineer Waterways Experiment Station
Vicksburg, Mississippi 39180 (USA)

Serves as Chief, Structural Analysis Group, Structural Mechanics Division (SMD), Structures Laboratory, U.S. Army Engineer Waterways Experiment Station (WES). This job involves directing and performing research in the areas of seismic analysis, strength design of reinforced hydraulic concrete structures, flow induced structural vibrations, soil-structure interaction and blast response of structures.

For more than 20 years, Dr. Hall has been involved in planning, directing and conducting research on problems concerned with numerical structural modeling, soil-structure interaction, dynamic structural analysis, computer-aided design and structural design criteria. Presently serves as the program manager for the Corps of Engineers' Concrete and Structural Engineering Research Program and for the structural aspects of the Corps' Earthquake Engineering Research Program. Serves as the principal investigator for the Federal Aviation Administration in seismic evaluation of their complete inventory of facilities, technical advisor to B.C. Hydro for the Seven Mile Dam Investigation, and as consultant for the Panama Canal Commission for the seismic evaluation of the Panama Canal's structures.

Other notable functions and experiences include: invited as a team member to survey seismic damage following the January 17, 1995 Kobe Earthquake, Japan; a member of the Federal Emergency Management Agency's Hazard Mitigation Survey team following the October 17, 1989, Loma Prieta Earthquake, California; a member of ASCE's technical committee on Seismic Effects; served as Chair of the ASCE's Government Engineers Section/Branch Involvement Committee; a member of the Society of American Military Engineers; a member of the Technical Program Committee for the 1993 National Earthquake Conference; serves on the Advisory Committee for the Waterways Experiment Station Graduate Center; serves as an Adjunct Professor for Mississippi State University, Alcorn State University, University of Missouri at Columbia and the University of Puerto Rico; represents the Corps of Engineers on the U.S.-Japan Cooperative Program National Resources Panel on Wind and Seismic Effects as a co-chair of the technical committee on "Earthquake Engineering for Dams;" invited by the National Science Foundation (NSF) and the Chinese government to participate in experiments (1991 and 1998) in China on the dynamic response of a concrete arch dam; authored or co-authored more than 100 technical publications in the area of earthquake engineering, computer-aided design and structural dynamics; received several honors and awards such as Chi Epsilon, Sigma Xi, National Deans List, Phi Kappa Phi, numerous annual performance awards, Achievement Medal for Civilian Service, and Directors 1996 R&D Achievement Award.

IZZAT M. IDRISS

Date of Birth: December 28, 1935

Birthplace: Damascus, Syria



Education: B.S., Rensselaer Polytechnic Institute, 1958.
M.S., California Institute of Technology, 1959.
Ph.D., University of California at Berkeley, 1966.

Position: Professor of Civil Engineering
Department of Civil & Environmental Engineering
University of California at Davis,
Davis, California 95616-5294 (USA)

I. M. Idriss is Professor of Civil Engineering at the University of California at Davis (UCD). His areas of teaching, research and practice are: earthquake geotechnical engineering; soil mechanics and foundation engineering; earthfill and rockfill dam engineering; applications of probabilistic procedures to geotechnical problems; and numerical modeling. He joined the faculty at UCD in 1989 following 20 years at Woodward-Clyde Consultants in San Francisco, Santa Ana and Oakland where he was a senior Principal, and five years as a member of the teaching and research staff of the geotechnical engineering group at the University of California at Berkeley, where he completed his Ph. D. degree in 1966. Prior to that he had completed an MS degree at Caltech in 1959 and a BCE degree at Rensselaer Polytechnic Institute in 1958.

He has been involved in post earthquake investigations since the occurrence of the 1964 Great Alaska earthquake and has done comprehensive post earthquake investigations of some ten earthquakes from Anchorage to Kobe. He has developed or co-developed many of the currently used procedures for evaluating liquefaction, site response, and behavior of earthfill and rockfill dams during earthquakes.

He has provided and continues to provide consulting services on many projects in the USA and other countries. He has served and continues to serve on several consulting or review boards for US and International companies and for State and Federal Agencies. He has received many awards and honors over the past thirty years, including election to the US Academy of Engineering in 1989, receipt of the first H. Bolton Seed Medal from ASCE in 1995, and the Distinguished Public Service Award from the University of California at Davis for 1998-1999.

JOSEPH P. KOESTER



Date of Birth: July 6, 1956

Birthplace: Lexington, Kentucky (USA)

Education: B.S. in Civil Engineering, University of Kentucky, 1978.
M.S. in Civil Engineering, University of Kentucky, 1979.
Ph.D. in Civil Engineering, University of Colorado, 1992.

Position: Civil Engineer
Earthquake Engineering and Geosciences Division
Geotechnical Laboratory
U.S. Army Engineer Waterways Experiment Station
Vicksburg, Mississippi 39180 (USA)

Dr. Koester began his career with the Waterways Experiment Station (WES) in March, 1980, as a Research Civil Engineer in the Earthquake Engineering and Geophysics Division. During his tenure at WES, Dr. Koester has directed and performed various military and civil projects involving the development and use of geophysical surveying equipment and procedures, design and application of geotechnical and environmental in situ test equipment and procedures, and the seismic stability evaluation of earth- and rock-fill dams. His dissertation research examined cyclic strength and pore pressure generation characteristics (during earthquake shaking) of fine-grained soils, and Dr. Koester continues to develop improved analytical procedures and test equipment for evaluation of the response of various types of soil to cyclic loading. During the period July – December 1994, Dr. Koester managed intermediate- and long-range Military Research, Development, Testing and Evaluation (RDT&E) programs and plans as Corps of Engineers Liaison Officer to the Assistant Secretary of the Army (Research, Development and Acquisition), at the Pentagon.

Dr. Koester is an active member of the Society of American Military Engineers, the U.S. Committee on Large Dams of the International Commission on Large Dams, and the American Society of Civil Engineers, where he serves on the Soil Dynamics Committee. He is also a member of the Sigma Xi, Tau Beta Pi, and Chi Epsilon engineering honorary societies. Dr. Koester serves on the WES Dam Safety Committee and the Subcommittee for Natural Disaster Reduction of the National Science and Technology Council. Dr. Koester is the author or a co-author of twelve refereed papers and over 30 technical reports.

ENRIQUE E. MATHEU

Date of Birth: March 20, 1964

Birthplace: Cordoba, Argentina



Education: B.Sc. in Civil Engineering,
National University of Cordoba, 1988.
M.Sc. in Civil Engineering,
University of Puerto Rico, 1992.
Ph.D. in Engineering Mechanics,
Virginia Polytechnic Institute & State University, 1997.

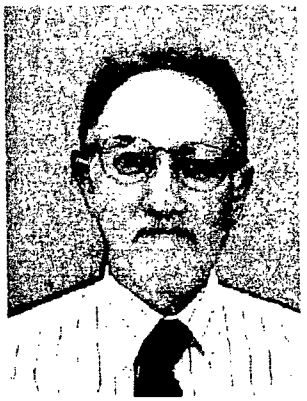
Position: Research Assistant Professor
Department of Engineering Science and Mechanics
Virginia Polytechnic Institute & State University
Blacksburg, Virginia 24060 (USA)

Enrique E. Matheu recently joined the Department of Engineering Science and Mechanics at the Virginia Polytechnic Institute & State University (Virginia Tech) as a Research Assistant Professor. His areas of research interest include structural dynamics and control, earthquake engineering, and finite-element applications. During his doctoral studies at Virginia Tech, he carried out research in active and semi-active control strategies for the reduction of the seismic response of civil engineering structures. Part of his current research is focused on the application of nontraditional control techniques (neural networks and fuzzy logic) for vibration control of buildings.

His professional experience includes a two-year fellowship with the National Council of Scientific and Technological Research (Argentina), where his work focused on the development of numerical procedures for the dynamic analysis of embankment dams. He has also collaborated as a Visiting Research Scientist at the U.S. Army Engineer Waterways Experiment Station (Vicksburg, MS), where he conducted and directed research on the area of seismic response of concrete dams.

He has authored or co-authored over 30 journal articles, conference papers, and technical reports. He is a member of the American Academy of Mechanics (AAM), the American Society of Civil Engineers (ASCE), the American Society for Engineering Education (ASEE), the Earthquake Engineering Research Institute (EERI), the Society for Industrial and Applied Mathematics (SIAM), and the United States Committee on Large Dams (USCOLD).

RICHARD L. MUNOZ



Date of Birth: December 24, 1951

Birthplace: El Paso, Texas (USA)

Education: B.Sc. in Civil Engineering,
University of Texas at El Paso.

Position: Structural Engineer
Concrete Dams Structural Analysis Group
Bureau of Reclamation
Denver, Colorado 80225 (USA)

Richard L. Munoz is a structural engineer with the United States Bureau of Reclamation in Denver, Colorado. Mr. Munoz has worked in the Concrete Dams Structural Analysis Group for nearly 20 years and has been involved in the analysis of numerous dams such as Horse Mesa, Nambe Falls, Deadwood, Parker, Friant, and Arrowrock Dams. Mr. Munoz received his Bachelor of Science in Civil Engineering from The University of Texas at El Paso.

RICHARD S. OLSEN



Date of Birth: March 5, 1954

Place of Birth: Portland, Oregon (USA)

Education: B.S. in Civil Engineering,
Oregon State University, 1976.
M.S. in Geotechnical Engineering,
University of California at Berkeley, 1977.
Ph.D. in Geotechnical Engineering,
University of California at Berkeley, 1994.

Position: Research Geotechnical Earthquake Engineer
Earthquake Engineering and Geosciences Division
Geotechnical Laboratory
U.S. Army Engineer Waterways Experiment Station
Vicksburg, Mississippi 39180 (USA)

Dr. Olsen has worked for FUGRO (Ertec), Harding-Lawson Assoc, and Dames & Moore before joining the Waterways Experiment Station in February 1982 as a research civil engineer in the Earthquake Engineering and Geosciences Division. His research has resulted in numerous techniques for evaluating Cone Penetrometer Test (CPT) data and site characterization. Specifically, he is known for developing CPT based techniques to predict static and dynamic soil properties, soil classification, and stress normalization parameters. Over 400 researchers world-wide have requested his 1994 PhD dissertation. He developed the stress focus theory in 1992 which accounts for confining stress effects (i.e. stress normalization) on different strength parameters and measurements for all strength levels, soil types, and stress levels (1 to 4000 KPa). The stress focus theory has been used with the CPT cone resistance, Standard Penetration Test (SPT), shear wave velocity, modulus, liquefaction resistance, sand friction angle, and recently K_α. He developed a unique CPT based technique for prediction of liquefaction resistance (using the cone resistance and friction ratio), originally published in 1984 with updates/improvements in 1986, 1988, 1995, 1996, & 1998.

He was one of the original developers of the SCAPS probing system to detect hydro-carbon contamination in situ using fiber optic transmitted laser induced fluorescence (1987-1992). He was in charge of CPT technology, data acquisition, data evaluation, computer hardware, and all software development. He developed all the techniques for detecting and characterizing fluorescence signatures and 3D visualization techniques (for displaying CPT-predicted soil layers and predicted equivalent diesel fuel distribution). He designed and fabricated a 9-meter boat for rapid CPT investigations (up to 25 soundings per day) in shallow extremely soft sea floor soils off the Texas coast (1994-1995). This work also required writing custom software for CPT and vane shear data acquisition, dynamic GPS position monitoring, and high resolution 2D characterization.

Some of his other accomplishments are seismic stability evaluation of 12 large earth dams (performed over the last 18 years), development of 2D stratigraphic (and statistical) techniques/software for CPT data analysis, web master for www.liquefaction.com, and development of a PC-based system for geophysical detection of tunnel activity (1986-1988). Dr. Olsen is a member of the American Society of Civil Engineers and other societies and is author of 28 conference publications and over 14 technical reports.

MICHAEL K. SHARP



Date of Birth: November 7, 1958

Birthplace: Union, Mississippi (USA)

Education: B.S. in Biology,
University of Mississippi, 1982.
B.S. in Civil Engineering,
Texas A&M University, 1987.
M.S. in Civil Engineering,
Mississippi State University, 1992.

Position: Research Civil Engineer
Earthquake Engineering and Geosciences Division
Geotechnical Laboratory
U.S. Army Engineer Waterways Experiment Station
Vicksburg, Mississippi 39180 (USA)

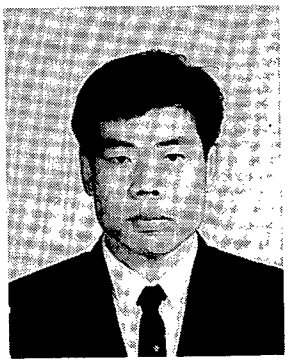
Mr. Sharp is currently pursuing a Ph.D. in civil engineering at Rensselaer Polytechnic Institute under the direction of Professor Ricardo Dobry. His main interest of study is the dynamic effects of soils and centrifuge modeling. Mr. Sharp has been a civil engineer in the Engineering Geophysics Branch of the Earthquake Engineering and Geosciences Division since December, 1987. He has performed research studies utilizing geophysical methods to assist in solving geotechnical and environmental problems.

Mr. Sharp is a member of the American Society of Civil Engineers and the Society of Exploration Geophysicists. He is the co-author of 5 refereed journal articles and over 30 technical reports.

List of Speakers

Japan-Side

PERSONAL CAREER



NAME: Zengyan CAO

POSITION: Senior Research Engineer
Technical Division 1
Scientific System Department
Kaihatsu Computing Service Center Ltd.

ADDRESS: 2-2-18, Fukagawa, Kotoku, Tokyo 135-8451, JAPAN
Tel. +81-3-3642-9771
Fax. +81-3-3642-9796

DATE OF BIRTH: September 27, 1960

EDUCATION: Ph.D. (1995) of Earthquake Engineering, Saitama University

MAJOR SUBJECT: Numerical Analysis of Structures, Dam Engineering

MAJOR AREA OF EXPERIENCE:

1981-1983	Engineer, Institute of Hebei Water Resources Research, China
1986-1992	Research Engineer, Earthquake Engineering Research Center, China Institute of Water Resources and Hydropower Research (IWHR)
1995 -	Senior Research Engineer, Technical Division 1, Scientific System Department, Kaihatsu Computing Service Center Ltd.

TRAVEL ABROAD: P. R. China, USA, Mexico

MAJOR PUBLICATIONS:

"Upstream Boundary of Reservoir in Dynamic Analysis", Journal of Engineering Mechanics, ASCE, Vol.124, April, 1998

"An Investigation on the Radiation Damping of 3-D Dam-Foundation-Reservoir System", 10th Japan Symposium of Earthquake Engineering, November, 1998

"Investigation on the Earthquake Response and Basic Characteristics of a Rockfill Dam", Large Dams, No.163, JANCOLD, April, 1998

"Dynamic Behavior of a Rockfill dam and its Material Properties", Proceedings of the 19th Congress of International Committee on Large Dams (ICOLD), Q.73, R.40, May, 1997

"Comparison Between Substructure Method and Direct Analysis", Proceedings of 24th Japan Earthquake Engineering Conference, June, 1997

"Dynamic Behavior of Faced Rockfill Dam - Reservoir System", Proceedings of 24th Japan Earthquake Engineering Conference, June, 1997

"Vibration Modes of Rockfill Dams Based on the Observations of Microtremors and Earthquakes", Journal of Science and Technology, Samasat University, 1996

"Elemental Three Dimensional Dynamic Behavior of a Fill Dam", Proceedings of 11th World Conference on Earthquake Engineering, June, 1996

"Hydrodynamic Pressure and Reservoir Boundary Treatment", Proceedings of 9th Japan Earthquake Engineering Symposium, November, 1994

PERSONAL CAREER



NAME : Shojiro KATAOKA

POSITION : Research Engineer, Ground Vibration Division,
Earthquake Disaster Prevention Research Center,
Public Works Research Institute (PWRI),
Ministry of Construction (MOC)

ADDRESS : 1, Asahi, Tsukuba-Shi, Ibaraki-Ken, 305-0804, JAPAN
Tel. +81-298-64-4963
Fax. +81-298-64-0598

DATE OF BIRTH : January 1, 1970

EDUCATION : B. S. in Civil Engineering, Tokyo Institute of Technology (1992)
M. S. in Earthquake Engineering, Tokyo Institute of Technology (1994)
Ph.D. in Earthquake Engineering, Tokyo Institute of Technology (1996)

MAJOR SUBJECT : Earthquake Engineering, Engineering Seismology

MAJOR AREA OF EXPERIENCE :

1994–1997	Research Fellow of the Japan Society for the Promotion of Science
1996–1997	Postdoctoral Scholar in Civil Engineering, Division of Engineering and Applied Science, California Institute of Technology
1997–1998	Lecturer, Tokyo Institute of Technology
1998–	Research Engineer, Ground Vibration Division, Earthquake Disaster Prevention Research Center, PWRI, MOC

TRAVEL ABROAD : UK, Greece, Austria, Switzerland, Mexico, USA, Philippines

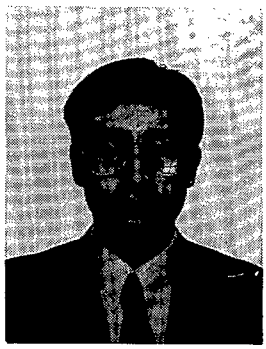
MAJOR PUBLICATIONS :

"Synthetic earthquake motion of 2-D irregular ground in near-field", Proceedings of the 11th World Conference on Earthquake Engineering (1996)

"3-D simulation of near-field ground motion of the 1995 Hyogo-ken Nanbu earthquake", Proceedings from the 6th U. S. – Japan Workshop on Earthquake Resistant Design of Lifeline Facilities and Countermeasures against Liquefaction (1996)

"Earthquake response of 2-D concrete gravity dam interacted with foundation and reservoir", Proceedings of the International Symposium on Seismic and Environmental Aspects of Dams Design: Earth, Concrete and Tailings Dams (1996)

PERSONAL CAREER



NAME : Kentaro KIDO

POSITION : Senior Research Engineer
Concrete Dam Division
Research Institute
Water Resources Development Public Corporation
(WARDEC)

ADDRESS : 936, Jinde, Urawa-Shi, Saitama-Ken, 338-0812,
JAPAN
Tel. +81-48-853-1785
Fax. +81-48-855-8099

DATE OF BIRTH : January 28, 1964

EDUCATION : Master(1988) of Civil Engineering, Kyoto University

MAJOR SUBJECT: Dam Engineering

MAJOR AREA OF EXPERIENCE:

1988-1992	Engineer, Urayama Dam Construction Office, WARDEC
1992-1994	Assistant Chief, Water Quality Management Div., Water Quality Bureau, Environment Agency
1994-1995	Research Engineer, Concrete Dam Div., Research Institute, WARDEC
1996-	Senior Research Engineer, Concrete Dam Div., Research Institute, WARDEC

TRAVEL ABROAD: Spain

MAJOR PUBLICATIONS:

"A Study of Thermal Control on RCD Dam", Intl. Symposium of Roller Compacted Concrete Dams(1995)

"Dynamic Analysis of Hitokura Dam during the 1995 Hyogoken-Nambu Earthquake", ICOLD 19th Congress(1997)

"A Study of the Influence of Longitudinal Joints on the Behavior of Concrete Gravity Dams", ICOLD 19th Congress(1997)

PERSONAL CAREER

NAME: Osamu Matsuo

POSITION: Head
Soil Dynamics Division
Earthquake Disaster Prevention
Research Center

ADDRESS: Asahi-1, Tsukuba, Ibaraki
305-0804 Japan
(tel) 0298-64-2933
(fax) 0298-64-2576



DATE OF BIRTH: March 17, 1954

EDUCATION: Master of Engineering
Kyushu University

MAJOR SUBJECT: Soil Dynamics and Earthquake Engineering

MAJOR AREA OF EXPERIENCE:

1979-1990 Research Engineer
Soil Dynamics Division, PWRI
1990-1993 Assistant Director
Research and Programming Division
Economic Cooperation Bureau
Ministry of Foreign Affairs
1993- Head
Soil Dynamics Division

TRAVEL ABROAD: Argentine, Bolivia, China, Colombia, Equador, Fiji, Ghana, Indonesia, Ivory Coast, Mexico, Nepal, Thailand, Tonga, U.S.A.

MAJOR PUBLICATIONS:

Matsuo, O. et al.: Shaking table tests and analyses of geosynthetics-reinforced soil retaining walls, Geosynthetics International, Special Issue (Vol.5, No.1), International Geosynthetics Society, 1998.

Matsuo, O. et al.: Evaluation of cone penetration testing as an in situ liquefaction resistance measurement, Proc. 1st Intl. Conf. on Site Characterization, 1998.

Matsuo, O. et al.: Numerical simulation of seismic failure of embankments founded on liquefiable soils, Proc. 9th Intl. Conf. of the Intl. Assoc. for Computer Methods and Advances in Geomechanics, 1997.

Matsuo, O. et al.: Revised liquefaction potential evaluation procedure and seismic design treatment of liquefaction for bridge foundation, Proc. 12 th U.S.-Japan Bridge Engineering Workshop, 1996.

Matsuo, O. et al.: Deep mixing method as a liquefaction prevention measure, Proc. IS-Tokyo'96/ 2nd Intl. Conf. on Ground Improvement Geosystems, 1996.

Koga, Y. and O. Matsuo: Shaking table tests of embankment resting on liquefiable sandy ground, Soils and Foundations, 1990.

PERSONAL CAREER



NAME: Norihisa MATSUMOTO
POSITION: Director, Engineering Department I
Japan Dam Engineering Center(JDEC)
ADDRESS: Mesonic 39 Mori BLDG.
Azabudai 2-4-5, Minatoku
Tokyo, 106-0041 JAPAN
Phone: +81-3-3433-7811
Fax: +81-3-3432-6204
e-mail: matsu@jdec.or.jp

Date of Birth: March 2, 1944

EDUCATION: Bachelor(1966) of Civil Engineering, Univ. of Tokyo

MAJOR SUBJECT: Dam Engineering

MAJOR AREA OF EXPERIENCE:

1972-1977 Research Engineer, Filldams Division, PWRI, MOC
1977-1978 Visiting Researcher, Bureau of Reclamation
1978-1979 Chief Research Engineer, Dam Structural Division, PWRI
1979-1991 Head, Filldams Division, PWRI
1991-1994 Chief Research Engineer, JDEC
1994-1995 Director, Dams Department, PWRI
1995- Director, Engineering Division Ⅰ, JDEC

ACTIVITIES ABROAD: USA, CHINA, KOREA, TAIWAN, INDONESIA, VENEZUELA, INDIA, TURKEY, SWITZERLAND, BRAZIL, UAE, ITALY,

MAJOR PUBLICATIONS:

"Comprehensive Inspections of Dams and Reservoirs in Japan" Symposium on Rehabilitation of Dams, ICOLD Annual Meeting, New Delhi, Nov. 1998

"Effects on Dams" Special Issue of Soils and Foundations, Japanese Geotechnical Society, Jan. 1996

"Comparisons of Deformation Characteristics of Rockfill Materials using Monotonic and Cyclic Loading Laboratory tests and in situ tests" Canadian Geotechnical Journal, Vol.31, 1994

"Behaviors of Foundations for Fill Dams during Construction and First Filling of Reservoirs in Japan" ICOLD 17th Congress, Vienna, 1991

"Experience and Problems of Construction of Dams on Soft Rock Foundations in Japan" Proc. International Symposium on Weak Rock, ISRM, Tokyo, 1981

PERSONAL CAREER



NAME : Isao NAGAYAMA

POSITION : Head of Dam Structure Division
Dam Department
Public Works Research Institute (PWRI)
Ministry of Construction (MOC)

ADDRESS : 1, Asahi, Tsukuba-Shi, Ibaraki-Ken, 305, JAPAN
Tel. +81-298-64-2402
Fax. +81-298-64-2688

DATE OF BIRTH : April 26,1951

EDUCATION : Bachelor(1974) of Civil Engineering, University of Tokyo

MAJOR SUBJECT : Dam Engineering

MAJOR AREA OF EXPERIENCE :

1974-1976	Engineer, Kawaji Dam Construction Office, Kanto Regional Construction Bureau, MOC
1976-1983	Research Engineer, Dam Structure Div. Dam Dept., PWRI, MOC
1983-1988	Senior Research Engineer, Dam Structure Div. Dam Dept., PWRI, MOC
(1984-1985	Visiting Researcher, ER Center Bureau of Reclamation, US Dept. of the Interior)
1988-	Head of Dam Structure Div., Dam Dept. PWRI, MOC

TRAVEL ABROAD : USA, P.R. of China, Indonesia, Republic of South Africa, Spain, Italy

MAJOR PUBLICATIONS :

"Study on Dynamic Behavior of Concrete Dam during Earthquake with Hydrodynamic Interaction", ICOLD Intl. Symposium on Earthquake and Dams (1987)

"A Study on Control of Temperature Cracks in Large Roller Compacted Concrete Dams", ICOLD 16th Intl. Congress (1988)

"A Study on the Compaction Mechanism of RCD Using Large-sized Specimens and Standard Specimens", Int. Symposium of Roller Compacted Concrete Dams (1995)

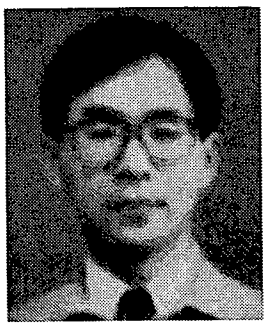
"Safety of Dams during Hyogoken-Nambu Earthquake on January 17, 1995 in Japan" 11th WCEE (1996)

"A Study on Mixture Design of RCD Concrete Using Standard Specimen Compaction Device", ICOLD 19th Congress (1997)

"Behavior of Dams during the Hyogoken-Nambu Earthquake on January 17, 1995 in Japan", ICOLD 19th Congress (1997)

"Case Study about Vertical Seismic Motion Effects on Stress in Concrete Gravity Dam", ICOLD Symposium on Rehabilitation of Dams (1998)

PERSONAL CAREER



NAME : Tatsuo NISHIUCHI

POSITION : Senior Researcher
Structure Department
Central Research Institute of
Electric Power Industry (CRIEPI)

ADDRESS : 1646, Abiko, Abiko-Shi, Chiba-Ken, 270-1194, JAPAN
Tel. +81-(0)471-82-1181
Fax. +81-(0)471-83-2962

DATE OF BIRTH : May 9, 1964

EDUCATION : Master(1989) of Civil Engineering, University of Tokyo

MAJOR SUBJECT : Concrete Engineering

MAJOR AREA OF EXPERIENCE :

1989-1992	Researcher, Material Section, Earthquake Dept., CRIEPI
1992-1995	Research Engineer, Construction Material Group, Structure Dept., CRIEPI
1995-1997	Senior Researcher, Construction Material Group, Structure Dept., CRIEPI
1997-	Senior Researcher, Structure Dept., CRIEPI

TRAVEL ABROAD : Italy, France, Canada, Taiwan

MAJOR PUBLICATIONS :

"A Study on Shear-Slip Failure Criterion of Concrete Blocks Joints" ; CRIEPI Report No.U94051(1995)

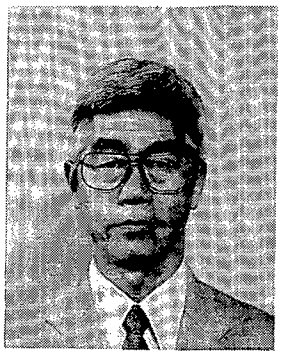
"A Study on the Effect of Shear Key Blocks on the Behavior of Vertical Joints in Arch Dams"; CRIEPI Report No.U94052(1995)

"Effect of Stiffness of Boundary Rock and Uplift Change on Behavior of Arch Dam" ;CRIEPI Report No.U96048(1997)

"Investigation on the Static Behavior of an Aged Arch Dam Using Non-Linear Finite Element Method" ;CRIEPI Report No.U97060(1998)

"3D Finite Element Analysis of Arch Dam Modeling Non-linear Behavior of Contraction Joints";The Sixth East Asia-Pacific Conference on Structural Engineering & Construction(1998)

PERSONAL CAREER



NAME : Tatsuo OHMACHI

POSITION : Head and Professor, Department of Built Environment
Interdisciplinary Graduate School of Science and
Engineering, Tokyo Institute of Technology

ADDRESS : 4259 Nagatsuta-cho, Midori-ku, Yokohama 226-8502
Tel. +81-045-924-5605
Fax. +81-045-924-5574
E-Mail: Ohmachi@enveng.titech.ac.jp

DATE OF BIRTH : August 3, 1945

EDUCATION : 1969-1974 Graduate School of Civil Engineering, University of Tokyo
1965-1969 Department of Civil Engineering, University of Tokyo

MAJOR SUBJECT : Earthquake Engineering
Civil Engineering
Engineering Seismology

MAJOR AREA OF EXPERIENCE :

1987 to date : Professor, Tokyo Institute of Technology
1979 - 1987 : Associate Professor, Tokyo Institute of Technology
1974 - 1979 : Electric Power Development Co. Ltd.

TRAVEL ABROAD : USA, China, Korea, Chile, India, Philippines, Mexico, Austria

MAJOR PUBLICATIONS :

"A FE-BE Method for Dynamic Analysis of Dam-Foundation-Reservoir Systems in the Time Domain", Earthquake Engineering and Structural Dynamics (1993)

"Model Analysis of a Dam-foundation System Based on an FE-BE Method in the Time Domain", Earthquake Engineering and Structural Dynamics (1994)

"Assessment of Ultimate Earthquake Stability of Rockfill Dams with Vertical Clay Core", 18th ICOLD (1994)

"Experimental Study of Hydrodynamic Pressure inside Narrow Cracks", Dam Engineering, Japan Society of Dam Engineering (1998)

"2 Dimensional Analysis of Seismic Cracking in Concrete Gravity Dams", Dam Engineering, Japan Society of Dam Engineering (1998)

PERSONAL CAREER



NAME : Yoshio Ohne

POSITION : Professor of
AICHI INSTITUTE of
TECHNOLOGY.

ADDRESS : 1,247, Yachigusa, Yagusa-cho,
Toyota-shi, Aichi-ken, JAPAN.
Tel. +81−565−48−8121
Fax. +81−565−48−3749

DATE OF BIRTH: Feb, 7, 1934

EDUCATION: Bachelor(1956)and Dr, degree(1968)at
Tokyo Institute of Technology.

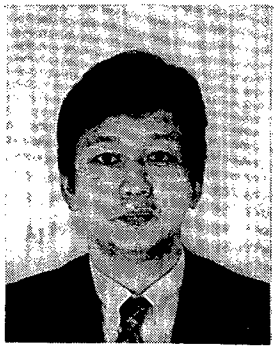
MAJOR SUBJECT: Geotechnical and Dam Engineering.

MAJOR AREA OF EXPERIENCE:
- *1956−1965 Aichi Water Resource and Irrigation Public Corporation.
- *1964−1965 West Germany.
- *1965−1968 Sanyu Consaltants Co,.
- *1968−present: prof.of A. I. T.

TRAVEL ABROAD:
European countries, Mexico, Brazil, USA and others.

MAJOR PUBLICATION:
- *Design and constraction of fill-type dams.
- *Hand-book of geotechnical engineering(1980)
- *Treatment of groundwater at the excavation(1981).
- *Hand-book of civil engineering(1985).
- *Other 38 papers on dam engineering.

PERSONAL CAREER



NAME : Takashi SASAKI

POSITION : Senior Research Engineer
Dam Structure Division
Dam Department
Public Works Research Institute (PWRI)
Ministry of Construction (MOC)
The Japanese Government

ADDRESS : 1, Asahi, Tsukuba City,
Ibaraki Prefecture, 305, JAPAN
Tel. +81-298-64-4283
Fax. +81-298-64-2688

DATE OF BIRTH : January 26, 1965

EDUCATION : 1987 Bachelor (1987) and Master Degree (1989) of Civil Engineering, Tokyo Institute of Technology

MAJOR SUBJECT : Civil Engineering (Dam Engineering)

MAJOR AREA OF EXPERIENCE:

1989-1996	Research Engineer, Dam Structure Div., Dam Dept., PWRI, MOC
1996-	Senior Research Engineer, Dam Structure Div., Dam Dept., PWRI, MOC
(1997.12-1998.12	Visiting Scholar, University of California at Berkeley, USA)

TRAVEL ABROAD : U.S.A., P.R. of China, Mexico

MAJOR PAPERS :

"Direct Tensile Strength of Concrete for Dams" (with I. Nagayama et al.), Technical Memorandum of PWRI, No. 3223, 1993 (in Japanese)

"A Study on the Mixture Design of RCD Concrete Using Large-sized Specimens and Standard Specimens" (with I. Nagayama et al.), Intl. Workshop on Construction and Management Technology for Dams, and Enhancement of the Dam Lake Basin Environment for the Next Generation, 1994

"Seismic Response Properties of Concrete Gravity Dam with Interaction of Dam and Foundation Rock" (with I. Nagayama), UJNR 27th Joint Meeting of U.S. and Japan Panel on Wind and Seismic Effects at PWRI, 1995

"Safety of Dams during Hyogoken-Nambu Earthquake on January 17, 1995 in Japan" (with A. Nakamura et al.), 11th World Conference on Earthquake Engineering, 1996

"Effects of Vertical Seismic Motion on Structural Stability of Concrete Gravity Dams" (with I. Nagayama), 1st U.S.- Japan Workshop on Advanced Research on Earthquake Engineering for Dams at WES, 1996

"Experimental Study on Tensile Strength of Concrete for Dams" (with I. Nagayama), UJNR 29th Joint Meeting of U.S. and Japan Panel on Wind and Seismic Effects at PWRI, 1997

"A Study on Stress in Concrete Gravity Dam using Seismic Data during Kobe Earthquake" (with T. Uesaka and I. Nagayama), UJNR 30th Joint Meeting of U.S. and Japan Panel on Wind and Seismic Effects at NIST, USA, 1998

"Case Study about Vertical Seismic Motion Effects on Stress in Concrete Gravity Dam" (with T. Yokotsuka, T. Uesaka and I. Nagayama), Symposium in Rehabilitation of Dams, 66th ICOLD Annual Meeting, New Delhi, 1998

PERSONAL CAREER



NAME: Choshiro Tamura

POSITION: Professor
Department of Civil Engineering
College of Industrial Technology
Nihon University

ADDRESS: 1-2-1, Izumi-cho, Narashino-City,
Chiba-Prefecture, 275 Japan
Tel. +81-474-74-2428
Fax. +81-474-74-2449

DATE OF BIRTH: June 26, 1930

EDUCATION: Bachelor (1954) and Master Degree (1959) of Engineering,
University of Tokyo
Doctor Degree of Engineering, University of Tokyo

MAJOR SUBJICT: Earthquake Resistance of Dams
Earthquake Resistance of Underground Structures
Earthquake Engineering

MAJOR AREA OF EXPERIENCE:

1959-1965	Design Engineer, Nihon-Construction-Consultant Ltd.
1965-1966	Assistant, Institute of Industrial Science (IIS), University of Tokyo
1966-1975	Assistant Professor, IIS., University of Tokyo
1975-1991	Professor, IIS., University of Tokyo
1991-	Professor Emeritus, University of Tokyo
1991-	Professor, College of Industrial Technology, Nihon University

TRAVER ABROAD: USA, China, GB, Chile, Italy, India, Spain, Turkey

MAJOR PUBLICATIONS:

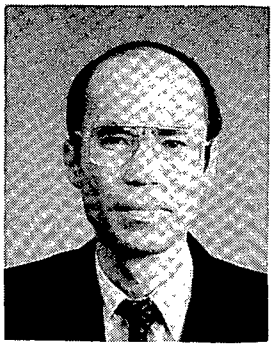
Dynamic Behavior of Earth Dam During Earthquakes (co-author), Report of IIS., 1966

Dynamic Behavior of a Submerged Tunnel During Earthquakes(co-author) Report of IIS., 1975

Static and Dynamic Behavior of Kurobe Dam (co-author), Tokyo University Press, 1988

Earthquake Damages and Dynamic Characteristics of the Ground, San-kaidou, 1996

PERSONAL CAREER



NAME :Hiroo SHIOJIRI
POSITION :Professor
Civil Engineering Department
College of Science and Technology
Nihon University

ADDRESS :1-8.Kanda-Surugadai,Chiyoda-Ku,Tokyo,101-8303,JAPAN
DATE OF BIRTH :December 10,1945
EDUCATION :Master(1970) of Engineering, University of Tokyo
MAJOR SUBJECT:Earthquake Engineering
MAJOR AREA OF EXPERIENCE:

1970-1978	Research Engineering, Structure Section, Central Research Institute of Electric Power Industry(CRIEPI)
1979-1986	Senior Research Engineer, Nuclear Structure Section, CRIEPI
1987-1991	Research Fellow, Seismic Isolation Section, CRIEPI
1992-	Professor, Civil Engineering Department, college of Science and Technology, Nihon University

TRAVEL ABROAD :USA,P.R. of China, R.of China, Philippine, R.of Korea,
MAJOR PUBLICATIONS:

"A Method for Time Domain Analysis of Semi-Infinite Foundation-Structure-Water Systems", Numerical Methods in Geomechanics Nagoya, (1985)

"Simulation Analysis of Forced Vibration Response of Arch Dam", Proc. JSCE No.605(1994)

"A Method for the Analysis of Porous Media", Civil Engineering Confference,Philippine,(1996)

"Modified Iterative Extended Kalman Filterling for the Identification of Wave Propagation Problem", Probability and Structural Safety,(1997)

"A Time-Domain Method for the Analysis of Two-Phase Media", Proc 10th Earthquake Engineering Conference(1998)

PERSONAL CAREER



NAME: Tsuneo UESAKA

POSITION: Director, Dam Department
Public Works Research Institute
Ministry of Construction

ADDRESS: 1, Asahi, Tsukuba-shi, Ibaraki-ken
305-0804, Japan
TEL 0298-64-2211
FAX 0298-64-2688

DATE OF BIRTH: January 1, 1948

EDUCATION: Bachelor (1970) and Master Degree (1972) of Engineering, Osaka University

MAJOR FIELD: Dam Engineering

MAJOR AREA OF EXPERIENCE

1988-1990	Director, Miyagase Dam Construction Office, Kanto Regional Construction Bureau
1990-1992	Senior Officer for Construction, River Development Division, River Bureau
1992-1993	Director, Water Resources Survey Division, National Land Agency
1993-1995	Director, Tone River Upper Reaches Work Office, Kanto Regional Construction Bureau
1995-1997	Director, Water Resources Planning Division, National Land Agency
1997-	Director, Dam Department, Public Works Research Institute

TRAVEL ABROAD: USA, Philippine, Korea, Thailand, Nepal, Brazil

MAJOR PUBLICATIONS

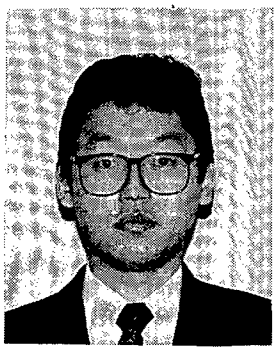
"Construction of Multi-purpose Dams", Dam Engineering Center (1987)

"Present Problems and Future View of Rationalized Construction Methods for Dams", Dam Engineering (1991)

"Concrete of Optimum Design for Aggregate", Cement & Concrete (1992)

and many other papers and publications

PERSONAL CAREER



1. NAME : Yoshikazu YAMAGUCHI

2. TITLE : Senior Research Engineer, Fill Dam Division, Dam Department, Public Works Research Institute, Ministry of Construction

3. ADDRESS : 1, Asahi, Tsukuba-shi, Ibaraki-ken 305-0804, JAPAN
Tel. +81-298-64-4326, Fax. +81-298-64-0164
e-mail: yamaguti@pwri.go.jp

4. DATE OF BIRTH : February 6, 1961

5. EDUCATION : 1984 Bachelor of Engineering, Osaka University.
1993 Doctor of Engineering, Osaka University.

6. MAJOR SUBJECT : Dam Engineering, Rock Mechanics.

7. TRAVEL ABROAD : USA, Canada, Peru, Bolivia, Portugal, Austria, Singapore.

8. MAJOR AREAS OF PROFESSIONAL EXPERIENCE :
1984-1993 Research Engineer, Fill Dam Division, PWRI.
1991-1992 Visiting Research Engineer, USAE Waterways Experiment Station.
1993- Senior Research Engineer, Fill Dam Division PWRI.

9. MAJOR TECHNICAL REPORTS & PUBLICATIONS

"Deformation of foundation and change of permeability due to fill placement in embankment dams", Proc. 6th Int. Congr. Rock Mech., 1987.

"Field testing method for resistance laws of highly permeable rock foundations in laminar and turbulent flow conditions", Proc. JSCE, No.454, 1992.

"Fundamental study on seepage failure potential of dam foundations", Journ. JSEG, 35-2, 1994.

"Seepage control and underseepage monitoring for dam foundations with multiple aquifers", Proc. 18th Congr. ICOLD, 1994.

"Development of Fracture Direction Controlled groting", Proc. IS-TOKYO'95, 1995.

"Filter design and problems in Japanese rockfill dams", Proc. GEOFILTERS'96, 1996.

"Permeability evaluation of jointed rock masses using high viscosity fluid tests", Proc. NYRocks'97, 1997.

"Survey of seepage through heightened earthfill dam with high-density electrical prospecting method", Proc. 4th CHIGE, 1998.

"Improved surface-treated cements for cement powder grouting", Ground Improvement, 2-2, 1998.

"Resistivity measurement of cement-based grouts", Proc. GI98, 1998.

and many other papers & publications.

PERSONAL CAREER



NAME: Hitoshi YOSHIDA

POSITION: Head, Fill-type Dam Division
Dam Department
Public Works Research Institute
Ministry of Construction

ADDRESS: 1, Asahi, Tsukuba-shi, Ibaraki-ken
305-0804, Japan
Tel. 0298-64-2413
Fax. 0298-64-0164

DATE OF BIRTH: April 23, 1954

EDUCATION : Bachelor (1977) and Master Degree (1979) of Civil Engineering,
Kyoto University

MAJOR SUBJECT: Research on Embankment Dam Engineering

MAJOR AREA OF EXPERIENCE:

1984-1987 Director, Research and Investigation Section,
Nukui Dam Construction Office,
Tyugoku Regional Construction Bureau, Ministry of Construction

1987-1989 Director, River Planning Division,
Tyugoku Regional Construction Bureau, Ministry of Construction

1989-1991 Dam Instructor, Planning and Research Administration Department,
Public Works Research Institute, Ministry of Construction

1991-1993 Director, Ryumon Dam Construction Office,
Kyusyu Regional Construction Bureau, Ministry of Construction

1993-1996 Director, Second Research Department,
Foundation of River & Basin Integrated Communications, JAPAN

1996- Head of Fill-type Dam Division, Dam Department,
Public Works Research Institute, Ministry of Construction

TRAVEL ABROAD: Indonesia, USA, Taiwan, China, Korea

MAJOR PUBLICATIONS:

"Construction of Multi-purpose Dams" , Japan Dam Engineering Center(1987)
"Handbook of Dam Construction" , Sankai-Dou(1991)

Keynote Lectures

Present States of Construction and Maintenance of Dams in Japan

Tsuneo UESAKA

ABSTRACT

Present states of construction and maintenance of dams in Japan are introduced in this paper. First, natural and social characteristics in Japan are described. This information explains the necessity of the construction of many dams well. After progress of dam construction in Japan by purpose of dam is explained, damage to dams due to major earthquakes and changing seismic design standards for dams are introduced. Finally, problems to tackle in the construction and maintenance stages are summarized.

Key Words: *Dam, Earthquake, Environmental conservation, Rationalization, Maintenance, Redevelopment*

1. Natural Characteristics

1.1 Topographic Characteristics of rivers in Japan

About 75% of the total $377 \times 10^3 km^2$ of Japan is mountains. Because of this, rivers generally have steep slopes and short lengths of river channels (Fig.1-1). The remaining flat lands are mostly comprised of flood plains formed by the deposition of soil and rocks transported form the mountains by these rivers.

1.2 Characteristics of floods and disaster

Japan is spread across a difference in longitude of about 31 degrees and a difference in latitude of about 25 degrees, and the climate varies considerably between the southern and northern parts of Japan. Most of the nation has a temperate climate with much rain and high humidity.

The annual precipitation of Japan is about 1,800 mm, which is much larger than the world mean value of 800mm. As shown in Fig.1-2, precipitation varies greatly with location; it is about 1,000mm in Setouchi district and the eastern part of Hokkaido, but it amounts to almost 4,000mm in the southwest area near the Pacific Ocean.

In addition, tropical cyclones develop on the Pacific Ocean and become typhoons from summer to autumn, and about 3 to 4 typhoons reach Japan, resulting in large rainfalls in a wide area. Torrential rains due to fronts and typhoons have frequently caused large floods and disasters throughout the country.

1.3 Characteristics of Runoff

The form of runoff in Japan has the following characteristics;

1) Flash Flood
2) Large peak discharge of flood
3) Sharp hydrographs
4) Extremely unstable flow regime
5) Large volume of runoff sediment

Director, Dam Department, Public Works Research Institute (PWRI), Ministry of Construction, Tsukuba Science City, 305-0804, Japan.

1.4 Earthquakes

Fig.1-3, a map of the epicenters of major earthquakes around the world, shows that compared with other parts of the world, large earthquakes occur with relatively high frequency on the lands along the coast of the Pacific Ocean from the Japanese Archipelago to the west coast of the United States. And Fig.1-4 is a map of the distribution of the epicenters of large earthquakes occurring in Japan during historical times. It reveals that strong seabed earthquakes in the 8.0 magnitude class occur frequently under the Pacific Ocean and that so-called shallow intraplate earthquakes in the 6.5 magnitude class occur often beneath the land.

Fig.1-5 shows the distribution of tectonic plates near Japan. It shows that the Japanese Archipelago is located on the eastern edge of the Eurasian Plate. As the Pacific Plate approaches from the east and the Philippine Sea Plate moves toward Japan from the southeast, they are forced down under the Japanese Archipelago in the Japan Sea Deeps and the South Sea Trough respectively. The Pacific Plate moves to the west at a rate of about 10 cm per year and the Philippine Sea Plate is moving northwest at a rate of about 4 cm per year. Earthquakes occur at the boundaries between these ocean plates that are sinking under the land from the ocean at a gentle angle and the plate above them. In Japan, lively earthquake activity occurs from the plate boundaries to the land plate under the nation's landmass. One result of this activity is the formation of many faults under and around Japan that are shown in Fig.1-6.

Fig.1-7 shows the locations of those Japanese dams under the jurisdiction of the Ministry of Construction that are now being operated or under construction. At this time, about 382 dams are being operated and about 310 are under construction (at the end of 1997). There are many more dams that are not under the jurisdiction of the Ministry of Construction. For all these reasons, it is extremely important to guarantee the earthquake safety of dams in Japan.

2. Social Characteristics

The population of Japan is 120 million. Population density is 314 person per 1km^2, one of the highest population densities in the world. However, the area of low land and plateaus that can be utilized relatively easily is only about 25% of land area, or 92,000km^2, and thus actual population density is extremely high. In addition, the greater part of the population and property is concentrated in the alluvial plains which were formed by the deposition of transported sediment of rivers and are likely to be flooded (Table 2-1). About 58% of the total population live in the inundation areas of rivers which amount to about 10% of land, and (75% of the gross national assets) are concentrated in these areas. This means that Japan has the potential for tremendous disasters due to floods.

To cope with these situations and to improve the safety of the nation, the government is required to promote the flood control projects. Flood control by dams is becoming an important part of flood prevention schemes in river basins.

Annual mean precipitation in this country is about 1,800 mm which is 2.5 times the world mean and is relatively high but, in terms of water utilization, the rainfall per capita is only 1/5 of the world mean so that it cannot be said water resources in Japan are sufficient.

The precipitation per capita varies considerably with locality and, especially in the southern Kanto and Keihanshin area where

population and industries are concentrated, the precipitation per capita, is only about 1/7 of the national mean, so that there is a local imbalance between the demand for water and available water resources (Fig.2-1).

The water demand varies by locality and the rainfall varies greatly by locality so that shortage of water occurs in certain areas in drought years.

As outlined above, because of the social characteristics of river basins in this country, there is a strong need for dam construction for both flood control and development and utilization of water resources.

3. Dams in Japan

For many centuries in Japan raising rice crops in paddy fields has been commonly performed and irrigation water extensively taken from rivers. Most of the land had been already developed for the raising of rice crops. Therefore, in order to take in additional river water on a stable basin, it has now become necessary to construct water resources development facilities such as dams for most rivers. In Japan the dam construction works are executed with the purpose of water resources development and flood control. Progress of dam construction in Japan by purpose of dam will be explained hereinafter(Fig.3-1).

- Dams for irrigation

Many dams for irrigation were built before World War II but fewer dams were built exclusively for irrigation after the war as a result of a decrease in the area of paddy fields due to the conversion of farm lands into house lots and a sudden decrease in the number of agricultural workers.

- Dams for electric power generation

From the period of economic reconstruction after World War II to the early stage of high economic growth (around 1965), many dams for power generation were constructed and became a driving force for the industrial development. However, proper sites for large-scale hydro-power generation have decreased and thermal power plants and atomic power plants have increased in number, so that now only a small number of dams related to pumped storage power stations are built and the number of dams built exclusively for power generation is decreasing.

- Dams for municipal and industrial water

Ever since the high economic growth age started in this country around 1965, the demand for water for municipal and industrial use increased considerably in order to develop the economy and enhance the living standard, and many dams were constructed for these purposes. However, after 1975 when stable economic growth began, multipurpose dams rather than dams for exclusive use have been constructed in greater numbers.

- Dams for flood control

Dams for flood control built under the control of the Ministry of Construction gradually increased in number as flood control projects were promoted after the war, and now these dams are working very effectively for the prevention of disaster.

Flood control by dams has become an extremely effective flood control measure in Japan as flood prevention by river improvement by the outward displacement of levees has become increasingly difficult in downstream areas of rivers with vigorous industrial activity and high population densities.

4. Earthquakes and Damage to Dams

4.1 Historical Earthquake Records and Damage to Dam Facilities

Damage to dams due to histrical earthquakes is described below. But these dams are all either dams constructed before present seismic design methods were established or dams not designed in accordance with these design methods. Only slight damage has been found on dams constructed based on modern design and execution methods.

(1) Great Kanto Earthquake (September 1, 1923 ; M7.9)

The Great Kanto Earthquake damaged the Ono Dam in Yamanashi Prefecture and the Lower Murayama Dam in Tokyo Prefecture. The Ono Dam, an earth dam completed in 1914, is about 51 km from the epicenter. The damage included settlement up to about 30 cm at the center of the dam crest and a crack with a length of 22 m and maximum width between 18 and 21 mm on the dam crest. At the Lower Murayama Dam, an earth dam completed in 1927 (61 km from the epicenter), 3 longitudinal cracks with a length of 70 m, maximum widths of 2.4 cm, and maximum depths of 10 m formed on the top surface of the dam body that was then under construction.

(2) Niigata Earthquake (June 16, 1964 ; M7.5)

The Niigata Earthquake damaged the Minase Dam (concrete facing rockfill dam completed in 1964) located in Akita Prefecture about 145 km from the epicenter, breaking the expansion joint on the impervious concrete slab at the surface for 10 m and causing 14 cm of settlement of its crest.

(3) Nagano-Ken-Seibu Earthquake (September 14, 1984 ; M6.8)

The Nagano-ken-seibu Earthquake damaged the Makio Dam (rockfill dam completed with a central core in 1961) located in Nagano Prefecture at a distance of 4 km from the epicenter, forming a crack with a depth of 1.5 m at the dam crest in the axial direction of the dam and causing settlement between 50 and 100 mm and displacement of 50 mm to the upstream side at a point on the upstream side. An October 3 aftershock caused settlement between 10 mm and 15 mm.

(4) Hokkaido Nansei-Oki Earthquake (July 12, 1993 ; M7.8)

The Hokkaido Nansei-Oki Earthquake damaged the Niwaikumine Dam (earth dam completed in 1927 and repaired in 1934) located in Hokkaido about 74 km from the epicenter, forming a longitudinal crack of about 120 m and a maximum width of about 50 cm on the dam crest. It also caused a 100 cm settlement and a crack with a depth of 70 cm on the upstream side, and bulging of the dam body parallel to the dam axis at a point about 1/3 of the height of the upstream side slope. Sand boiling and cracks were also seen on the bottom of reservoir near the upstream side slope of the dam body.

(5) Hyogoken-Nambu Earthquake (January 17, 1995 ; M7.2)

The Hyogoken-Nambu Earthquake damaged the Kitayama Dam (earth dam completed in 1968) located in Hyogo Prefecture at a distance of 31 km from the epicenter, causing the shallow slippage of 100 m of a riprap layer on the upstream side slope.

4.2 Changing Seismic Design Standards for Dams

The history of the seismic design of dams in Japan begins with the 1925 proposal by Mononobe of a seismic design method for gravity dams based on the seismic coefficient

method, a proposal prepared in response to the Great Kanto Earthquake of 1923. The first dam designed based on the seismic coefficient method in Japan was the Komaki Dam (now owned by Kansai Electric Power Co., Inc.) completed in 1930. In 1934, Mononobe proposed seismic design methods for other types of dams.

After World War II, a series of large dams were constructed for electric power generation, flood control, and water resources development in order to contribute to the recovery from the devastation brought by the war. This activity contributed to the acceleration of the systemization of dam design methods in Japan. In 1953, the Japanese Committee of the International Commission on Large Dams (Now the Japan National Committee on Large Dams) formed the Dam Design Standards Subcommittee, which published the Dam Design Standards in 1957 stipulating the seismic design of dams based on the seismic coefficient method. This set of standards stipulated separate standards for strong earthquake zones and for weak earthquake zones. Then in 1971, the Japan National Committee on Large Dams revised the Dam Design Standards. This revised standard classifies the seismic coefficient as the ground seismic coefficient and the dam body seismic coefficient and stipulates that for arch dams that bend easily, the dam body seismic coefficient must be twice the ground seismic coefficient.

As structures that span rivers, dams are also legally restricted by provisions of the River Law. In conformity with provisions of the River Law, the Dam Structure Standards and Details of the Dam Structure Standards were issued in 1968 as a notification of the River Bureau of the Ministry of Construction. The present system of design standards for dams was finally completed with the 1976 publication of Cabinet Order Concerning Structural Standards for River Administration Facilities, etc. and the accompanying Execution Regulations. This Structural Standards stipulates that seismic design of dams must be based on the seismic coefficient method and provides separate design seismic coefficients for strong earthquake zones and weak earthquake zones. The Execution Regulations were partly revised in 1981 to provide for medium earthquake zones, and have not been revised since.

4.3 Behavior of Dams During the Hyogoken-Nambu Earthquake

In the early morning of January 17, 1995, the Hyogoken-Nambu Earthquake whose epicenter was in the northern Awaji Island inflicted the severe damage in the Hanshin and Awaji Areas. In some parts of the areas, a seismic intensity of 7 was recorded by the Japan Meteorological Agency. A lot of buildings collapsed by the earthquake or were consumed in the fire which followed it. The Hanshin expressway, the Shinkansen line, lifelines such as gas and water, and other many public facilities were also destroyed. Table 4-1 shows the outline of the Hyogoken-Nambu Earthquake and Fig.4-1 shows the distribution of the seismic intensity recorded by the Japan Meteorological Agency.

About 50 dams are located within 50 km of the epicenter of the earthquake. Fig.4-2 shows the distribution of the horizontal peak accelerations recorded at the dam foundations during the earthquake. The dam closest to the earthquake fault, called the Nojima Fault, was the Tokiwa Dam (about 800 m from the Nojima Fault). There are also a number of old dams in Kobe City, where the earthquake damage was most severe. The Gohonmatsu Dam was built in 1900 as the first concrete gravity dam (rubble masonry structure) in

Japan.

Immediately after the earthquake, site offices of the dams carried out the special safety inspection of dams within about 200 km of the epicenter. The Ministry of Construction also dispatched dam experts immediately after the earthquake in order to inspect the dam safety and to collect the acceleration records. The inspections confirmed that no dams suffered severe damage that required emergency protective countermeasures, while some dams were slightly damaged.

In view of the extensive damage caused by the earthquake, the Ministry of Construction organized the Committee on Evaluation of Earthquake Resistance of Dams to examine the safety of dams designed with the present design criteria for dams in Japan.

The Hyogoken-Nambu Earthquake of January 17, 1995 inflicted severe damage in Hanshin and Awaji Areas such as has be never experienced in Japan in recent years. The safety inspection of dams conducted by the site offices and dam experts immediately after the earthquake, however, showed that there was no severe damage affecting the safety of dams, although slight damage was observed in several dams. The survey after the earthquake showed that the peak accelerations at dam sites were much smaller than the accelerations at soil sites. The dams were constructed at hard bed rock, which contributed to the safety of dams during the earthquake.

The Ministry of Construction organized the Committee on Evaluation of Earthquake Resistance of Dams after the earthquake to examine the earthquake resistance of dams designed with the present design criteria. The Committee has reconfirmed that dams designed with the present design criteria are safe.

In Japan, dam site are selected after a detailed geological survey. The dams are designed with careful structural analyses based on the design criteria, and are constructed under strict management with high quality of materials. This careful survey, design and construction effort helps ensure the safety of the dams.

The dams are large, important structures which must not fail, so the earthquake resistance design of dams should be improved further with the reinforced measurement system of the earthquake motion.

5. Challenges in Dam Construction

5.1 Environmental Conservation

Before a dam is constructed, an environmental impact study is carefully performed to forecast its effects on the environment. It is important to minimize the extent that the construction of the dam alters the environment, and when alteration of the environment is unavoidable, it is also important to adopt appropriate restoration measures to minimize the effects of the construction of the dam. It is also vital to go beyond merely minimizing its effects to include measures to create diverse breeding areas and habitats for living organisms in order to improve the environment around the dam site.

Table 5-1 shows are concrete measures adopted for environmental conservation purposes.

In recent years, golden eagles, Hodgson's hawk eagle, and other rare birds of prey have approached extinction in Japan as a consequence of a decline in their reproduction rate caused by the deterioration of their living environment and the disappearance of suitable habitats. And because these birds stand at the top of the food chain in the regions they

inhabit they are, as an index of the soundness of the environment, considered to be extremely important for environment impact assessment and environment monitoring purposes.

If the area where a dam project is to be executed is closely linked to the habitat of birds of prey of this kind, there is good reason to fear that the project will effect them, because the execution will take a long time to complete and will alter their habitat.

In the future, it will be important to both survey the living conditions and habitats of rare birds of prey at an early stage of project planning in order to study measures to protect them from the effects of the project and to plan and implement appropriate conservation measures during the project.

5.2 Technology Challenges

The construction of large dams in Japan began in the 1950s, and since that time it has been transformed by continuous technology development.

New technologies have been developed in order to build safer dams more economically, and in recent years, particular importance has been given to technology to minimize the effects of dam construction on the natural environment. The key words for new technology development are "guaranteeing safety," "pursuing economy," and "minimizing the environmental impact."

The goals of technological development categorized by dam construction element are "rationalization of materials," "rationalization of design," and rationalization of execution." Formerly studied as unrelated matters, these three types of technological rationalization will be unified, permitting greater progress in technological development than possible in the past.

①Rationalization of design

The rationalization of dam design that has contributed to the more economical construction of safer dams includes the construction of parabolic arch dams thanks to the development of numerical analysis methods, seismic design of dams based on dynamic analysis techniques, and stability analysis of foundation ground using finite element analysis. But future development must go beyond new analysis technology to encompass the establishment of new design systems based on a more comprehensive perspective that incorporates the rationalization of both materials and execution. The development of the new dam design method based on CSG that is discussed below corresponds to rationalization of this kind.

②Rationalization of execution

In the past, the greatest efforts have been devoted to achieving more rational dam executions. The safety of dams has been improved without reducing their performance thanks to the development of the RCD method and the ELCM method. And the remarkable improvement in execution safety achieved through the use of these execution methods is an outstanding result of their development. The RCD method can now be used for 1 m lift execution by combining it with the thin layer spreading method and the newly developed vibrating roller compaction; a new combined method that has been used efficiently at the Miyagase Dam, Gassan Dam, Urayama Dam, and many other dams. The execution of discharge control facilities, gate rooms, passageways inside dam bodies and other steel reinforced construction parts or narrow parts has become more efficient and its labor requirements cut by, in addition to using precast members, using high fluidity concrete in place of stiff consistency concrete. Research is now in progress in an effort to sharply

reduce the labor required for dam construction by finding ways of executing dam bodies with high fluidity concrete.

③Rationalization of materials

Measures to rationalize materials include the improvement of concrete execution properties by using super retarders and by relaxing temperature control measures through the development of low heat cement and developing lean mix concrete such as RCD use concrete, but the next important goal is the development of ways to make extensive use of low quality aggregates. Through the separate production of aggregate, it will be possible to use aggregate that does not satisfy previous standards to make concrete that forms the interior of gravity concrete dams, and to lower costs and minimize the load on the environment by reducing the quantity of waste rock produced at borrow area. In order to clarify what kinds of aggregate can be used as aggregate for interior dam concrete, aggregates made from waste rock are being used to perform various physical tests, concrete tests, freeze-thaw testing without water, and freeze-thaw testing with the freezing rate controlled. In addition, efforts are being made to reduce environmental loads by using materials produced at dam sites as aggregate material.

A new material called CSG that is made by adding cement to materials produced on site has been developed. CSG can be used for many applications ranging from temporary structures to permanent structures, and its use comprehensively rationalizes materials, execution, and design. CSG was used to make a permanent structure for the first time at the Nagashima Sediment Dam, where river bed gravel deposited at the dam site was used as concrete aggregate without being cleaned or crushed. The only processing was the minimum mechanical stabilization needed to guarantee the specified concrete strength required by the dam. A continuous mixer was used and the compaction method employed by the RCD construction method adopted to sharply increase the efficiency of the execution. The use of CSG is sure to spread thanks to its potential to rationalize the material, execution, and the design aspects of dam construction. Fig.5-1 presents an overview of new technologies developed in recent years.

6. Problems at the Management Stage

6.1 Reservoir Sedimentation Management

In Japan, a dam is planned so that its reservoir capacity is adequate to handle the sediment likely to be deposited in the reservoir during a 100 year period. In other words, the flood control and water use plans are prepared by setting the one-century sediment capacity as part of the reservoir capacity so that this portion of the capacity will initially have no water storage function.

The effects of sedimentation at a dam on the river upstream and downstream from the dam include effects on human activities, namely flood control and water utilization, plus its effects on ecosystems. Its downstream effects are not necessarily limited to the river course because they may extend to the seashore. And deposition in a dam reservoir is only one element that effects the flow of sediment. It is necessary to plan comprehensive sediment control measures based on the new concept of the entire area where sediment moves from the mountains including their forests all the way to the seacoast as a "sediment system."

A dam reservoir controls the speed of the cycle of the water flowing in a river at the same time as it is used to supply water for

human use and to control flood conditions, but it cannot only adjust flowing water. It has the potential to be a sediment control facility that mitigates the flow of excessive sediment to supply appropriate quantities of sediment.

(1)Present state of reservoir sedimentation

In reservoirs with a total capacity in excess of 1 million m^3, the quantity of deposition is measured once a year and a report on the quantity deposited and the quantity excavated and removed is submitted to the Ministry of Construction. Fig.6-1 is a map that plots the distribution of annual average sedimentation in the 709 dams with deposition greater than zero from among the 782 dams reported (dams less than zero are all dams completed during the past decade). Here, annual average sedimentation is total sediment in 1996 divided by number of years since completion of the dam.

The figure also shows the principal geological structures, revealing that dams with a high annual average sedimentation are distributed in the vicinities of major Japanese tectonic lines: the Itoigawa-Shizuoka Prefecture tectonic line, and the central tectonic line, indicating that mountains in these regions are susceptible to erosion. These are also regions that receive relatively heavy annual rainfall. The total sedimentation reached about 1.2 billion m^3, with the two regions accounting for about 60% of that total.

Nationwide annual average sediment deposition between 1986 and 1996 equals approx. 20 million m^3/year. The average reservoir capacity of the dams studied is about 23 million m^3/year. This means that every year, enough sediment is deposited to fill a single dam. This indicates that sediment deposition measures are an important way to guarantee sustained use of dam reservoirs. The average deposition as a percentage of total reservoir capacity was approximately 7% in 1996, making the loss of reservoir capacity a critical overall problem, but it is a particularly urgent dilemma in the Chubu Region and other designated parts of Japan.

(2)Reservoir Sedimentation Management Measures

In the past, sedimentation management measures for dam reservoirs were deposition measures categorized as "reducing the quantity of sediment entering a reservoir" and "removing sediment from reservoirs."

From Fig.6-2, measures to supply sediment to the downstream river are sediment bypass, sediment flushing, and turbid water discharge.

①Sediment Flushing

Sediment deposition occurs inside reservoirs because the water flows extremely slowly. For this reason, if a way can be found to lower the reservoir water level enough to restore the form of the original river, it is possible for the natural force of the flowing water to discharge the accumulated sediment. This is called sediment flushing.

Fig.6-3 shows an example of the change in the deposited sediment in the reservoir of the Dashidaira Dam (dam height: 76.7 m, total reservoir capacity: 9 million m^3) operated by Kansai Electric Power Co. on the Kurobe River caused by flushing. The change in the deposition surface was created by an imbalance in the quantity of flowing sediment between the flow sections. If the quantity of sediment flowing through the said section is larger than that flowing from upstream, the deposition surface declines and if the quantity of sediment is smaller than that flowing from upstream, the deposition surface rises. In the case of the Dashidaira Dam, the water level was reduced throughout a large scale reservoir, making this the largest flushing performed in

Japan. Similar flushing is planned for the Unazuki Dam (dam height 97 m and total reservoir capacity of 24.7 million m^3) now under construction downstream from the Dashidaira Dam. Fig.6-4 shows the linked flushing that will be performed simultaneously at the two dams.

②Effects of a sediment bypass

Along with sediment flushing, a sediment bypass is another typical method of using natural forces to transport sediment. The Miwa Dam (dam height of 69.1 m and total reservoir capacity of 34 million m^3) on the Tenryu River where a sediment bypass has been studied is a gravity concrete dam completed in 1959. A series of large-scale floods have deposited far more sediment than originally estimated. By 1988, total deposition in its reservoir reached 11 million m^3, which exceeded 30% of the total reservoir capacity, and sedimentation appeared to be increasing. Judging from past sedimentation at the Miwa Dam, the annual average sediment inflow is estimated to be 68.5 million m^3, and plans call for a sediment bypass to be used to bypass 52.5 million m^3 of wash load that accounts for about 77% of this total sediment inflow.

③Control of sediment supply

Not all sediment that enters a reservoir is deposited on its bed. Fine-grained sediment is a constituent of the sediment removed along with water discharged from the spillway etc. If positive measures can be taken to discharge sediment through such discharge facilities, the quantity of fine sediment deposited in the reservoir will be reduced and sediment will be supplied to the downstream river.

6.2 Management of Reservoir Environments

In order for a dam to obtain adequate quantities of water for various human uses and to maintain the downstream river and at the same time to allow the full exercise of the hydrophilic functions of a dam reservoir, the quality of the water in the reservoir must be maintained at a high level.

The major water quality phenomena that appear as a consequence of the creation of large-scale reservoirs by the construction of dams include the cold water phenomenon, long term turbidity phenomenon, and the eutrophication phenomenon.

①Cold Water Protection Measures

Because the temperature of the water near the surface of a reservoir is generally much higher than the temperature of the river water flowing into the reservoir, in cases where the only problem is cold water, it can be resolved by installing a surface intake system to take in surface water. And at reservoirs effected by long term turbidity and by eutrophication as well as the problem of cold water, a comprehensive study of the state of the water quality must be conducted so the water is removed at an appropriate depth. In such cases, a flexible water intake system allowing the dam manager to freely choose the intake level is installed.

②Long term turbidity measures

Measures implemented inside reservoirs that lower the turbidity of a river downstream from a dam include restricting the inflow of turbid water into the reservoir accompanied by the discharge of turbid water that has entered the reservoir.

③Selective Intake

Another reservoir measure in wide use is the selective intake device that permits discharge to be controlled to reduce the quantity of turbid water flowing downstream. During the flood period when highly turbid

water flows into the reservoir, the system is operated to discharge the turbid water from the reservoir as quickly as possible in order to leave only clear water in the reservoir, then after the end of the flood period, the system is operated in order to minimize the quantity of highly turbid water discharged.

④Reservoir Bank Slope Preservation Facilities

The slopes on the banks of reservoirs are prone to collapse or erode under the effects of water level fluctuations, rainfall, and waves. The collapse and erosion of these banks also contribute to turbidity of the water. To prevent this problem, slope stabilization work is executed where a slope is unstable and slope reforestation work and slope protection work are carried out at locations where a slope is susceptible to erosion.

⑤Eutrophication Measures

Technology to be used to develop new eutrophication prevention measures is now underway. This includes the development of the "flow control system" at the Public Works Research Institute.

⑥Flow Control System

The flow control system will suppress the abnormal growth of blue-green algae by blocking the supply of nutrient salts and sunlight to blue-green algae that inhabit the surface layer of the water by forming a 15 to 20 meter deep circulating mixed layer that usually consists of warm water near the surface of a dam reservoir and in which there is a uniform distribution of the water temperature near the surface. The flow control system will also maintain this layer during medium and small scale flood periods. Fig.6-5 is a schematic diagram of the flow control system.

6.3 Effective Use of Existing Dams

(1)Redevelopment of existing dams

The number of appropriate dam sites has been continually decreasing with the progress of dam construction, yet the demand for flood control and water utilization remains unbated with the sophistication of socio-economic needs. Under these circumstances, attempts are being made to improve flood control and water utilization functions through the redevelopment of existing dams in areas having a wealth of effective dam sites.

Basically, the following two general methods are used to develop existing dams:

1) Reservoir capacity increase

2) Reservoir operation rules changes

Specific methods for 1) include heightening of dams. Those for 2) include changes of reservoir operation by installing or remodeling the intakes or outlets equipment.

①Heightening of dam

This consists of raising the levees of an existing dam and using the extra effective capacity obtained for flood control and water utilization. It has the advantage of a great increase of effective capacity that can be achieved with only slight enlargement of dam and the ability to form certain prospects from the geological point of view. However, it involves ,matters requiring careful study, such as the fairly advanced techniques needed to connect the new and old dam bodies, improve the foundation, and the difficulty of maintaining normal functioning of existing dams during the period construction.

② Remodeling of Intakes and Discharge Equipment

This consists of installing or remodeling the intakes or outlets equipment of existing dams thereby changing the rules of flood control and

using either the capacity that has thus become unnecessary or the capacity that was not formerly usable for flood control or water utilization. It has the advantages of the effective use of the reservoir capacity and the relative freedom from compensation but involves the advanced techniques necessary to install or remodel intakes or outlets equipment for the dam body and other matters requiring careful study.

(2)Reorganization of dams

Dams are reorganized by changing the operation rules for existing dams when new dams are constructed in order to provide the effective operation between the existing and new dams in the same river system and the optimum combination of dams in the river system as a whole.

Fig.6-6 shows the project of the Nagasaki Urgent Flood Control Dams. This project are summarized as follows:

①For Nakanoshima River, the required flood control capacity will be secured by changing the capacities of Hongouchi-Kobu Dam and Nishiyama Dam, existing dams in upper reach built exclusively for domestic water. (Two dams are deteriorated and thus will be remodeled.)

②For Uragami River, the required flood control capacity will be secured by changing the capacity of Uragami Dam, an existing dam in upper reach built exclusively for domestic water.(Renovation of outlets and others)

③For the water utilization functions which will be lost by this project, new dams will be built in the Yukiura River and Hachiro River, nearby rivers damaged also by the torrential rains, and the lost functions will be regained together with the flood control functions.

④The above dams supply the deficiency and required flood control capacity at each river since the disaster on July 1982.

Table 2-1 Progress of population and property in river areas in Japan

	Items	1965		1975		1980	
		Net value	Share	Net value	Share	Net value	Share
Area (km^2)	Nationwide	377,700	100	377,700	100	377,700	100
	River inundation area	38,000	10	38,000	10	38,000	10
Population ($\times 10^4$)	Nationwide	9,828	100	11,194	100	11,706	100
	River inundation area	4,500	45.8	5,321	46.7	5,640	48.2
Properties ($\times 10^9$yen)	Nationwide	197	100	494	100	593	100
	River inundation area	116	59	334	68	427	72

Table 4-1 Outline of Hyogoken-Nambu Earthquake

Earthquake Name	1995 Hyogoken-Nambu Earthquake
Date/Time	05:46:52 a.m. January 17, 1995
Epicenter	North latitude 34 ° 36', East longitude 135 ° 03'
Epicenter Depth	14 km
Magnitude	7.2 (Japan Meteorological Agency)

Table 5-1 Environmental Conservation Method

Item	Environmental Conservation	Concrete Measure
Minimization of alteration	・Planning a dam with little impact on the environment ・Environmental planning based on a zoning plan	
Restoration of altered	・Restoring the lost environment ・Guaranteeing migration/movement routes	・Guaranteering substitute land ・Restoring vegetation ・Guaranteering routes for animals to travel/migrate ・Installing fish ladders
Improving the environment	・Providing diverse breeding areas and habitats ・Environmental management and public education	・Biotope creation ・Installation of floating island ・Provision of habitats for animals ・Releasing fish native to the region

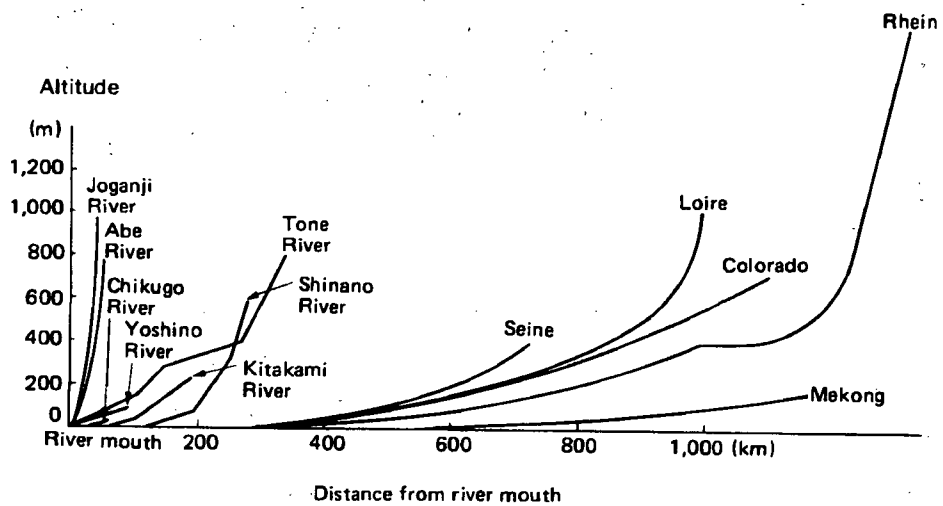


Fig.1-1 Comparison of main rivers in the world

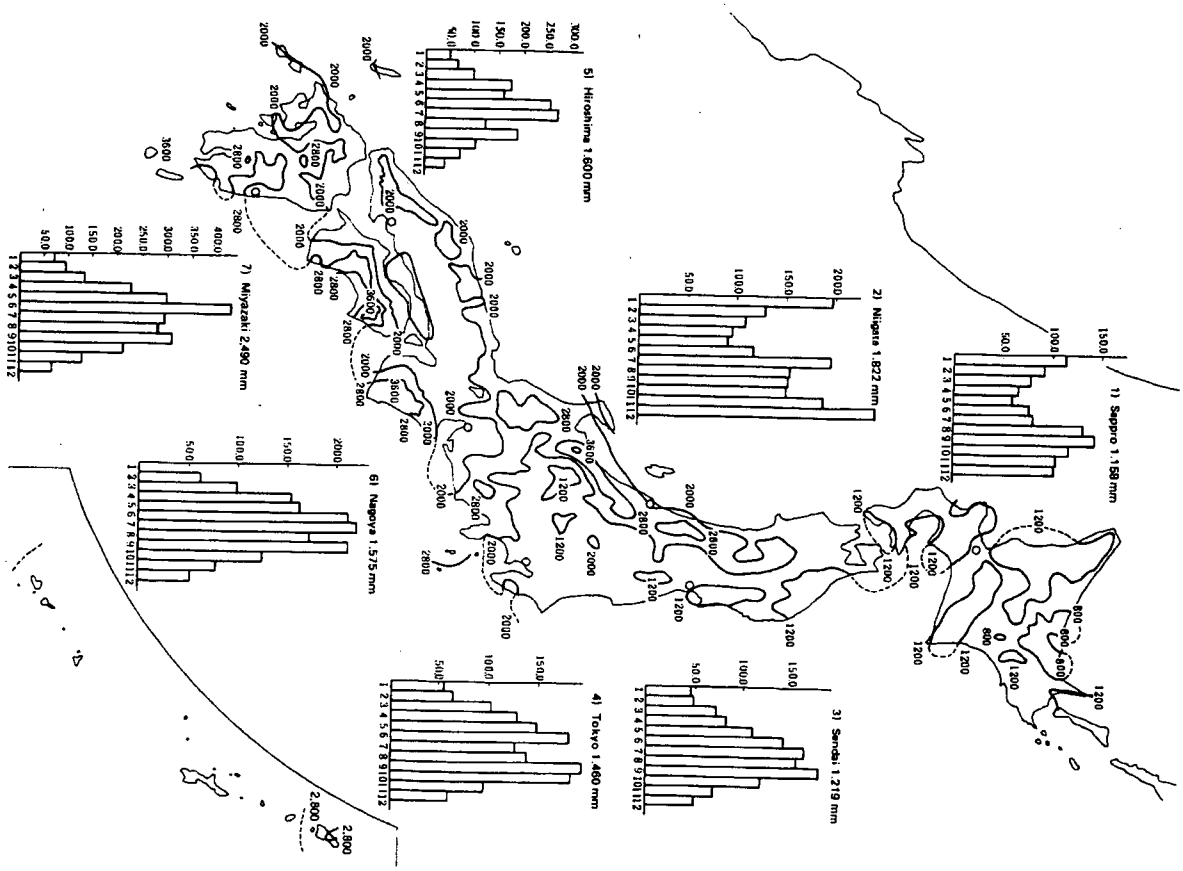


Fig.1-2 Regional distribution of annual precipitation

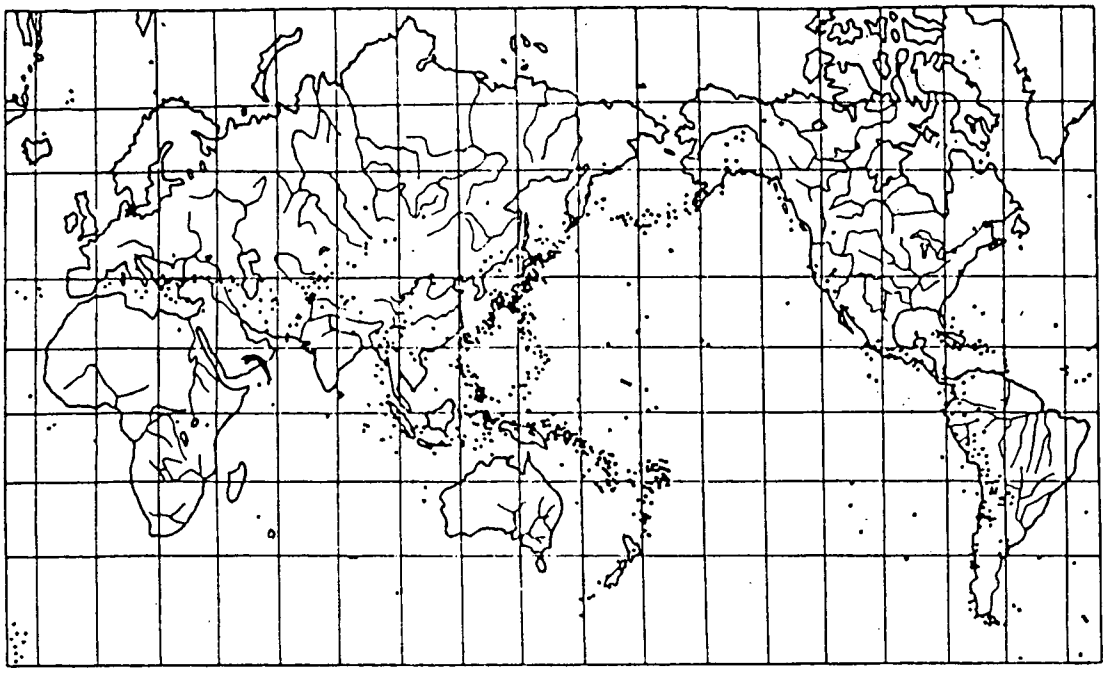


Fig.1-3 Epicenters of major earthquakes around the world

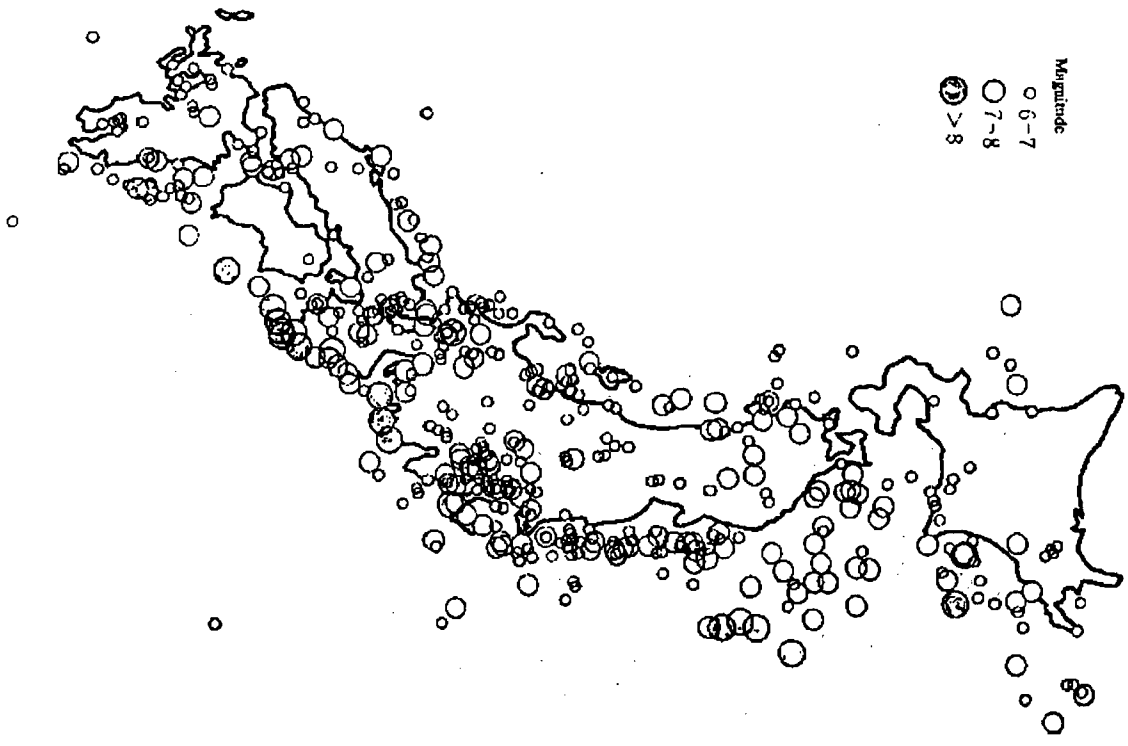


Fig.1-4 Distribution of the epicenters of large earthquakes occurring in Japan during histrical time

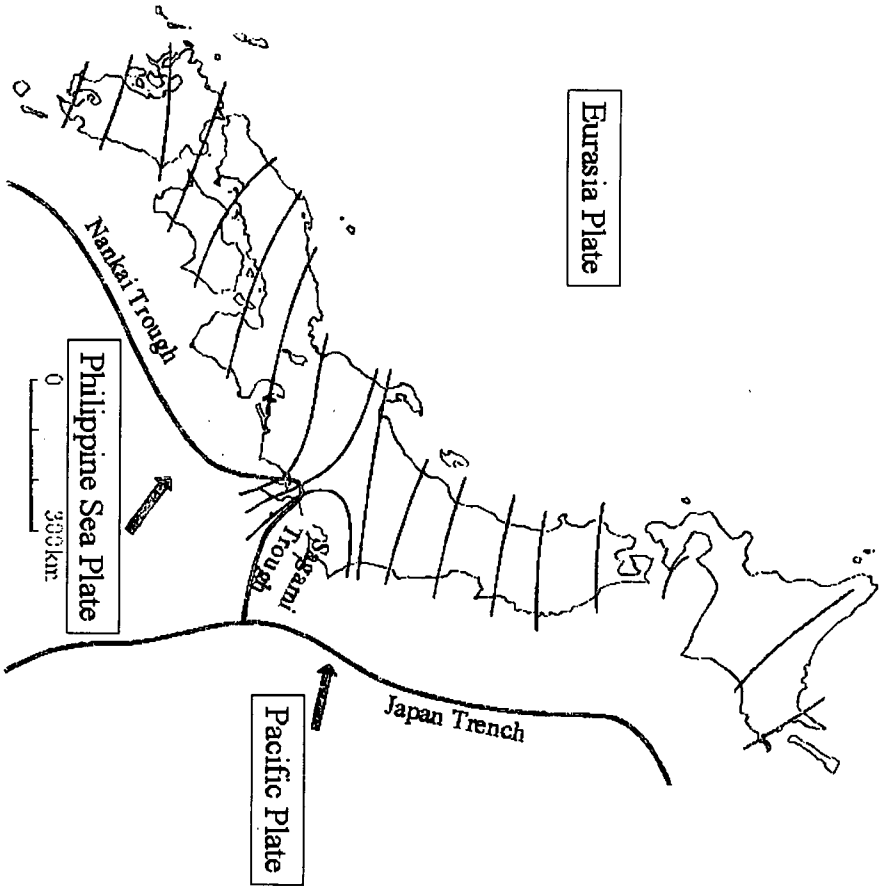


Fig.1-5 Distribution of tectonic plates near Japan

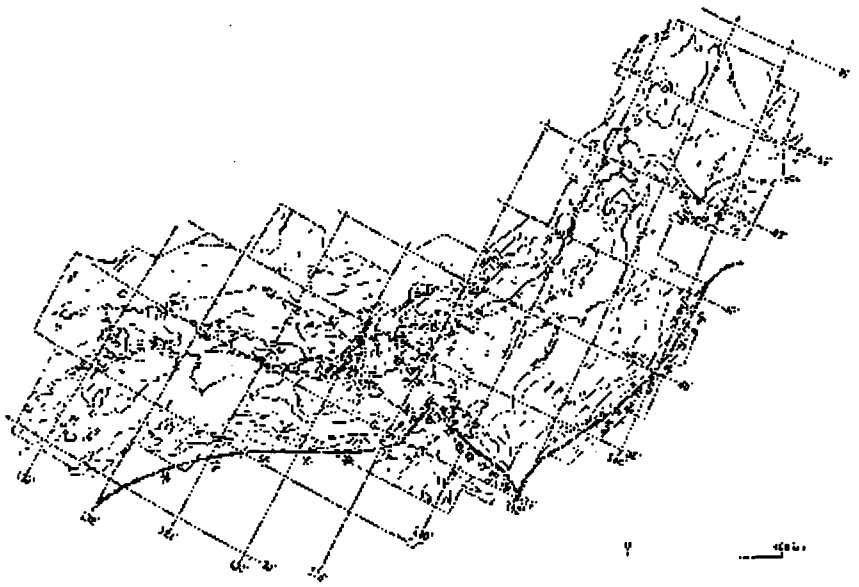
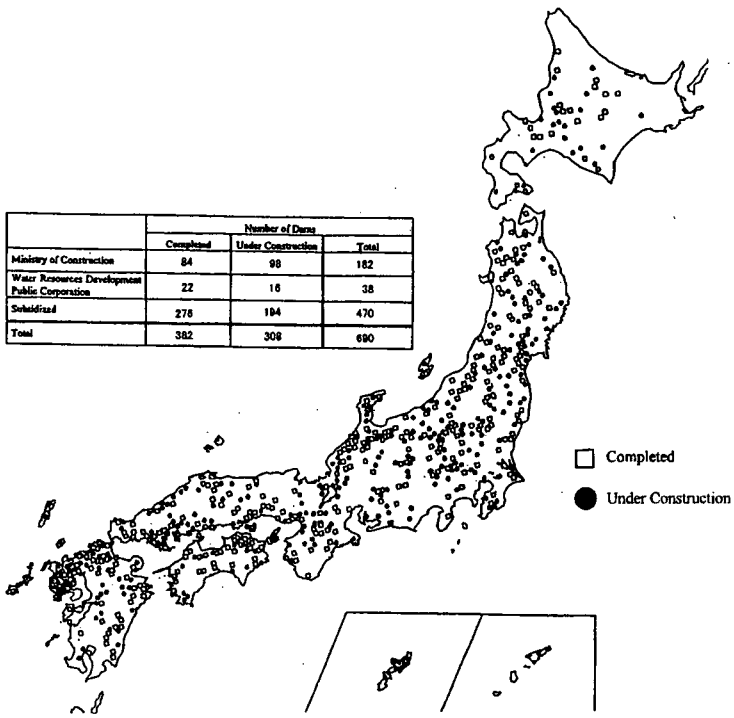


Fig.1-6 Faults under and around Japan



	Number of Dams		
	Completed	Under Construction	Total
Ministry of Construction	84	98	182
Water Resources Development Public Corporation	22	16	38
Subsidized	276	194	470
Total	382	308	690

Fig.1-7 Location map of dams Japan

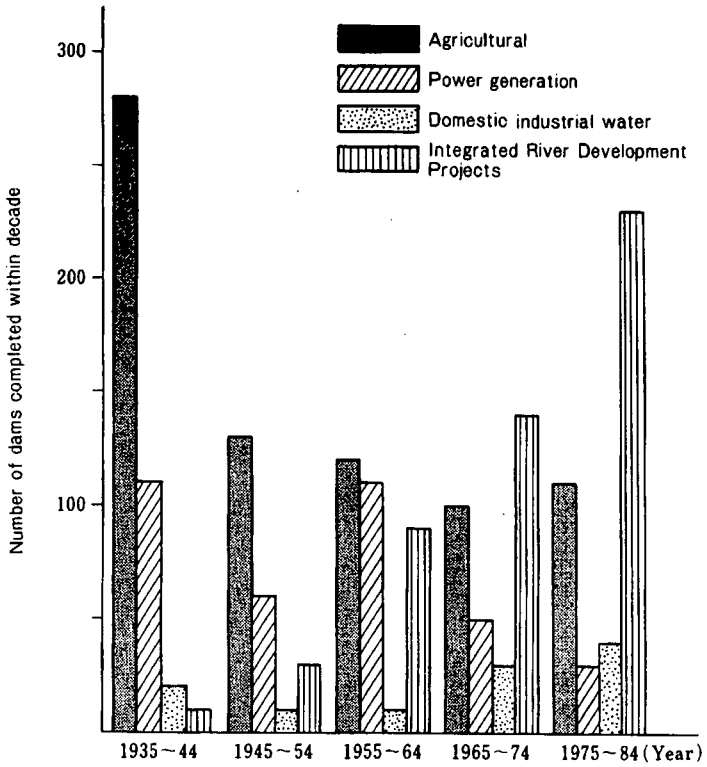


Fig.3-1 Progress in the number of completed dams by purpose

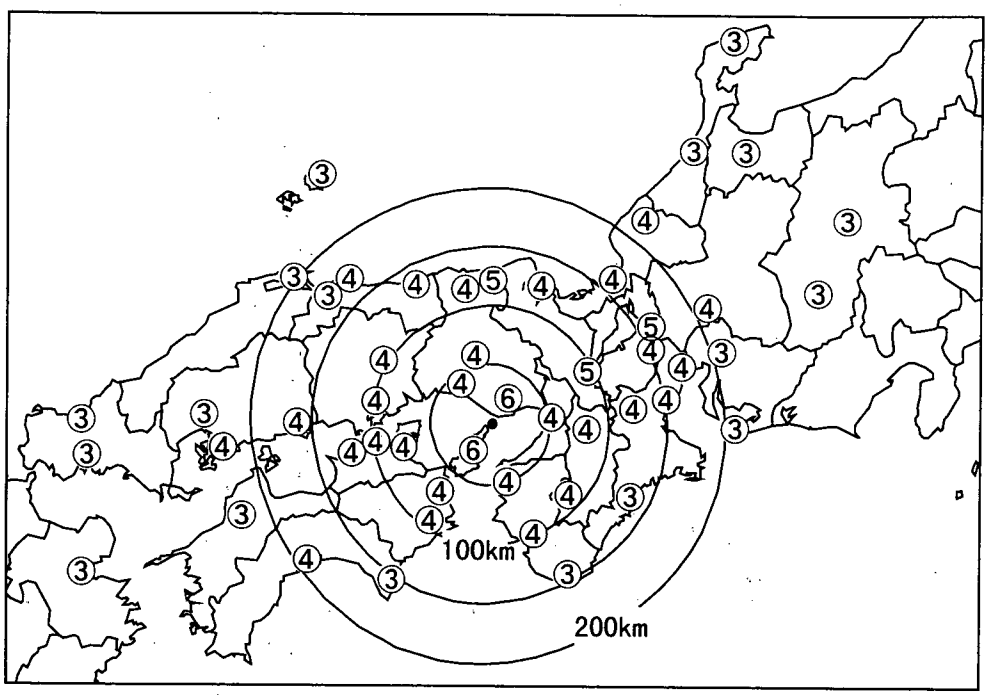


Fig.4-1 Map of seismic intensity of Hyogoken-Nambu Earthquake
(Values reported by Japan Meteorological Agency)

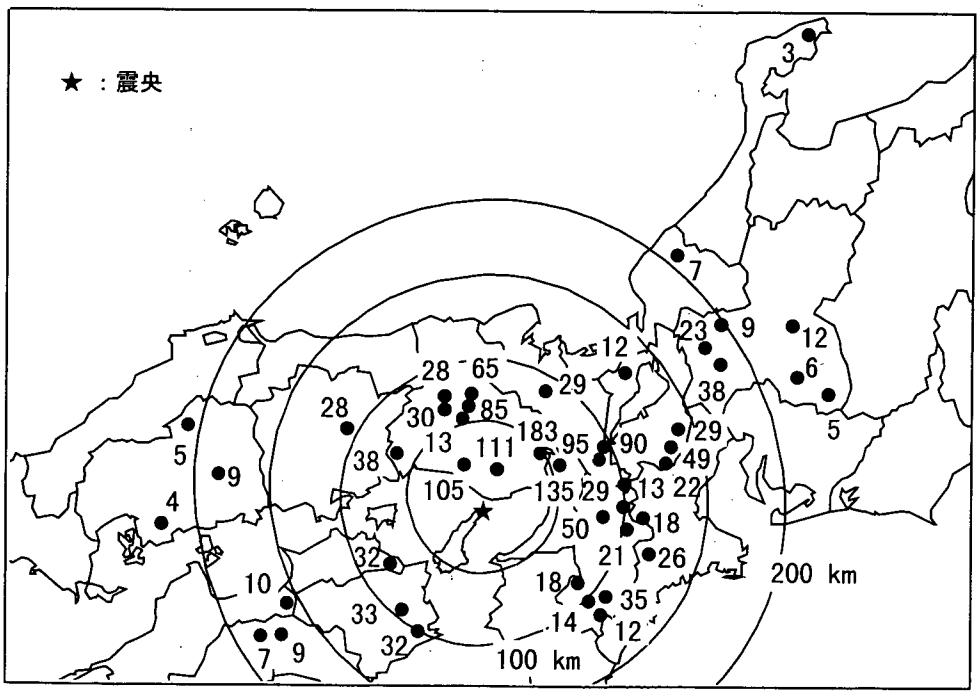


Fig.4-2 Map of horizontal peak acceleration at dam foundation

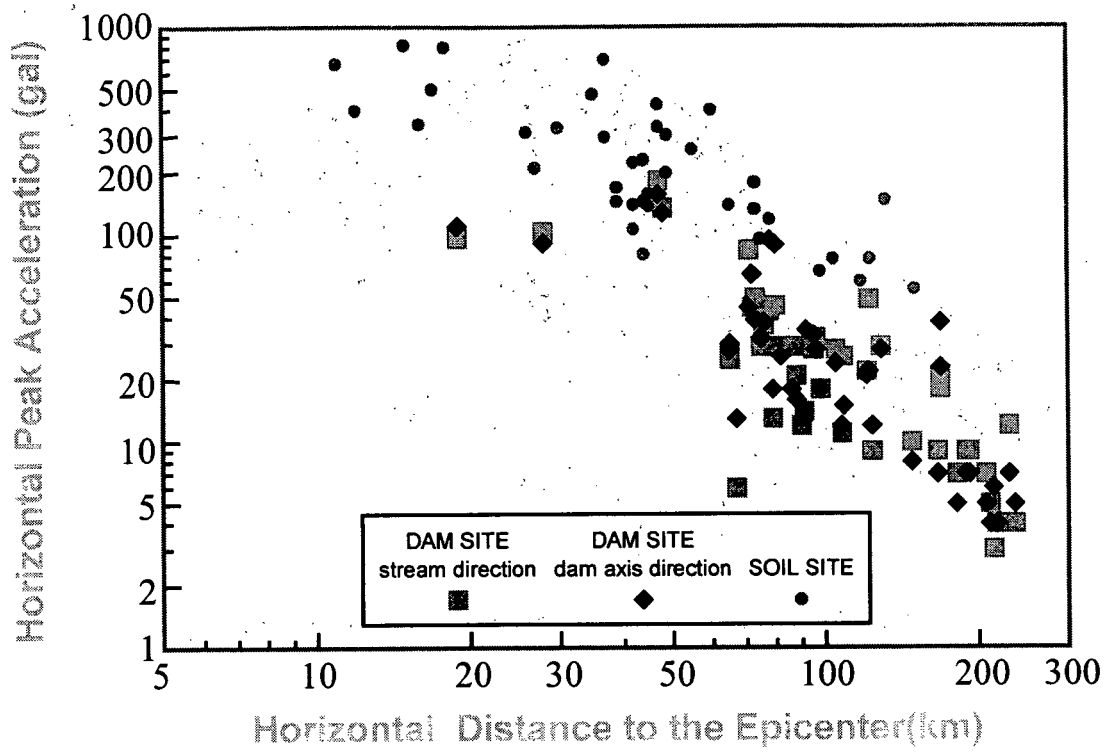


Fig.4-3 Attenuation of horizontal acceleration

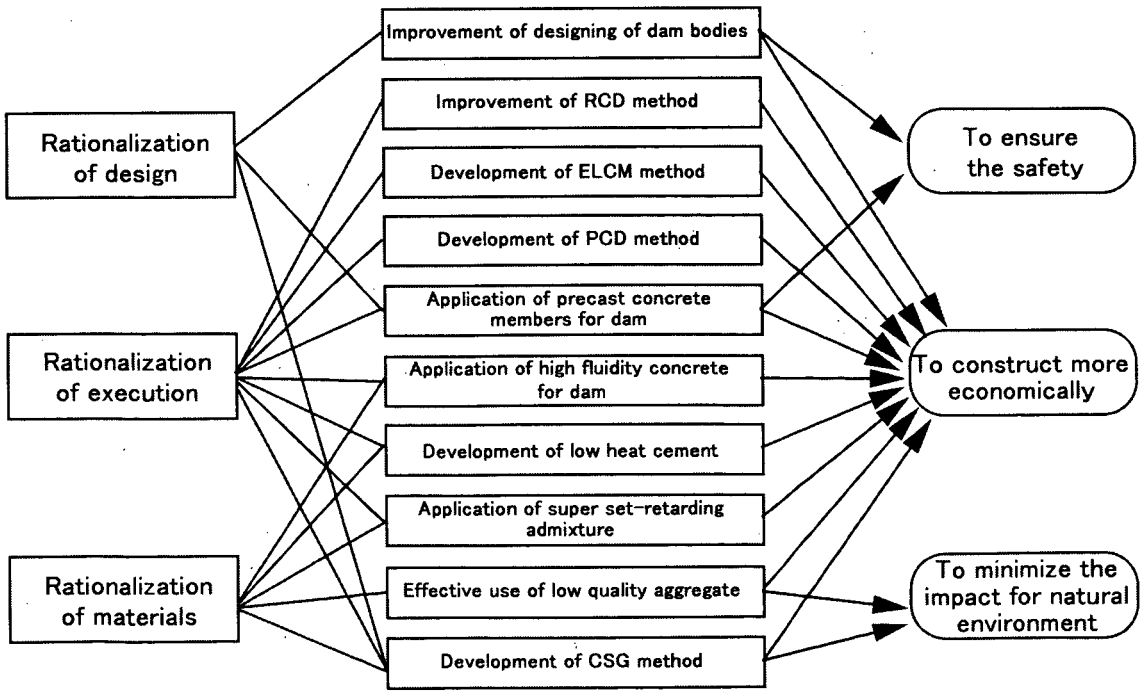


Fig.5-1 New technologies developed in recent years

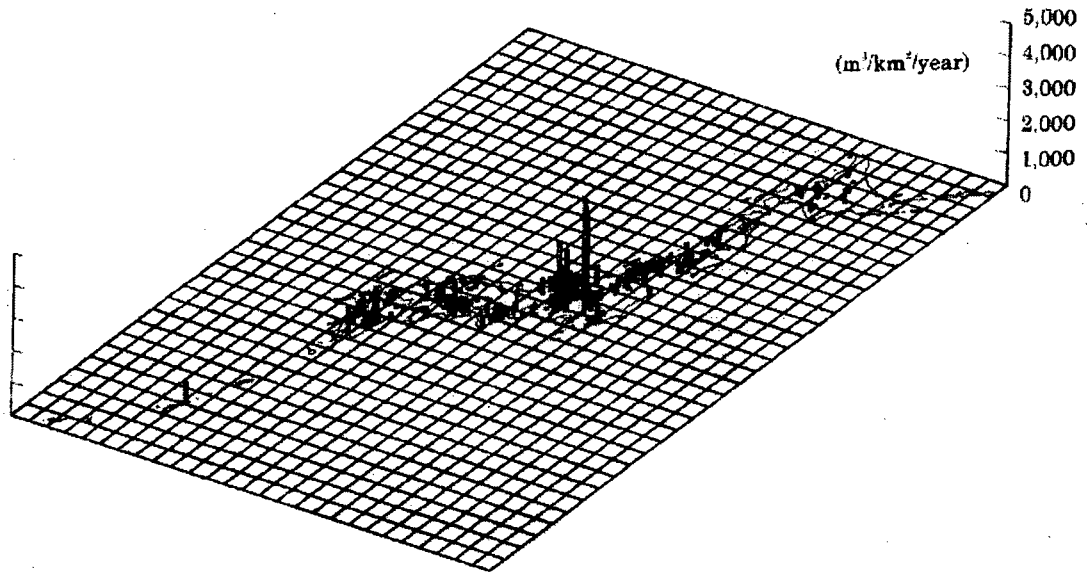


Fig.6-1 Specific Sediment Yield of Catchment Basins on Japanese Reservoirs

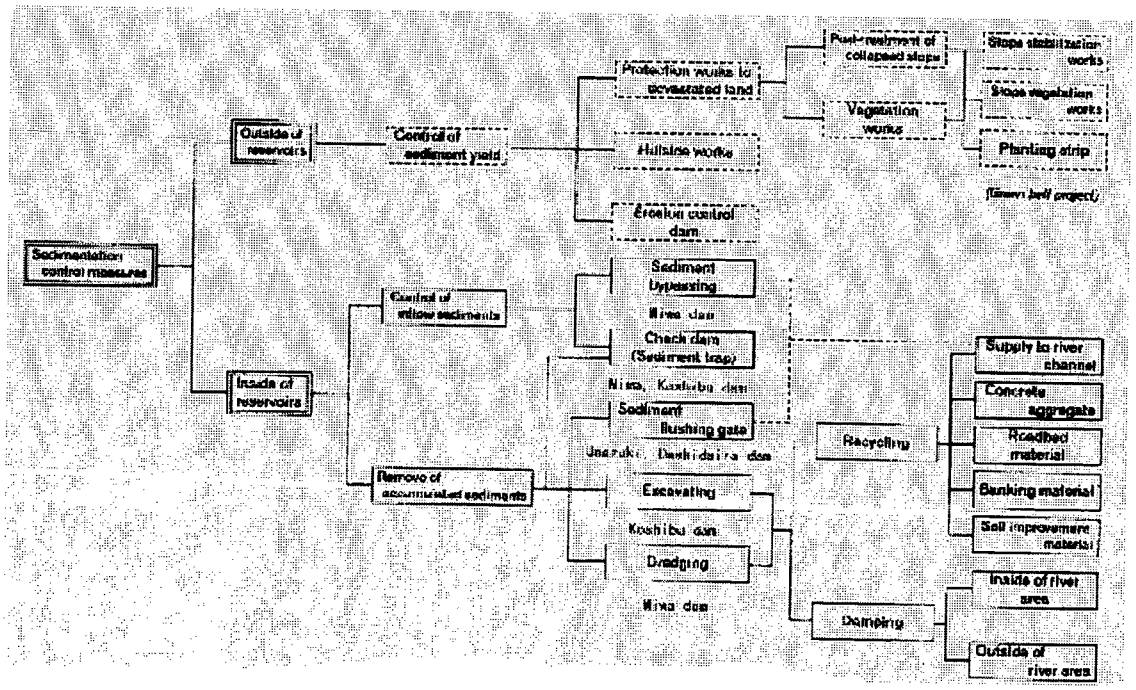


Fig.6-2 Sediment Control Measures in Japan

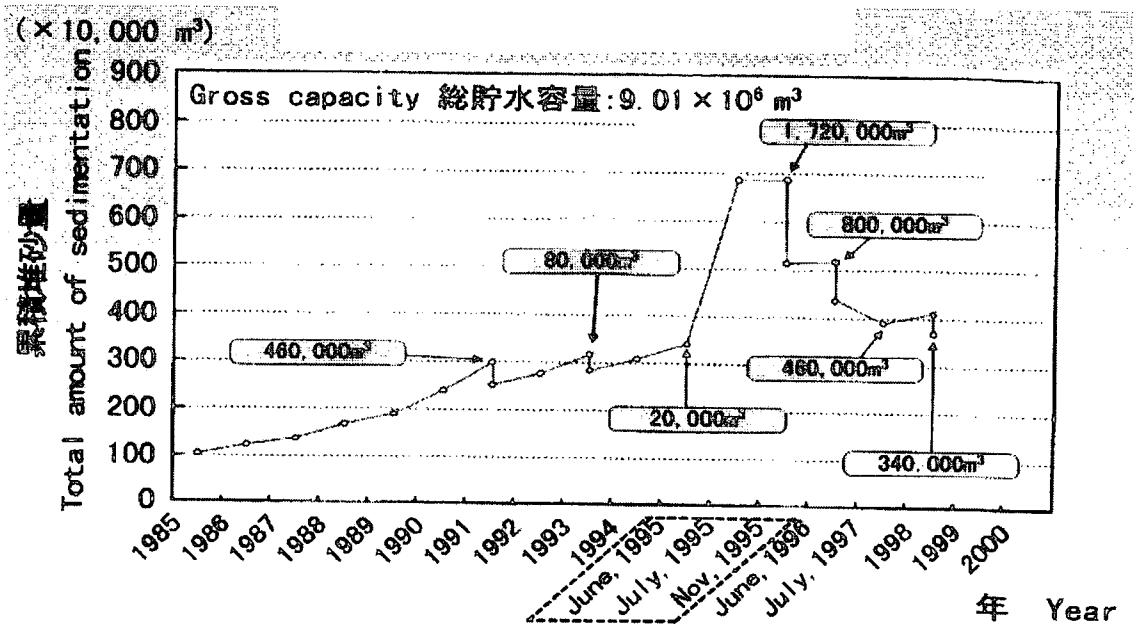


Fig.6-3 Annual Amount of Sedimentation –Dashidaira Dam-

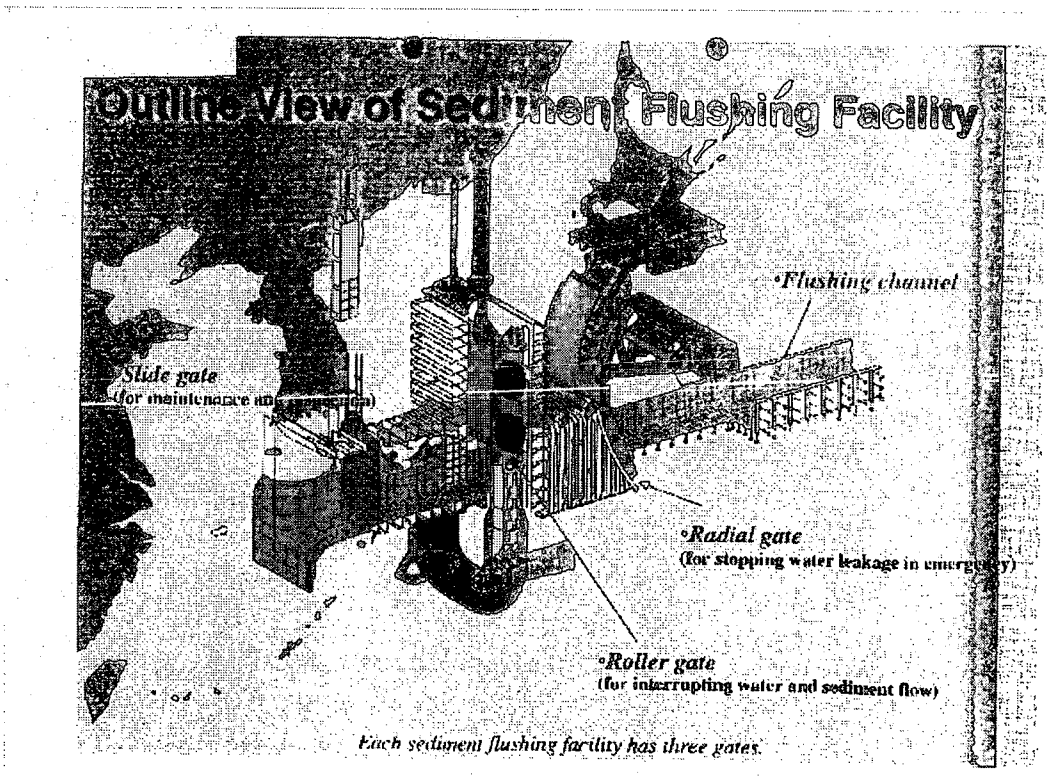


Fig.6-4 Outline View of Sediment Flushing Facility

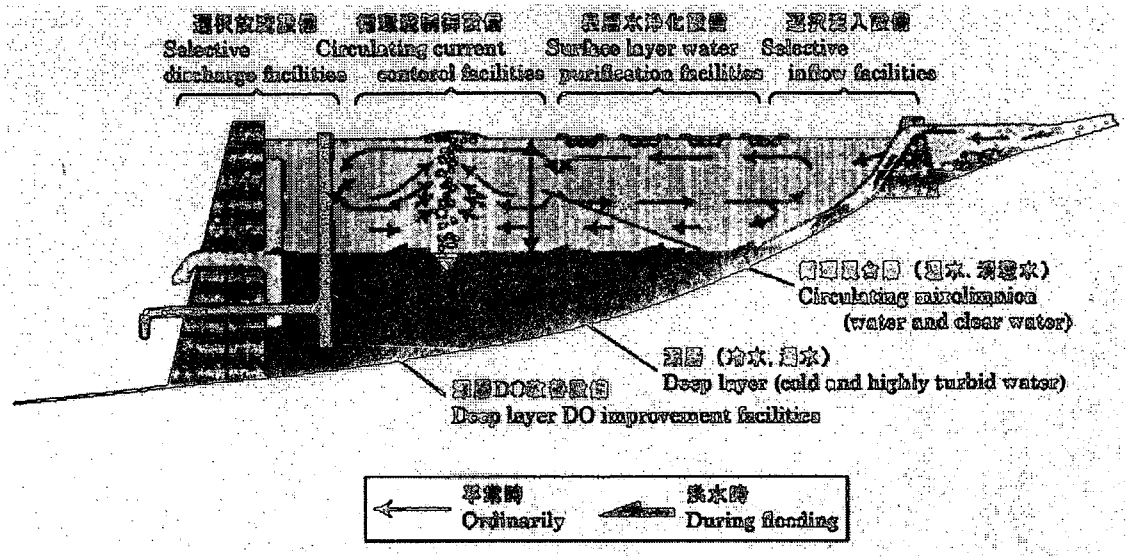


Fig.6-5 Reservoir Water Quality Environment Creation

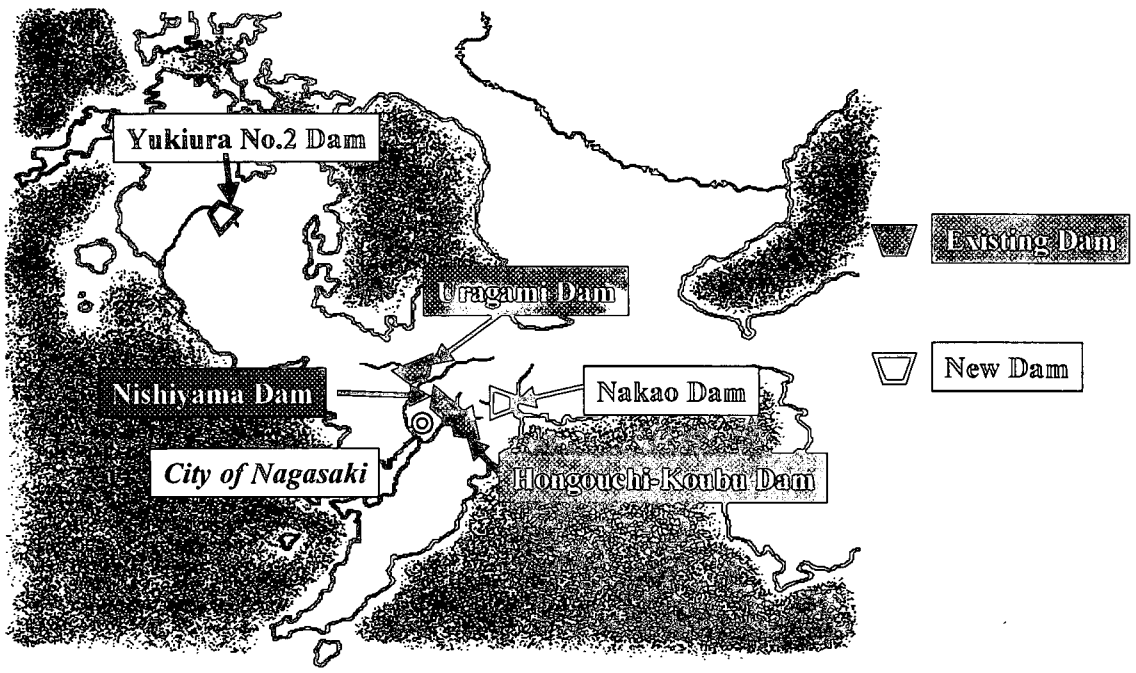


Fig.6-6 Nagasaki Urgent Flood Control Dams

Status of Construction and Safety of Dams in the United States

by

Robert L. Hall[1]

ABSTRACT

The construction of new dams in the United States has been strongly opposed for the past 20 years. However, the need for new dams does currently exist and will exist in the future. This need is demonstrated by the current construction of three of the largest dam projects in the history of the United States: The construction of the $1.9 billion Eastside project; the $220 million Seven Oaks project; and the $1.3 billion Olmsted project. The two rock-fill dams at each end of a 7.2-km-long valley are the main structures of the Eastside Project, and they will contain over 84 million m^3 of embankment material. The reservoir at this project will contain over 987 million m^3 of water. The Seven Oaks Dam, a U.S. Army Corps of Engineers project, is an earth- and rock-fill dam with a maximum height of 167.6 meters. The Olmsted Locks and Dam (L&D) is the largest civil works project undertaken by the U.S. Army Corps of Engineers to modernize navigation facilities for the 21st century. In contrast, most of the dams in the United States are over 30 years old, and many of these have reached or exceeded their 50-year design life. Twenty-eight percent of the Corps' 569 dams have been identified as being hydrologically or seismically deficient. The cost to retrofit these structures ranges between $1.3 to $6.5 billion. Risk-based dam safety procedures are currently being developed to assist engineers in identifying the most critical deficiencies. The Corps in the assessment of the Alamo and Bluestone Dams has recently used preliminary procedures. These procedures will assist in developing a risk management policy to ensure public safety and protect the national investment in infrastructure.

KEYWORDS: concrete dams; earth- and rock-fill dams; construction; safety; environmental impacts; risk procedures.

1. INTRODUCTION

Dam projects have a significant impact on their surrounding environment. These effects must be considered when building a large dam project. For example, dams cause the water upstream to flow at a slower rate, resulting in silting problems. The water flow on the downstream side of the dam is also reduced, resulting in a change of water temperature, quality, and quantity. Dams without fish ladders have stopped migration of fish in the rivers (Figure 1). Because of environmental concerns, dams in North Carolina, Vermont, and Wisconsin have already been removed. Many environmental problems are associated with any large construction project, and this is also true with any dam construction project.

Unfortunately, many false environmental impacts have been charged against dam projects. Just 20 years ago, the general public in the United States considered dams the solution for water management and energy. People have claimed that dam projects can alter local climate and weather of an area. The massive weight of the water in the reservoir has been said to affect the geology of the area. Recently, a NASA geophysicist claimed that the weight of the world's collective reservoir is speeding up the earth's rate of spin and is changing the shape of the earth's magnetic field [1]. Most of these accusations come from North America or Europe, where hydroelectric potential has largely been exploited, and where the consumption of energy has no restrictions [2].

Hydropower remains the most economically feasible renewable energy. The World Bank reports that hydroelectric dams totaling an output of 135,000 MW are under construction. In addition to hydropower, dams provide water for drinking, industry, irrigation, recreation, and river navigation. The U.S. Committee on Large Dams reports that the number of new dams that are more than 15-m

[1] Supervisory Research Structural Engineer, Structural Mechanics Division, Structures Laboratory, U.S. Army Engineer Research and Development Center, Vicksburg, MS 39180 (USA)

high is actually increasing in the world, as well as in the United States. Out of the 1,242 dams under construction in 1994, 79 percent exceeds 100 m. Most construction is occurring in developing countries as the following number of new dams indicates: China, 311; Turkey, 190; Japan, 140; Republic of Korea, 125; India, 76; and USA, 55. The present number of dams worldwide (36,000) will not provide the necessary water supply by the year 2030. Therefore, safer, environmentally responsible, and socially acceptable dams will be needed in the near future [3].

2. EASTSIDE PROJECT

The Metropolitan Water District of Southern California is currently constructing the largest earth- and rock-fill dam in the history of the United States. This $1.9 billion project will double the surface water storage capacity in all of Southern California. This storage capacity is needed to meet emergency drought and seasonal storage needs of a projected population growth of an additional 5 million people in the next 30 years.

The Eastside Reservoir will be formed by two earth- and rock-fill dams, 7.2-km apart, and a third smaller saddle dam in the north rim (Figure 2). The earthwork volume of over 84-million cubic meters makes this the largest earth- and rock-fill dam project in the U.S. history. The dam project also has several appurtenant structures, including an inclined inlet/outlet tower, pumping plant, pressure tunnel, and pressure-control facility. The West Dam is 2.7 km long and 87 m above the original ground level. The rock fill embankment has an alluvial core, 5 filter/drainage zones, and a rock outer shell. The exterior slopes of one vertical to two horizontal are the result of high seismic considerations. The foundation was excavated 26 m down to alluvial material, and then a cutoff wall was constructed by the bentonite slurry trench method. The East Dam is a zoned embankment 3.2-km long and 56 m above the original ground level. The cross section is similar to the West Dam. Because the foundation material had the potential to liquefy from earthquake ground motions, the foundation materials were excavated down to bedrock. Water from the Colorado River Aqueduct will be diverted to the reservoir by the San Diego Canal and then into a 617,000-m^3 forebay before being pumped into the reservoir. The pumping plant contains twelve 4,500-kW pumps, with a total capacity of 59.5 m^3/sec [4].

3. SEVEN OAKS PROJECT

The U.S. Army Corps of Engineers (USACE) Seven Oaks project is located in the Upper Santa Ana River and is a single-purpose flood-control project. It is a part of the Santa Ana River (California) Mainstream Project (Figure 3). The project is planned to operate in conjunction with the Prado Dam located 60-km downstream on the Santa Ana River, to provide flood protection to Orange County, California. During the early part of each flood season, runoff will be stored behind the dam in order to build a debris pool to protect the outlet works. Small releases of the pool will be made on a continual basis in order to maintain the downstream water supply. During a flood, Seven Oaks will store water destined for the Prado dam for as long as the pool at the Prado Dam is rising. When the flood threat at the Prado Dam has passed, Seven Oaks will begin to release its stored floodwater at a rate which does not exceed the downstream channel capacity. At the end of the flood season, the Seven Oaks reservoir will be gradually drained, and the Santa Ana River will flow through the project unhindered.

The project will consist of a 167.6-metre-high earth- and rock-fill dam, a complex outlet system consisting of an inclined intake structure (Figure 4), and a regulating outlet gate chamber encased in the rock abutment. The intake structure has an inclined geometry due to the severe seismic threat in this area. The dam will be constructed in a region of high seismicity between the two branches of the San Andreas Fault. The site is located approximately 2-km upstream from the mouth of the Santa Ana River Canyon near the South Branch of the San Andreas Fault. According to the Corps of Engineers assessment, the North Branch of the Fault crosses the reservoir about 1-km upstream from the dam site.

4. OLMSTED PROJECT

The Olmsted L&D is one of the largest civil works projects undertaken by the USACE to lead the modernization of Corps navigation facilities for the 21st century (Figure 5). The Olmsted L&D project is being constructed on the Ohio River, 25-km upstream from the confluence of the Ohio and the Mississippi

Rivers. The new L&D project will replace L&Ds 52 and 53 on the lower Ohio River. The project will include twin 365.8-metre by 33.5-meter lock chambers with a design lift of 6.4 meters, a 426-metre-long navigation pass, and a 201-metre section of tainter gates. The dam is constructed of raised gates. The 1:5-scale model of the gates is shown in Figure 6. The project is also approximately 26 km from the New Madrid seismic zone. The high seismic design ground motion results in this being the first L&D project in which the seismic load case controls the design.

5. DAM SAFETY

Both old and new dams must be operated and maintained in a safe manner. The U.S. dam safety program strives to protect the public from the dangers of hazardous dams and helps owners to recognize deficiencies. The dam safety program has resulted in the USACE identifying the following facts about their 569 dams:

- 64 percent are over 30 years old.
- 28 percent have reached or exceeded their 50-year design life.
- 65 dams have been identified as being hydrologically or seismically deficient, based on current methodologies.
- The cost to retrofit these deficiencies is approximately $6.5 billion.

These retrofit costs exceed the USACE operation and maintenance budgets and require that each deficiency be carefully prioritized. This has resulted in the development of draft guidance for risk assessment for dam safety. The intent of these guidelines is to assist practicing engineers and researchers in using risk methods for assessing dam safety. The methods are based on a systems approach for dams that include risk assessment and control.

The USACE, as an owner, builder, and operator of dams, has a responsibility for developing a risk management policy to ensure public safety and protect the nation's investment in infrastructure. The adopted policy uses risk-based economical and decision analysis for major infrastructure expenditure decisions and allocations. The policy separates safety decisions from economic decisions by performing separate analyses.

The current USACE dam safety guidance, ER1110-2-1155, determines the population at risk with and without dam failure. It also considers loss of life by establishing project hazard-rating categories. This guidance has the following deficiencies:

- It does not account for the occurrence likelihood of events, such as failure due to floods or earthquakes, in assessing dams.
- It does not make a distinction between loss of lives as a result to dam failure and loss of lives due to other reasons.
- Computational procedures are based on deterministic parameters when the parameters can only be properly defined probabilistically.
- Hazard rating is ambiguous since it is not linked to an event.
- The term base safety condition (BSC) is only vaguely defined.
- It allows the use of economic risk analysis of dams for floods greater than the corresponding BSC flood.
- It does not provide procedures for assessing structural and geotechnical failure probabilities of dams from specified natural hazards.

These deficiencies have resulted in the development of a draft guidance for risk-based methods for assessing dam safety [5].

6. RISK-BASED ANALYSIS OF THE ALAMO DAM

The Alamo Dam is located in the State of Arizona on the Bill Williams River approximately 63-km upstream from the river's confluence with the Colorado River at Lake Havasu City. The Alamo Dam and reservoir is a multipurpose facility providing flood control, water supply, and conservation, recreation, and fish and wildlife enhancement (Figure 7). The dam is an earth- and rock-fill structure that is 86-meters high, with a crest length of 297 meters. A recent hydrologic study indicated that the Probable Maximum Flood would result in floodwaters overtopping the dam by 17.3 feet. The flood could cause erosion of the toe of the dam from spillway flows, crest erosion from wave action, and erosion of the spillway. The risk-based analysis procedures considered raising

the embankment, lowering and widening the spillway, adding fuse gates, constructing an Ogee crest spillway, constructing auxiliary spillways, and hardening the embankment face and combinations. The risk-based analysis determined a low probability of failure and loss of life and that the structure meets or exceeds life-safety criteria for ANCOLD, Bureau of Reclamation, and British Columbia Hydro.

7. RISK-BASED ANALYSIS OF THE BLUESTONE DAM

The Bluestone Dam is located on the New River near Hinton, West Virginia (Figure 8). The project was constructed in the 1940's and is operated and maintained by USACE. The structure is a concrete gravity dam, 50-meter high and 624-meter long. The project was originally designed for flood control and for hydroelectric power generation. Six 5.8-metre-diameter penstocks were constructed, but hydropower generators were never installed. Recent hydrologic studies of the Bluestone Basin indicate that the design storm event (51,200-m^3/sec) is significantly greater than the original design storm (12,200 m^3/sec). The new design storm would result in overtopping the dam by 4.6 meters and would result in an unstable structure. The most significant failure mechanism is reported to be deep-seated sliding along the near-horizontal bedding foundation planes. The risk-based analysis procedure considered raising the dam 6.7 meters to prevent overtopping; constructing an auxiliary spillway; raising the dam 4 meters and utilizing the six existing penstocks for spilling the reservoir; and installing post-tensioned anchors and/or passive toe blocks. The risk-based analyses indicated no significant differences in risk between the remedial alternatives. This resulted in selecting the least costly alternative to raise the dam 4 meters and use the existing penstocks for spilling the floodwaters.

8. CONCLUSIONS

Dams are, and will always be, important structures. The environmental and social objections will continue to keep the number of new dams at a minimum in the United States. The most significant challenge for the United States is maintaining and retrofitting existing inventory of dams.

The risk-based analysis procedures will assist the engineers in selecting the safest and least-costly retrofits and will correctly prioritize the projects that require remediation.

9. ACKNOWLEDGMENTS

This work was sponsored by the Civil Works Earthquake Engineering Program of the U.S. Army Engineer Research and Development Center (ERDC) in Vicksburg, MS. We appreciate the cooperation of the authorities at the ERDC, which permitted the preparation and presentation of this paper. Permission to publish this paper was granted by the Chief of Engineers, U.S. Army Corps of Engineers.

10. REFERENCES

1. "Dams alter earth's orbit," Ottawa Citizen, 3 March 1996, page D8.

2. Armistead, Thomas F., "Dam Conflicts Threaten Global Growth," Engineering News Record, 14 September 1998.

3. Veltrop, Jan, "Benefits of Dams," USCOLD Newsletter, March 1995, page 3.

4. Majors, Dennis G., Ehasz, Joseph L., and Ruotolo, Donn, "$1.9 Billion Eastside Reservoir Project Concept to Construct in 5 years," Metropolitan Water District Publication, 1996.

5. Ayyup, Bilal M., Baecher, Gregory A., Ebeling, Robert M., Ellingwood, Bruce R., Johnson, Peggy M., and Leggett, Mary A., Draft-State-of-the-Art Report on Risk Assessment for Dam Safety, USACE.

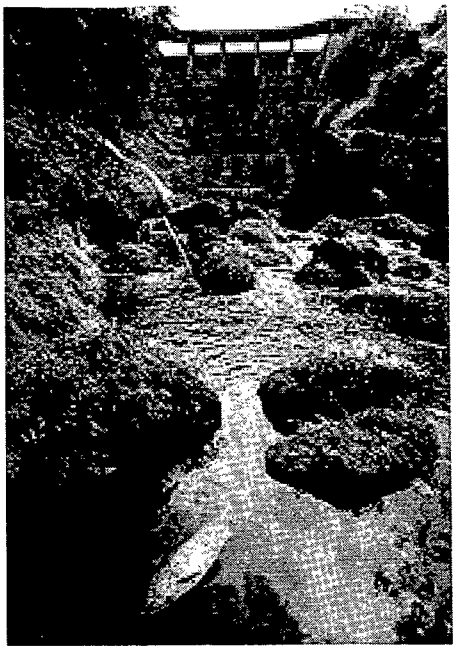


Figure 1. Dam without fish ladder

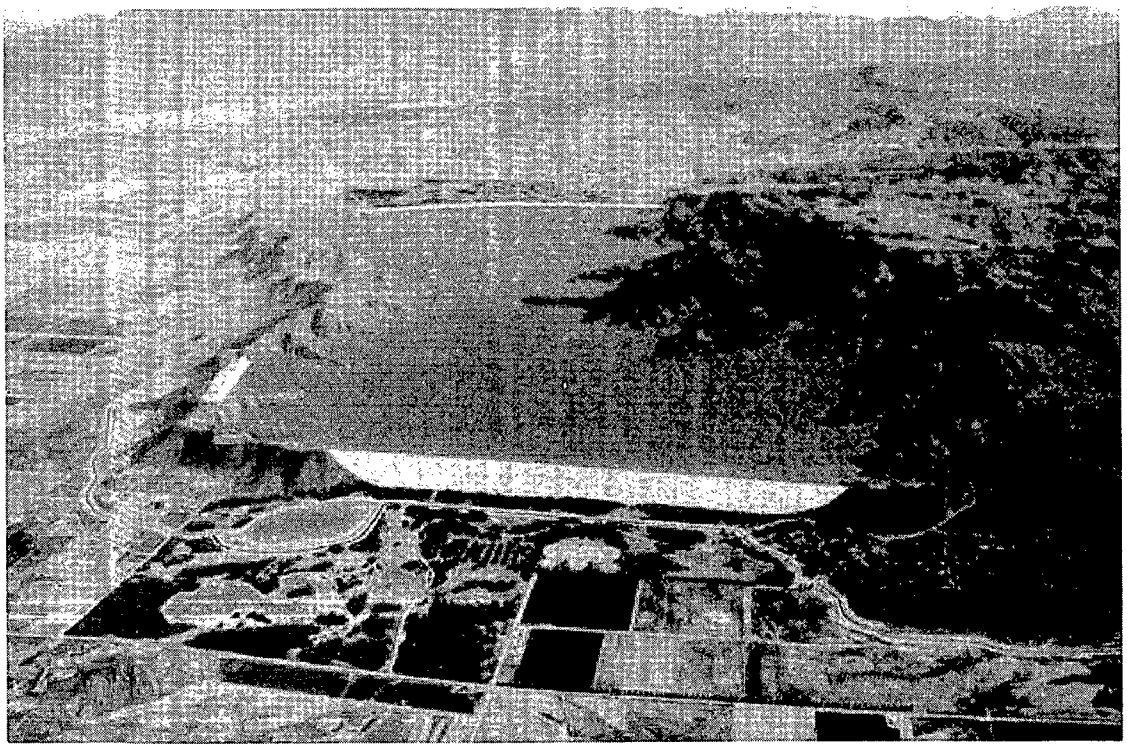


Figure 2. Eastside Project

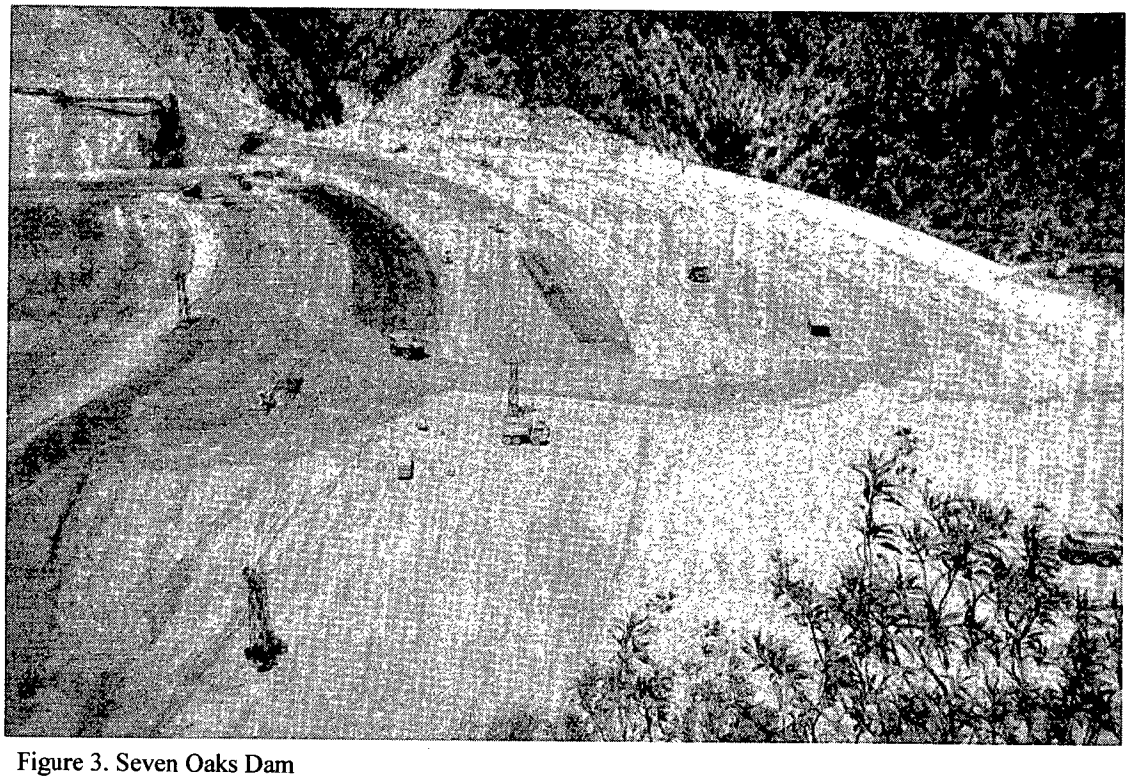


Figure 3. Seven Oaks Dam

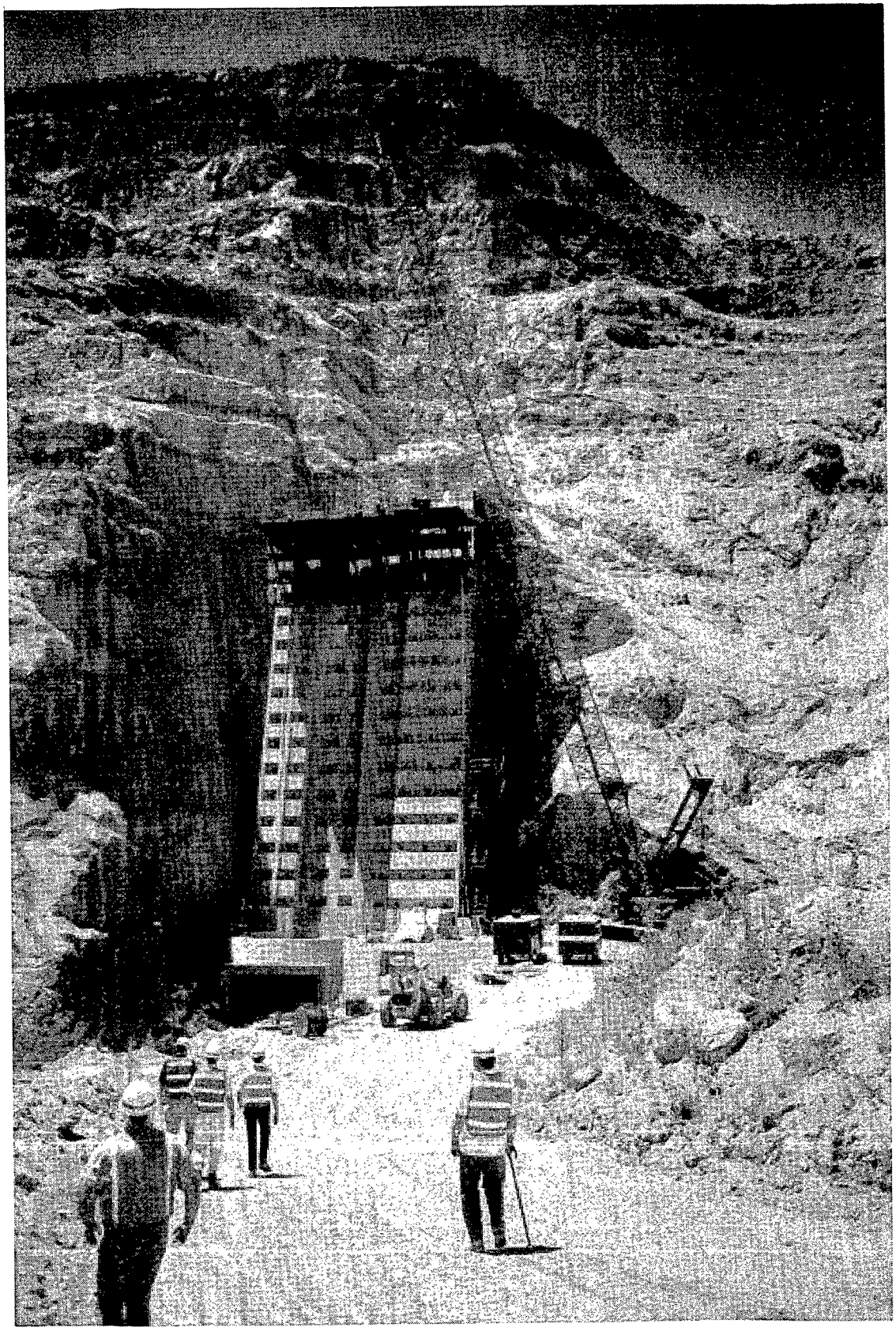


Figure 4. Seven Oaks Intake Tower

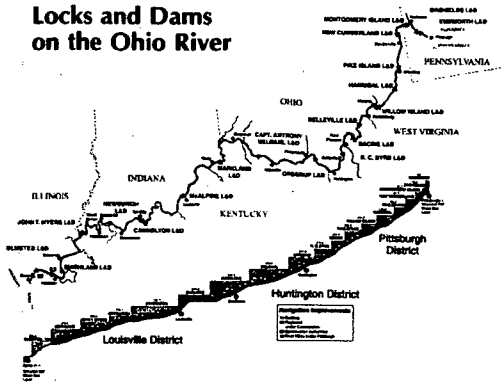


Figure 5.Olmsted Locks and Dam Project

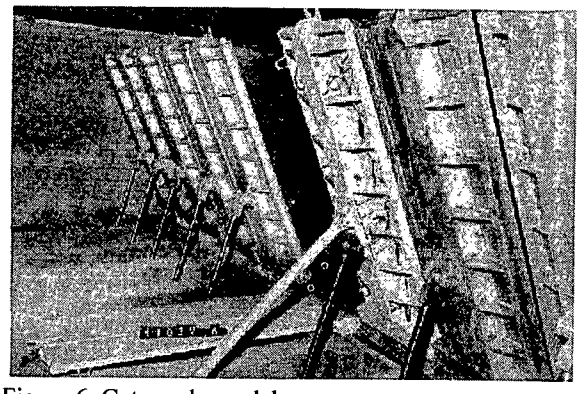

Figure 6. Gate scale model


Figure 7. Alamo Dam

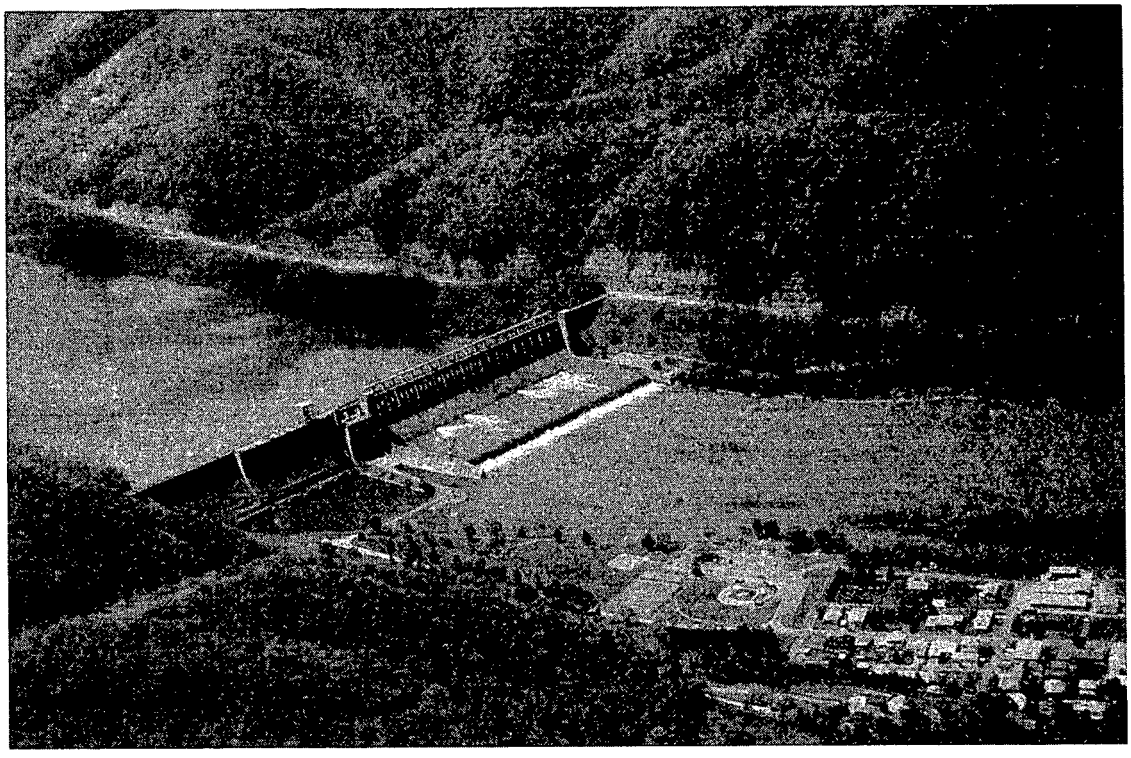


Figure 8. Bluestone Dam

On the Behavior of Large Dams near the Epicenter during Earthquakes in Japan

Choshiro TAMURA

Let me begin by expressing my great pleasure on the opening of this second workshop on earthquake engineering for dams. The first workshop was held three years ago at the Waterways Experiment Station in Vicksburg, Mississippi. As a recall that workshop was a very enjoyable and cordial meeting.

Now as everyone here is well aware, earthquakes frequently rattle Japan as if the entire country were sitting on a shaking table. It is said the energy in the earthquakes that occur in Japan and the surrounding region account for as much as 10 or more percent of the total energy of all earthquakes worldwide, in spite of the relatively very small area. Taking earthquakes into account is a fundamental condition whenever we think about the safety of all structures in Japan.

Next to the seismic resistance of Japan's nuclear power plants, the seismic resistance of dams is regarded as the most important concern. As was already explained earlier by Mr. Uesaka in his keynote address, the Japan Commission on Large Dams conducted an investigation of the behavior of large dams in Japan when struck by a powerful earthquake. The results of this investigation have recently been published. These results have great significance for understanding the actual seismic resistance features of dams. While a great expenditure of time and academic study is necessary for the analysis of this data, I have begun to analyze this data and would like to speak about this with you today.

Because behaviors during an earthquake are so complex, the one propriate method for assessing the seismic resistance of not just dams but any structure is thought to be deep surveying on the actual phenomena when they occur. It is probably quite correct to note that it's unfortunate, but in recent years we have been able to meet with not so few examples of large dams in or near the epicentral regions. Some examples can be cited, including Koyna dam during the Koyna Earthquake (M=7.0) in 1967, the Lower Van Normann dam and others during the San Fernando Earthquake (M=6.6) in 1971, the Dou He dam in the Taishan Earthquake (M=7.8) in 1976, the Makio Dam during the Naganoken-seibu Earthquake (M=6.8) in 1984, La Villita dam during the Michoacan Earthquake (M=8.1) in 1985, the Austrian dam and others during the Loma Prieta Earthquake (M=7.2) in 1989, and the Ambuklao dam and others during the Luzon Earthquake (M=7.8) in 1990. To this we can add new resource materials from a dam near the fault of the Hyogoken-nanbu Earthquake (M=7.2) in 1995. In Japan we have been

Professor Emeritus of University of Tokyo, Professor of Nihon University

conducting research on the seismic resistance of dams while studying these past examples. We believe that in order to firmly grasp the principal factors in seismic resistance, understanding the behavior of large dams when they are struck by a powerful earthquake is fundamental.

I'd like to begin by first showing you the construction conditions of dams built in Japan in recent years. Figure 1 shows the number of dams built, by construction period and purpose of the dam. The horizontal axis shows the period of construction. 1868 is the first year of the Meiji Era. The bar graph shows the number of dams completed during each period in question; the coordinates on the left-hand axis show the number of large dams constructed and the coordinates on the right-hand axis show the total number of large dams. In 1867 there were 508 dams for irrigation purposes, but by 1995 there were 2,605 such dams, approximately a five-fold increase. In the lower section of the figure is information showing how the Standard for Seismic Design for dams has changed historically. From about 1950, you can see that Seismic Design Standards have been laid down and developed in succession in each sector. Before that time small-scale dams for agricultural (irrigation) purposes accounted for the majority of all dams and were built using traditional design and construction methods, and it is believed there were not major changes in the seismic resistance of dams before around that era. Thereafter, small-scale dams built for local irrigation purposes were classified into dams completed before 1956 and all other dams, and began to be treated separately. Let's look at dams completed after 1900 regarding present dam conditions and extant information of dams. The dams that were the subject of the Japan Commission on Large Dams' study are shown in Table 1. As you can see from this table, only those dams that have received strong vibrations were targeted. All together 273 dams were the subjects of the study, with dams completed after 1900 accounting for approximately 13% of the total. Here I will discuss dams that have been subject to severe tremors of earthquakes of magnitude 6.5 or larger. This encompasses 182 dams, or 8.7% of the total.

First, let's eliminate the small-scale local irrigation dams explained earlier. If we select the principal earthquakes that have subjected dams to strong seismic shocks, Table 2 is the result. The symbols for the dam categories follow the ICOLD designations. PG indicates a gravity dam, ER indicates a rockfill dam, TE refers to an earthfill dam, VA an arch dam, and HG indicates a hollow gravity dam. A total of 32 dams were subject to the Hyogoken-nanbu Earthquake in 1995; nearly all escaped damage, with only light damage occurring at dams in only several locations. Below this on the table the results of the 1984 Naganoken-seibu Earthquake, the 1969 central Gifu Prefecture Earthquake (M=6.6) are shown in order, followed by others such as the 1987 earthquake in the northern part of the Hidaka mountains (M=7.0).

Figure 2 shows the 32 dams that were hit by the Hyogoken-nanbu Earthquake in 1995, indicated by dam type, height of dam and epicentral distance. The length of the fault that has acted during this earthquake is conjectured to be about 45-50km. Dams that are situated on the ground above or near this fault are indicated with an "X" mark. In addition, the triangle (△) is the distance from the active fault to the dam concerned. At the earthfill dam indicated as Number 17, it has been confirmed that the riprap on the upstream face slid downwards by 20-30 centimeters. The dam indicated as Number 1 is a gravity dam used for watersupply that was completed in 1900 and has a typical triangular-shaped cross section. Repairs are being made to stop water leaks because leaks increased as a result of the earthquake, but this is unrelated to the stability of the dam body. This dam is located only several dozen meters from the Nunobiki fault,one of the component faults in the Rokko fault system . Although small changes in the conditions of several other dams have been reported, overall the results of the survey are believed to show that the dams possessed a high level of strength against this earthquake.

Figure 3 shows the situation for the 1984 Naganoken-seibu Earthquake. The data are shown in the figure using the same conventions as Figure 2. There are 30 dams within a distance of 50km from the epicenter. The Makio Dam (number 17 in the figure) located 4km from the epicenter received light damage, but no structural damage occurred to the dam body. This dam is a rockfill dam with a height of 104.8m, and was constructed in 1961 as a multipurpose dam. Vibration rollers were used in the compaction of the dam body.

The situation for the 1964 Niigata Earthquake (M=7.5) is shown in Figure 4. No dams were located in the epicentral region because the earthquake epicenter was approximately 25km off the coast of Niigata Prefecture. Of a total of 11 dams, damage was reported at two dams (Number 1 and 9 in the figure). Dam Number 1 was a concrete gravity dam with a height of dam of 82.5m. An increase in leaks between the blocks on the left bank side was confirmed and repaired. Number 9 was completed in 1964 and is a concrete facing type rockfill dam. Although it was more than 100km from the earthquake epicenter, it is included in the figure because it did suffer damage from the quake. The joints of concrete facing slabs on the upstream face were damaged, resulting in an increase in water leakage, and the dam had to be repaired.

Figure 5 shows the local irrigation dams that were constructed before 1956 that were damaged at the time of the same Niigata Earthquake. All of these were earthfill dams. When compared with the data in Figure 4, the fact that the circumstances in which damage to the dams occurred are extremely different is plainly evident.

As shown here, we can infer that the years around

1956 represent a boundary that marks large improvements in the seismic resistance of local irrigation dams. Looked at from the behavior of dams that received strong earthquake shocks, it is presumed that dams designed and constructed following current standards for seismic design for dams have a high level of seismic resistance. Taking that earthquake resistance of dams – particularly the seismic resistance of Embankment Dams – is the overall result of dam design as well as factors such as materials, construction methods and foundation conditions into consideration, I think that not only analytical but also synthetic study will be useful and fundamental to clarify the characteristics of earthquake resistance of dams.

Table 1 Magnitude of Earthquake and Area around the Epicenter to be surveyed for Investigation on Seismic Resistance of Large Dams

Magnitude of Earthquake	Radius of surveyed area
5.5≦M<6.5	30 km
6.5≦M<7.5	50 km
M≧7.5	100 km

Table 2 Number of large Dams surveyed

The number does not include the number of local irrigation dams completed before 1956.

1) 1995 Hyogoken-nanbu Earthquake (M=7.2)

Total number of dam : 32

PG				ER			TE		
15m≦	30m≦	60m≦	100m≦	15m≦	30m≦	60m≦	15m≦	30m≦	60m≦
19	16	3	0	6	3	0	7	2	0

2) 1984 Naganoken-seibu Earthquake (M=6.8)

Total number of dam : 30

PG				ER				VA				HG
15m≦	30m≦	60m≦	100m≦	15m≦	30m≦	60m≦	100m≦	60m≦	100m≦	150m≦	200m≦	69.0m
21	15	6	0	3	2	1	0	5	3	1	0	1

3)Earthquake at central part of Gifu-prefecture (1969,M=6.6)

Total number of dam : 23

PG				VA	ER		HG
15m≦	30m≦	60m≦	100m≦	133.0m	100m≦	150m≦	69.0m
19	12	5	0	1	2	0	1

4)Kitamino Earthquake (1961, M=7.0)

Total number of dam : 13

PG				ER
15m≦	30m≦	60m≦	100m≦	131.0m
12	5	3	0	1

5) 1964 Niigata Earthquake (M =7.5)

Total number of dam :11

PG			TE			ER	HG
30m≦	60m≦	100m≦	15m≦	30m≦	60m≦	66.5m	46.0m
4	3	0	5	3	0	1	1

6) Earthquake at northern part of the Hidaka-mountains (M=7.0)

Total number of dam : 8

PG				ER	VA
15m≦	30m≦	60m≦	100m≦	102.8m	61.2m
6	5	1	0	1	1

7) 1983 Nihonkai-chubu Earthquake (M=7.7)

Total number of dam : 6

PG	TE		ER
72.0m	15m≦	30m≦	66.5m
1	4	0	1

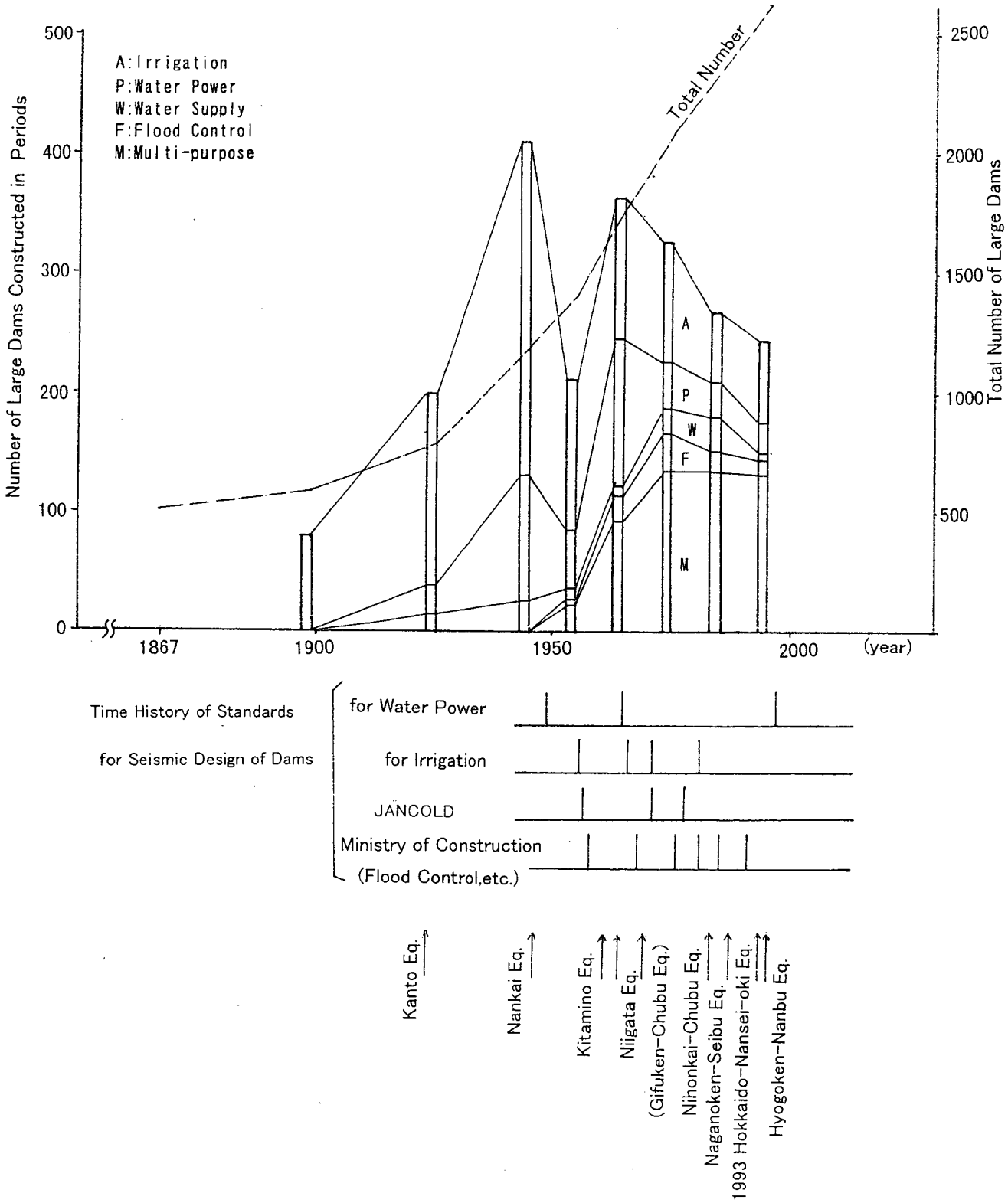


Fig.1 Number of Large Dams in Japan (1867～1995)

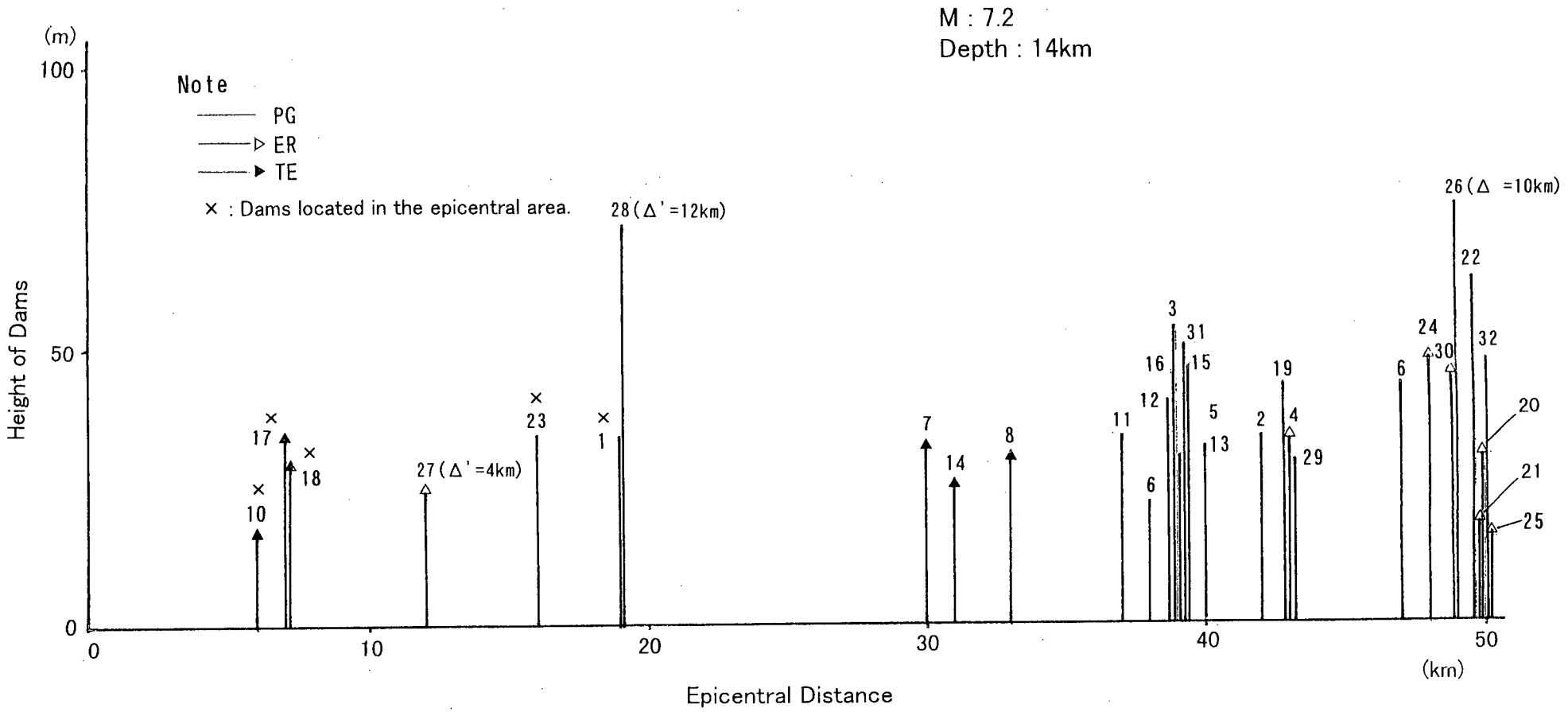


Fig.2 Height and Epicentral Distance of Dams, Hyogoken-Nanbu Earthquake, Jan.17, 1995

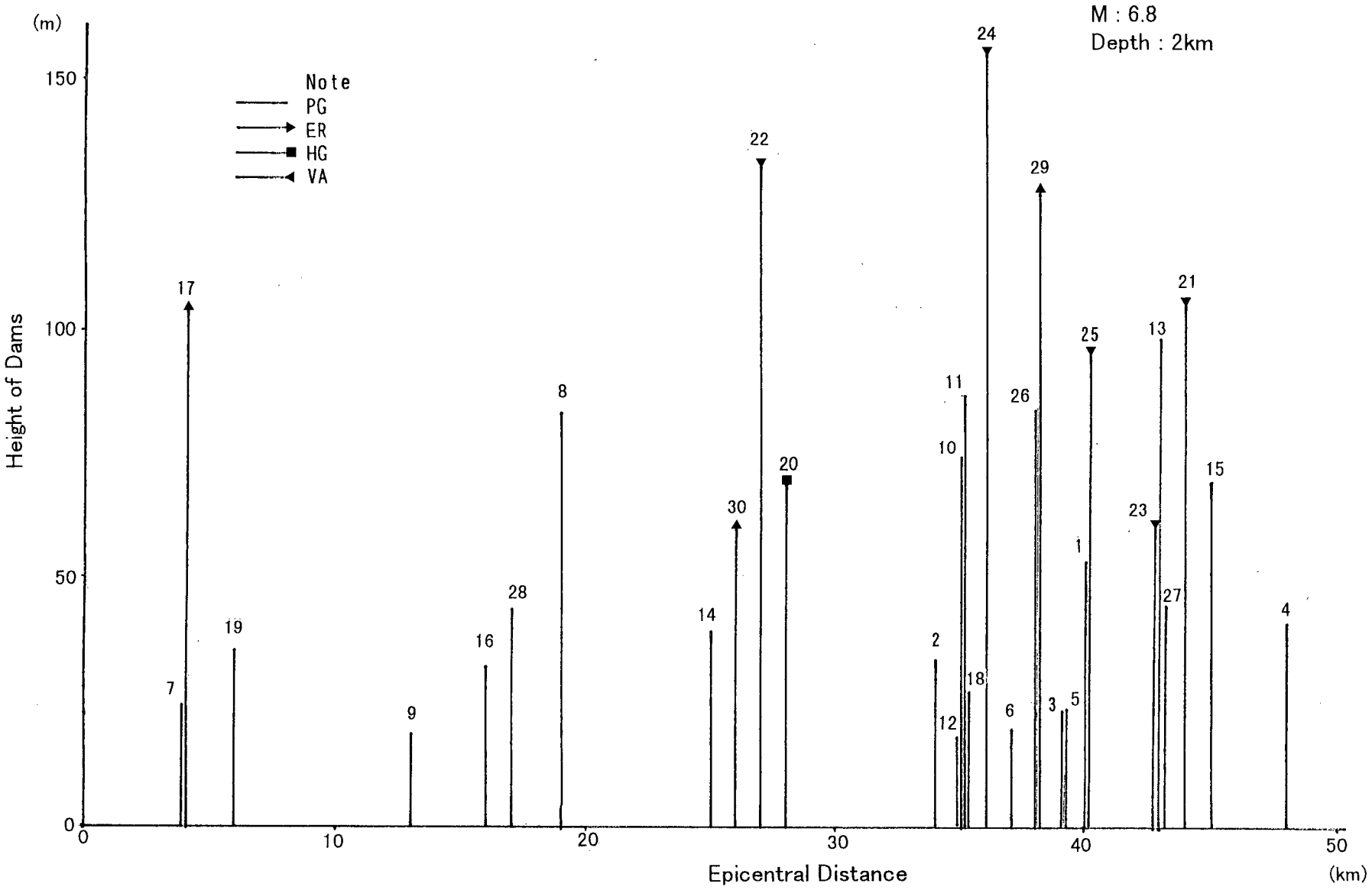


Fig.3 Height and Epicentral Distance of Dams, Naganoken-seibu Earthquake, Sep.14,1984

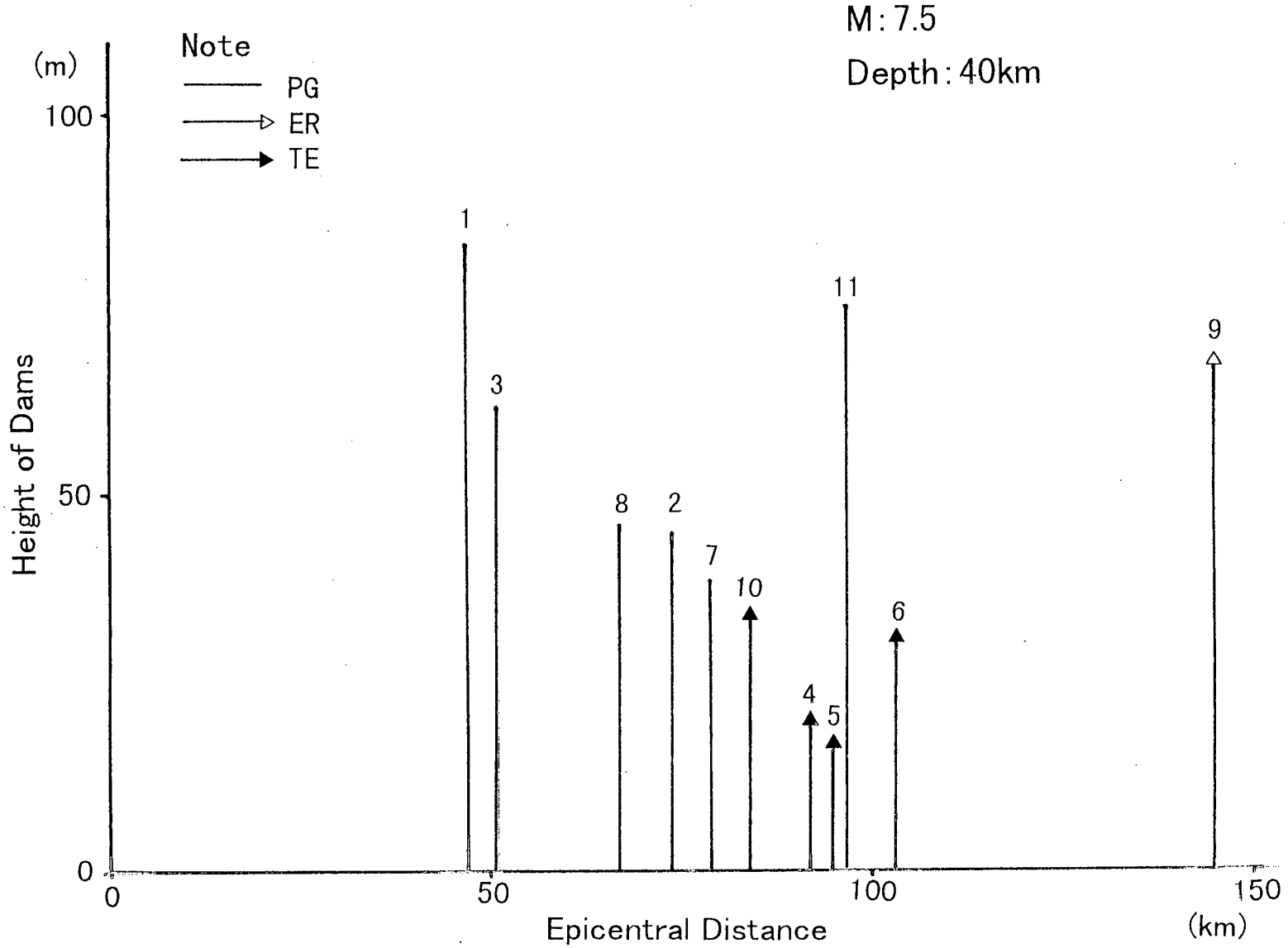


Fig.4 Height and Epicentral Distance of Dams, Niigata Earthquake, June.16, 1964 (No-1)

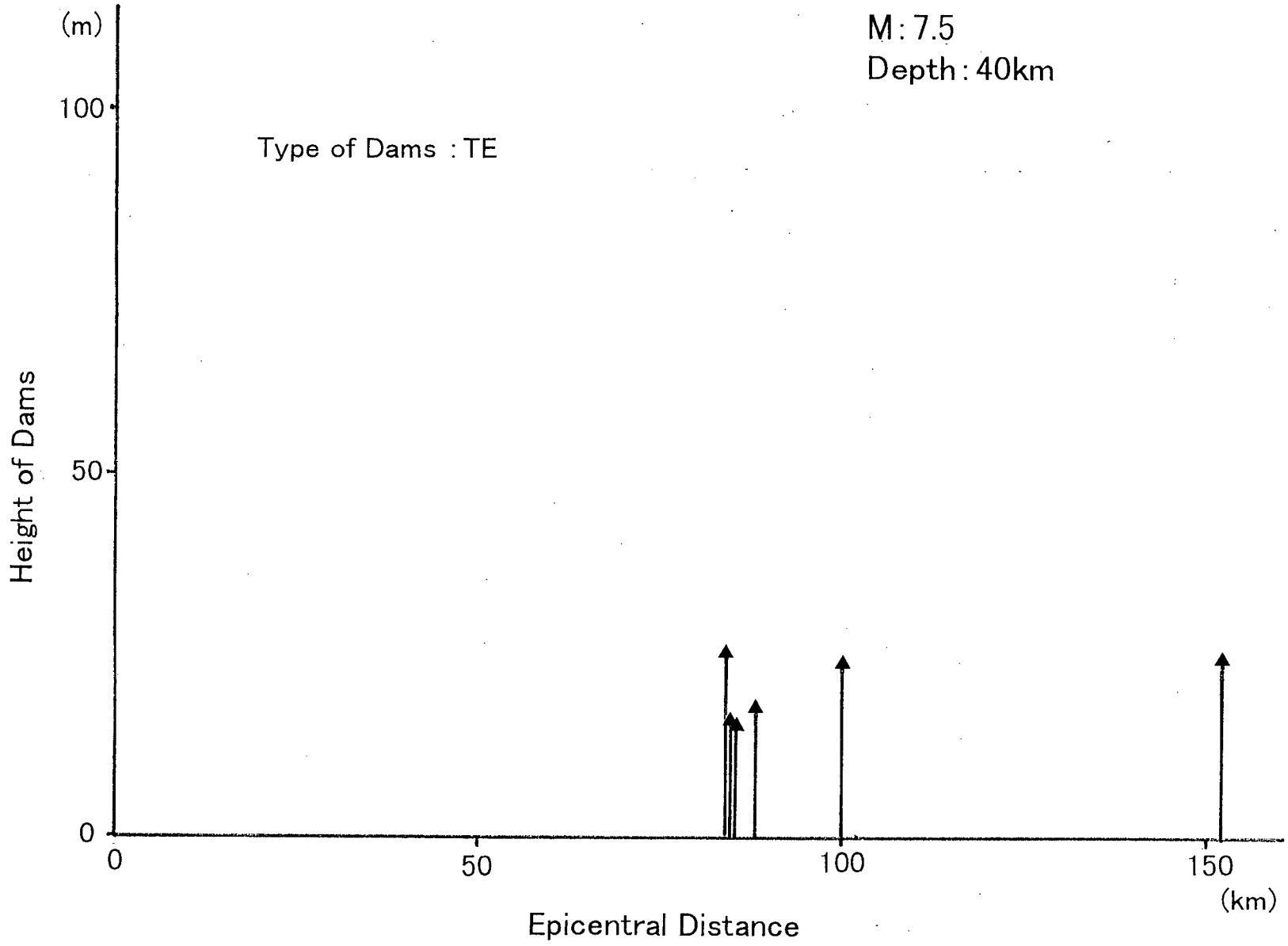


Fig.5 Height and Epicentral Distance of Dams, Niigata Earthquake, June.16, 1964 (No-2)

Technical Session 1

Concrete Dams (1)

Vibration Tests and Earthquake Response Observation of Concrete Dams

by

Hiroo SHIOJIRI[1], Minoru UEDA[2], Yukihiro TOYODA[3]

ABSTRACT

Vibration tests , observation of earthquake responses are conducted on two arch dams . The accelerations of dams and foundation rock as well as hydrodynamic pressures on upstream face of one dam are measured. The numerical analyses are conducted to establish correlation to observations and experimental results.

Key Word :*Arch Dam,*
Earthquake Response,
Vibration Test,
Numercal Analysis.

1. INTRODUCTION

It is necessary for designing safe dams to predict accurately the performance of the dams during earthquake. The accuracy of the prediction depends on the numerical modeling. The validity of modeling is verified by comparing the analytical results with the experimental results conducted on prototype and/or response observations.

In this paper , the simulation analyses of the vibration tests conducted on two arch dams and measurements of earthquake responses of the dams are introduced. Based on the comparison of analytical and measured results, the validity of the modeling rules is discussed.

2. ANALYTICAL METHOD

The dam and foundation rock are discretized by 20 nodes 3-D solid finite elements. The viscous boundary derived by virtual work[1] is applied at the far end of foundation rock. As to the reservoir water, the governing equation is assumed to be written using velocity potential[2] as follows:

$$\frac{1}{c^2}\frac{\partial^2\phi}{\partial t^2}=\frac{\partial^2\phi}{\partial x^2}+\frac{\partial^2\phi}{\partial y^2}+\frac{\partial^2\phi}{\partial z^2} \qquad (1)$$

,in which c denotes sound velocity in water, ϕ denotes velocity potential, and x,y,and z are Cartesian coordinates, where z is measured in upward direction and y in upstram direction. The boundary condition at the free surface is given by:

$$\frac{1}{g}\frac{\partial^2\phi}{\partial t^2}-\frac{\partial\phi}{\partial z}=0 \qquad (2)$$

,where z denotes the acceleration of gravity. The boundary condition on the reservor bottom or side is given considering partial absorbtion and reflaction of sound wave as:

$$\frac{\partial\phi}{\partial t}+c\beta\left(\frac{\partial\phi}{\partial n}-\frac{\partial U_{gn}}{\partial t}\right)=0 \qquad (3)$$

,where β, $\frac{\partial}{\partial n}$, ρ and U_{gn} denote the acoustic normal direction to boundary ,the density of

1)Dr.Eng.,Professor,Nihon University, Tokyo,Japan
2)Dr.Eng. Chubu Electric Power Company, Nagoya,Japan
3)M.Eng.Centrl Research Institute of Electric Power Industry, Abiko,Japan

water, the density of material ,and the impedance ratio at the boundary, derivative in displacement of reservoir bottom normal to the boundary, respectively.

The boundary condition on the dam surface is :

$$\frac{\partial \phi}{\partial n} = \frac{\partial U_n}{\partial t} \tag{4}$$

, where U_n denotes the velocity of dam surface normal to the surface. The boundary condition at the far end of the reservoir is assumed to be:

$$\frac{\partial \phi}{\partial t} + c\frac{\partial \phi}{\partial y} = 0 \tag{5}$$

The hydrodynamic pressure is given as:

$$P_d = -\rho \frac{\partial \phi}{\partial t} \tag{6}$$

Based on the weak form formulation of the governing equation, and using the 20 nodes isoparametoric shape functions, the finite element for water and the corresponding discetized boundary conditions are derived as follows.

$$\frac{\rho}{c^2}\int_{V_e}[N_L]^T[N_L]dv\{\ddot{\phi}\}_e + \rho\int_{V_e}[B]^T[B]dv\{\phi\}_e$$

$$= -\frac{\rho}{g}\int_{S_e}[N_N]^T[N_N]ds\{\ddot{\phi}\}_e \text{ (water surface)}$$

$$= -\frac{\rho}{c\beta}\int_{S_e}[N_N]^T[N_N]ds\{\dot{\phi}\}_e + \rho\int_{S_e}[N_N]^T[N_N]ds\{\dot{U}_g\}_e$$

(reservoir bottom) (7a)

$$= -\frac{\rho}{c}\int_{S_e}[N_N]^T[N_N]ds\{\dot{\phi}\}_e \text{ (far end of reservoir)} \tag{7b}$$

$$= \rho\int_{S_e}[N_N]^T[N_N]ds\{\dot{U}\}_e \text{ (on dam surface)} \tag{7c}$$

,where

$$[N_L] = \begin{bmatrix} N_1 & & & N_2 & & & \cdots & N_N & & \\ & N_1 & & & N_2 & & \cdots & & N_N & \\ & & N_1 & & & N_2 & \cdots & & & N_N \end{bmatrix},$$

$$[N_N]^T = (n_x \quad n_y \quad n_z)[N_L]$$

$$[N] = [N_1 \quad N_2 \quad \cdots \quad N_N]$$

$$\{\phi\}_e = (\phi_1, \phi_2, \cdots \phi_N)^T$$

$$[B] = \begin{bmatrix} \frac{\partial N_1}{\partial x} & \frac{\partial N_2}{\partial x} & \cdots & \frac{\partial N_N}{\partial x} \\ \frac{\partial N_1}{\partial y} & \frac{\partial N_2}{\partial y} & \cdots & \frac{\partial N_N}{\partial y} \\ \frac{\partial N_1}{\partial z} & \frac{\partial N_2}{\partial y} & \cdots & \frac{\partial N_N}{\partial z} \end{bmatrix}$$

and $(n_x \quad n_y \quad n_z)$, $\{U_g\}_e$, $\{U_e\}$, N_i, ϕ_i are the normal unit vector of the surface ,the displacement vector of the reservoir bottom, the displacement vector of the dam surface., a shape function, and a nodal value of velocity potential, respectively.

The nodal forces applied on the dam surface by reservoir water is given by:

$$\{f\}_e = -\rho\int_{S_e}[N]^T[N]ds\{\ddot{\phi}\} \tag{8}$$

3. SIMULATION OF VIBRATION TEST

(1)Takane arch dam

Takane dam is constructed in 1969,and owned by Chubu Electric Power Company. The height is 130m,and crest length is 275m. The vibration test was conducted in 1971, when reservoir is full.(Fig.1) The frequency range of the test is from 2Hz up to 6Hz. The increment of the frequency is 0.1Hz except near resonant frequencies, where the increment is 0.05Hz. The vibration properties obtained by the test is shown in Table. 1.

The material properties to be used, and the effects of extent of mesh division, of mesh size, and of boundary conditions are examined in the simulation analysis[3].

a)The effect of discrtization

The mesh size should be determined considering wave length. The mesh size and the ratio of the size to the wave length at 6Hz is shown in Table 2.

i)Discretization of dam

The computed responses for different mesh size of the dam are shown in Fig.2 The mesh size of 15m(10 meshes in a wave) seems sufficient, because difference between the responses with mesh size 15m and those with mesh size 10m is small.

ii)Discretization of foundation rock

The effects of the extent of the foundation rock meshes are demonstrated in Fig.3. It seems that the 120m deep foundation rock model is sufficient,i.e. the depth about the same as the

height of the dam. The effects of the mesh size of foundation rock are shown in Fig.4. The mesh size of 30m seems to give sufficiently accurate results, which is about 1/10 of the wave length.

iii)Discretization of Reservoir Water

The effects of reservoir model length and of mesh size are observed in Fig.5 and in Fig.6. The computed responses is the same if the model length exceeds 275m, i.e. twice as much as the dam height. The mesh size of 17.5m gives the best correlation with the measured values. It is about 1/15 of the wave length at 6 Hz. The reason why the reservoir needs smaller mesh width is that the variation of the hydrodynamic pressure near the dam surface in radial direction is much larger than the average values in the reservoir.

b) Material properties

i)Dam concrete

The strain-rate dependence of elastic modulus of concrete is negligible for the strain-rate expected during earthquake. The elastic modulus for the simulation analysis is estimated to be equal to the tangent modulus at 0 strain obtained from uni-axial static tests of specimens[4].

ii)Foundation rock

The elastic modulus of rock can be estimated by several methods. They are the in-situ loading tests, the measurement of the elastic wave velocities generated by explosives, and the measurement of S-wave velocities of earthquake wave. The last one is conducted assuming the direction of the incident earthquake wave. The estimated value by one method differs from that by other method. The reason of discrepancy may be caused by the difference of the magnitude of the strain of rock during the measurements. The comparison of computed results with measured ones is shown in Fig.7. The modulus obtained from S-wave velocity gives the best correlation.

c)Miscellaneous

i)Impedance ratio at reservoir bed and bank

The reservoir bed or bank is made of rock covered by soil. Besides, there is sediments at the bottom of the reservoir.
Impedance ratio of soil or sediments is about 1,while that of rock is about 5.

The comparison of computed and measured results are shown in Fig.8. It is observed that the impedance ratio of rock is most appropriate for the boundary condition of reservoir bed or bank.

ii)Foundation rock

The computed results with and without mass of rock are plotted in Fig.9 along with measured values ,where fixed boundary at the far end of foudation rock is assumed. Both results are larger than the measured one. The results with massless rock are better than those with rock mass.

The results with the abutment fixed are plotted in Fig.10. The computed resonant frequency is much higher than the measured one.

iii)Compressibility of water

The computed results with and without consideration of compressibility of water are plotted in Fig.11, along with the measured ones. The results without water compressibility differ from the measured ones in high frequency range.

vi)Damping

The estimated material damping of concrete is about 1.5%. The value of material damping of rock has insignificant effects on the response of dams.

d)Vibration Mode

The measured and computed vibration modes are compared in Fig.12. The good correlation is obtained.

(2)Kawaore arch dam

Kawaore dam is constructed and owned by Chubu Electric Power Company. The hight is 107.5m, and the crest length is 341.2m. The construction is finished in October of 1992. After the completion of the dam, the reservoir water is accumulated , and water surface reached high water level in December of 1994. The vibration

tests were conducted at the water levels of 70m below high water level, 26.5 m below high water level(low water level), and high water level.

The accelerometers and pressure meters are installed in the dam and in the foundation rock.(Fig. 13) The pressure meters are designed such that only the dynamic component of pressure is measured. (Fig.14) The resolution is smaller than 10 Pascal, while the expected maximum hydrodynamic pressure during vibration tests is 3-4 hundred Pascal. The measured results are compared with computaional results.[4)]

a) Finite element mesh

The finite element mesh of Kawaore dam is shown in Fig.15. The mesh sizes are kept less than 1/10 of shortest wave length(wave length at 10Hz). The depth of foundation rock mesh is 120m, i.e. nearly the same as the height of the dam. The minimum horizontal distance between dam and the far end of rock model is taken as 170m,i.e. about half of dam crest length.

The preliminary computation shows the results is the same if the distance is increased up to 1.5 times as much as the crest length.

b)Material properties

i)Dam

The elastic moduli are equal to the tangent moduli at strain 0 obtained by static tests of specimens. The material damping of concrete is assumed to be 1%.

ii)Foundation Rock

The elastic moduli are estimated based on the velocity of S-wave of earthquake. Since the effects of the material damping of rock on the dam response is negligible, the same material damping as dam concrete is assumed for rock.

c) Boundary condition

The impedance ratio at the sides of reservoir model is assumed to be 1, because reservoir extends further in the transverse direction. There exists bank at the upstream end. The computed results with the impedance ratio 1.0 at the upstream (assuming water extends infinitely) and 5.3(corresponding to bank) are plotted in Fig. 16,and 17 along with measured value. It is shown that the value of impedance ratio at far end of the reservoir has significant influence on the response of the dam.

d)Comparison of computational and measured results.

The displacement amplitudes obtained by the tests at low water level and at high water level are compared with the corresponding computational results.(Fig.18,19) The agreements are good for both case. The mode shapes at high water level are shown in Fig.20.Again, the agreements are good.

The comparison of the computed and the measured hydrodynamic pressure are shown in Fig.21. The two results agree well.

(3)Earthquake response

The response of Kawaore arch dam to the earthquake ground motion occurred on March 16 in 1997 are measured. Maximum acceleration response of Kawaore arch dam was 120Gal. The response of the dam is simulated numerically,[5)] where the high frequency component above 10Hz were filtered out.

a)Finite element mesh

It is observed that the thickness of the rock model and the horizontal distance between the dam and outer end of the rock model should be 1.5 times as much as those adopted in the simulation analyses of vibration tests after parametric computations.

b)Material properties

The elastic moduli of dam concrete and foundation rock are the same as used in the simulation analyses of vibration tests. The material damping of the concrete has great influence on the dam response. The material damping of foundation rock affects the free ground motion of foundation rock and has significant effects on the response of the dam.

The material damping of concrete and rock is considered to be strain amplitude dependent

When the response amplitudes are small ,the of damping is estimated to be 1% for both concrete and foundation rock based on the correlation to vibration tests(Case1). After parametric simulation analysis, it is shown that the best correlation to observation is obtained if value of material damping of concrete is set to be 5.8% and that of rock 3% during the 10sec. of large acceleration response(Case 2).

c)Comparison of computational and measured response

The computed acceleration response is compared with the observed one(Fig.22,23) The agreements are fairly good for both large amplitudes and small amplitudes.

4. EFFECT OF WATER LEVEL ON NATURAL FREQUENCY

The natural frequencies of Kawaore dam with different water levels are shown in table 3.
The natural frequencies corresponding to high water level and low water level agree well with linear analysis results as described above. Linear analysis predicts that the fundamental natural frequency increases as water level decreases. But, the fundamental natural frequency decreases as the water level decreases further below low water level.

It is caused by nonlinearity such as opening of joints , and nonlinear analysis is necessary to simulate it.

5. CONCLUSION

The results of linear analytical methods for arch dam are compared with vibration test results and earthquake observation in which maximum acceleration is 120 Gal. The results of numerical modeling described here are in good agreement with measured values when water levels are not too low. When water level is very low ,the effects of nonlinearity must be taken into account.

REFERENCES

1)MIURA,F. and OKINAKA,H.: Dynamic analysis method for 3-D soil-structure interaction systems with the viscous boundary based on the principle of virtual work, Proc.JSCE,No.404/I-11,pp.385-404,1989.(in Japanese)

2)SHIOJIRI,H. and AOYAGI,S. : Earthquake response of concrete gravity dams and arch dams, Proc. 8th WCEE, Prentice Hall Inc., New Jersey, Vol.V,pp.87-94,1989.

3)UEDA,M.,OKUDA,H.,SHIOJIRI,H. and TAMURA,C.: Simulation analysis of forced vibration response of arch dam, Proc. JSCE, No.501/I-29,pp.203-212,1994(in Japanese)

4)SATO,M.,UEDA,M.,OKUDA,H. and KONDO,H.:On the velocity of earthquake waves in concrete, Proc. 48th Annual Conference of JSCE,1,pp.318-319,1993.

5)UEDA,M.,TAMURA,C.,SHIOJIRI,H. and KONDO,H.:Simulation analysis of dynamic water pressures and displacements measured on forced vibration test of arch dam, Proc. JSCE, No.605/I-45,pp.15-28,1998.(in Japanese)

6)TOYODA,Y.,UEDA,M,M.,TUNEKAWA,K. and SHIOJIRI, H.:Validation of 3-D time history analysis procedure for computing earthquake response of arch dam-foundation rock-reservoir water systems based on experimental results, Proc. 10th Earthquake Engineering Symposium, pp.2027-2032, 1998. (in Japanese)

7)UEDA,M.,TSUNEKAWA,K.,YOKOI,M. and SHIOJIRI,H.:Simulation analysis of earthquake response of prototype arch dam, Proc.24th JSCE Earthquake Engineering Symposium,pp.513-516, 1997. (in Japanese)

Table 1. Vibration characteristics of Takane dam

mode	Natural freq. (Hz)	Damping (%)
Asymmetric 1st	2.7	2.0
Symmetric 1st	4.4	3.0

Table 2. Mesh size(m)

Num.of meshes in a wave length	Dam	Rock	Reservoir water
5	28	53	47
10	14	27	23
15	9	18	16
20	7	13	12

Table 3.Water level vs. natural frequency (Hz)

Water level (*belowHigh Water Leve*)	-70m	-26.5m (*L.W.L.*)	0 (*H.W.L.*)
Symmetric 1st	2.88	2.95	2.42
Asymmetric 1st	3.19	3.29	2.81
Symmetric 2nd	4.33	4.60	4.03
Asymmetric 2nd	5.53	6.01	4.40

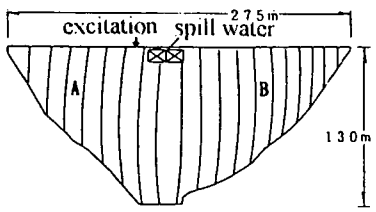


Fig.1.Down stream face of Takane dam

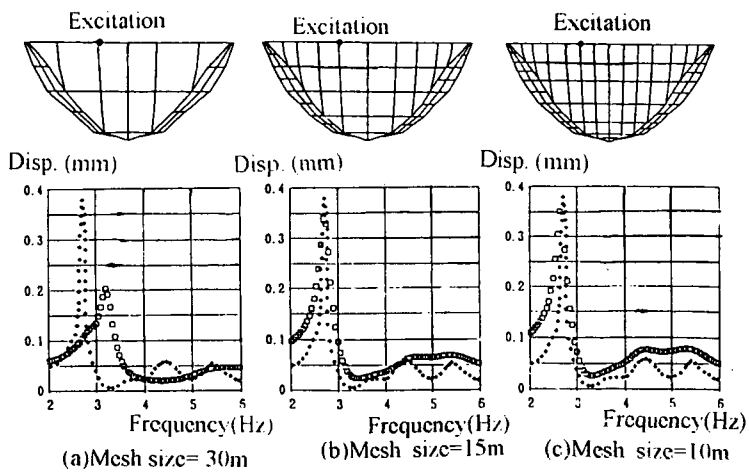


Fig.2.Effect of mesh size in dam

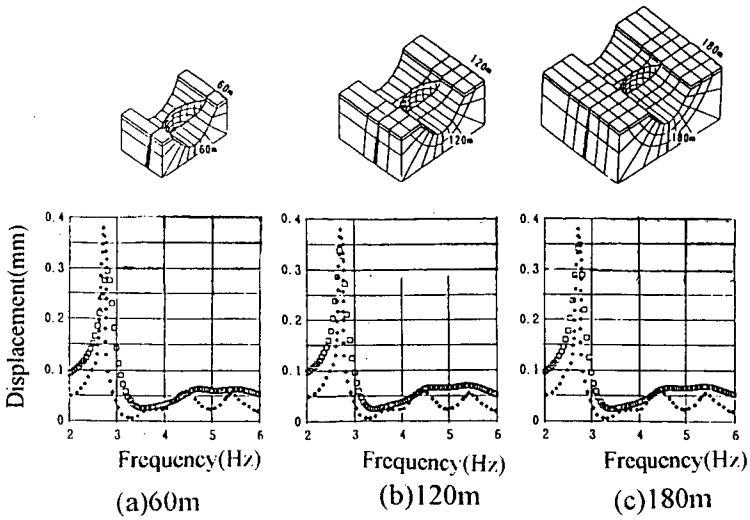


Fig.3. Effect of extent of foundation rock model

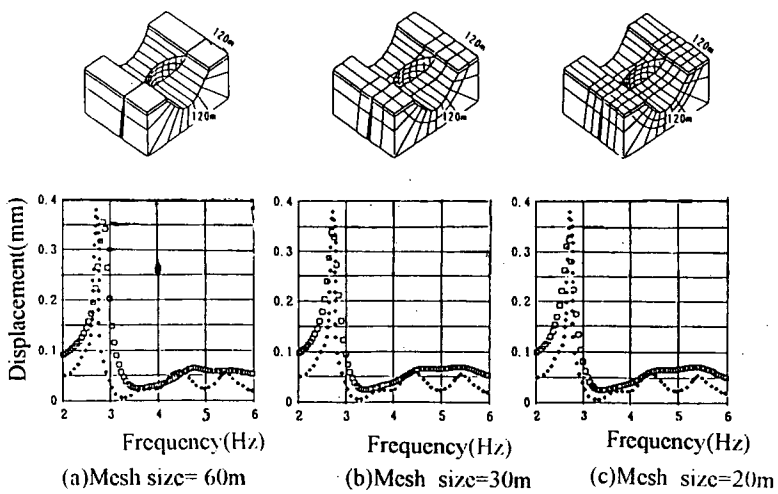


Fig.4.Effect of mesh size in rock

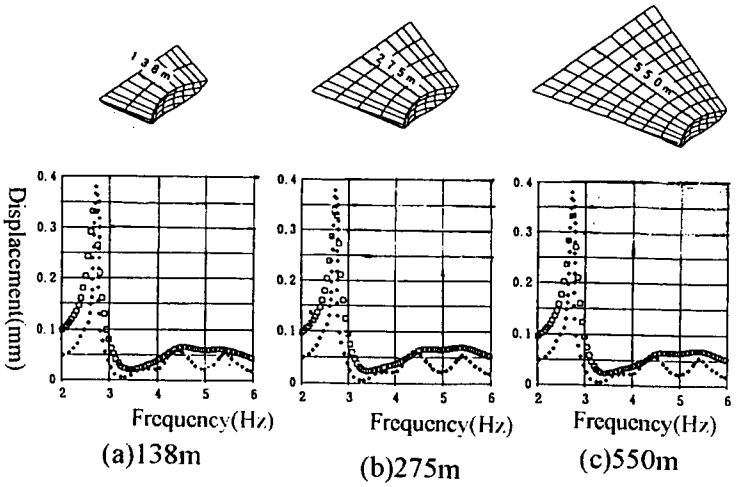


Fig.5.Effect of extent of reservoir model

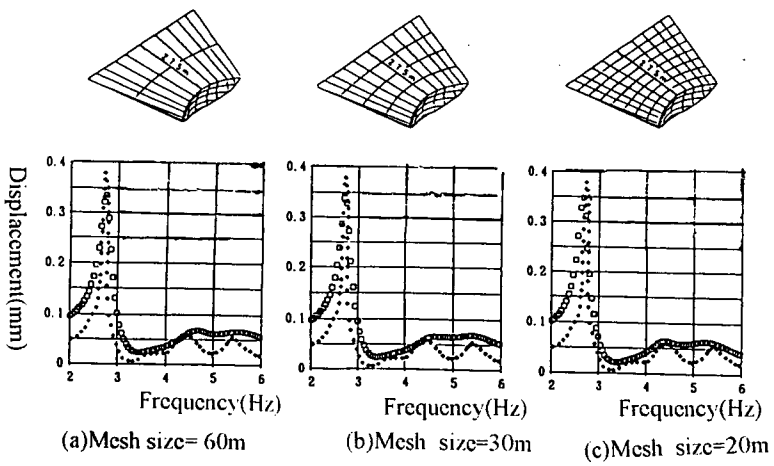


Fig.6.Effect of mesh size in reservoir

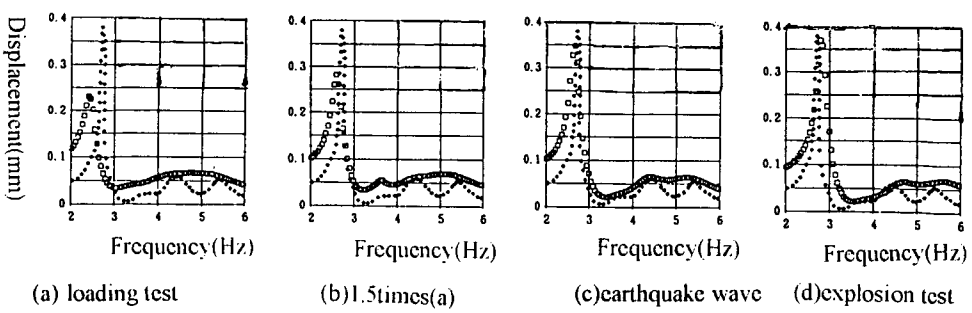
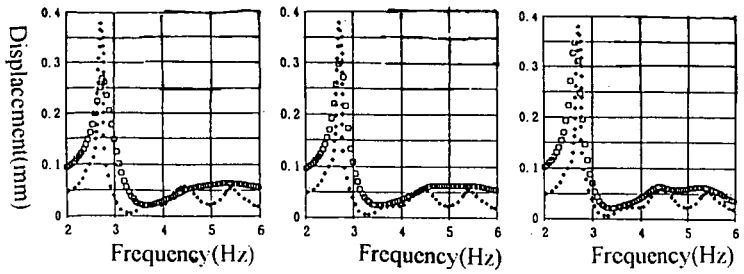
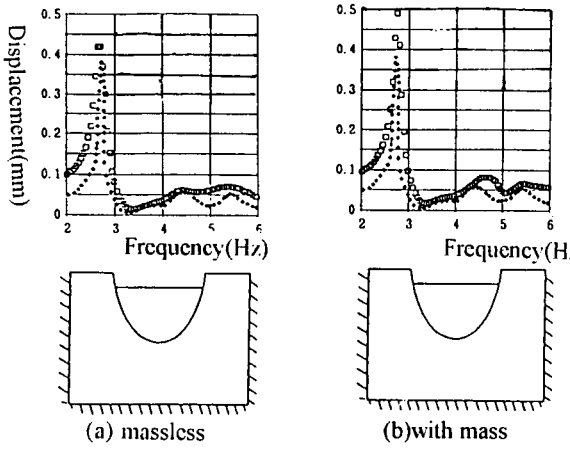


Fig.7.The effect of velocity of shear wave in rock



(a)β=1.0 (b) β=3.0 (c) β=5.0

Fig.8.Effect of impedance ratio β at reservoir bed



(a) massless (b)with mass

Fig.9.Effect of mass of rock model (fixed boundary)

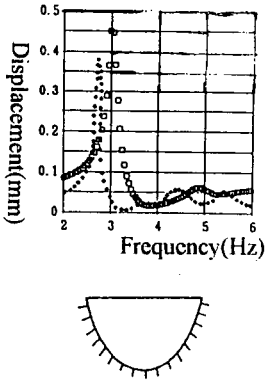


Fig.10.Response of dam with fixed abutment

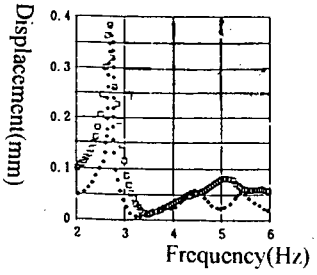


Fig.11. Response of dam with incompressive reservoir water

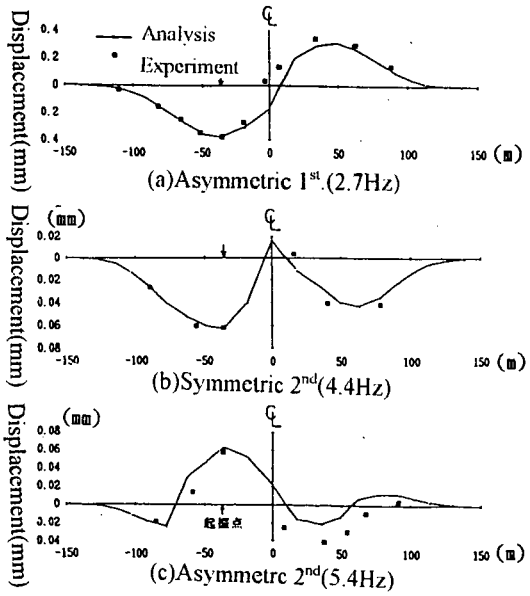


Fig.12.Mode shape

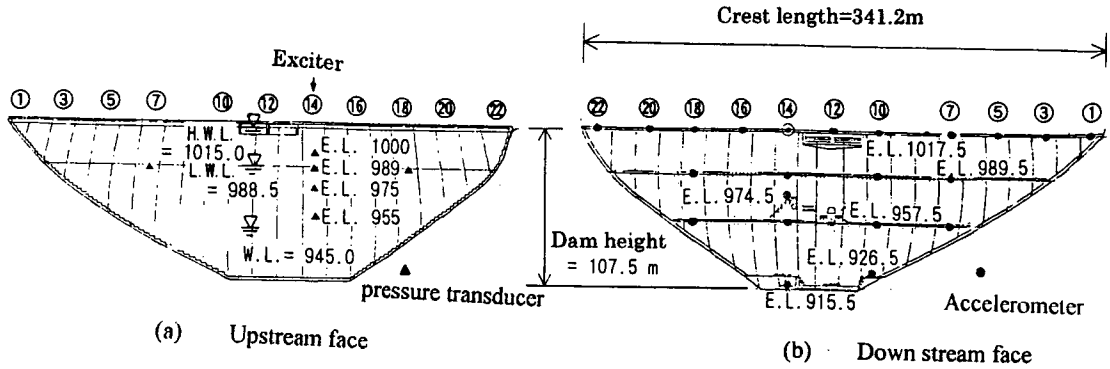


Fig.13. Dam face of Kawaore dam

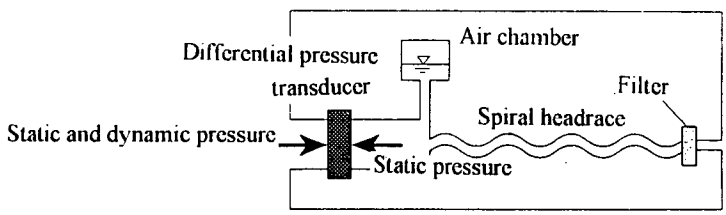
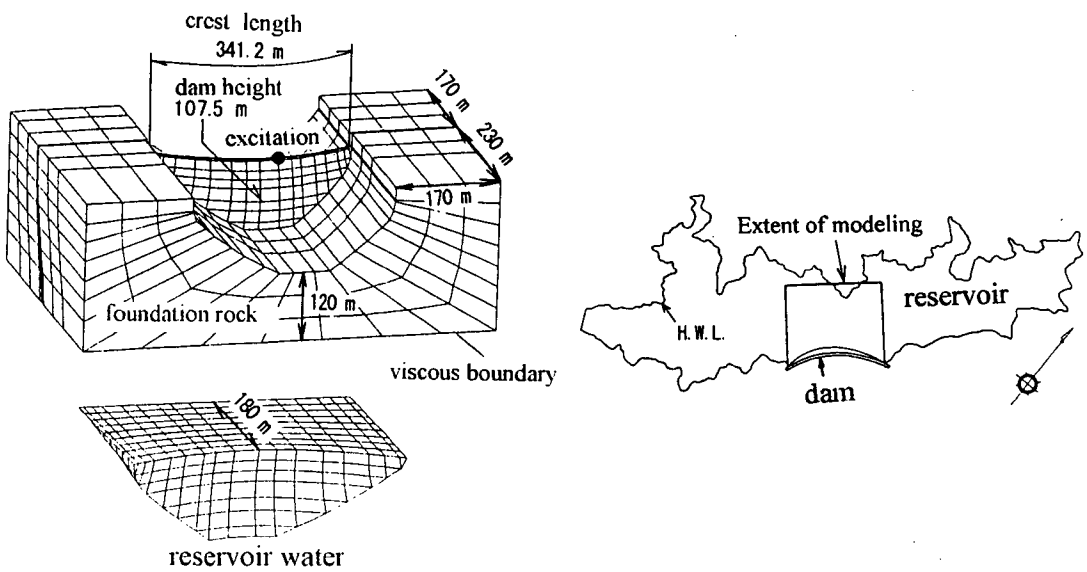


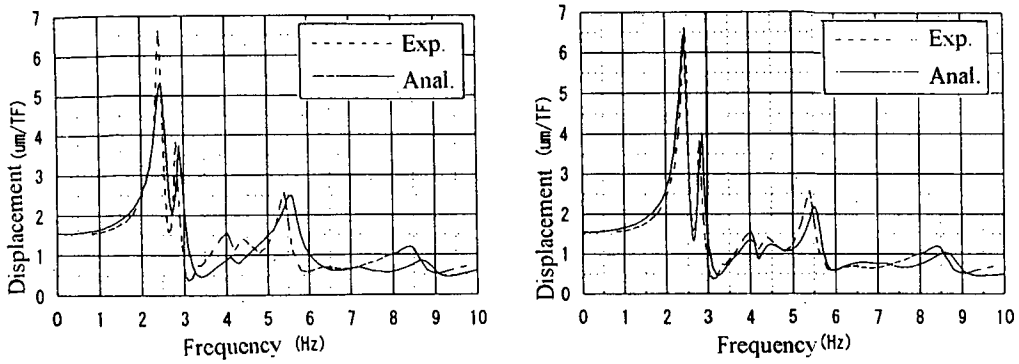
Fig.14.Illustration of pressure transducer



(a) FEM modeling

(b) Extent of modeling

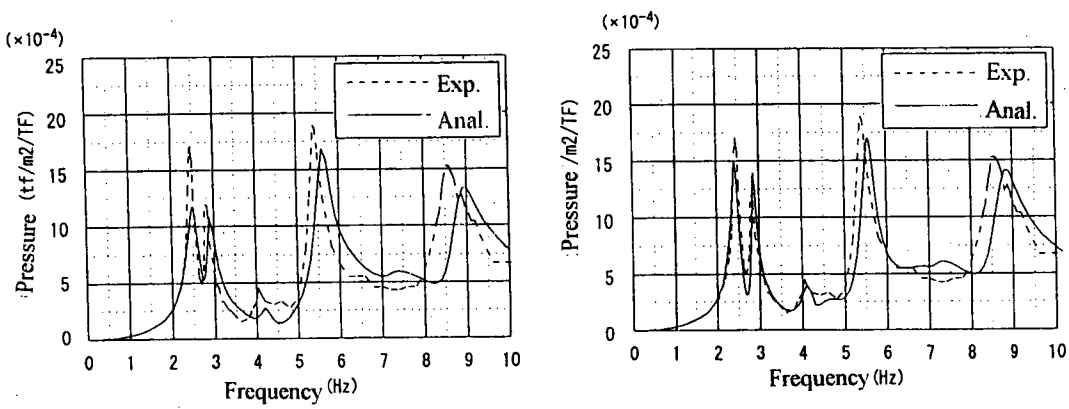
Fig.15. Modeling



(a) β=1.0(infinite water)

(b)β=5.3(bank)

Fig.16.Effect of impedance ratio
at upstream end of reservoir
on dam displacement(H.W.L.)



(a) β=1.0(infinite water)

(b)β=5.3(bank)

Fig.17.Effect of impedance ratio
at upstream end of reservoir
on hydrodynamic pressure(H.W.L.)

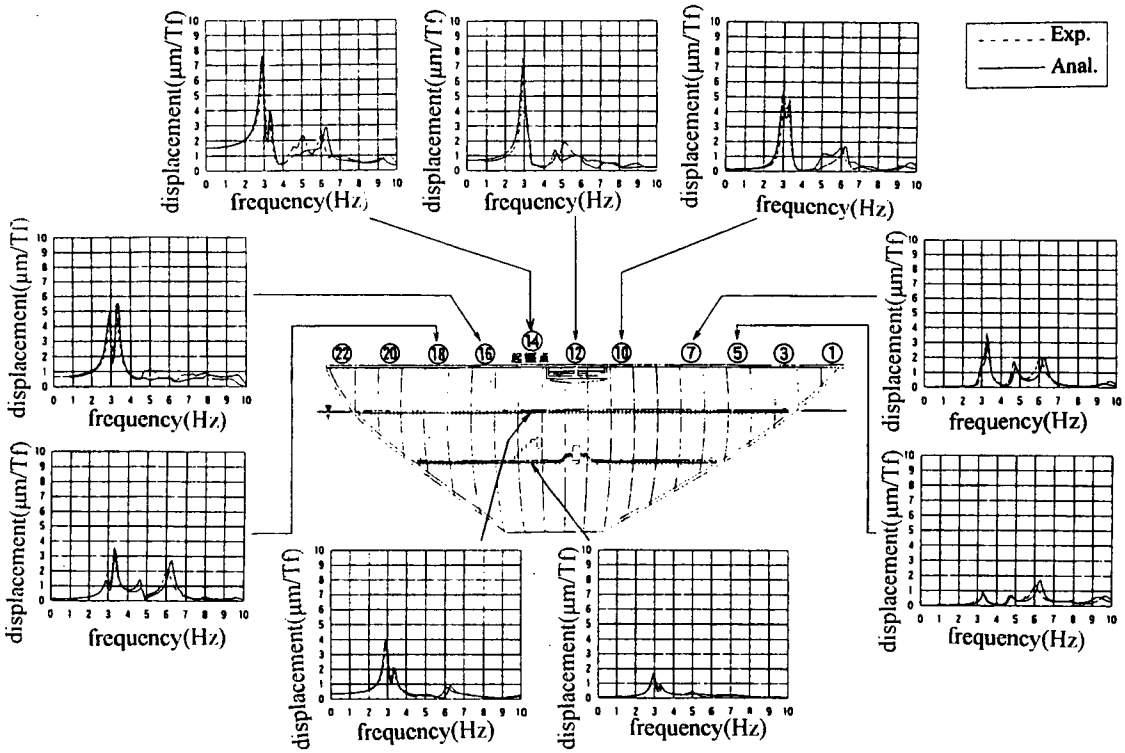


Fig.18.Comparison of analytical and experimental results(L.W.L.) (displacement)

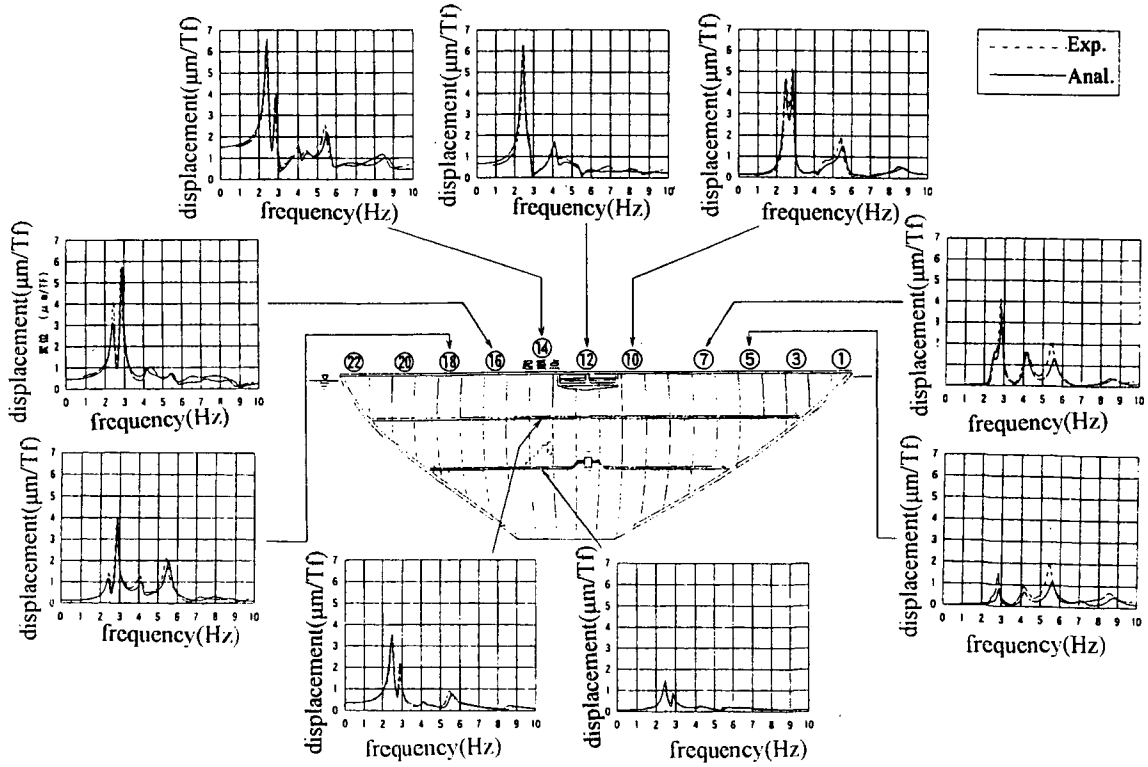


Fig.19.Comparison of analytical and experimental results(H.W.L.) (displacement)

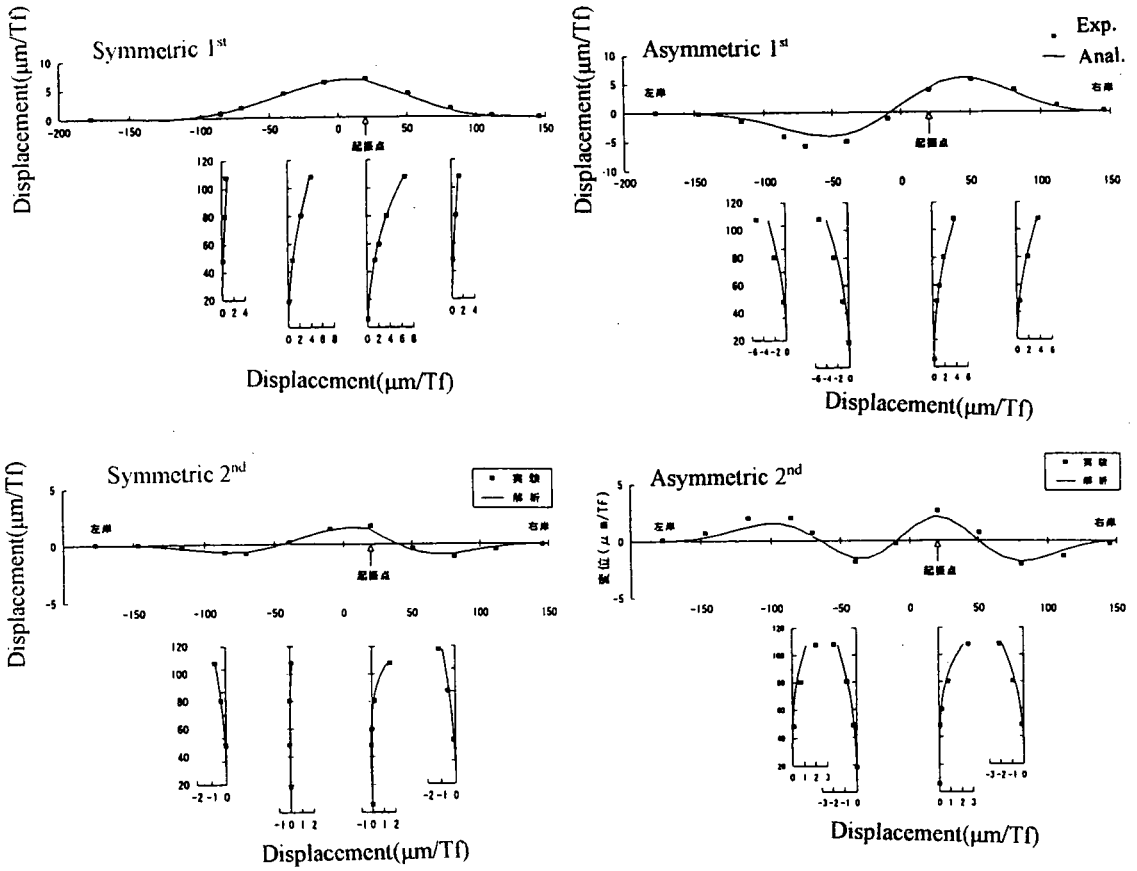


Fig.20.Mode shape(H.W.L.)

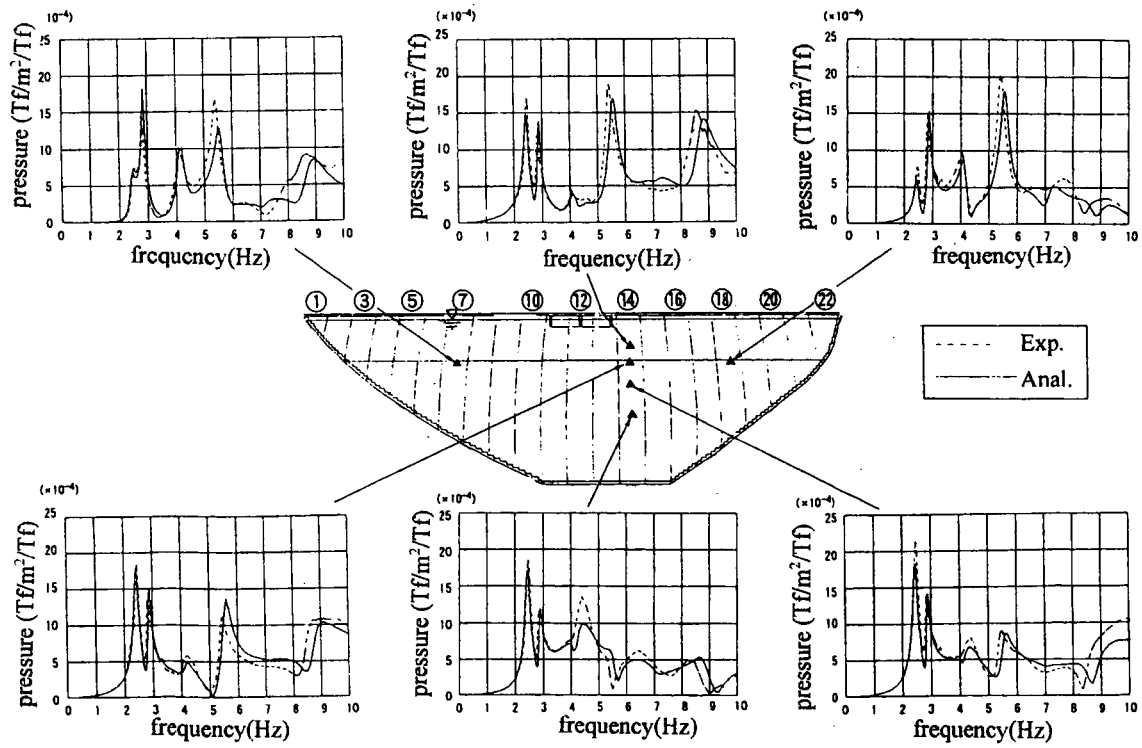


Fig.21.Comparison of analytical and experimental results(H.W.L.) (hydrodynamic pressure)

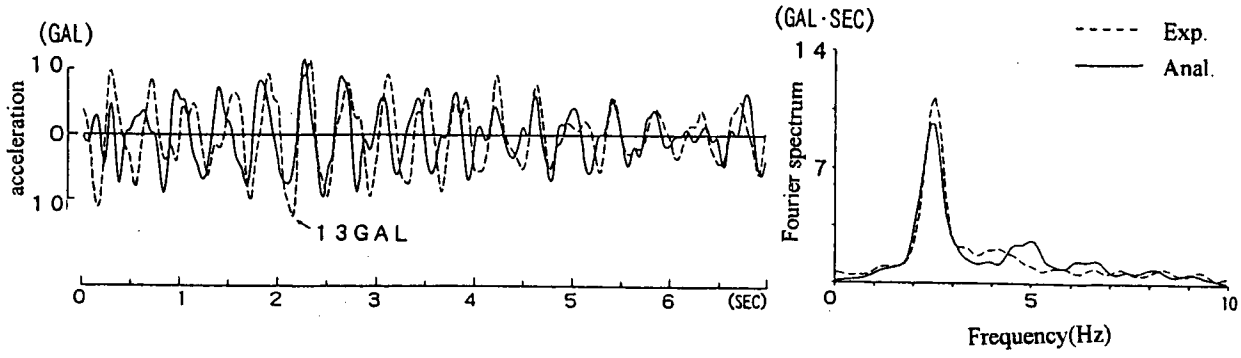


Fig.22. Comparison of analytical and experimental results
(damping of rock=1.0%, of concrete=1.5%)

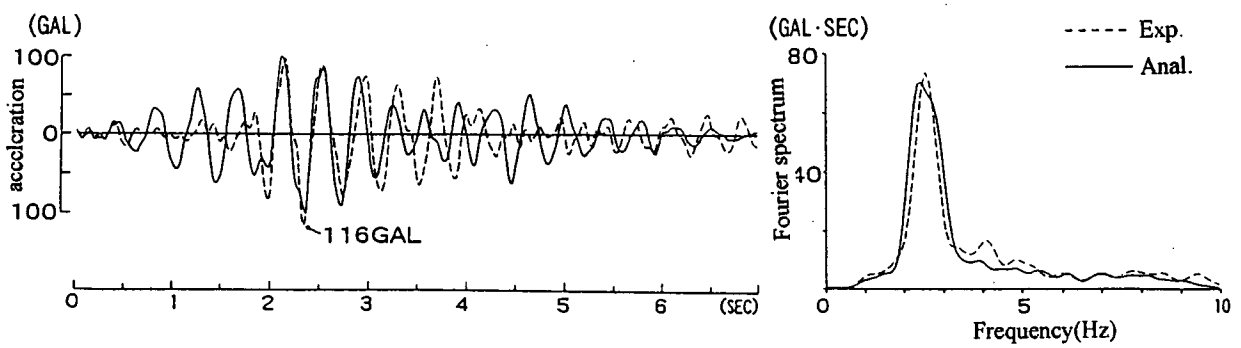


Fig.23. Comparison of analytical and experimental results
(damping of rock=3.0%, of concrete=5.8%)

FIELD MEASUREMENTS OF DYNAMIC INTERACTON AT LONGYANGXIA DAM

Yusof GHANAAT*

ABSTRACT

This paper describes an experimental study of dam-water-foundation interaction conducted at Longyangxia Dam in China. In the primary tests, the dam and its retained water were excited by detonating large explosive charges in shallow water upstream from the dam. The dam and water responses to the explosives were recorded by accelerometers, pressure sensors, as well as by three-component seismographs. In the secondary test series, the reflection coefficient of the reservoir boundaries was measured using a newly developed procedure based on the acoustic reverberation concept. The results obtained indicate that explosive detonations appear to be the best means for exciting the dam-water-foundation system, and that acoustic reverberation technique offers a practical procedure for measuring an overall reflection coefficient for the entire reservoir boundary.

1. INTRODUCTION

This paper describes field measurements of dam-water-foundation interaction effects that was performed in October 1998 on Longyangxia Dam -- a gravity arch dam located in Gonghe County, Qinghai Province, China. This study was done as the most recent phase of a continuing cooperative research program funded by the US National Science Foundation under the US-China Protocol on Earthquake Studies. The collaborating organizations in this research project are QUEST Structures of Orinda, California, Institute of Water Conservancy and Hydroelectric Research (IWHR) of Beijing, China, and the US Army Engineers Waterways Experiment Station (WES), Vicksburg, Mississippi. Dr. Yusof Ghanaat of QUEST Structures and Professor H.-Q. Chen of IWHR are co-principal investigators, with Professors R.W. Clough of UC Berkeley and K.T. Zhang of Tsinghua University acting as Project Advisors. Other researchers from the United States who participated in the field measurements included Dr. Robert Hall of WES, who directed dam response measurements and Mr. Bruce Redpath, who served as principal geophysicist.

The objectives of the research were:

- To develop new testing procedures for exciting dynamic response of the entire dam-water-foundation system
- To explore new and improved procedures for in-situ measurement of the reflection coefficient of the reservoir bottom materials
- And to obtain measured data that would enable better validation of the current analytical procedures for predicting earthquake response of arch dams

The basic concept in the field measurements was to excite the dynamic response of the dam and its retained water by detonating explosive charges buried in the foundation rock downstream from the dam or in shallow water. The extremely narrow and steep gorge immediately downstream of the dam did not permit for the use of explosives buried in bore holes. As a result of this difficulty the explosive charges were detonated in shallow water at about 1.2 km upstream from the dam. In the primary program tests, large charges fired in water were intended to excite the dam-water interaction by blast-generated waves travelling through the foundation rock and water. In a secondary test series, the dam-water interaction mechanism was excited by small explosive charges (blasting caps) suspended in the forebay. A major purpose of the secondary tests was to determine the contribution to the dam-water interaction resulting from reflection and refraction of vibratory waves at the

* Principal, QUEST Structures, Orinda, California

forebay bottom and sides, taking account of any sediment deposited at the bottom.

2. TEST STRUCTURE / INSTRUMENTATION

Longyangxia Dam selected for this experiment, is a 178 m-high concrete gravity arch dam located in Gonghe County, Qinghai Province, in northwest China. Figure 1 shows an artist conception of the dam and associated power station, which closely matches the completed project. The arch section of the dam is 396 m long at the crest level with a crest and base thickness of 15 m and 80 m, respectively. The dam also includes two 30 m high concrete gravity blocks at each end of the arch, beyond which auxiliary dams are provided on both banks. The total water front length of the dam structures therefore reaches a length of more than 1,223 meters.

Completed in 1986, Longyangxia is the first dam in a cascade of seven dams planned for the upper reaches of Yellow River. With a reservoir storage capacity of 24.7 billion cubic meters and installed power capacity of 1,280 MW, Longyangxia Dam is currently the largest hydropower project in China. As shown in Figure 1, the dam includes an overflow spillway on the right abutment, two lower outlets on the right side near the base, and an intermediate outlet at mid-height near the left abutment.

The primary instrumentation used in recording the dynamic interaction were three sets of dynamic water pressure gages (hydrophones) installed on the face of the dam, within the forebay, and at the forebay entrance. A second instrumentation system consisting of accelerometers was employed to measure the dam response. The third response recording system included a set of digital seismograph units positioned in galleries near the dam-foundation interface. Each of these instrumentation systems is described next.

2.1 Water pressures on dam surface

Two strings of hydrophones were lowered from the dam crest and positioned on the face of the dam as shown on upper graph of Figure 2. Only hydrophones shown as filled rectangles were working and could be used. Both hydrophone strings were positioned approximately near the ¼ span locations, mainly because the center portion of the dam is covered by the intake and trash rack structure.

2.2 Water pressures within forebay

Two additional strings of hydrophones were suspended from a support cable stretched along the river channel at mid-section of the dam to measure pressures within the forebay. These strings were attached at distances 25 m and 67 m from the dam face. Again only functioning hydrophones shown as filled rectangles (lower graph of Figure 2) were used. These hydrophones and those suspended on the face of the dam were connected to the PC-based data acquisition system located on the crest of the dam.

A third array of hydrophones discussed later was stretched across the forebay entrance to measure blast-generated waves travelling toward the dam. This horizontal array included 12 hydrophones spaced at 3m intervals with a 24-channel EG&G Geometrics Seismograph as the recording unit.

2.3 Dam accelerations

Instrumentation system used to measure the dam response consisted of 17 accelerometers and a PC-based digital recording system. As shown in Figure 3, seven of these accelerometers (A1 to A7) were positioned along the crest of the dam and were oriented such that to sense the radial component of dam accelerations. The remaining 10 accelerometers were installed inside the galleries at three lower elevations, and were again oriented to measure the radial component of dam accelerations. The PC-based data acquisition system was placed in a room at the center of the dam crest.

In addition to this recording system, more than 12 digital seismograph units were also employed. Five of these strong motion seismographs were mounted across the dam crest, and the rest were positioned in galleries near the dam-foundation interface to

provide some indication of the blast generated waves applied to the dam and foundation rock.

3. TEST PROGRAM

Blast excitation tests were conducted by detonating four different explosive charges in shallow water. Initially, a preliminary charge of 50kg was detonated 2 km from the dam to calibrate the prediction of the resulting ground motion based on empirical equations. This calibration test indicated that the blast-generated signals for a 50 kg charge were very small compared to the level of ambient signals produced by turbine generators and other machinery. Subsequently, main blast tests consisting of a single 100 kg, a single 300 kg, and a double 300 kg charge were detonated at a distance of 1.2 km from the dam. Figure 4 is a plan view of the dam site showing crest and water level contour lines with location of the shots, which was aligned approximately along the dam centerline. Note that the water level during the tests was 47.5 m below the dam crest due to a recent draught in the region. The water depth therefore was only slightly more than 2/3 of the dam height. In each test the explosive charges were lowered from a boat and detonated at the lake bottom in 30 m deep water. As shown in Figure 5, each explosion generated a large plume of water.

In the secondary test series the reflection coefficient of the reservoir boundaries at Longyangxia Dam was measured using a newly developed procedure based on the acoustic reverberation concept. Unlike our previous seismic reflection and seismic refraction techniques (Ghanaat et al., 1993; Ghanaat and Redpath, 1995) that measure reflection coefficient at a spot or small region, acoustic reverberation employed in this experiment was an exploratory attempt to obtain an overall reflection coefficient for the entire forebay region. In acoustic reverberation tests, the body of water near the dam (forebay) was excited and brought to a steady state condition using an underwater energy source. The decaying response produced by turning off the source was then measured by hydrophones to obtain the reverberation time, from which the reflection coefficient for any surface or combination of surfaces could be determined.

4. SUMMARY OF MEASURED DATA

This experiment has produced a complete set of measured data for the study of dam-water-foundation interaction effects. A total of 27 pressures, 17 accelerations, and 36 components of strong motion seismograph records have been collected for each of the three explosion tests. A comprehensive analysis and interpretation of all recorded signals is in progress and will be documented in our final report to the U.S. National Science Foundation. Only a few representative measured data are presented and discussed in this paper.

4.1 Recorded water pressures

Figure 6 is an example of water pressure recorded at the forebay entrance using EG&G Seismograph. The recorded pressure signal suggests two explosions, even though only a single charge of 100 kg with no delay was used. Based on the time interval, water depth, and the size of charges, we believe that the second set of pulses in the pressure record is the result of gas bubble collapse. Also note that the high-frequency pulses at the start of the record indicate wave arrival through the foundation rock, whereas the accompanying lower frequency pulses are those propagating through the water. The computed power spectral density (PSD) of the pressure signal (lower graph of Figure 6) indicates that the water blast energy is dominant in the range of 5 to 8 Hz. Accordingly, vibration modes with frequencies in this range are expected to dominate the dam response.

Figure 7 shows an example of the recorded water pressure on the face of the dam induced by the single 100 kg blast. Despite the high-amplitude ambient pressures present in this record, the blast-induced pressures are clearly visible in the time window of 7.5 to 10 seconds. Also shown in Figure 7 is PSD of this pressure record, indicating numerous resonant peaks, some of which can be identified as frequencies of the dam and the

impounded water. We are currently investigating the nature and characteristics of such resonant peaks to determine dam-water interaction mechanism. The results will be described and presented in the final project report.

4.2 Recorded dam accelerations

An example of the recorded signals for the "*zero-time*" or firing pulse and the radial acceleration of the dam response at the center of the crest is shown in Figure 8. The firing pulse was recorded so that the exact detonation time and therefore wave travelling times through foundation rock and water could be determined. This pulse was transmitted by wire over a distance of 1.2 km to the recording center. The velocity and displacement histories, also shown in Figure 8, were computed by successive integration of the recorded acceleration in the frequency domain. The results indicate that maximum dam accelerations of about 0.002 g and 0.008 g were obtained for the 100 kg and 300 kg shots, respectively.

The recorded acceleration signals exhibit three distinct parts. The first part starting at zero and lasting about 7.5 seconds shows the dam response to ambient noise caused by turbine generators, wind, and other machinery. The second part with high-amplitude pulses starting at about 7.5 seconds (consistent with the firing pulse) and lasting for about 3 seconds represents dam response to the blast-generated waves. The remaining part beyond the 11 seconds again represents the dam response to ambient noise, except that vibration of the lower outlet-gate towers produce stronger excitation from 15 to 22 seconds.

4.3 Dynamic characteristics of dam

One important result of this experiment is identification of dynamic characteristics of the dam system. Dynamic properties of a dam such as the resonant frequencies, damping, and mode shapes can be identified from transfer functions, if input signal to the structure is available. In the absence of the input signal, PSD of the measured dam response can be used to obtain the dam properties. In that case, a PSD peak at any response point can be interpreted either as a resonant frequency of the dam or a peak in the excitation spectrum. To distinguish between the spectral peaks representing the dam modes and those corresponding to peaks in the input spectrum, one can take advantage of the fact that all points on a structure responding in a lightly damped normal mode of vibration are either in phase or 180 degrees out of phase.

In order to facilitate and improve the ability to identify dynamic properties of the dam, in addition to the customary amplitude and phase spectral analysis discussed above, spectrogram of the measured dam accelerations were also developed for all 17 acceleration response points. As displayed in Figure 9, a spectrogram is a three-dimensional plot of the power spectra with respect to frequency and time. The spectrogram of the recorded acceleration at the dam crest in this figure clearly indicates that the blast signals excite the dam in the time window of 7.5 -to-10.5 seconds and contain energy in the frequency range of 5 to 9 Hz. The 3-Hz spectral peaks observed beyond the 15 seconds closely correspond to fundamental mode of the dam, as being excited by vibration of the lower outlet gate towers.

Spectrograms can also be developed for the dam velocity or dam displacement response. One difference between the acceleration and displacement spectrograms is that the higher frequency spectral peaks dominate the acceleration spectrogram, whereas the displacement spectrogram tends to highlight the lower frequency peaks. Thus the acceleration spectrogram may be used to identify higher modes while displacement spectrogram will be more suitable for the lower modes.

Acceleration spectrograms were used to fully characterize the recorded dam acceleration responses in terms of their frequency content at any given time windows, and variation of spectral amplitudes with time for any given frequency. This is clearly illustrated in the two-dimensional spectrogram shown in Figure 10. The top graph in

this figure shows the measured dam acceleration signal and the bottom graph is the corresponding spectrogram exhibiting variation of PSD with time and frequency. Produced from the spectrogram cross-section at 8 seconds, the second graph from the top demonstrates frequency content of the signal at the time of 8 seconds. Whereas the second graph from the bottom obtained from the cross-section at 3.1 Hz, indicates variation of spectral amplitudes with time of a 3.1 Hz signal present in the recorded acceleration. Using such information the measured acceleration records were decomposed into dominant single-frequency records from which the dam response could be animated and its mode of vibration determined.

Following the above procedure, 10 modes of vibration were identified, as displayed in Figure 11 (Mode 10 not shown). Mode 1 at 3.17 Hz is the fundamental symmetric mode of the dam. Mode 2 with a frequency of 4.39 Hz represents the fundamental anti-symmetric mode of the dam. Mode 3 at 5.25 Hz is similar to the fundamental symmetric mode, except that it is accompanied by the second cantilever bending mode of the dam. Higher modes exhibit more complicated deflected shapes, but in general they consist of higher order bending of the arch sections combined with the second and higher cantilever bending modes.

4.4 Acoustic reverberation test results

The acoustic reverberation tests at Longyangxia Dam utilized an array of 10 blasting caps as the excitation source and an array of 12 hydrophones as detectors, as illustrated in Figure 12. Assembled at intervals of 3 m, the blasting caps were suspended in water and detonated sequentially from bottom to top using delays of 100 ms and 50 ms. The resulting water pressures were recorded by the array of 12 hydrophones stretched across the forebay entrance and connected to the EG&G Seismograph (lower graph of Figure 12).

Reverberation time, the parameter of interest in the acoustic reverberation tests, refers to the amount of time required for the sound field in a space to decay 60 dB, or to one millionth of the original power. In simple terms this refers to the amount of time it takes for sound energy to bounce around a reservoir before being absorbed by the reservoir boundary materials. Closed spaces that don't have materials that absorb sound have long reverberation times, and very absorbent spaces have short reverberation times. Top graph of Figure 13 shows a pressure signal recorded by one of the 12 hydrophones during the reverberation tests. This graph illustrates that the sequential detonation of 10 blasting caps did in fact produced a reasonably sustained signal, which then decayed nicely at the conclusion of the blasts. The bottom graph illustrates the procedure employed to determine the reverberation time. For this purpose the measured pressure signals were squared and averaged across all channels and then plotted in logarithmic scale. From the logarithmic graph it can easily be determined that an energy decay of 60 dB corresponds to a reverberation time of 1.6 seconds.

Knowing the reverberation time and volume and total surface areas of the forebay, a reflection coefficient of 0.82 was obtained using the well-known Sabine equation. This reflection coefficient value appears to be quite reasonable for a rock site with very little or no accumulated sediments.

5. SUMMARY OF CORRELATION STUDIES

Another objective of this study was to obtain measured data for validation of the current analytical procedures. For this purpose Longyangxia Dam, a portion of the foundation rock, and the impounded water were modeled using the GDAP (Ghanaat, 1993) and EACD-3D (Fok et al., 1986) programs. Both programs employ the same finite-element models for the dam and foundation rock, but GDAP assumes incompressible water while EACD-3D accounts for water compressibility and the reservoir bottom absorption effects to represent the impounded water.

Models for the dam and foundation rock were developed in accordance with the standard finite-element procedures using shell and solid elements. The impounded water, however, was constructed to match the measured bottom topography of the reservoir. Assuming water is incompressible, the GDAP model was used to compute vibration frequencies and mode shapes for the combined dam-water-foundation system. In order to obtain a relatively close match between the measured and computed frequencies, the modulus of elasticity for the concrete and foundation rock were increased by about 35%. This appears to be reasonable considering that the measured modulus values used initially had been determined under slow rate of loading and are not appropriate for dynamic loading. The mode shapes and frequencies computed in this manner show good agreements with the measured mode shapes discussed earlier.

More correlation studies are still progressing and only limited preliminary results can be discussed at this time. These include frequency response functions of the dam computed by EACD-3D for two compressible reservoir water models: one based on the measured reservoir topography, and another using a standard prismatic model. The results obtained so far indicate that the prismatic reservoir model produces higher dam response. Another preliminary finding is that the frequencies computed on the basis of water compressibility provide slightly better match with the measured values.

6. CONCLUSIONS

Based on the data analyses and correlation studies conducted so far the following preliminary conclusion can be drawn:

1. This experiment has shown that detonating explosive charges in the water can successfully excite large arch dams and their retained lakes.
2. Dynamic properties of the dam can be obtained from such tests, provided that appropriate data processing techniques are employed.
3. Acoustic reverberation technique to determine an effective overall reflection coefficient for the reservoir boundary works and can provide reasonable data.
4. Water compressibility and reservoir topography appear to be important for this dam, even though the water level was low.

REFERENCES

Fok, K.-L., Hall, J.F., and Chopra, A.K. (1986). "EACD-3D, A computer program for three-dimensional analysis of concrete dams," Earthquake Engineering Research Center, University of California, Berkeley, Report No. UCB/EERC-86/09.

Ghanaat, Y. (1993). "GDAP, Graphics-based Dam Analysis Program," US Army Corps of Engineers, Waterways Experiment Station, Vicksburg, Mississippi.

Ghanaat, Y., Chen, H.-Q., Redpath, B.B., and Clough, R.W. (1993). "Experimental Study of Dongjiang Dam for Dam-Water-Foundation Interaction," QUEST Report No. QS93-03 submitted to the US National Science Foundation.

Ghanaat, Y. and Redpath, B.B. (1995). " Measurements of reservoir-bottom reflection coefficient at seven concrete dam sites," QUEST Report No. QS95-01, submitted to the US Army Corps of Engineers, Waterways Experiment Station and US Bureau of Reclamation.

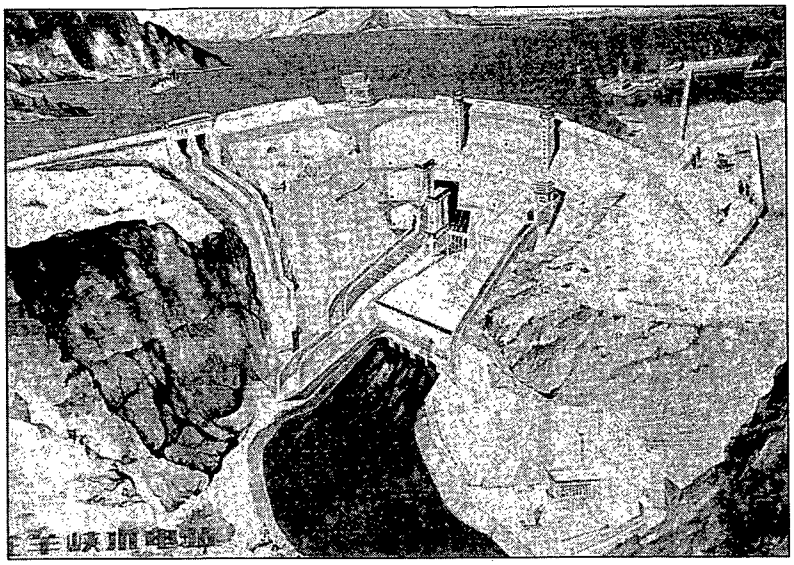
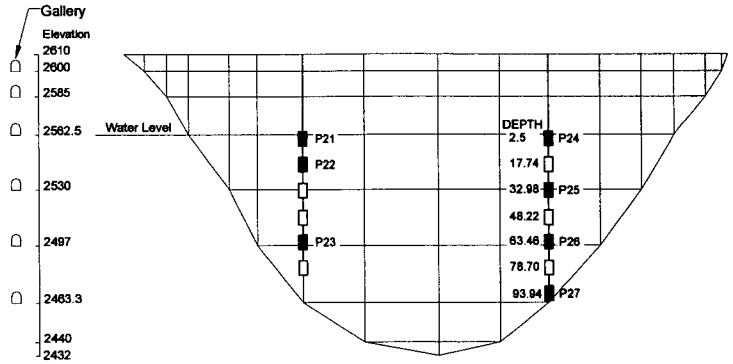
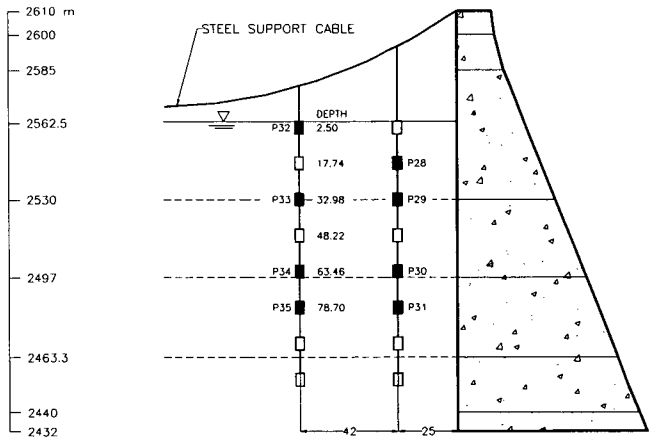


Figure 1
Artist conception of
Longyangxia Dam and
Hydropower Station



Location of hydrophones suspended on dam face
(Looking downstream)

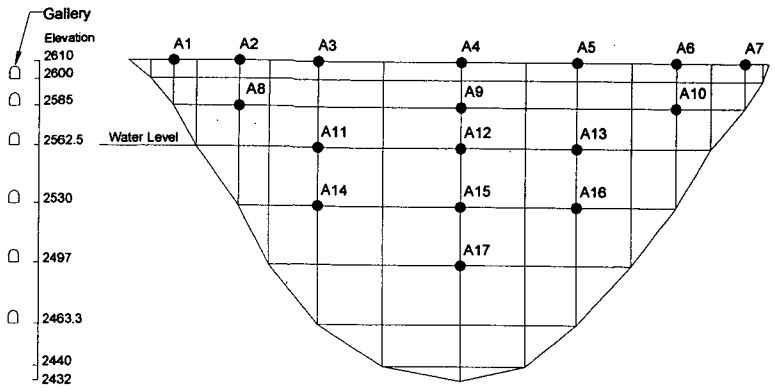
■ Hydrophones used (P21 to P27)



■ Hydrophones used

□ Hydrophones not used or functioned

Figure 2 Location of hydrophones on dam surface and within forebay



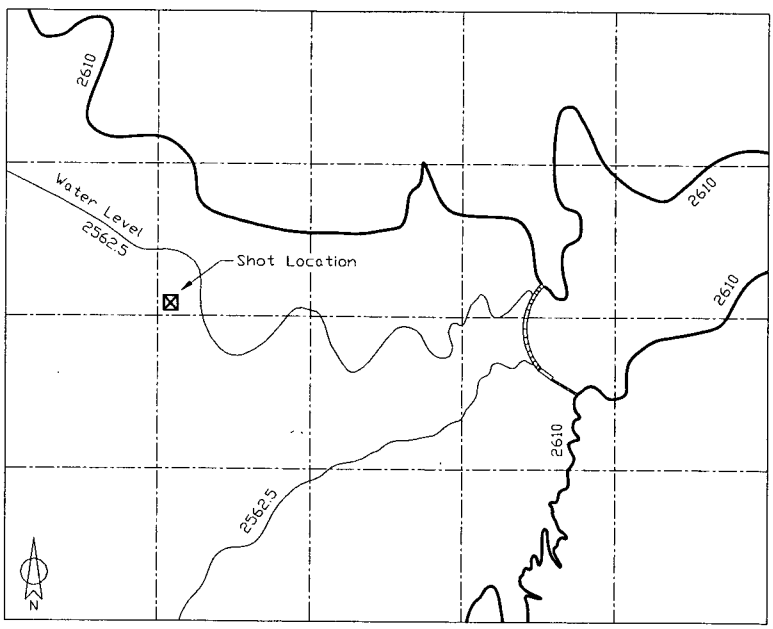
Locatin of accelerometers for measuring dam response
(Looking downstream)

Figure 3

Location of accelerometers used to measure dam response

Figure 4

Plan view of Longyangxia Dam and its retained water showing dam crest and water level contours and water blast location



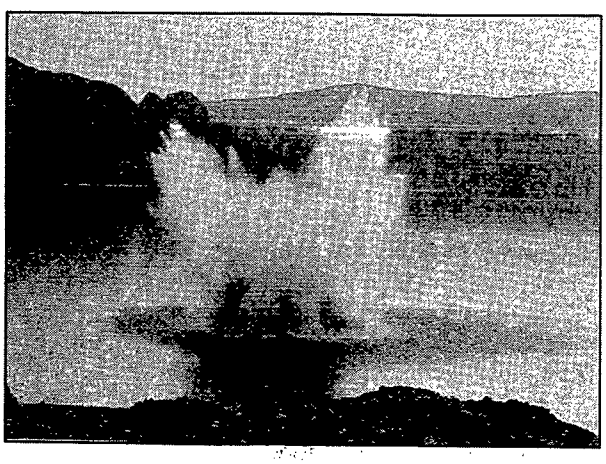


Figure 5

Plume of water generated by 300kg blast

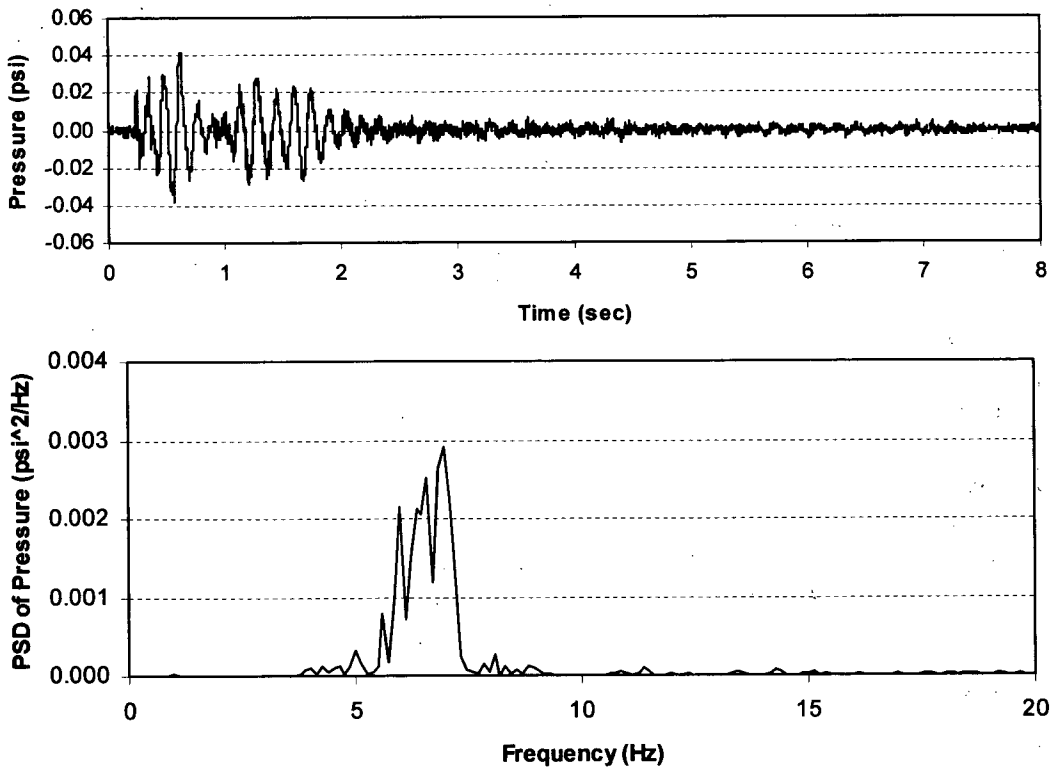


Figure 6 Recorded water pressure at forebay entrance with computed PSD due to single 100kg blast

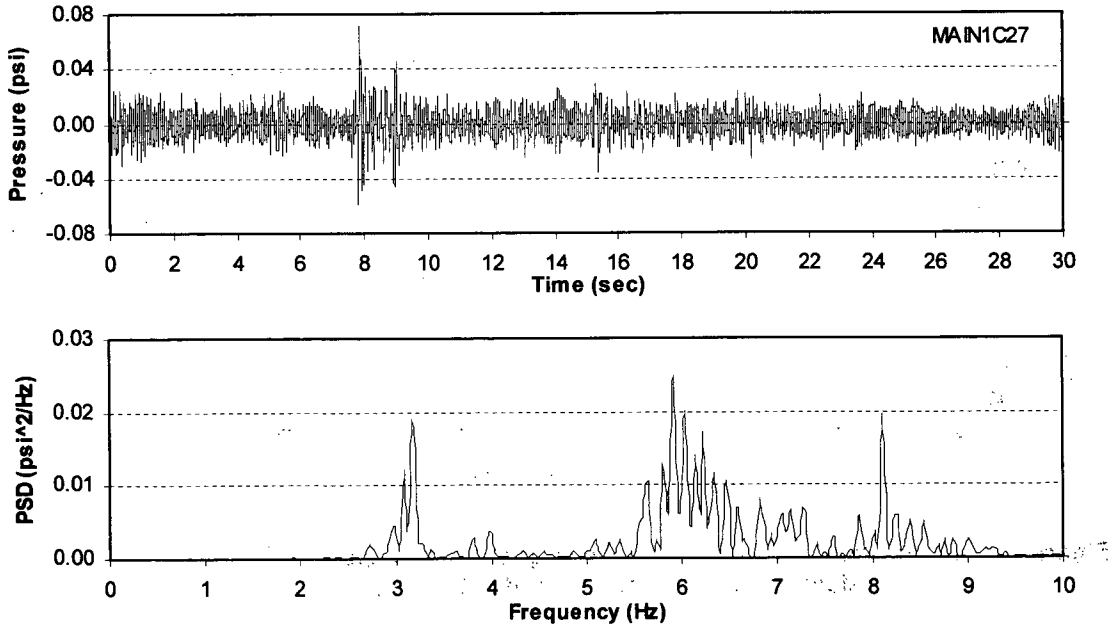


Figure 7 Recorded water pressure on dam surface with computed PSD due to single 100kg blast

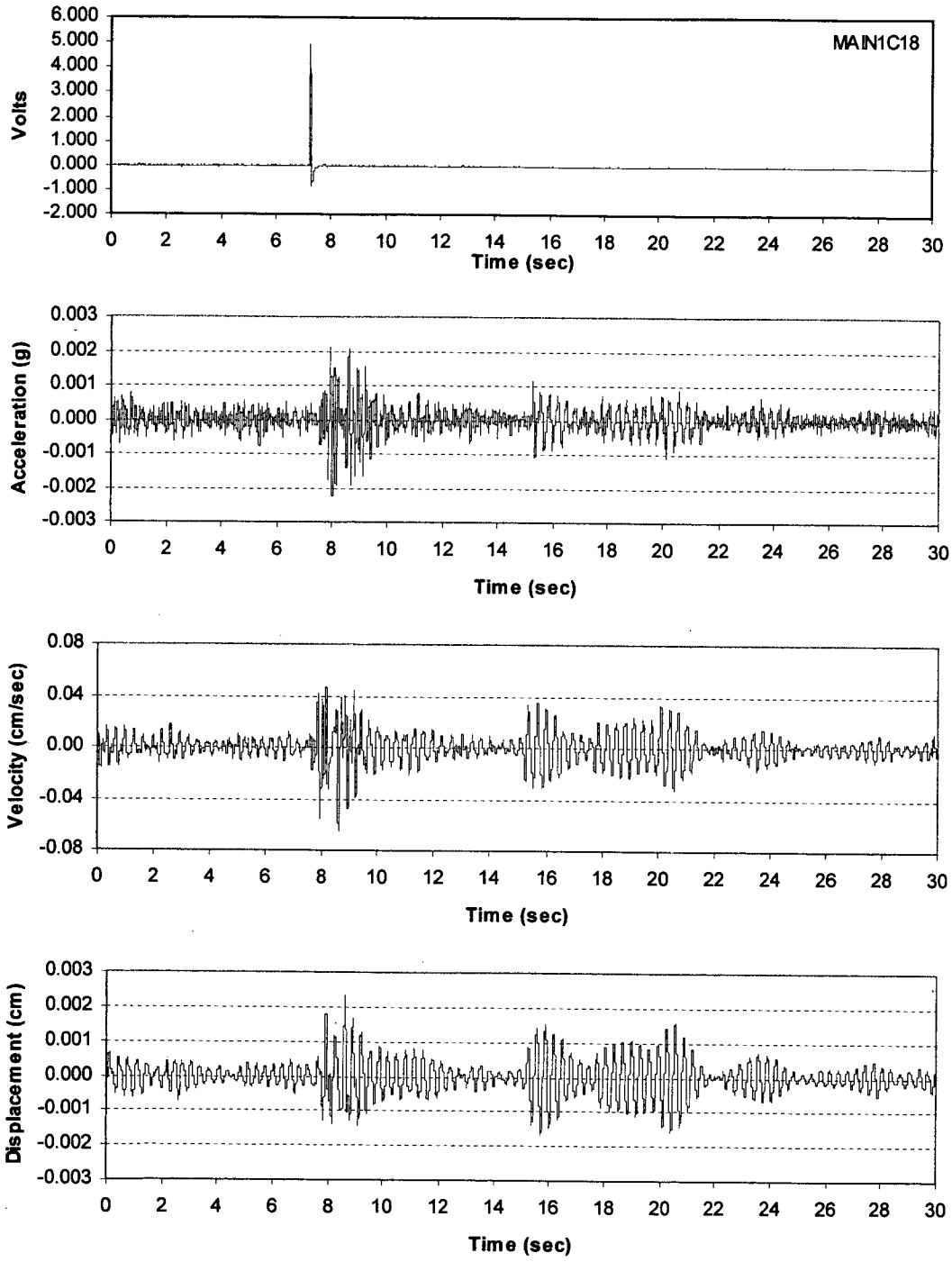


Figure 8 Recorded zero-time and acceleration signals with computed velocity and displacement histories at center of dam crest due to single 100kg blast

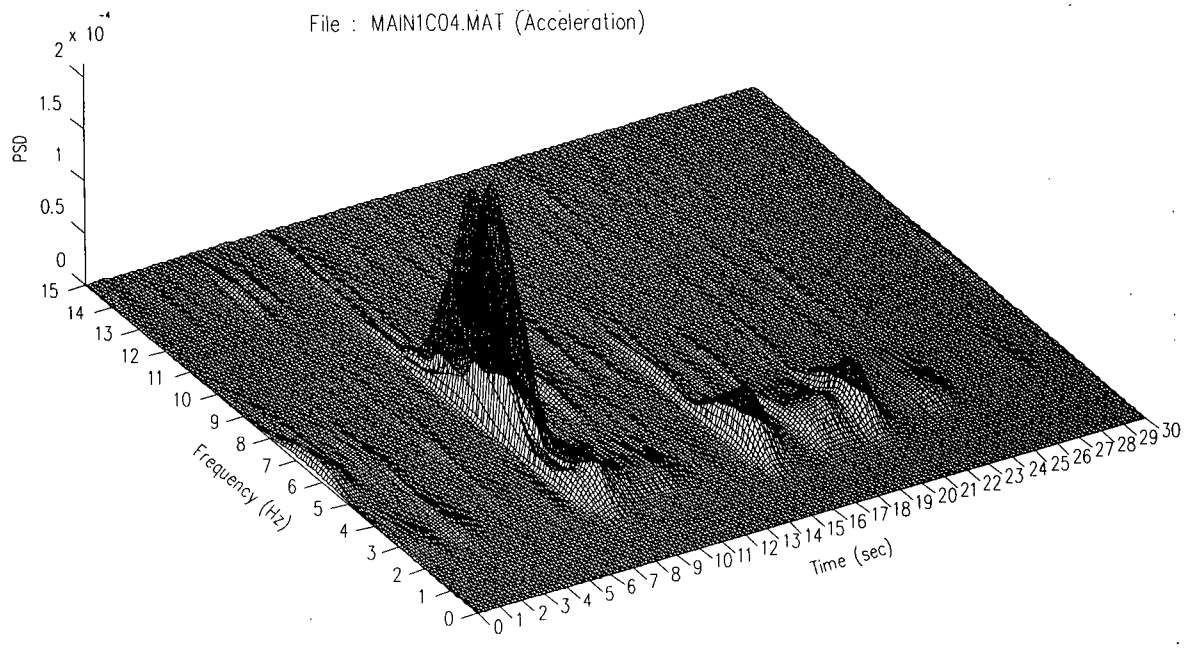


Figure 9 3D spectrogram of recorded acceleration

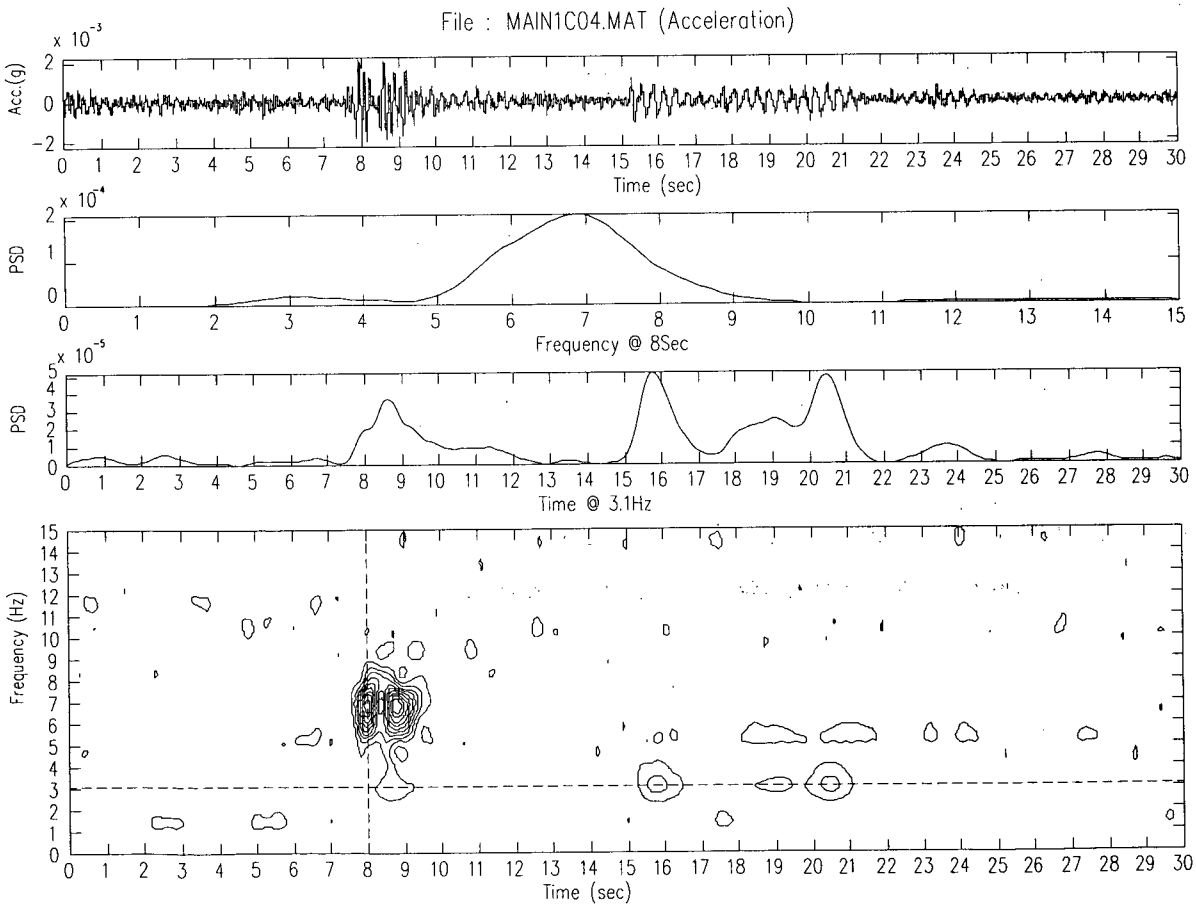


Figure 10 2D Spectrogram of recorded dam acceleration

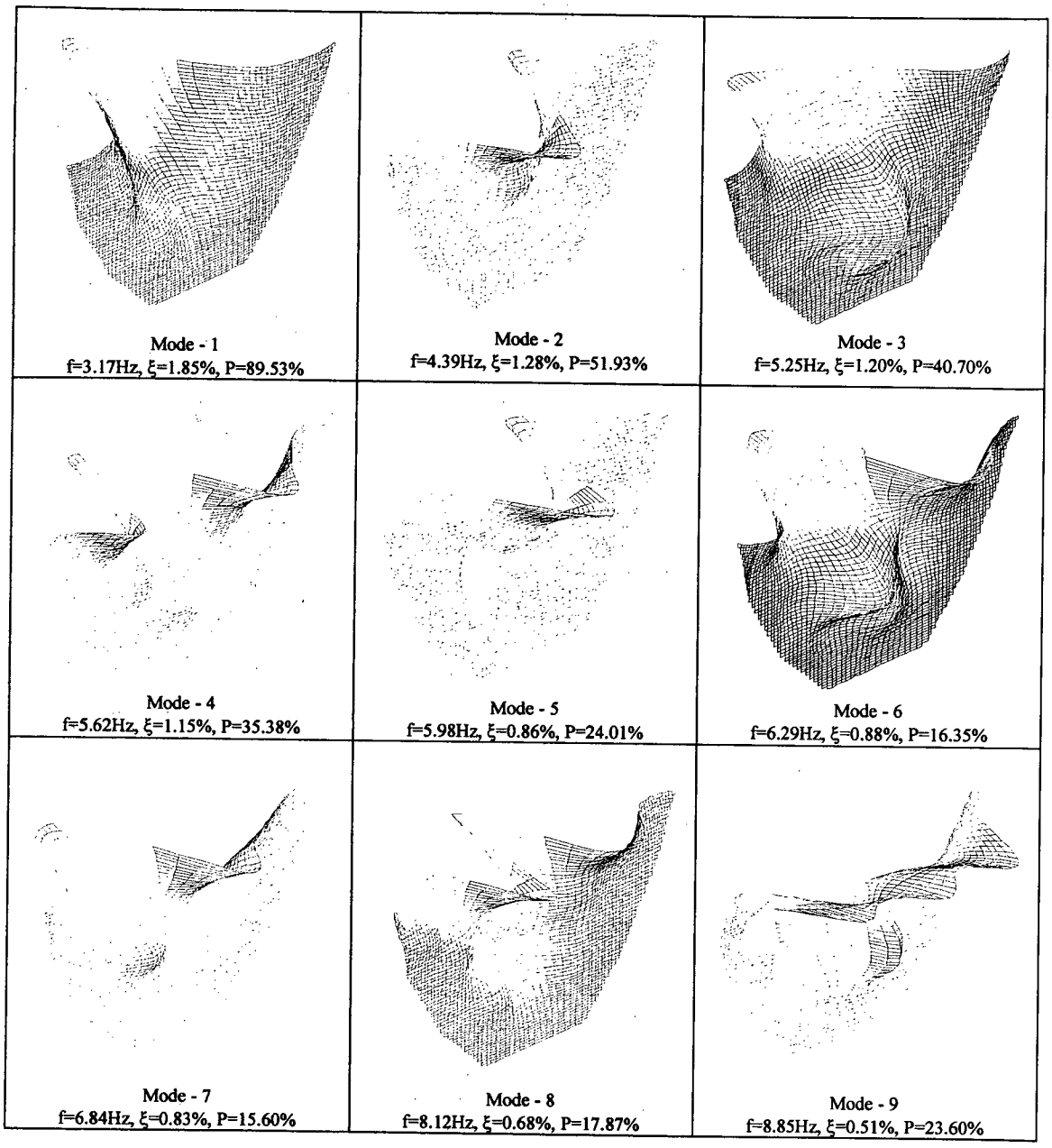


Figure 11 Measured mode shapes, frequencies, and modal damping ratios

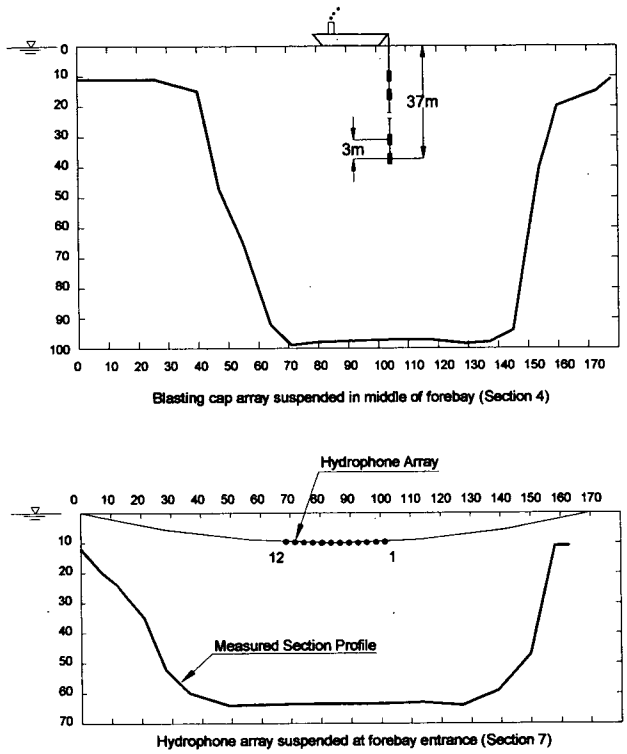


Figure 12 Acoustic reverberation test setup

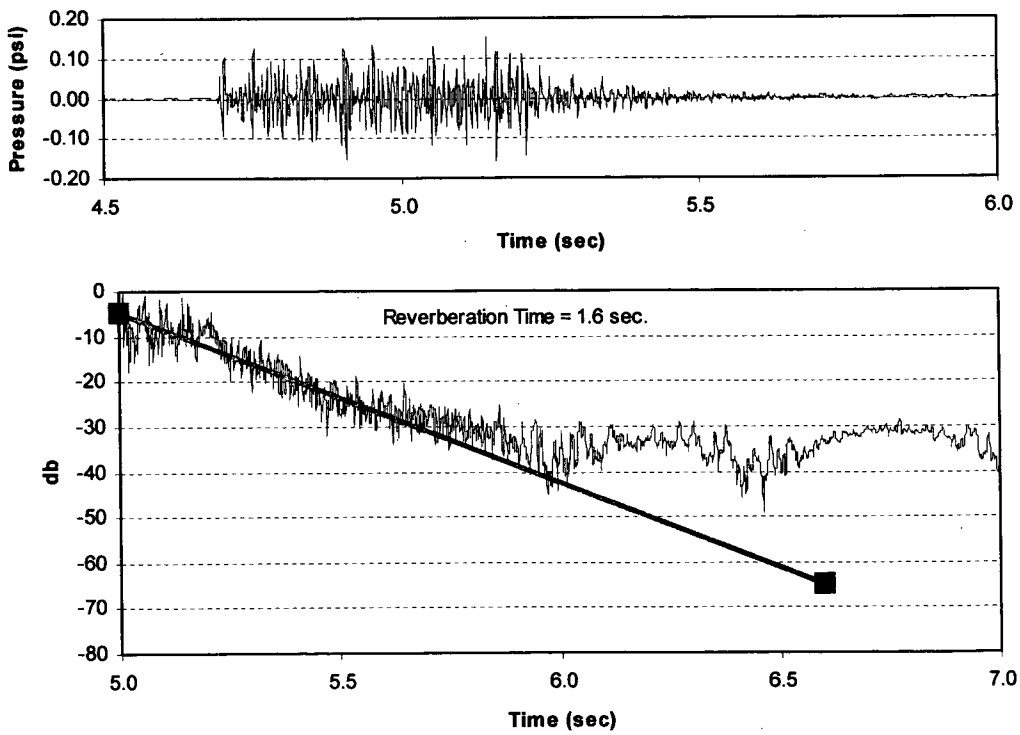


Figure 13 Measured reverberation time at Longyangxia Dam

Influence of the 1995 Hyogoken-Nambu Earthquake on Hitokura Dam Foundation Rock

by

Kentaro KIDO[1] and Tomonobu SUGIURA[2]

ABSTRACT

The influence of the 1995 Hyogoken-Nambu Earthquake on the foundation rock of Hitokura Dam was examined, focusing primarily on changes in permeability, by using measurement data for leakage from foundation drain holes and uplift pressures obtained during the period from the initial stages of the filling to 1998.

Leakage from many foundation drain holes one year after the earthquake was higher than in the year preceding the earthquake. Leakage rates, however, were within the range of values observed during the initial stages of filling. It is therefore thought that strong ground motions caused local changes in permeability of the foundation rock, thereby causing a temporary return to the initial stages of the filling.

Two years after the earthquake, leakage from many drains began to show a tendency to decrease, and leakage rates have now returned to the pre-earthquake levels.

Key Words: *Hyogoken-Nambu Earthquake, Hitokura Dam, foundation leakage, permeability.*

1. INTRODUCTION

Hitokura Dam is a 75-meter-high concrete gravity dam constructed on the Ina River in the Yodo River system. The filling of the reservoir behind the dam began in 1982.

During the Hyogoken-Nambu Earthquake (Jan. 17, 1995; magnitude 7.2; hereafter referred to simply as the "earthquake"), a horizontal acceleration (in the upstream-downstream direction) of 183 Gal was recorded at Hitokura Dam, which is located 47 km northeast of the epicenter. This is the highest acceleration that has been recorded in dam foundation rock during the earthquake (Committee on Evaluation of Earthquake Resistance of Dams 1995). The location of the dam is shown in Figure 1, data on the dam are summarized in Table 1, and seismic waves observed at the lower inspection gallery are shown in Figure 2.

Immediately after the earthquake, the dam body was inspected by the personnel of the Hitokura Dam Operation and Maintenance Office. We, the authors, carried out a dynamic analysis of the dam body by use of observed seismic waves and analytically demonstrated that the dam body was sufficiently safe even during the earthquake (K. Kido et al. 1997).

The reservoir level at the time of the earthquake, however, was down at EL.117.44 m, and the reservoir depth was 38.44 m, which is only about 55% of the water depth (70 m) at normal water level. The Operation and Maintenance Office, therefore, decided to monitor the dam body, until normal water level (EL.149.0 m) was reached for the first time since the earthquake, in the manner practiced at the initial stages of impoundment.

In April 1997, two years following the

1) Senior Research Engineer, Concrete Dam Division, Research Institute of Water Resources Development Public Corporation, Urawa, Japan

2) Assistant Chief, Operation and Maintenance Section, Tomisato Dam Construction Office, Iyomishima, Japan

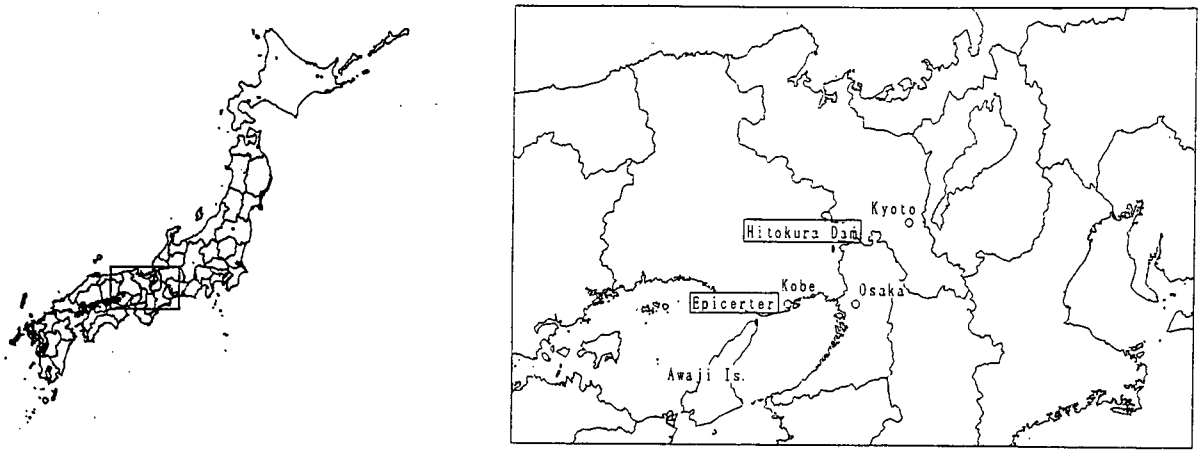
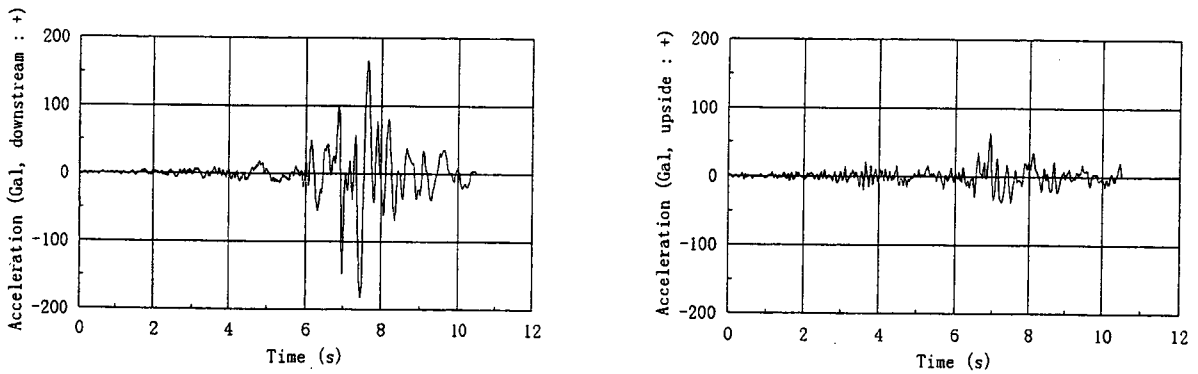


Figure 1 Location of Hitokura Dam



Upstream-downstream direction Vertical direction

Figure 2 Seismic waves observed at lower inspection gallery

earthquake, the reservoir reached normal water level for the first time after the earthquake, and the monitored condition of the dam body did not indicate any problem. All measurements taken during the reservoir level variations in 1997, such as dam body deformations measured with plumb lines and total leakage from the foundation rock, indicated behavior similar to the pre-earthquake behavior in 1994 (Y. Furukawa et al. 1998).

Table 1 Data on Hitokura Dam

Location	Kawanishi C. Hyogo Pref.
Dam type	Concrete gravity dam
Dam height	75.00m
Crest length	285.00m
Volume of dam	410,000m^3
Elevation of top of dam	EL.154.00m
Elevation of foundation rock	EL. 79.00m
Downstream slope	1:0.79
Upstream slope	(<EL.100.00m) 1:0.70
	(>EL.100.00m) Vertical
Design flood level	EL.152.50m
Surcharge water level	EL.152.00m
Normal water level	EL.149.00m
Critical water level during flood season	EL.135.30m
Minimun operating level	EL.108.00m

2. PURPOSE OF STUDY

From the results mentioned in the preceding section, it can be considered that Hitokura Dam, even after undergoing the earthquake, is sufficiently safe. Measured values, however, of leakage from the foundation drain holes and of uplift pressure show increases and decreases, which vary among drain holes. It is suspected that strong ground motions somehow affected the permeability of the foundation rock.

In this study, first we conduct a detailed analysis of the leakage and uplift pressure measurement data collected at Hitokura Dam before and after the earthquake to examine changes in permeability characteristics of the foundation rock caused by the earthquake. Then, we compare the measurement data with previously obtained measurement data, which were collected during the 15-year period from 1983 (initial stage of filling), to evaluate the influence of the earthquake under changing conditions (transition to equilibrium) over the long time period from the commencement of reservoir filling to the present.

3. SCOPE AND METHOD OF STUDY

(1) Foundation rock

Figure 3 shows the geological profile of the dam foundation rock. The foundation rock is composed of sandstone and slate belonging

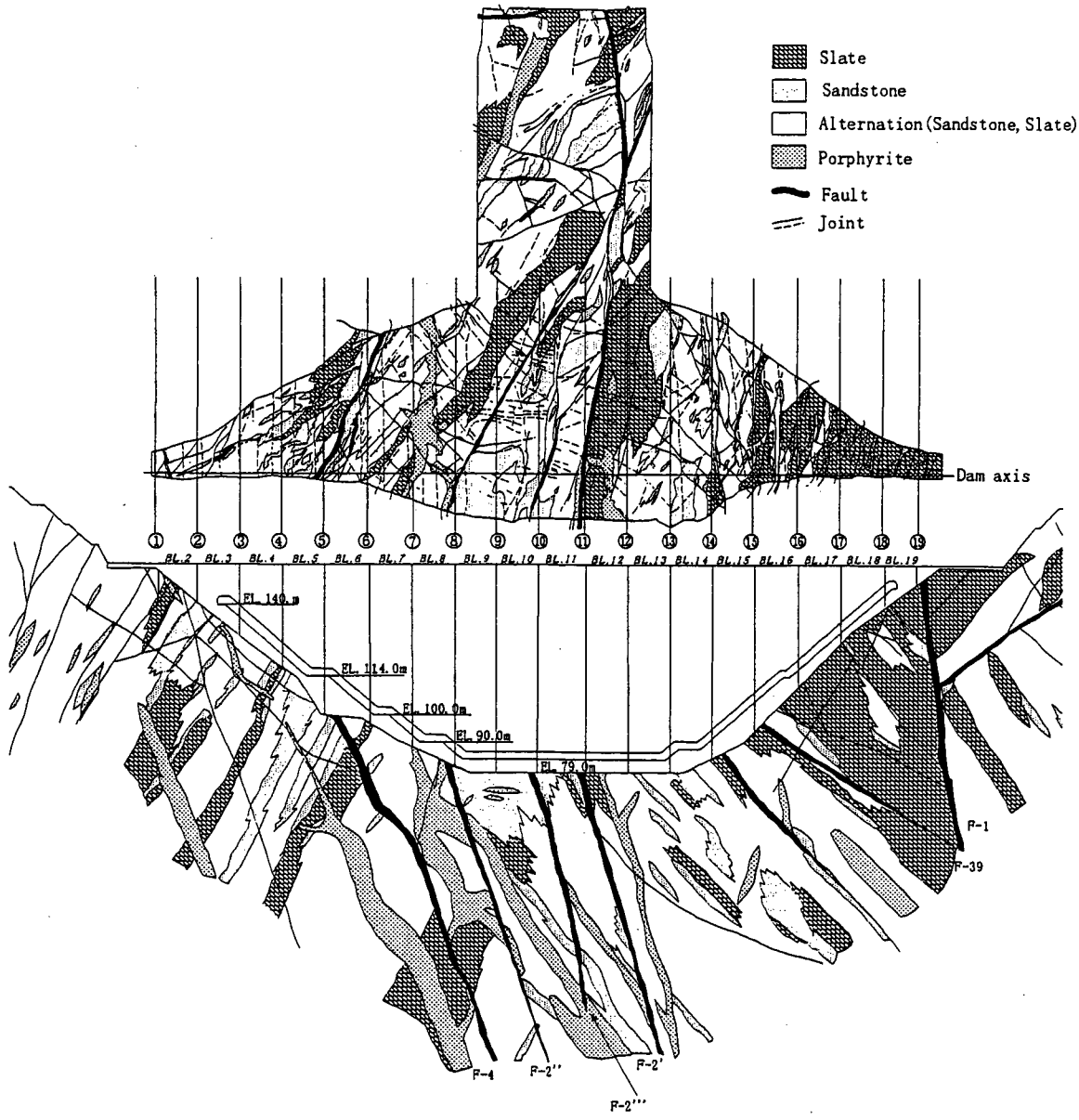


Figure 3 Geological plan of the foundation rock

to a Paleozoic group called the Tamba group and alternations of sandstone and slate. The foundation rock is also interspersed with porphyrite intrusions. These rocks have the following characteristics:

a) Sandstone: Compact and hard. Cracks are more widely spaced than in slate, but are concentrated locally. Apertures of cracks begin to loosen as deterioration progresses. If apertures open, strength falls sharply, causing a rise in permeability.

b) Slate: Highly jointed. Rock fragments themselves are quite hard. As weathering progresses, this slate becomes softer and brittler and is argillized.

c) Porphyrite: Intrusions in Paleozoic strata in the bedrock. Fresh porphyrite is harder than sandstone. There are extensive fine apertures, and permeability is locally high.

There are no major faults, but continuous faults in the upstream-downstream direction include F-1 fault (fracture width: 0.5 m) on the right bank, F-2' fault (fracture width: 1 to 1.5 m) and F-2" fault (fracture width: 0.5 to 1.5 m) in the river bed, and F-4 fault (fracture width: 0.5 to 2 m) on the left bank.

(2) Instrumentation

Measurement items concerning the behavior of the foundation rock are displacement measured with an inverted plumb line, leakage from foundation drains and from ground, uplift pressure at foundation drains, and pore water pressure. Figure 4 shows the arrangement of the measuring instruments.

Bourdon tube gauge measurement of foundation drain leakage and uplift pressure is usually carried out once a month. After an earthquake and during a period of high water level following an earthquake, the measurement is carried out at frequencies of once a day to once a week. The last measurement before the earthquake was made on December 16, 1994, and the first post-quake measurement was made on January 18, 1995, the day after the earthquake. Measurements using other instruments are carried out once a day.

The measuring instruments at the dam have been in use for nearly 20 years after the monitoring of the dam began. The measuring performance of many instruments, however, remains satisfactory with only small percentages of missing or anomalous measurements.

(3) Study method

Measurement items that indicate the behavior of the dam foundation rock include displacement, leakage, and uplift pressure. The data obtained from the reverse plumb line measurement at Hitokura Dam do not show displacements due to the earthquake. The leakage and uplift pressure data show similar patterns of change, indicating that basically their changes are caused by the same factors.

Using the measurement data, therefore, this study focuses primarily on foundation drain leakage and response to reservoir level

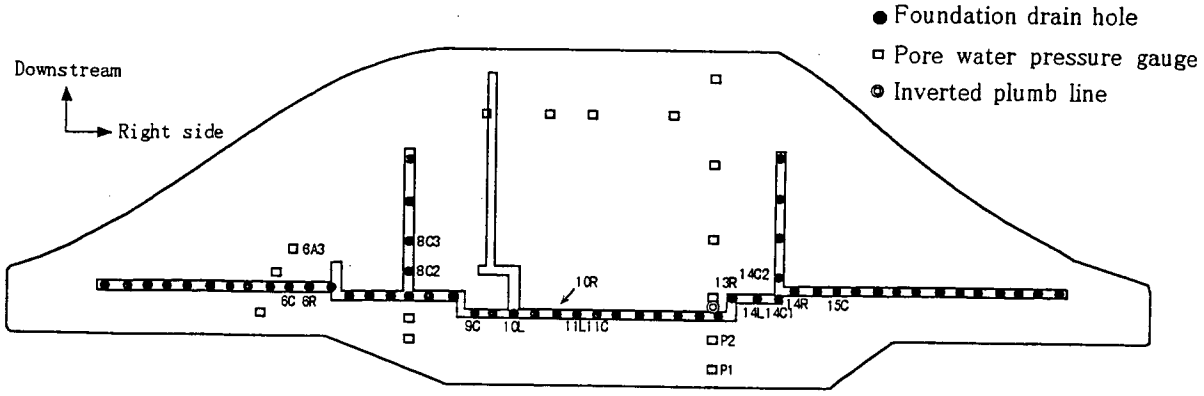


Figure 4 Locations of measuring instruments

before and after the earthquake. By comparing these results with the behavior observed at the initial stages of the filling, the study also investigates possible factors affecting changes at drain holes, the influences of the earthquake on the foundation rock, their relationships with the geological conditions, and the permeability of the foundation rock.

As for the annual reservoir level variation (hereafter referred to as "one cycle") at Hitokura Dam, the reservoir revel usually begins to rise in January and peaks in April or May. Then, the reservoir level becomes lower until the flood season (June 16 to October 15) and stays more or less constant from autumn to winter. There are many years in which the normal water level is not reached even when the water has peaked. In this study, 1994 (highest water level: EL.148.44 m on April 2) is used as a representative pre-quake year for comparison with the post-quake conditions.

4. GENERAL TENDENCY OF CHANGES IN FOUNDATION LEAKAGE

(1) Total foundation leakage

Figure 5 shows total foundation leakage (sum total of leakage from all foundation drain holes) before and after the earthquake. The figure shows the following characteristics:

a) Little change is observed on the day after the earthquake.

b) As water level rises in the first cycle (1995) after the earthquake, leakages increases and shows values greater than the pre-quake values.

c) As water level rises in and after the second cycle (1996), leakage does not increase sharply and shows values that are similar to the pre-quake values.

(2) The day after the earthquake

Figure 6 shows the distribution of foundation drain leakage rates from different drain holes and their changes. The figure indicates the following tendencies:

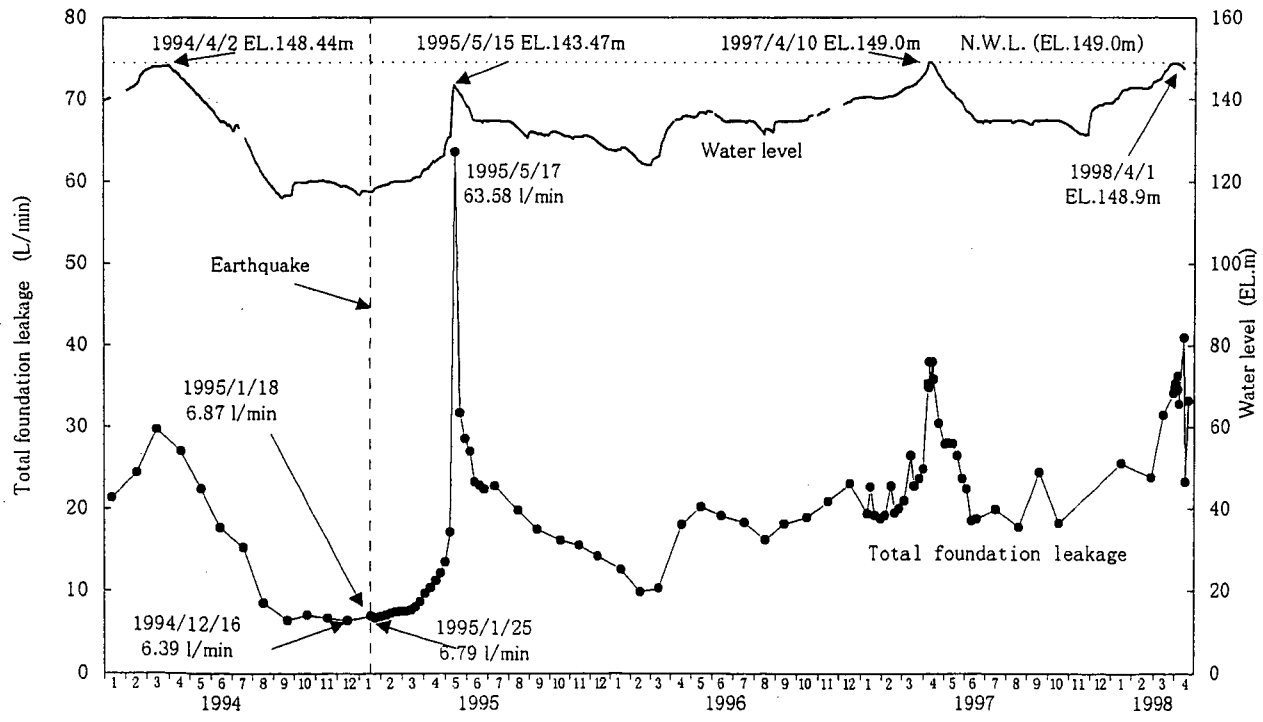


Figure 5 Changes with time in leakage rate at foundation drain holes before and after the earthquake

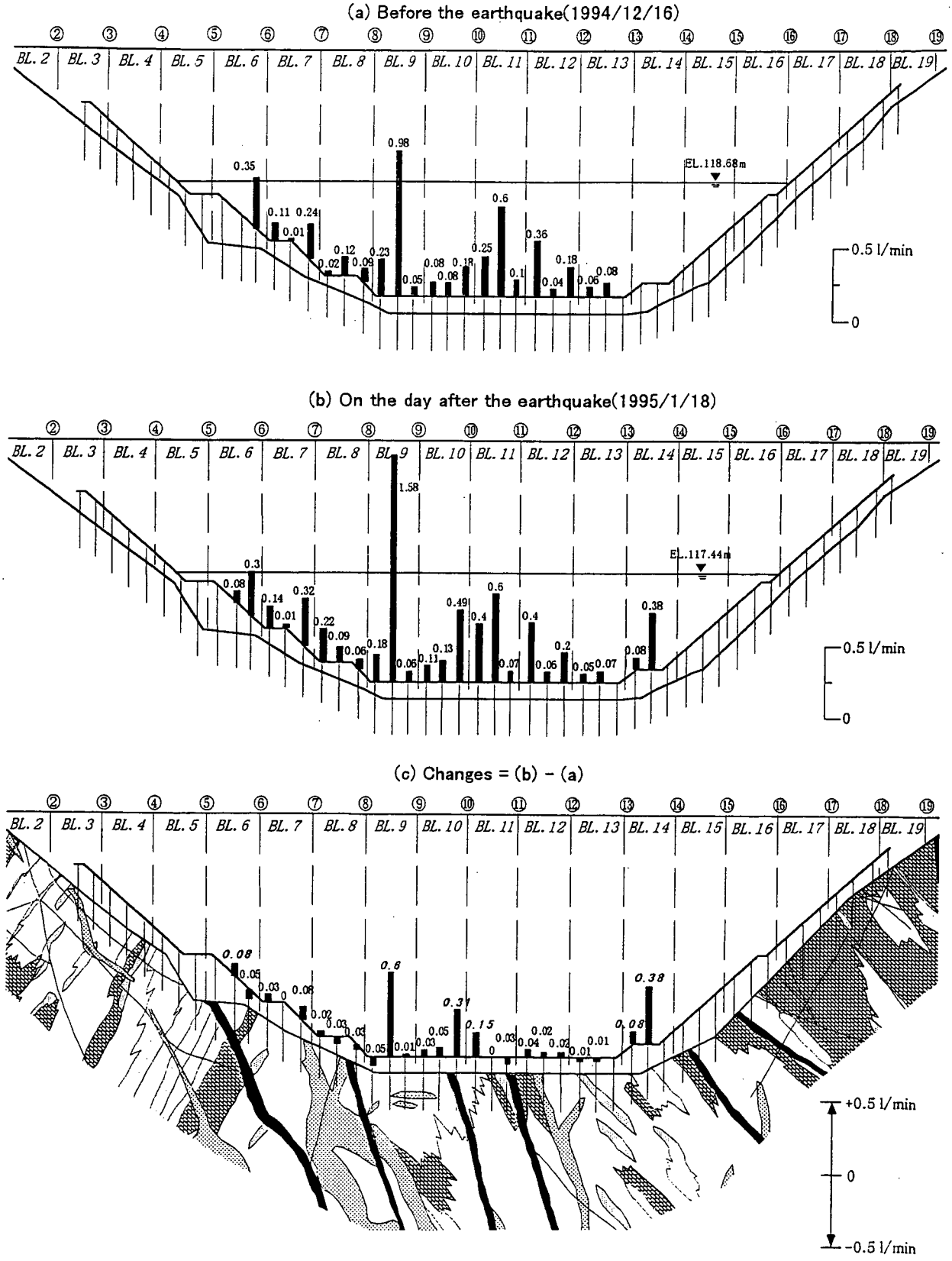


Figure 6 Changes in leakage rate at foundation drain holes on the day after the earthquake

a) Some foundation drain holes show decreases in leakage, and others show increases, although both decreases and increases are small in absolute amount.
b) Drain holes 9C to 11L and 14L to 4C2 located in the sandstone continuous to the upstream face of the dam show relatively high rates of increase (up to 0.6 L/min at 9C), while 11C to 13R located in alternating layers at similar elevations show lower rates of increase. The holes drilled in the porphyrite in block 8 tend to show relatively high rates of decrease (up to 1.4 L/min at 8C3).
c) Holes 6C, 9C, and 14C1, which show relatively high rates of increase, tend to show high rates of increase in leakage at the initial stage of the reservoir filling.

(3) First cycle after the earthquake

Figure 7 compares the leakage rates at different holes in the first cycle after the earthquake with the leakage rates before the earthquake and at the initial stage of the filling (first cycle in 1983 after the filling began) corresponding to the same water levels. The data shown here were taken from values obtained at the time of the highest water level in the first post-quake cycle. Figure 7 shows the following tendencies:
a) Even at 6C, at which the highest leakage rate in the first post-quake cycle was recorded, the highest leakage rate is 8 L/min or less. Leakage rates at individual holes are very low, and most holes show values not greater than 1 L/min.
b) Leakage rates in the first post-quake cycle from almost all holes are higher than the pre-quake values. They are lower, however, than in the first cycle after the commencement of the filling.

(4) At normal water level

Figure 8 compares leakage rates at normal water level in 1994 (before the earthquake), in 1997 in which normal water level was reached for the first time after the earthquake, and in 1983 (initial stage of filling). The data shown here were taken from values roughly corresponding to normal water level. Figure 8 shows the following tendencies:
a) Even at 6C, which shows the highest leakage rate at the time of normal water level after the earthquake, the leakage rates were about 10 L/min, and leakage from individual holes was very low.
b) On the whole, the post-quake leakage rates at the time of normal water level were close to the pre-quake values, except at 6C. Almost all holes show values equal to or less than those in the first cycle after the commencement of the filling.

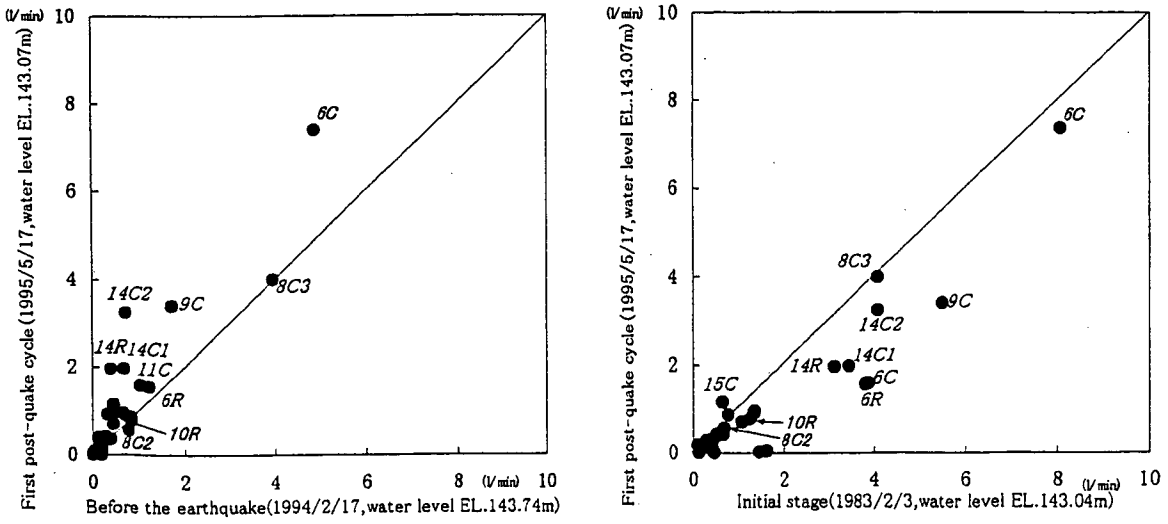


Figure 7 Comparison of leakage rates at foundation drain holes in the first post-quake cycle

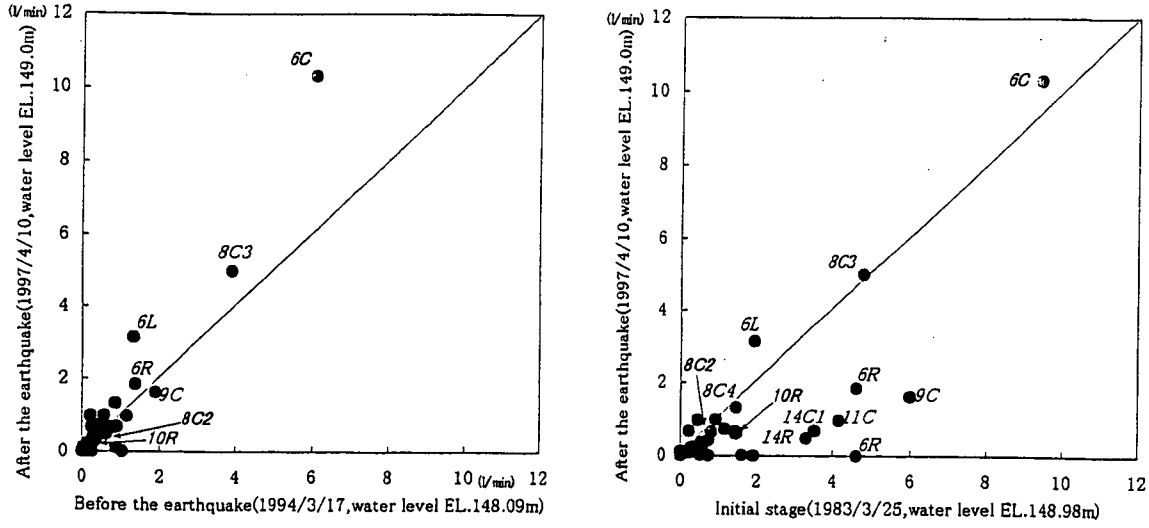


Figure 8 Comparison of leakage rates at foundation drain holes at normal water level before and after the earthquake

(5) Discussion

Leakage rates at drain holes changed although reservoir level showed little change immediately after the earthquake. We think that strong ground motions affected local permeability of the foundation rock locally. To be more specific, we suspect that the properties (width of opening, degree of clogging) of apertures in the rock, through which water moves, have changed locally.

The fact that leakage rates at most drain holes at the time of the highest water level in the first cycle after the earthquake and at the time of normal water level in 1997 were higher than the pre-quake leakage rates indicates that the earthquake caused the local permeability of the rock at many locations.

As for the relationship between changes in permeability and geology, the rates of increase in leakage from holes located in sandstone layers that are continuous from upstream to the hole zone were relatively high, and the rates of leakage from alternated layers and porphyrite tended to increase more slowly or even decrease. This indicates that differences in water channel characteristics (e.g., aperture spacing, aperture width, continuity) depending on rock type may be reflected in the changes in permeability caused by strong ground motions. Since, however, the foundation rock has been grouted, the examination of this point requires the evaluation and analysis of the groutability of the rock.

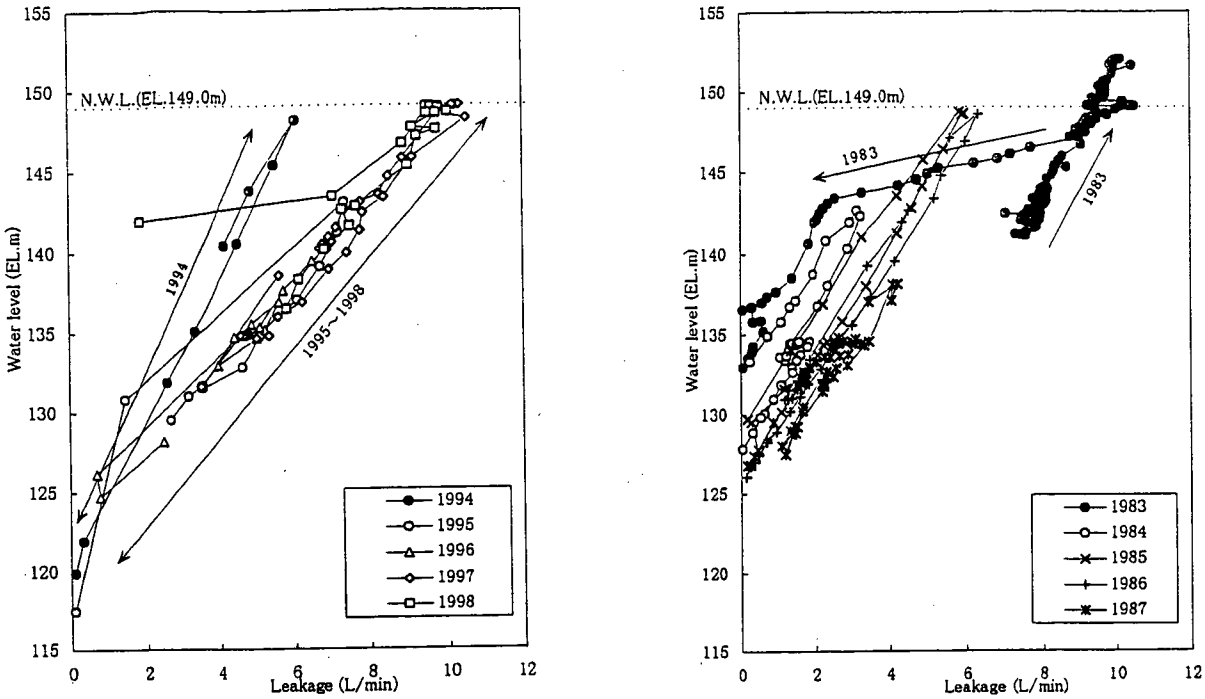
The changes under consideration here account for a very small percentage of total leakage. In addition, the post-quake leakage rates are similar to the values at the times of the corresponding water levels, that is, previously recorded values. Those changes, therefore, do not pose any problem from the viewpoint of the safety of the foundation rock.

5. PATTERN OF LEAKAGE RATE CHANGES BY DRAIN HOLE

(1) Most leaky hole: 6C

Figure 9 shows the correlations between the leakage rate at hole 6C, the most leaky hole in Figures 7 and 8, and reservoir level from 1994 (before the earthquake) to 1998. For comparison, data for the early stages (1983 to 1987) of the reservoir filling are also shown in Figure 9. The figure reveals the following tendencies:

a) Post-quake leakage rates are higher than pre-quake leakage rates corresponding to the



Before and after the earthquake(1994-1998) Early stages(1983-1987)

Figure 9 Correlations between leakage rates at foundation drain holes and reservoir level (hole 6C)

same water levels. The ratio of the leakage rate to water level rise (the reciprocal of the slope of the graph) for the post-quake data is higher than that for the pre-quake data. The maximum leakage rate, however, is about 10 L/min.

b) The post-quake leakage rates show linear correlations with reservoir level, indicating stability of behavior.

c) The correlations with the post-quake leakage rates resemble the correlations in the first cycle (1983) after the commencement of the filling.

(2) Hole that shows a typical pattern: 10R

Figure 10 shows correlations between the leakage rate and reservoir level between 1994 (before the earthquake) to 1998 for hole 10R, a hole which shows a representative pattern of changes, although the absolute rates of leakage are small. For comparison, Figure 10 also shows values for the early stages of the filling (1983 to 1987). As shown, the following tendencies are noted:

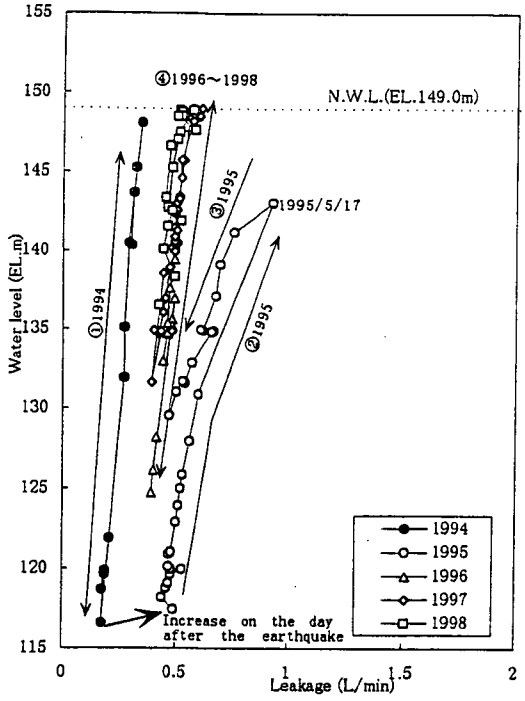
a) Both pre-quake and post-quake values show clear correlations with reservoir level for each year.

b) Leakage rates increase on the day after the earthquake.

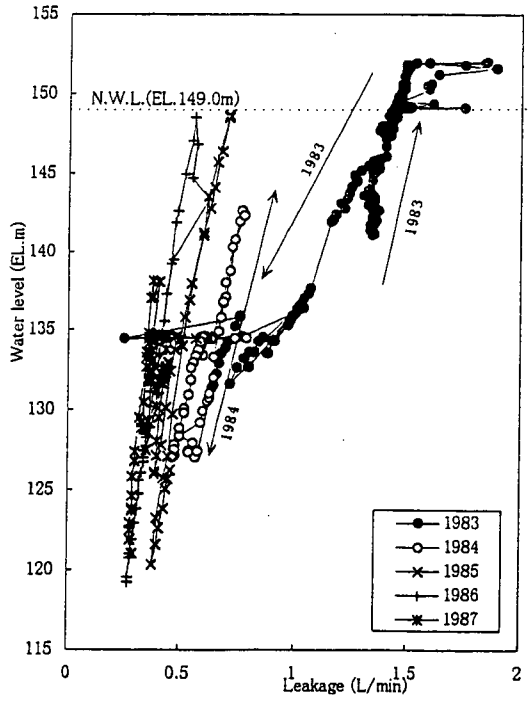
c) The leakage rates in the first post-quake cycle are higher than the pre-quake leakage rates at the same water levels, and the rates of increase of leakage rate due to water level rise in the first post-quake cycle are higher than the rates of increase before the quake. The leakage rates, however, are lower than those at the initial stages of the filling.

d) The leakage rates during water level decline in the first post-quake cycle are lower than those during water level rise in the same cycle.

e) The second and subsequent post-quake cycles show leakage rates that are slightly higher than the pre-quake leakage rates. The second and subsequent post-quake cycles, however, show linear correlations with reservoir level and also show similar values during water level rise and during water level decline.



Before and after the earthquake(1994-1998)



Early stages(1983-1987)

Figure 10 Correlations between leakage rates at foundation drain holes and reservoir level (hole 10R)

f) Leakage rates before the earthquake are lower than those at the early stages of the filling, and the first post-quake values are close to the values at the early stages of the filling.

(3) Discussion

High leakage rates at hole 6C are thought to be due to high permeability of the surrounding rock, which was increased by the earthquake and then stabilized. The fact that the correlations with reservoir level resemble those in the first cycle after the commencement of the filling indicates that the earthquake caused the rock to return to the conditions at the initial stages of the filling rather than to change the properties of the rock to new properties. Thus, it is suspected that the clogging materials accumulated in apertures in the rock over the years after the reservoir was filled were "loosened" by the strong ground motions, resulting in a return to the initial permeability.

Leakage rates in the early stages of the filling fell sharply during the period of waterlevel decline in 1983. Two or three years later, leakage rates showed tendency to increase again and stabilize, but such tendency did not occur after the earthquake. The reason for this phenomenon is unknown.

At hole 10R, which showed a typical pattern, permeability of the surrounding rock seemed to have increased temporarily under the influence of the strong ground motions, as in the case of hole 6C. In the process of water level rise and fall in the first post-quake cycle, however, permeability decreased again. A similar decrease in permeability occurred in the first cycle after the commencement of the filling. Such permeability declines are thought to be due to gradual clogging of apertures in the rock. It is probably as a result of such clogging that the present permeability shows a stable pattern resembling a typical pattern observed several years after the commencement of reservoir filling.

6. CHANGES IN UPLIFT PRESSURE

(1) Day after the earthquake

Figure 11 shows the distribution of uplift pressures at foundation drain holes on a day before the earthquake (December 16, 1994) and on the day after the earthquake (January 18, 1996), along with changes in uplift pressure. This figure shows leakage rate tendencies which show fair resemblance to the leakage rates mentioned earlier (Figure 4).

(2) In the first post-quake cycle and at time of normal water level

Figure 12 compares uplift pressures in the first post-quake cycle at different holes with those before the earthquake (1994) and at the initial stage of the reservoir filling (first cycle after commencement of filling, 1983). Figure 13 compares uplift forces at the time of normal water level at different holes in 1994 (before the earthquake) and in 1997, the year in which normal water level was reached for the first time after the earthquake.

Figures 12 and 13 show the following tendencies:

a) At almost all holes and measuring instruments, uplift pressures in the first post-quake cycle are greater than the pre-quake uplift pressures at the corresponding reservoir levels.

b) The 1997 (post-quake) values are similar to the pre-quake values, except at hole 6C.

Thus, uplift pressures in the first post-quake cycle are greater than the pre-quake values, except at hole 6C, but those high uplift pressures decreased to the pre-quake level by 1997, when normal water level was reached for the first time after the earthquake.

(3) Pattern of changes at hole 6C

Figure 14 shows the correlations between uplift pressure at hole 6C, which shows high uplift pressures during the period of normal water level after the earthquake, and reservoir level from 1994 (before the earthquake) to 1998.

As shown, as in the case of leakage rates (Figure 7(1)), the post-quake uplift pressures are greater than the pre-quake values at the corresponding reservoir levels, and the rates of increase corresponding to water level rises are also greater than the pre-quake values. Since, however, the correlations with water level rise are linear and behavior is stable, these greater values are not problematic.

(4) Pattern of changes at hole 10L

Figure 15 shows the correlations between uplift pressure at hole 10L, which, although the quantities involves are small in absolute terms, shows a typical pattern of changes, and reservoir level from 1994 (before the earthquake) to 1998.

This figure shows the following tendencies:

a) Both pre-quake and post-quake values show correlations with reservoir level for each year.

b) Uplift pressures rise on the day after the earthquake.

c) Uplift pressures in the first post-quake cycle are greater than the pre-quake values at the corresponding reservoir levels, and the rates of increase corresponding to water level rise are also greater than the pre-quake values.

d) Uplift pressures in the second and subsequent cycles are similar to the pre-quake values and show stable behavior.

(5) Discussion

The results shown above indicate that uplift pressures at foundation drain holes show patterns resembling those of leakage rate changes in terms of overall tendency of changes and patterns of changes at individual holes.

To evaluate the stability of the dam body, we made stability calculations, using measurement data obtained on April 10, 1997, from piezometers installed in 13 blocks. The stability calculations gave an average safety factor of shear sliding along the base of 4.05, confirming that the dam body satisfies the design requirements even after the earthquake.

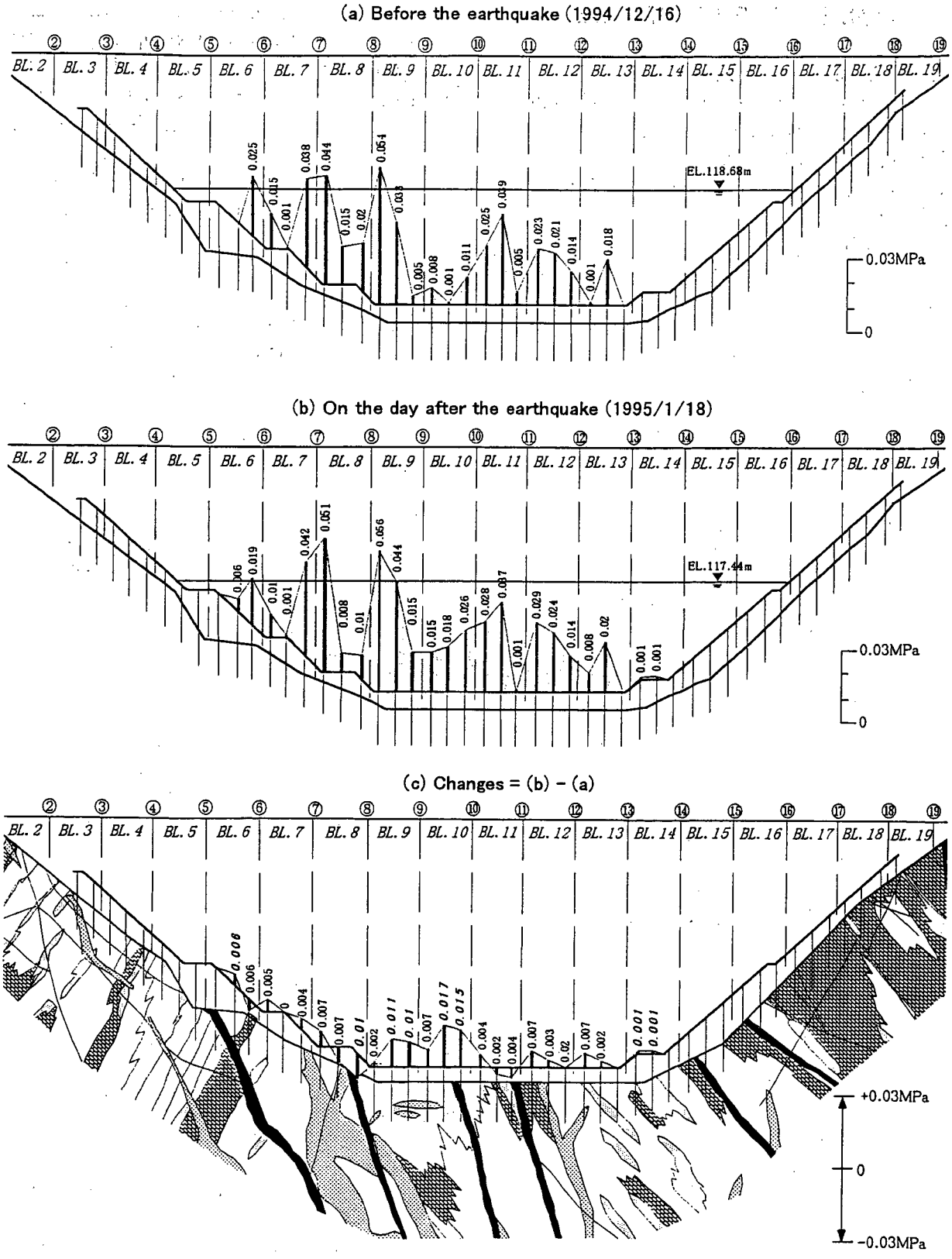


Figure 11 Changes in uplift pressure at foundation drain holes on the day after the earthquake

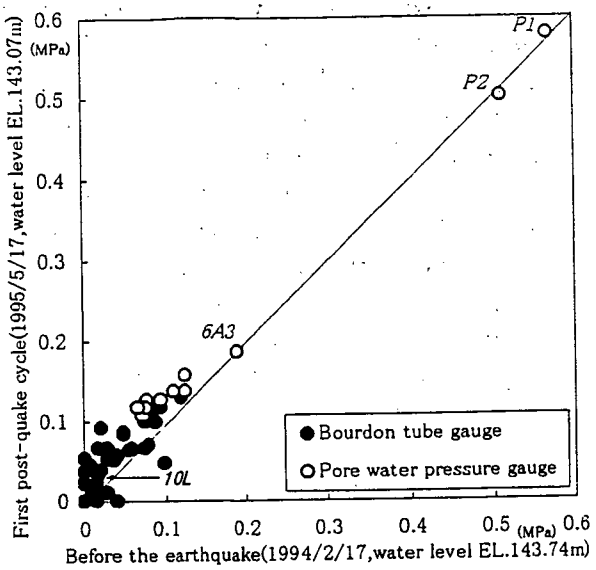


Figure 12 Comparison of uplift pressures at foundation drain holes in the first post-quake cycle

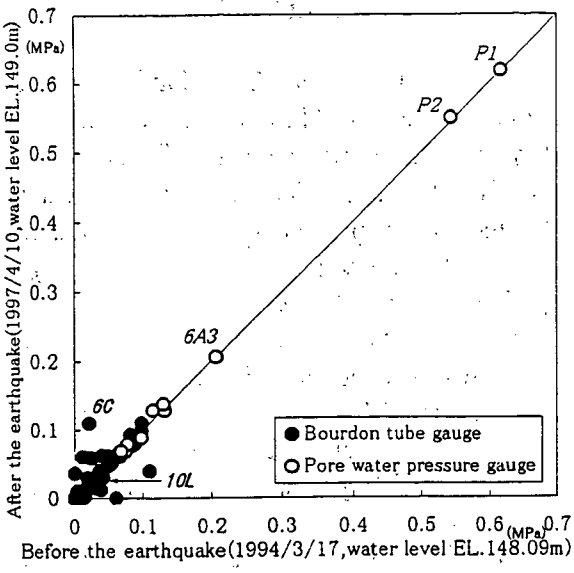


Figure 13 Comparison of uplift pressures at foundation drain holes at normal water level before and after the earthquake

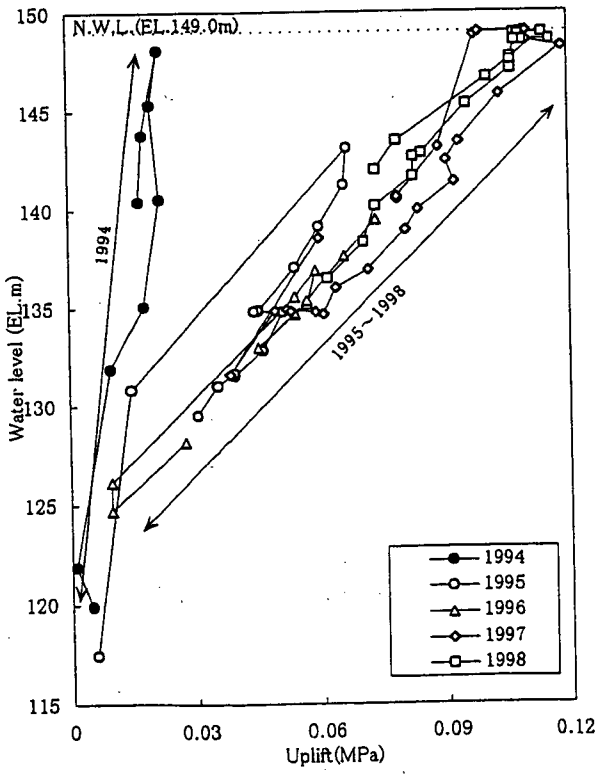


Figure 14 Correlations between uplift pressures at foundation drain holes and reservoir level (hole 6C)

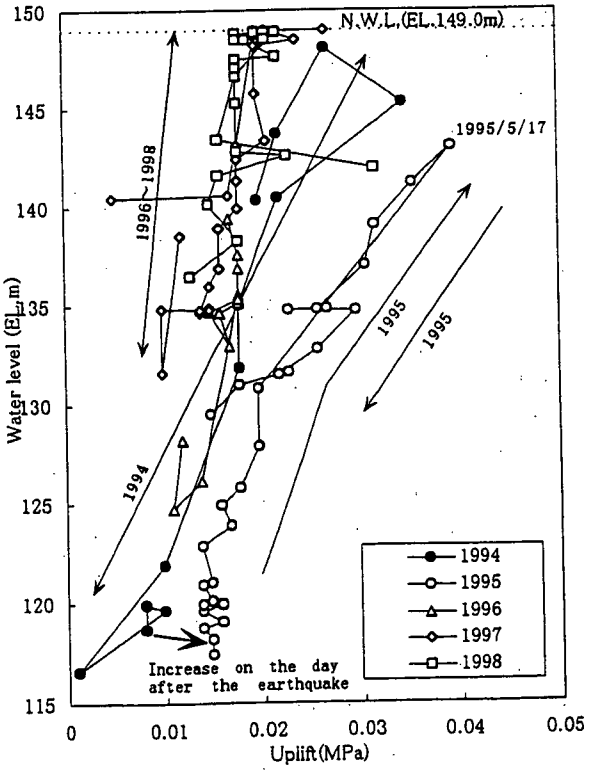


Figure 15 Correlations between uplift pressures at foundation drain holes and reservoir level (hole 10L)

7. CONCLUSIONS

Characteristics of the behavior of the foundation rock of Hitokura Dam after the earthquake can be summarized as follows:

a) On the day after the earthquake, leakage rates and uplift pressures at the foundation drain holes increased or decreased, although only slightly in absolute terms.

b) The earthquake caused local increases in permeability and increases in leakage rate and uplift pressure. These increases, however, are smaller than the values at the initial stages of the reservoir filling and can be said to be within the range of previously observed values. Subsequently, permeability began to decrease again, and both leakage rates and uplift pressures decreased.

c) Some of the measured values in the second and subsequent cycles after the earthquake differ from the pre-quake values. After the earthquake and during the periods of normal water level, many holes and many measuring instruments showed values equal to or smaller than the pre-quake values. Even the values differing from the pre-quake values stabilized in the second and subsequent cycles after the earthquake.

d) Under the influence of the earthquake, permeability of the foundation rock tended to return to the level at the initial stages of the filling.

e) Changes in permeability due to the earthquake show tend to vary to some degree with geological conditions.

f) Changes in permeability due to the earthquake are thought to have resulted primarily from changes in the condition (e.g., aperture width, degree of clogging) of apertures which function as channels of water flow.

8. CONCLUDING REMARKS

A series of studies reported above showed that the permeability of the foundation rock of Hitokura Dam, which underwent strong ground motions of the Hyogoken-Nambu Earthquake, showed a tendency to return temporarily to the level at the initial stages of the reservoir filling and later stabilize again.

In order to evaluate the behavior and stability of a similar foundation rock, it is necessary to carry out measurements at close time intervals, at least in the first cycle of reservoir level rise and fall following the earthquake. It can be said, therefore, that the decision to carry out the monitoring of the dam body pursuant to the test filling standards until normal water level was reached for the first time after the earthquake was appropriate.

The measurement data reported on in the present paper were obtained by using the greatest number of measuring points and with the highest measurement frequency ever used in the monitoring of a dam that has been in service for many years. The measurement data also capture behavioral changes due to strong ground motions. The data, therefore, will provide valuable information that can be used to further research on the earthquake resistance of dams.

REFERENCES

1) Committee on Evaluation of Earthquake Resistance of Dams: Report of Committee on Evaluation of Earthquake Resistance of Dams, 1995. (in Japanese)

2) K.Kido,Y.Sugimura,M.Morita,K.Hiraki: Dynamic Analysis of Hitokura Dam During the 1995 Hyogoken-Nambu Earthquake, 19th Congress on Large Dams, Vol.I,C.16, ICOLD, 1997.

3) Y.Furukawa,Y.Sugimura,K.Kido,T.Sugiura: The Behavior and Safety of Hitokura Dam after the 1995 Hyogoken-Nambu Earthquake, Water Technology, No.3, Water Resources Development Public Corporation, 1998. (in Japanese)

Experimental Study on Dynamic Tensile Strength of Concrete using Splitting Tensile Tests

by

Takashi SASAKI *, Isao Nagayama **, Masahiro HATANO *** and Yuji KANEKO ****

ABSTRACT

In order to evaluate the seismic resistance of concrete dams, several studies have been conducted about dynamic tensile strength of concrete.

This paper presents results of splitting tensile tests for concrete under the fast rate loading and examines the effects of loading rates, initial stress and loading pattern on the tensile strength of concrete. The following results were obtained:

1) The tensile strength of concrete obeys the cement water ratio theory, regardless of loading rate.
2) A higher rate of loading results in a larger tensile strength. The rate of increase of strength due to the loading rate is not affected by the cement water ratio.
3) The tensile strength is not affected by the initial stress before the fast rate loading. The rate of loading at the time of failure determines the tensile strength of concrete.

Keywords : *Concrete, Splitting Tensile Test, Tensile Strength, Rate of Loading*

1. PREFACE

The present Japanese design criteria using the seismic coefficient method specifies the middle-third condition for concrete gravity dams and the stress in the dam calculated according to this criteria should be compressive or zero. However, large tensile stress in the dam body is induced during earthquakes in the dynamic analysis of concrete dams, and the detailed investigation of the tensile strength of concrete is therefore important to secure the seismic resistance of concrete dams. The investigations of the tensile strength of concrete have been conducted by many researchers until now[1)], and the tensile strength of concrete is said to be effected by several parameters, for example cement-water ratio, the size of the specimen for tests, loading rate and so on. For the seismic safety of concrete dams, the effect of dynamic loading on tensile strength is the most important.

* Senior Research Engineer, Dam Structure Division, Dam Department, Public Works Research Institute, Ministry of Construction, Tsukuba Science City, 305-0804, Japan

** Head ,ditto

*** Research Engineer, ditto

**** Assistant Research Engineer, ditto

This paper discusses the results of splitting tensile tests of concrete with different mix proportions under various loading rates and loading patterns.

2. TEST METHODS

Splitting tensile tests were conducted in this study. This test method is widely used for evaluating the tensile strength of concrete.

The test equipment is shown in Figure 1. Acrylic plates were set up between the top of the specimen and the upper loading plate and between the bottom of the specimen and the lower loading plate.

The applied load on a specimen was measured with loading cells and the loading rate was controlled at a specified value by the computer. The strain of the specimen was measured using three strain gages stuck on a circular surface of the specimen perpendicular to the loading direction (see Figure 2).

The specimens were cylinders of 19 cm in diameter and 19 cm in height.

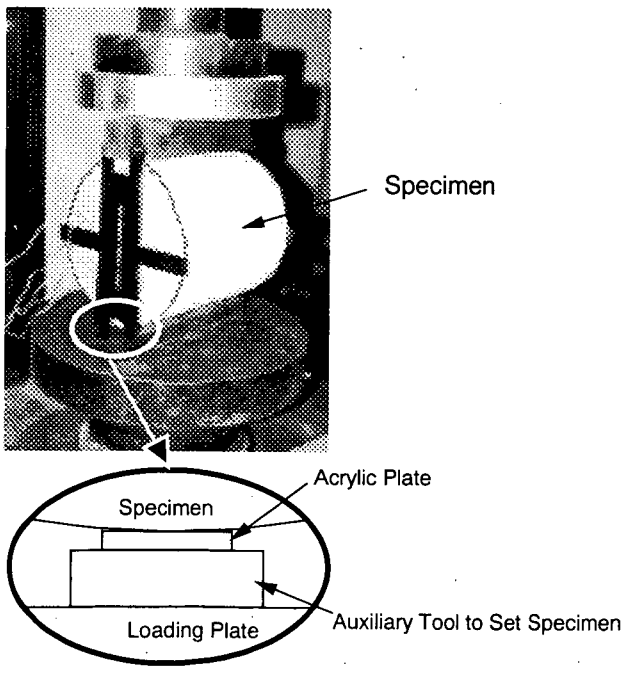


Figure 1 Test Equipment

3. TEST CONDITION

3.1 Tests for evaluation of effects of cement-water ratio and loading rate

(1) Mix proportions of concrete

Table 1 shows the mix proportions of concrete used in the tests for the evaluation of the effects of cement-water ratio and loading rate. Three types of mix proportions were selected. The cement-water ratios were 1.25, 1.67 and 2.00. The cement-water ratio of 1.25

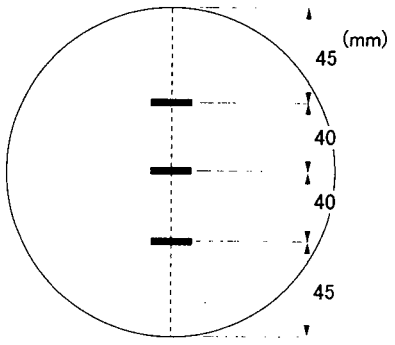


Figure 2 Location of strain gages

Table 1 Mix Proportions of Concrete

(Tests for evaluation of effect of cement-water ratio and loading ratio)

MSA (mm)	Slump (cm)	Air (%)	s / a (%)	C / W	Unit Content (kg/m^3)				
					W	C	S	G	Admixture
10	4±1	8±1	51.0	2.00	164	328	876	853	0.164
10	4±1	8±1	53.0	1.67	169	282	924	830	0.141
10	4±1	8±1	57.0	1.25	179	224	1006	769	0.112

corresponds to the mixture of RCD concrete, that of 1.67 corresponds to the mixture for concrete gravity dams and that of 2.00 corresponds to the mixture for concrete arch dams.

(2) Loading rate

The following four different loading rates were used in the tests in order to investigate the effect of the loading rate on tensile strength;

Loading Rate :

0.01, 0.1, 1, 50 N/mm^2/sec

The loading rate was constant during a test for a specimen. The loading rate was defined by the increasing rate of the normal stress in the horizontal direction at the center of the specimen.

3.2 Tests for evaluation of effects of loading pattern

(1) Mix proportions of concrete

Table 2 shows the mix proportion of concrete used in the tests for the evaluation of the effects of loading pattern. The cement-water ratio is 1.67 for all test cases.

(2) Loading pattern

Three loading rates, 0.1, 2.5, 50 N/mm^2/sec were set and they were named "Low Speed", "Middle Speed" and "High Speed" respectively. Tests were conducted under eight patterns of loading. The loading patterns are shown in Table 3. The loading rate was changed during loading at the time when the

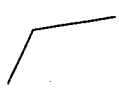
Table 2 Mix Proportions of Concrete

(Tests for evaluation of effects of loading pattern)

MSA (mm)	Slump (cm)	Air (%)	s / a (%)	C / W	Unit Content (kg/m^3)				
					W	C	S	G	Admixture
10	4±1	8±1	53.0	1.67	161	268	943	846	0.148

Table 3 Loading Patterns

(Tests for the evaluation of the effects of loading pattern)

Case #	Initial Loading Rate (N/mm^2/s)	Stress at Point of Change of Loading Rate (N/mm^2)	Latter Loading Rate (N/mm^2/s)	Measurement Interval (msec)	Number of Specimen	Schematic Pattern of Loading
1	0.1(Low)	0	0.1(Low)	10	21	
2	50(High)	0	50(High)	0.5	21	
3	0.1(Low)	1	2.5(Middle)	2	21	
4	0.1(Low)	1	50(High)	1	21	
5	0.1(Low)	2	2.5(Middle)	4	21	
6	0.1(Low)	2	50(High)	2	21	
7	50(High)	3	0.1(Low)	2	21	
8	50(High)	3	2.5(Middle)	0.5	21	

stress at the center of a specimen was 1, 2, or 3 N/mm^2 (Case 3~8). In Table 3, "Initial Loading Rate" signifies the loading rate before the change of loading rate and "Latter Loading Rate" signifies the loading rate after the change of loading rate, and "Stress at Point of Change of Loading Rate" signifies the horizontal normal stress at the center of the specimen where the loading rate was changed.

4. TEST RESULTS

4.1 Tests for evaluation of effects of cement-water ratio and loading rate

(1) Comparison of compressive strength and tensile strength at slow loading rate

Figure 3 shows the relationship between cement-water ratio and compressive strength of concrete for loading rate of 0.2 N/mm^2/sec (almost static loading), Figure 4 shows the relationship between cement-water ratio and tensile strength for loading rate of 0.01 N/mm^2/sec (almost static loading). Both of compressive strength and tensile strength obey the cement-water ratio theory.

Figure 5 shows the relationship between compressive strength and tensile strength. The ratio of tensile strength to compressive strength is about 1:9 to 1:11. The ratio of tensile strength to the compressive strength becomes lower due to the increase of cement-water ratio. It mean that the increasing ratio of tensile strength due to the increase of cement-water ratio is lower than that of compressive strength.

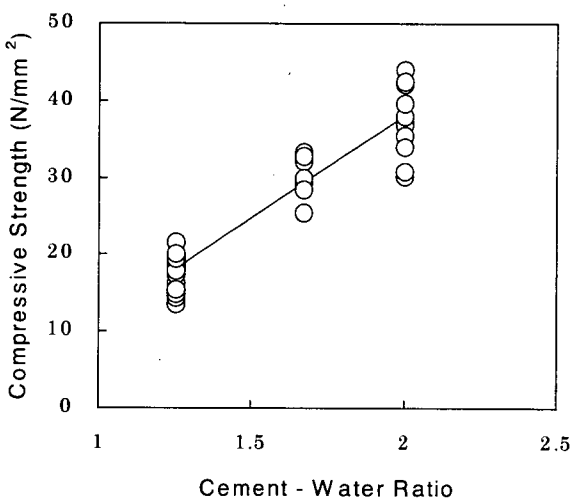


Figure 3 Cement-Water Ratio and Compressive Strength

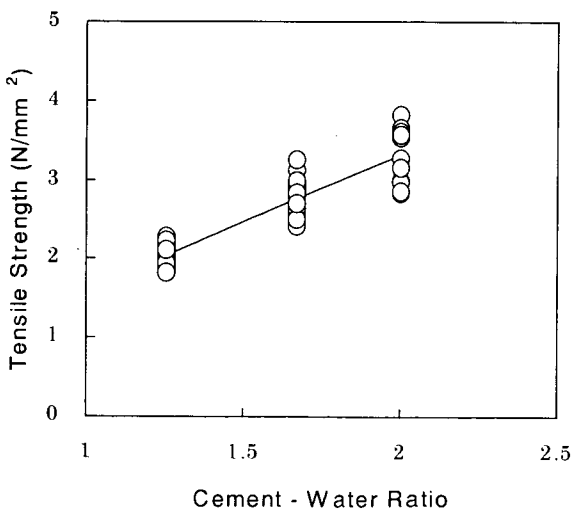


Figure 4 Cement-Water Ratio and Tensile Strength

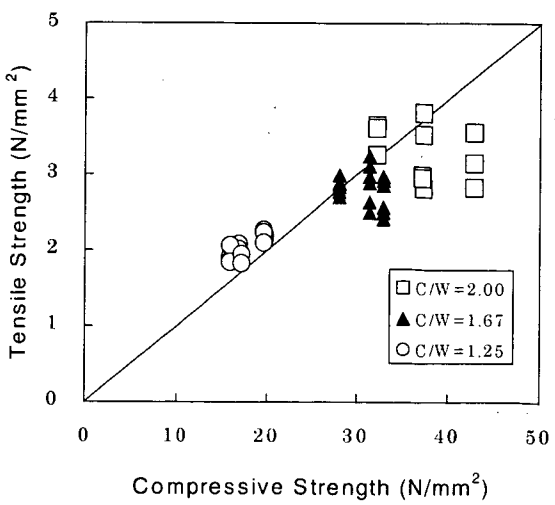


Figure 5 Compressive Strength and Tensile Strength

(2) Relationship between cement-water ratio and tensile strength

Figure 6 shows the relationship between cement-water ratio and tensile strength for all loading cases. For any loading rate, tensile strength obey the cement-water ratio theory, and the higher the loading rate is, the higher tensile strength is.

Figure 7 shows the normalized strength by setting the tensile strength for the cement-water ratio of 1.25 as the unit value. Regardless of the loading rate, the normalized strength is the same when the cement-water ratio is the same.

(3) Relationship of loading rate and tensile strength

Figure 8 shows the relationship between of the loading rate and tensile strength for each cement-water ratio. For any cement-water ratio, the tensile strength gets larger as the loading rate becomes faster.

Figure 9 shows the normalized strength by setting the tensile strength for the loading rate of 0.01 $N/mm^2/sec$ as the unit value. Regardless of the cement-water ratio, the normalized strength is the same when the loading rate is the same.

(4) Characteristic of elastic modulus

Using the strain ε_x in the direction perpendicular to the loading direction (namely, horizontal direction on the circular surface) at three points on the splitting plane shown in Figure 2, the modulus of elasticity E is obtained by the following equation :

$$E = \frac{2P}{\varepsilon_x \pi dH}\left\{1+\nu\left(\frac{2d}{d-2y}+\frac{2d}{d+2y}-1\right)\right\}$$

Here, d : the diameter of the specimen,
H : the height of the specimen,
y : the distance from the center of specimen along the splitting direction
P : the loading force
ν : the Poisson's ratio (assumed to be 0.2 in this study)

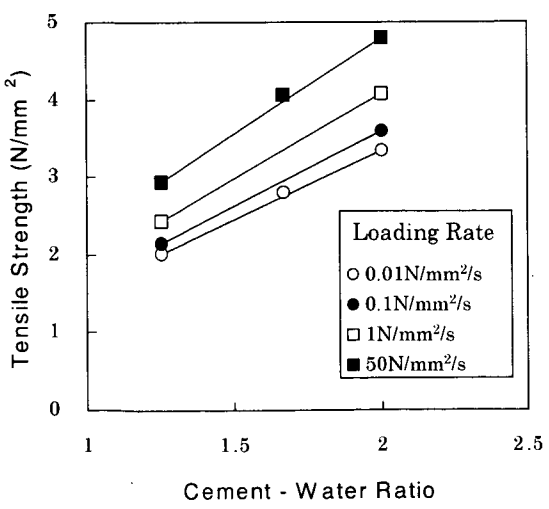


Figure 6 Cement-Water Ratio and Tensile Strength (All Loading Rates)

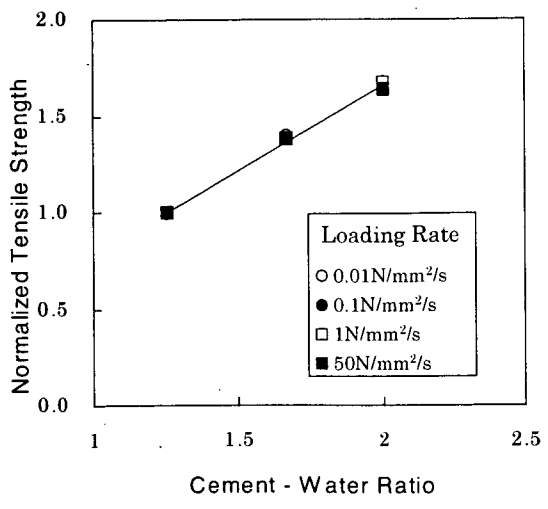


Figure 7 Cement-Water Ratio and Normalized Tensile Strength

Figure 10 shows the relationship between the loading rate and the modulus of elasticity. The modulus of elasticity in this figure is the secant modulus when the horizontal normal stress is correspond to 30 % of the tensile strength. The figure shows that the modulus of elasticity doesn't seems to have a loading-rate-dependency. While the tensile strength changes largely in response to the change of the loading rate, this feature is very different from the loading-rate-dependency of the tensile strength. It means that the tensile strain capacity (the strain limit) gets larger as the loading ratio becomes higher.

4.2 Tests for evaluation of effects of loading pattern

(1) Cases of Initial loading rate of "Low Speed"

In regards to the cases that "initial loading rate" was "Low Speed", Figure 11 shows the relationship between the "latter loading rate" and the tensile strength of Case 1, 3 and 4 ("stress at point of change of loading rate" is 1 N/mm^2), and Figure 12 shows that of Case 1, 5 and 6 ("stress at point of change of loading rate" is 2 N/mm^2). These figures show that the tensile strength gets larger as "latter loading rate" becomes higher.

(2) Cases of Initial loading rate of "High Speed"

In regards to the cases that "initial loading rate" was "High Speed", Figure 13 shows the relationship

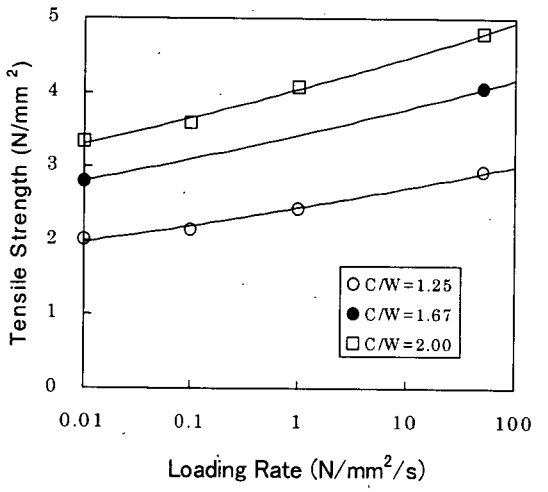


Figure 8 Loading Rate and Tensile Strength

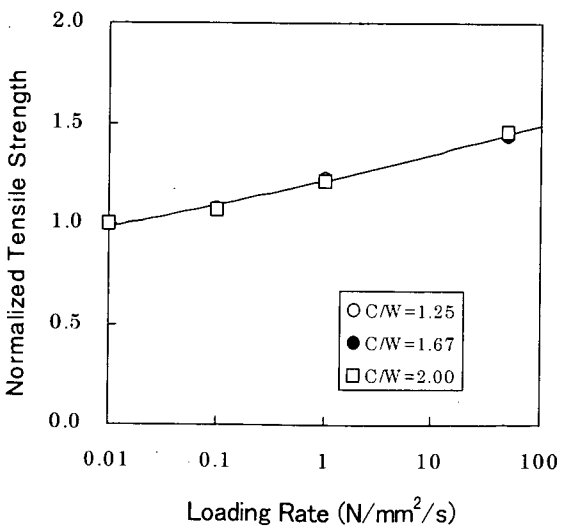


Figure 9 Loading Rate and Normalized Tensile Strength

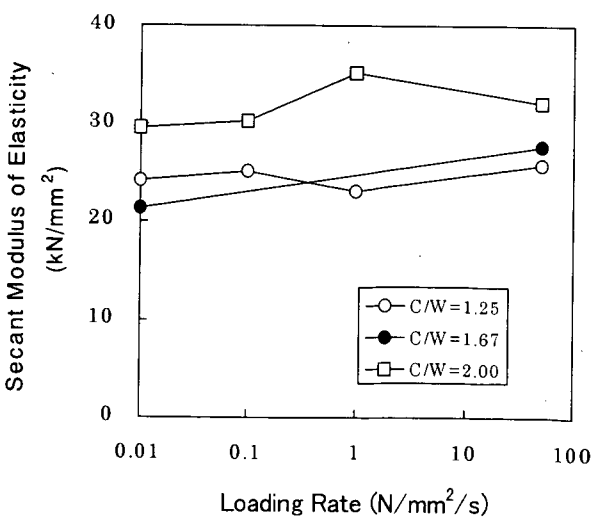


Figure 10 Loading Rate and Modulus of Elasticity

between "latter loading rate" and the tensile strength of Case 2, 7 and 8 ("stress at point of change of loading rate" is 3 N/mm^2). This figure shows that the tensile strength gets smaller as "latter loading rate" becomes lower.

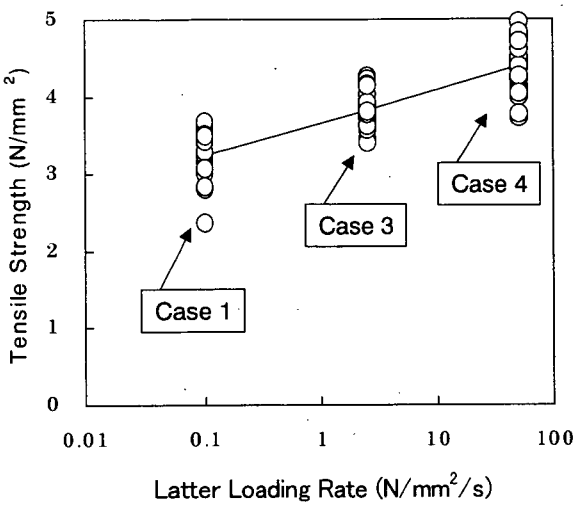


Figure 11 Latter Loading Rate and Tensile Strength
(Initial loading rate : Low Speed)
(Stress at point of change of loading rate : 1 N/mm^2)

(3) Relationship between "latter loading rate "and tensile strength for all cases

Figure 14 shows the relationship between "latter loading rate" and the tensile strength for all test cases. This figure shows that the tensile strength is the same when "latter loading rate" is the same irrespective of loading pattern.

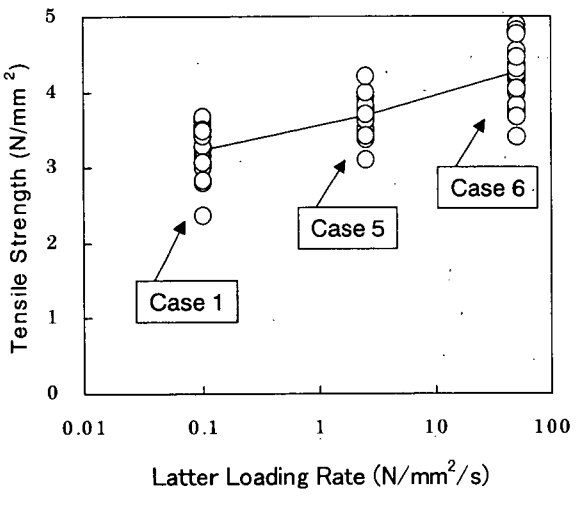


Figure 12 Latter Loading Rate and Tensile Strength
(Initial loading rate : Low Speed)
(Stress at point of change of loading rate : 2 N/mm^2)

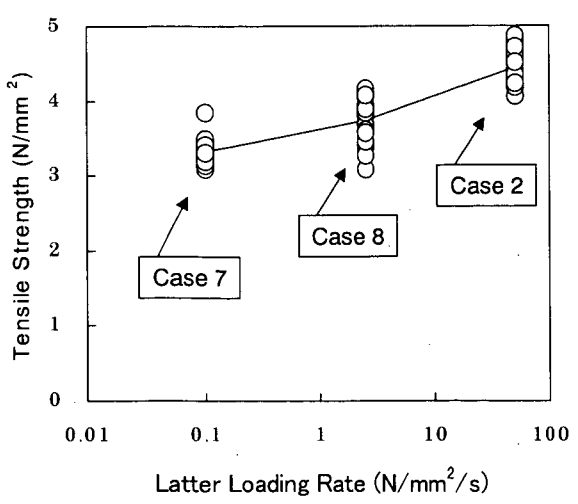


Figure 13 Latter Loading Rate and Tensile Strength
(Initial Loading Rate : High Speed)
(Stress at point of change of loading rate : 3 N/mm^2)

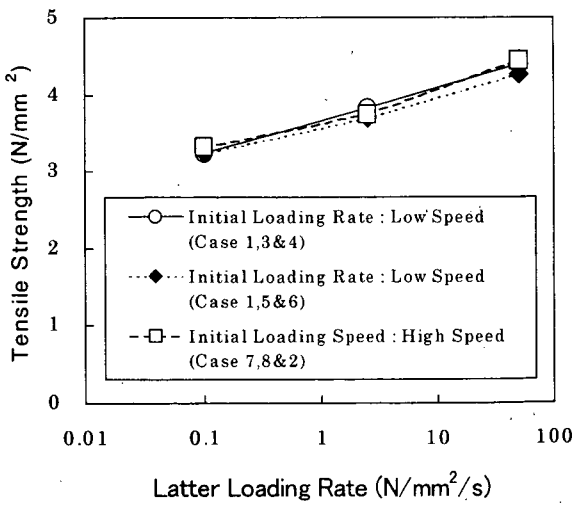


Figure 14 Latter Loading Rate and Tensile Strength
(All loading cases)

(4) Effects of "stress at point of change of loading rate" on the tensile strength

Figure 15 shows the relationship between "stress at point of change of loading rate" and the tensile strength. From this figure, it can be considered that there is no effect of "stress at point of change of loading rate" on the tensile strength.

4. CONCLUSION

The following conclusions are derived from the tensile strength tests.

From the tests for the evaluation of the effect of cement-water ratio and loading rate :

1) The tensile strength of concrete increases as the loading rate increases.

2) The tensile strength has a linear relationship to the cement-water ratio for all loading rates. That is to say, the tensile strength of concrete obeys the cement-water ratio theory regardless of loading rate.

3) The increasing rate of strength as the increase of loading rate is not affected by the cement-water ratio.

4) The modulus of elasticity is not affected by the loading rate.

Then, from the tests for the evaluation of the effects of loading pattern :

5) The tensile strength is affected only by "latter loading rate". That is to say, the loading rate at the time of failure determines the tensile strength.

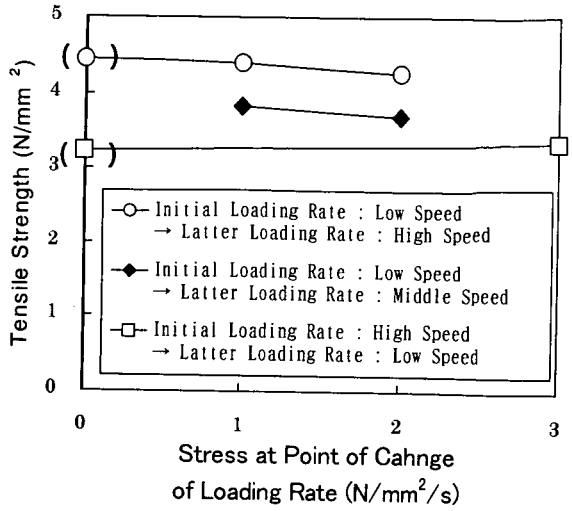


Figure 15 Stress at point of change of loading rate and tensile strength

6) Stress where the loading rate is changed have no effect on the tensile strength.

In regards to test cases where initial loading rate is "Low Speed", the stress where the loading rate is changed can be considered as the initial stress (needless to say, it is momentary stress) before fast rate loading. The initial stress, therefore, doesn't affect the tensile strength.

Meanwhile, during actual earthquakes, the loading rate for concrete of dams changes every moment. In the instant when tensile stress of concrete is the highest, it is possible that the loading rate becomes almost 0. In such a occasion, the increase of the tensile strength may not be expected. It seems to be suggested by the results of test cases that the initial loading rate was "High Speed" in this paper.

REFERENCES

1) For Example;
Tadashi HATANO, T : "Dynamic Behavior of Concrete Under Impulsive Tensile Load", Technical Reports No. C-6002, Technical Laboratory of the Central Research Institute of Electric Power Industry, Japan, Nov. 5, 1960
Jerome M. Raphael : "Tensile Strength of Concrete" : Technical Paper No. 81-17, ACI Journal, March-April, 1984
3) Isao NAGAYAMA, Kazuo WATANABE, Takashi SASAKI and Masahiro HATANO : "Experimental Study on Tensile Strength of Concrete for Dams", Proc. of The 27th Joint Meeting of UJNR Panel on Wind and Seismic Effects, Tsukuba, May 1997.

Technical Session 2

Embankment Dams (1)

Hydraulic Fracturing in Fill-type Dams during Earthquake

Yoshio OHNE*), Kunitomo NARITA*)
Yoshio NAKAMURA**) and Yuji MURASE***)

ABSTRACT: In addition to the safety against sliding failure of embankment slopes, safety against internal erosion caused by hydraulic fracturing has been another important issues to be discussed in the seismic resistant design of fill-type dams. This paper concerns the mechanism and its possibility of occurrence of hydraulic fracturing in earth and rock fill dams during earthquake. Laboratory seepage fracture tests were conducted on erosive soils under various conditions of water pressure and confining stresses to know what are to be influential factors on seepage failure, and FEM dynamic response analysis was made for different cases of embankment configuration to study the extent of damages and development process of hydraulic fracturing during earthquake.

Key words: *hydraulic fracturing/ earthquake/ hydraulic gradient/ dynamic analysis/ stress ratio*

1. INTRODUCTION

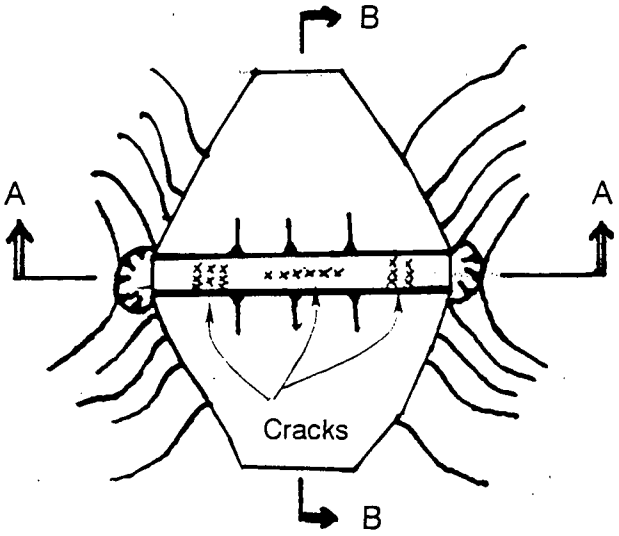
Stability evaluation of fill-type dams during earthquake has mostly focused on the sliding failure of embankment slopes. FEM dynamic response analysis has been an effective and useful tool commonly applied in the study of seismic behavior of dam body during earthquake.

In the First US-Japan Workshop on Advanced Research on Earthquake Engineering for Dams (Nov. 1996), the authors have proposed a practically useful method of stability evaluation of embankment, by taking into account response shear strain as a failure criterion.[1] Because the proposed method necessarily does not require the dynamic shear strength of construction materials, it seems to be applicable with high accuracy in the evaluation of slope stability of earth and rock fill dams.

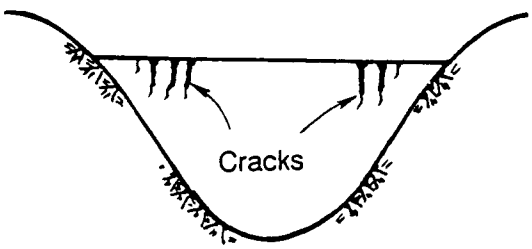
In the earthquake resistant design of fill-type dams, however, not only stability against sliding failure of embankment slope but also that against internal erosion and water leakage through the core is necessary to ensure when the reservoir water is filled during dam operation. Cut-off wall trench construction and severe selection of core and filter zone materials are for instance to be effective measures to prevent such hydraulic fracturing damages.

In this study, laboratory seepage fracture tests were conducted to investigate failure criterion of hydraulic fracturing by paying attention on the relationship between the confining stress and hydraulic gradient in the core zone. FEM dynamic response analysis was then made on the longitudinal section of embankment dams to find stress distribution and hydraulic gradient in the core. The computed values were compared with those by tests to examine the possibility of the occurrence of hydraulic fracturing. The results presented the fact that hydraulic fracturing tends to occur in the upper part of the sharp abutment and near the turning point of the abutment slope.

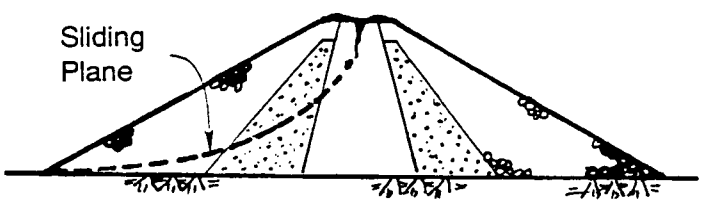
*) *Professor, Aichi Institute of Technology*
**) *Chief Eng., AICO Consulting co. ltd.*
***) *Chief Eng., DAIME Eng. Service co. ltd.*



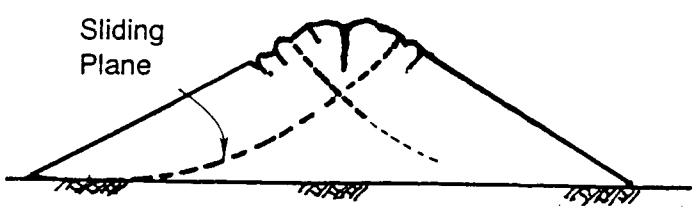
(a) Plan View of Rock Fill Dam



(b) A-A Section



(c) B-B Section



(d) Cracking and Sliding in Earth Dam

Fig.2.1 Damage of Fill-type Dams caused by Earthquake

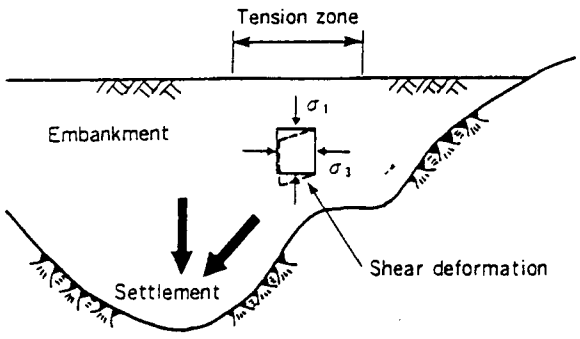
2. DAMAGE OF FILL-TYPE DAMS CAUSED BY EARTHQUAKE

According to the recent investigation reports on the damages of fill-type dams caused by big earthquakes, seismic damages can be classified into two categories; (1) the transverse cracking at the crest of a dam near the abutment foundation, as shown in Figs.2.1(a) and (b), and (2) the longitudinal cracking to cause sliding failure of embankment slopes, as shown in Figs.2.1(c) and (d).[2] The former type of cracking could lead leakage of the reservoir water and internal erosion through the core.

3. MECHANISM OF HYDRAULIC FRACTURING [3][4]

Hydraulic fracturing takes place due to the decrease in confining stress acting on the soil, which in turn is caused by the differential settlement in the core. In Fig.3.1(a), for instance, differential settlement is induced by the earthquake force near the abutment foundation, and it causes reduction in the lateral confining pressure (σ_3). In Fig.3.2(a), settlement near the turning point of the core width induces arching action and decrease in the vertical confining pressure (σ_1), which must be the cause of hydraulic fracturing. Fig.3.1(b) and Fig.3.2(b), respectively, represents these stress conditions with Mohr's stress circles. As indicated by the dotted lines, reduction in the confining pressure may shift the stress circle left and get it closer to the failure envelope to lead a state of hydraulic fracturing.

(a)



(b)

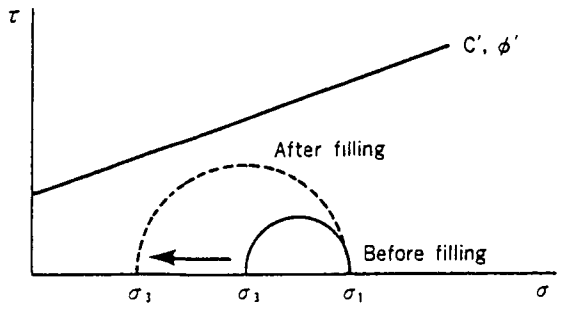
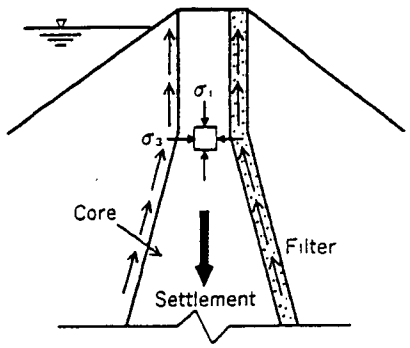


Fig.3.1 Stress Change due to Differential Settlement

(a)



(b)

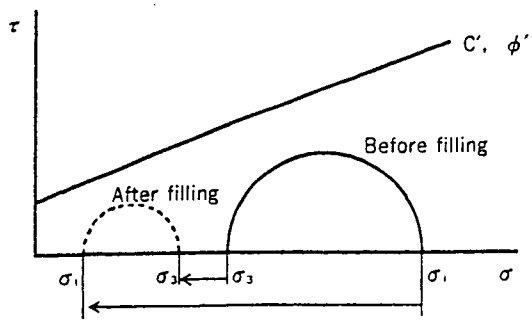


Fig.3.2 Stress Change due to Arch Action

3.1 Laboratory tests on hydraulic fracturing

In order to discuss the possibility of hydraulic fracturing for different situations mentioned above, the following two series of tests were carried out in this study.

Test-1: from the initial uniform stress state of $\sigma_1 = \sigma_3$ in the tri-axial compression apparatus, the minor principal stress σ_3 on the specimen is decreased gradually, under a seepage condition of constant hydraulic gradient, to produce the final state of seepage fracture, which realizes the stress states shown in Fig.3.1.

Test-2: seepage fracture tests are conducted under a constant effective vertical stress (σ'_v), by increasing the hydraulic gradient step by step to obtain the final value (if) at fracture, which realizes the stress states in presented Fig.3.2.

3.2 Apparatus and soil samples

Schematical illustrations of the apparatus for Test-1 and Test-2 series are shown in Fig.3.3 and Fig.3.4, respectively. The water flows from one side to the other in Fig.3.3 and from the center to the two end points in Fig.3.4, with a head difference Δh.

Grain size distributions of the materials used in the tests are shown in Fig.3.5, in which the material of a) SM and b) SC are used for Test-1 and Test-2, respectively. The specimens are prepared in the laboratory to satisfy the specified Proctor compaction conditions of dry density and water content, as shown in Fig.3.6, of points B, C and D in Test-1 and the point E in Test-2 series. Details of the test conditions are summarized in Table-3.1.

3.3 Test results in Test-1 series

The results of Test-1 series are summarized in Figs.3.7 and 3.8. The relationship between the discharge (q) and the effective stress ratio ($\overline{ob}/\overline{oc}$) defined in the column is shown in Fig.3.8. It is clearly seen in the figure that the discharge from the specimen increases due to the increase in the stress ratio, showing an abrupt

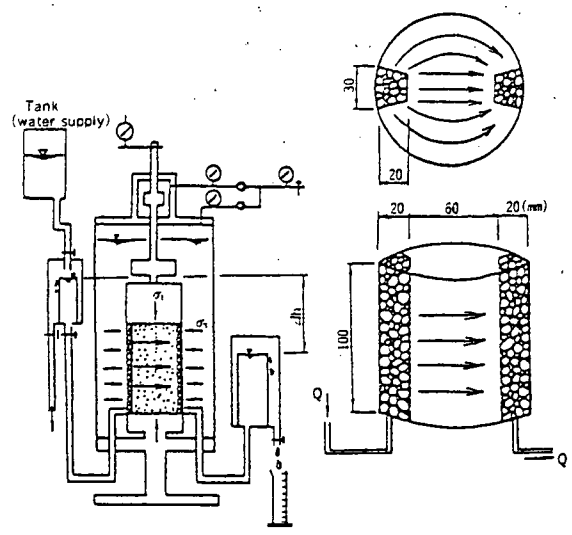


Fig.3.3 Seepage Test Apparatus for Test-1 Series

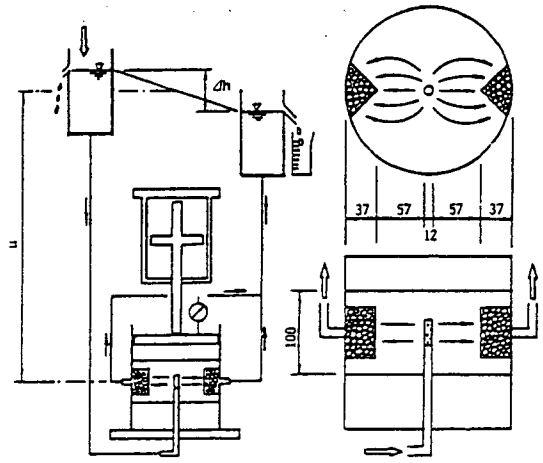


Fig.3.4 Seepage Test Apparatus for Test-2 Series

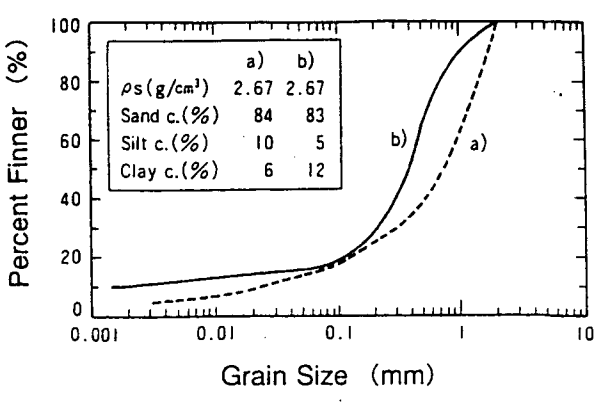


Fig.3.5 Grain Size Distribution of Fill Materials used in Tests

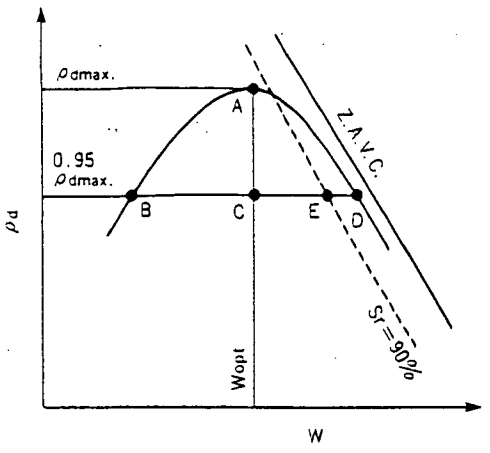


Fig.3.6 Compaction Conditions of Test Specimens

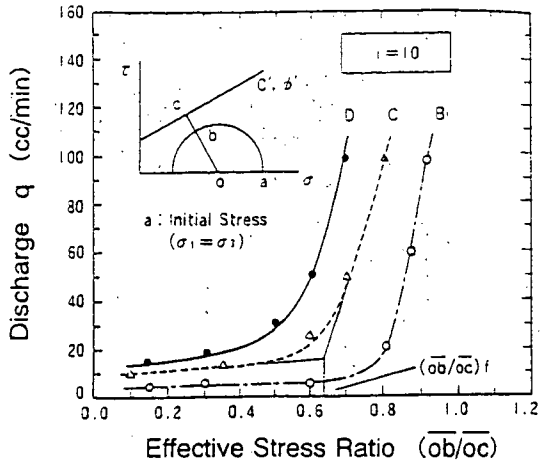


Fig.3.7 Discharge versus Stress Ratio Relation (Test-1)

Table-3.1 Summary of Seepage Test Conditions

		Test-1	Test-2
Stress and Seepage Conditions		Initial State : $\sigma_1=\sigma_2$ σ_1 = 1, 2, 3 (kgf/cm²) i = 5, 10, 20 σ_3 : gradually decreasing	σ_v = 0.5 (kgf/cm²) σ_v'= 0.1, 0.2, 0.4 i : gradually increasing
Specimen	Test Point	B C D	E
	Density	0.95 × ρ_{dmax} (ρ_{dmax} = 1.86g/cm³)	0.95 × ρ_{dmax} (ρ_{dmax} = 1.85g/cm³)
	Water Content W (%) Deg. of Sat. Sr (%)	9.4 13.7 16.8 49.1 71.6 87.8	17.6 90.0

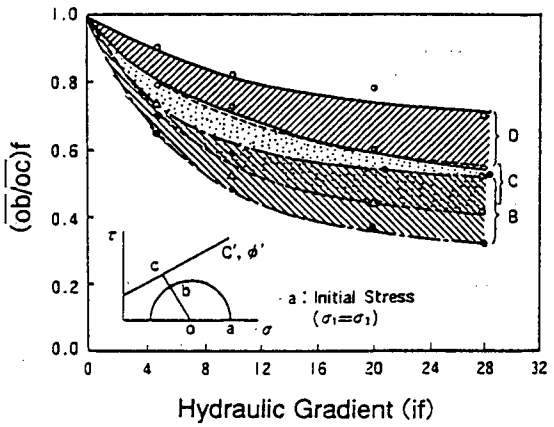


Fig.3.8 Stress Ratio at Failure (Test-1)

change at a certain condition. The values of the critical stress ratio $(\overline{ob}/\overline{oc})_f$ defined by the point are plotted against the value of the hydraulic gradient at failure (if) in Fig.3.8 for different compaction conditions. It is recognized in the figure that for samples having the same dry density a higher resistance can be expected to achieve against hydraulic fracturing as the material is compacted in the wet side of the optimum.

3.4 The test results in Test-2 series

A representative test result of σ'_v= 0.4kgf/cm² is shown in Fig.3.9, taking the discharge (Q) from the specimen on the ordinate and the hydraulic gradient (i) on the abscissa, in which solid lines are drawn in reference to the constant coefficient of permeability, which satisfies the Darcy's law of v=ki for the state of the laminar flow. It is seen that solid circle plots move along these straight lines of constant k-value in the early stage of the test, showing however an abrupt change in the discharge (Q) in the vicinity of i ≒ 40. The critical value of the hydraulic gradient (if) can then be defined at the point of if=40 for the case of σ'_v=0.4kgf/cm². The relation between the values of if and σ'_v is summarized in Fig.3.10, for the results of the present study by solid circles and for other tests on SM to CL materials by open circles.

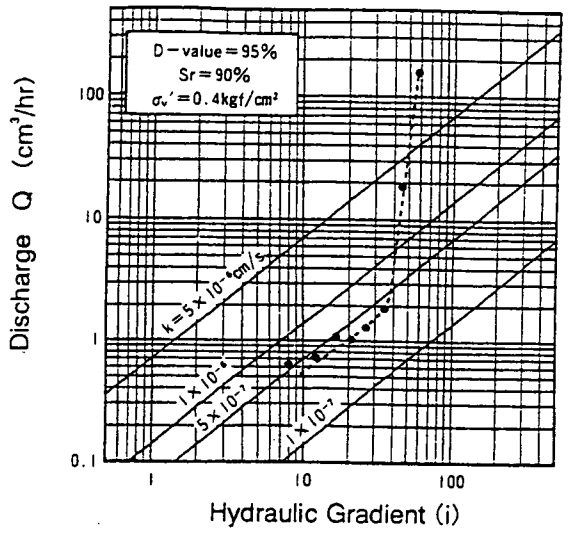


Fig.3.9 Discharge versus Hydraulic Gradient Relation (Test-2)

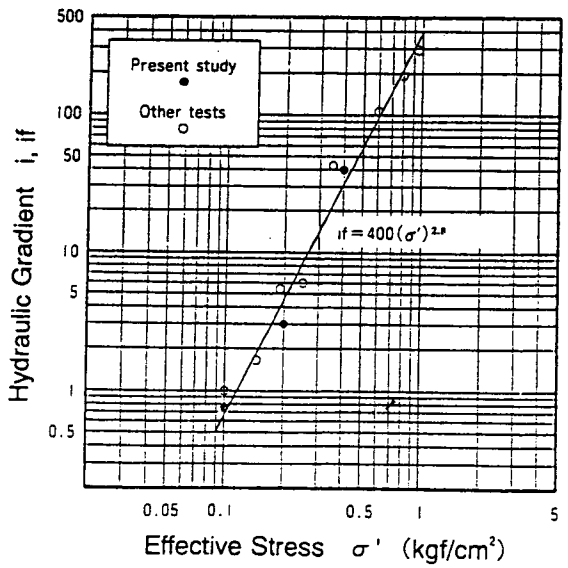


Fig.3.10 Hydraulic Gradient at Failure (Test-2)

4. FEM DYNAMIC RESPONSE ANALYSIS

4.1 Analysis procedure

The aim of this study is to examine the possibility of hydraulic fracturing in fill-type dams when earthquake forces act upon the core with the reservoir filled with water. FEM dynamic response analysis is now conducted on simple embankment models for different types of harmonic excitation. Analysis procedures and conditions employed here are summarized below.

1) The analysis is done for a standard type of rock fill dam with a centrally located core of 100m in height, as presented in Fig.4.1, by changing abutment configuration in four cases.

2) Two-dimensional analysis may be reasonable as a first step to understand dynamic behavior of fill-type dams and to evaluate their possibility of hydraulic fracturing during earthquake. Analysis is therefore made for harmonic excitation of acceleration with a frequency of 1Hz.

3) The analytical procedure adopted here is basically the same as the QUAD-4 program, where non linear material properties of dynamic behavior are represented by the Hardin-Drnevich model in the following forms.

$$G/G_0 = \frac{1}{1+(\gamma/\gamma_r)\gamma}$$

$$h/h_0 = \frac{\gamma/\gamma_r}{1+(\gamma/\gamma_r)}$$

where $G_0 = 510\ \sigma'^{0.47}$

$\gamma_r = 4.8 \times 10^{-3}\ \sigma'^{0.75}$

4.2 Results of dynamic response analysis

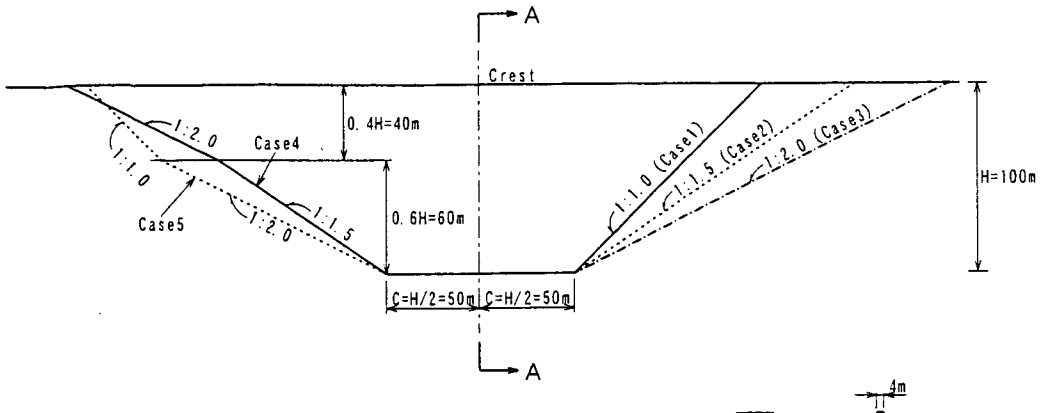
1) Dynamic response of embankment

In Table-4.1, values of the input and response acceleration calculated at the base and the crest are compared, with the natural frequency obtained for the primary mode of vibration of the embankment. It is clear that the response acceleration at the crest is about 3.5 to 4.0 times larger than the base acceleration.

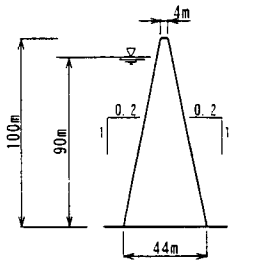
Primary mode of vibration and distribution of the response acceleration in embankment are drawn in Fig.4.2 for a representative case of the abutment slope of 1 to 1.5 (case-2). Such results for others cases as case-1, 3, 4 and 5 are almost same as that of case-2 one's.

2) Evaluation of hydraulic fracturing

Possibility of the hydraulic fracturing during earthquake is examined here by applying the following two criteria.



Case No.	H	C	Gradient (1:b)	
			(0～0.6)H	(0.6～1.0)H
Case-1	100	50	1.0	1.0
Case-2			1.5	1.5
Case-3			2.0	2.0
Case-4			1.5	2.0
Case-5			2.0	1.0



Section of core zone A-A

Fig.4.1 Abutment Configuration Employed in Dynamic Response Analysis

Table 4.1 Response Acceleration at Dam Crest

Case No.	Base Acceleration (1Hz)		
	50 gal	100 gal	200 gal
Case-1	214.3 (1.05)	414.5 (1.02)	754.9 (0.97)
Case-2	218.4 (0.95)	407.8 (0.93)	707.6 (0.90)
Case-3	200.9 (0.90)	373.1 (0.89)	667.7 (0.86)
Case-4	200.9 (0.90)	372.6 (0.89)	666.1 (0.86)
Case-5	201.9 (0.91)	373.6 (0.89)	666.7 (0.86)

( ) shows natural frequency (Hz) at the first mode

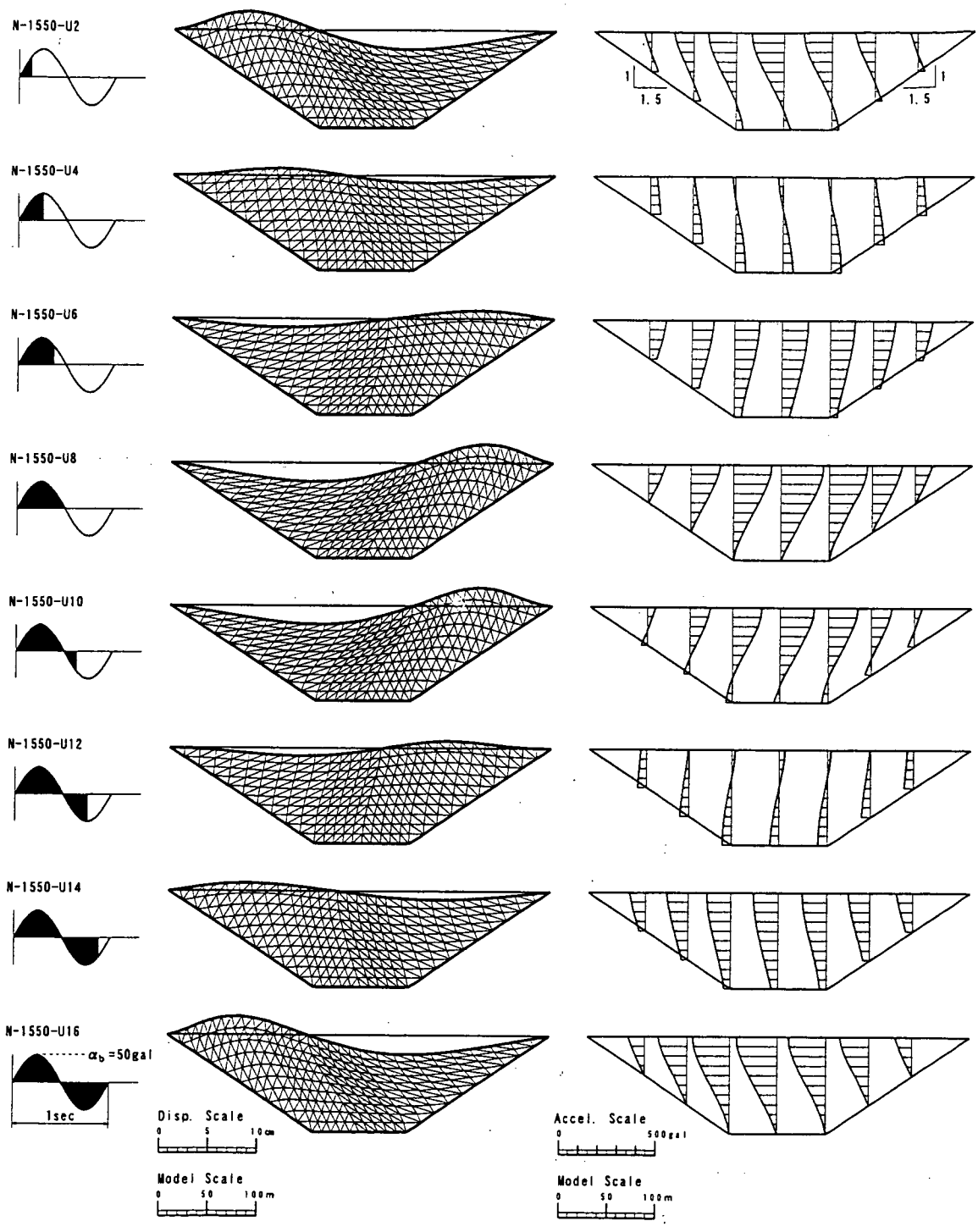


Fig.4.2 Deformation mode along dam axis

(a) Safety evaluation proposed in this paper

Evaluation of safety factor against hydraulic fracturing is explained in Fig.4.3, which is redrawn from Fig.3.8 in a more precise form. In this figure, the stress ratio which leads to hydraulic fracture is obtained corresponding to the value of the hydraulic gradient at failure (i_f), and the safety factor can be evaluated as the ratio of the value of the stress ratio at failure to that at the present state. Assuming that $i_f = 2.0$ for the soil compacted in the state of B, for example, the value of the stress ratio at failure can be determined from the upper solid line as $(\overline{ob}/\overline{oc})_f = 0.95$. If the value of the stress ratio calculated in the dynamic response analysis is taken as $(\overline{ob}/\overline{oc}) = 0.93$, the safety factor (Fs) becomes to be $Fs = 0.95/0.93 \fallingdotseq 1.02$, suggesting a little safety against hydraulic fracturing.

(b) Safety evaluation by Seed[5),6)]

Seed et al. (1976) have presented the following criteria to evaluate possibility of hydraulic fracturing in the Teton dam failure.

$$\sigma_3' \leqq u$$

where σ_3' and u are the minor principal stress and pore water pressure, respectively, at a certain point.

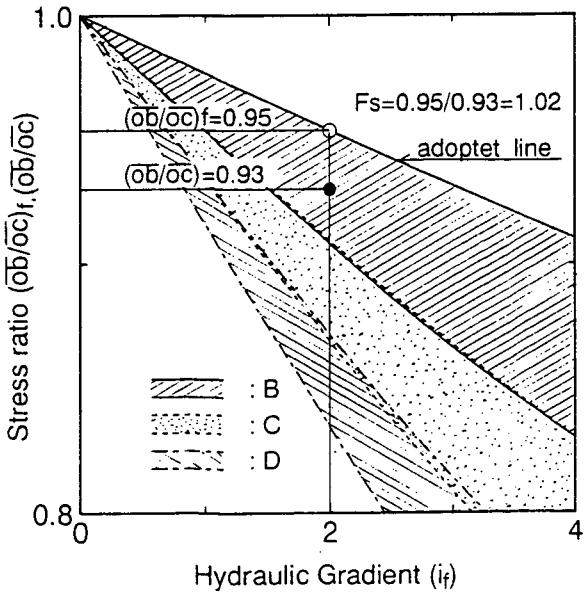


Fig.4.3 Safety Evaluation with Stress Ratio

5. DISCUSSIONS ON POSSIBILITY OF HYDRAULIC FRACTURING

Possibility of hydraulic fracturing in the core zone is discussed now by comparing the results from two methods of safety evaluation presented above; one is the criterion proposed in this paper and the other by Seed et al.

5.1 Safety evaluation proposed in this paper

Distributions of the response acceleration and the safety factor against hydraulic fracturing in the embankment are presented in Fig.5.1 through Fig.5.10 for all cases of abutment configuration. Discussions are summarized in the following.

(a) In the embankment with abutment slope of 1:1.5, hydraulic fracture appears initially in the upper part near the abutment foundation, and it develops to the lower part as the response acceleration increases.

(b) Possibility of fracturing becomes lower as the abutment slope is gentle.

(c) In the case the abutment foundation has a turning point of slope inclination, hydraulic fracture takes place first near the point and it extends widely upwards.

(d) In the case the abutment slope is steeper in the upper part than the lower (U-shaped valley), fracture starts near the turning point of slope and it extends upwards and much more widely than the above case along the upper steep abutment. This result is not a matter of worrying about, because the confining stress in the core is much higher than the above case in the static state.

5.2 Safety evaluation by Seed method

Distributions of the minor principal stress σ_3 and the pore water pressure u in embankment are given in Fig.5.11 through Fig.5.15. Tendency of hydraulic fracturing is almost the same as presented above except the shape and extent of the rapture zone. It is clear that the criterion presented by Seed is rather loose as compared with that proposed in this paper.

6. SUMMARIES

Possibility of hydraulic fracturing during earthquake was discussed in this paper through laboratory seepage fracture tests and FEM dynamic response analysis. Focus of the present study is placed on to know the threshold of the hydraulic fracturing, and satisfactory results were obtained to discuss on the safety evaluation of embankment against hydraulic fracture. It is necessary, however, much more follow-up study to apply the proposed method for the actual dam design: i.e., more rigorous 3D dynamic analysis and seepage fracture tests under vibration are required for a future precise study on hydraulic fracture.

REFERENCES

1) Ohne, Y. et al (Nov. 1996). Evaluation of seismic slope stability of earth and rock fill dams, *First U.S-Japan Workshop on Advanced Research on Earthquake Eng. for Dams.*

2) Ohne,Y. (1985). Seismic behavior of MAKIO dam, *A report of specialty session of NAGANO-KEN SEIBU Earthquake, the 20th JSSMFE annual meeting.* (in Japanese)

3) Ohne, Y. & Narita, K. (1978). Some considerations of the Teton Dam failure. *Technical report of Aichi Inst. of Technology,* No.13: pp.217-229.

4) Murase, Y. et al (Aug. 1995). Study on hydraulic fracturing of core-type rock fill dams. *The MWA International Conf. on Dam Engineering*, pp.363-371.

5) Teton Dam Failure Interior Review Group. 1976a. *First interim report on the Teton Dam failure.*

6) Teton Dam Failure Interior Review Group. 1976b. *Second interim report on the Teton Dam failure.*

7) Narita, K. et al (1997). Centrifuge model tests on hydraulic fracturing in earth and rockfill dams. *Proc. 9th Int. Conf. of IACMAG*, vol.3, pp.2291-2294.

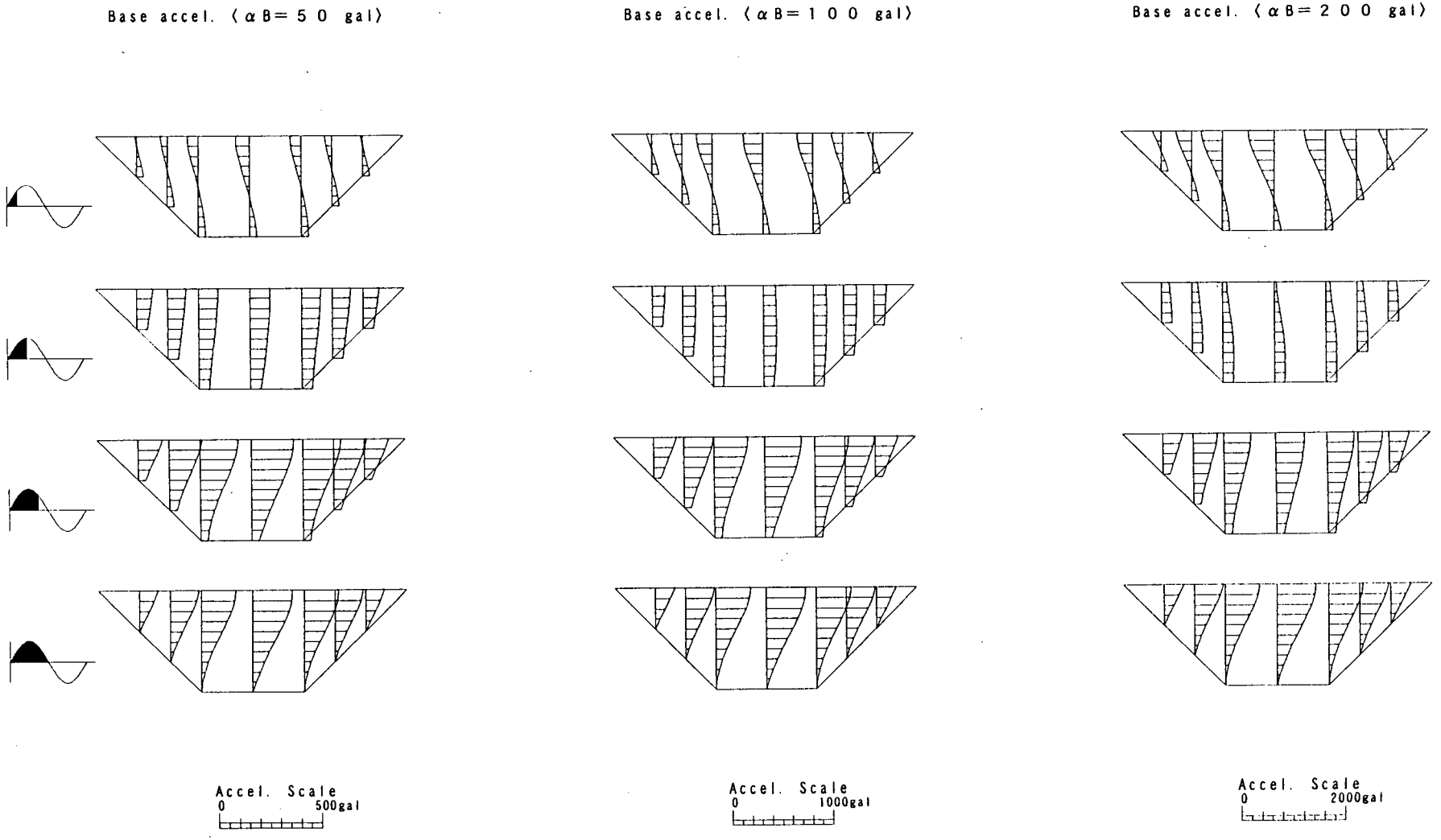


Fig. 5.1 Distribution of response acceleration [abutment 1:1.0]

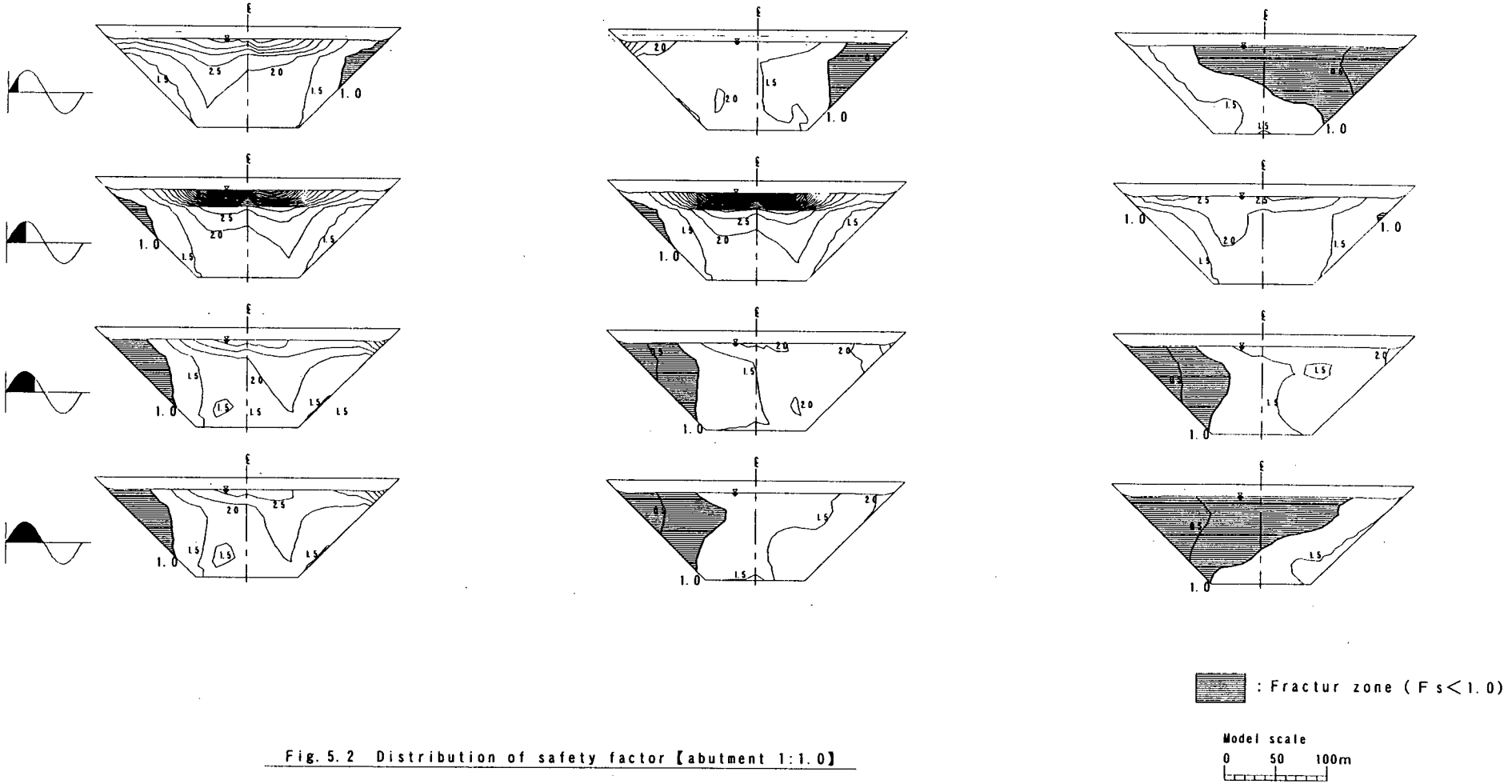


Fig. 5.2 Distribution of safety factor 【abutment 1:1.0】

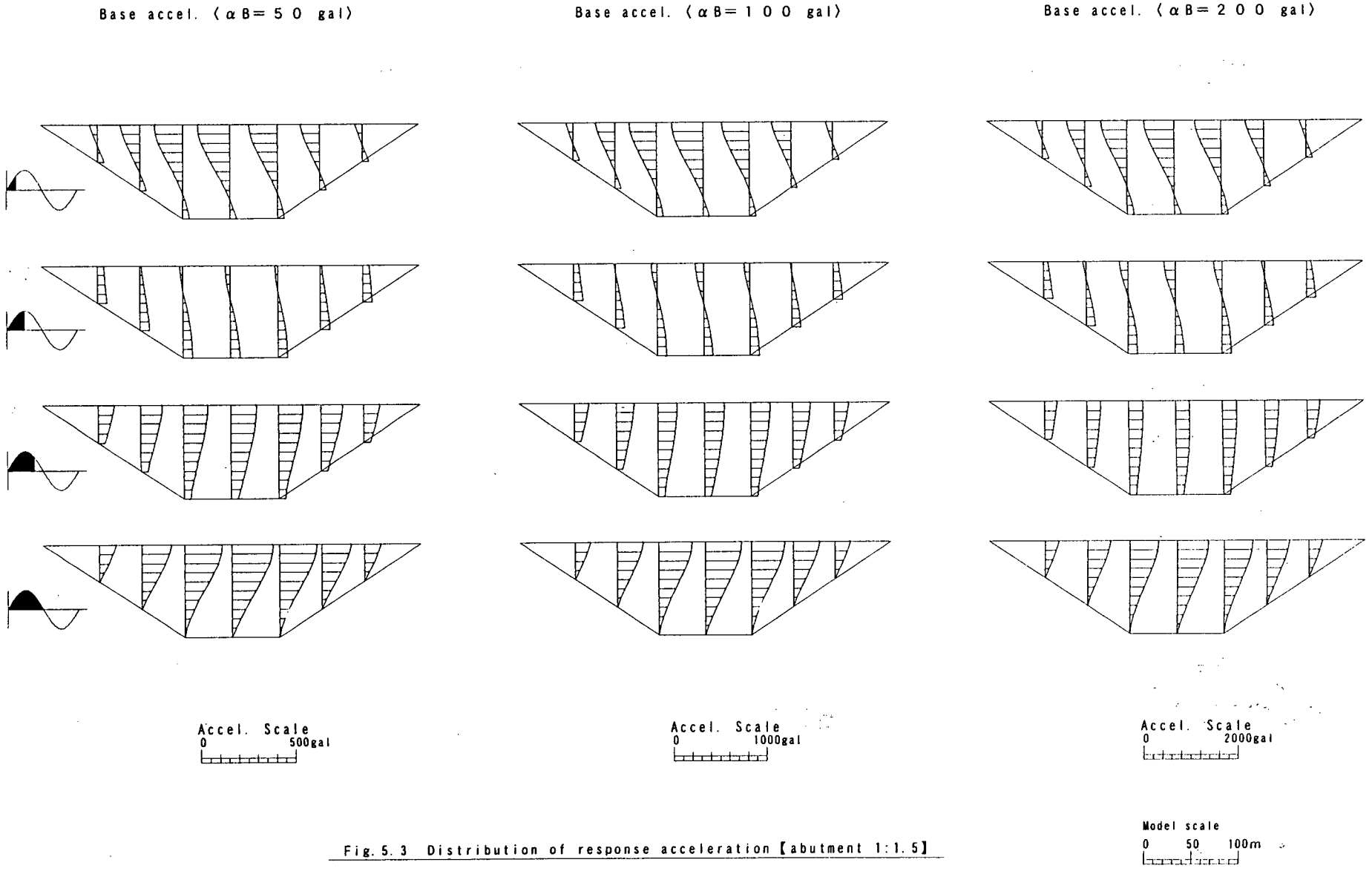


Fig. 5.3 Distribution of response acceleration [abutment 1:1.5]

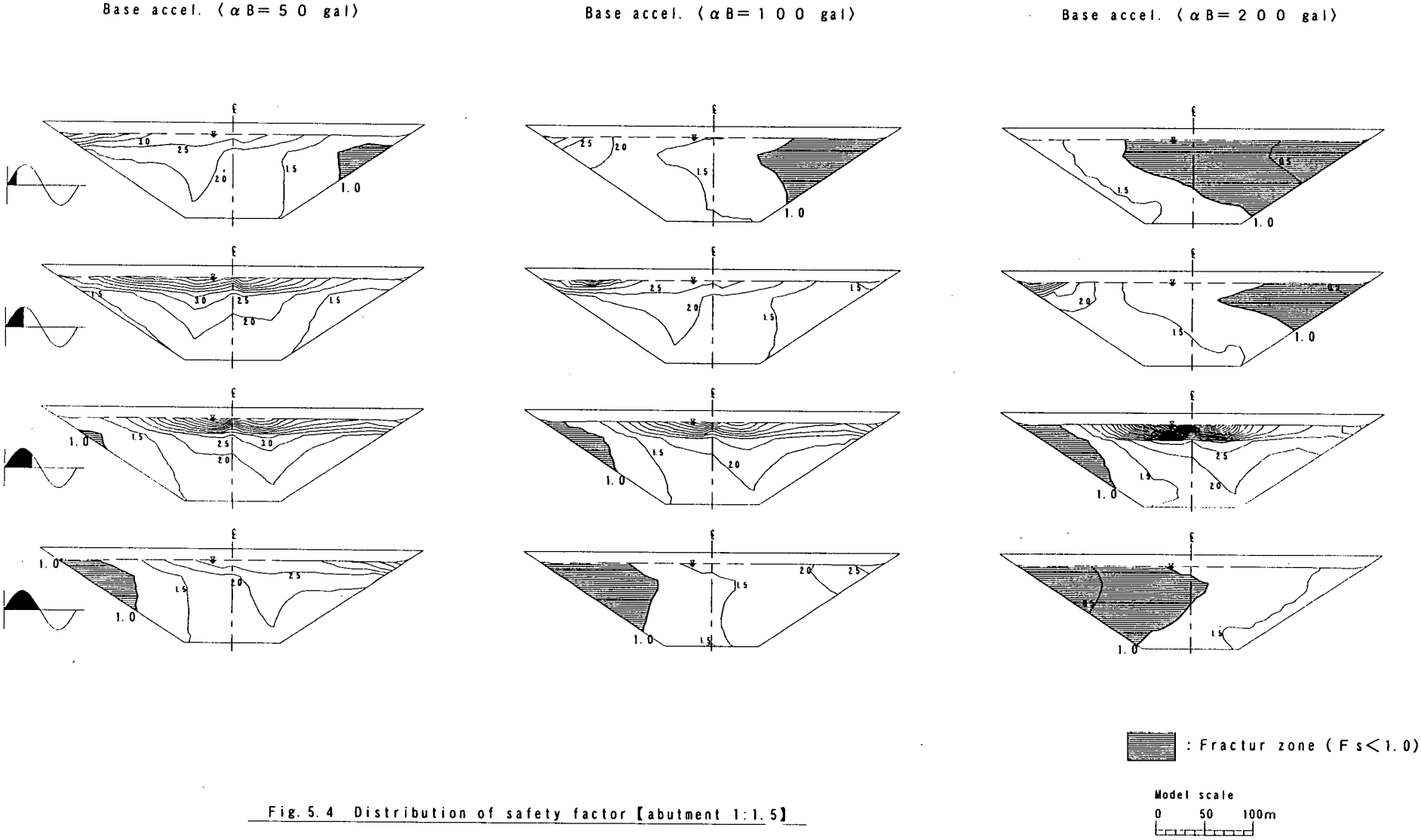
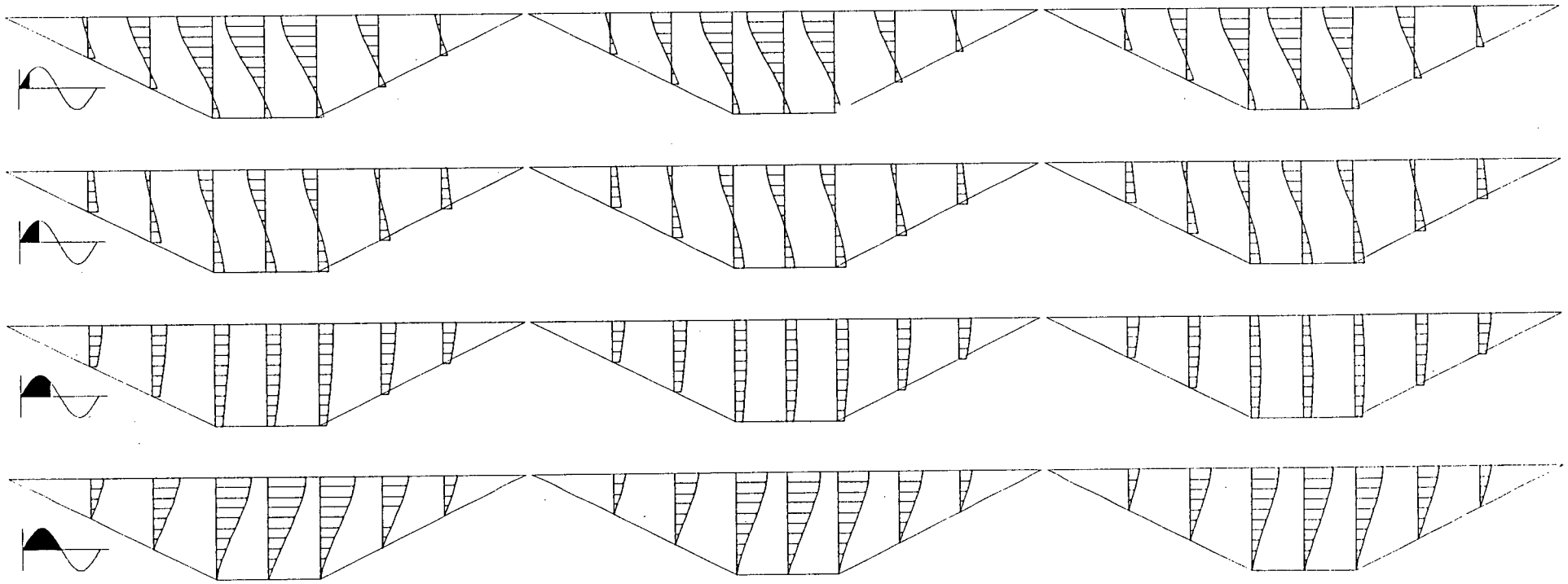


Fig. 5. 4 Distribution of safety factor [abutment 1:1. 5]

Base accel. 〈αB=50 gal〉

Base accel. 〈αB=100 gal〉

Base accel. 〈αB=200 gal〉



Accel. Scale
0 500gal

Accel. Scale
0 1000gal

Accel. Scale
0 2000gal

Model scale
0 50 100m

Fig. 5.5 Distribution of response acceleration 【abutment 1:2.0】

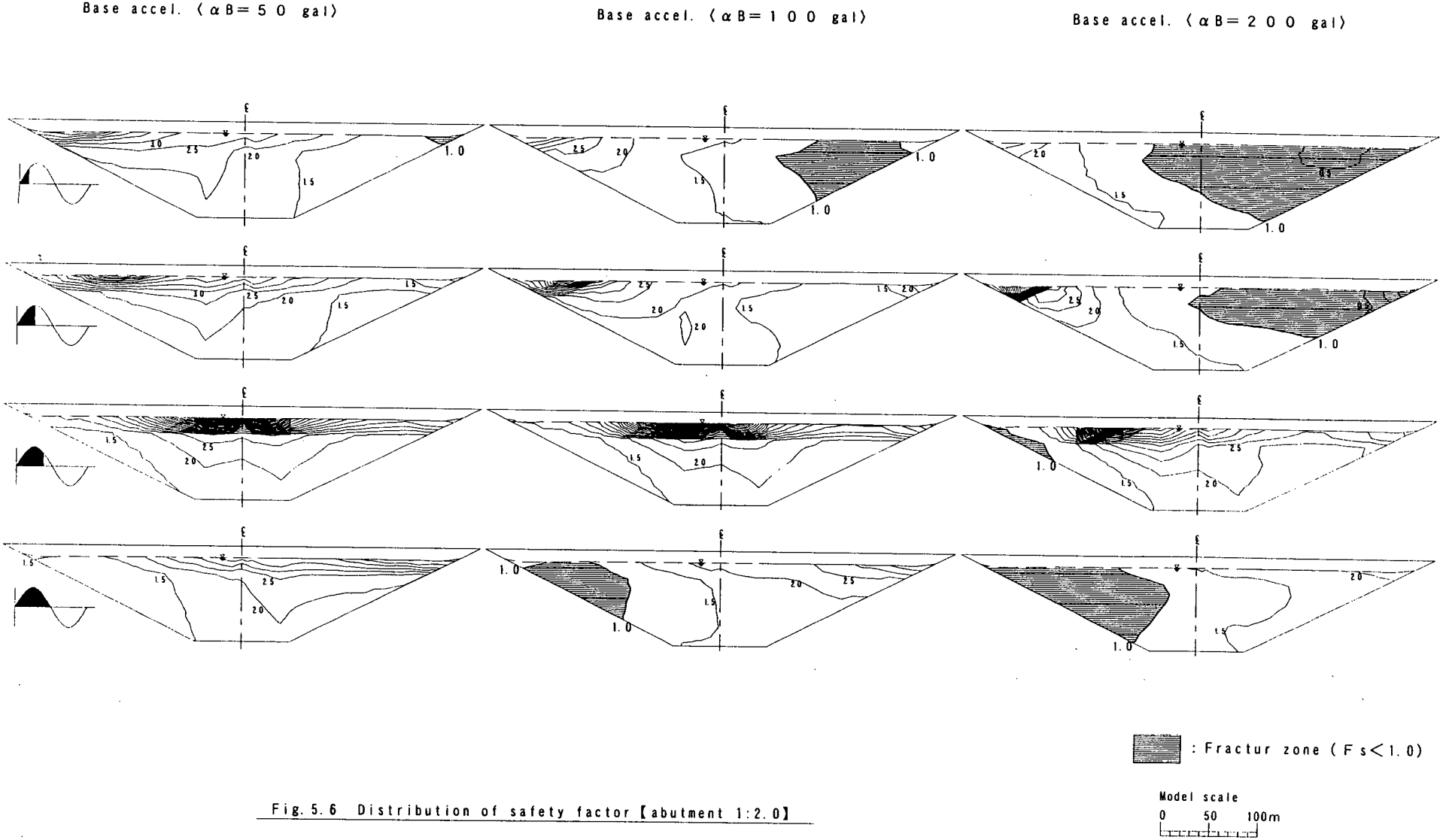


Fig. 5.6 Distribution of safety factor [abutment 1:2.0]

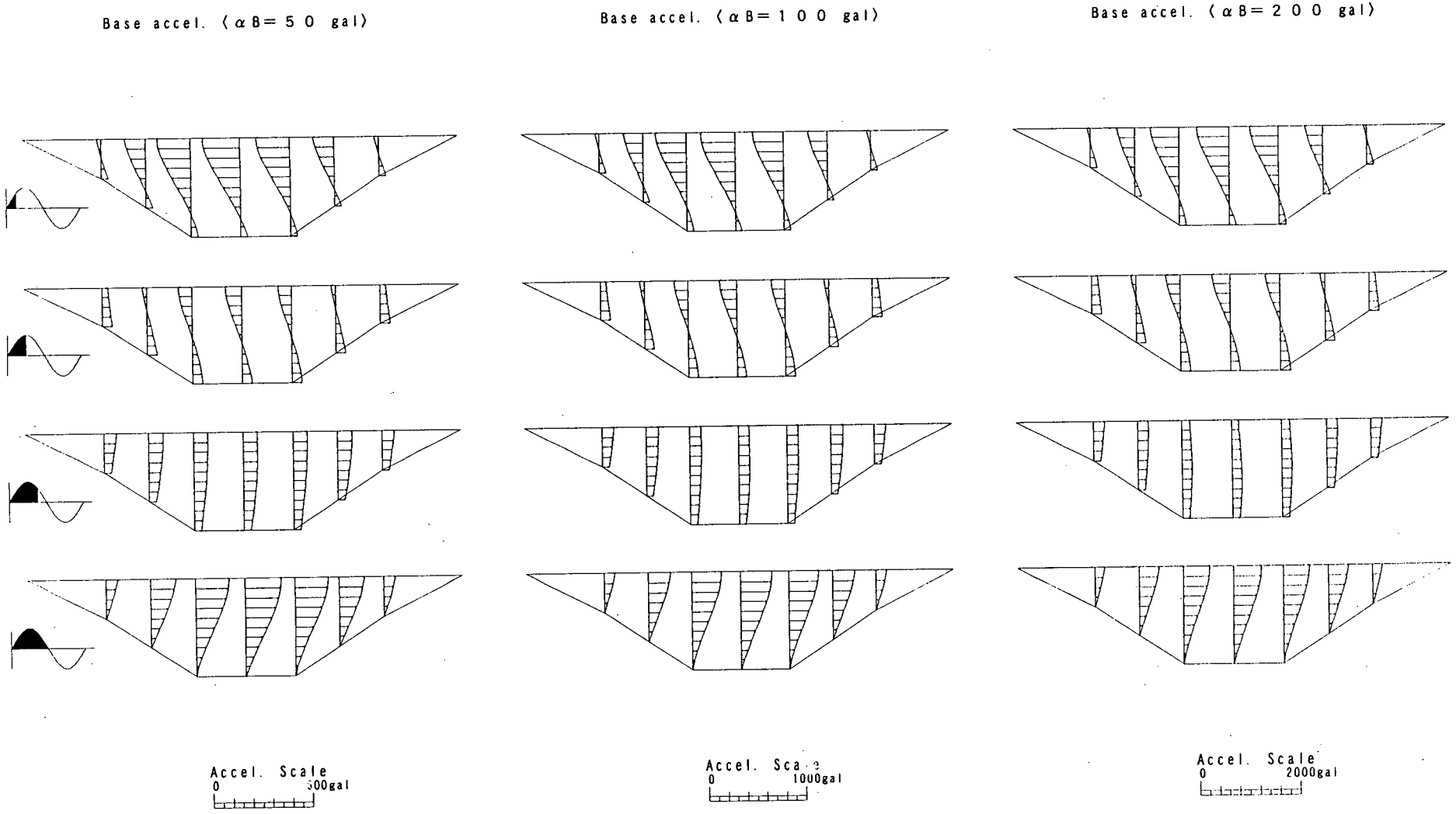


Fig. 5.7 Distribution of response acceleration [abutment 1:S(1.5, 2.0)]

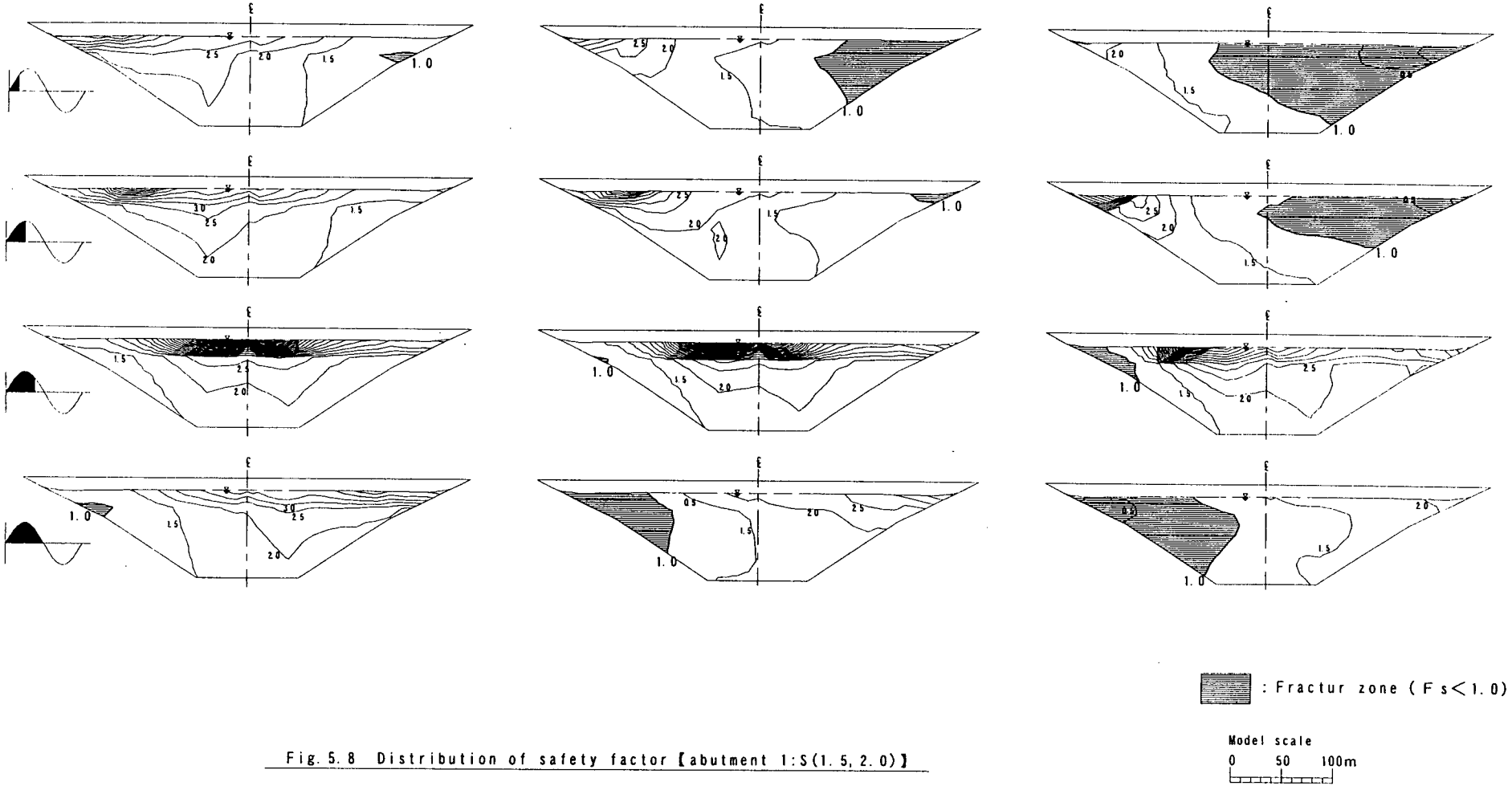


Fig. 5.8 Distribution of safety factor [abutment 1:S(1.5, 2.0)]

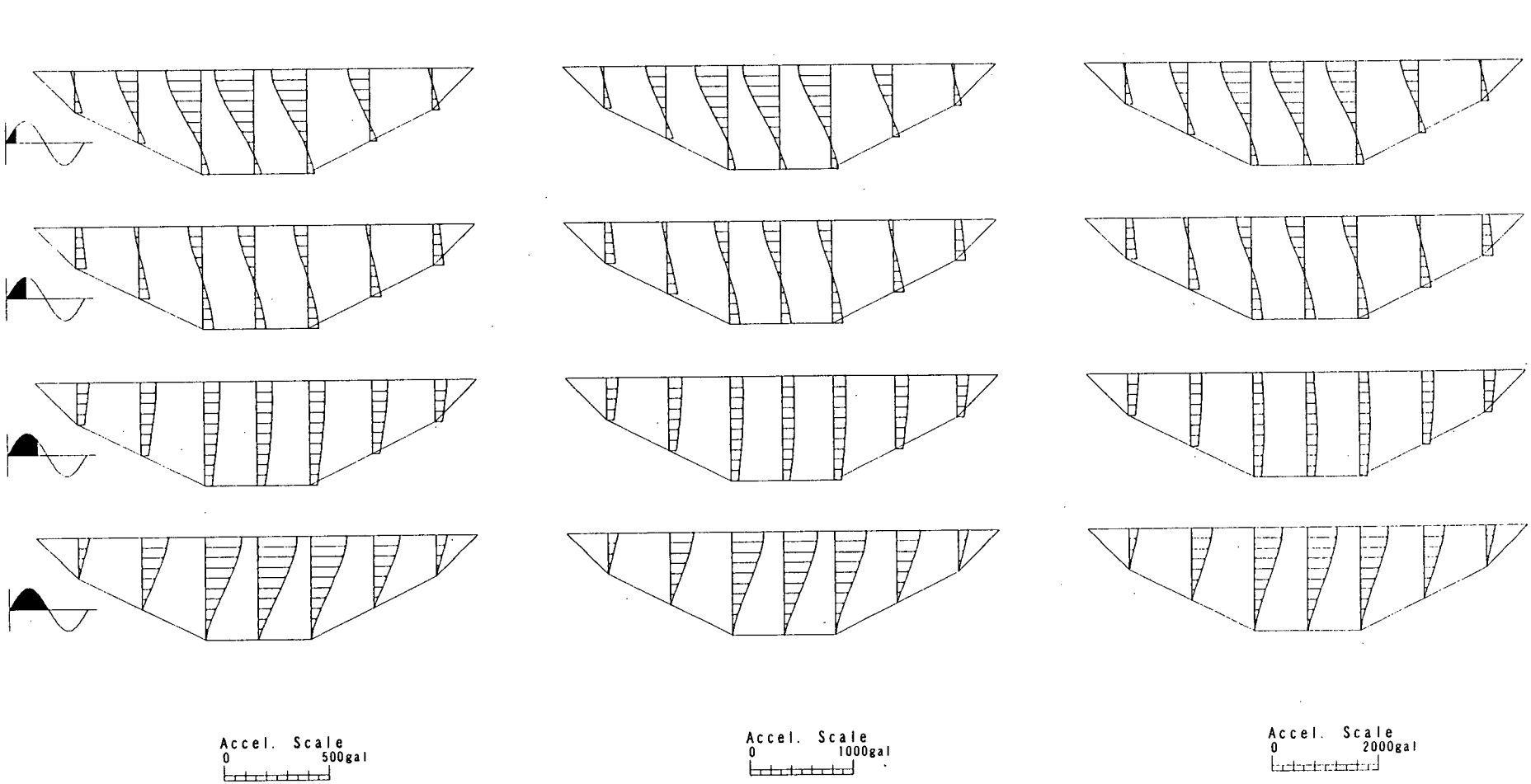


Fig. 5.9 Distribution of response acceleration【abutment 1:SS(2.0, 1.0)】

Base accel. 〈αB＝５０ gal〉

Base accel. 〈αB＝１００ gal〉

Base accel. 〈αB＝２００ gal〉

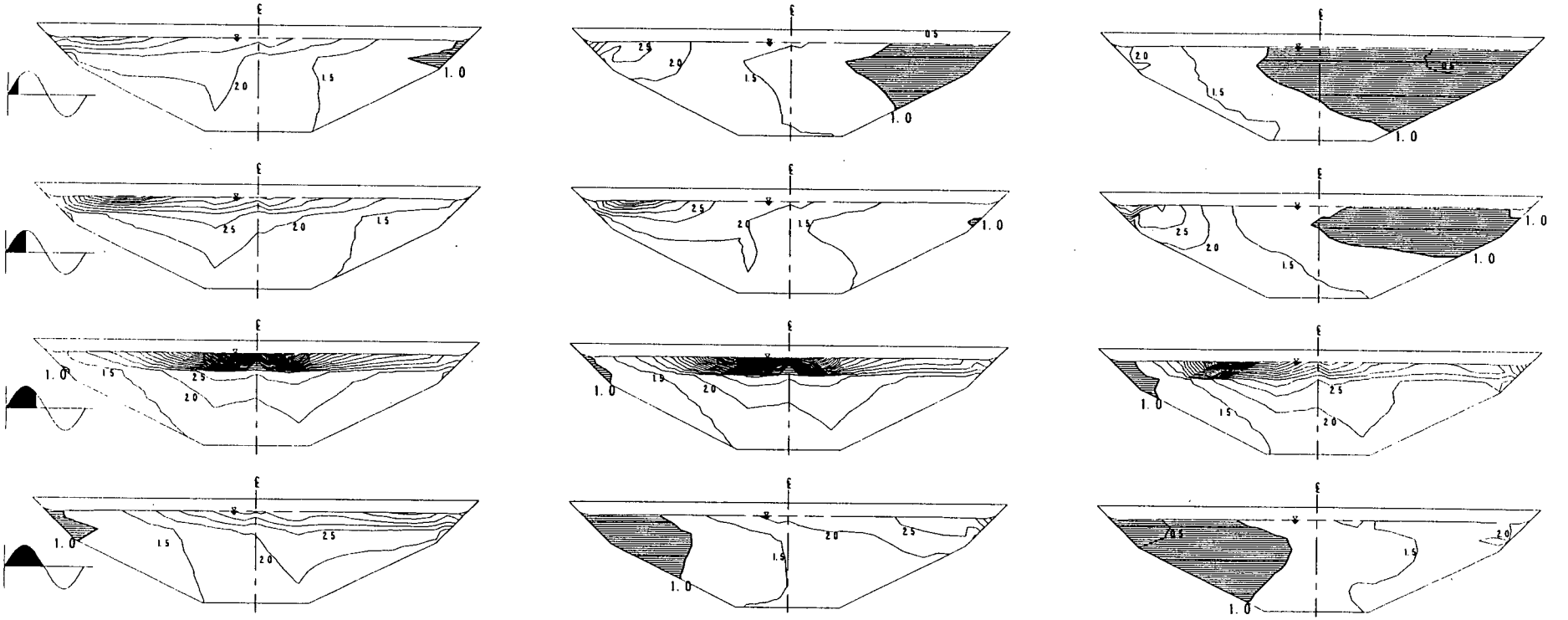


Fig. 5.10 Distribution of safety factor 【abutment 1:SS(2.0, 1.0)】

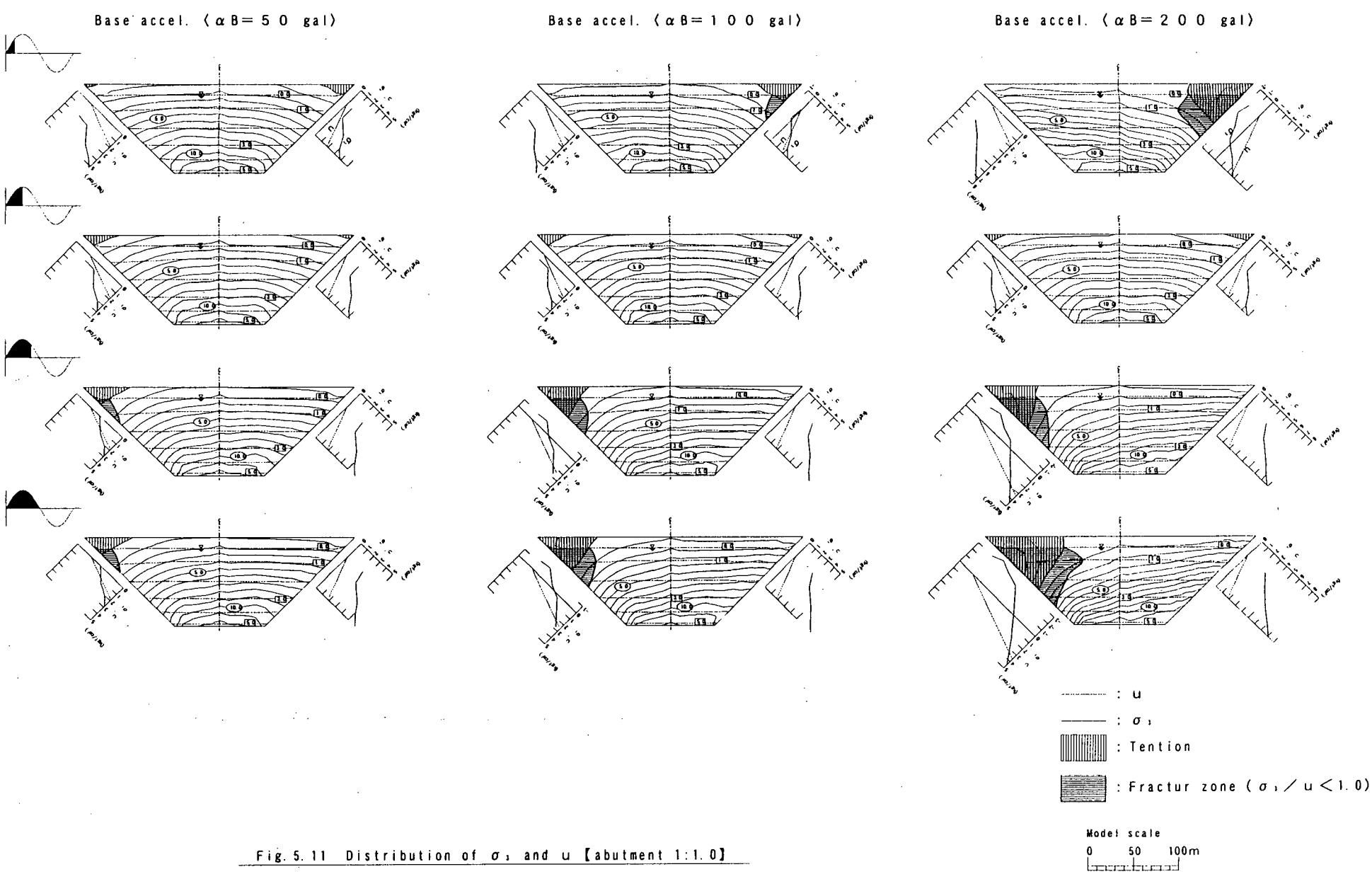


Fig. 5.11 Distribution of σ_1 and u 【abutment 1:1.0】

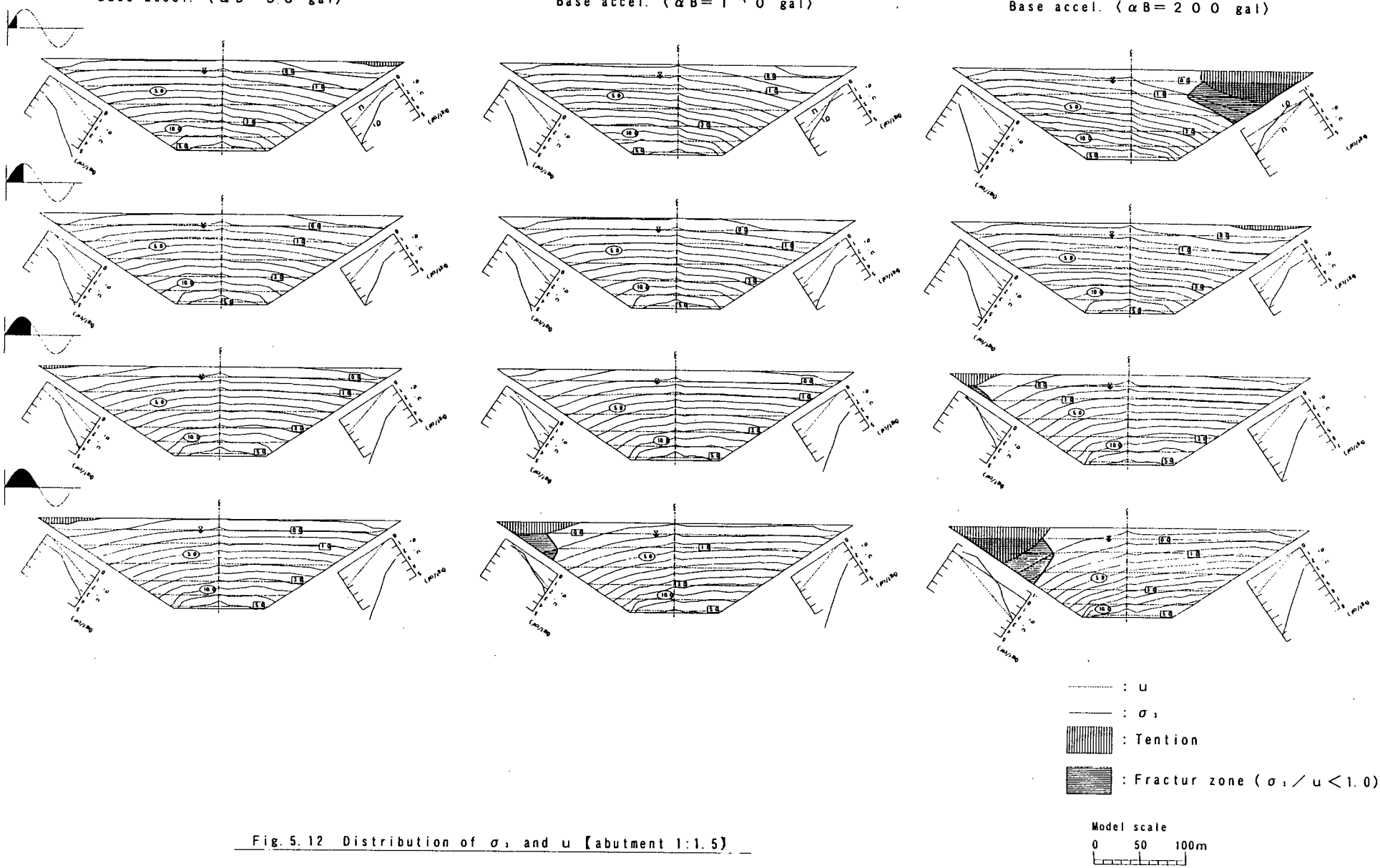


Fig. 5.12 Distribution of σ_1 and u 【abutment 1:1.5】

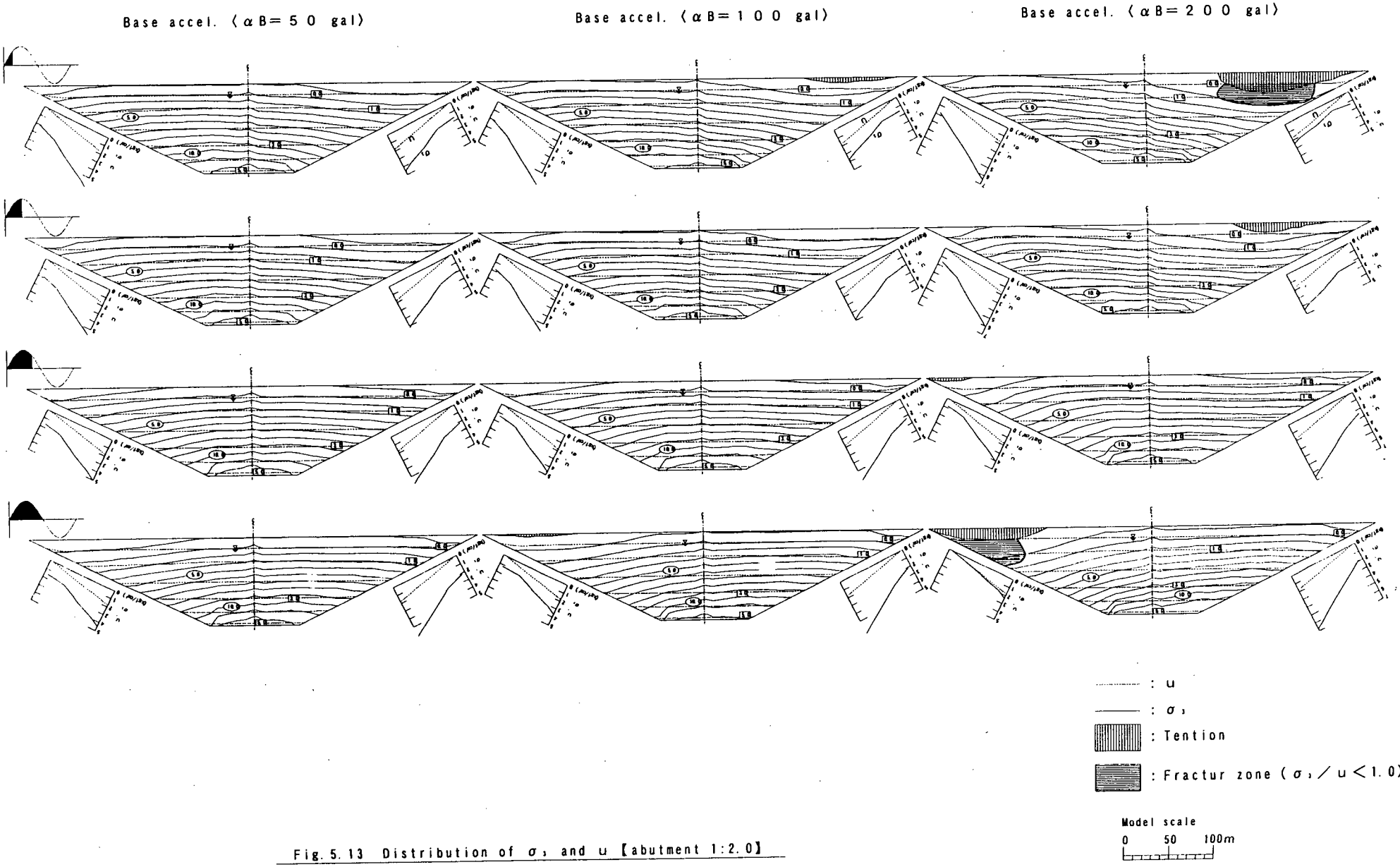


Fig. 5.13 Distribution of σ_3 and u 【abutment 1:2.0】

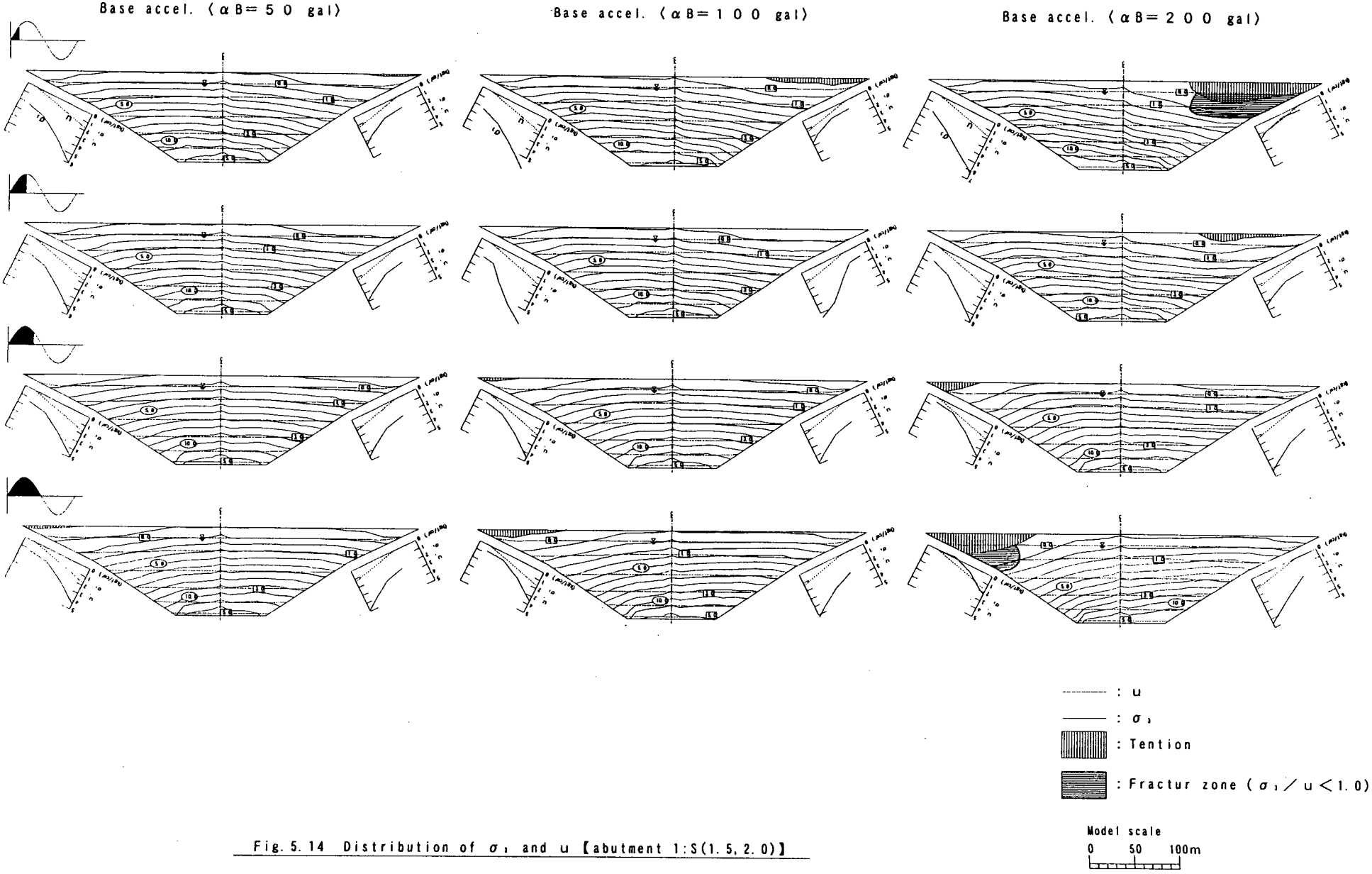


Fig. 5.14 Distribution of σ_1 and u 【abutment 1:S(1.5, 2.0)】

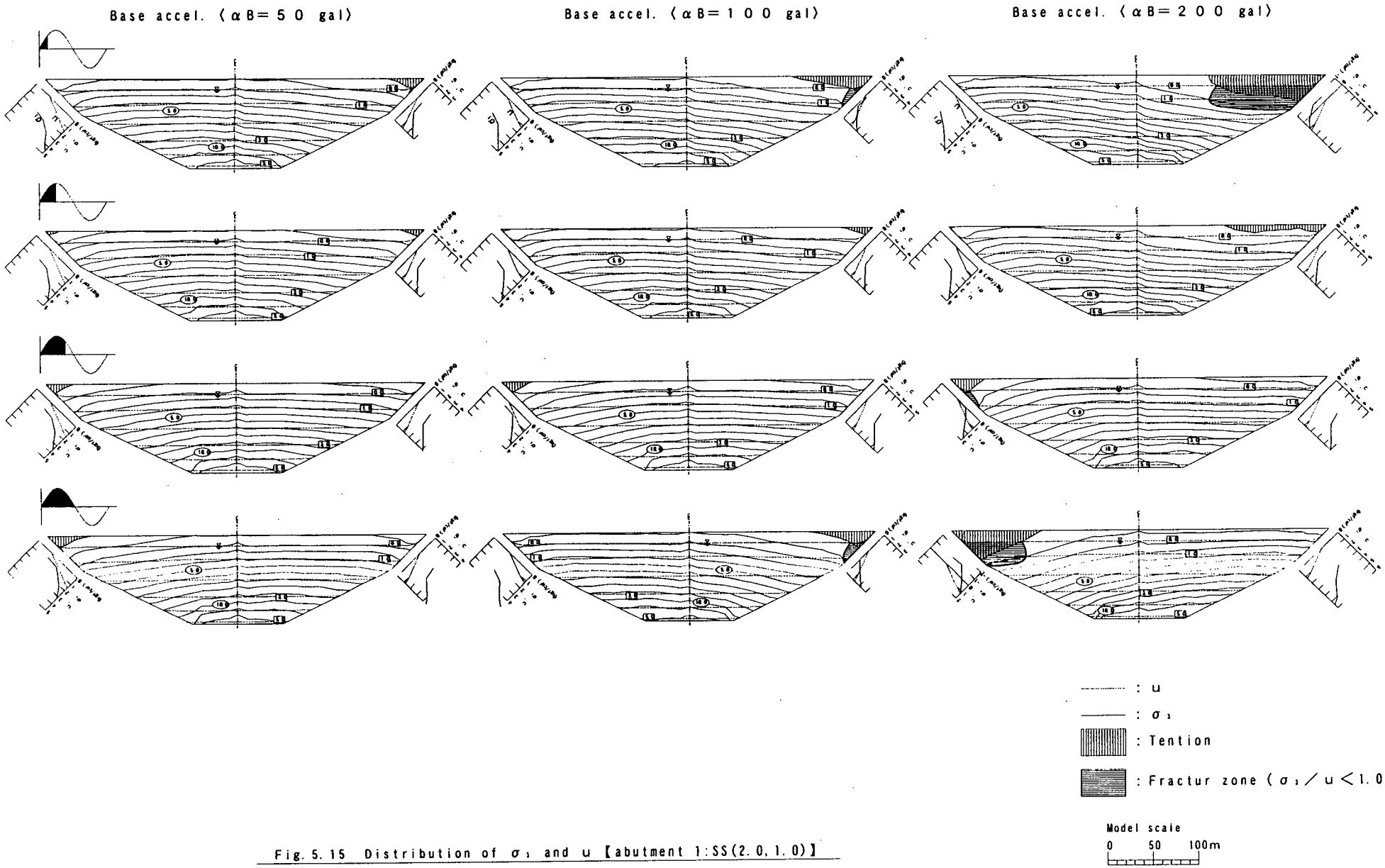


Fig. 5.15 Distribution of σ_3 and u 【abutment 1:SS(2.0, 1.0)】

INFLUENCE OF CONFINING STRESS ON LIQUEFACTION RESISTANCE

Mary E. Hynes and **Richard S. Olsen**

U.S. Army Engineer Waterways Experiment Station
3909 Halls Ferry Road
Vicksburg, Mississippi 39180-6199 (USA)
E-mail: olsenr@ex1.wes.army.mil

ABSTRACT

The confining stress factor K_s is used in liquefaction evaluations to extend empirical charts for liquefaction resistance to confining stresses higher than the empirical field-performance database, approximately 1 atm. Estimates of K_s from Harder (1988) and Hynes (1988) indicated relatively large reductions in liquefaction resistance ratios with increasing confining stress. Laboratory work by Vaid and colleagues (1985, 1995) indicated higher values of K_s. In this study, a database was developed to investigate the reasons for the broad scatter in K_s. From our study we conclude that: 1) K_s is strongly influenced by method of deposition, stress history, aging effects, and density; 2) reconstructed, pluviated specimens in the laboratory may represent recently deposited dredged materials or recently liquefied materials; however, 3) high quality undisturbed samples are needed to determine field-relevant values of K_s. The MCEER International Liquefaction Committee (Youd and Idriss 1997) adopted the K_s recommendations from this study.

Deformation Characteristics of Coarse-grained Materials in Cyclic and Monotonic Loading Triaxial Tests

Yoshikazu YAMAGUCHI[1], Tsuneo UESAKA[2], Hitoshi YOSHIDA[3]
Tomoya IWASHITA[1] and Jun MATSUURA[4]

ABSTRACT

Cyclic and monotonic loading triaxial tests on coarse-grained materials were performed. The effects of bedding errors at the top and bottom ends of specimens on the test results were evaluated by comparing axial strains measured externally and locally. As the strain of a soil material is larger, its stiffness decays, which indicates strain-dependency of the stiffness. The effects of the loading pattern for the testing, the grain shape of tested materials and the relative density of specimens on the strain-dependency of the Young's modulus of coarse-grained materials were also evaluated. In addition, the strain-dependency of the Young's modulus of coarse-grained materials was compared with that of fine sands.

Key Words: *bedding error,*
coarse-grained materials,
triaxial test,
Young's modulus.

1. INTRODUCTION

It is important to evaluate the non-linear deformation properties of granular materials such as rockfill and gravel materials for earthquake response analyses of rockfill dams and structures constructed on gravel deposits. The deformation properties of coarse-grained materials in a range of shear strains less than 0.1% are very significant input material properties for dynamic analyses. Because the deformation properties of coarse-grained materials have been evaluated with large-scale triaxial tests, it is essential to improve the precision of the material stiffness measurement with triaxial tests. When axial displacement is measured externally, the axial strain may be over-estimated due to the bedding error between the ends of the specimen and the cap and pedestal of the triaxial cell. The bedding error is caused by the looseness at the ends of the specimen and a poor fit between the specimen ends and the cap or the pedestal. The effect of the bedding error is larger for the tests on dense specimens of coarse-grained materials prepared in the laboratory than for tests on fine sands

1)Senior Research Engineer, Fill Dam Division, Public Works Research Institute (PWRI), Ministry of Construction, Tsukuba, Japan.
2) Director, Dam Department, PWRI, ditto.
3) Head, Fill Dam Division, PWRI, ditto.
4) Research Engineer, ditto.

(Tatsuoka *et al.*, 1992). This study confirms the effect of the bedding error in large-scale triaxial tests on coarse-grained materials having angular and round grain shapes. As the strain of a soil material increases, its stiffness decays, which indicates strain-dependency of the stiffness, that is, non-linear deformation properties. The strain-dependency of stiffness is affected by the difference in materials, specimen conditions, and testing methods, etc. We evaluate the effect of the loading pattern for the testing, the grain shape of materials and the relative density of specimens on the strain-dependency of Young's modulus of coarse-grained materials. We also compare the strain-dependency of Young's modulus of coarse-grained materials with that of fine sands.

2. TESTED MATERIALS

Two kinds of coarse-grained materials were prepared for the test. One is crushed rock (CRR) with angular shape, the other is riverbed gravel (RBG) with round shape. The physical properties of both materials are shown in **Table 1**. The grain size distribution curve of both materials is the same as shown in **Figure 1**.

3. EXPERIMENTAL METHOD

Triaxial tests on large specimens with a diameter of 300 mm and a height of 600 mm were performed. **Photo. 1** shows the triaxial testing apparatus. A load cell installed inside the triaxial cell and combined with the cap of a specimen measured the axial load free from the effect of piston friction. The local and external axial strains in a small range were measured. The local axial strains were measured by means of a local deformation transducer (LDT). The LDT is a thin strip of phosphor bronze on which a couple of strain gauges are attached at the central part of each side of the surface. The LDT strip is 500 mm long, 5 mm wide, and 1.2 mm thick, as shown in **Photo. 2**, and measured the deformation of the central part (approx. 470 mm) of the lateral surface of the specimen excluding the ends of the specimen, as shown in **Photo. 3**. The external axial strains (EXT) were measured from the displacement of a specimen cap to which a couple of targets were attached, using gap sensors installed on column standings fixed on the base of the triaxial cell, as shown in **Photo. 4**.

The specimens were prepared by the compaction of materials with an electric vibrator in six layers. The specimens were set up in two kinds of relative density Dr of 50% (loose) and 85% (dense) for CRR, only 85% (dense) for RBG. The top and bottom ends of the specimens were in contact with a porous stone disk fixed to the cap and pedestal. The specimens were then saturated until a B-value of at least 0.95 was reached.

Consolidated drained triaxial tests were carried out with two loading patterns of cyclic loading (CL test) and monotonic compression loading (ML test). The CL tests were performed by staged confining pressure testing in the each stage of which the confining pressure $\sigma c'$ was gradually increased from lower pressure to higher pressure, that is, 0.1, 0.2, 0.39, 0.59 MPa. **Figure 2** shows a schematic figure of the process of the staged loading. At each loading stage with the constant confining pressure, twelve cycles of symmetric sinusoidal cyclic axial stresses with constant amplitude of deviator stress were applied at a loading frequency of 0.1 Hz on the specimen. As the stiffness of the specimen, the equivalent

Young's modulus *Eeq* was obtained using the hysteresis loop of the tenth cyclic loading as shown in **Figure 3** (a). The data of loads and displacements were filtered for more than 1.0 Hz and less than 0.0001 Hz. In the ML tests, a constant axial strain rate of 0.5 %/min was used. At the start of an operation, the loading piston and the triaxial chamber piston were separated to avoid the strain history acting on the specimen during the action of combining the pistons. At the time of the pistons contacting and load acting on a specimen just after the start of operation, the strain was defined as zero. The data of loads and displacements were fed at a sampling frequency of 200 Hz, and were filtered for more than 2.0 Hz. As the stiffness of the specimen, the secant Young's modulus *Esec* was obtained for each sampling data as shown in **Figure 3** (b).

4. TEST RESULTS

(1) Effects of Bedding Error

The effects of the bedding error on strain measurements of gravels obtained from triaxial tests have been reported by several researchers (Tatsuoka *et al.*, 1994, Hamano *et al.*, 1995, Tanaka *et al.*, 1995). We compared the strain measurements from the LDT and the EXT for the tests on CRR and RBG. **Figure 4** shows the relationships between *Eeq* and the single amplitude axial strain $(\varepsilon a)sa$ from the CL tests on dense CRR and dense RBG, and **Figure 5** shows the relationships between the deviator stress $(\sigma_1 - \sigma_3)$ and the axial strain εa from the ML tests. The Young's modulus *Eeq* and the deviator stress $(\sigma_1 - \sigma_3)$ measured by the LDT are greater than those by the EXT for both the CL and ML tests. At an elastic range of $(\varepsilon a)sa$ of 10^{-5} or less, the differences of the stiffness are between 5% and 25% for the CL tests on both CRR and RBG.

(2) Comparison of Stiffness from Cyclic Loading and Monotonic Loading Tests

Figure 6 shows the strain-decay curves of the Young's moduli *Eeq* and *Esec* from the CL and ML tests plotted against $(\varepsilon a)sa$ for the CL tests and εa for the ML tests respectively. The axial strains measured by the LDT are used for the arrangement of the figure. For a range of small axial strain less than 10^{-5}, the Young's modulus from the CL test and that from the ML test almost agree for both CRR and RBG. The moduli at the small strain are constant, which means that the behavior is elastic.

The rates of decay of the two Young's moduli *Eeq* and *Esec* from the CL and ML tests respectively begin to differ for a range of axial strain more than about 5×10^{-5}. On the loose specimen, whose relative density Dr = 50%, the decay in the Young's modulus with increase in axial strain is smaller in the CL tests than in the ML tests. On the dense specimen, whose Dr = 85%, the decay in the Young's modulus with increase in axial strain is, however, a little larger in the CL tests than in the ML tests. **Figure 7** shows hysteresis loops with single amplitude axial strain $(\varepsilon a)sa$ of about 2×10^{-4} from the CL tests on CRR specimens with Dr of 50% and 85%. The cyclic strain of the loose specimen moves to the compressive side, so the hysteresis loop is not closed. The equivalent Young's modulus *Eeq* in **Figure 6 (a)**, thus, is somewhat overestimated, but only by about 3%, and the decay of *Eeq* is unchanged from the tendency noted above.

Several researchers (Tatsuoka *et al.*, 1994, Hamano *et al.*, 1994) have reported the

comparisons between the locally measured stiffness of sand from the CL and the ML tests. **Figure 8** shows the strain decay curves of the Young's moduli, *Eeq* and *Esec*, from the CL and the ML tests on loose (Dr = 45%) and dense (Dr = 70%) Toyoura sand which is Japanese fine sand (Tatsuoka *et al.*, 1994). It can be seen from **Figure 8** that, on sand also, the Young's modulus *Eeq* from the CL tests agrees well with the *Esec* from the ML tests in a range of axial strain less than about 10^{-5}. The strain-dependency of Young's moduli *Eeq* and *Esec* of sands, however, differs from that of coarse-grained materials shown in **Figure 6**. Regardless of the relative density of the sand specimens, the strain-dependency of Young's modulus of sand is smaller in the CL tests than in the ML tests in a range of more than about 5×10^{-5}.

Comparing **Figures 6** and **8**, the strain-dependency of Young's moduli *Eeq* and *Esec* of dense coarse-grained materials differs from that of dense sands. The strain-decay of Young's modulus of dense coarse-grained materials is a little larger in the CL tests than in the ML tests. On the other hand, the strain-decay of dense sands is smaller in the CL tests than in the ML tests. Dong *et al.* (1994) also reported similar results from the tests on several gravels having nearly maximum density, with the results for this set of tests on both the dense CRR and RBG specimens. Dong *et al.* explained these phenomena as follows. This difference between the deformation properties of sands in the CL tests and the ML tests is primarily due to the effect of cyclic strain-hardening; i.e., the increase in the stiffness due to the change in the structure by drained cyclic loading itself. In the case of CL tests on dense gravels with constant confining pressure, however, due to the high stiffness, as the cyclic strain amplitude becomes large, a reduction in the axial stress (thus the reduction in the mean stress) when loaded in triaxial extension becomes very large. This mechanism overwhelms the effect of cyclic strain-hardening. The main reason why the strain-decay of Young's modulus of loose CRR specimens is similar to that of sands is that the effect of cyclic strain-hardening overwhelms the effect of a reduction in the mean stress.

5. CONCLUSIONS

The test results of the cyclic and monotonic triaxial tests on loose and dense coarse-grained materials are summarized as follows.

[1] Due to the bedding error, the Young's modulus externally measured from the displacement of a cap was 5% to 25% smaller than the locally measured modulus for this test set on coarse-grained materials.

[2] The Young's modulus from cyclic loading and that from monotonic loading tests almost agreed in a range of small axial strain less than 10^{-5}.

[3] The strain-decay of Young's moduli *Eeq* and *Esec* of dense coarse-grained materials from cyclic loading and monotonic loading tests differed from that of loose coarse-grained materials. Comparing the results of coarse-grained materials with that of sands, the strain-decay of Young's modulus in cyclic loading and monotonic loading tests on loose coarse-grained materials was similar to that of the sands. The strain-decay of Young's modulus of dense coarse-grained materials, however, was different from that of sands.

REFERENCES

Dong, J., Nakamura, K., Tatsuoka, F. and Kohata, Y. (1994): Deformation Properties of Gravels in Triaxial Compression Tests and Cyclic Triaxial Tests, *Pre-failure Deformation of Geomaterials*, Balkema, pp.17-23.

Hamano, M., Toriihara, M. and Hirama, K. (1994): Comparison between Static and Dynamic Modulus of Deformation Using Small Strain Gauge, *Proc. the 29th Japan National Conference on Soil Mechanics and Foundation Engineering*, Japanese Society of Soil Mechanics and Foundation Engineering, pp.763-764. (in Japanese)

Hamano, M., Toriihara, M. and Hirama, K. (1995): Dynamic Deformation Properties of Gravel Changed Grain Size Using Small Strain Gauge, *Proc. the 30th Japan National Conference on Soil Mechanics and Foundation Engineering*, Japanese Society of Soil Mechanics and Foundation Engineering, pp.957-958. (in Japanese)

Tanaka, Y., Kokusho, T., Okamoto, T. and Kudo, K. (1995): Effect of Non-uniformity on Dynamic Deformation Properties of Gravel, *Proc. the 50th Annual Conference of Japan Society of Civil Engineers*, Vol. Ⅲ, pp.460-461. (in Japanese)

Tatsuoka, F. and Shibuya, S. (1992): Deformation Characteristics of Soils and Rocks from Field and Laboratory Tests, *Report of the Institute of Industrial Science*, The University of Tokyo, Vol.37, No.1.

Tatsuoka, F., Teachavorasinskun, S., Dong, J., Kohata, Y. and Sato, T. (1994): Importance of Measuring Local Strains in Cyclic Triaxial Tests on Granular Materials, *Dynamic Geotechnical Testing*, Vol. Ⅱ, ASTM STP 1213, pp.288-302.

Table 1 Physical properties of the tested materials

		CRR	RBG
Density of soil particles	ρ s (g/cm^3)	2.93	2.56
Water content	w (%)	0.54	1.03
Maximum void ratio	Emax	0.569	0.432
Minimum void ratio	Emin	0.142	0.167
Maximum grain size	Dmax (mm)	63.0	63.0
50% passing grain size	D50 (mm)	10.2	10.2
Uniformity coefficient	Uc	30	30
Grain shape		angular	round

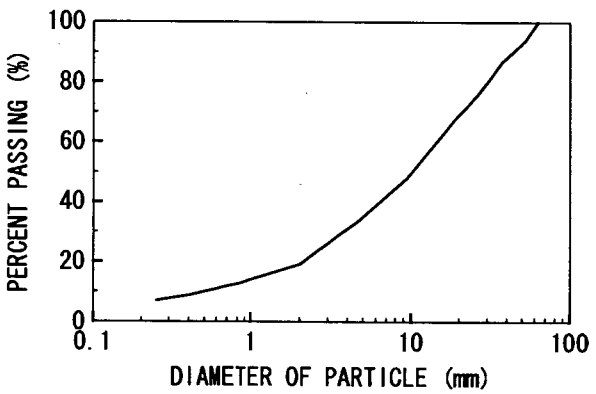


Figure 1 Grain size distribution curve of the tested materials

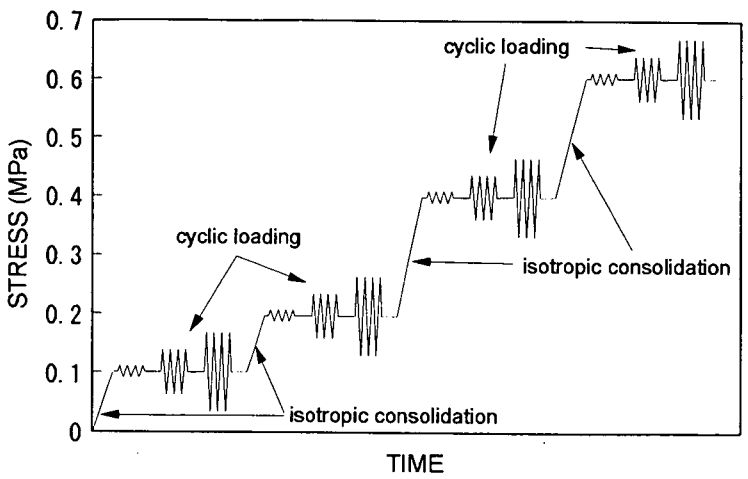


Figure 2 Illustration of process of cyclic loading test

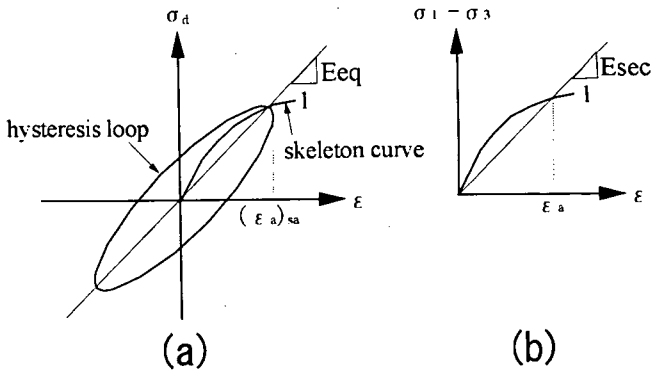


Figure 3 Definitions of Young's moduli from (a) cyclic and (b) monotonic loading

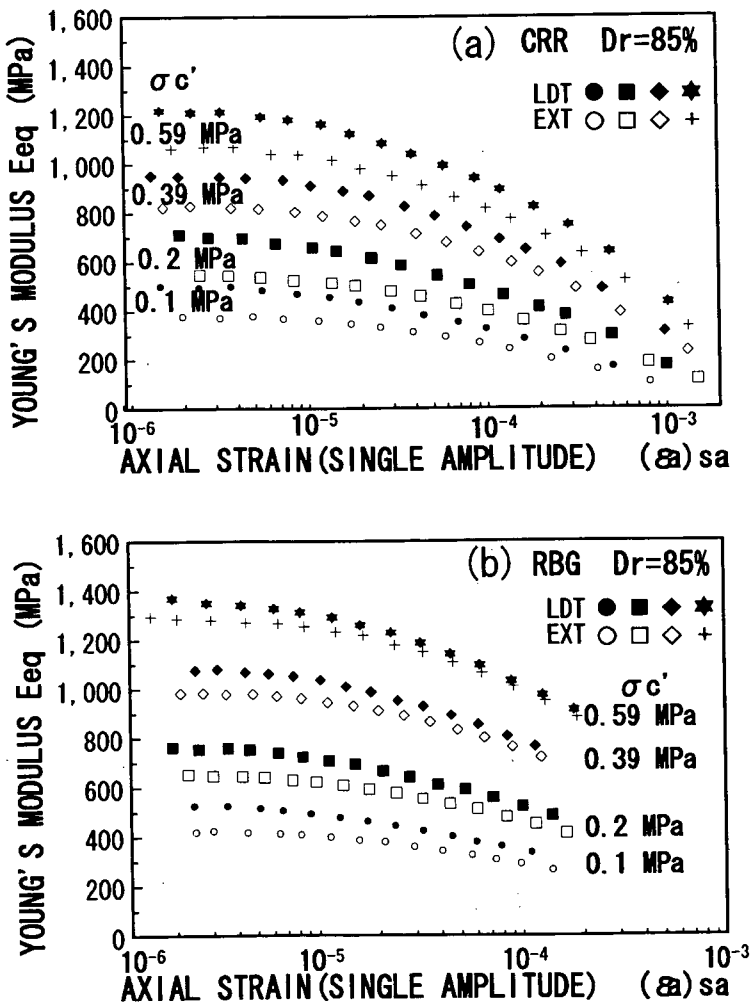


Figure 4 Comparisons of *Eeq-(εa)sa* measured locally and externally in cyclic loading triaxial tests; (a) dense CRR and (b) dense RBG

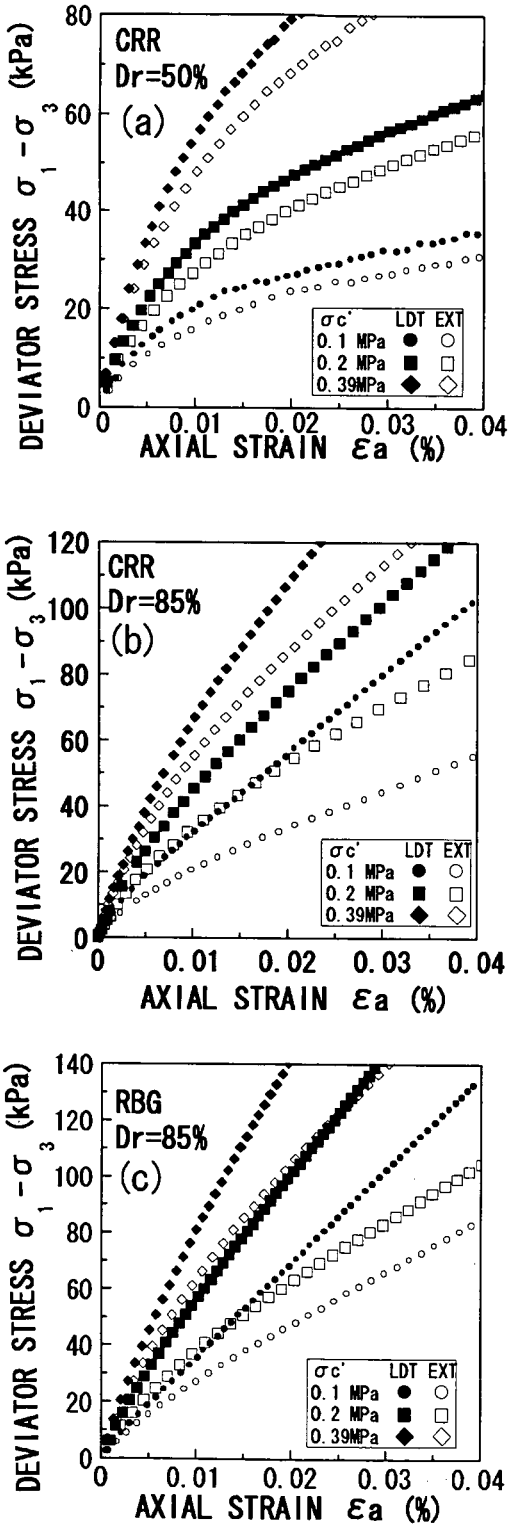
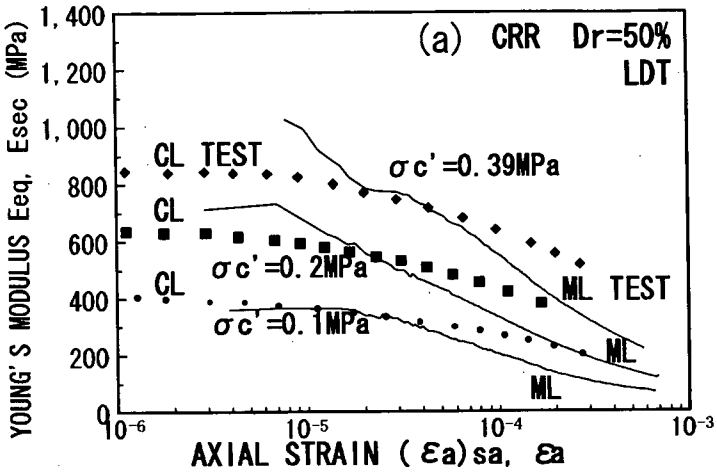
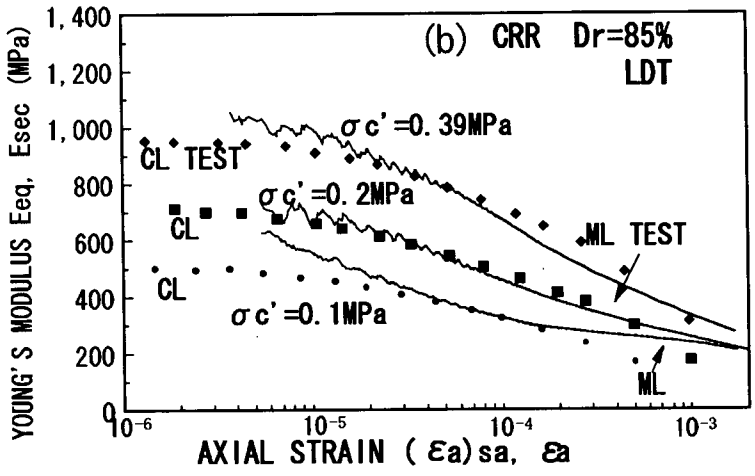


Figure 5 Comparisons of deviator stress- εa measured locally and externally in monotonic loading triaxial tests; (a) loose CRR, (b) dense CRR and (c) dense RBG





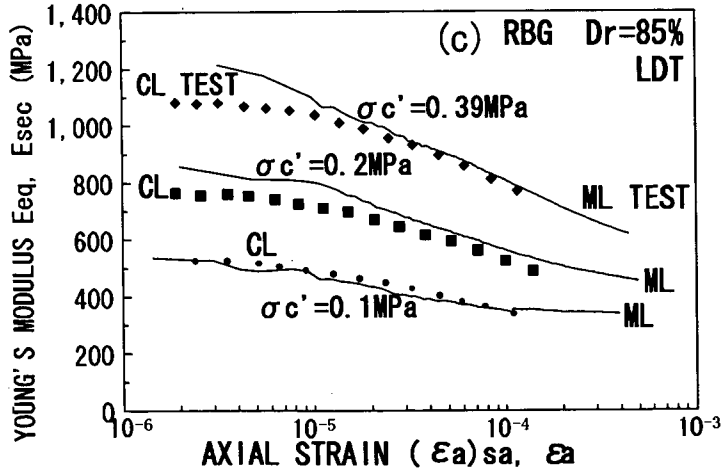


Figure 6 Comparisons of *Eeq-(εa)sa* from cyclic loading tests and *Esec-εa* from monotonic loading tests; (a) loose CRR, (b) dense CRR and (c) dense RBG

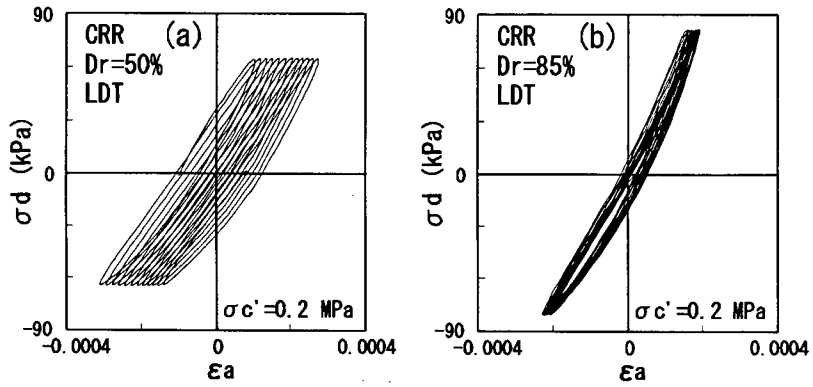


Figure 7 Hysteresis loops from cyclic loading tests at $(\varepsilon a)sa = 2 \times 10^{-4}$; (a) loose CRR and (b) dense CRR

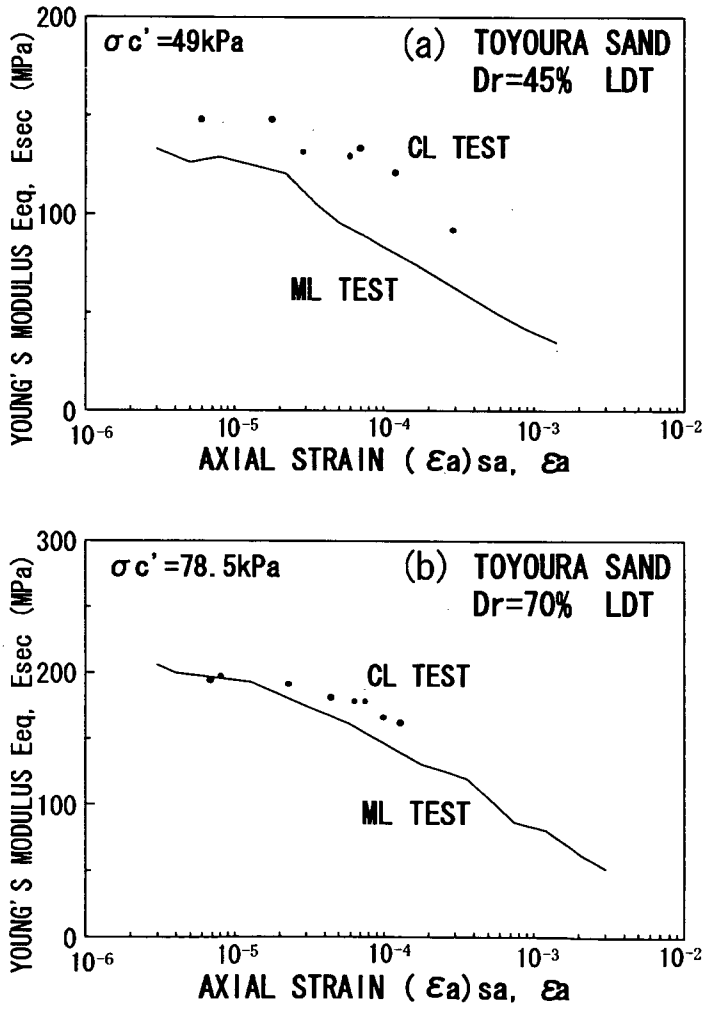


Figure 8 Comparisons of *Eeq-(εa)sa* from cyclic loading tests and *Esec-εa* from monotonic loading tests; (a) loose Toyoura sand and (b) dense Toyoura sand (Tatsuoka *et al.*, 1994)

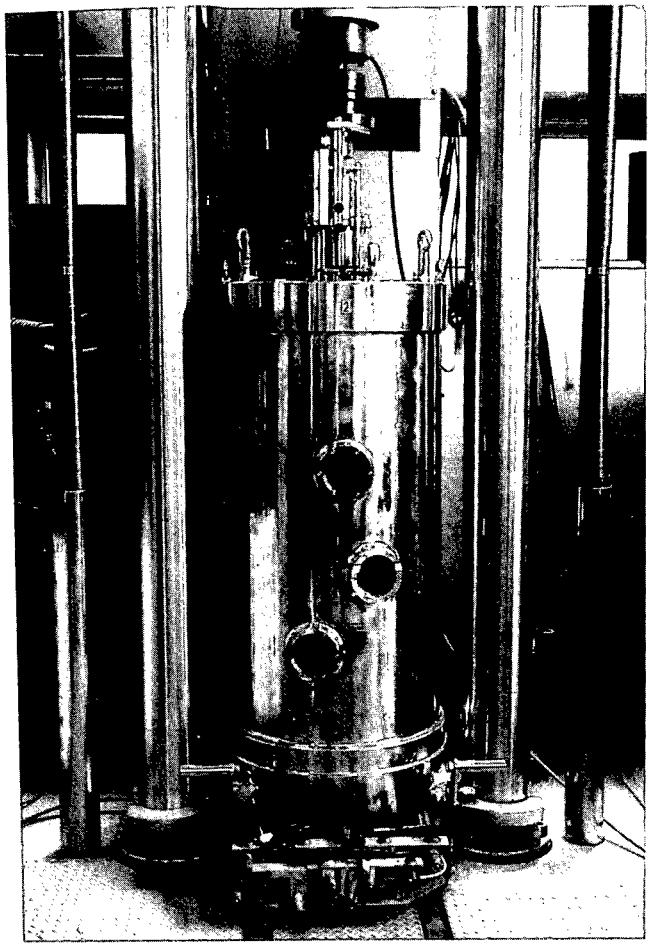


Photo. 1 External view of large-scale triaxial testing apparatus

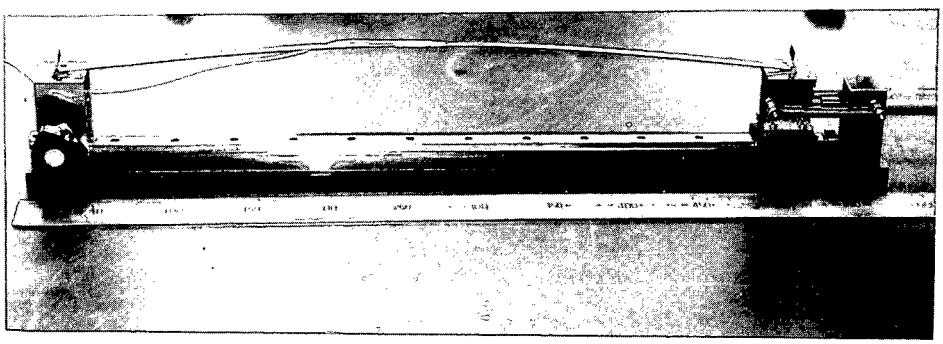


Photo. 2 Local deformation transducer (LDT)

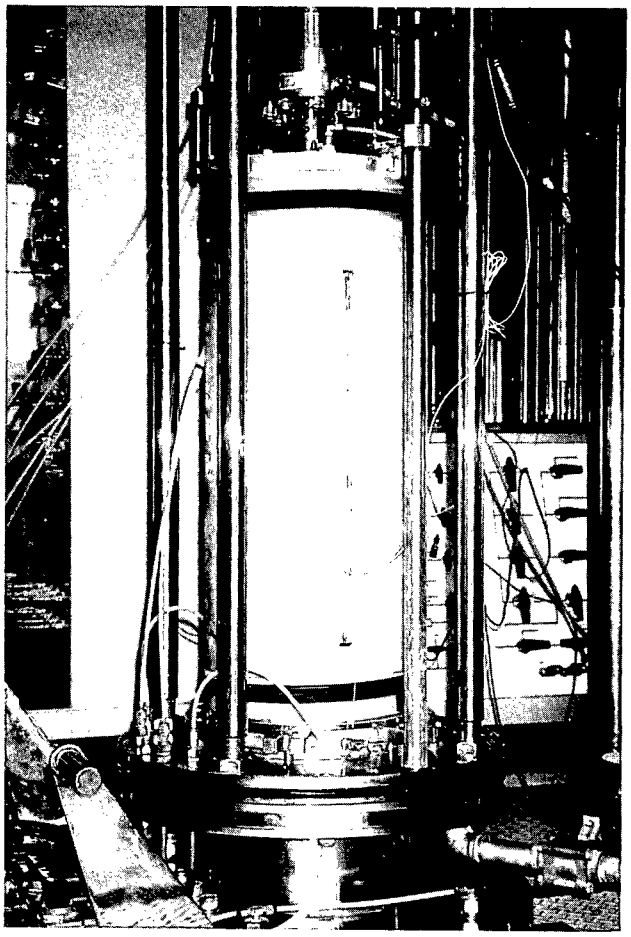


Photo. 3 LDT attached on the side of a specimen of coarse-grained materials

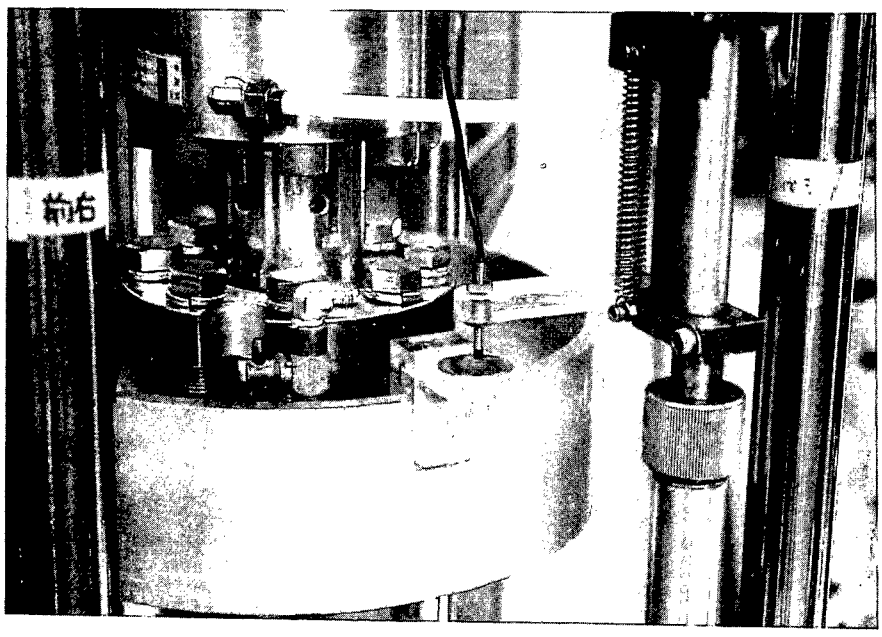


Photo. 4 Gap sensor and target attached on the top cap of a specimen

Technical Session 3

Embankment Dams (2)

PENETRATION TESTING OF LIQUEFIED GRAVELS AT SEWARD, ALASKA

Joseph P. Koester[1], Chris Daniel[2], and Michael L. Anderson[3]

(Adapted from draft report submitted for publication at Transportation Research Board Annual Meeting, January 2000)

ABSTRACT

A series of dynamic in situ penetration tests were performed in deep alluvial gravel deposits at Seward, Alaska that were shaken and apparently liquefied by the March 27, 1964 Alaska Earthquake. Both a US Standard Penetration Test split spoon and a larger diameter drive sampler were used, and dynamic cone penetrometers of two sizes were also driven into the gravels near the mouth of the Resurrection River that had exhibited settlement and lateral spreading consequent to earthquake shaking. Two safety hammers were employed (nominally 140 lbs, or 623 N, and 300 lbs, or 1334 N), and the energy delivered using various hammer and penetrometer combinations was measured throughout all tests. Limited measurements were also made of hammer velocity, using a radar system developed for that purpose, to allow for kinetic energy determination. Soils recovered in the split spoon samplers were sent to the US Army Engineer Waterways Experiment Station Soils Research Facility in Vicksburg, Mississippi, where they were evaluated for classification (gradation and index properties). This paper summarizes the sampling and testing procedures used at the Seward site, as well as preliminary analysis of the various penetration test results. Comparisons are also made to penetration resistance measurements made by the Alaska Highway Department immediately following the 1964 earthquake. Results of this investigation will be adapted to guide future practice for in situ determination of liquefaction resistance in coarse alluvial soils.

KEYWORDS: liquefaction, gravels, penetration test, dynamic energy measurement

ACKNOWLEDGMENTS

The tests described and the resulting data presented herein, unless otherwise noted, were obtained from research conducted under the Earthquake Engineering Research Program of the United States Army Corps of Engineers. Permission was granted by the Chief of Engineers to publish this information. The authors are grateful to the participants in the field study, namely:

---

[1]Research Civil Engineer, Geotechnical Laboratory, U.S. Army Engineer Research and Development Center, Vicksburg, MS (ATTN: CEWES-GG-H), Phone: (601) 634-2202; Fax: (601) 634-3453; e-mail: koestej@wes.army.mil

[2]Research Assistant, In Situ Testing Group, Civil Engineering Department, University of British Columbia, 2324 Main Mall, Vancouver, BC, Canada V6T 1Z4Phone: (604) 822-2637; Fax: (604) 822-6901; e-mail: Daniel@civil.ubc.ca

[3]Civil Engineer, US Army Engineer District, Alaska, Anchorage, AK (CEPOA-EN-G-SG) Phone: (907) 753-2686; Fax: (907) 753-2688; e-mail:Michael.L.Anderson@poa02.usace.army.mil

Messrs. Dan Ackerman and Erick St. Clair, the drilling equipment operators, from the US Army Engineer District, Alaska (CEPOA), whose conscientious and patient attention to a variety of demanding details assured the integrity of the data; Mr. Frank Dieckgraeff, owner of Metco, Inc., for site access and an abundant water supply; BC Hydro and Klohn-Crippen Consultants, Ltd. of Vancouver, BC, for the loan of the energy measurement system and radar devices, respectively; and the financial support and participation of Conetec Investigations, Ltd. and Dr. W. D. Liam Finn of Vancouver, BC, and Prof. John Howie of the Civil Engineering Department of the University of British Columbia, Vancouver, BC. Professor Howie also assisted with the planning of penetration tests and design of push rod subassemblies and adapters and cone penetrometers that were machined by CEPOA for use at the test site.

1. INTRODUCTION

In situ material properties of soils containing gravels and cobbles, including inference of liquefaction resistance and residual strength, are currently estimated by converting results of any of several dynamic penetration tests (Becker Hammer Penetration Test, BPT, Large Penetration Test, LPT, and site-specific variations) to equivalent Standard Penetration Test (SPT) blowcounts. BPT/SPT correlations employed to date for U. S. Army Corps of Engineers projects have considered Becker (diesel combustion) efficiency (in the manner described by Harder and Seed, 1986 and Harder, 1988). Field measurements using Pile Driving Analyzer (PDA) equipment have also shown that BPT efficiency is strongly influenced by mechanical energy losses, including friction acting along the driven casing (Sy, 1993, Sy and Campanella, 1993 and Sy and Campanella, 1994). Improved correlative techniques are needed for interpretation of the results of penetration tests for a variety of situations where post-earthquake stability is of concern.

The U. S. Army Engineer Waterways Experiment Station (WES) is investigating in situ testing methods applied to gravelly soils to determine their response to earthquake ground motions as part of a research program on seismic stability evaluation of reservoir dams. A limited program of dynamic in situ penetration tests was performed in deep alluvial gravel deposits at Seward, Alaska that were shaken and apparently liquefied by the March 27, 1964 Alaska Earthquake. Both a US Standard Penetration Test split spoon and a larger diameter drive sampler were used, and dynamic cone penetrometers of two sizes were driven into the gravels near the mouth of the Resurrection River that had exhibited settlement and lateral spreading consequent to earthquake shaking. It was the author's original intention to perform BPT's in the Seward gravels, but mobility costs for a suitable BPT rig were prohibitively high.

2. BACKGROUND

Liquefaction and consequent post-earthquake instability has been observed during moderate to strong earthquakes in loose to medium dense gravels, both naturally deposited and placed by various artificial processes. Table 1 lists field occurrence data on liquefaction in gravels during earthquakes worldwide during the last 20 years. Unless the gravels known to have liquefied were at or near the ground

surface, there were no in situ testing procedures available prior to the last two decades to confirm or deny the occurrence of liquefaction in gravels in the subsurface. The use of the BPT is widespread, but not standardized as relates to interpretation of test results for liquefaction potential evaluation. Density tests are extremely valuable, but are usually impractical to conduct in saturated gravel deposits at depths greater than about 10 ft (3.05 m). Sampling and testing of gravels is difficult; in situ freezing techniques such as those employed in Japan (e.g., Tanaka, et al., 1989) hold great promise for recovery of high-quality specimens of coarse-grained soils.

3. OBJECTIVES

The objectives of the field test series discussed in this paper were to compare results from a variety of penetration tests performed in a gravelly deposit known to have experienced earthquake-induced liquefaction. This is only one component of the research project, which includes additional field experiments and laboratory chamber investigations of penetration resistance and other engineering measurements in gravels. The overall goals of the sponsoring research project are: to develop and validate procedures to properly adapt penetration test results to estimate in situ cyclic and residual strengths of soils empirically, and to evaluate the adaptation of alternate in situ testing technologies for measuring in situ parameters needed for analysis, such as density or void ratio, to characterize dynamic strength.

4. PREVIOUS INVESTIGATIONS

The experiment site was selected based on reports of 1964 Good Friday Earthquake damage to the bridges along the Alaska Railroad and those along the Anchorage-to-Seward highway that resulted from liquefaction and lateral spreading of the gravelly soils beneath and along the streambanks at each abutment (McCulloch and Bonilla, 1970). The bridge piers at each crossing of a triple stream channel of the Resurrection River at Seward were founded on piles driven to roughly 40 ft (12.19 m) depth. As a result of 1964 earthquake shaking, these piles were displaced streamward without rotation, suggesting pervasive and deep-seated liquefaction. The Alaska State Highway Department performed a limited series of dynamic penetration tests at the site following the 1964 earthquake, but no other in situ tests have been conducted there until the experiments discussed herein. The previous dynamic penetration tests, reported by McCulloch and Bonilla (1970) consisted of continuous driving of a 2.5-inch (0.064 m) diameter solid cone (essentially a plugged split- spoon penetrometer of the same size) using a 342-lb (1521 N) safety hammer (the actual sliding weight, not including anvil and driving rod is 294 lbs, or 1308 N) and a 30-inch (0.762 m) hammer drop, with blows per foot recorded and published in their report as N-values, as well as Standard Penetration Tests and sampling using a 140-lb (623 N) safety hammer and a 2-inch (0.051 m) diameter sample spoon with a 30-inch (0.762 m) drop (Figure 1). Those tests indicated loose, gravelly sands and sandy gravels to significant (greater than 75 ft, or 22.86 m) depth. Depth to bedrock in this filled fjord of the Exit Glacier is not known.

The soils are mainly normally consolidated alluvial outwash from one or more upland glaciers in the area.

5. FIELD PROCEDURE SUMMARY

The field exercise described in this paper took place at Seward, Alaska, during the period 28 August - 5 September 1998. Figure 2 is an aerial photo of the Resurrection River - Mineral Creek floodplain showing three prospective test sites for this project. The site is on property owned by the Metco Construction Materials Company, a gravel and aggregate harvesting operation at Seward. A drill crew from the U. S. Army Engineer District, Alaska (CEPOA), deployed and operated a tracked drill rig (Figure 3) and the various safety hammer and rod assemblies used in this study. The hammers, samplers, and drive points used in this study are shown in Figure 4.

The first penetration test was conducted in the riverbed itself, in a gravel bar about 400 ft (121.92 m) upstream from the bridge at Seward Highway mile 3.3. This first hole was sampled continuously using a standard split spoon (2-inch, or 0.051 m O.D., 1.4-inch, or 0.036 m I.D.) and a 4-inch (0.102 m) I.D. hollow stem auger (HSA). Driving energy was measured and recorded for every hammer blow, using a dynamic energy measurement transducer (Figure 5) provided by British Columbia Hydropower Authority (BC Hydro) and operated by Mr. Chris Daniel of the University of British Columbia. Water level was kept at the level of the ground surface during all drilling operations, especially during removal of the sand plug, or pilot bit. Hole depths were always measured after pilot bit removal, to determine whether any heave had occurred; heave at the site was generally less than 0.1 ft (0.03 m) using this procedure. The first hole was drilled to 60 ft (18.29 m) below ground surface; most sampling drives retained material (predictably low retention with the small, standard spoon); all sampled soil was shipped to WES for gradation and other index testing.

Upon completion of the first penetration test in the river bed, which served to develop field procedures and check out operation of all of energy measurement gear and establish careful drilling procedures (including conscientious observance to tighten every rod connection and adapter fitting within the rod string using two wrenches, resulting in excruciatingly slow progress), the drill rig was relocated to an abutment area of the highway bridge at mile 3.3. Overnight subsequent to the move, heavy rains caused the braided stream to rise four feet and remain at a high water stage for two days. Such rapid variation of flow is typical at this site, and indicates the depositional energy associated with the gravel bed placement. Initial plans to install grouted PVC casing to support crosshole seismic velocity surveys at the bridge abutment were abandoned due to insufficient hole clearance within the hollow stem auger. All remaining penetration tests were conducted in the vicinity of the bridge abutment. Table 2 is a summary of drilling operations conducted during the experiment series. The Alaska Fish and Game Commission pre-approved the exclusive use of clean tap water (no river drafting was allowed due to the presence of spawning salmon), and each hole was plugged with one or more bags of bentonite chips on abandonment.

6. TEST RESULTS

Penetration test results for all variations of procedure used at the Seward site are shown in Figure 6, uncorrected for differences in equipment or procedure. In all cases, three turns of rope were wrapped around the drill rig cathead winch; drop heights and hammer weights are noted in Table 3. The first test (SEWA9801) was performed in the river bed (termed as Site 2 in the figure), as discussed earlier, and depth is shown offset by 15 ft (4.57 m) to account for the fact that the surface elevation is lower here than at the bridge abutment, where the remainder of tests were performed. The tests were performed along an upstream-to-downstream line, so as to avoid lateral variations in streambed deposition as much as possible. It appears from Figure 6 that this strategy paid off, as there is remarkable correspondence between penetration resistance, even uncorrected, measured at the two sites. Abbreviations used in the plot are explained in Table 2.

In the raw data plot of Figure 6, it is evident that penetration resistance is strongly dependent on probe size in the gravelly sand and sandy gravels at the Seward site. Penetration resistance was higher among the drive sampler tests when the smaller diameter SPT was employed, but higher penetration resistance was recorded for the larger of the two driven solid cones. Larger particles may govern penetration resistance for intruding probes when no sample is obtained, creating essential an increased footprint for a given driving energy input. The reverse is true, however, with drive samplers, since larger particles are captured within larger cutting shoe areas and do not impede penetration to any proportional degree. Large particles increase the footprint of the cutting shoe if they will not fit inside. The zone of relatively low blowcounts observed in the Site 1 LPT and SPT, and Site 2 SPT in Figure 6 was reflected in the penetration testing performed following the 1964 earthquake, as shown in Figure 1.

Energy delivered by the safety hammers to the top of the drill rod string was dynamically measured for every test in this study, using the BC Hydro transducer system. An "energy ratio," was developed using data reported by the system, defined as the percentage of delivered energy relative to the theoretical maximum energy delivered by free-fall of the safety hammer used through the height specific to each test. Preliminary analysis was performed as of the date of this paper to adjust blowcounts for variations in driving energy. Figure 7 replots the results shown in Figure 6 after each raw blowcount was multiplied by the equipment-specific energy ratio and divided by 60. Numerous corrections or adjustments have been developed to account for variations among SPT data alone, given variability in procedures and equipment employed for that one, so-called "standard" test (e.g., Youd and Idriss, 1997). The cursory adjustment applied in Figure 7 is intended only to indicate the nature of the energy adjustment applied for the equipment used in this study; it is by no means a rigorous consideration of all variables, nor is it intended to allow for future comparison with results from tests where other equipment may be used.

A radar system was also employed during selected tests in this study, to measure the actual falling velocity of the safety

hammers. Kinetic energy delivered at impact should theoretically be the half of the product of the falling mass and the square of the velocity at impact. For the limited data set produced in this field study, the energy at impact as measured by the BC Hydro transducer system was generally slightly higher than the energy calculated from velocity of falling safety hammers.

7. CONCLUSIONS AND FUTURE PLANS

A limited set of field data was produced from penetration tests conducted in gravels liquefied by the 1964 Alaska Earthquake. These data represent the first collection of a variety of types of penetration tests in gravels where energy was measured to support adjustment of the results for varying equipment and procedures. Subsequent, more rigorous evaluation of the data will follow, in support of a research program to develop improved field procedures and interpretation methods for in situ determination of cyclic strength and behavior of coarse-grained soils. The data set is maintained by the principal author and may be made available to interested researchers in the near future.

Crosshole seismic surveys are planned at the site to complement this unique data set. Two cased boreholes will be installed during the summer of 1999 in which shear and compression wave velocities will be measured. Those data will also be unique, as such measurements have not been made in formerly liquefied coarse-grained soils in the US. Results of this study and the overarching research project will have implications to several engineering purposes.

8. REFERENCES

Coulter, H.W. and Migliaccio, R.R. 1966. "Effect of the earthquake of March 27, 1964 at Valdez, Alaska, U.S. Geological Survey Professional Paper 542-C.

Harder, L.F. 1988. "Use of penetration tests to determine the liquefaction potential of soils during earthquake shaking," PhD Thesis, University of California, Berkeley, CA.

Harder, L.F. and Seed, H.B. 1986. "Determination of penetration resistance for coarse-grained soils using the Becker hammer drill," Report No. UCB/EERC-86/06, University of California, Berkeley, CA.

Ishihara, K. 1985. "Stability of natural slopes during earthquakes," *Proceedings, 11th International Conference on Soil Mechanics and Foundation Engineering,* San Francisco, CA, Vol. 1, 321-376.

Kokusho, T., Tanaka, Y., Kudo, K. And Kawai, T. 1995. "Liquefaction case study of volcanic gravel layer during 1993 Hokkaido-Nansei-Oki earthquake," *Proceedings, 3rd International Conference on Recent Advances in Geotechnical Earthquake Engineering and Soil Dynamics,* St. Louis, MO, 235-242.

Maurenbrecher, P.M., Den Outer, A. And Luger, H.J. 1995. "Review of geotechnical investigations resulting from the Roermond April 13, 1992 earthquake," *Proceedings, 3rd International Conference on Recent Advances in Geotechnical Earthquake Engineering and Soil Dynamics,* St. Louis, MO, 645-652.

McCulloch, D.S. and Bonilla, M.G. 1970. "Effects of the earthquake of March 27, 1964, on the Alaska Railroad," Geological Survey Professional Paper 545-D, U.S. Department of the Interior, Washington, D.C.

Sy, A. 1993. "Energy measurements and correlations of the Standard Penetration Test (SPT) and the Becker Penetration Test (BPT)," PhD Thesis, Department of Civil Engineering, University of British Columbia, Vancouver, BC.

Sy, A., and Campanella, R.G. 1993. "Dynamic performance of the Becker Hammer drill and penetration test," *Canadian Geotechnical Journal*, 30(4): 607-619.

Sy, A., and Campanella, R.G. 1994. "Becker and standard penetration tests (BPT-SPT) correlations with consideration of casing friction," *Canadian Geotechnical Journal*, 31(3): 343-356.

Tanaka, Y., Kokusho, T., Yoshida, Y., and Kudo, K. 1989. "Dynamic strength evaluation of gravelly soils," *Proceedings of Discussion Session on Influence of Local Conditions on Seismic Response, Twelfth International Conference on soils Mechanics and Foundation Engineering*, International Society of Soil Mechanics and Foundation Engineers, Rio de Janeiro, Brazil, 1989.

Tokimatsu, K. And Yoshimi, Y. 1983. "Empirical correlation of soil liquefaction based on SPT N-value and fines content," *Soils and Foundations*, 23(4): 56-74.

Wang, W.S. 1984. "Earthquake damages to earth dams and levees in relation to soil liquefaction and weakness in soft clays," *Proceedings of the International Conference on Case Histories in Geotechnical Engineering,* St. Louis, MO, Vol. 1, 511-521.

Yegian, M.K., Ghahraman, V.G. and Harutiunyan, R.N. 1994. "Liquefaction and embankment failure case histories, 1988 Armenian earthquake," *Journal of Geotechnical Engineering,* ASCE, 120(3): 581-596.

Youd, T.L. , Harp, E.L., Keefer, D.K. and Wilson, R.C. 1985. "The Borah Peak, Idaho earthquake of October 28, 1983 - liquefaction," *Earthquake Spectra*, EERI, 2(1): 71-89.

Youd, T. L., and Idriss, I.M. eds. 1997. "Proceedings of the NCEER Workshop on Evaluation of Liquefaction Resistance of Soils," Report No. NCEER-97-0022, State University of New York at Buffalo, Buffalo, NY, viewable on the World Wide Web at http://mceer.buffalo.edu., 1997.

YEAR	M	EARTHQUAKE	REFERENCE
1981	7.9	Mino-Owari, Japan	Tokimatsu and Yoshimi (1983)
1943	7.3	Fukui, Japan	Ishihara (1985)
1964	9.2	Valdez, Alaska	Coulter and Migliaccio (1966)
1975	7.3	Haicheng, PRC	Wang (1984)
1976	7.8	Tangshan, PRC	Wang (1984)
1978	7.4	Miyagiken-Oki, Japan	Tokimatsu and Yoshimi (1983)
1983	7.3	Borah Peak, Idaho	Youd, et al. (1985), Harder (1988)
1988	6.8	Armenia	Yegian, et al. (1994)
1992	5.8	Roermond, Netherlands	Maurenbrecher, et al. (1995)
1993	7.8	Hokkaido, Japan	Kokusho, et al. (1995)
1995	6.8	Kobe, Japan	Kokusho, et al. (1995)

Table 1. Observations of liquefaction in gravelly soils (adapted from personal communication, Alex Sy, Klohn-Crippen Consultants, Ltd, Richmond, BC, Canada, 1996)

Test Identification/ Location	Date	Test Type*	Hammer Weight, lb. (N)/Drop Height, in. (m)	Maximum Depth, ft (m)	Test Spacing
SEWA9801 / Site 2	Aug. 29 - 31	1.52 in. (0.039 m) ID Split Spoon (SPT)	137 (609 N)/30 (0.762 m)	59.57 (18.16 m)	Continuous to 30 ft (9.14 m), followed by 5 ft (1.52 m) spacing
SEWA9802 / Site 1	Aug. 31 - Sept. 2	1.52 in. (0.039 m) ID Split Spoon (SPT)	137 (609 N)/30 (0.762 m)	79.15 (24.12 m)	5 ft (1.52 m) starting at 15 ft (4.57 m) depth
SEWA9803 / Site 1	Sept. 2 - 3	2.52 in. (0.064 m) ID Split Spoon (LPT)	294 (1308 N)/34 (0.864 m)	78.9 (24.05 m)	5 ft (1.52 m) starting at 15 ft (4.57 m) depth
SEWA9804 / Site 1	Sept. 3 - 4	3.5 in. (0.089 m) OD Dynamic Cone (LDCPT)	294 (1308 N)/34 (0.864 m)	43 (13.11 m)	Continuous starting at 15 ft (4.57 m) depth
SEWA9805 / Site 1	Sept. 4	2.32 in. (0.059 m) OD Dynamic Cone (DCPT)	294 (1308 N)/30 (0.762 m)	50 (15.24 m)	Continuous starting at 15 ft (4.57 m) depth
SEWA9806 / Site 1	Sept. 5	2.52 in. (0.064 m) ID Split Spoon (LPT)	294 (1308 N)/34 (0.864 m)	81 (24.69 m)	5 ft (1.52 m) starting at 15 ft (4.57 m) depth
SEWA9807 / Site 1	Sept. 5 - 6	3.5 in. (0.089 m) OD Dynamic Cone (LDCPT)	294 (1308 N)/34 (0.864 m)	39.5 (12.04 m)	Continuous starting at 15 ft (4.57 m) depth

Table 2. Field test summary, Seward site

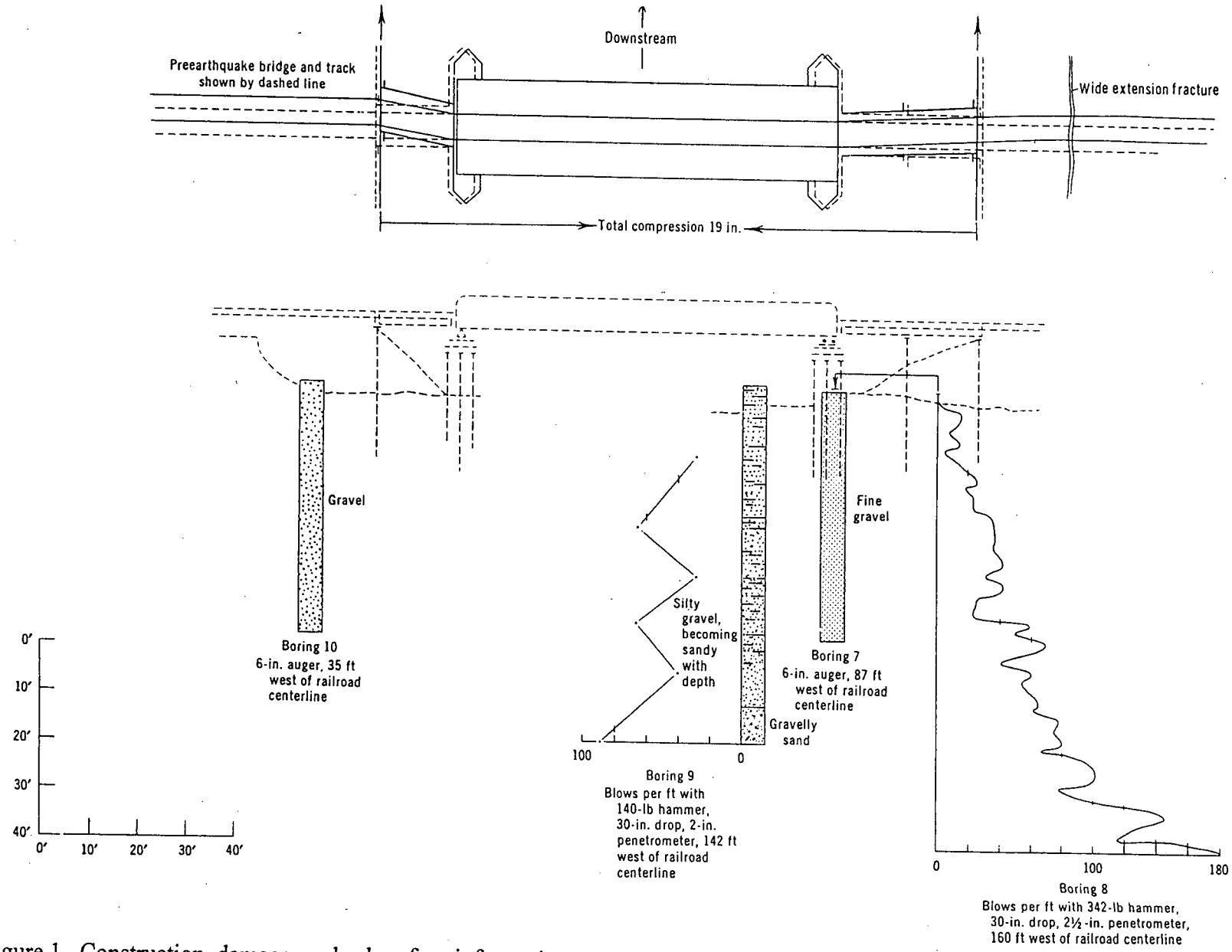


Figure 1. Construction, damage, and subsurface information, Bridge 3.3, Seward, Alaska (McCulloch and Bonilla, 1970)

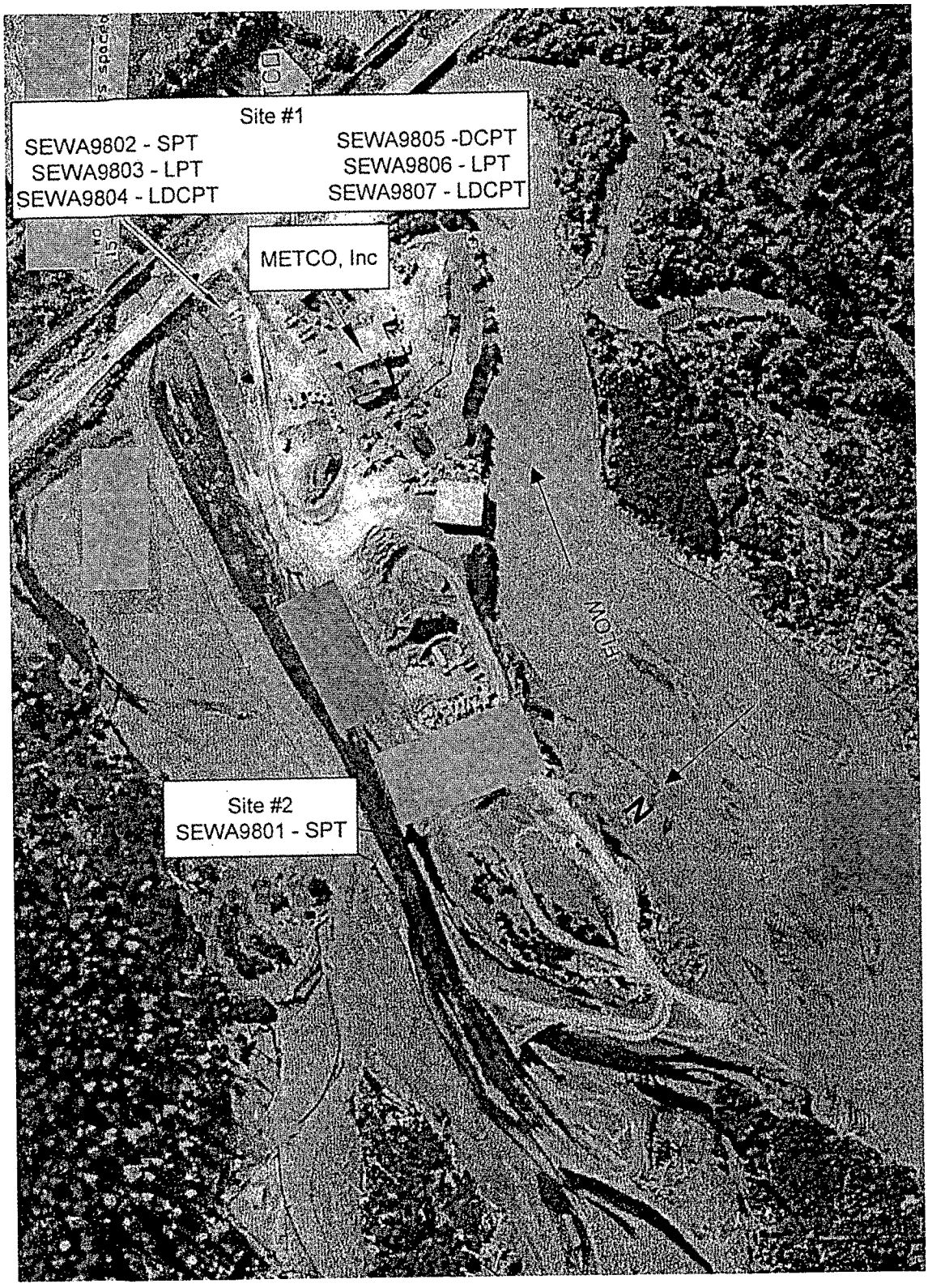


Figure 2. Aerial view of Seward, Alaska, test site

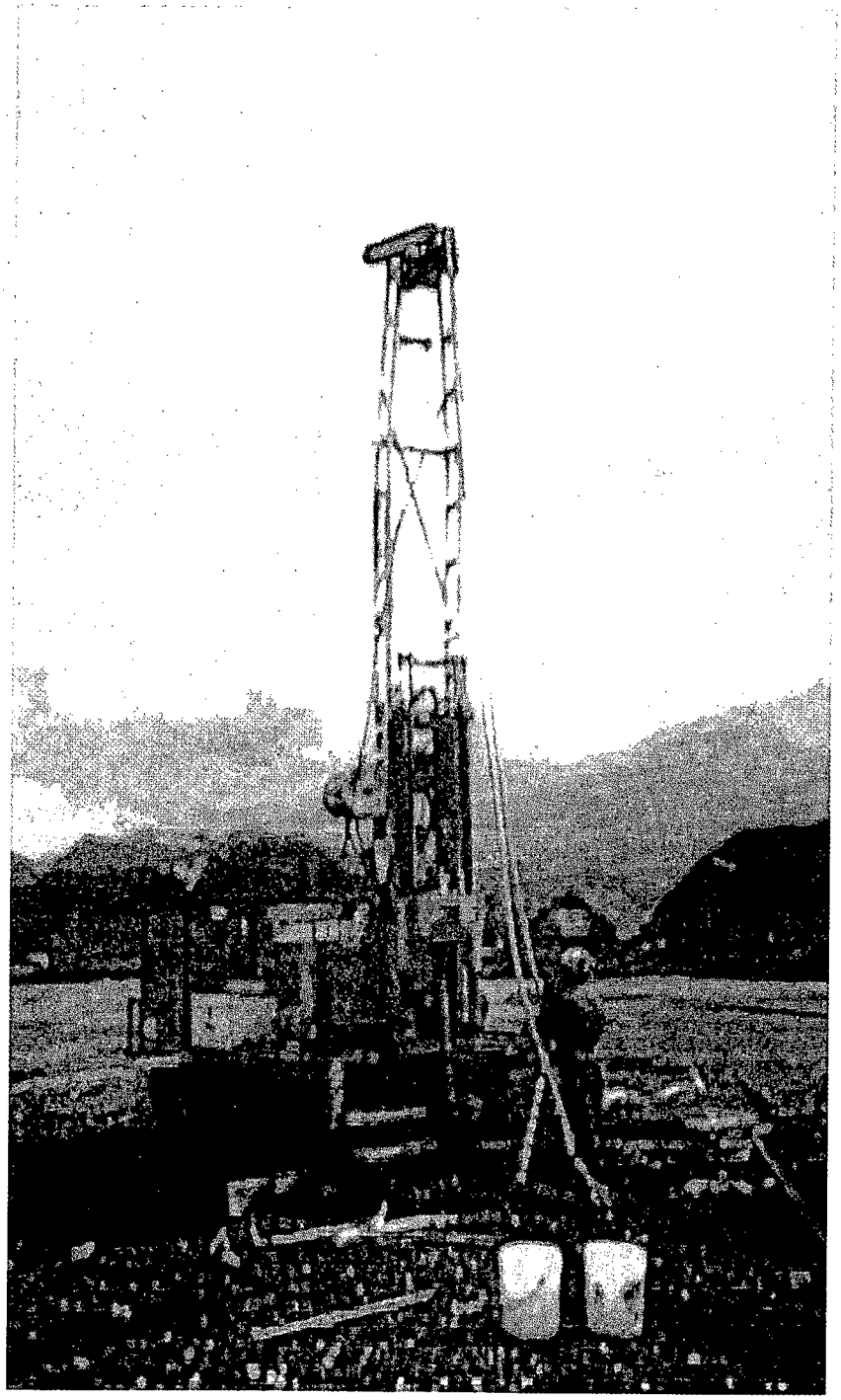


Figure 3. Tracked drill rig used with hollow stem augers

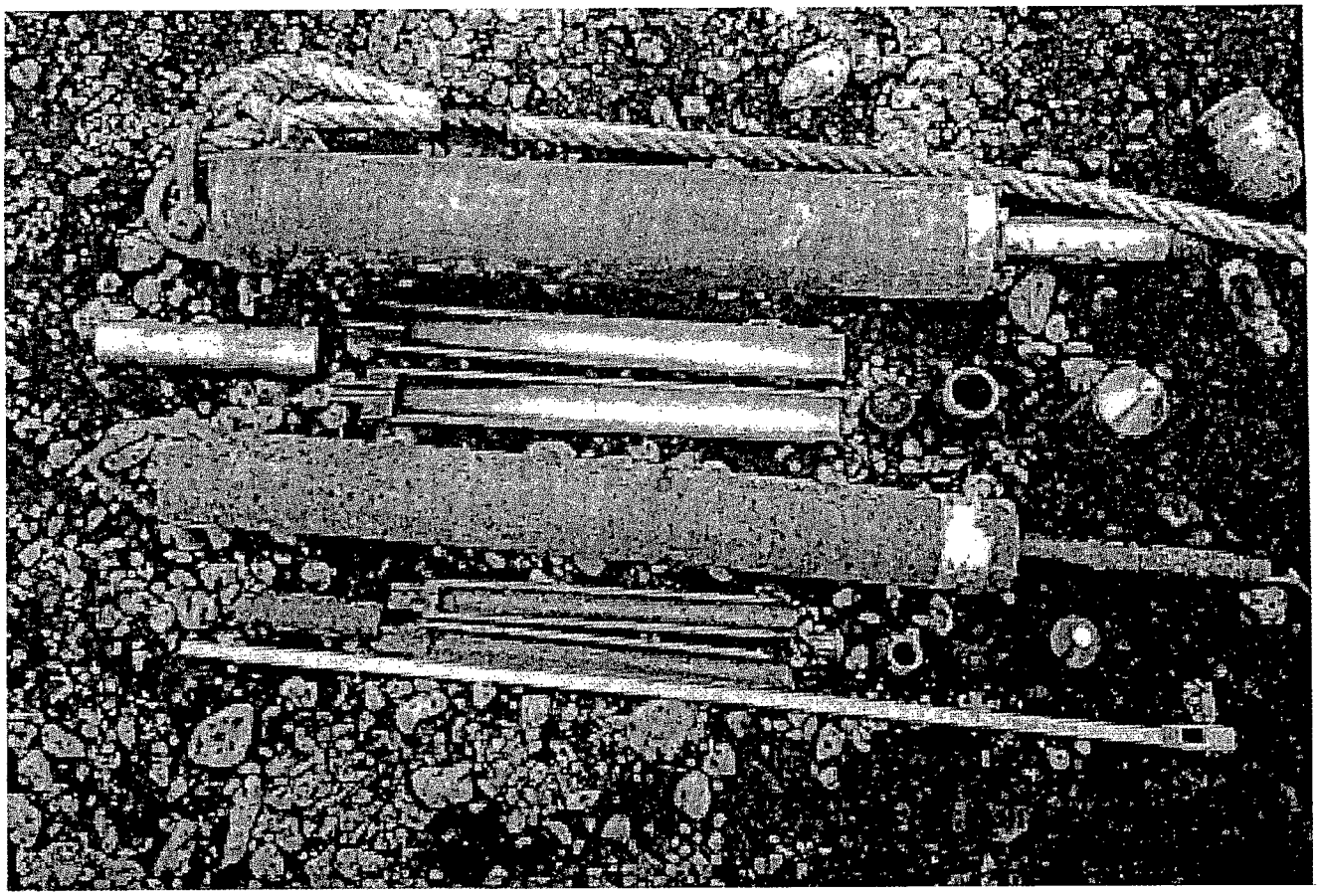


Figure 4. Safety hammers, split spoon samplers, and solid drive tips used in this study.
From top to bottom, central: 300 lb hammer; 2.5 in. I.D. sampler; 140 lb hammer; 1.5 in. I.D. sampler
Also shown, center right, is the 3.5 in. diameter LDCPT tip; the 2.5 in. diameter DCPT tip is at lower right
(1 lb = 4.45 N; 1 in. = 0.0254 m)

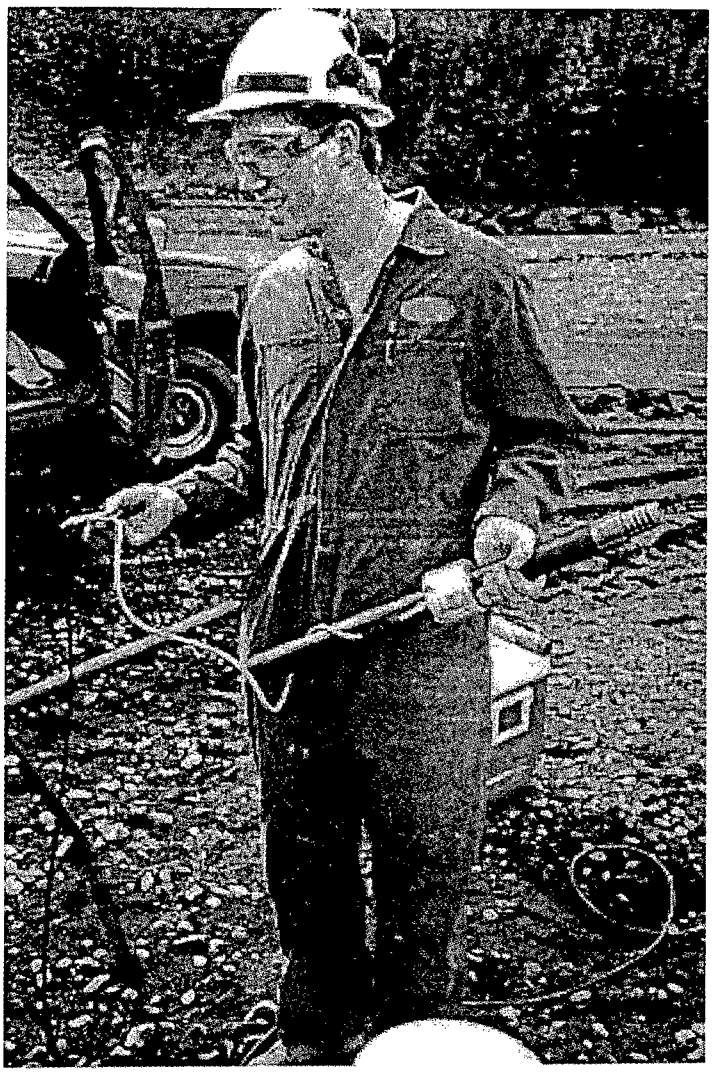


Figure 5. Dynamic energy measurement transducer, loaned by British Columbia Hydropower Authority

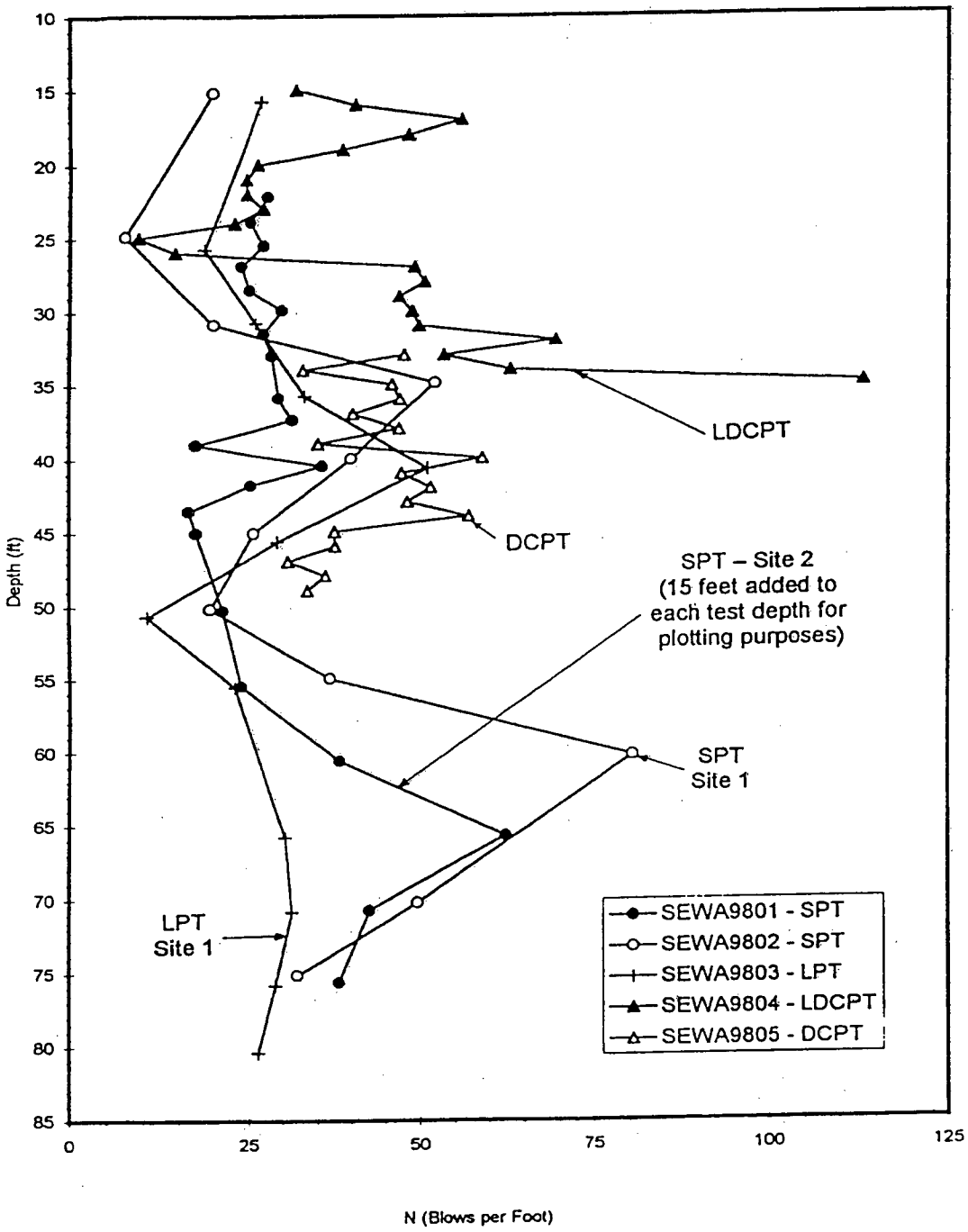


Figure 7. Penetration test data at Seward site, adjusted to 60% of maximum potential energy, specific to test parameters (1 ft = 0.3048 m)

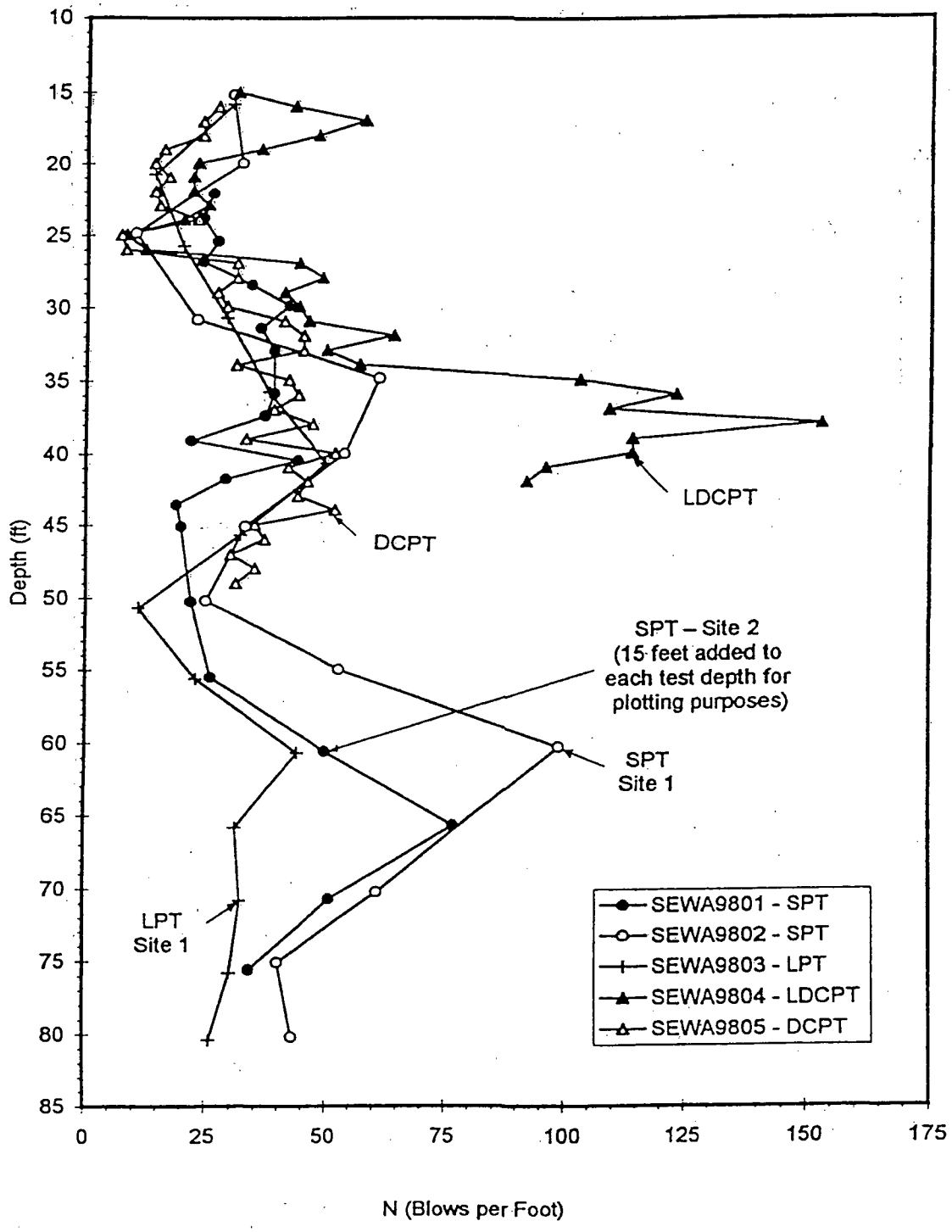


Figure 6. Raw penetration test results at Seward site
(Legend data in Table 2; 1 ft = 0.3048 m)

Dynamic Deformation and Strength Properties of Rockfill Materials

By

Nario Yasuda[1], and Norihisa Matsumoto[2]

This paper is the abbreviated version of Journal of Research, Public Works Research Institute, Vol.32, "A Study on dynamic deformation and strength properties of rockfill materials and their applicability to the seismic analysis of the embankment dams", published in March, 1997. The contents in this paper were conducted while the authors worked for PWRI.

ABSTRACT

In evaluating the stability of rockfill dams during earthquakes, dynamic deformation and strength properties of materials are important. In this paper we compared the deformation properties of compacted rockfill materials obtained from laboratory tests with those from in-situ geophysical logging tests. We also tested the deformation and strength properties of undisturbed and reconstituted specimen for dense gravel deposits. Both triaxial and simple torsional shear testing apparatus were used and the results were compared. We clarified dynamic deformation and strength properties of compacted rockfill for the use of seismic stability analysis of embankment dams.

KEYWORDS: Rockfill
Dynamic modulus
Shear strength
Cyclic triaxial test

1. PREFACE

The embankment dams in early history in Japan were all earthfill dams, such as legendary Kaerumata Ike, built in AD. 162, and Mannnoh Ike in AD. 1128. The first rockfill dam in Japan was constructed in 1953, and it was Ishibuti Dam with concrete face as an impervious element. After that, most high embankment dams were constructed with using rockfill as shell materials, since Japan is one of most seismically active counties in the world and rockfill structure have been considered to be strong to earthquakes. However, data on dynamic deformation and strength properties of rockfill materials are limited because of the difficulty of including the coarse size of rockfill in the laboratory specimen. Therefore we have conducted a series of large-scale triaxial and simple shear laboratory testing in both monotonic and cyclic loading for

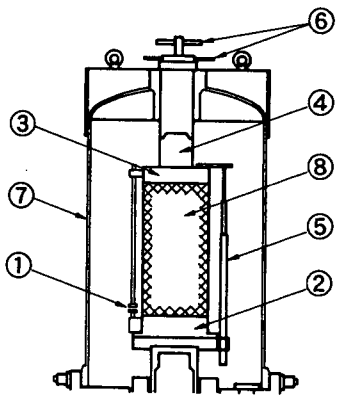
1) Director, Yunisigawa Dam Project Office, Ministry of Construction, former Chief Research Engineer, Filldams Division, Public Works Research Institute, MOC
2) Director, Engineering Division, Japan Dam Engineering Center, former Head, Filldams Division, Public Works Research Institute, MOC

compacted rockfill. We also identified the deformation and strength properties of riverbed gravel deposit using undisturbed specimen acquired by freezing sampling method, and compared them with the results obtained from disturbed specimen.

2. DYNAMIC DEFORMATION PROPERTIES OF ROCKFILL MATERIAS

Testing method

The testing apparatus used for the study was developed by the laboratory of PWRI to perform large-scale shear tests on rockfill materials. With a hollow cylindrical specimen of 80 cm outer diameter, 40 cm inner diameter and 80 cm in height, the apparatus is capable of applying torsional shear stress under monotonic loading and sinusoidal cyclic loading at a maximum rate of 0.3Hz. Monotonic and cyclic loading triaxial tests can be conducted with a solid specimen of 40 cm in diameter and 80 cm in height by changing an attachment. A schematic view of the testing equipment is shown in Figs. 1 and 2. The small displacements are measured by using eddy current type transducer with a maximum measurement length of 4 mm and a resolution of 0.16% as shown in Fig. 2.



① GAP SENSER
② CAP
③ PEDESTAL
④ LOAD CELL
⑤ DISPLACEMENT TRANSDUCER
⑥ LOAD CELL STOPPER
⑦ TRIAXIAL CELL
⑧ SPECIMEN

Fig. 1 Schematic diagram of triaxial testing apparatus

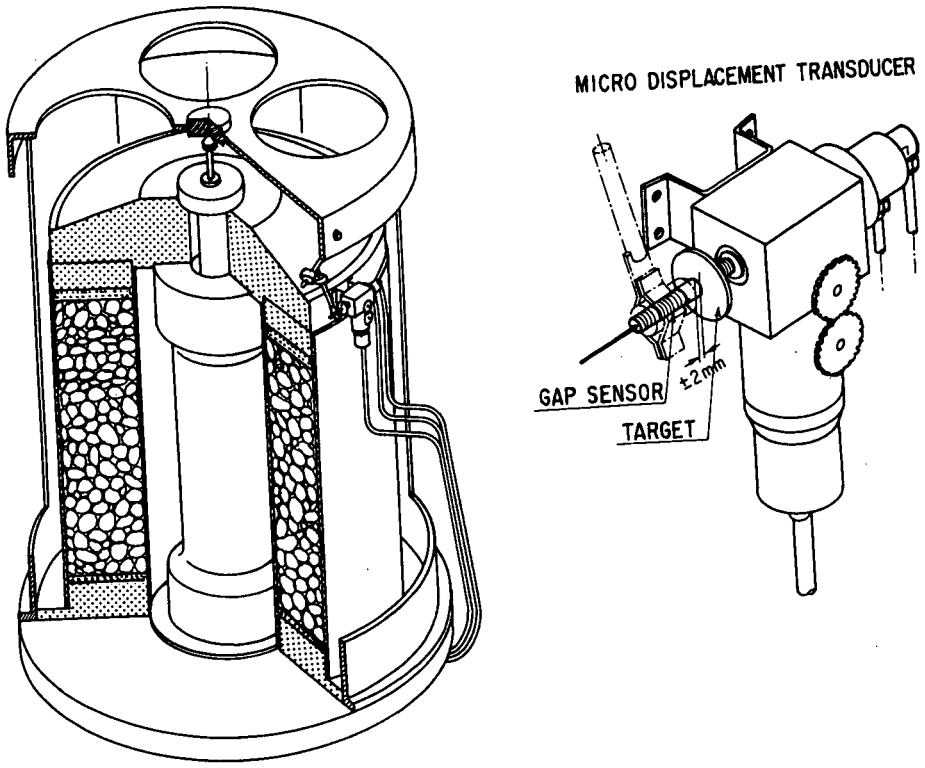


Fig. 2 Schematic diagram of torsional shear apparatus

Tests results for Toyoura sand

Before performing tests for rockfill materials, we conducted tests of Toyoura sand, and the tests results were compared with the past test results for shear modulus G, and damping ratio h that are dependent on shear strain γ, confining stress σ_c, and void ratio e.

Fig. 3 shows shear modulus of Toyoura sand obtained from past studies and authors', indicating that there is a good agreement between shear modulus G obtained from authors' cyclic torsional simple shear tests(CTSS) and cyclic triaxial tests(CTX), and authors' results coincide with those from resonant column tests in the past study with γ less than 10^{-4} and with tests results from CTSS with γ more than 10^{-4}. However, damping ratio by CTSS was a little greater than that by CTX, which are not illustrated in this abbreviated version.

Tests for rockfill materials

Fig. 4 shows the relationship between G and σ_c, where G is normalized by eliminating the effect of void ratio e, and σ_c is initial confining stress. The data are plotted on the straight lines of $K(\gamma)$ at gradients $m(\gamma)$ for each γ value. Therefore G of rockfill materials can be represented by the following formula over a wide strain range.

$$G=K(\gamma)\cdot\alpha\cdot\sigma_c^{m(\gamma)} \quad (1)$$

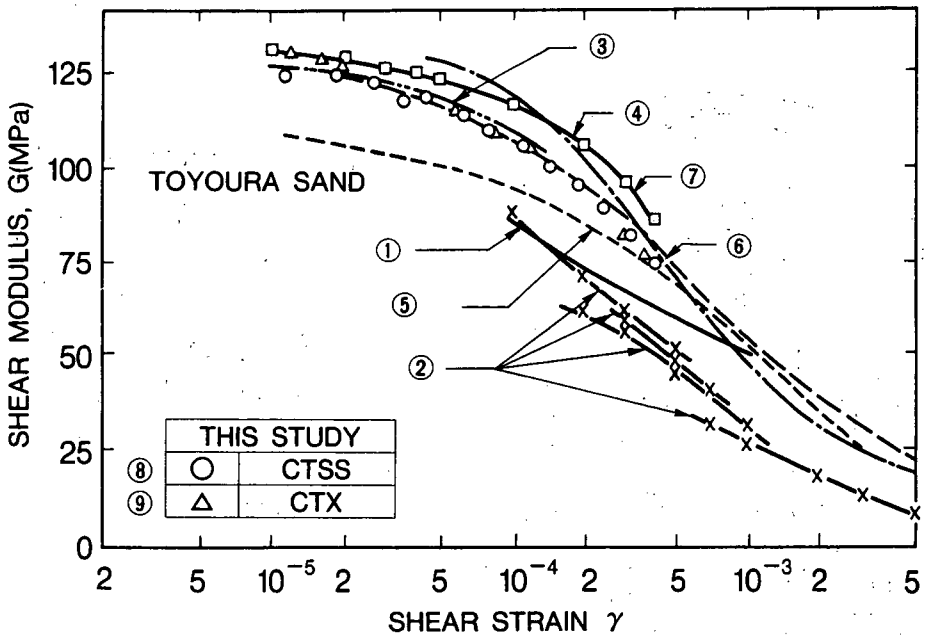


Fig. 3 Shear modulus versus shear strain of Toyoura sand

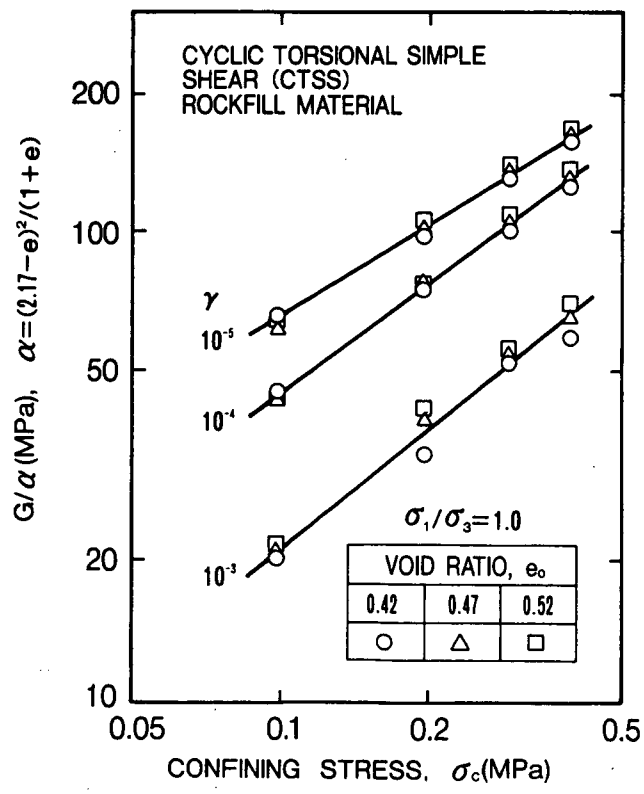


Fig. 4 Shear modulus versus confining stress of rockfill

Fig. 5 illustrates the relationship between damping ratio h and void ratio e, where h is normalized by eliminating the effect of confining stress. There is linear relationship between normalized h and e, hence h can be expressed by the following formula.

$$h=L(\gamma)\cdot(0.4+1.5ec)\cdot \sigma_c^{n(\gamma)} \quad (2)$$

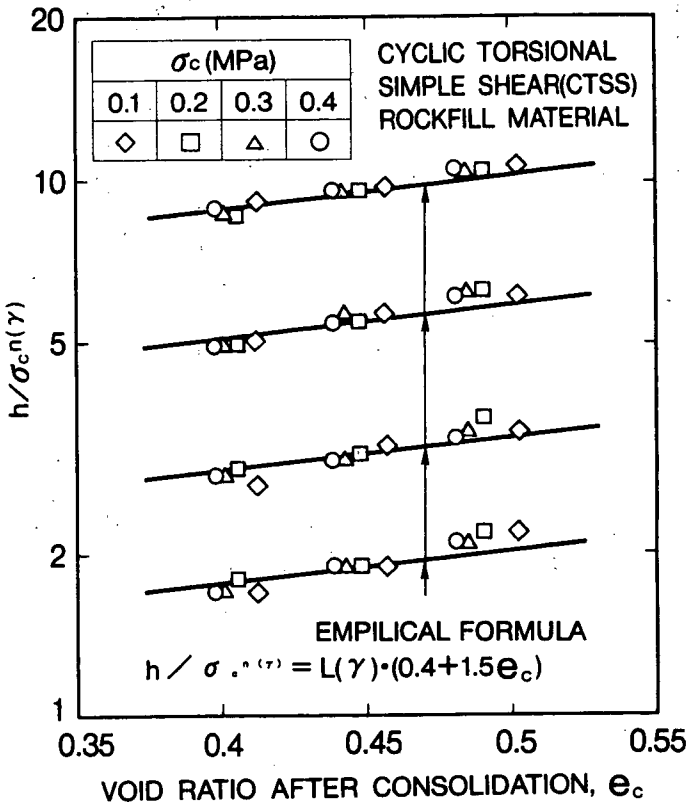


Fig. 5 Damping ratio versus confining stress of rockfill

The test results show that G is dependant on the value of mean principal stress σ_m (=($\sigma_1+\sigma_2+\sigma_3$)/3), and effects of σ_1/σ_3 on G is small. The effects of σ_1/σ_3 on h is also small. Consequently G and h obtained from laboratory tests with isotropic consolidation can be applied for the analysis, provided the in-situ mean confining stress is taken into account. The same G and h were given for four different cyclic loading frequencies of 0.01, 0.05, 0.1, and 0.2 Hz, and hence there is no frequency dependency of G and h.

Fig. 6 shows the shear strain dependent curves of G by CTSS and CTX. G by CTSS is larger than that by CTX at any confining stress, and the difference increases, as the confining stress increases. The cause of the difference can be attributed to the different intermediate stress.

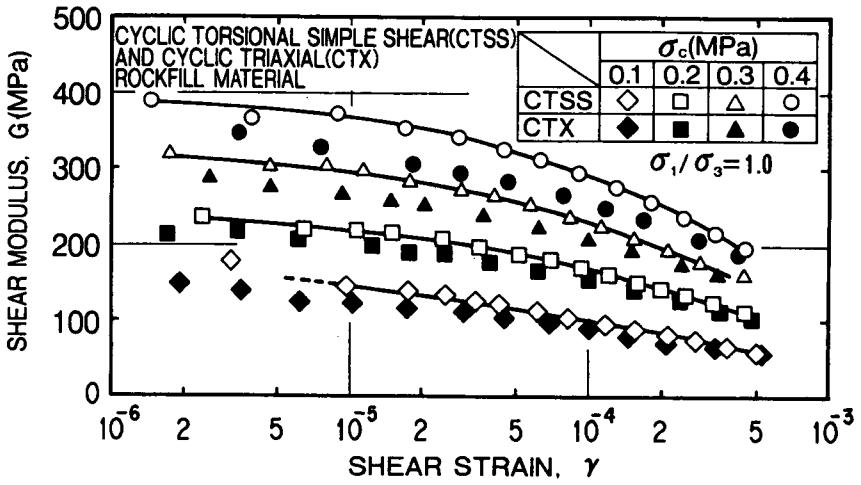


Fig. 6 Shear modulus of CTSS and CTX tests

Fig. 7 indicates the comparison of damping ratio h between CTSS and CTX tests. The h value obtained from CTSS is larger than that from CTX, where the difference increases as strain γ increases.

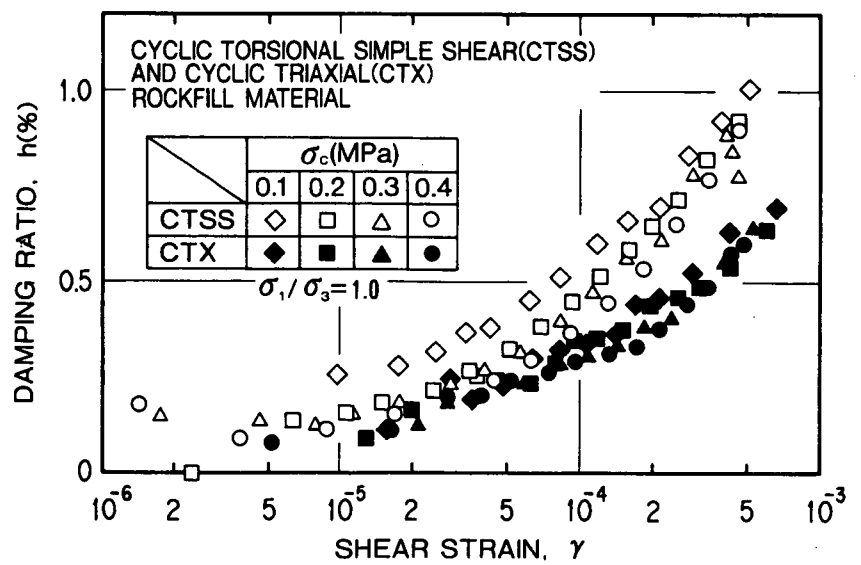


Fig. 7 Damping ratio of CTSS and CTX tests

3. DYNAMIC DEFORMATION PROPERTIES OF GRAVEL DEPOSIT

Gravel deposits are often left in-place, and they are used as the foundations for embankment dams. We sampled the undisturbed specimen by freezing method in Cyubetu River, and brought it to the laboratory to test. We also conducted in-situ geophysical tests to measure the shear wave velocity.

Test procedures

The riverbed deposit consists of two geologically different strata: the lower layer of the Pleistocene and upper layer of the Holocene. The boundary is 10.7 m below the ground level. The grain size distribution of two layers was very similar, but the lower layer contained more weathered gravel and better indurated. Undisturbed specimens of 30 cm diameter were sampled from the gravel deposit by using liquid nitrogen of −196℃. After the ground was frozen, a core tube of 34 cm external diameter was used to extract a core of 30 cm diameter, and both ends of the core ware cut, then sealed in an insulated vessel at the site and transported by a refrigerated vehicle. The surfaces of the specimens were very smooth with no irregularities, in spite of containing a lot of coarse gravel. It seemed that sampling process did not disturb the specimens. The average diameter D_{50} of the deposit both of lower and upper layer was about 70 mm, and fine content of lower and upper layer was 1% and 2.5% respectively. The void ratio of lower layer was 0.21, and that of upper was 0.25 in average.

We also prepared the reconstituted specimen by forming the grain size distribution completely parallel to that of in-situ materials. The density of the reconstituted specimens was adjusted to have the same one with that of the upper layer deposit.

Tests results

Fig. 8 shows the G versus γ relationship for a confining pressure of 0.005Mpa. The G value of the undisturbed specimens is about twice as large as that of reconstituted specimens. Fig. 8 also indicates that G of lower layer is much higher than that of upper layer. The larger value of G was probably caused by the cementation effects of the materials during the geologic age. The G/G_0 versus γ relationship was marked by almost identical tendencies in both the undisturbed and reconstituted specimens.

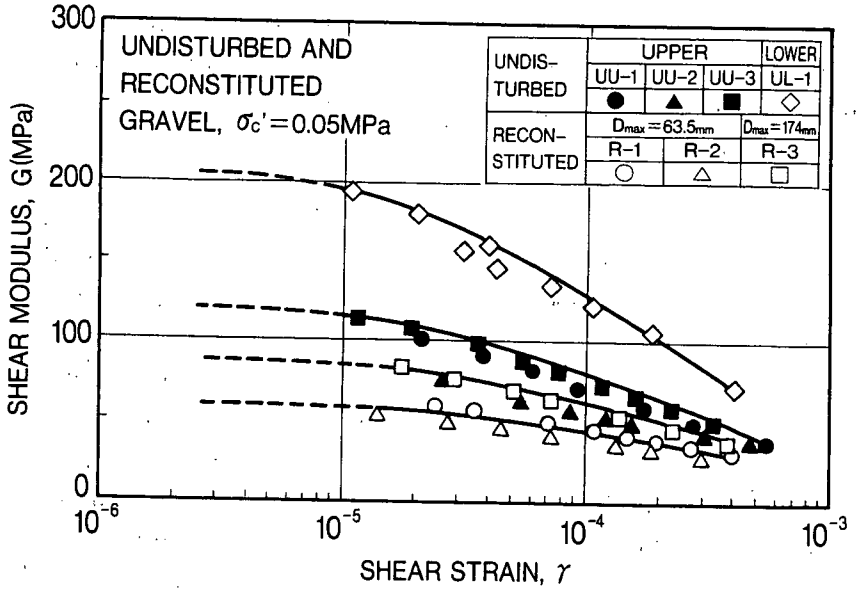


Fig. 8 Shear modulus of undisturbed and reconstituted specimen

Damping ratio h is shown in Fig. 9 for undisturbed and reconstituted specimens. It indicates h is more dependent on the confining pressure in the lower layer deposit than in the upper. The value h seems to have little difference in between the undisturbed and reconstituted samples.

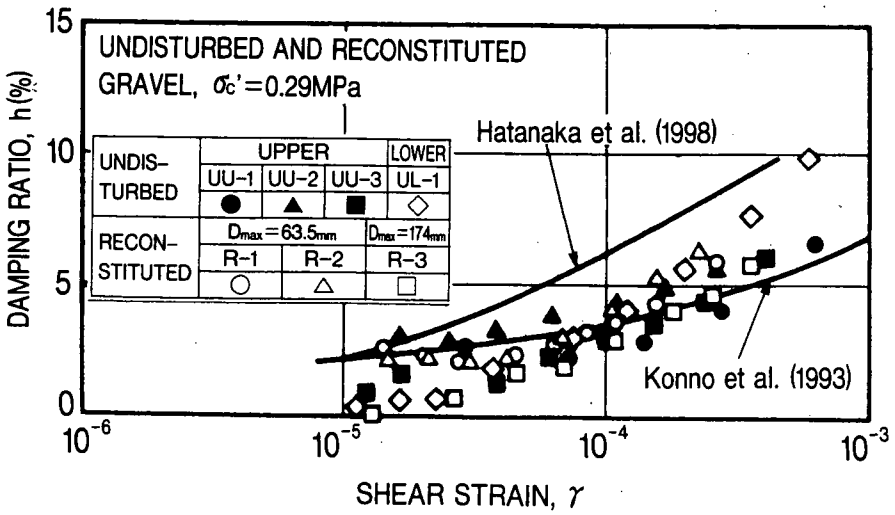


Fig. 9 Damping ratio of gravel deposit for undisturbed and reconstituted specimen

We performed geophysical P-S logging tests using boreholes drilled adjacent to the freezing sampling site. The P-waves were generated by striking the ground near the borehole vertically with a mallet, where the S-waves produced by hitting the board fixed to the ground firmly near the borehole. The P and S-waves thus generated were monitored by three component geophones placed at the depths of the boreholes. Fig. 10 compares the in-situ S-wave velocity V_s obtained from the PS-logging with V_s obtained from cyclic deformation testing in the laboratory. Here, laboratory V_s was computed from the initial shear modulus G_0 using the relation $G_0=\rho \cdot V_s^2$. As the figure indicates V_s values obtained from the laboratory undisturbed tests for the lower gravel layer are identical to the in-situ geophysical V_s, while undisturbed laboratory Vs for upper layer was about 70% smaller than that of in-situ V_s.

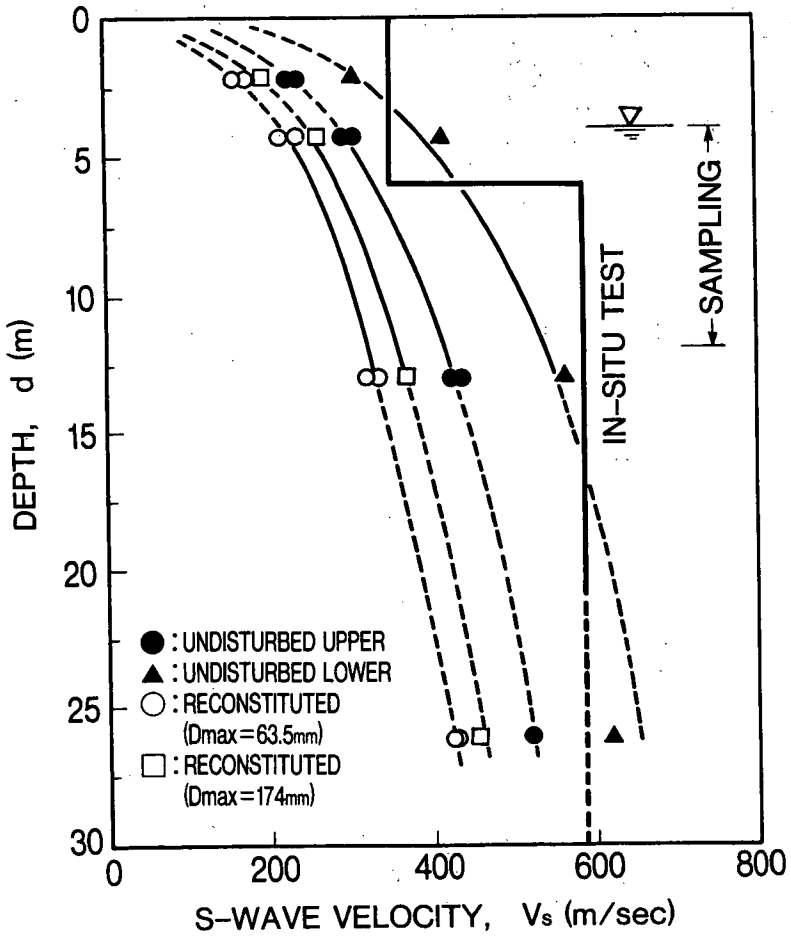


Fig. 10 Distribution of S-wave velocity with depth from laboratory and in-situ tests

4. COMPARISON OF DYNAMIC DEFORMATION PROPERTIES OF ROCKFILL MATERIALS IN LABORTORY AND IN-SITU TESTS

Miho Dam

Miho Dam is a 95 m high rockfill dam with a central impervious core as shown in Fig. 11. The elastic wave velocity was measured by small scale blasting at intervals of 2.5m utilizing holes for measurement of settlements and through reception points at intervals of 2.5 m on the two lines of the downstream slope surface. The test results of shear wave velocity were shown in Fig. 12. In this figure also V_s obtained from laboratory CTX test was included, and corresponds well with that of the geophysical exploration.

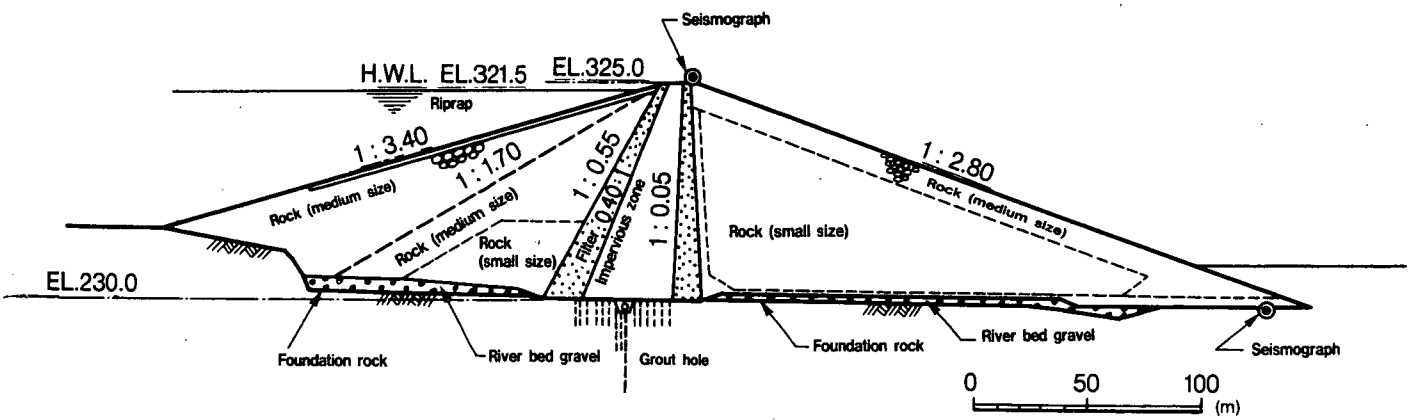


Fig. 11 Maximum section of Miho Dam

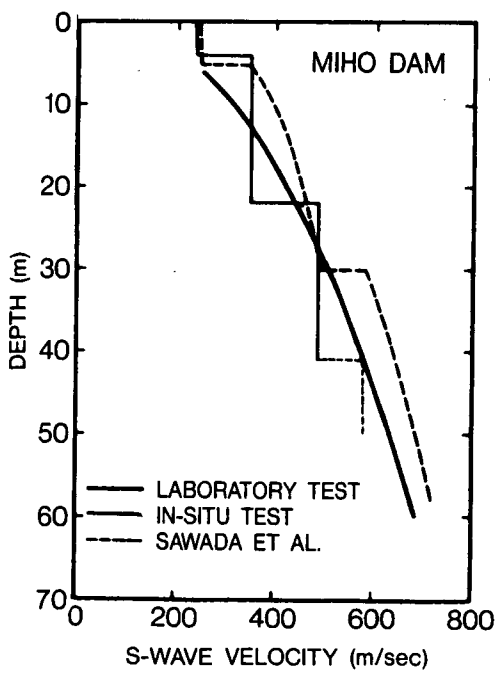
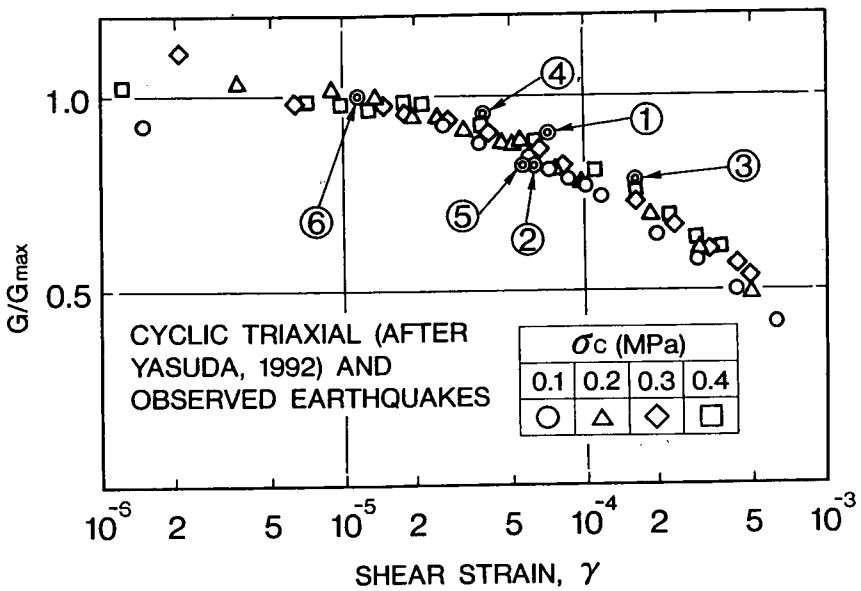


Fig. 12 Distribution of S-wave velocity with depth in Miho Dam

The earthquake is one of the large-scale in-situ tests. At Miho Dam, fifty events of earthquake had been recorded after the completion of the dam. We analyzed the strain dependency of shear modulus of the embankment materials by using major six accelerograms recorded at Miho Dam. The average shear modulus G_0 was computed assuming it be proportional to the square root of first natural frequency of the dam, and the maximum strain in the dam be proportional to the maximum displacement of the crest of the dam that can be obtained from peak acceleration and natural frequency. Fig. 13 shows the G versus γ relation for Miho dam obtained from measured accelerograms and laboratory CTX test. Therefore strain dependency of G in the laboratory testing seems to be supported by the largest-scale in-situ tests.



No.	Date	Magnitude	Natural Frequency
①	June 29,1980	6.7	1.95
②	April 14, 1981	4.5	1.86
③	August 8, 1983	6.0	1.81
④	December 17, 1987	6.7	2.00
⑤	August 2, 1990	5.1	1.86
⑥	February 2, 1992	5.7	2.05

Fig. 13 G/G_0 versus strain relationship obtained from earthquake records and laboratory tests

Shichigasyuku Dam

Schichigasyuku Dam is also a 93 m high rockfill dam with a central impervious core, as shown in Fig. 14. At the dam, shear wave velocity and longitudinal wave velocity were measured using the boreholes in the dam body during construction. Four stages of in-situ measurement were conducted at various construction stages. V_s values obtained from third and forth in-situ test were illustrated in Fig. 15, and laboratory results were also given in the figure. The comparison also suggests the cyclic laboratory test be able to reproduce in-situ properties.

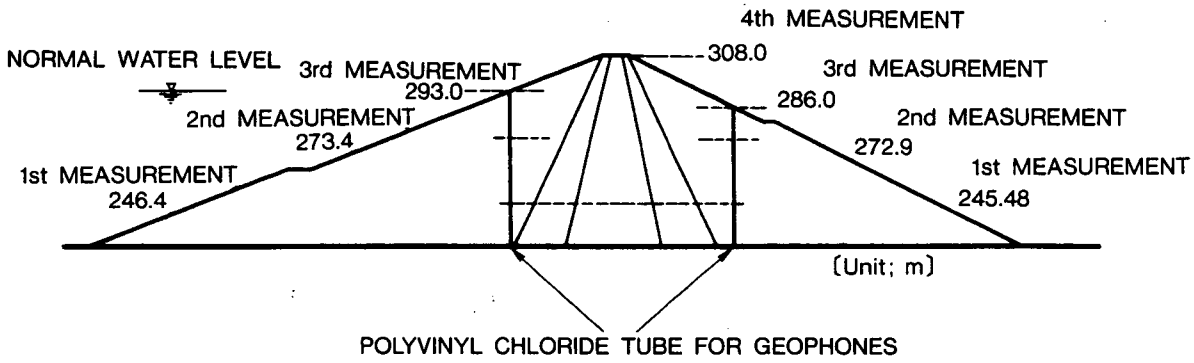


Fig. 14 Cross section of Schitigasyuku Dam and locations of measurement boreholes

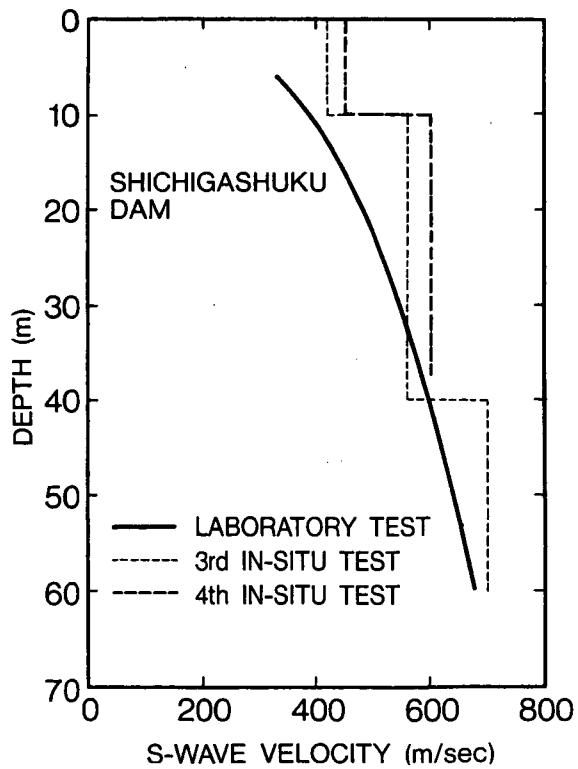


Fig. 15 Shear wave velocity with depth in Schitigasyuku Dam

5. STRENGTH OF GRAVEL DEPOSIT

Cyclic undrained strength test procedure for undisturbed and reconstituted specimen of gravel deposit

Cyclic undrained tests were performed for the specimens obtained by freezing sampling method as stated in chapter 3 and compared to the reconstituted specimen. The specimens were shaped and the membranes were attached inside a freezer set at −20℃. A sketch was made of each specimen just before it was placed on the triaxial cell. Each specimen was prepared as follows:

1. The pedestal and cap attached to the specimen are cooled to the same temperature as the specimen.
2. The carrying case is removed, and the surface of the specimen is cleaned of ice flake, dust, and loose materials. The surface with thin plastic sheet is sketched and photographed.
3. Its weight, diameter, and length are measured, and documemted as the initial value of the specimen.
4. The specimen is placed on the pedestal, and any chips, depression, or protrusions on its surface including either end and side are covered with fine sand to make the surface as smooth as possible. The cap is placed on the end, and a rubber membrane with a thickness of 2 mm is attached around it.
5. The specimen is taken from the freezer and installed inside the triaxial cell. The loading piston and load cell are set, and the cell water is injected to apply a confining pressure of 294kPa, then the specimen is left for 24 hours to thaw out.
6. When the pressure inside the specimen reaches −294 kPa by vacuuming, the confining pressure is released. After drainage of cell water, the cell is removed, and negative pressure of −294kPa enables the specimen to stand itself.
7. Protrusions and depressions appear on the surface of the specimen resulting from the melting of ice lumps. To avoid membrane penetration, silicon rubber is used to fill up the depressions and another rubber sleeve is placed over it.
8. The cell is set again and filled with water again. As the confining pressure of 294kPa is applied, the negative pressure inside the specimen is removed. The void air in the specimen is replaced with CO_2 gas passed through the bottom of the specimen at a pressure of 147kPa for three to four hors. Then deaerated water is supplied through the bottom of the specimen for 24 hours at a water head of 2 m(19.6kPa). A back pressure of 0.2MPa is applied. After confirming B value to exceed 0.95, consolidation is started.
9. When consolidation is completed, the drained volume and displacement of the specimen are measured, and then cyclic loading is applied.

After completing cyclic tests for undisturbed frozen specimens, reconstituted specimen were prepared and tested using the materials of upper gravel layer. The grain size distribution are parallel to that of in-situ material, and moisture content and void ratio are simulated to the average of undisturbed upper layer specimen. The effective mean principal stress for dynamic strength tests was 0.1, 0.29, and 0.59MPa for the upper

layer specimen, and 0.29MPa for lower layer specimen. Cyclic loading with a frequency of 0.1Hz was applied to the specimen so that the amplitude of the compression and extension is the same, and loading continues until double amplitude axial strain reaches 5%.

Test results of cyclic undrained loading for gravel deposit

Fig. 16 represents the time histories of cyclic deviator stress, axial stress, and pore water pressure for an effective mean principal stress of 0.29MPa. Fig.17 compares the cyclic shear stress ratio of undisturbed and reconstituted specimens at the mean confining pressure of 0.29MPa. The cyclic shear stress ratio of the reconstituted specimen is about 40% of that of undisturbed lower layer specimen and 80% of undisturbed upper layer specimen at 20 cycles and axial strain of 2%.

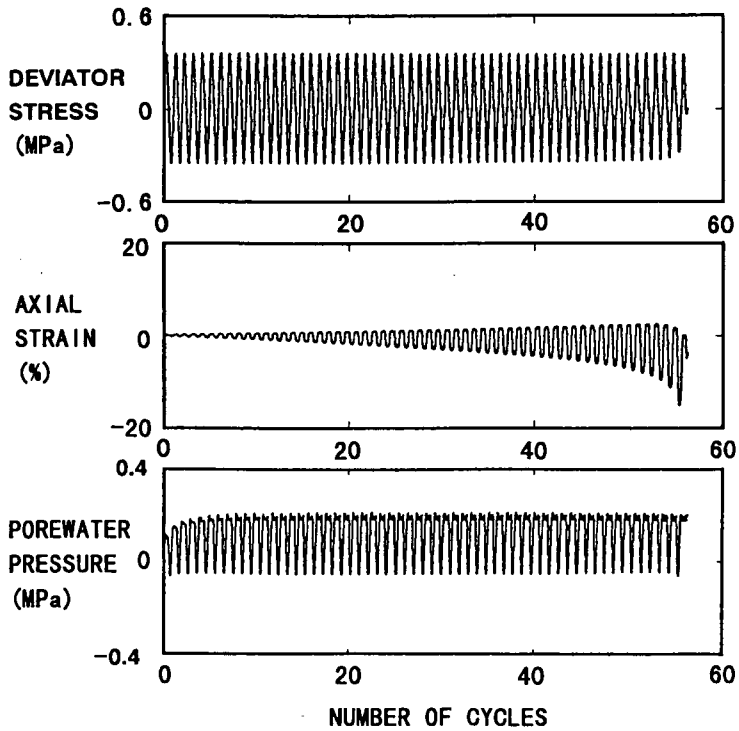


Fig. 16 Deviator stress, axial strain, and porewater pressure of undisturbed lower gravel layer

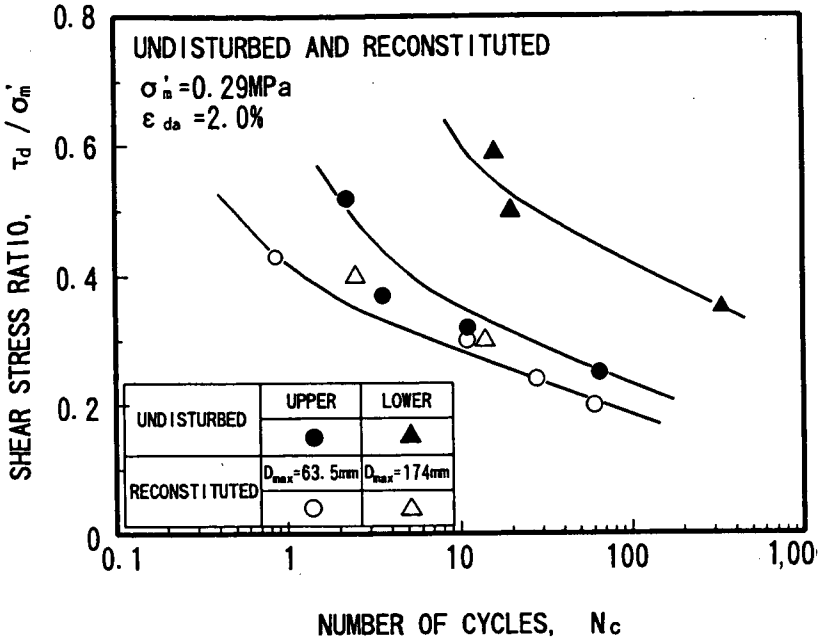


Fig. 17 Shear stress ratio of undisturbed and reconstituted specimen

Monotonic loading tests

Drained monotonic loading tests were carried out for undisturbed and reconstituted specimens. Fig. 18 illustrates the maximum deviator stress versus void ratio at three different confining stresses. There is not much difference in maximum deviator stress for different specimen as it is for cyclic stress ratio. It seems that the effect of void ratio is dominant on the monotonic strength.

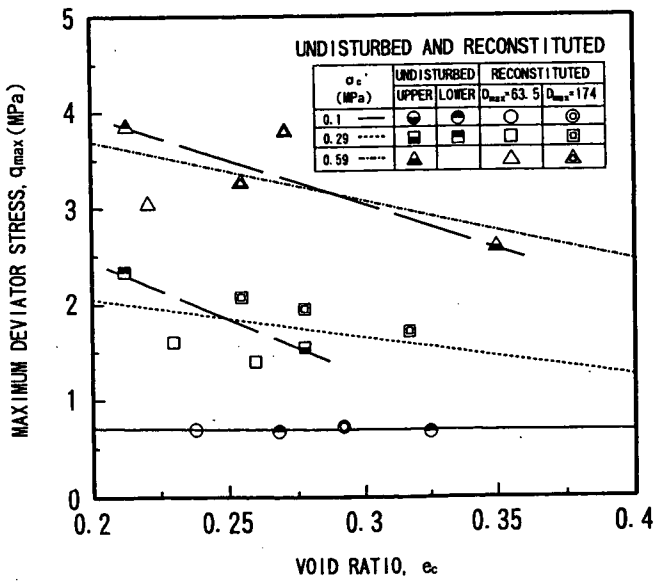


Fig. 18 Maximum deviator stress and void ratio in monotonic loading

6. MONOTONIC AND CYCLIC STRENGTH OF COMPACTED ROCKFILL MATERIALS

Test procedure

The materials borrowed at Sagurigawa Dam were used for a series of the tests to identify the strength of monotonic and cyclic strength of compacted rockfill. The parent rock of the materials is gabbro and of high quality. The maximum grain size contained in specimens is 63.5 mm and average diameter is 10 mm with minimal content of fines. The apparatus described in chapter 2 was used, and specimen was prepared by the same way as described in the previous chapter.

Test results

The effect of initial confining stress on cyclic stress ratios at the 20th cycle, i.e. SR_{20}, to reach shear strain of 1.0% is shown in Fig. 19(CTX tests). In case the relative density is over 85%, SR20 increases greatly with the decrease of confining stress. However, in case the relative density is 60 or 70%, shear stress ratio depends little on the initial confining stress. Fig. 20 shows the relationship between cyclic shear stress ratio and relative density(CTX tests). The shear stress ratio increases remarkably with the increase of relative density over 85% for each strain level. This tendency is more pronounced with the anisotropic consolidation than with the isotropic consolidation specimen.

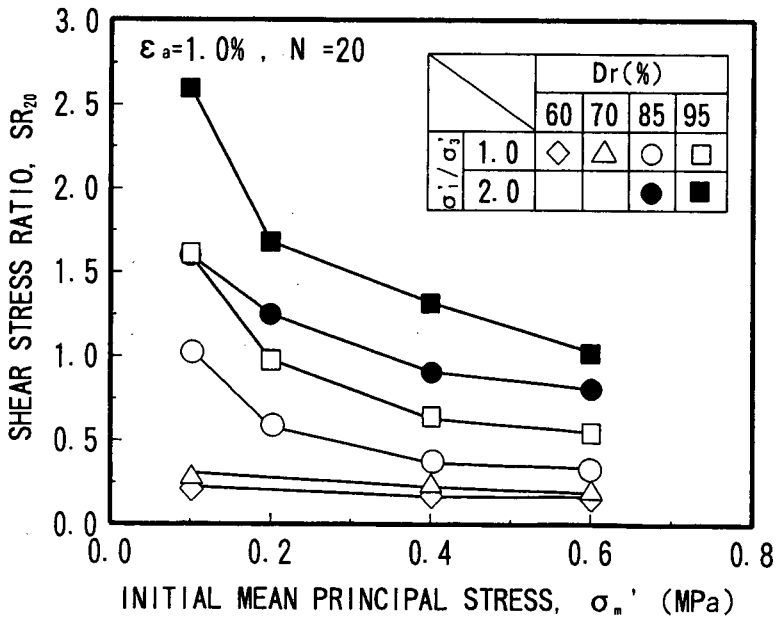


Fig. 19 Shear stress ratio and initial confining stress with different relative density

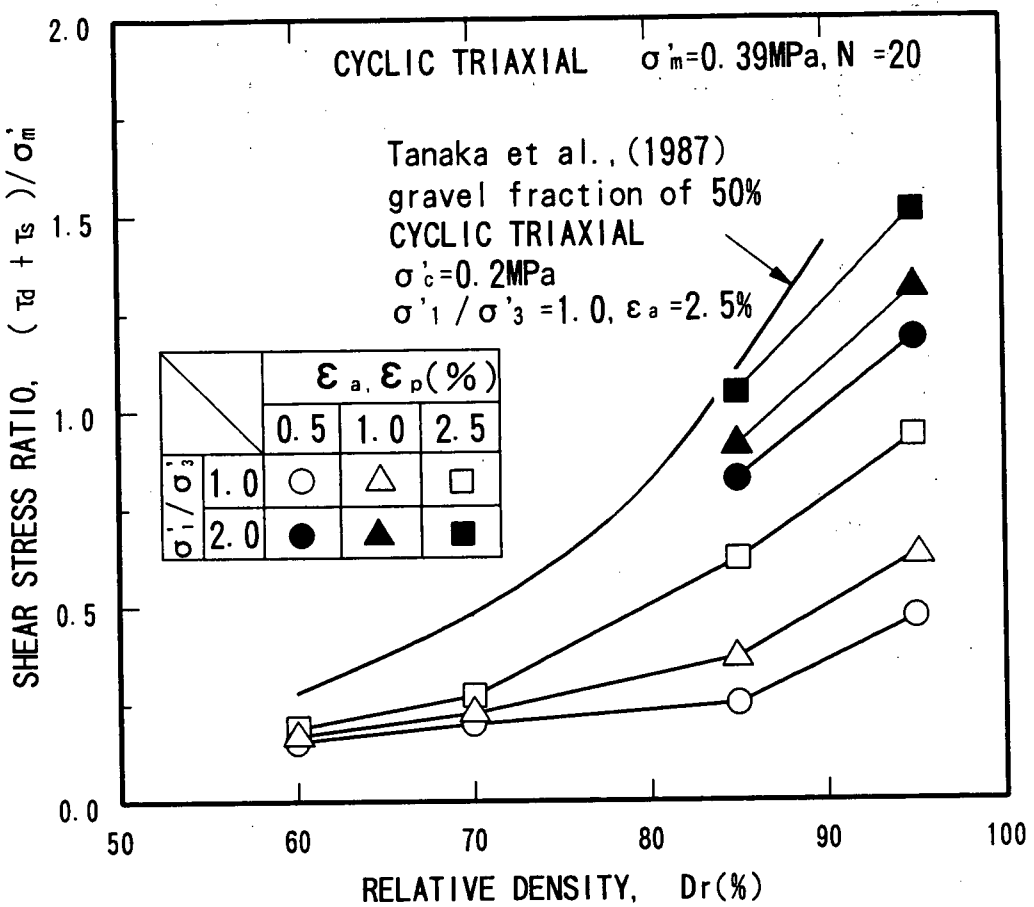


Fig. 20 Shear stress ratio versus relative density of rockfill at cyclic undrained CTX tests with isotropic and anisotropic consolidation

Next the undrained strength of rockfill by cyclic torsional simple shear tests will be described. Fig. 21 shows the relationship between the shear stress ratio and the number of cyclic loading in a consolidation stress ratio ranging from 1.0 to 2.0 with the shear strain of single amplitude of 1.0%. The figure indicates that shear stress ratio depends on the mean initial confining pressure and does not on the initial stress ratio. Fig. 22 shows the development of shear strain in CTSS tests for monotonic and cyclic loading. When the initial shearing stress is 0.25MPa, cyclic shear stress to cause the same strain exceeds that of drained test and almost the same as monotonic undrained loading.

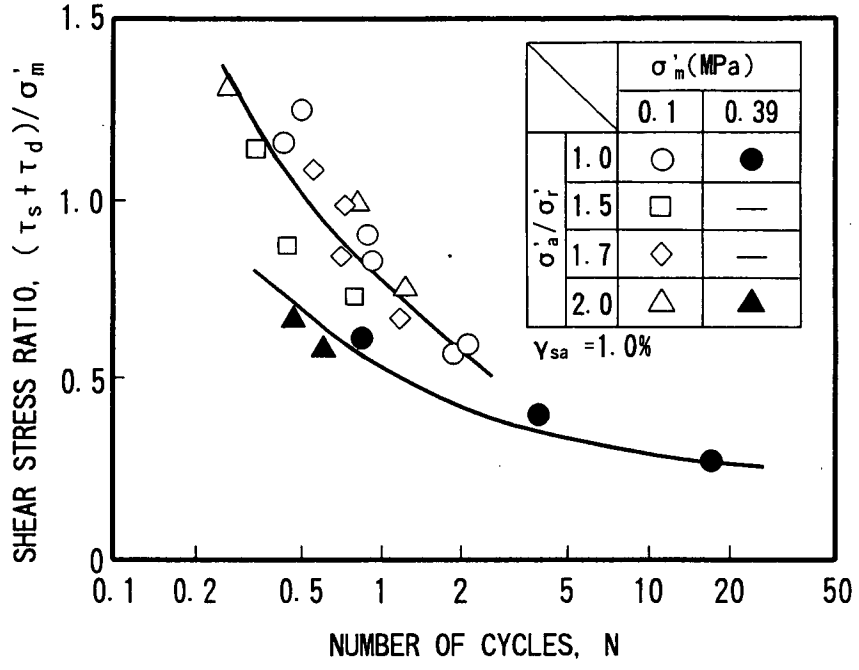


Fig. 21 Shear stress ratio versus number of cycles of rockfill at CTSS tests with isotropic and anisotropic consolidation

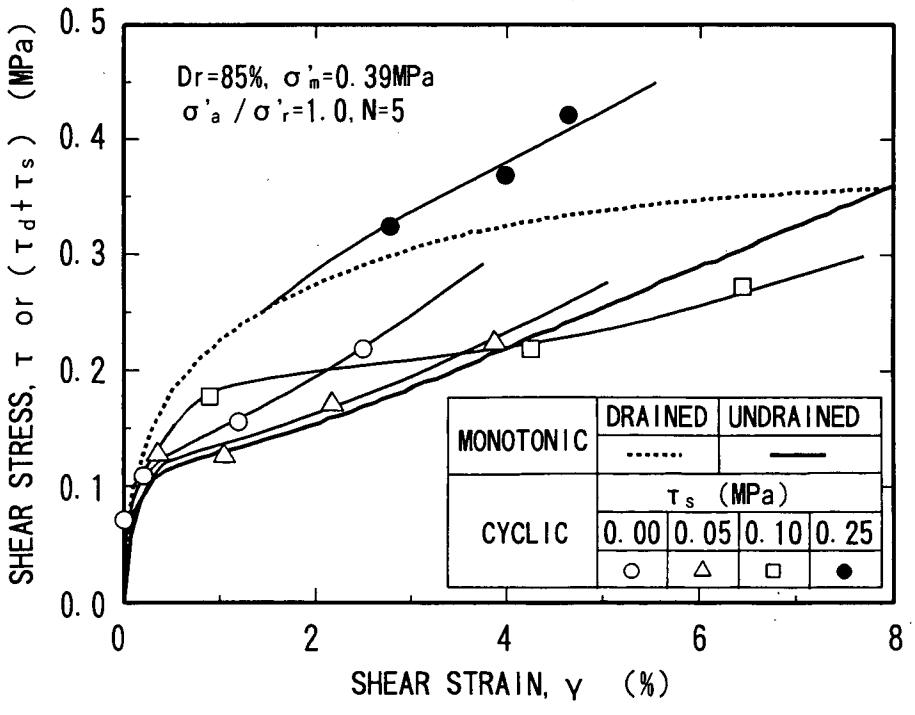


Fig. 22 Shear stress and shear strain in cyclic and monotonic loading(CTSS)

The comparison was made between CTX and CTSS for compacted rockfill. Fig. 23 shows shear stress ratio curve with the number of cycles. When the initial confining pressure is 0.1MPa, CTX gives larger strength, but when it is 0.39MPa, CTX strength is almost same as CTSS.

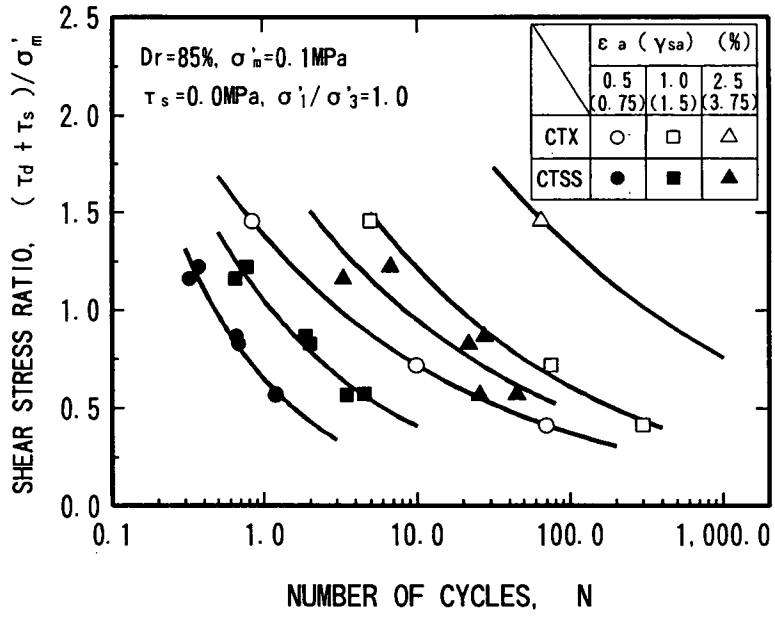


Fig. 23(a) Strength of CTX and CTSS test(initial mean confining pressure=0.1MPa)

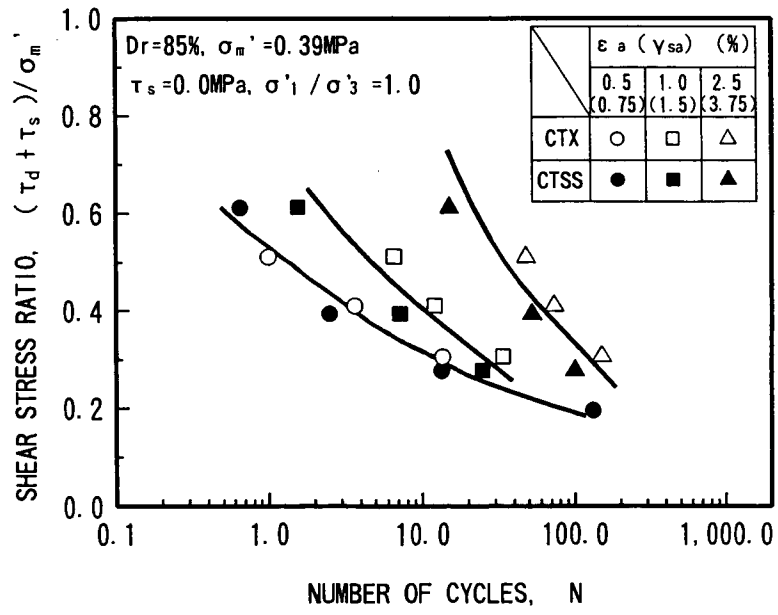


Fig. 23(b) Strength of CTX and CTSS test(initial mean confining pressure=0.39MPa)

Fig. 24 illustrates the failure stress at the plane of 45 degrees to the direction of principal stress in an specimen in relation with the normal stress on that plane. Here, the failure is designated as when maximum deviator stress occurs in monotonic loading, and when strain reaches 2.5% in 20 cycles in cyclic loading. It can be stated that the cyclic strength is less than the static undrained strength. However, cyclic undrained strength with anisotropic consolidation is greater than static drained strength, when the normal stress is less than 0.5MPa. Here, the reference strain for cyclic loading is taken to be 2.5%. However, larger reference strain can be tolerated, and much more dynamic strength can be expected for compacted rockfill.

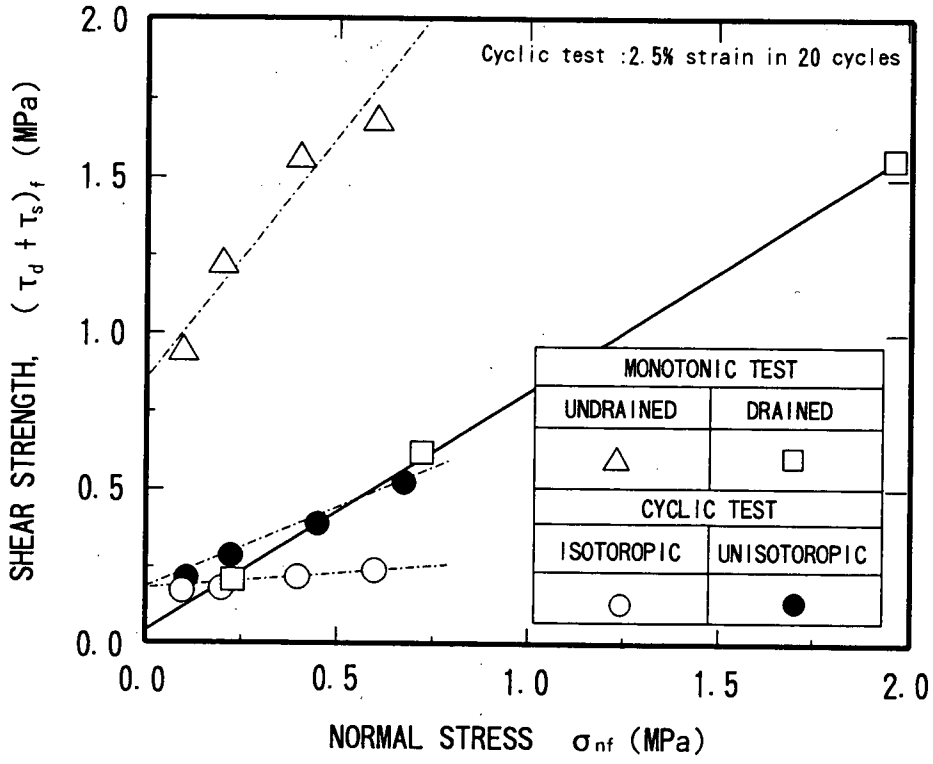


Fig. 24 Monotonic and cyclic strength of rockfill in drained and undraiend condition

References

1. N. Yasuda, N. Matsumoto, "A study on the deformation and strength properties of rockfill materials and their applicability to the seismic analysis of the embankment dams", Journal of Research, PWRI, Vol. 32, March, 1997
2. N. Yasuda, N. Matsumoto, "Comparison of deformation characteristics and cyclic loading laboratory tests and in situ tests", Canadian Geotechnical Journal, J. 31, 1994, pp.162-174

The paper is abbreviated version of reference No. 1. For further references, please refer to its references.

Seismic Stability and Deformations of Embankment Dams

by
Gonzalo Castro, Ph.D., P.E.[1]

Seismically induced failures of earth dams generally involve relatively loose sandy soils in the dams or their foundations. The failures can be divided into: a) those caused by a loss of stability and b) those in which limited but sufficiently large deformations accumulate during the earthquake to constitute cause of "failure" for structures or lifelines. In Case a) the deformations are very large and occur mostly following the earthquake. In Case b) the earth structure has not actually failed in the sense of a loss of stability, and the deformations occur mostly during the earthquake.

UNSTABLE CASE

A typical case of a loss of stability is the slide of the Lower San Fernando Dam caused by the 1971 San Fernando earthquake. Cross sections of the dam prior to and after the slide are shown in Figure 1. Detailed descriptions of the slide are presented in Seed et al. (1975) and Castro et al. (1989). The slide was caused by the loss in strength of the soil in the lower part of the hydraulic fill shell, which is shown darkened in Figure 1. This zone of the hydraulic fill consists of silty sands and sandy silts with standard penetration test (SPT) blowcounts mostly in the range of 15 to 20 blows/foot and cone tip resistance typically in the range of 50 to 100 tsf.

A review of the stability of the dam for pre-earthquake conditions indicates that the shear stresses within the failure zone in the hydraulic fill average about 900 psf. Computations of the dynamics of the movement of the center of gravity of the sliding mass indicated that the average shear resistance in the same zone during the slide was about 500 psf (Davis et al. 1988). The peak seismic shear stresses in the same zone were estimated by Seed et al. (1975) to be about 2000 to 3000 psf. Based on this information, one can infer that the stress strain behavior of the soil in the lower part of the hydraulic fill was as shown in Figure 2 and that it represents undrained behavior. Thus, even though the dam was stable since its construction in 1915 until the 1971 earthquake, there was a potential for instability because the undrained strength available at large strains was lower than the statically applied shear stresses. However, actual instability occurred only when 1) an earthquake occurred causing rapid enough loading so that the soil behaved undrained, and 2) the earthquake was large enough to overcome the peak strength and to strain the soil sufficiently so that the mobilized shear resistance became lower than the statically applied shear stresses. At that point, the slide movements were driven by the static and not the seismic shear stresses. Note that during the slide the available strength in the hydraulic fill of about 500 psf was a small fraction of the drained strength of about 3500 psf, i.e., the soil was strongly contractive and large pore pressures were present in the soil.

In the type of failure discussed above, the key soil parameter is the soil shear strength at large strains. The value of this strength determines whether instability could be triggered by the earthquake. The soil behavior can be assumed to be undrained given the relatively short duration of the movements and the relatively low permeability of the soil. In the Lower San Fernando Dam case, the undrained strength at large strains is a small fraction of the drained strength; however, the available strength is not zero. Poulos (1971) defined the steady state strength as, "the state in which the soil mass is continuously deforming at constant volume,

[1]Principal, GEI Consultants, Inc., Winchester, MA 01890 (USA)

constant normal effective stress, constant shear stress, and constant velocity." Even though in the case of the seismically induced failure discussed above, the velocity of deformation was not constant, the effect of rate deformation on the value of undrained steady state strength has been shown to be negligible (Castro et al. 1982). Thus, the strength that governs the seismically induced failure discussed above is the undrained steady state strength (referred to as S_{us}). Laboratory determinations of S_{us} indicate that S_{us} is only a function of void ratio for a given soil and also that it is a sensitive function of void ratio. For sandy soils, changes in values of S_{us} by a factor of 10 correspond to changes in void ratio, typically of 0.08 to 0.15.

The determination of *in situ* values of S_{us} must consider the heterogeneity of natural soil deposits and the changes in void ratio that even the most careful sampling procedure will cause in "undisturbed" soil samples. A procedure was proposed by Poulos et al. (1985) to account for these factors.

The results of the application of the Poulos et al. procedure to the hydraulic fill from the Lower San Fernando Dam are presented in Figure 3. The results presented were obtained from tests performed by two laboratories, indicating no significant difference among the two laboratories. More importantly, the results are in good agreement with the strengths estimated from the mechanics of the actual slide thus providing verification of the soundness of the method used to determine *in situ* values of S_{us}.

The laboratory investigation performed to determine S_{us} provided also information on the shear strains required to trigger the failure (about 0.5 percent) and on the strains at which S_{us} was reached (about 20 percent). Given a thickness of the failure zone of about 35 feet one can estimate the corresponding displacements of the failure mass as follows:

Table 1. Lower San Fernando Dam Slide - Strains in Critical Layer

Displacement of Failure Mass (ft)	Shear Strain in Layer (%)	Event
0.2	0.5	Triggering Strain
7	20	Steady State Reached
150	400	Movement Stopped

Note that very small displacements are sufficient to trigger the failure. Thus in cases of potential instability resulting from low S_{us} values in sands, either the deformations are very small if the earthquake is not sufficient to trigger the failure, or become very large if instability is triggered. An analysis of earthquakes that caused significant shaking of the Lower San Fernando Dam prior to the 1971 event and a review of detailed surveying records at the time of these events indicated negligible deformations. This observation is in agreement with the very small deformations that are required to trigger a major failure.

STABLE CASE

The response of an earth structure to seismic shaking would be quite different than the observed response of the Lower San Fernando Dam, if the S_{us} values are sufficiently high so that the earth structure would remain stable even if the strengths were reduced to S_{us}. In such case, the stress strain behavior in the sands would be as shown schematically in Figure 4. The deformations would be limited, but potentially damaging. Because of the limited deformations, the pre- and post-earthquake driving shear stresses are about the same. The movements would occur mostly during shaking and the dam would be stable at the end of shaking. Displacements are typically less than 3 m and often substantially lower.

DAM REMEDIATION

When providing remediation to reinforce loose sands in an earth dam or its foundation one needs to consider what behavior one is trying to improve. An example of the proposed remediation for an earth dam is shown in Figure 5. The loose sand in the foundation was found to have low enough S_{us} values that it was potentially unstable and it was further determined that the earthquake would cause sufficiently large strains that the loose sand strength would be reduced to S_{us}.

Thus, a failure of the type observed at the Lower San Fernando Dam was likely. The deep soil mixed columns are arranged as continuous rows transverse to the axis of the dam, forming "shear walls." The purpose of these walls is to provide sufficient strength in the loose sand layer so that the dam would remain stable even if the loose sand strength were reduced to S_{us}. The arrangement of the columns would be different if their purpose were to limit the strains in the loose sand within and adjacent to the reinforced zone, so that the sand would not develop pore pressure increases and/or a reduction in strength to S_{us}. In such a case, one would arrange the columns in a grid of both transverse and longitudinal walls or in a pattern of cells.

REFERENCES

Castro, G., Poulos, S.J., France, J.W. & Enos, J.L. (1982). Liquefaction induced by cyclic loading, report by Geotechnical Engineers, Inc. to the National Science Foundation, Washington, D.C. March, 1-80.

Castro, G., Keller, T.O. & Boynton, S.S. (1989). Re-evaluation of the Lower San Fernando Dam, report 1, an investigation of the Feb. 9, 1971 slide, 2 Vols. GEI Consultants, Inc., U.S. Army Corps of Engineers Contract Report GL-89-2, September.

Davis, A.P., Castro, G., & Poulos, S.J. (1988). Strengths backfigured from liquefaction case histories, the *Second International Conference on Case Histories in Geotechnical Engineering*, Rolla, Missouri.

Poulos, S.J., Castro, G., & France, J.W. (1985). Liquefaction evaluation procedure, *Journal of Geotechnical Engineering*, ASCE, Vol.III, GT6, 772-791.

Seed, H.B., Lee, K.L., Idriss, I.M. & Makdisi, F.I. (1975). The slides in the San Fernando Dams during the earthquake of February 9, 1971, *Journal of the Geotechnical Engineering Division*, ASCE, Vol. 101, GT7, 651-688.

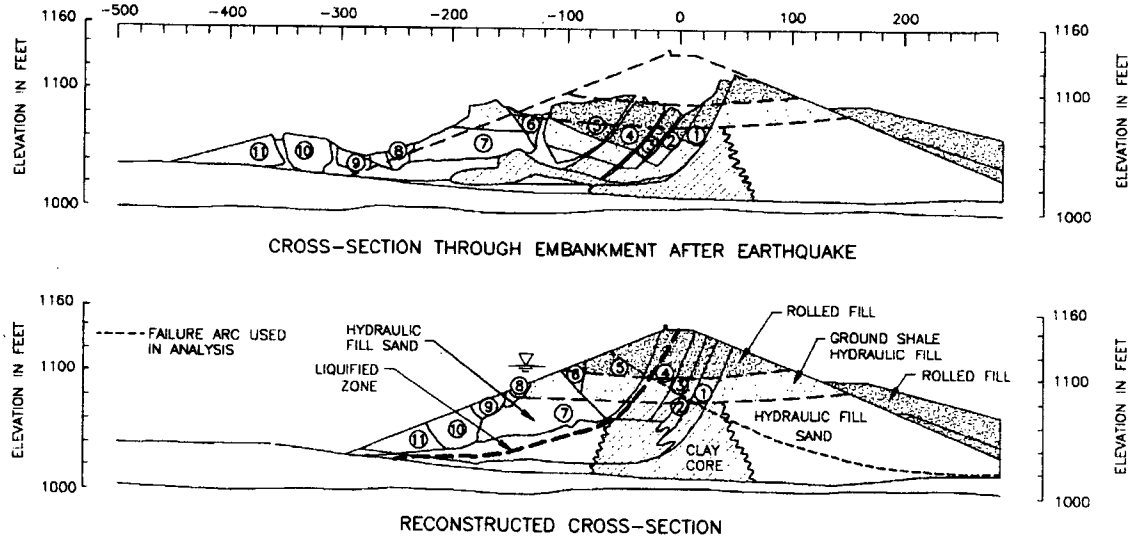


Figure 1: Lower San Fernando Dam slide.

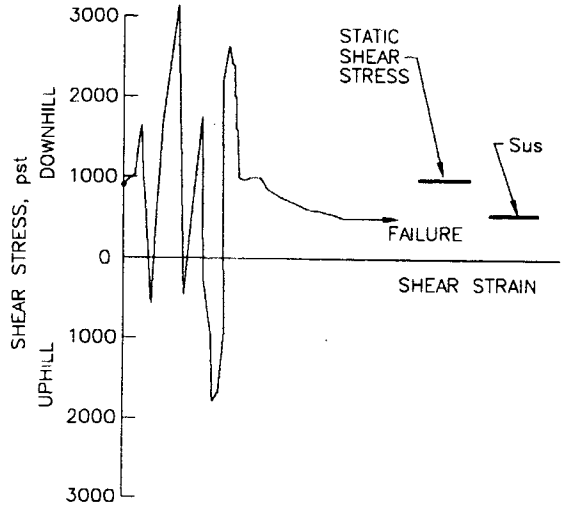


Figure 2: Stress strain diagram for the unstable case - Lower San Fernando Dam.

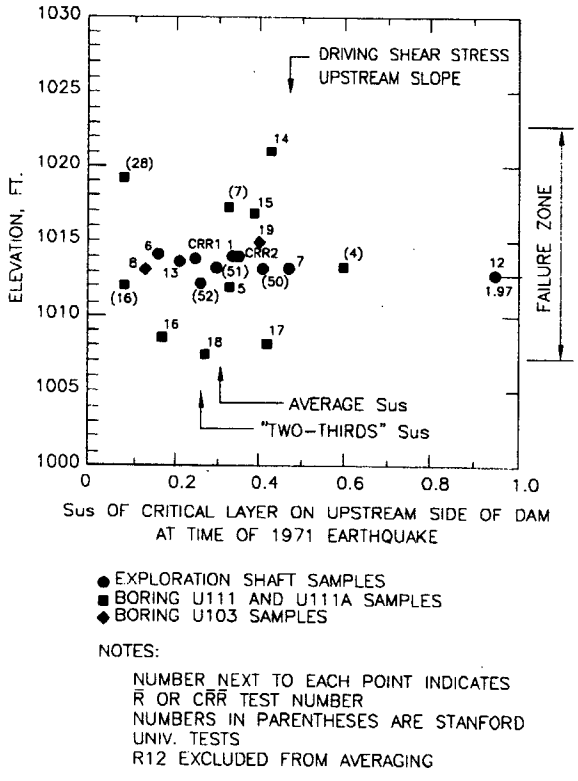


Figure 3: Determination of undrained steady state strength in laboratory.

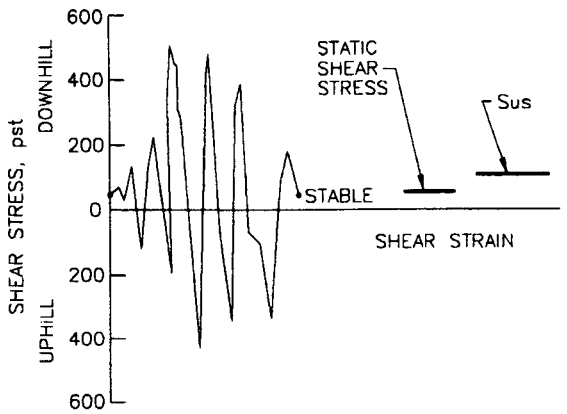


Figure 4: Stress strain diagram for the stable case.

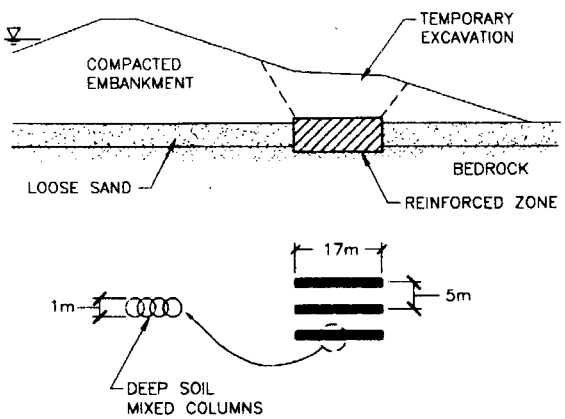


Figure 5: Remediation of embankment dam on loose sand foundation.

Factor Analysis of Damage to Small Earth Dams due to the 1995 Hyogoken-Nambu Earthquake

Hitoshi YOSHIDA[1], Tsuneo UESAKA[2], Tomoya IWASHITA[3], Jun MATSUURA[4] and Norihisa MATSUMOTO[5]

ABSTRACT

This paper discusses damage to small earth dams due to the Hyogoken-Nambu Earthquake of January 17, 1995. Investigations of 266 dams were conducted in the area where the JMA seismic intensity was 5 or higher, and which were located within about 50 kilometers from the earthquake source fault. Small earth dams suffered various forms of damage such as longitudinal cracking, transverse cracking, settlement and deformation of the dam body. The damage to small earth dams was classified into five grades from no damage to severe damage such as a complete failure. The damage grade was analyzed by several factors such as distance from the fault, topography and geology, intensity of quake motion, direction of dam axis against the fault, year of completion, and height of dam. The characteristics of factors affecting damage to small earth dams were evaluated.

Key Words: *Dam, Damage, Earthquake, Fault, Geology, Site investigation.*

1. INTRODUCTION

The Kobe area of Japan was struck by a major earthquake, the Hyogoken-Nambu Earthquake, with a Japan Meteorological Agency (JMA) magnitude of 7.2 on January 17, 1995. This earthquake was a large intra-plate earthquake. A JMA seismic intensity of 7 was recorded in the Kobe urban area and in the northern part of Awaji Island for the first time since the Fukui Earthquake in 1948. The maximum horizontal acceleration of 818 gal was recorded on the stiff ground (JMA Kobe station) a few hundred meters near the source fault. From the observed records, the maximum earthquake motions observed in the earthquake source field within ten kilometers were 300 to 800 gal in acceleration and 80 to 180 kine in velocity on the soft ground, and acceleration of 400 to 820 gal in acceleration and velocity of 40 to 90 kine in velocity on the solid ground (Iwasaki, 1996).

1) Head, Fill Dam Division, Public Works Research Institute, Tsukuba, Japan
2) Director, Dam Department, PWRI, ditto
3) Senior Research Engineer, Fill Dam Division, ditto
4) Research Engineer, ditto
5) Technical Counselor, Japan Dam Engineering Center, Tokyo, Japan

Buildings and infrastructures suffered severe damage on the strong quake zones while soil structures such as banks, small earth dams and river levees suffered damage over a wide area. We analyzed the factors that affected the damage to small earth dams. We reported the performance of and damage to earth dams caused by the event. The earth dams investigated are small-scale embankment dams for mainly irrigation, and do not include rockfill dams and large dams higher than twenty meters under the River Law of Japan. Most damaged dams were earth dams lower than fifteen meters. The well-engineered dams with a height of more than twenty meters, that were designed and constructed according to the recent design criteria, did not suffer serious damage affecting their safety (Matsumoto *et al.*, 1996).

Numerous small earth dams are distributed throughout Awaji Island (about 24,000 dams), the Kako river basin in the west of Kobe City, and the Muko river and Ina river basins in the east of Kobe City. Since the strong quake zones in which the JMA seismic intensity of 7 was recorded were in urban areas, there were few earth dams in the areas. An earth dam, Niteko Dam, near the zone of seismic intensity 7 collapsed. In the Kako river basin that is located in the west of Kobe City, small earth dams were severely damaged, although there was little damage to buildings and other infrastructures. On Awaji Island, many small earth dams were damaged in Hokudan-cho where passed the Nojima Fault and in Ichinomiya-cho leaded from the southern end of the fault. Damage to earth dams in Sumoto City was comparatively slight in spite of an observed seismic intensity of 6. On Honshu Island (Main Island), damage to earth dams was concentrated in the source fault area of Itami City, Takarazuka City, Nishinomiya City and the plain of Akashi City, Kakogawa City and the western part of Kobe City. In the northern area of the Rokko mountain region, damage was relatively slight.

The materials of most of the investigated small earth dams were silty sand or clayey sand, mostly composed of decomposed granite. The water levels in the reservoirs of most earth dams were very low, since the event occurred in the farmer's slack season. Damage to the small earth dams would have been severer if the reservoir water level had been higher in the farmer's busiest season. An earth dam on Awaji Island failed due to the liquefaction and overtopped shown in **Photo. 1**. The sand boils were found out at the bottom of the reservoir. We could find sand boils at the reservoir bottom of other dams, yet it was not clear that damage to these dams occurred due to the liquefaction.

In northern Awaji Island, inflow to several dams rapidly increased probably because of groundwater fluctuations after the event. In several earth dams on the mountainous slopes in Tsuna-cho, cracks occurred on the bottom of the reservoirs and the reservoirs became empty, in spite of no damage to the dam bodies themselves. The same phenomenon reported just after the Nankai Earthquake that occurred about 150 km south of Awaji Island in December, 1946.

2. OUTLINE OF INVESTIGATIONS

We investigated small earth dams in the area where the seismic intensity was 5 or higher, and which were located within about 50 kilometers from the earthquake source fault. Here, the earthquake source faults are the Nojima Fault on Awaji Island and the aftershocks area on Honshu Island. It is estimated that maximum

acceleration on the ground in the investigated area exceeded 100 gal from the observed records. We gathered little data on undamaged or slightly damaged earth dams far from the source fault, because of giving priority to investigation of severely damaged earth dams. A total of 266 small earth dams was investigated in detail; 143 on Awaji Island and 123 on Honshu Island. The locations of the investigated earth dams are shown in **Figure 1**. We collected the following data: the survey of main profiles such as heights, widths and lengths of the crest, slope gradients, axial directions, years of completion, etc., the inspection of slope protections, spillways, sluice ways, leakage and reservoir slopes, the observation of the materials of dams and the geology of foundations and abutments, the measurement of settlements, the mapping of cracks and bulging, and the finding of sand boils. We also sampled the soil materials of the several dam bodies and made various soil tests on the samples.

We also investigated the performance of tombstones during the Hyogoken-Nambu Earthquake to estimate the distribution of the intensity of the earthquake motion in the northern part of Awaji Island (Iwashita *et al.*, 1996). We surveyed the state of 3,545 overturned tombstones for a total of 79 graveyards. We selected only rectangular-shaped tombstones and excluded specially shaped and structured ones. We calculated the ratio of overturned tombstones for each graveyard and estimated the intensity of the quake motion at each site.

3. FACTORS AFFECTING DAMAGE TO DAMS

We classified the damage to small earth dams into five grades from no damage (Grade 0) to failure (Grade 4). The classification of the damage grades was conducted on the basis of the damage criterion shown in **Table 1**. This criterion was modified from that of the earthquake induced damage of the river levees in "Technical Manual for Earthquake Disaster Restoration on Civil Engineering Structures (draft)" (Ministry of Construction, 1986). Typical views of damaged dams classified as Grade 4, 3 and 2 are shown respectively in **Photos 1**, **2**, **3** and **4**. We describe the analysis results of several factors affecting damage to small earth dams in the following.

(1) Forms of Damage

Earth dams suffered various forms of damage such as longitudinal cracking, transverse cracking, settlement, deformation of the dam body and liquefaction. The piping of the dam body and foundation occurred due to a failure of aged sluiceways.

We classified the forms of major damage to small earth dams into seven types: longitudinal cracks, transverse cracks, settlement, damage of spillways, damage of sluice ways, damage of slope protections, and leakage. **Figure 2** shows the number of dams for each damage form: (a) indicates on Awaji Island and (b) on Honshu Island. The most common form of damage was longitudinal cracks. Over sixty percent of damaged earth dams occurred longitudinal cracks. Most of the dams damaged severely (over Grade 3) were those of the longitudinal cracks. The damage of the dams in the area over 30 km away from the aftershocks area on Honshu Island was mainly to slope protections, but the damage was slight (Grade 1).

Figure 3 shows the percentage of each major

damage form for each range of axial direction of dam. It seems that there is no special relationship between the form of damage and axial direction of dams.

(2) Effect of Distance from the Fault

Figure 4 shows the relations between damage grade of earth dams and the closest horizontal distance from the fault: (a) indicates on Awaji Island and (b) on Honshu Island. The lateral axis in **Figure 4** indicates the distance from the Nojima Fault on Awaji Island, and the distance from the centerline of the aftershocks area on Honshu Island. Symbols in **Figure 4** differ by the geological stratum of the foundation of each dam shown in **Table 2**.

Awaji Island

The damage grade of dams decreases with increase in distance from the fault, for the dams on the stratum prior to the Osaka group over 10 km away from the fault. Even within a few kilometers of distance from the fault, there was no dam damaged in Grade 4 severely, and some of these dams suffered no damage. The earthquake ruptures of the Nojima Fault passed just near about ten earth dams. In spite of the location, these ten dams suffered damage, the grades of which were only Grade 1 to 3. None of the dams collapsed and some of the dams were undamaged. A small dam directly above the Nojima Fault suffered a failure of the spillway and only a medium damage to the downstream body.

Honshu Island

The attenuation of damage to dams was not observed clearly because we focused our investigation on severely damaged earth dams far away the fault. In spite of the long distance from the fault, several dams on alluvium, terrace deposit and diluvium of the Osaka group suffered severe damage. Three earth dams on the Osaka group of 20 to 30 km away from the fault suffered large-scale slides (Damage Grade 4). The view of one of them is shown in **Photo. 2**. These dams were constructed over 70 years ago and had steep slopes.

(3) Effect of Geological Stratum of Foundation

The geological classification of the investigated area is indicated in **Table 2**. An earthquake motion due to the rupture of fault progresses up to the ground surface and amplifies during progression through the ground. Generally, the response of the motion becomes larger in a softer ground layer, that is a younger stratum. Therefore, the geological stratum of a dam foundation affects the intensity of the incident quake motion of the dam. The following can be said from **Figure 4** that shows the attenuation of damage grade for each geological stratum of dam foundation.

Awaji Island

There are few earth dams on alluvium or terrace deposits because the distribution of the alluvium and terrace deposits on Awaji Island is limited to narrow areas. The younger the geological stratum of a dam foundation and the longer the distance from the Nojima Fault to the dam, the severer the damage to the dam, for the dams on the stratum of the Pre-Quaternary Age. Next, the dams with a foundation prior to the Tertiary Age suffered only slight damage of under Grade 1 if over two kilometers from the Nojima Fault.

Honshu Island

The earth dams with higher damage than Grade 2 were limited to those constructed on alluvium, terrace deposits and the Osaka group. The earth dams with geological foundations prior to the

Tertiary Age were not damaged or limited to slight damage.

(4) Effect of Intensity of Earthquake Motions

Figure 5 shows the distribution map of the ratio of the number of overturned tombstones against a total of the tombstones obtained from our investigation at the northern part of Awaji Island. The geological cross section (Mizuno *et al.*, 1990) of the line A-A' drawn in **Figure 1** (a) is shown in **Figure 6**. The damage grades of earth dams and the percentages of overturned tombstones at graveyards near the line A-A' are also shown in **Figure 6**. We compared **Figure 5** with the distribution map of damaged dams in **Figure 1** (a) and evaluated **Figure 6**. The percentages of overturned tombstones exceeded eighty percent in the areas where the damage to dams was over Grade 3. This suggests that very strong earthquake motions were experienced in those areas.

(5) Effect of Topography

We classified the topography of dam sites into plains, hills, foothills, steep slopes of mountain, and gentle slopes of mountain. **Figure 7** shows the percentage of each topography for each damage grade.

Awaji Island

The damage to earth dams was severer in the order of plains > hills > gentle slopes of mountain > foothills > steep slopes of mountain from **Figure 7**, although the number of investigated dams is different for each topography. Damaged dams of over Grade 3 are concentrated in plains and hills, which is also related to their geology.

Honshu Island

Most of the damaged dams were constructed on plains or hills. Earth dams at gentle slopes and steep slopes of mountains suffered practically no damage, although few dams were investigated at the topographical areas. Topography of plains reflects that the foundation geology consists of the alluvium deposit.

(6) Effect of Axial Direction of Dam

Figure 8 shows the relation between axial direction of dam and distance from the fault with damage grade of 2 or higher. The axial direction of dams indicates the differential direction from the north. The differential direction ranges within $\pm 90^\circ$; a plus sign indicates clockwise from the north and a minus sign counterclockwise.

Awaji Island

The axial directions of damaged dams were concentrated in the direction of around 30° to 40° from the north even for the dams over ten kilometers away from the fault, with the exception of the damaged dams within a few kilometers from the fault. These directions agree with the direction of the Nojima Fault. The predominant directions of the earthquake motions due to the rupture of the fault make right angles with the fault. Hence, **Figure 8 (a)** indicates that the predominant direction of earthquake motions agreed with the stream direction of the dams.

Honshu Island

The axial direction of dams was not clearly related to the damage to dams in **Figure 8 (b)** about Honshu Island.

(7) Effect of Year of Completion

The construction method of an earth dam and the structure of a dam body depend on banking techniques, tools and machines available at the time of the construction of dams. The year of completions of an earth dam can thus be used as an index for evaluating the dam structure, construction method and especially the degree of compaction. We divided it roughly into three periods of before 1925, 1925 to 1950 and after 1950. **Figure 9** shows the percentages of the period of the completion year for each damage grade.

Awaji Island

The small earth dams damaged in Grade 3 or higher were old dams constructed before 1925.

Honshu Island

The small earth dams damaged in Grade 2 or higher were old dams constructed before 1925. Two dams on the alluvium deposit in Kakogawa City suffered the damage of longitudinal cracks at the crest and suffered damage of Grade 1, although they were constructed after 1950. Both of them had heights of lower than three meters and steep slopes of 1:1.6 to 1:1.0.

The old small earth dams constructed before the early twentieth century were banked by human-power under inadequate construction management and have steep slopes in their cross sectional shapes, that is poor-engineered. The relatively recent earth dams constructed after the 1950's were compacted probably by machines and well engineered. Hence, they were not damaged or very slightly damaged (Grade 1) in spite of the few number of investigated dams.

(8) Effect of Dam Height

Figure 10 shows the relations between height of dams, damage grade and distance from the fault for the damaged dams of over Grade 2.

Awaji Island

The dams damaged severely of over Grade 3 were limited to the dams with a height of fewer than ten meters excluding the dams just near the Nojima Fault.

Honshu Island

Most of the damaged earth dams exceeding Grade 2 were less than 10 m in height. Although two earth dams with a height of over 10 m suffered severe damage of Grade 3, both of them had extremely steep slopes of 1:1.6 to 1:1.4. One of the two had a thick extra-banking on the dam body itself for a crest road.

Most of the severely damaged earth dams were limited to those with a height of under about 10 m. The high earth dams were not damaged or very slightly damaged except for a few special dams mentioned above. This was because the structure and banking method of large earth dams are different from those of low and small dams with a height of fewer than 10 m.

4. CONCLUSIONS

We investigated damage to small earth dams due to the Hyogoken-Nambu Earthquake. We evaluated the effect of several factors on the characteristics and grades of the damage to dams. The findings are summarized as follows.

[1] Longitudinal cracking was the most common form of damage to small earth dams.

[2] The earth dams constructed on old geological foundations of the Pre-Quaternary Age suffered little damage. The dams on young geological foundations such as the alluvium or diluvium of the Osaka group suffered severe damage.

[3] The earth dams in low lands of plains or hills were seriously damaged. The earth dams in mountainous areas suffered little or only slight damage. This reflects the foundation geology stated in [2].

[4] Almost all the severely damaged earth dams on Awaji Island and Honshu Island were low dams with a height of lower than ten meters and were old dams constructed before the 1920's. The dams constructed after the 1950's were undamaged or very slightly damaged.

ACKNOWLEDGEMENTS

We wish to acknowledge valuable cooperation of the field survey with Mr. Shinji Yokoyama of CTI Engineering Co., LTD.

REFERENCES

Iwasaki, Y. (1996): Records of Strong Earthquake Motions, *Report on Investigation of the Great Hanshin-Awaji Earthquake Disaster*, Vol.1, Japanese Geotechnical Society, Japan, pp. 43-57. (in Japanese)

Iwashita, T., A. Nakamura, N. Matsumoto and S. Yokoyama (1996): Characteristics of earthquake motion near a fault during the 1995 Hyogoken-Nambu Earthquake from the overturning of tombstones, *Proc. of Conference on the Great Hanshin-Awaji Earthquake Disaster*, Japan Society of Civil Engineers, pp. 17-22. (in Japanese with English summary)

Matsumoto, N., A. Nakamura, T. Sasaki and T. Iwashita (1996): Effects on Dams, *Special Issue on Geotechnical Aspects of the January 17 1995 Hyogoken-Nambu Earthquake, Soils and Foundations*, Japanese Geotechnical Society, pp. 273-281.

Ministry of Construction, Japanese Government (1986): River Facilities, *Technical Manual for Earthquake Disaster Restoration on Civil Engineering Structures (draft)*, pp.96-113. (in Japanese)

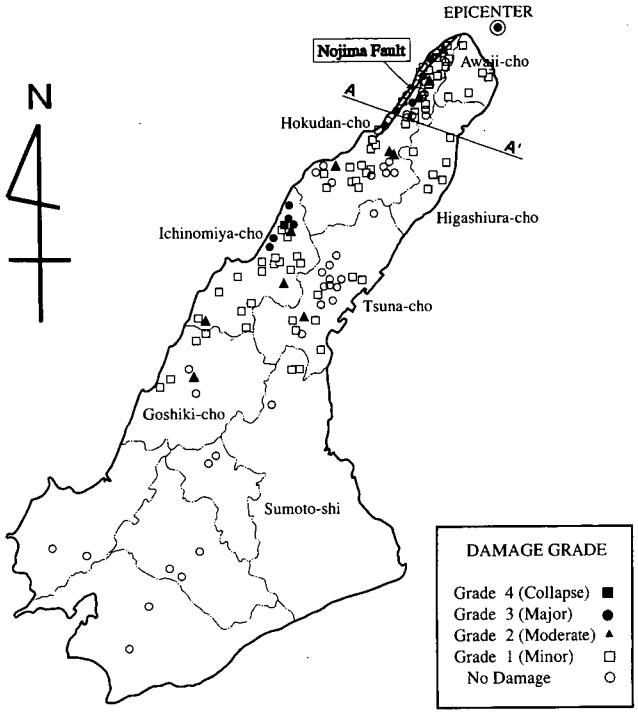
Mizuno, K. *et al.* (1990): Geology in Akashi Area, *Report on local geology*, Vol. 83. (in Japanese)

Table 1 *Criterion for evaluation of damage grade of small earth dams*

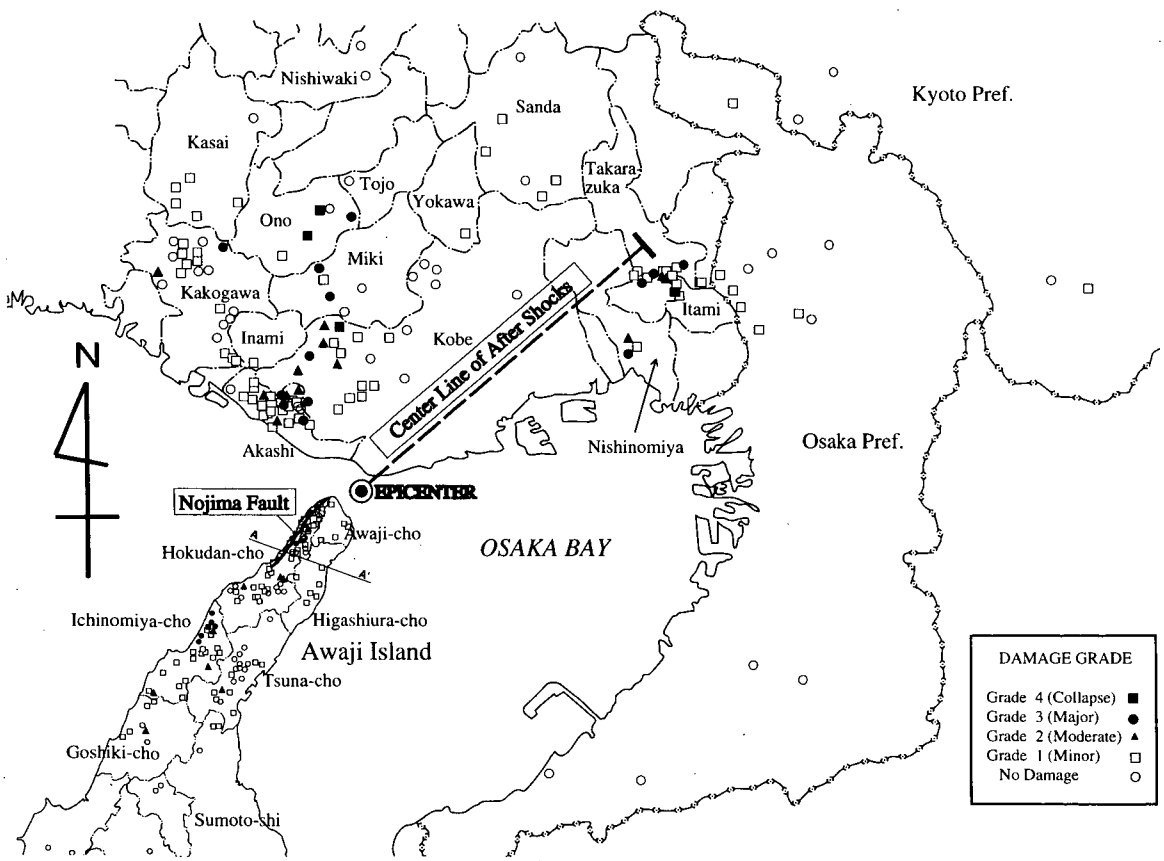
Form	Classification		Grade	Notes
Longitudinal crack	Deep crack	Over 20 cm wide or Differential settlement of over 30 cm	4, 3	・Large-scale slide ・Collapse of a part of dam (Grade 4)
		10 to 20 cm wide or Differential settlement of 20 to 30 cm	2	
		Under 10 cm wide and Differential settlement of under 15 cm	1	
	Shallow crack	Over 10 cm wide or Differential settlement of over 15 cm	2	・Small-scale slide ・Shallow slide
		Under 10 cm wide and Differential settlement of under 15 cm	1	
Transverse crack	Leakage route due to continous cracks from upstream to downstream	(Over 20 cm wide or Differential settlement of over 30 cm)	4, 3	・Overall judgment from condition of leakage ・Collapse of a part of dam (Grade 4)
		(10 to 20 cm wide or Differential settlement of 15 to 30 cm)	2	
	Discontinuous cracks from upstream to downstream	(Under 10 cm wide and Differential settlement of under 15 cm)	1	
Settlement・Deformation	Large deformation		4, 3	・Liquefaction ・Collapse of a part of dam (Grade 4)
	Uniform settlement	Settlement of over 100 cm	3	
		Settlement of 50 to 100 cm	2	
		Settlement of under 50 cm	1	
Damage to appurtenant works	Severe damage		3	・Appurtenant works indicate spillway, sluice way, slope protection, etc. ・Judgment considering aging of structures
	Medium damage		2	
	Slight damage		1	
Leakage	Increase of drainage Leakage due to piping		4～1	・Overall judgment with other damage factors

Table 2 *Geological classifications in the investigated area*

Geological time		Stratum			Rock	Outcrop area
Quaternary	Holocene	Alluvium	a		Clay, Sand, Gravel	Hyogo Pref. Osaka Pref. Awaji Island
	Pleistocene	Terrace deposit	t			
Tertiary	Pleistocene ～Oligocene	Osaka group	Og			
	Miocene	Kobe group	K		Mudstone, Sandstone, Conglomerate	Kobe
					Tuff	Kobe, Awaji Island
Cretaceous		Rokko granite	Ng	PrT	Biotite granite	Kobe
		Ryoke granite	Nrg		Granite, Granodiorite	Awaji Island
		Izumi group	Ial		Sandstone, Shale	Awaji Island
		Arima group	A		Rhyolite, Pyroclastic rock	Hyogo Pref.
Jurassic ～ Carboniferous		Tanba group	T		Sandstone, Slate, Shale	Hyogo Pref.

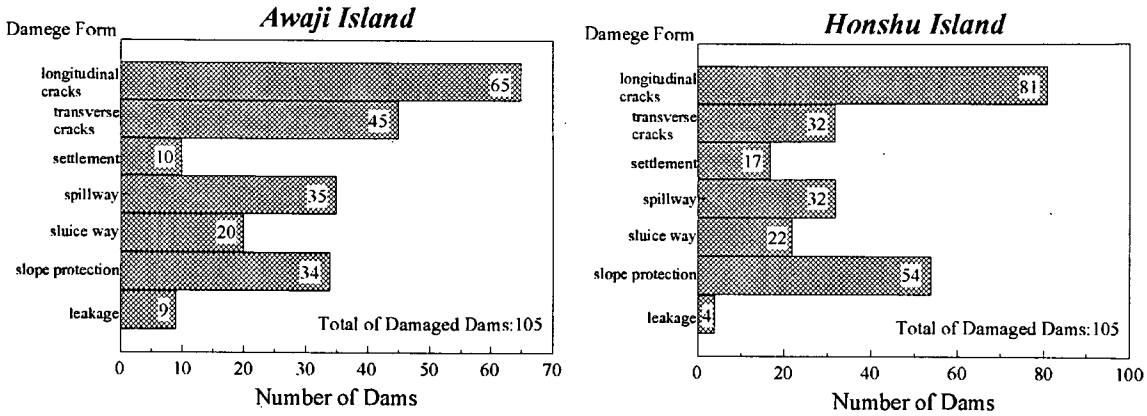


(a) Awaji Island



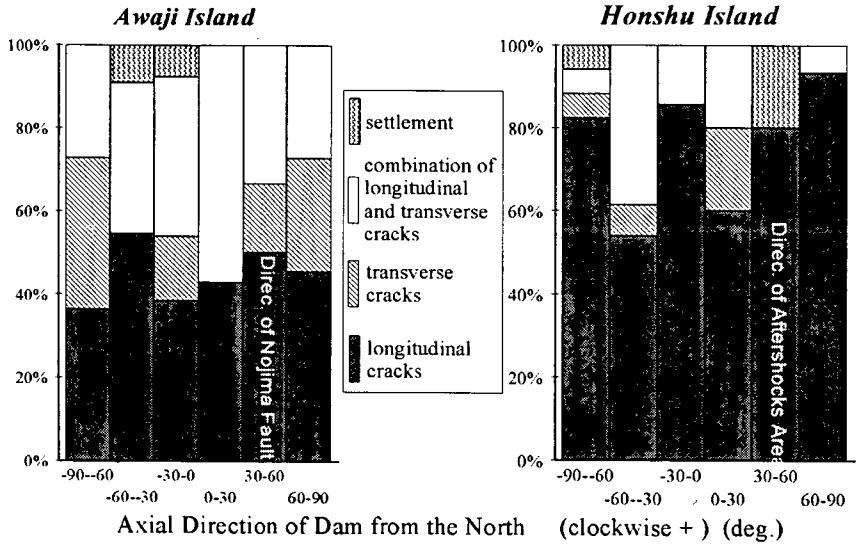
(b) Honshu Island

Figure 1 *Locations and damage grade of investigated earth dams*



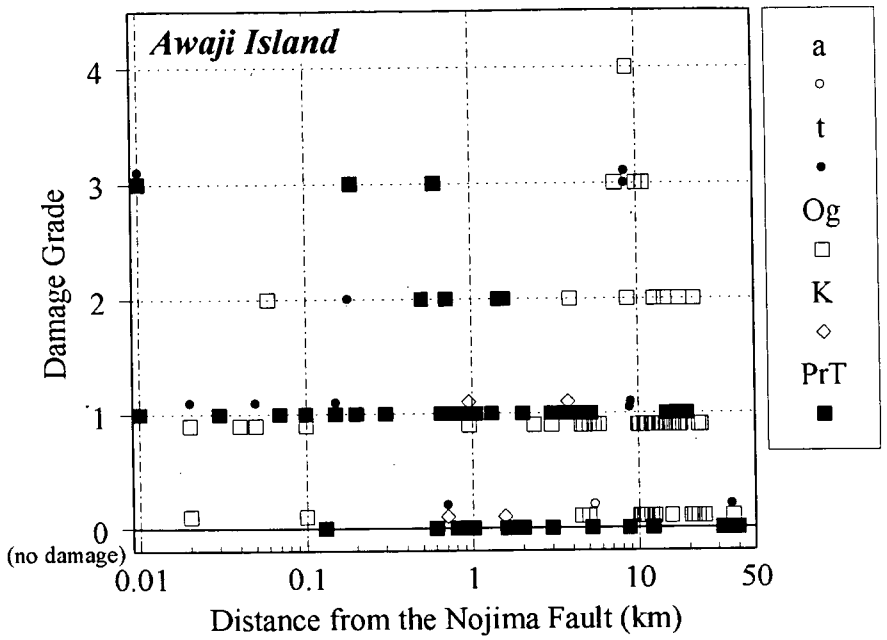
(a) Awaji Island *(b) Honshu Island*

Figure 2 *The number of earth dams for each damage form*

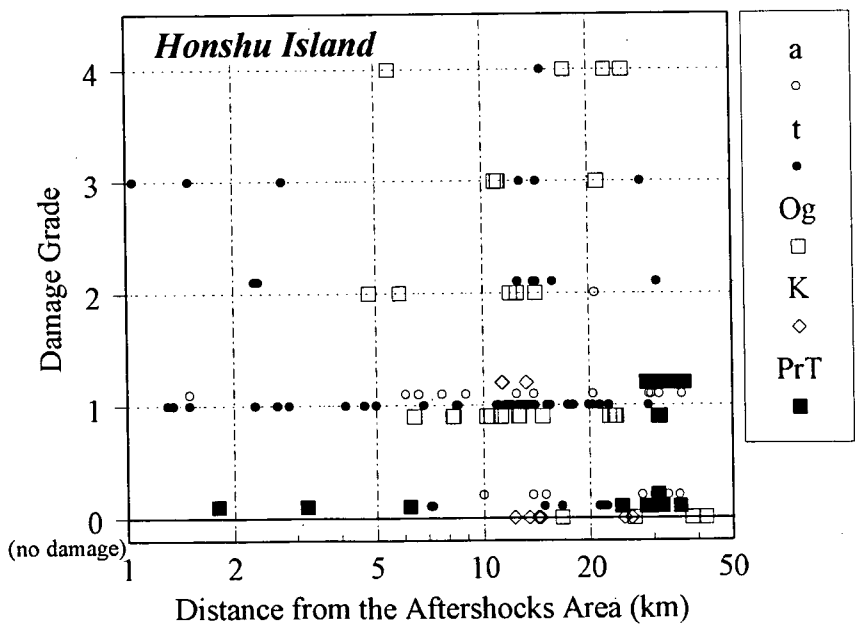


(a) Awaji Island *(b) Honshu Island*

Figure 3 *Relations of damage forms with axial direction of damaged earth dams*



(a) Awaji Island



(b) Honshu Island

Figure 4 *Relations of damage grade of earth dams with distance from the fault and geological stratum of dam foundation*

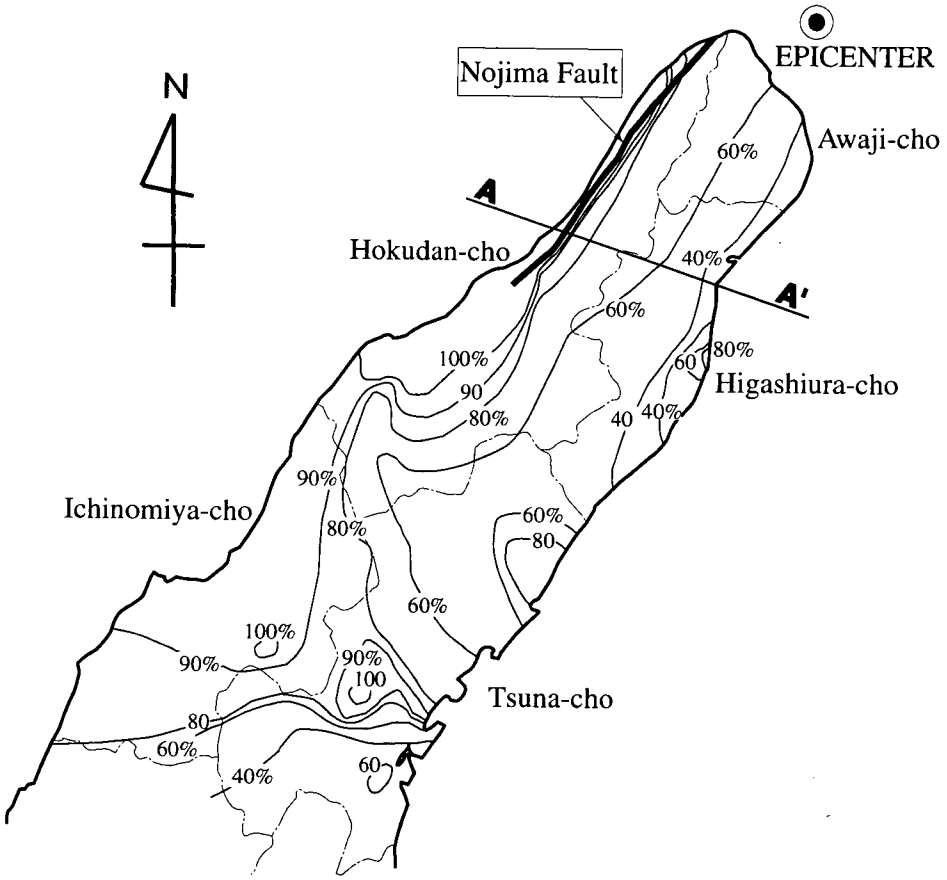


Figure 5 *Distribution of the ratio of the number of the overturned tombstones against a total of the tombstones surveyed at each graveyard in the northern part of Awaji Island*

Figure 6 *Distribution of damage grade of earth dams and the ratio of the number of the overturned tombstones in the geological cross section (Mizuno et al., 1990) of line A-A' shown in Figure 1 (a) and Figure5 of north Awaji Island*

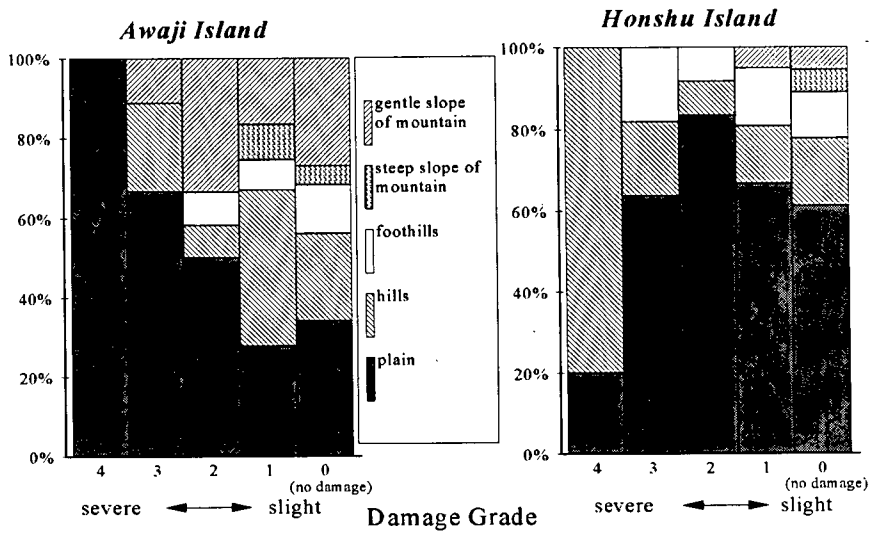
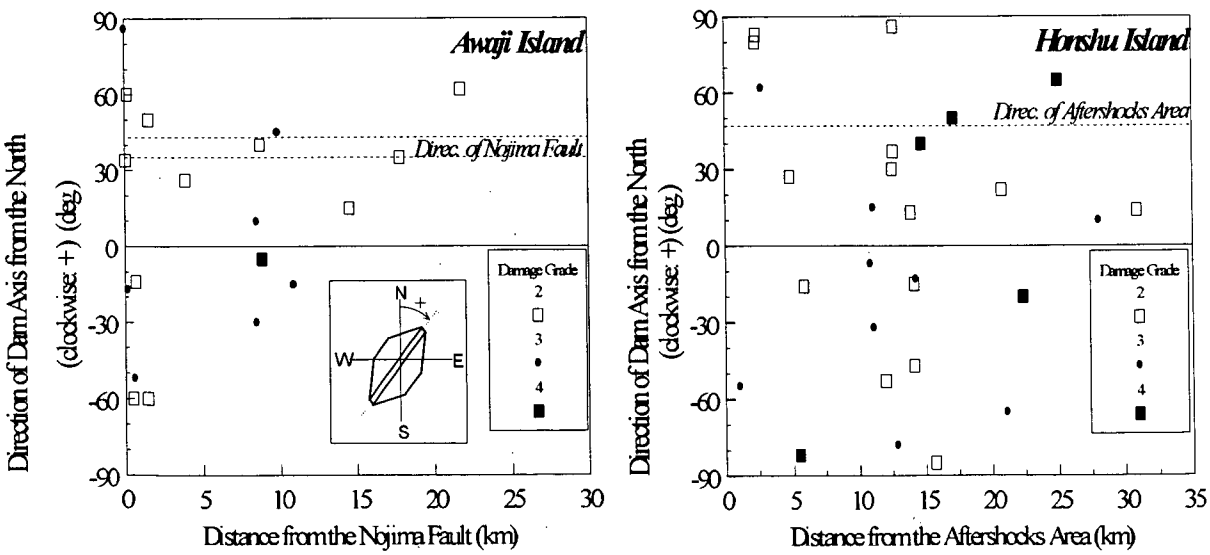
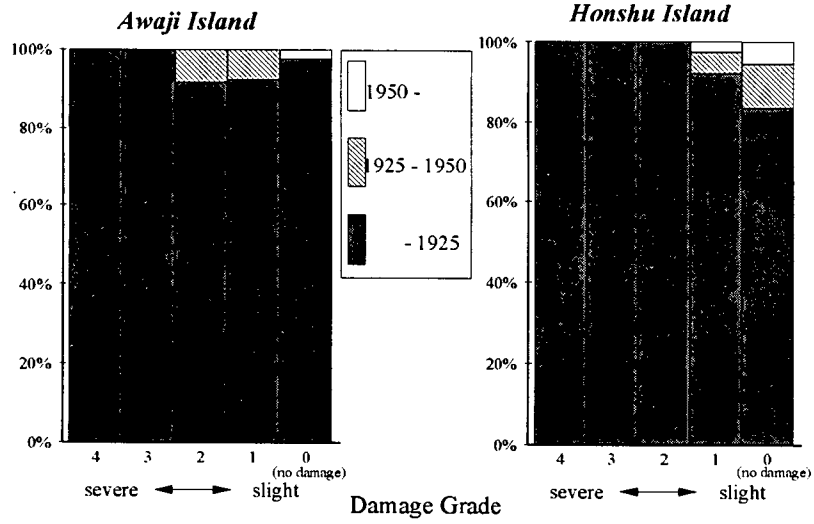


Figure 7 *Relations of damage grade of earth dams with topology at dam sites*



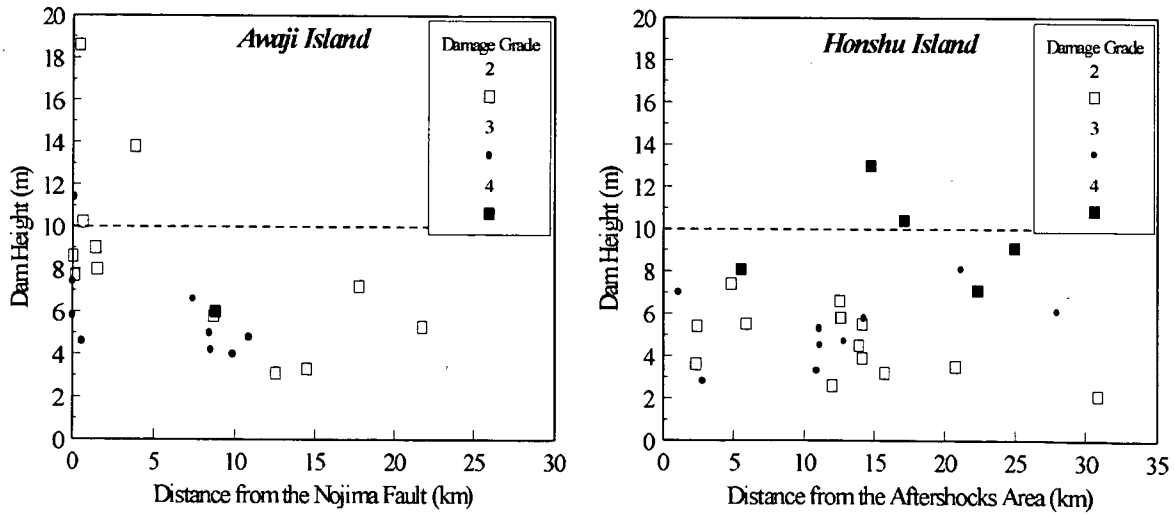
(a) Awaji Island *(b) Honshu Island*

Figure 8 *Distribution of axial direction of damaged earth dams*



(a) Awaji Island *(b) Honshu Island*

Figure 9 *Relations of damage grade of earth dams with year of completions*



(a) Awaji Island *(b) Honshu Island*

Figure 10 *Relations of damage grade of earth dams with dam height*



Photo. 1 *A liquefied earth dam of Grade 4 (Ichinomiya-cho on Awaji Island)*



Photo. 2 *A slide earth dam of Grade 4 (Ono City on Honshu Island)*



Photo. 3 *A damaged earth dam of Grade 3 (Ichinomiya-cho on Awaji Island)*



Photo. 4 *A damaged earth dam of Grade 2 (Akashi City on Honshu Island)*

Technical Session 4

Concrete Dams (2)

Seismic Response of Gravity Dams in Near Field During the 1995 Hyogoken-Nanbu Earthquake

By

T. Ohmachi[1], A. Jalali[2], and H. Kawana[3]

ABSTRACT

During the 1995 Hyogoken-Nanbu earthquake (often referred to Kobe earthquake), Nunobiki and Karasubara dams were struck in the close proximity of the fault rupture. Seismic response of the dams was evaluated by using artificially generated ground motions. The result of analysis shows that no cracks or any other serious damages may occur in the dams, which has been validated by post-earthquake observations. The directional differences in frequency contents and amplitude of ground motions in the near-field region and their effect on maximum tensile stress have been also discussed. Due to effect of polarized motion, the amount of increase in maximum tensile stress is not similar for all elements throughout the dam, and varies between 30% and 200%.

Keywords: Gravity Dams, Near-Field Ground Motion, Earthquake Damages, Kobe Earthquake, Tensile Stresses.

INTRODUCTION

Located inside the Kobe city (as shown in Figure 7), Nunobiki and Karasubara dams were shaken by 1995 Hyogoken-Nanbu earthquake (M 7.2). Although the rupture of the Kobe earthquake directly into downtown Kobe inflicted severe damages to buildings and other structures, almost all of the dams (about 50 dams within 50 km from the epicenter of the Kobe earthquake) have survived without any major damages that could be harmful for dam safety. There was not any instrumentation program on the sites of the Nunobiki and Karasubara dams, consequently real recordings are not available for these dams.

This paper reports on the artificially generating of the ground motions on dam sites and seismic behavior of the dams due to these ground motions. Because of rupture directivity in near-field region, we have also discussed these effects and their relevance from a structural engineering point of view.

RESPONSE OF DAMS TO KOBE EARTHQUAKE

Nunobiki Dam

Nunobiki dam, gravity type, height 33.3 m, crest length 110 m, crest thickness 3.62 m, and base thickness 23.82 m, located inside Kobe city, survived the 1995 magnitude 7.2 earthquake with no apparent damages.

Reportedly, the amount of drainage water increased slightly after the earthquake, but

1) Professor, Department of Built Environment, Interdisciplinary Graduate School of Science and Engineering, Tokyo Institute of Technology, Yokohama, Japan
2) Ph. D. Student, ditto
3) Formerly Graduate Student, ditto

the amount of increase was small and stabilized later. Although constructed in 1900, Nunobiki dam was well built and is still in good condition today.

Karasubara Dam

Karasubara dam, curved gravity type, height 32 m, crest length 124 m, crest thickness 3.64 m, and base thickness 26 m, located in northwest part of Kobe city. There was reportedly no damage, and no increase in drainage water.

AMBIENT VIBRAION TEST

Ambient vibration tests (microtremor measurements) are a well-known technique for evaluating the dynamic characteristics of structures. However, attention should be called to the fact that the small level of energy from ambient excitation does not always allow obtaining of measurable vibrations in all of the frequency range of interest. The impossibility of noise measurement may lead to difficulties in interpretation of experimental data. Consequently, ambient vibration tests in dams are mainly applied as a preliminary phase. Microtremor measurements of the Nunobiki Dam, and Karasubara Dam were carried out at the reservoir water level of -3.17m, and –3.83m (below the dam crest) respectively. To identify the dynamic properties of the dams from microtremor measurements different methods are available. In this study we have used auto-regressive modeling methods.

The auto-regressive modeling method is a parametric system identification approach for estimating the vibration properties of a linear system. This approach involves minimizing the error between the output signal and input signal, in the least squares sense, for the various parameters of the auto-regressive model (Ljung, 1987). This section presents briefly the results of applying the method for identifying the modal frequencies of the both dams. Details of the theoretical background for the method can be found elsewhere (Safak, 1988, 1989a, 1989b, 1991). Frequency response function, and poles and zeroes for Nunobiki dam are shown in Figure 1.From this model and frequency response function we can identify the modal frequencies and damping ratios. For this dam the first mode is identified with a frequency of 10 Hz.

Figure 2 shows frequency response function, and auto correlation of residuals of output, cross correlation of input and output for Karasubara Dam. The first identified mode for Karasubara dam from frequency response function (Figure 2) is 10 Hz.

FE-BE MODEL, AND ANALYSIS

The computer program EACD3D-96 developed at the University of California, Berkeley (Tan et al., 1996) was used for earthquake analysis of Nunobiki and Karasubara dams.

To model Nunobiki Dam, 17 isoparametric solid elements are used. The boundary element mesh of the foundation rock consists of 9 rectangular isoparametric surface elements. Fluid region consists of 17 three-dimensional finite elements. The water level is considered to be at –8.77m (below the dam crest) during the earthquake. The finite element idealization of the dam and the boundary element idealization of the foundation rock are shown in Figure 3.

Finite element mesh of Karasubars Dam uses 28 three-dimensional solid elements. 12 rectangular surface elements with quadratic shape functions are employed for boundary element idealization of foundation rock. 28 three-dimensional finite elements are used in water domain. The water level was at -9.80m (below the crest) during the earthquake. Figure 4 shows the finite element and boundary element idealization of the dam and foundation rock. The material properties used for concrete and foundation rock for both dams are shown in Table 1.

Calculated Resonance Frequency of Dams

We have checked calculated modal frequencies of the dams by obtaining the

Table 1- Material properties used in analysis

	Modulus of elasticity(Mpa.)	Poisson's ratio(υ)	Damping ratio(ξ)
Concrete	29000	0.2	0.05
Foundation rock	10400	0.2	0.05

frequency response functions for a point at the crest of the both dams and by comparing with microtremor measurements. Figure 5 shows frequency response functions for Nunobiki and Karasubara dams, for which the water level is at the same level as it was during the microtremor measurements (-3.17m and -3.83m). As it can be seen in Figures 1, 2, and 3 there is a fairly good agreement between measured and calculated results.

INPUT GROUND MOTION

Since there has been no instrumentation program in the Nunobiki and Karasubara dam, we have to use synthesized ground motion for estimating seismic response of both of the dams. There are several methods for artificially generating the ground motion, and we have used some of these methods for both dams, based on the availability of the proper data. Following are a brief explanation of the process for generating the ground motions.

Estimating from the Observed Data in the Area (Method 1)

There was ground motions recorded at the basement of thirty-seven stories building during the Kobe earthquake. This building is almost the nearest point (about 700m) to the Nunobiki dam, for which ground motion data is available. These data could not be considered as free-field ground motion, because these include soil-structure interaction effects. To obtain free-field ground motion, we conducted microtremor measurements at the free- field and the basement. For these signals we carefully constructed transfer function. By applying transfer function to the recorded data at the basement during the 1995 Kobe earthquake, we were able to obtain the free-field ground motion at the building site. Finally we have produced ground motions at Nunobiki dam by source inversion from strong ground motion obtained at the free field, by using multiple reflection theory and considering attenuation of seismic waves according to following equations (Akamatsu, 1980):

$$u_d(f) = u_o \frac{r_o}{r_d} \exp(\pi f (\frac{r_o - r_d}{Q(f) v_s})) \qquad (1)$$

$$Q(f) = 110\sqrt{f} \qquad (2)$$

In which, u_o, r_o, and u_d, r_d, are acceleration and distances from hypocenter for observation and destination points. Q is a dimensionless factor, and f is frequency. We will call this record N1 for Nunobiki dam hereafter. Three components of this record along with E-W and N-S variation of acceleration are shown in Figure 6.

Empirical Green's Function Procedure (Method 2)

The empirical Green's function method was suggested by Hartzell (1978) for the first time. In this method, rupture propagation and radiation pattern are specified deterministically and the source radiation and propagation effects are included empirically by assuming that the motions observed from an aftershock contain this information. The methods proposed by Hadley and Helmberger (1980) and Irikura (1983) are modifications of Hartzell's method of summing empirical Green's functions. This method requires an adequate sampling in both distance and source depth of empirical Green's functions, which is difficult to obtain in most regions. In order

to overcome this limitation, researchers have proposed different approaches. We have have followed Irikura's approach. According to Irikura (1997):

$$U(t) = \sum_{i=1}^{l \times m} c \frac{r}{r_i} F_i(t) * u_i(t) \tag{3}$$

$$F_i(t) = \delta(t - t_i) + \frac{1}{n'(1 - e^{-1})} \sum_{j=1}^{(N-1)n'} e^{-(j-1)/(N-1)n'} \delta[t - t_i - (j-1)\tau/(N-1)n'] \tag{4}$$

$$t_\xi = \frac{r - r_{ij}}{v_s} + \frac{\xi_{ij}}{v_r} \tag{5}$$

U (t) and *u (t)* is the ground motion for a large event and observed record of a small event used as the EGF, respectively. The terms *r, r_{ij},* are distances from the site to the hypocenter of a small event, and from the site to the *(i, j)* th sub-fault, respectively. The term ξ_{ij} is the distance between the starting point and *(i, j)* th sub-fault, v_s is the share wave velocity, v_r, is the rupture velocity, τ is the rise time of the large event, c is the stress drop ratio for the large and small events, and *n'* is constant number. δ is Dirac delta and * is convolution operator. The scaling number N is obtained from the following equation:

$$(M_{om} / cM_{os})^{1/3} = N = l = m \tag{6}$$

Where, M_{om} and M_{os} are the seismic moments for the large and small events, respectively. l and m show the number of elements, assuming that we break up the fault plane into l and m elements (of length ΔL) along the length and m elements (of width ΔW) along the width of the fault plane.

To apply the EGF method to simulate strong ground motion, we have used the source model which has adopted by Kamae et al., 1997. The detailed information about small events and source parameters are shown in Tables 2 and 3. The location of dams and faults of the main event and sub-events are shown in Figure 7. The resulted ground motion from this method for Karasubara dam will be called K1. The time history, and. E-W, N-S variation of acceleration of K1 are shown in Figure 8.

Broadband Strong-Ground Motion Modeling Procedure (Method 3)

For using empirical Green's functions, appropriate ground motion records of small events from the target source area, which are considered as Green's functions, must be available. Unfortunately, it is rare to have suitable ground motion records of such small events, especially in the target source area prone to future large earthquakes. As an alternative way to avoid this limitation is the use of synthetic Green's functions that are calculated based on a hybrid scheme that

Table 2- Small events used in EGF method

	Date	Epicenter		Depth(km)	Magnitude(M)
		Lat.	Long.		
Small event 1	96/05/11, 14:46	34.528		11	3.8
small event 2	96/09/01, 13:49	34.694	135.194	15	3.7

Table 3- Source parameters used in EGF Method

	Fault size (L × W) (km × km)	M_o (dyne × cm)	σ (bar)	Strike(°)	Dip(°)	Rake(°)
Sub-event 1	8 × 8	$.34 \times 10^{26}$	163.0	N53° E	90.0	233.0
Sub-event 2	11 × 16	1.0×10^{26}	86.0	N45° E	82.0	198.0
Sub-event 3	8 × 8	$.18 \times 10^{26}$	86.0	N233° E	85.0	0.0

v_s =3.5 (km/s), v_r =2.8 (km/s), τ =0.6 (sec)

combines different methods for calculating the low-and high-frequency parts of the Green's functions (Kamae K., et al., 1990). The low- frequency part (less than 1Hz) is calculated by 3D-Simulation (Kataoka S., 1996). The high frequency part (higher than 1Hz) is calculated using the stochastic simulation method of Boore (1983). The synthetic Green's function is then calculated by combining the low-and high-frequency parts of the motion. Finally, strong ground motions from a large earthquake are obtained by the summation of the hybrid Green's functions following the empirical Green's function procedure. This method is usually called hybrid procedure, because it computes the low –frequency and high-frequency ranges separately and then combines the two to produce a single time history.

To produce high-frequency part in this case, we have made small events (about M 5.0) and synthesized by empirical Green's function to consider rupture propagation. Finally we have produced the ground motions at both dam sites. We have shown these records by N2, and K2 for both Nunobiki and Karasubara dams respectively. Figures 9 and 10 show time histories along with E-W and N-S variations of accelerations for N2, and K2. Table 4 summarizes the methods used for simulating ground motions for each dam and their corresponding names.

SEISMIC RESPONSE OF THE DAMS

Rotation of Ground Motion Components

The synthesized ground motions for dams are in the N-S, and E-W directions. In order to analyze the dams, we have rotated the horizontal components of the ground motion according to their orientation with respect to N-S, and E-W directions by using the following equation:

$$\alpha_\theta = \alpha_1 \cos(\theta - \theta_1) + \alpha_2 \cos(\theta - \theta_2) \quad (7)$$

θ, θ_1, and θ_2, are azimuth angles of an arbitrary direction, and components, respectively, measured from the North. Amplitudes of components are shown by α_1 and α_2. After rotating the ground motions we obtain two set of input for each dam, one for actual orientation of dams, and the other for case when the fault normal direction coincides with stream direction of the dams. Consequently we have four set of input ground motions in the horizontal direction for each of the dams.

Analysis Results

The seismic responses of the dams are evaluated by using two sets of input ground motions. These ground motions are

Table 4- Methods used for synthetically generated ground motions

Method	Nunobiki Dam	Karasubara Dam	Record No.
Method 1	yes	no	N1
Method 2	no	yes	K2
Method 3	yes	yes	N2 and K2

synthesized by different methods for both dams in two cases; case1, the orientation of the dams is actual; case2, the orientation of the dams has changed in a way that fault-normal and fault-parallel directions coincide with upstream and cross-stream directions of dams, respectively.

At present the process of evaluating the seismic performance of concrete dams using results of linear elastic numerical analyses, involves comparing the computed levels of stress with levels that are considered acceptable based on considerations of concrete strength. If computed levels of stress are generally less than or equal to levels considered acceptable, the seismic performance and safety of the dam are considered acceptable. If computed levels of stress exceed acceptable levels; the seismic performance of the dam may be considered unacceptable. For evaluation of seismic performance of Nunobiki and Karasubara dams we have focused on tensile stress level throughout dam bodies.

Case1

Figures 11-12 show the envelope of the maximum principal stresses on the upstream and downstream faces of the Nunobiki and Karasubara dams, viewed looking upstream, due to N1, N2, K1, and K2 synthesized ground motions for actual orientation of dams.

The maximum principal stress on the upstream face of the Nunobiki dam due to N1 is about .65 MPa. on the elements 1 and 8 at the left abutment of the dam. In the case of downstream face, maximum principal stress is .75 MPa. and occurs on element 1. The stress level for all elements on the downstream face is much higher than the upstream face. The maximum principal stress due to N2 on the upstream face of the Nunobiki dam is about .6 MPa., and occurs on element 8, but for downstream, it is about .64 MPa., and occurs on elements 8, and 13 in the left and right abutments. Again the stress level on the downstream is higher than the upstream for all elements.

For Karasubara dam the maximum principal stress due to K1 is about .4 MPa., and .6 MPa. on the upstream and downstream faces of element 1, respectively. But, again similar to Nunobiki dam case, the stress level is much higher than the upstream face. In the case ground motion K2, the maximum principal stress on the upstream face is about .45 MPa. on element 1, but it reaches to .65 MPa. on the downstream face of element 19. It can be seen that the level of stress on the downstream face is much higher than the upstream face.

The maximum dynamic tensile stress calculated in the dam bodies is less than 1 MPa. It is supposed that these gravity dams can withstand such dynamic stresses. Observation of the dams shortly after the Kobe earthquake also verifies these calculation results.

Case 2

Regarding the effect of the orientation of the dams on seismic response, we have considered both dams by using only N2, and K2 ground motions. After rotating the horizontal components of N2, and K2 to fault-normal and fault-parallel directions, we have recognized two different orientations

for dam with respect to horizontal components. One, when the stream direction coincides with the fault-normal component (the most critical orientation). Second, when the stream direction is the same as the fault-parallel direction (the least critical orientation). To show the effect of polarization of ground motion on stress we have calculated principal stresses of both dams due to N2, and K2, for two critical orientations. We will explain the polarization effect on stress level mainly by comparing the stresses of two critical orientations in terms of amount of increase in percent. Figures 13-14 shows Maximum principal stresses on the upstream and downstream face of the Nunobiki and Karasubara dams for each critical orientation respectively. In the case of Nunobiki dam, the maximum principal stress on the upstream face of the dam for two critical orientations is .8 MPa. and .5 MPa. which occur on element 8 and 10, respectively. In this regard, the maximum increase on stress level amounts to 60%. But for most critical elements (elements with largest stresses) the increase on stress level is about 75%. In other elements the average increase is more than 40%. For downstream face of Nunobiki dam the maximum principal stresses for two critical orientation occur on elements 8-17 and the increase is about 25%. The maximum principal stresses in this case are .75 MPa. and .60 MPa. The average increases for all elements are not so high and remain below 20%.

For upstream face of Karasubara dam the maximum principal stresses are .60 MPa. and .30 MPa., which occur on element 28. The increase is about 100%. But in the case of other elements, for example element 15, the increase is about 205%. And still stress level is fairly high (about .5 MPa.). In this case the increase on stress level is much more than other cases, and in elements 25-28 (elements connected to foundation rock at the lower part of the dam) is more than 110%. On average the increase of stress is more than 75% for all elements. The maximum principal stresses on the downstream face are .70 MPa. for element 8, and .50 MPa. for elements 19-22. The increase is about 40%. For elements 8, 16, 23, and 24 the increase is about 125%, but stress is not critical (about .50 MPa.).

CONCLUSIONS

The calculated stress level is well below the maximum tensile strength of concrete for dams, so we do not expect any kind of damage, as it was the case during the 1995 Kobe earthquake.

The analysis results for both dams in case 1 indicate maximum tensile stress occurs near the elevation of the downstream face, where its slope changes. This is in agreement with observed and experimental behavior of gravity dams.

According to our findings in case 2, the dynamic response of structures will be influenced by their orientation relative to the ground motion and by their proximity to causative fault.

Regarding the variation of maximum stress with respect to orientation of structure there has been increases up to two times depending on the location of stress point on the dam.

In the near field, the acceleration response spectra in the fault-normal and fault-parallel are significantly different. This difference increases in long periods. This implies that maximum tensile stress will increase much more in higher dams according to their orientation than lower dams.

ACKNOWLEDGMENTS

Kobe municipal official provided data and information needed in this study for Nunobiki and Karasubara dams. They also provided access to dam sites for microtremor measurements. Their cooperation is sincerely appreciated. JMA and K-net provided ground motion recordings of building and free field used for ground motion simulation. This is gratefully acknowledged.

REFERENCES

Ljung, L. (1987). *System Identification*: Theory for the User, Prentice-Hall, Englewood Cliffs, NJ.

Safak, E. (1988). *Analysis of Recordings in Structural Engineering: Adaptive Filtering, Prediction, and Control,* Open-file Report 88-647, U.S. Geological Survey, Menlo Park, CA.

Safak, E. (1989). "Adaptive Modeling, Identification, and Control of Dynamic Structural System. I. Theory," *Journal of Engineering Mechanics*, ASCE, 115(11), 2386-2405.

Safak, E. (1989). "Adaptive Modeling, Identification, and Control of Dynamic Structural System. II. Applications," *Journal of Engineering Mechanics*, ASCE, 115(11), 2406-2426.

Safak, E. (1991). "Identification of Linear Structures Using Discrete-time Filters," *Journal of Structural Engineering,* ASCE, 117(10), 3064-3085.

Tamura K., Honda T. (1998). Investigation of soil characteristics at JMA, Kobe. Public Works Research Institute Report. Vol. 3586.

Akamatsu, J. Attenuation, (1980). property of seismic waves and source characteristics of small earthquake. Bull. Disaster Res. Inst. Kyoto Univ., Vol.30 pp50-80.

Hartzell, S.H. (1978). Earthquake Aftershocks as Green's Functions. Geophys. Res. Lett., 5: 1-4.

Hadley, D.M. and Helmberger, D.V. (1980). Simulation of Strong Ground Motions. Bull. Seism. Soc. Am., 70:617-630.

Irikura, K. (1983). Semi-empirical Estimation of Strong Ground Motions during Large Earthquakes. Bull. Disaster Res. Inst. Kyoto Univ., 33:63-104.

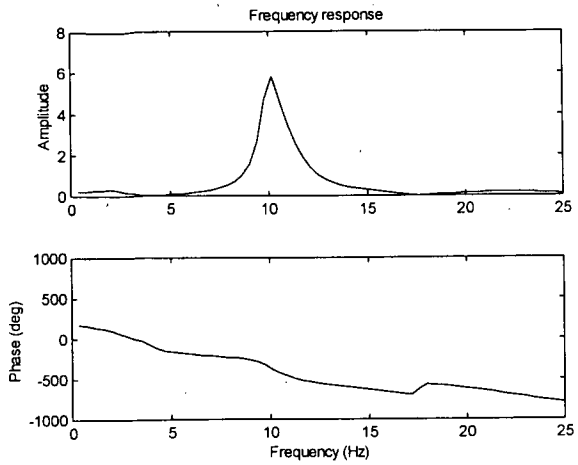
K. Irikura, T. Kagawa, H. Sekiguchi (1997). Revision of the Green's function method by Irikura (1986), Program and Abstracts. The Seismological Society of Japan, 2, B25.

K. Kamae and K. Irikura, (1998). Source Model of the 1995 Hyogoken-Nanbu Earthquake and Simulation of Near-Source Ground Motion, Bull.Seism.Soc.Am.88, pp.400-412.

Boore, D.M. (1983). Stochastic simulation of high-frequency ground motion based on seismological model of the radiated spectra Bull.Seism.Soc.Am. Vol.73 pp.1865-1894.

K. Kamae, K. Irikura, Y. Fukuchi (1990). Prediction of strong ground motion for M7 Earthquake using regional scaling relations of source parameters, Jounal of Struct. Const. Eng, AIJ, No.416, pp.57-69.

Kataoka S. (1996). Simulation of the 1995 Hyogoken-Nanbu Earthquake by a 3-D BEM, Technical Report, No.54, Department of Civil Engineering Tokyo Institute of Technology.



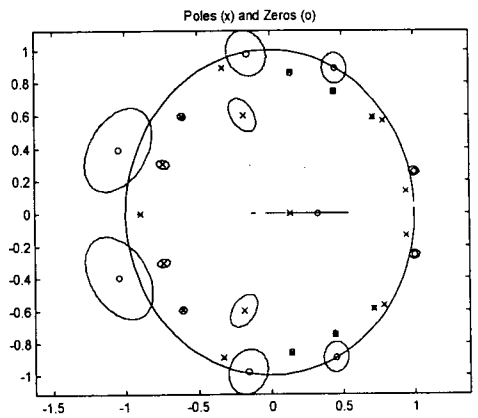
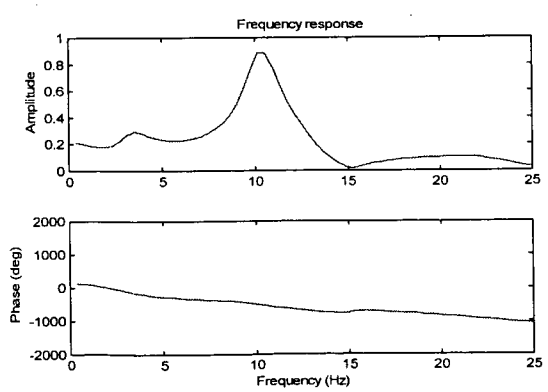


Figure 1. Frequency response function, along with poles and zeroes for Nunobiki Dam.



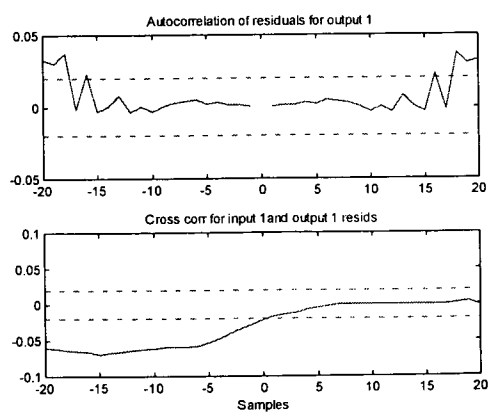


Figure 2. Frequency response function, along with auto correlation of residuals, and cross correlation of input and output.

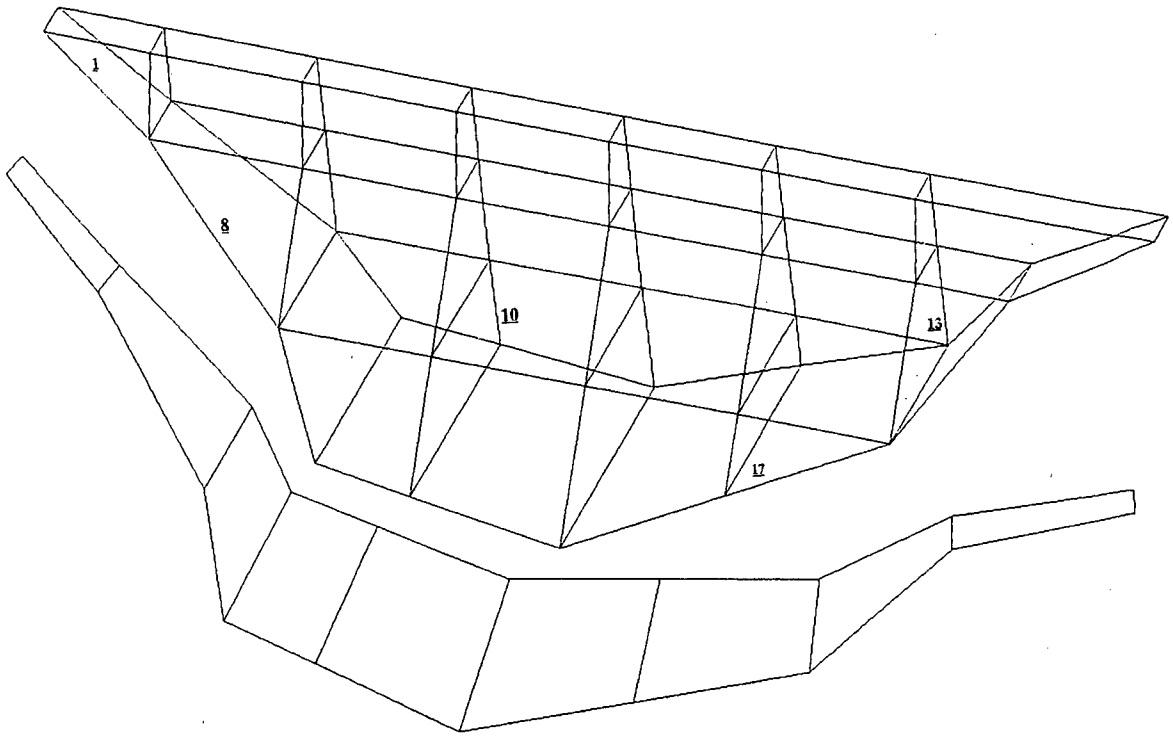


Figure 3. Finite element and boundary element mesh of the dam body and foundation rock for Nunobiki Dam.

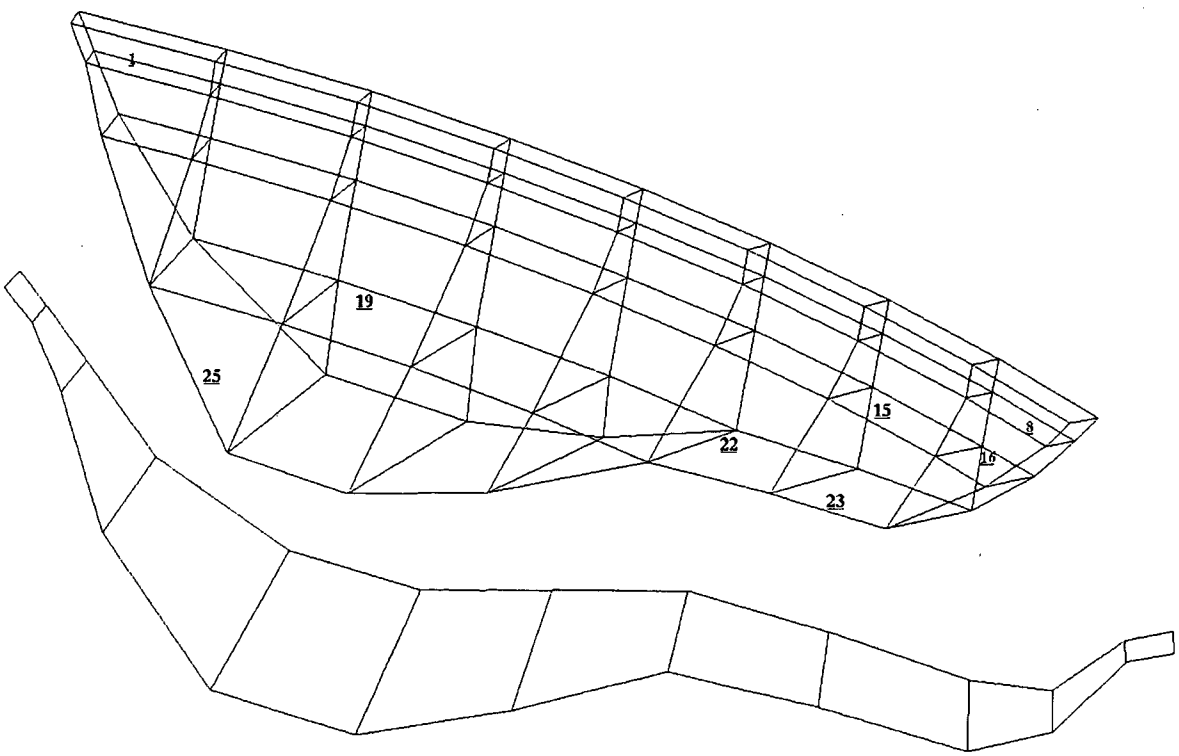


Figure 4. Finite element and boundary element mesh of the dam body and foundation rock for Karasubara Dam.

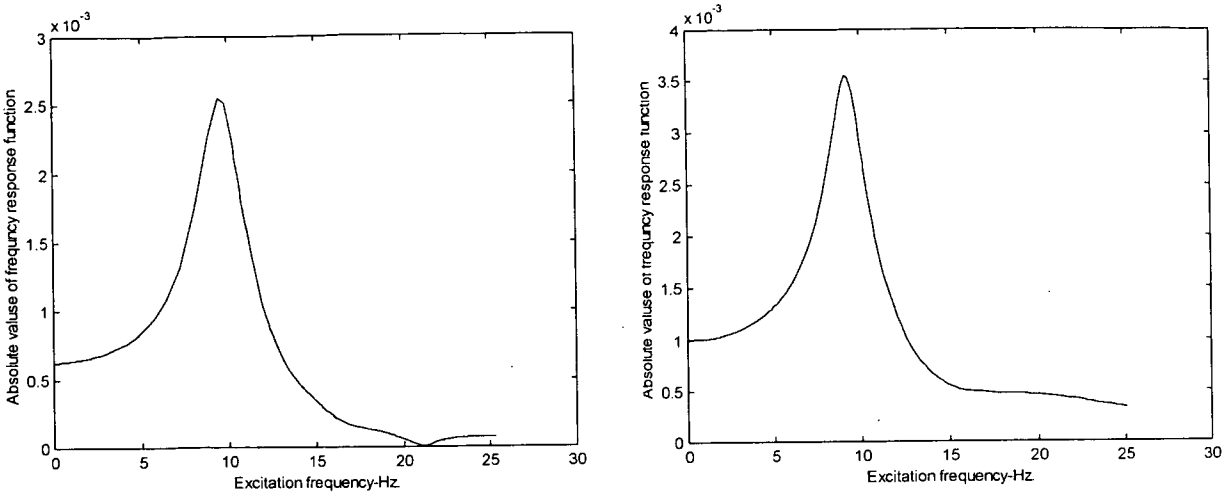


Figure 5. Frequency response functions for Nunobiki dam (left) and Karasubara dam (right).

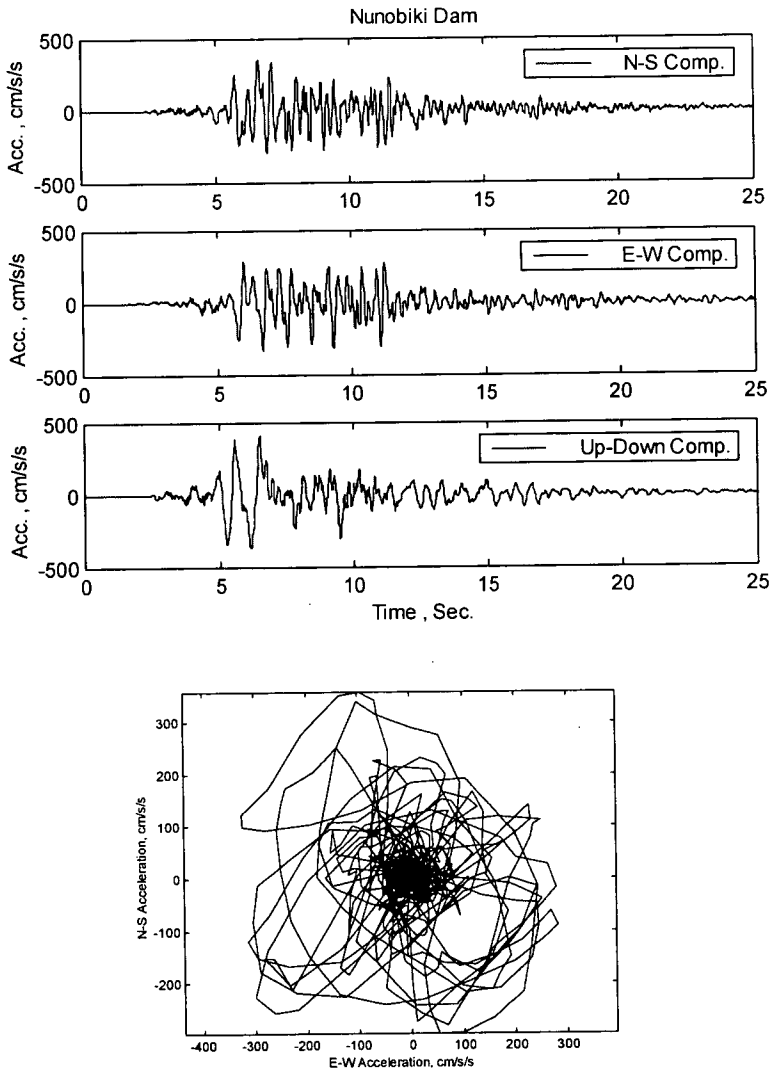


Figure 6. Time history (top), and E-W, N-S variation of acceleration (down) of N1.

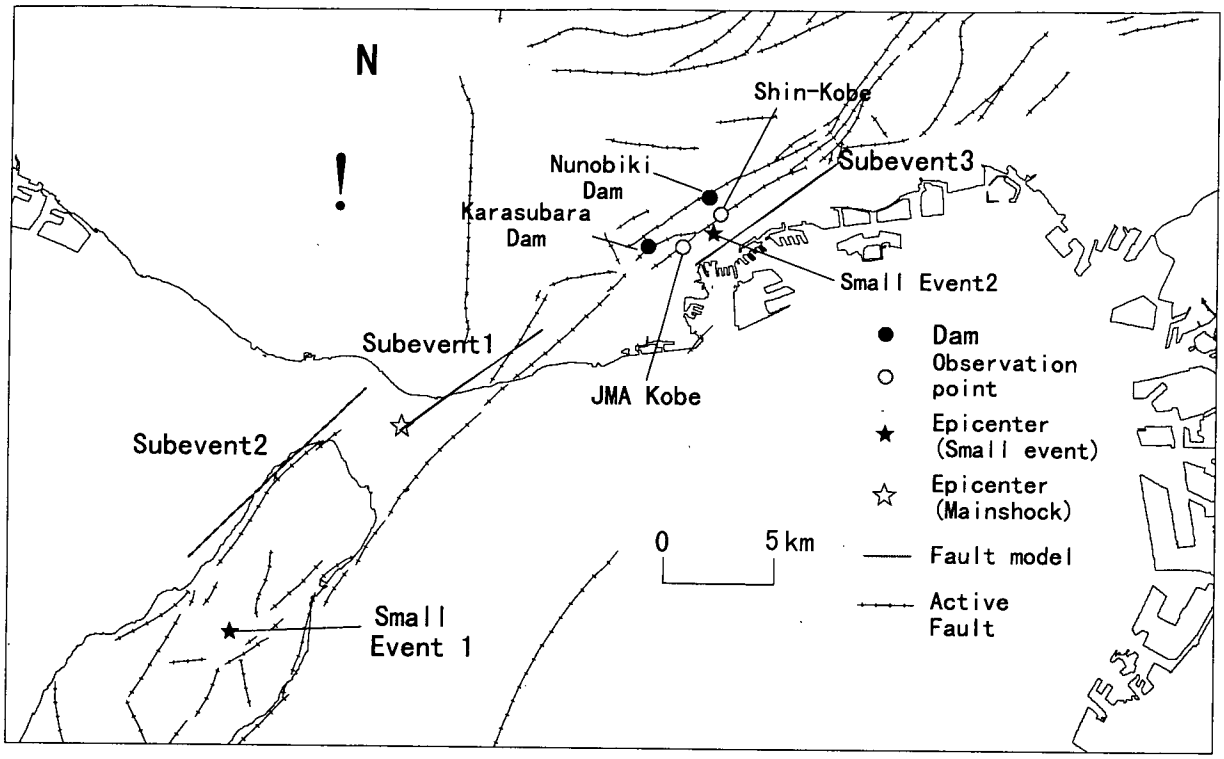


Figure 7. Location of dams, faults of the main event and sub-events used in generating the ground motions.

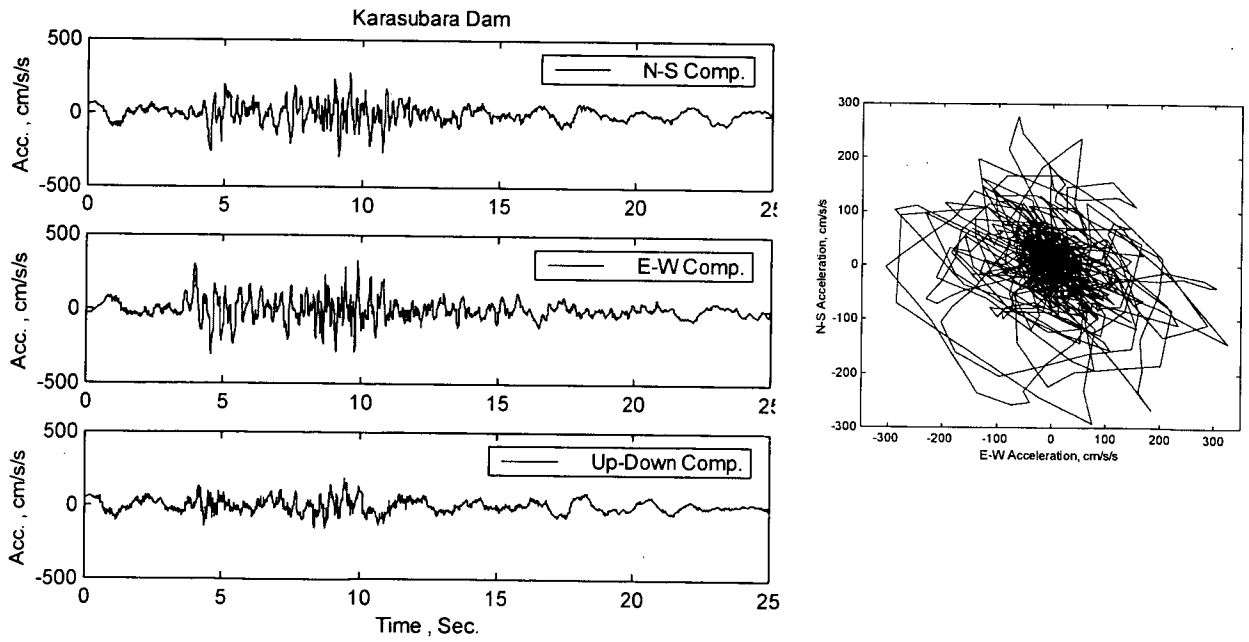


Figure 8. Time history, and E-W, N-S variation of acceleration of K1.

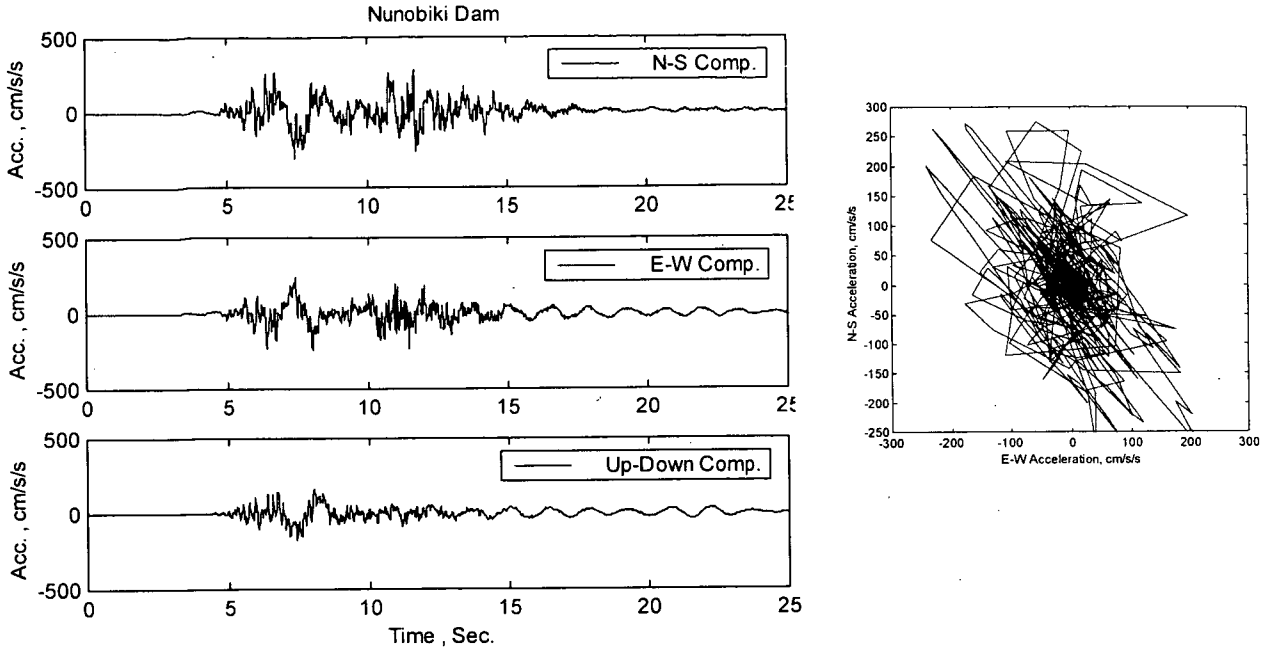


Figure 9. Time history, and E-W, N-S variation of acceleration of N2.

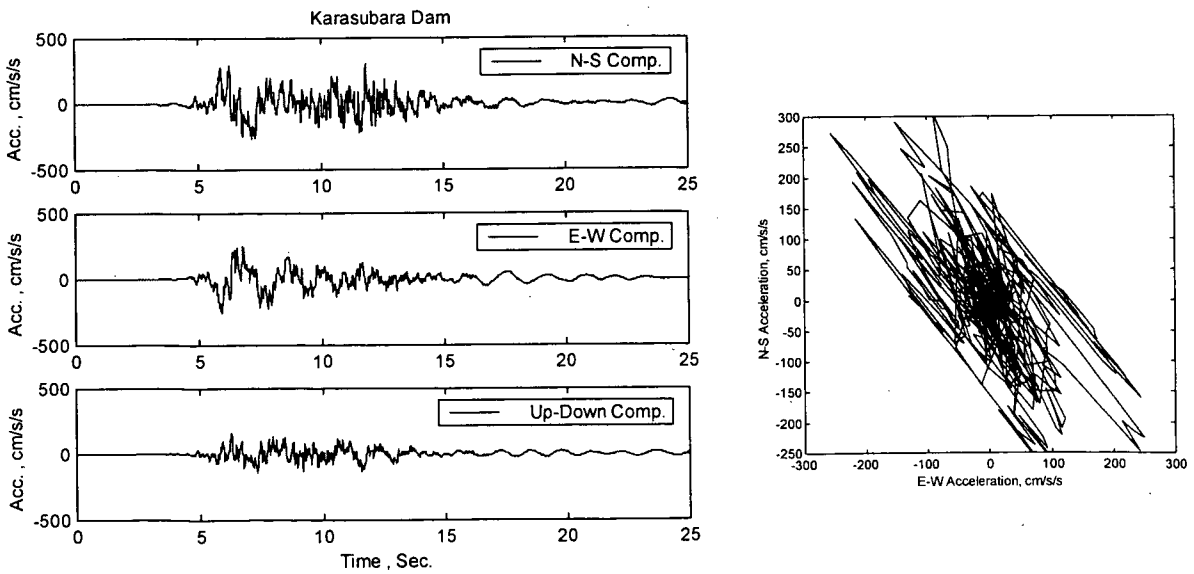


Figure 10. Time history, and E-W, N-S variation of acceleration of K2.

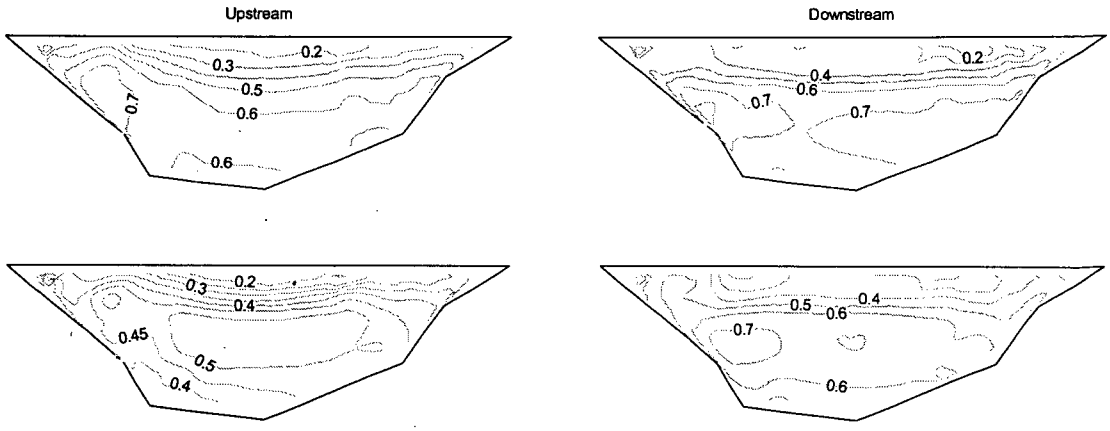


Figure 13. Envelopes of maximum principal stresses on the upstream and downstream face of the Nunobiki Dam due to N2 ground motion for most critical (up) and least critical (down) orientations of the dam (in MPa.).

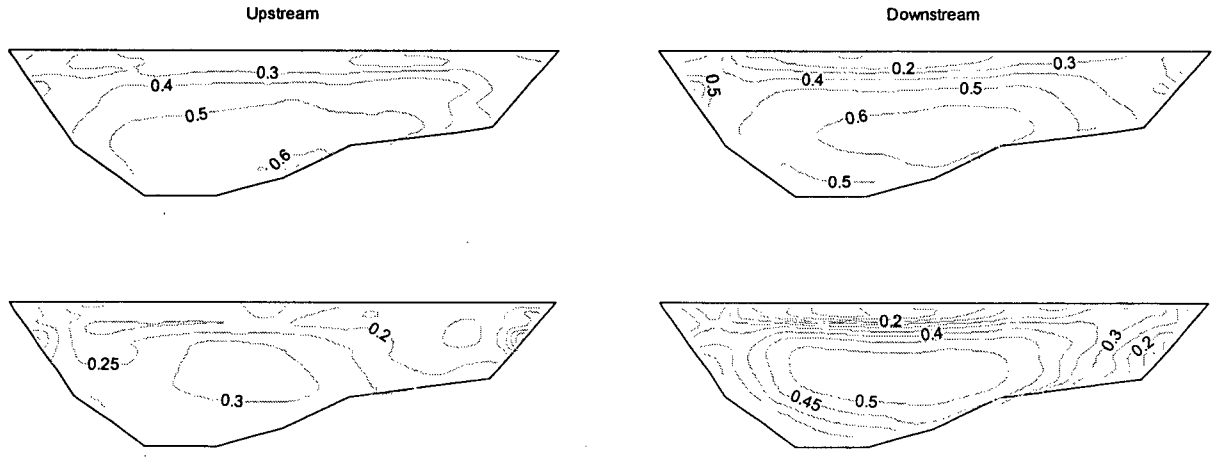


Figure 14. Envelopes of maximum principal stresses on the upstream and downstream face of the Karasubara Dam due to K2 ground motion for most critical (up) and least critical (down) orientations of the dam (in MPa.).

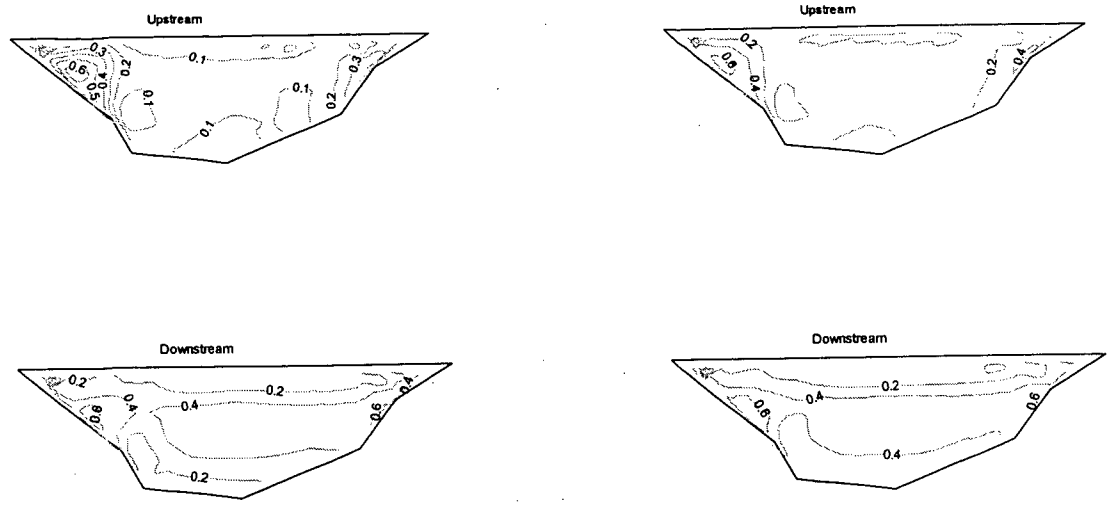


Figure 11. Envelopes of maximum principal stresses on the upstream and downstream face of the Nunobiki Dam due to N1 (left) and N2 (right) ground motions for actual orientation of the dam (in MPa.).

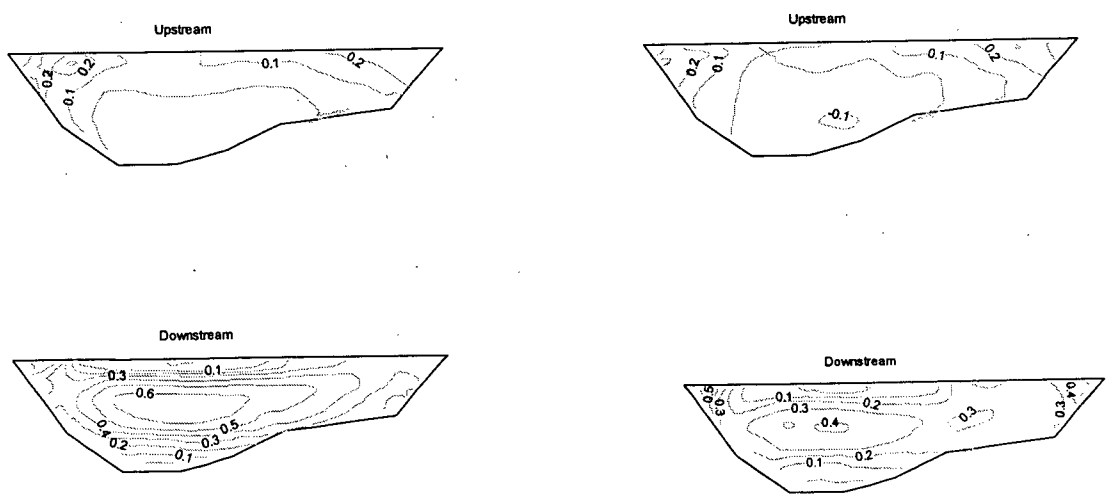


Figure 12. Envelopes of maximum principal stresses on the upstream and downstream face of the Karasubara Dam due to K1 (left) and K2 (right) ground motions for actual orientation of the dam (in MPa.).

Nonlinear Seismic Response of Concrete Gravity Dams

by

Enrique E. Matheu[1], Robert L. Hall[2] and Robert M. Ebeling[3]

ABSTRACT

This work is part of an ongoing research effort whose main objective is the development of computational tools and technical guidelines for the accurate evaluation and assessment of the performance of concrete gravity dams subjected to seismic excitations. During severe seismic motions, concrete dams are likely to experience cracking due to the low tensile capacity of plain concrete. The focus of this research work is to investigate the influence of the tensile behavior of concrete on the dynamic response characteristics of the system. The tensile behavior is represented using a smeared crack approach based on the fixed-orthogonal crack model. The effects of cracking at a given point are represented by the local adjustment of the stress field and the modification of the corresponding material parameters. A planar finite element model of a dam section is used to model the two-dimensional response of a single monolith. The structure selected for this numerical study corresponds to the tallest non-overflow monolith of Koyna Dam.

KEYWORDS: Concrete gravity dams; nonlinear response; tensile cracking; smeared crack model.

1. INTRODUCTION

The accurate evaluation of the seismic performance of concrete dams requires the development of numerical procedures that account effectively for the most critical factors controlling the response. The complex system constituted by the dam, the reservoir, and the foundation is characterized by an extensive spatial domain, with unavoidable uncertainties in the input characteristics and the material parameters. The response characteristics of the system are affected by various important factors, such as: 1) problem geometry (shape and dimensions); 2) spatial variability of the seismic input; 3) intensity and frequency content of the ground motion; 4) constitutive behavior of the different materials present in the system 5) presence of lift and contraction joints; and 6) dynamic interaction phenomena between the different sub-domains.

For a specific geometric configuration and for a given seismic excitation, the response of the dam-reservoir-foundation system is mainly governed by the concrete constitutive behavior and the interaction between the dam, the reservoir and the underlying foundation. The associated effects are usually functions of not only present but also past states of the system. The accurate modeling of the resulting nonlinear problem requires a time-domain formulation, usually in the form of a direct time integration procedure. Some researchers have also proposed hybrid time-frequency techniques as an alternative strategy for the solution of this problem. However, it is important to remark that analysis procedures based on linear assumptions are nevertheless capable of rendering valuable and insightful information. In spite of their limitations, these procedures constitute a useful tool, which can provide significant information

[1] Research Assistant Professor, Department of Engineering Science and Mechanics, Virginia Polytechnic Institute and State University, Blacksburg, VA 24060 (USA).
[2] Supervisory Research Structural Engineer, Structural Mechanics Division, Structures Laboratory, U.S. Army Engineer Waterways Experiment Station, Vicksburg, MS 39180 (USA).
[3] Civil Engineer, U.S. Army Engineer Waterways Experiment Station, Vicksburg, MS 39180 (USA).

regarding some of the main characteristics of the system's response.

Several extensive numerical studies based on linear models have evaluated the influence of the different interaction phenomena that influence the dynamic response. Many of these analyses have been performed with great efficiency in the frequency domain (Chakrabarti and Chopra, 1973; Chopra and Gupta, 1981; Hall and Chopra, 1982). However, it is clear that severe ground motions can trigger different response mechanisms not predicted by the linear analysis. For example, dynamic stresses caused by strong earthquakes may create areas of localized damage, mostly associated with the low tensile strength of the mass concrete.

The range of validity of the linear assumption for material behavior depends therefore on the severity of the excitation. For low-intensity ground motions, only minor cracking can be expected to develop within the mass concrete. The dominant response characteristics can be reasonably predicted assuming linear behavior and frequency-domain techniques can be used for this type of analysis in a very powerful and effective manner. However, in case of severe ground motions, substantial cracking is likely to develop across significant regions of the dam, and the overall dynamic response characteristics of the system could be substantially changed from those predicted using a linear analysis. For this level of ground excitation, the dynamic performance should be evaluated taking into account the effects of cracking.

There are two main approaches for the representation of tensile cracks in finite-element applications: 1) discrete crack model; and 2) smeared crack model.

In the discrete crack model (Ngo and Scordelis, 1967), the physical discontinuity caused by the crack is explicitly incorporated in the finite-element mesh. This model is closer to the real physical condition by capturing the localization of the crack. However, its implementation is rather challenging, because of the modification of the finite-element topology during the analysis. The works by Skrikerud (1986), and Ayari and Saouma (1990) can be cited as examples of the application of this model to the seismic analysis of gravity dams.

In the smeared crack model (Rashid, 1968), the crack is idealized as an infinite number of continuously distributed (smeared) micro-cracks. The implementation of this model is less expensive than the previous formulation. However, it represents only an approximation to the real phenomenon. The smeared crack model has been employed quite extensively for the analysis of concrete gravity dams. Pal (1986) studied the two-dimensional seismic response of the tallest non-overflow monolith of Koyna Dam (India) using this type of model to capture the tensile behavior of concrete. Similar studies were performed by Mlakar (1987), and Mao and Taylor (1997), focusing on the nonlinear response of different gravity dam sections subjected to seismic ground motion. The dam sections were selected to be representative of the most common designs corresponding to sections of different heights. The numerical simulations frequently showed that the example sections cracked completely across the width, with most of the cracking phenomena initiating at the upstream edge of the base, and at the locations of abrupt slope change along the downstream face. In general, the studies reported a similar pattern of behavior, with cracked areas usually concentrated near slope changes, which propagated almost instantaneously after initiation once the intensity of the excitation exceeded a critical value. The parametric studies demonstrated that the approximate representation of damage by means of additional damping added to the corresponding linear model does not capture the characteristics of the nonlinear response associated with a brittle material.

Vargas-Loli and Fenves (1989) carried out an extensive numerical study of the two-dimensional seismic response of Pine Flat Dam (USA) using a smeared crack model based on an equivalent tensile strength criterion. This study showed that diffuse cracking patterns are likely to occur near stress concentration areas. In most

cases, the ground excitation levels that induced crack initiation also generated severe damage by extensive crack propagation, forcing the structural system to reach its ultimate condition. Another comprehensive study of the nonlinear seismic response of Pine Flat Dam was presented by El-Aidi and Hall (1989a, b). The tensile behavior of the material was represented using the smeared crack approach, and crack propagation was governed by an element-dependent strength criterion applied to the elements ahead of the crack tip. The numerical simulation of the system response was performed in an interactive environment, where the propagation of cracks was ultimately controlled by the analyst, in an effort to avoid spurious cracking patterns.

The purpose of this work is to investigate the influence of the tensile behavior of concrete on the dynamic response characteristics of the system, using a smeared crack approach to model the tensile behavior of the material. The numerical results will be used to help in the design of a 1:20 scale model for a series of shaking table experiments, which in turn will be used for calibration of this and other constitutive models. The final objective of this research initiative is the development of guidelines that will help engineers and analysts in the identification of the validity and limitations of linear response methodologies, and the proper interpretation of nonlinear analyses.

2. CONCRETE CONSTITUTIVE MODEL

In general, the type and sophistication of the model used to describe the nonlinear behavior of concrete depends on the particular conditions of the problem. In this case, nonlinearities induced by dynamic compressive stresses are not as important as those associated with tensile cracking and frictional effects. Therefore, the constitutive model should be able to consider the formation of cracks and their behavior under cyclic loading (opening, closing, and re-opening). Additionally, the model should be able to account for the presence of planes of weakness, such as lift joints.

A two-dimensional smeared crack model is adopted in this work. The smeared crack model is a finite-element modeling approach intended to capture the characteristics of the response under tensile conditions. This model monitors the stress/strain conditions at pre-specified points in the finite-element mesh. Crack initiation and propagation are defined in terms of some appropriate local criteria. After cracking, the local material properties are modified by introducing an orthotropic constitutive model whose orientation depends on the cracking plane. Therefore, the finite-element mesh remains unmodified and the global tangent stiffness matrix is generated by the proper adjusting of the constitutive matrix, at element level.

After initiation of the cracking process, the initially isotropic stress-strain constitutive relationship is replaced by an orthotropic model, given by

$$\begin{Bmatrix} d\sigma'_x \\ d\sigma'_y \\ d\sigma'_{xy} \end{Bmatrix} = \begin{bmatrix} 0 & 0 & 0 \\ 0 & E & 0 \\ 0 & 0 & \beta G \end{bmatrix} \begin{Bmatrix} d\varepsilon'_x \\ d\varepsilon'_y \\ d\gamma'_{xy} \end{Bmatrix}$$

where the stress and strain components are referred to a rotated reference system (x',y'), which is aligned with the cracking plane. It is usual to retain some shear stiffness across the crack to account for aggregate-interlock effects, and the corresponding shear stiffness is defined in terms of a dimensionless parameter β, referred to as the shear retention factor (Suidan and Schnobrich, 1973).

Upon cracking, the current tensile stress normal to the crack is completely released. As mentioned by Bazant and Oh (1983), this assumption of abrupt stress drop is adequate only for those problems in which the cross section dimensions are sufficiently large with respect to the aggregate size. Alternatively, a gradual stress-release criterion could be enforced. Therefore, after a given integration point reaches the conditions for the initiation or the propagation of a crack, the element unloads locally normal to the plane of the crack, and this

induces a redistribution of the stress field at neighboring points. The local constitutive behavior is depicted in Figure (1).

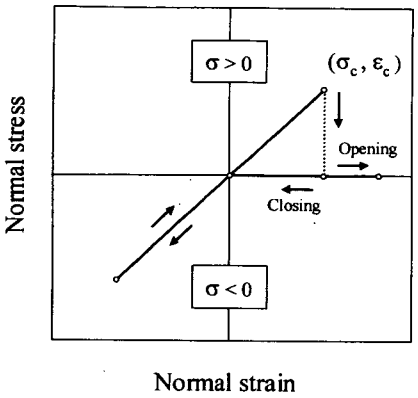


Figure 1: Stress-strain relationship.

The orientation of the cracking plane remains constant, and no rotation after cracking is considered. Therefore, the orientation of the cracking surface is fixed after crack initiation, with zero tensile strength assigned to its normal direction, and secondary cracking is allowed only in the corresponding orthogonal direction (fixed-orthogonal crack model). The sign of the strain component normal to the cracking plane governs any further closing and re-opening of the crack.

The crack initiation criterion is defined as follows:

$$c_p(\sigma_1,\varepsilon_1)=\frac{\sigma_1}{\sigma_f}+\frac{\varepsilon_1}{\varepsilon_f}-1$$

where σ_f and ε_f denote maximum admissible values for the corresponding principal values of stress and strain, respectively. The resulting criterion is a function of the two-dimensional state of stress at the point, and it can be written as follows:

$$c_p(\sigma_1,\sigma_2)=\sigma_1-\frac{\nu\bar{E}}{E+\bar{E}}\sigma_2-\frac{E}{E+\bar{E}}\sigma_f$$

where $\bar{E}=\sigma_f/\varepsilon_f$. The principal conditions of stress and strain are monitored for all integration points, and the corresponding crack initiation potential is evaluated for each step of the computations. This scheme allows the determination of a hierarchy between all prospective cracking points.

3. HYDRODYNAMIC EFFECTS

Based on the incompressibility assumption for the fluid domain, the hydrodynamic effects are incorporated using the generalized version of Westergaard's solution. Instead of adding lumped masses at each node along the fluid-structure interface, a consistent mass matrix is computed for each interface element based on the pressure distribution and the orientation of the local normal as follows:

$$\mathbf{M}_e=\int_{S_e}\overline{p}_{(s)}\mathbf{N}_{(s)}^T\Lambda_{(s)}\mathbf{N}_{(s)}ds$$

The coefficient $\overline{p}_{(s)}$ denotes the corresponding pressure coefficient, the matrix $\mathbf{N}_{(s)}$ indicates the shape function matrix evaluated along the element side S_e, and $\Lambda_{(s)}$ is the local orientation matrix, given by

$$\Lambda_{(s)}=\begin{bmatrix}\cos^2(\lambda_x) & \sin(2\lambda_x)/2\\ \sin(2\lambda_x)/2 & \sin^2(\lambda_x)\end{bmatrix}$$

in which λ_x defines the direction of the normal to the interface. The formulation therefore takes into account the slope of the upstream face of the dam, and it renders a non-diagonal added-mass matrix.

4. NUMERICAL RESULTS

The global equations of motion are integrated using a standard implicit iterative scheme. If the displacement configuration at time t_n is indicated by the vector $\mathbf{a}_n$, then the equations of motion for the system subjected to ground acceleration $\ddot{x}^g$ are given by

$$\mathbf{M}\ddot{\mathbf{a}}_n^{(k)}+\mathbf{C}_n^{(k)}\dot{\mathbf{a}}_n^{(k)}+\mathbf{p}_n^{(k)}=-\mathbf{M}\mathbf{r}\ddot{x}_n^g$$

where the subscript k indicates the iteration number. The matrix $\mathbf{M}$ is the global mass matrix, and $\mathbf{p}_n^{(k)}$ represents the internal force vector, which is approximated as follows:

$$\mathbf{p}_n^{(k)} \approx \mathbf{p}_{n-1}^{(k-1)} + \mathbf{K}_T^{(k-1)} \Delta \mathbf{a}_n^{(k)}$$

where $\mathbf{K}_n^{(k-1)}$ indicates the tangent stiffness matrix, and $\Delta \mathbf{a}_n^{(k)}$ denotes the corresponding displacement increment. The global damping effects are modeled by using a damping matrix $\mathbf{C}_n^{(k)}$ proportional to the tangent stiffness. This is done to eliminate fictitious damping forces that may appear on cracked elements. This proportional damping is introduced to account for energy dissipation effects not associated with the local opening and closing of cracks.

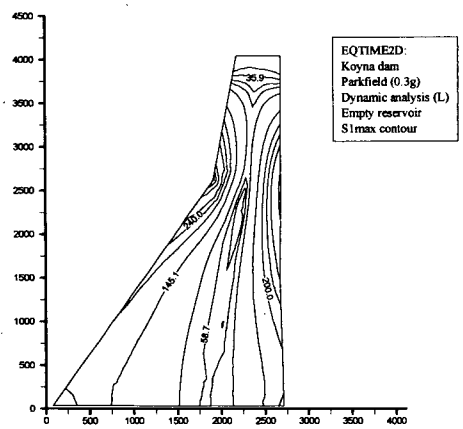


Figure 2: Principal stress contour (linear).

As a numerical example, the dynamic response of the tallest nonoverflow monolith of the Koyna Dam (India) is calculated. The ground excitation is a horizontal component of the Parkfield earthquake of 1966, with a peak ground acceleration value scaled to 0.3g. Figure (2) shows the envelope of maximum principal stresses. As expected, a concentration of high values of stress is observed in the area near the change of slope of the downstream face of the dam.

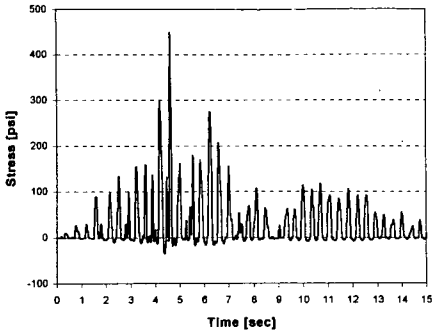


Figure 3: Principal stress time history (linear).

Figure (3) shows the time history of the maximum principal stress in one of the elements within the stress concentration area. It can be observed that the peak value of stress of occurs at about 4.5 sec, and it reaches almost 450 psi. This value largely exceeds the assumed tensile strength of the concrete at that elevation.

Figure (4) shows the envelope of maximum principal stress values obtained for the nonlinear case, using the smeared crack model to represent the tensile behavior of concrete. It is observed the development of a cracking zone in the area corresponding to the stress concentration region that was noticed in the previous linear analysis. The presence of this damaged area induces a modification of the stress field in neighboring regions.

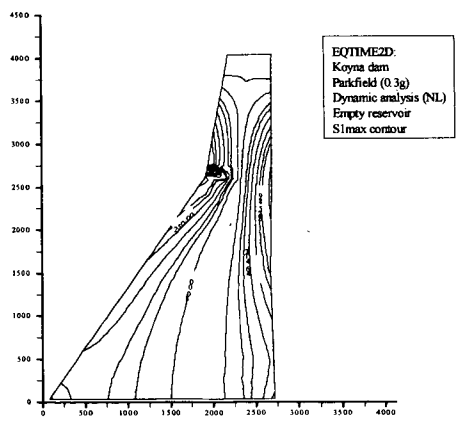


Figure 4: Principal stress contour (nonlinear).

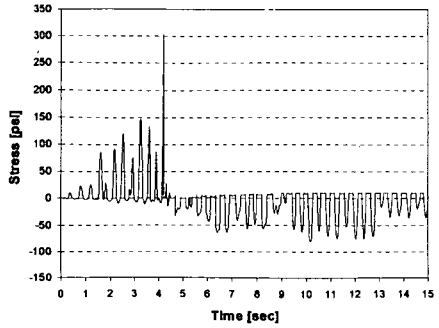


Figure 5: Principal stress time history (nonlinear).

Figure (5) shows the time history of the maximum principal stress in one of the elements within the cracked zone. Note that this is not the normal stress orthogonal to the crack plane, due to the continuous rotation of principal axes induced by the presence of shear stresses. After cracking, a sudden drop is observed in the value of the tensile component of subsequent principal stress cycles.

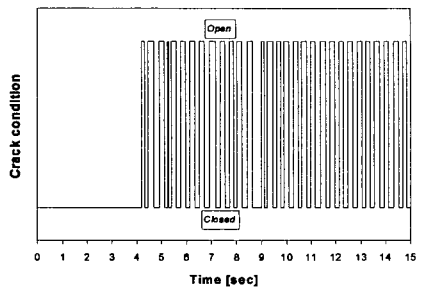


Figure 6: Cracking state.

The evolution of the corresponding cracking state is presented in Figure (6) as a function of time. It is observed that the post-cracking condition of the point oscillates between closed and re-opened conditions.

5. CONCLUSIONS

Depending on the level of the ground excitation, the response characteristics predicted by linear analysis procedures can differ substantially from those obtained by considering the nonlinear constitutive behavior. The rigorous seismic evaluation of concrete dams requires an accurate quantification of the damage that can occur under earthquake excitations. Therefore, the constitutive model should represent the main characteristics of the tensile behavior of concrete. These nonlinear analysis procedures can identify the ultimate capacity of existing concrete dams by taking into account the most critical phenomena controlling the response.

6. ACKNOWLEDGEMENTS

This study was sponsored by the Civil Works Earthquake Engineering Research Program of the U.S. Army Engineer Waterways Experiment Station in Vicksburg, MS. We appreciate the cooperation of the authorities at the U.S. Army Engineer Waterways Experiment Station, which permitted us to prepare and present this paper. Permission to publish this paper was granted by the Chief of Engineers, U.S. Army Corps of Engineers.

7. REFERENCES

Ayari, M. L., and Saouma, V. E., "A Fracture Mechanics Based Seismic Analysis of Concrete Gravity Dams using Discrete Cracks," *Engineering Fracture Mechanics*, Vol. 35, pp. 587-598 (1990).

Bazant, Z. P., and Oh, B. H., "Crack Band Theory for Fracture of Concrete," *Materials and Structures*, Vol. 16, pp. 155-177 (1983).

Chakrabarti, P., and Chopra, A. K., "Earthquake Analysis of Gravity Dams including Hydrodynamic Interaction," *Earthquake Engineering and Structural Dynamics*, Vol. 2, pp. 143-160 (1973).

Chopra, A. K., and Gupta, S., "Hydrodynamic and Foundation Interaction Effects in Earthquake Response of a Concrete Gravity Dam," *Journal of the Structural Division* (ASCE), Vol. 107, No. 8, pp. 1399-1412 (1981).

Dowling, M. J., and Hall, J. F., "Nonlinear Seismic Analysis of Arch Dams," *Journal of Engineering Mechanics* (ASCE), Vol. 115, No. 4, pp. 768-789 (1989).

El-Aidi, B., and Hall, J. F., "Nonlinear Earthquake Response of Concrete Gravity Dams

– Part 1: Modeling," *Earthquake Engineering and Structural Dynamics*, Vol. 18, pp. 837-851 (1989a).

El-Aidi, B., and Hall, J. F., "Nonlinear Earthquake Response of Concrete Gravity Dams – Part 2: Behavior," *Earthquake Engineering and Structural Dynamics*, Vol. 18, pp. 853-865 (1989b).

Hall, J. F. and Chopra, A. K., "Two-Dimensional Dynamic Analysis of Concrete Gravity and Embankment Dams including Hydrodynamic Effects," *Earthquake Engineering and Structural Dynamics*, Vol. 10, pp. 305-332 (1982).

Mao, M., and Taylor, C. A., "Nonlinear Seismic Cracking Analysis of Medium-Height Concrete Gravity Dams," *Computers and Structures*, Vol. 64, No. 5, pp. 1197-1204 (1997).

Mlakar, P., "Nonlinear Response of Concrete Gravity Dams to Strong Earthquake-Induced Ground Motion," *Computers and Structures*, Vol. 26, No. 1, pp. 165-173 (1987).

Ngo, D., and Scordelis, A. C., "Finite Element Analysis of Reinforced Concrete Beams," *Journal of the American Concrete Institute*, Vol. 64, No. 3, pp. 152-163 (1967).

Pal, N., "Seismic Cracking of Concrete Gravity Dams," *Journal of the Structural Division* (ASCE), Vol. 102, No. 9, pp. 1827-1844 (1976).

Rashid, Y. R., "Analysis of Prestressed Concrete Pressure Vessels," *Nuclear Engineering and Design*, Vol. 7, No. 4, pp. 334-344 (1968).

Skrikerud, P., "Discrete Crack Modeling for Dynamically Loaded, Unreinforced Concrete Structures," *Earthquake Engineering and Structural Dynamics*, Vol. 14, pp. 297-315 (1986).

Suidan, M., and Schnobrich, W. C., "Finite Element Analysis of Reinforced Concrete," *Journal of the Structural Division* (ASCE), Vol. 99, No. 10, pp. 2109-2110 (1973).

Vargas-Loli, L. M., and Fenves, G. L., "Effects of Concrete Cracking on the Earthquake Response of Gravity Dams," *Earthquake Engineering and Structural Dynamics*, Vol. 18, pp. 575-592 (1989).

PROPOSAL OF MODIFIED SEISMIC COEFFICIENT METHOD FOR CONCRETE GRAVITY DAMS

Isao NAGAYAMA*, Takashi SASAKI**

ABSTRUCT

The modified seismic coefficient method was proposed as the seismic resistance design method of concrete gravity dams after the discussion of theory of modal analysis and response spectrum method. The case study showed the stress obtained from the modified seismic coefficient method coincided well with the stress obtained from dynamic analysis.

Keywords : *modified seismic coefficient method*
concrete gravity dam
response spectrum
modal analysis
stress

1. PREFACE

Dams are important structures which store huge amount of water for the purpose of flood control, water supply and power generation, etc. Therefore, they should have high safety even when they are attacked by big earthquakes.

Seismic resistance of dams in Japan is now confirmed with the seismic coefficient method in their design stage. The reliability of seismic resistance of dams designed by this method has been proved empirically, since there have been no dams which have suffered significant damage during big earthquakes. However, it is well known that the uniform distribution of acceleration on dams, which is assumed in the seismic coefficient method, is completely different from the real behavior of dams during earthquakes. It is therefore considered that the safety of dams during earthquakes is assured by providing the appropriate margin of safety – for example, no tensile stress condition at the upstream surface of concrete gravity dams.

However, this fact cannot deny the rationality of the seismic coefficient method because it is the simplest way of the seismic analysis and the dams designed by this method have been safe enough during big earthquakes. Only disadvantage of this method is the discrepancy between the design assumption and the real behavior.

In this paper, the authors propose the modified seismic coefficient method for the seismic resistance design of concrete gravity dams. The proposed method preserves the simplicity of the seismic coefficient method, but the modified seismic coefficient is derived theoretically from the theory of dynamics.

2. THEORETICAL DERIVATION OF MODIFIED SEISMIC COEFFICIENT METHOD

(1) Equation of Vibration

Dynamic behavior of the structure is expressed by the Newton's second law. The equation of motion is expressed as follows, using technique of the finite element method.

$$[M]\{\ddot{x}\} = -[K]\{x\} - [C]\{\dot{x}\} \qquad (1)$$

where $[x]$: displacement, $[M]$: mass matrix,

* Head of Dam Structure Division, Public Works Research Institute, Ministry of Construction Asahi 1, Tsukuba, Ibaraki, 305-0804, Japan.
** Senior Researcher of Dam Structure Division, ditto

$[K]$: stiffness matrix and $[C]$: viscosity matrix (damping matrix).

In the vibration problem, the equation of motion is usually expressed by the relative displacement $\{u\}$ of the structure to the ground.

$$\{u\} = \{x\} - [I]\{v\} \tag{2}$$

or

$$\{u\} = \{x\} - \{i_x\}v_x - \{i_y\}v_y - \{i_z\}v_z \tag{3}$$

where $[I]$: unit matrix connecting the motion of the structure and the ground motion, $\{v\}$: displacement of ground and

$$[I] = [\{i_x\}, \{i_y\}, \{i_z\}] \tag{4}$$

$$\{v\} = \{v_x, v_y, v_z\}^T \tag{5}$$

Eq. (1) can be rewritten as follows, since $[C][I] = 0$ and $[K][I] = 0$.

$$[M]\{\ddot{u}\} + [M][I]\{\ddot{v}\} = -[K]\{u\} - [C]\{\dot{u}\} \tag{6}$$

or

$$[M]\{\ddot{u}\} + [M](\{i_x\}\ddot{v}_x + \{i_y\}\ddot{v}_y + \{i_z\}\ddot{v}_z) = -[K]\{u\} - [C]\{\dot{u}\} \tag{7}$$

Eq. (7) is usually expressed as follows.

$$[M]\{\ddot{u}\} + [C]\{\dot{u}\} + [K]\{u\} = -[M](\{i_x\}a_x + \{i_y\}a_y + \{i_z\}a_z) \tag{8}$$

where

$$\{\ddot{v}\} = \{\ddot{v}_x, \ddot{v}_y, \ddot{v}_z\}^T = \{a_x, a_y, a_z\}^T \tag{9}$$

Eq. (8) is called the equation of vibration.

It is often said that the seismic coefficient method is not appropriate because it is not dynamic but pseudo-dynamic. But this opinion is completely wrong because d'Alembert's principle approves that the dynamical problem can be converted into the static problem by introducing inertia force. Namely, Eq. (6) can be arranged as the equilibrium equation of applied force on the structure at any arbitrary time t.

$$-[K]\{u\} - [C]\{\dot{u}\} - [M]\{\ddot{x}\} = 0 \tag{10}$$

Furthermore, Eq. (10) can be arranged as follows.

$$[K]\{u\} = -[M]\{\ddot{x}\} - [C]\{\dot{u}\} \tag{11}$$

Here, $\{u\}$ means static displacement by the pseudo-dynamic force $-[M]\{\ddot{x}\} - [C]\{\dot{u}\}$ which applies on the structure at arbitrary time t. Therefore, the question is how to determine the pseudo-dynamic load of $-[M]\{\ddot{x}\} - [C]\{\dot{u}\}$.

(2) Modal Analysis

Here, the term of $\{i_x\}a_y + \{i_z\}a_z$ in Eq. (8) is omitted for convenience, taking account of the principle of superposition in the elastic system.

$$[M]\{\ddot{u}\} + [C]\{\dot{u}\} + [K]\{u\} = -[M]\{i_x\}a_x \tag{12}$$

The theory of the modal analysis can be applied when the structure is elastic. In this method, relative displacement of the system can be expressed as the summation of displacements for vibration mode $\{u_s\}$ $(s = 1,2,3,....)$.

$$\{u\} = \Sigma\{u_s\}\beta_{sx}\psi_{sx} \tag{13}$$

$\{u_s\}$ $(s = 1,2,3,....)$ is the eigen-vector of the following equation

$$[K]\{u\} = \omega^2[M]\{u\} \tag{14}$$

and β_{sx} $(s = 1,2,3,....)$ is the participation factor expressed by

$$\beta_{sx} = \frac{\{u_s\}^T[M]\{i_x\}}{\{u_s\}^T[M]\{u_s\}} \tag{15}$$

Vibration modes are orthogonal each other with regard to mass matrix, damping matrix and stiffness matrix. (Strictly speaking, the second equation in Eq. (16) is assumption.)

$$\begin{aligned} \{u_s\}^T[M]\{u_r\} &= \delta_{sr}M_s \\ \{u_s\}^T[C]\{u_r\} &= \delta_{sr}C_s \\ \{u_s\}^T[K]\{u_r\} &= \delta_{sr}K_s \end{aligned} \tag{16}$$

Substituting Eq. (13) for $\{u\}$ in Eq. (12) and utilizing Eq. (15) and (16), the following

equation is derived.

$$M_s\ddot{\psi}_{sx} + C_s\dot{\psi}_{sx} + K_s\psi_{sx} = -M_s a_x \quad (17)$$

Therefore, ψ_{sx} in Eq. (13) is the solution of Eq. (17).

The stress in the structure is given by the following equation, using the technique of the finite element method.

$$\{\sigma\} = [D][B]\{u\} \quad (18)$$

where $[D]$: elastic matrix and $[B]$: strain-displacement transforming matrix.

Substituting Eq. (13) for $\{u\}$ in Eq. (18), the following equation is derived.

$$\{\sigma\} = \Sigma[D][B]\{u_s\}\beta_{sx}\psi_{sx} \quad (19)$$

or

$$\{\sigma\} = \Sigma\{\sigma_s\}\beta_{sx}\psi_{sx} \quad (20)$$

where $\{\sigma_s\}$ $(=[D][B]\{u_s\})$ is called the vibration mode of stress.

Now, extract the term of $\{u_s\}\beta_{sx}\psi_{sx}$ from Eq. (12). Because of the orthogonality of $\{u_s\}$, it must be expressed as follows, where p_r $(r = 1,2,3,\ldots.)$ is a still unknown coefficient.

$$[M]\{u_s\}\beta_{sx}\ddot{\psi}_{sx} + [C]\{u_s\}\beta_{sx}\dot{\psi}_{sx} + [K]\{u_s\}\beta_{sx}\psi_{sx} = -[M]\Sigma\{u_r\}p_r a_x \quad (21)$$

Multiplying $\{u_m\}^T$ $(m = 1,2,3,\ldots.)$ from the left side of Eq. (21) and utilizing Eq. (16) and (17), then the following equation is derived.

$$[M]\{u_s\}\beta_{sx}\ddot{\psi}_{sx} + [C]\{u_s\}\beta_{sx}\dot{\psi}_{sx} + [K]\{u_s\}\beta_{sx}\psi_{sx} = -[M]\{u_s\}\beta_{sx}a_x \quad (22)$$

Eq. (22) expresses the equation of vibration for the s-th mode. Then, the response of stress to the vibration of Eq. (22) is given by

$$\{\sigma\}_s = [D][B]\{u_s\}\beta_{sx}\psi_{sx} \quad (23)$$

or

$$\{\sigma\}_s = \{\sigma_s\}\beta_{sx}\psi_{sx} \quad (24)$$

Here, it should be noted that the following equation is true. It can be derived comparing Eq. (22) with Eq. (12).

$$\{i_x\}a_x = \Sigma\{u_s\}\beta_{sx}a_x \quad (25)$$

Then, the absolute acceleration $\{\ddot{x}\}_s$ with regard to the s-th mode of vibration is given by

$$\{\ddot{x}\}_s = \{u_s\}\beta_{sx}(\ddot{\psi}_{sx} + a_x) \quad (26)$$

(3) Dynamic Response to Harmonic Ground Acceleration

Here, the following harmonic ground acceleration is assumed.

$$a_x = a_0 \exp(j\omega t) \quad (27)$$

Then, the response ψ_{sx} of Eq. (17) is given by

$$\psi_{sx} = R_s(\omega)a_0 \exp(j\omega t) \quad (28)$$

$R_s(\omega)$ is called the s-th frequency response function and is given by

$$R_s(\omega) = \frac{-1}{-\omega^2 + 2jh_s\omega\omega_s + {\omega_s}^2} \quad (29)$$

where ω_s is the s-th natural circular frequency and h_s is the s-th damping ratio, and they are given by

$$\omega_s = \sqrt{\frac{K_s}{M_s}}, \quad h_s = \frac{1}{2\omega_s}\sqrt{\frac{C_s}{M_s}} \quad (30)$$

Then, relative displacement and absolute acceleration of the structure, and stress in the structure for the s-th mode are given by

$$\{u\}_s = \{u_s\}\beta_{sx}R_s(\omega)a_0 \exp(j\omega t) \quad (31)$$

$$\{\ddot{x}\}_s = \{u_s\}\beta_{sx}(1-\omega^2 R_s(\omega))a_0 \exp(j\omega t) \quad (32)$$

$$\{\sigma\}_s = \{\sigma_s\}\beta_{sx}R_s(\omega)a_0 \exp(j\omega t) \quad (33)$$

Furthermore, relative displacement and absolute acceleration of the structure, and stress in the structure as whole system are given by

$$\{u\} = \Sigma\{u_s\}\beta_{sx}R_s(\omega)a_0 \exp(j\omega t) \quad (34)$$

$$\{\ddot{x}\} = \Sigma\{u_s\}\beta_{sx}(1-\omega^2 R_s(\omega))a_0 \exp(j\omega t) \quad (35)$$

$$\{\sigma\} = \Sigma\{\sigma_s\}\beta_{sx}R_s(\omega)a_0 \exp(j\omega t) \quad (36)$$

Now, consider the s-th vibration mode again. Here, it is assumed that h_s is smaller enough than 1 (It is true in general). Then, the response is the maximum approximately when

$\omega = \omega_s$. The maximum response of relative displacement and absolute acceleration of the structure, and stress in the structure for the s-th mode are given by

$$\{u\}_{s,\max} = \pm\{u_s\}\frac{\beta_{sx}a_0}{2h_s\omega_s{}^2} \tag{37}$$

$$\{\ddot{x}\}_{s,\max} = \mp\{u_s\}\frac{\beta_{sx}a_0}{2h_s} \tag{38}$$

$$\{\sigma\}_{s,\max} = \pm\{\sigma_s\}\frac{\beta_{sx}a_0}{2h_s\omega_s{}^2} \tag{39}$$

These maximum responses occur almost at the same time of $t = (N+1/2)\pi/\omega$ $(N = 0,1,2,...)$ (Strictly speaking, Eq. (38) occurs at the slightly different time from the others).

It is well known that the effect of high modes on the total response of displacement is small enough because Eq. (37) has the term of $1/\omega_s{}^2$. Therefore, in a practical sense, only the first few modes are enough to express the behavior of the structure. This conclusion can also apply to the response of stress because Eq. (39) has the term of $1/\omega_s{}^2$ (as shown in Section 3).

(4) Response Spectrum Method

Then, arbitrary ground acceleration a_x of earthquake is considered. Characteristics of ground acceleration a_x are usually expressed by response spectrum of absolute acceleration $S_A(T,h)$ and/or response spectrum of relative displacement $S_D(T,h)$ which express the maximum response of the system of one-degree of freedom with natural period $T = 2\pi/\omega$ and damping ratio h.

Utilizing Eq. (17), the response spectrum can be applied to the structure of multi-degrees of freedom. Then, the maximum responses of relative displacement and absolute acceleration of the structure, and stress in the structure for the s-th vibration mode are expressed as follows.

$$\{u\}_{s,\max} = \pm\{u_s\}\beta_{sx}S_D(T_s,h_s) \tag{40}$$

$$\{\ddot{x}\}_{s,\max} = \mp\{u_s\}\beta_{sx}S_A(T_s,h_s) \tag{41}$$

$$\{\sigma\}_{s,\max} = \pm\{\sigma_s\}\beta_{sx}S_D(T_s,h_s) \tag{42}$$

And the responses of the whole structure are expected as follows, from statistical approach.

$$\{u\}_{\max} = \pm\sqrt{\Sigma(\{u_s\}\beta_{sx}S_D(T_s,h_s))^2} \tag{43}$$

$$\{\ddot{x}\}_{\max} = \mp\sqrt{\Sigma(\{u_s\}\beta_{sx}S_A(T_s,h_s))^2} \tag{44}$$

$$\{\sigma\}_{\max} = \pm\sqrt{\Sigma(\{\sigma_s\}\beta_{sx}S_D(T_s,h_s))^2} \tag{45}$$

(This expression is not correct in a strict mathematical sense. In this paper, however, it is defined for sake of convenience that calculation should be made each component of vectors.)

It is well known that the effect of high modes on the total response of displacement is small enough because $S_D(T_s,h_s)$ is smaller when T_s is smaller. Therefore, in a practical sense, only the first few modes are enough to express the behavior of the structure.

(5) Pseudo-dynamic Analysis (Modified Seismic Coefficient Method)

Now, the equation of vibration for the s-th mode expressed by Eq. (22) is considered. Applying d'Lambert's principle to Eq. (22), the following equation is obtained at any arbitrary time t.

$$[K]\{u_s\}\beta_{sx}\psi_{sx} = -[M]\{u_s\}\beta_{sx}(\ddot{\psi}_{sx} + a_x) - [C]\{u_s\}\beta_{sx}\dot{\psi}_{sx} \tag{46}$$

This equation means that $\{u_s\}\beta_{sx}\psi_{sx}$ is the solution of the following pseudo-dynamic equation.

$$[K]\{u\}_s = -[M]\{u_s\}\beta_{sx}(\ddot{\psi}_{sx} + a_x) - [C]\{u_s\}\beta_{sx}\dot{\psi}_{sx} \tag{47}$$

Especially, when $\{u\}_s$ is the maximum, then $\dot{\psi}_{sx} = 0$. Therefore,

$$[K]\{u\}_{s.\max} = -[M]\{u_s\}\beta_{sx}(\ddot{\psi}_{sx} + a_x) \quad (48)$$

Furthermore, the following equation is derived from Eq. (23).

$$\{\sigma\}_{s.\max} = -[D][B][K]^{-1}[M]\{u_s\}\beta_{sx}(\ddot{\psi}_{sx} + a_x) \quad (49)$$

It means that $\{u_s\}\beta_{sx}(\ddot{\psi}_{sx} + a_x)$ is the seismic coefficient at time t when stress response is the maximum (In a strict sense, the seismic coefficient is not the acceleration of the structure but its rate to the acceleration of gravity $\{u_s\}\beta_{sx}(\ddot{\psi}_{sx} + a_x)/g$. However, for the sake of convenience, $\{u_s\}\beta_{sx}(\ddot{\psi}_{sx} + a_x)$ is called the seismic coefficient in this paper).

It should be noted that $-\{u_s\}\beta_{sx}(\ddot{\psi}_{sx} + a_x)$ in Eq. (48) and (49) is not the maximum acceleration in general because the time when the relative displacement is the maximum does not always coincide with the time when the absolute acceleration is the maximum. Therefore, the responses given by the following equations are larger than the responses given by Eq. (48) and (49).

$$[K]\{u\}_s = -[M]\{u_s\}\beta_{sx}(\ddot{\psi}_{sx} + a_x)_{\max} \quad (50)$$

$$\{\sigma\}_s = -[D][B][K]^{-1}[M]\{u_s\}\beta_{sx}(\ddot{\psi}_{sx} + a_x)_{\max} \quad (51)$$

It means that Eq. (50) and (51) are the equations on a safer side in evaluating the safety of the structure.

Now, consider the case where a_x is defined by the following harmonic vibration.

$$a_x = a_0 \exp(j\omega t) \quad (52)$$

Then,

$$(\ddot{\psi}_{sx} + a_x)_{\max} = \sqrt{\frac{\omega_s{}^4 + 4h_s{}^2\omega_s{}^2\omega^2}{(\omega_s{}^2-\omega^2)^2 + 4h_s{}^2\omega_s{}^2\omega^2}}\, a_0 \quad (53)$$

When h_s is smaller enough than 1 (it is true in general), then the resonance occurs almost when $\omega = \omega_s$, and

$$(\ddot{\psi}_{sx} + a_x)_{\max} = \frac{a_0}{2h_s} \quad (54)$$

Therefore, the maximum responses are the solutions of the following equations.

$$[K]\{u\}_s = [M]\{u_s\}\frac{\beta_{sx}a_0}{2h_s} \quad (55)$$

$$\{\sigma\}_s = [D][B][K]^{-1}[M]\{u_s\}\frac{\beta_{sx}a_0}{2h_s} \quad (56)$$

The solutions of Eq. (55) and (56) are equal to Eq. (37) and (39) respectively. These are proved easily because $\omega_s{}^2[M]\{u_s\} = [K]\{u_s\}$.

The above discussion is also available in the response spectrum method. In this case,

$$\ddot{\psi}_{sx} + a_x = S_A(T_s, h_s) \quad (57)$$

and therefore,

$$[K]\{u\}_s = [M]\{u_s\}\beta_{sx}S_A(T_s, h_s) \quad (58)$$

$$\{\sigma\}_s = [D][B][K]^{-1}[M]\{u_s\}\beta_{sx}S_A(T_s, h_s) \quad (59)$$

Here, the following relation is approximately true from the statistical approach.

$$S_D(T_s, h_s) = \frac{S_A(T_s, h_s)}{\omega_s{}^2} \quad (60)$$

and the following equation is available.

$$\omega_s{}^2[M]\{u_s\} = [K]\{u_s\} \quad (61)$$

Then, substituting Eq. (60) for $S_A(T_s, h_s)$ in Eq. (58) and (59) and utilizing Eq. (61), the following solutions are obtained.

$$\{u\}_s = \{u_s\}\beta_{sx}S_D(T_s, h_s) \quad (62)$$

$$\{\sigma\}_s = [D][B]\{u_s\}\beta_{sx}S_D(T_s, h_s) \quad (63)$$

Therefore, the solutions of Eq. (58) and (59) are equal to Eq. (40) and (42).

It is well known that the effect of high modes on the total response of displacement is small enough because $S_D(T_s, h_s)$ is smaller when T_s is smaller. Therefore, in a practical sense, only the first few modes are enough to express the behavior of the structure, and sometimes only the first mode is enough as in the case of concrete gravity dams which will be discussed afterward. In this case, The pseudo-dynamic equations are expressed as follows.

$$[K]\{u\} = [M]\{u_1\}\beta_{1x}S_A(T_1, h_1) \quad (64)$$

$$\{\sigma\} = [D][B]\{u\} \tag{65}$$

Here, the term of $\{u_1\}\beta_{1x}S_A(T_1, h_1)$ in Eq. (64) and (65) expresses the seismic coefficient.

(6) Effect of Reservoir Water (Effect of Hydrodynamic Pressure)

The effect of reservoir water was not included in the above discussion. In this section, the effect of reservoir water will be considered.

The equation of vibration of reservoir is expressed as the following Laplace's equation and its boundary condition.

$$\nabla^2 p = \frac{1}{c^2}\ddot{p} \tag{66}$$

$$\frac{\partial}{\partial n} p = -\rho_w \ddot{x}_n \tag{67}$$

where p: pressure, c: velocity of sound, ρ_w: density of water $\ddot{x}_n$: absolute acceleration normal to the upstream surface of dams.

These equations can be arranged as follows, using the technique of the finite element method.

$$[G]\{\ddot{p}\} + [H]\{p\} = [A][L]\{\ddot{x}\} \tag{68}$$

where $[G]$, $[H]$ and $[A]$ express the term of $1/c^2$, ∇^2 and $\partial/\partial n$ respectively, and $[L]$ is the matrix in relation to the directional cosine of the boundary.

If $\{\ddot{x}\}$ is expresses by the harmonic vibration as

$$\{\ddot{x}\} = \{a_1\}\exp(j\omega t) \tag{69}$$

then $\{p\}$ should be also expressed by the harmonic vibration as

$$\{p\} = \{p_1\}\exp(j\omega t) \tag{70}$$

Therefore, the following solution of Eq. (68) is obtained.

$$\{p\} = ([H] - \omega^2[G])^{-1}[A][L]\{a_1\}\exp(j\omega t) \tag{71}$$

Therefore, the nodal force $\{f\}$ which applies on the upstream surface of the dam is given by

$$\{f\} = [L]^T[A]^T([H] - \omega^2[G])^{-1}[A][L] \times \{a_1\}\exp(j\omega t) \tag{72}$$

Here, the force $\{f\}$ is proportional to acceleration $\{a_1\}\exp(j\omega t)$. Therefore, the following matrix $[M_W(\omega)]$ can be treated as a kind of the mass matrix.

$$[M_W(\omega)] = [L]^T[A]^T([H] - \omega^2[G])^{-1}[A][L] \tag{73}$$

So, the term $[M_W(\omega)]$ is called the additional mass matrix corresponding to hydrodynamic pressure. This additional mass matrix is not constant but the function of circular frequency of input acceleration.

Now, the following equation is considered in stead of Eq. (72).

$$\{f\} = [M_W(\phi)]\{a_1\}\exp(j\omega t) \tag{74}$$

It should be noted that the additional mass matrix $[M_W(\phi)]$ in Eq. (74) is not a function of circular frequency ω of input acceleration, but constant value defined by ϕ. If $\phi = 2\pi\sec^{-1}$, then $[M_W(2\pi\sec^{-1})]$ is called Westergaard's additional mass matrix, and if $\phi = 0$, then $[M_W(0)]$ is called the additional mass matrix of incompressive water.

Using the additional mass matrix, the equation of vibration can be expressed as if the mass matrix of the structure system were $[M] + [M_W(\phi)]$, namely

$$([M] + [M_W(\phi)])\{\ddot{u}\} + [C]\{\dot{u}\} + [K]\{u\} = -([M] + [M_W(\phi)])\{a_x\} \tag{75}$$

Then, pseudo-dynamic equations corresponding to Eq. (64) and (65) are

$$[K]\{u\} = [M]\{u_1\}\beta_{1x}S_A(T_1, h_1) + [M_W(\phi)]\{u_1\}\beta_{1x}S_A(T_1, h_1) \tag{76}$$

$$\{\sigma\} = [D][B]\{u\} \tag{77}$$

where $\{u_1\}$ and $\omega_1 = 2\pi/T_1$ are the eigen-vector and the eigen-value of

$$[K]\{u\} = \omega^2([M]+[M_W(\phi)])\{u\} \quad (78)$$

and

$$\beta_{1x} = \frac{\{u_1\}^T([M]+[M_W(\phi)])\{i_x\}}{\{u_1\}^T([M]+[M_W(\phi)])\{u_1\}} \quad (79)$$

0 or 2π $\sec^{-1}$ is usually adopted as the value of ϕ, but in a strict sense, $\phi = 2\pi / T_1$ is more precise.

3. Case Study

(1) Model Dam

The above-mentioned theory is examined using a model concrete gravity dam in this section. The configuration of a model dam and its physical properties are shown in Fig. 1 and Table 1. The effect of reservoir water is evaluated as the additional mass matrix of incompressive water in this analysis.

(2) Eigen-Value and Eigen-Vector

The vibration modes of displacement of the dam are shown in Fig. 2 for the first 6 modes, and their natural frequencies ($f_s = \omega_s / 2\pi$) and the participation factors are shown in Table 2, where the participation factors means the values when the maximum value of components of eigen-vector $\{u_s\}$ is 1.

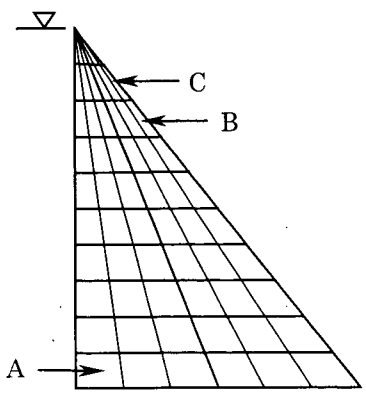


Fig. 1 Finite Element Model of Concrete Gravity Dam

(3) Response of Stress

The frequency response function of stress is given by

$$\{\sigma\}_s = [D][B]\{u_s\}\beta_{sx}R_s(\omega)a_0 \exp(j\omega t) \quad (80)$$

Therefore, if h_s is smaller enough than 1, its maximum response is approximately given by

$$\{\sigma\}_{s,\max} = \frac{[D][B]\{u_s\}\beta_{sx}a_0}{2h_s\omega_s^2} \quad (81)$$

when $\omega = \omega_s$.

Fig. 3 expresses the maximum response of

Table 1 Dimension and Properties of Dam

Dam:	
Height	100 m
Downstream Slope	0.8 to 1
Upstream Slope	vertical
Density	2300 kg / m^3
Modulus of Elasticity	30 kN / mm^2
Damping Ratio	0.1
Reservoir:	
Depth of Water	100 m
Density	1000 kg / m^3
Modulus of Elasticity	infinite (incompressive)

Table 2 Natural Frequency and Participation Factor

Mode s	Natural Frequency f_s (Hz)	Participation Factor $\max(\beta_{sx}\{u_s\})$
1	3.81	2.41
2	9.66	−2.57
3	12.90	−0.25
4	17.88	1.69
5	26.81	−0.28
6	27.99	−0.25

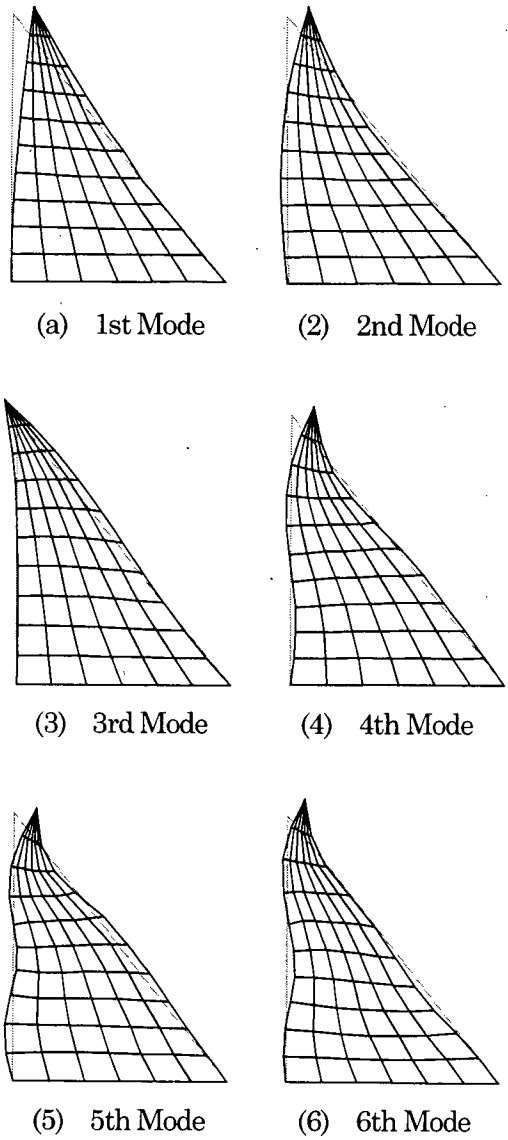


Fig. 2 Mode of Vibration

the first principal stress for each mode when $a_0 = 100\,\mathrm{gal}$. The location where the maximum stress occurs is shown in Fig. 1, namely Location A for the 1st mode, Location B for the 2nd mode and Location C for the 4th mode. From Fig. 3, it is understood that the effect of the 1st mode is predominant and that the effect of the other modes is small enough.

Then, the frequency response functions of

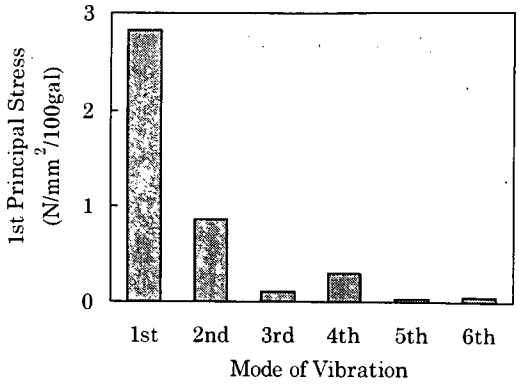


Fig. 3 Maximum Response of 1st Principal Stress for Each Mode

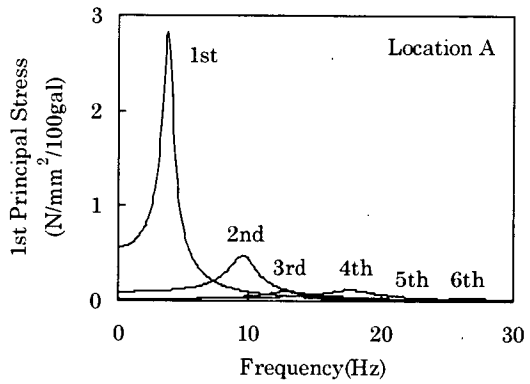


Fig. 4 Frequency Response Function of 1st Principal Stress at Location A

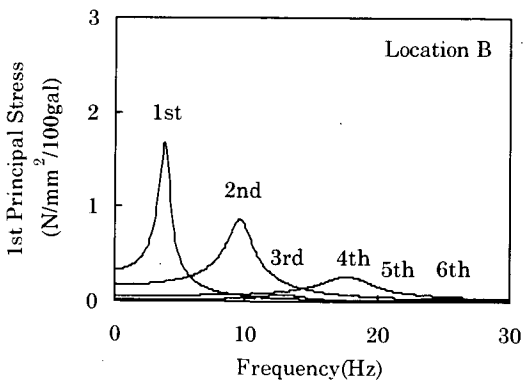


Fig. 5 Frequency Response Function of 1st Principal Stress at Location B

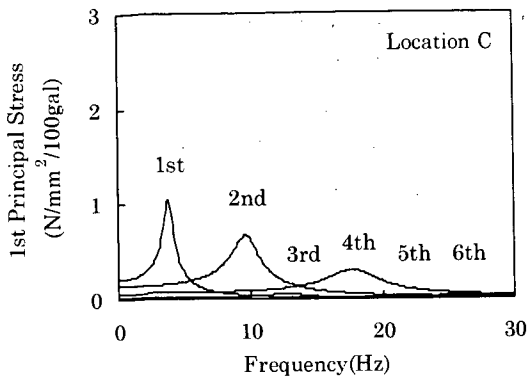


Fig. 6 Frequency Response Function of 1st Principal Stress at Location C

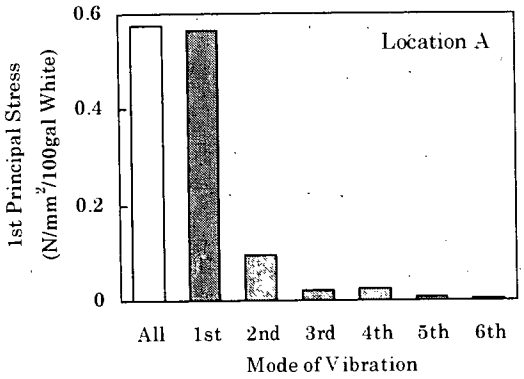


Fig. 7 Response of Stress to Acceleration with White Response Spectrum (Location A)

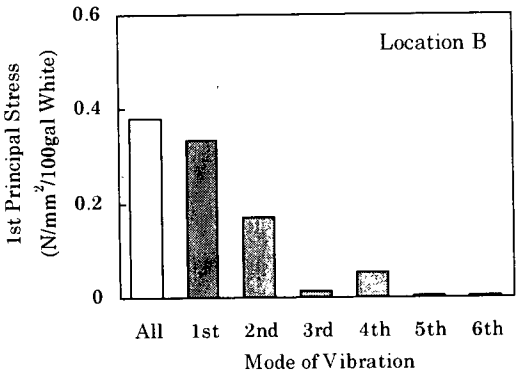


Fig. 8 Response of Stress to Acceleration with White Response Spectrum (Location B)

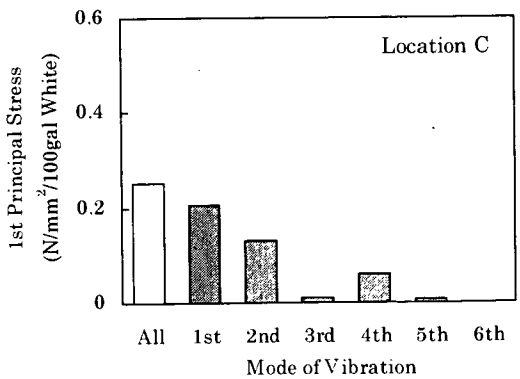


Fig. 9 Response of Stress to Acceleration with White Response Spectrum (Location C)

the first principal stress at Location A, B and C are shown in Fig. 4 to 6 (It should be noted that directions of the axis of the first principal stress are different each other and that their superposition is therefore impossible). From Fig. 5 and 6, it is found that the effect of the 1st mode is the largest even at Location B and C.

Next, the response of stress to the absolute acceleration with white response spectrum

$$S_A(T,h) = 100\,\text{gal} \qquad (82)$$

is considered. The response can be calculated from Eq. (42) and (45). The obtained principal stresses at Location A, B and C are shown in Fig. 7 to 9 respectively. In these figures, it is understood that the effect of the 1st mode is predominant and that the effect of the other modes is negligible in a practical sense. Difference between the stress for the 1st mode and the stress for all modes is 0.01 N/mm^2 at Location A and it is only 2 % of the maximum principal stress (0.58 N/mm^2).

Then, Fig. 10 shows the distribution of the first principal stress along the upstream surface of a dam, where the black symbol shows the result when only the 1st mode is considered and the white symbol shows the result when all modes are considered. Fig. 11 also shows the distribution of the first principal

stress along the downstream surface of a dam. These figures show that difference between the two results is almost negligible.

It should be noted, as previously discussed, that the results for the 1st mode are the same as the results of the pseudo-dynamic analysis where the modified seismic coefficient is $\{u_1\}\beta_{1x}S_A(T_1,h_1)$. It means that the pseudo-dynamic analysis using the modified seismic coefficient is useful in the seismic resistance design of concrete gravity dams.

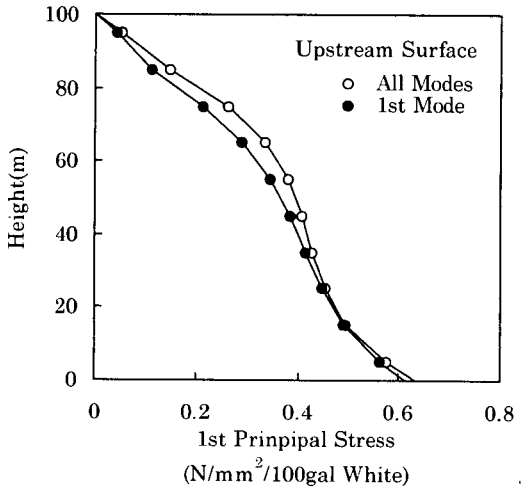


Fig. 10 Distribution of 1st Principal Stress along Upstream Surface of Dam.

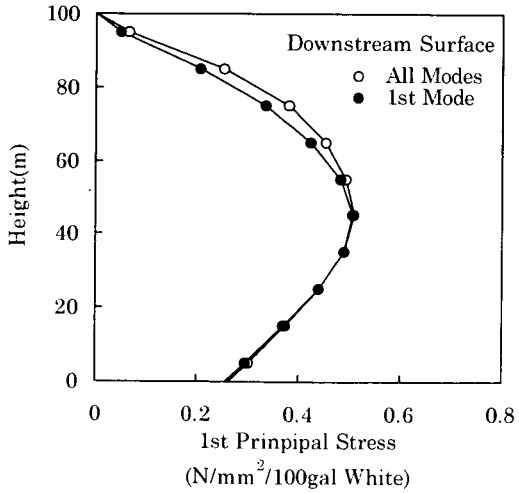


Fig. 11 Distribution of 1st Principal Stress along Downstream Surface of Dam.

It is known that the value of $\{u_s\}\beta_{sx}$ is independent on the height of a dam and that the shape of $\{u_s\}\beta_{sx}$ is similar regardless of dams because concrete gravity dams have a similar cross section. Then, in the practical manner, the authors propose the following approximation.

$$a(y) = 2.4\, S_A(T,h)\frac{y^2}{H^2} \tag{83}$$

$$T = \frac{H}{400\text{m/s}} \tag{84}$$

where $a(y)$: modified seismic coefficient, y: height from bedrock, $S_A(T,h)$: response spectrum of absolute acceleration, T: natural period of a dam with full reservoir, h: damping ratio ($\fallingdotseq 0.1$), H: height of a dam.

Remark:

In this paper, the authors defined that the seismic coefficient is the acceleration of the structure. However, the seismic coefficient is generally defined as the ratio of acceleration of the structure to acceleration of gravity. In this sense, Eq. (83) should be rewritten as follows.

$$k(y) = 2.4\frac{S_A(T,h)}{g}\frac{y^2}{H^2} \tag{85}$$

where $k(y)$: modified seismic coefficient, g: acceleration of gravity.

Reference

1. Bylaw Concerning Structural Standards for River Administration Facilities, 1976
2. Isao Nagayama, Sigeharu Jikan: Study on Dynamic Behavior of Concrete Dams during Earthquake with Hydrodynamic Interaction, Int. Symp. on Earthquake & Dams, China, 1987
3. Isao Nagayama: Present States and Future of Seismic Resistance Design of Concrete Dams, 3rd. Lecture of Japan Society of Dam Engineers, 1998.

Effect of Foundation and Reservoir Parameters on Dynamic Results for Arch Dams Using EACD-3D-96[1)]

By Richard L. Munoz[2)]

ABSTRACT

The Structural Analysis Section of the Bureau of Reclamation has adopted the EACD-3D-96 computer program, which was developed at the University of California at Berkeley, as the preferred method for the dynamic analysis of arch dams. EACD-3D-96 has capabilities beyond those of previous general purpose linear-elastic finite element structural analysis programs used at Reclamation. These capabilities, associated with the modeling of the reservoir and foundation, may have a significant influence on resulting dynamic stresses. The effect these parameters have on dynamic results is of interest in better understanding EACD-3D-96 and in better evaluating the behavior of arch dams. This report presents sensitivity studies that have been performed on several arch dams using EACD-3D-96. Three studies are presented which investigate; 1) the effect of variations in the dam modulus/foundation modulus ratio, 2) the effect of including foundation interaction, and, 3) the effect of including reservoir interaction. Comparisons are made based on dynamic results presented as envelope contour plots of maximum upstream arch stresses and in tabular form for maximum arch and cantilever stresses at specific output locations.

Key Words: Arch Dam Analysis
EACD-3D-96
Reservoir Interaction
Foundation Interaction

I. INTRODUCTION

The Bureau of Reclamation has for many years employed various linear-elastic finite element methods to analyze concrete arch dams under static and dynamic loading. These methods have, in general, employed certain common features in terms of modeling the dam, reservoir, and foundation. Dams have often been modeled with 3-D brick elements and hydrodynamic reservoir loading has been approximated by lumped masses based on a Westergaard distribution or an incompressible fluid model. The foundation has been modeled as a finite region having stiffness but without mass.

Over the past 3 years the Bureau has used the computer program EACD-3D-96 for the dynamic analysis of concrete arch dams. The EACD-3D-96 program differs from previous methods used at Reclamation in several respects: the dam is modeled with shell elements, the reservoir is modeled as a compressible fluid, and the foundation is modeled with boundary elements and includes mass effects such as radiation damping and inertia.

---

1) Submitted for presentation at U.S.-Japan Dam Earthquake Engineering Workshop, May 7-8, 1999, Tokyo, Japan.

2) Richard L. Munoz, Structural Engineer, Bureau of Reclamation, Structural Analysis Group (D-8110), PO Box 25007, Denver, Colorado 80225-0007, (303) 445-3230.

Dams that have been analyzed include: Deadwood Dam, Horse Mesa Dam, Monticello Dam, Morrow Point Dam, and Hoover Dam. Analyses of these dams have in some cases shown significant changes in dynamic stress results when compared to analyses completed using other linear-elastic approaches such as SAP-IV. Although some sensitivity studies were made for these dams, a rigorous investigation of the sensitivity of certain modeling and material parameters has never beet attempted. Such studies might reveal a better understanding of the expected behavior of arch dams.

2. OVERVIEW OF STUDIES

Three sets of studies were conducted on selected arch dams using the computer program EACD-3D-96 [1]. The three sets of studies included; 1) foundation interaction (mass effects) and compressible reservoir, 2) foundation flexibility (no mass effects) and compressible reservoir, and 3) foundation interaction (mass effects) and incompressible reservoir. Each study was conducted over a range of foundation-to-dam modulus ratios (foundation modulus varied while dam modulus was held constant). From the results of these studies the following three comparisons were made; 1) the effect of varying the foundation modulus when foundation interaction is included in the analysis, 2) the effect of including foundation interaction in the analysis versus not including foundation interaction, and 3) the effect of modeling the reservoir as a compressible fluid versus an incompressible fluid.

Results are shown for each of the studies as plots of maximum (tensile) stress envelope contours on the upstream face and as tables of maximum tensile stress in elements on the upstream and downstream faces of the dams. Evaluations were based on the maximum upstream dynamic stress results

2.1 DAMS STUDIES

Sensitivity studies were performed on three dams: Deadwood Dam, Monticello Dam, and Morrow Point Dam [2]. Brief descriptions of the dams follows; plots of the finite element meshes are shown in figure 1.

Deadwood Dam: Deadwood Dam is a 148.0 foot high, single curvature, arch dam having a crest width of 9.0 feet, a base width of 62 feet, and a crest length of about 450 feet. The model analyzed contains 54 shell elements in the dam and 16 boundary elements in the foundation. Ground motions used in the analysis of Deadwood Dam are from the Cerro Prieto, Mexico earthquake selected specifically for the dam.

Monticello Dam: Monticello Dam is a 305.0 foot high, single curvature, arch dam having a crest width of 12.0 feet, a base width of 100 feet, and a crest length of about 800 feet. The model analyzed contains 121 shell elements in the dam and 22 boundary elements in the foundation. Ground motions used in the analysis of Monticello Dam are from the Synthetic earthquake selected specifically for the dam.

Morrow Point Dam: Morrow Point Dam is a 468.0 foot high, double curvature, arch dam having a crest width of 12.0 feet, a base width of 52 feet, and a crest length of about 330 feet. The model analyzed contains 38 shell elements in the dam and 14 boundary elements in the foundation. Ground motions used in the analysis of Morrow Point Dam are from the Cabin Creek earthquake selected specifically for the dam.

2.2 MATERIAL PROPERTIES

Material properties used in the studies include modulus of elasticity, poisson's ratio, unit weight and damping ratio for both the dam

(concrete) and foundation (rock). The range of foundation properties used in these studies was based on test results of rock at numerous dam sites [3]. The concrete modulus selected represents a point between the low and high foundation modulus values such that the E_f/E_c ratio can be varied from 1/2:1 to 2:1. Properties used for the reservoir include unit weight and reflection coefficient. All values, with the exception of the foundation modulus of elasticity, were held constant for every study. The values are considered typical for arch dams and foundations and are summarized in table 1.

3. ANALYSIS RESULTS

Results are first presented as maximum (tensile) stress contour envelope plots in the arch and cantilever directions on the upstream face of each dam. Such plots provide a pattern of stress based on the maximum value at each integration point over the duration of an earthquake. These plots can show any change in stress due to a change in an analysis parameter. Furthermore, these plots can show any change in pattern which may indicate a change in modal contribution resulting from a change in an analysis parameter. Results are also summarized in tables showing the maximum stress that occurs on the upstream face of each dam for the three parametric studies.

The results of the various studies can most easily be discussed for each dam separately from which general conclusions will be drawn. The discussion will begin with the parametric study of foundation modulus when foundation interaction is included in the analysis. Next a discussion of the effect of the foundation model, with and without foundation interaction, will be made. Finally, the effect of reservoir model, compressible versus incompressible fluid, will be discussed.

3.1 DEADWOOD DAM

Foundation Modulus: Maximum arch stress contour plots for the foundation modulus study of Deadwood Dam are shown in the left column of figure 2. Results show little difference in contour pattern or stress magnitude for the range of foundation modulus values studied.

Foundation Model: The left and middle columns of figure 2 show the contour plots for the three foundation modulus values with and without the inclusion of foundation interaction (mass effects). Results show a 30 percent difference in stress for the low comparison and less than 10 percent difference for the equal and high comparisons.

Reservoir Model: The effect of compressible versus incompressible fluid is shown in the contour plots in the left and right columns of figure 2. A comparison of the stress patterns and magnitudes indicates that reservoir model has little effect on the dam.

3.2 MONTICELLO DAM

Foundation Modulus: Maximum arch stress contour plots for the foundation modulus study of Monticello Dam are shown in the left column of figure 3. Results show an increase in stress of about 20 percent between the low and high foundation modulus values.

Foundation Model: The left and middle columns of figure 3 show the contour plots for the three foundation modulus values with and without the inclusion of foundation interaction (mass effects). Results range from a 40 percent difference in stress for the low comparison to a 10 percent difference for the high comparison.

Reservoir Model: The effect of compressible versus incompressible fluid is shown in the contour plots in the left and right columns of figure 3. These results indicate that the compressible fluid model increases stress over the incompressible fluid by up to 25 percent for the high foundation modulus.

3.3 MORROW POINT DAM

Foundation Modulus: Maximum arch stress contour plots for the foundation modulus study of Morrow Point Dam are shown in the left column of figure 4. Stress results increase from the low to the equal modulus values then decrease for the high modulus value while contour patterns are similar in all three cases.

Foundation Model: The left and middle columns of figure 4 show the contour plots for the three foundation modulus values with and without the inclusion of foundation interaction (mass effects). Results show a 50 percent difference in stress for the low comparison and less than 10 percent difference for the equal and high comparisons.

Reservoir Model: The effect of compressible versus incompressible fluid is shown in the contour plots in the left and right columns of figure 4. Results indicate that the compressible fluid model decreases stress over the incompressible fluid by up to 17 percent for the high foundation modulus.

4. EVALUATION OF RESULTS

Results of these studies can best be evaluated by separating the effects of varying the foundation modulus of elasticity from the effects of foundation and reservoir modeling. This is possible by making comparisons within each column of figures 2, 3, and 4 to investigate foundation modulus effects and making comparisons across each row to determine modeling effects. The left and middle columns of figures 2, 3, and 4 show a comparison between foundation interaction included and not included in the studies. The left and right columns of figures 2, 3, and 4 show the comparisons between a reservoir modeled as a compressible or incompressible fluid. Furthermore, while evaluations of each dam are possible, of greater interest are observations that hold true for all three dams.

4.1 DAM/FOUNDATION MODULUS RATIO

Results for the three dams show no consistent trend when foundation modulus is varied and foundation interaction is included. This is in sharp contrast to results when foundation modulus is varied and foundation interaction is not included where a higher modulus leads to lower stresses. Since no consistent behavior is seen in these results, sensitivity studies of foundation modulus should be conducted when foundation interaction is included in the analysis. The uncertainty generally associated with foundation modulus of elasticity measurements makes such sensitivity studies even more prudent.

It should be noted, however, that variations in the foundation modulus of elasticity have a two-fold effect on resulting stresses. First the foundation is softened or stiffened relative to the dam thus changing the natural frequencies of the system. This will shift the frequencies of the system relative to the response spectrum of the earthquake and lead to a change in stresses. The second effect is to change the response amplitude of the system and thus increase or decrease the resulting stress in the dam. This second effect is more important in understanding the behavior of the structure since it is a property of the structure and not dependent on the earthquake loading. Studies have not been completed to determine

the contribution these two effects have on resulting stresses.

4.2 FOUNDATION MODEL

The effect of foundation modeling provides the most dramatic conclusion for the three dams studied. The inclusion of foundation interaction results in a significant reduction in dynamic stresses for the low E_f/E_c ratio. The reduction in stress is less for the equal E_f/E_c ratio and quite small for the high E_f/E_c ratio. These results emphasize the importance of an accurate determination of material properties and the need to perform sensitivity studies over a range of material property ratios to account for uncertainties in measured values.

4.3 RESERVOIR MODEL

The results of the reservoir modeling study show no consistency among the three dams. The comparison of compressible reservoir to incompressible reservoir shows little effect for Deadwood Dam, an increase in stress for Monticello Dam, and a decrease in stress for Morrow Point Dam.

5. FUTURE STUDIES

The evaluations presented in this report are based on dynamic stress results from the three arch dams each analyzed for a specific earthquake ground motion. It might be convenient for the dam analyst to evaluate arch dam behavior based on its structural response, a property of the dam/foundation/reservoir system, rather than the stress results for a specific earthquake. Response amplitude plots at specific nodes will be generated for these studies. Results will compare changes in response amplitude and system frequencies for the lower modes of each dam.

Results also show little sensitivity for the high E_f/E_c ratio studies. Repeating these studies using a higher concrete modulus and a range of E_f/E_c ratios from 1/4:1 to 1:1 would be beneficial.

6. REFERENCES

Tan, Hanchen; Chopra Anil K., "*EACD-3D-96: A Computer Program for Three-Dimensional Earthquake Analysis of Concrete Dams,*" Department of Civil and Environmental Engineering, University of California, Berkeley, California, October 1996.

"Water and Power Resource Service Project Data," United States Department of the Interior, 1991.

"Rock Mechanics Properties of Typical Foundation Rock Types," Engineering and Research Center, Bureau of Reclamation, July 1974.

Table 1 - Material Properties					
	Modulus of Elasticity (psi)	Poisson's Ratio	Unit Weight (pcf)	Damping Ratio (% of Critical)	Wave Reflection Coefficient
Foundation	1,500,000 3,000,000 6,000,000	0.20	165.0	0.05	
Dam	3,000,000	0.22	150.0	0.05	
Reservoir			62.4		0.7

Table 2 - Summary of Maximum Upstream Stresses for Deadwood Dam							
Upstream Face	Res.	Ef / Ec Ratio	U/S Arch Stress (psi)	Element		U/S Cant. Stress (psi)	Element
Foundation Flexibility (With Mass)	Compr	Low	1033	19		654	52
	Compr	Equal	1023	19		729	51
	Compr	High	985	19		753	51
Foundation Flexibility (Massless)	Compr	Low	1350	19		1031	12
	Compr	Equal	1099	19		797	51
	Compr	High	1021	19		788	51
Reservoir Model	Compr	Low	1033	19		654	52
	Compr	Equal	1023	19		729	51
	Compr	High	985	19		753	51
	Incompr	Low	1006	19		632	52
	Incompr	Equal	971	19		703	51
	Incompr	High	976	19		722	51

Modulus Ratio: Low - Ef/Ec=1/2, Equal - Ef/Ec= 1, High - Ef/Ec= 2

Table 3 - Summary of Maximum Downstream Stresses for Deadwood Dam							
Downstream Face	Res.	Ef / Ec Ratio	D/S Arch Stress (psi)	Element		D/S Cant. Stress (psi)	Element
Foundation Flexibility (With Mass)	Compr	Low	869	11		522	51
	Compr	Equal	679	23		497	51
	Compr	High	635	5		507	42
Foundation Flexibility (Massless)	Compr	Low	1282	12		781	12
	Compr	Equal	782	11		550	42
	Compr	High	714	9		544	42
Reservoir Model	Compr	Low	869	11		522	51
	Compr	Equal	679	23		497	51
	Compr	High	635	5		507	42
	Incompr	Low	847	11		489	43
	Incompr	Equal	642	23		471	42
	Incompr	High	633	9		520	31

Modulus Ratio: Low - Ef/Ec=1/2, Equal - Ef/Ec= 1, High - Ef/Ec= 2

Table 4 - Summary of Maximum Upstream Stresses for Monticello Dam							
Upstream Face	Res.	Ef / Ec Ratio	U/S Arch Stress (psi)	Element		U/S Cant. Stress (psi)	Element
Foundation Flexibility (With Mass)	Compr	Low	1340	15		934	71
	Compr	Equal	1535	15		994	71
	Compr	High	1606	15		1068	64
Foundation Flexibility (Massless)	Compr	Low	1872	15		1260	71
	Compr	Equal	1834	15		1159	64
	Compr	High	1775	15		1232	64
Reservoir Model	Compr	Low	1340	15		934	71
	Compr	Equal	1535	15		994	71
	Compr	High	1606	15		1068	64
	Incompr	Low	1280	14		781	64
	Incompr	Equal	1255	14		845	64
	Incompr	High	1265	14		983	64

Modulus Ratio: Low - Ef/Ec=1/2, Equal - Ef/Ec= 1, High - Ef/Ec= 2

Table 5 - Summary of Maximum Downstream Stresses for Monticello Dam							
Downstream Face	Res.	Ef / Ec Ratio	D/S Arch Stress (psi)	Element		D/S Cant. Stress (psi)	Element
Foundation Flexibility (With Mass)	Compr	Low	1538	11		857	71
	Compr	Equal	1611	11		927	69
	Compr	High	1647	12		976	69
Foundation Flexibility (Massless)	Compr	Low	2041	11		1317	71
	Compr	Equal	1995	11		1113	72
	Compr	High	1823	12		1028	69
Reservoir Model	Compr	Low	1538	11		857	71
	Compr	Equal	1611	11		927	69
	Compr	High	1647	12		976	69
	Incompr	Low	1438	11		839	71
	Incompr	Equal	1453	11		856	70
	Incompr	High	1499	11		990	70

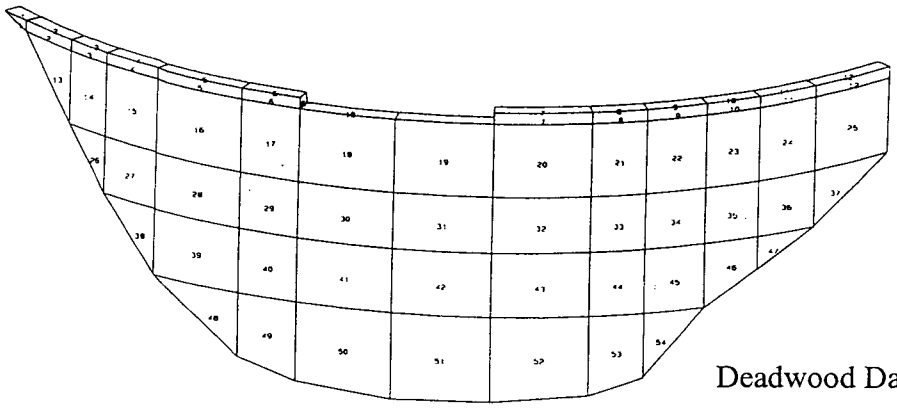
Modulus Ratio: Low - Ef/Ec=1/2, Equal - Ef/Ec= 1, High - Ef/Ec= 2

Table 6 - Summary of Maximum Upstream Stresses for Morrow Point Dam							
Upstream Face	Res.	Ef / Ec Ratio	U/S Arch Stress (psi)	Element		U/S Cant. Stress (psi)	Element
Foundation Flexibility (With Mass)	Compr	Low	1807	6		1090	14
	Compr	Equal	1949	6		1014	9
	Compr	High	1645	9		981	9
Foundation Flexibility (Massless)	Compr	Low	2740	6		1913	14
	Compr	Equal	2234	6		1353	14
	Compr	High	1629	5		925	9
Reservoir Model	Compr	Low	1807	6		1090	14
	Compr	Equal	1949	6		1014	9
	Compr	High	1645	9		981	9
	Incompr	Low	1805	6		809	14
	Incompr	Equal	2160	6		1012	9
	Incompr	High	1876	9		1017	9

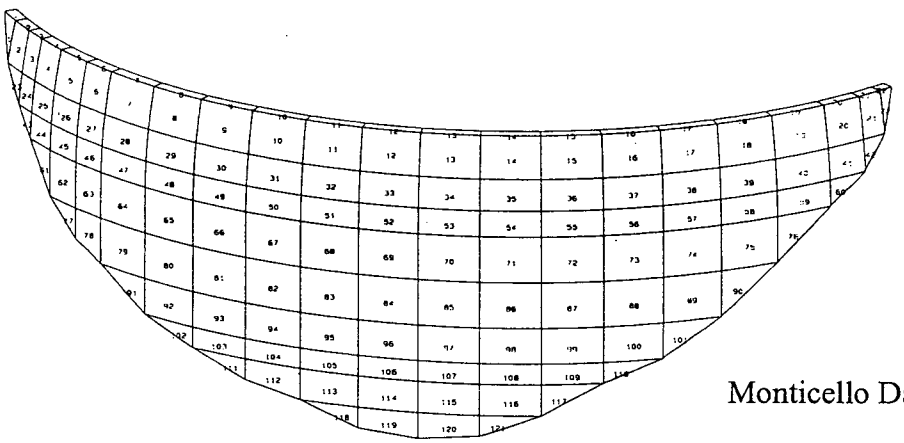
Modulus Ratio: Low - Ef/Ec=1/2, Equal - Ef/Ec= 1, High - Ef/Ec= 2

Table 7 - Summary of Maximum Downstream Stresses for Morrow Point Dam							
Downstream Face	Res.	Ef / Ec Ratio	D/S Arch Stress (psi)	Element		D/S Cant. Stress (psi)	Element
Foundation Flexibility (With Mass)	Compr	Low	1680	14		682	11
	Compr	Equal	2430	9		923	9
	Compr	High	2143	9		898	9
Foundation Flexibility (Massless)	Compr	Low	2065	8		1317	1
	Compr	Equal	2288	16		908	16
	Compr	High	2046	16		915	9
Reservoir Model	Compr	Low	1680	14		682	11
	Compr	Equal	2430	9		923	9
	Compr	High	2143	9		898	9
	Incompr	Low	2062	9		940	1
	Incompr	Equal	2617	9		1065	9
	Incompr	High	2520	9		1017	9

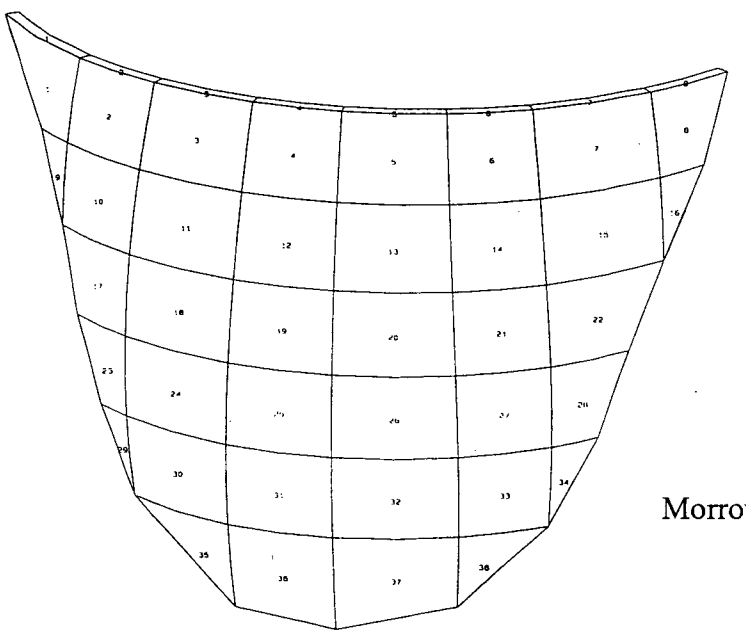
Modulus Ratio: Low - Ef/Ec=1/2, Equal - Ef/Ec= 1, High - Ef/Ec= 2



Deadwood Dam

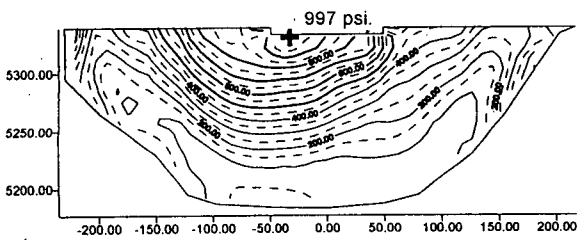


Monticello Dam

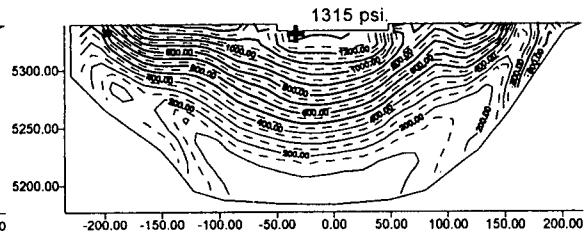


Morrow Point Dam

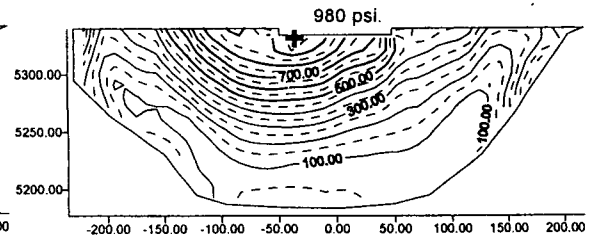
Figure 1



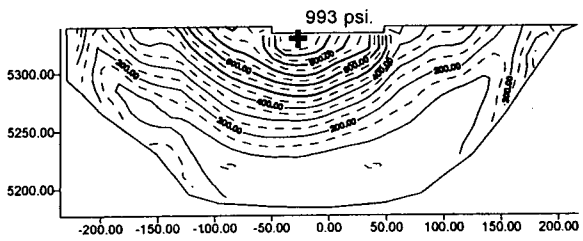
DEADWOOD DAM - UPSTREAM FACE
MAXIMUM ARCH CONTOURS
Ef=1,500,000 psi. Ec=3,000,000 psi. (With Mass)



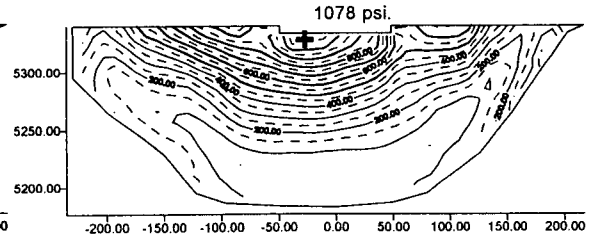
DEADWOOD DAM - UPSTREAM FACE
MAXIMUM ARCH CONTOURS
Ef=1,500,000 psi. Ec=3,000,000 psi. (No Mass)



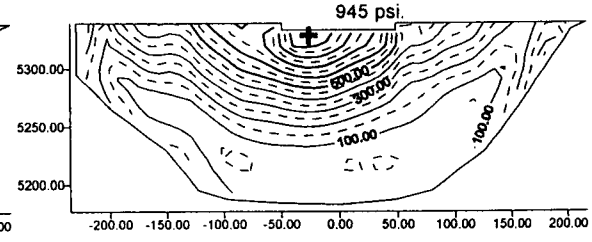
DEADWOOD DAM - UPSTREAM FACE
MAXIMUM ARCH CONTOURS
Ef=1,500,000 psi. Ec=3,000,000 psi. (With Mass/Incompressible)



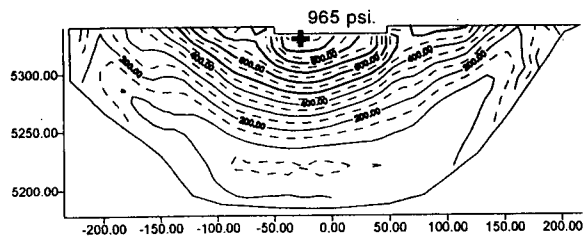
DEADWOOD DAM - UPSTREAM FACE
MAXIMUM ARCH CONTOURS
Ef=3,000,000 psi. Ec=3,000,000 psi. (With Mass)



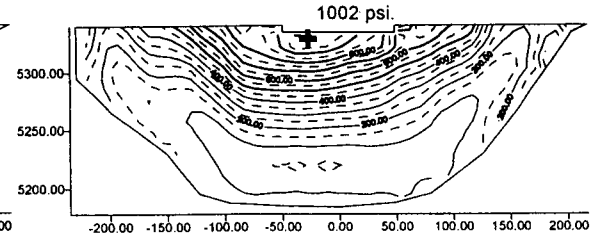
DEADWOOD DAM - UPSTREAM FACE
MAXIMUM ARCH CONTOURS
Ef=3,000,000 psi. Ec=3,000,000 psi. (No Mass)



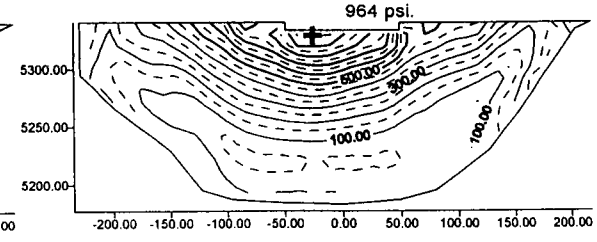
DEADWOOD DAM - UPSTREAM FACE
MAXIMUM ARCH CONTOURS
Ef=3,000,000 psi. Ec=3,000,000 psi. (With Mass/Incompressible)



DEADWOOD DAM - UPSTREAM FACE
MAXIMUM ARCH CONTOURS
Ef=6,000,000 psi. Ec=3,000,000 psi. (With Mass)



DEADWOOD DAM - UPSTREAM FACE
MAXIMUM ARCH CONTOURS
Ef=6,000,000 psi. Ec=3,000,000 psi. (No Mass)



DEADWOOD DAM - UPSTREAM FACE
MAXIMUM ARCH CONTOURS
Ef=6,000,000 psi. Ec=3,000,000 psi. (With Mass/Incompressible)

Figure 2

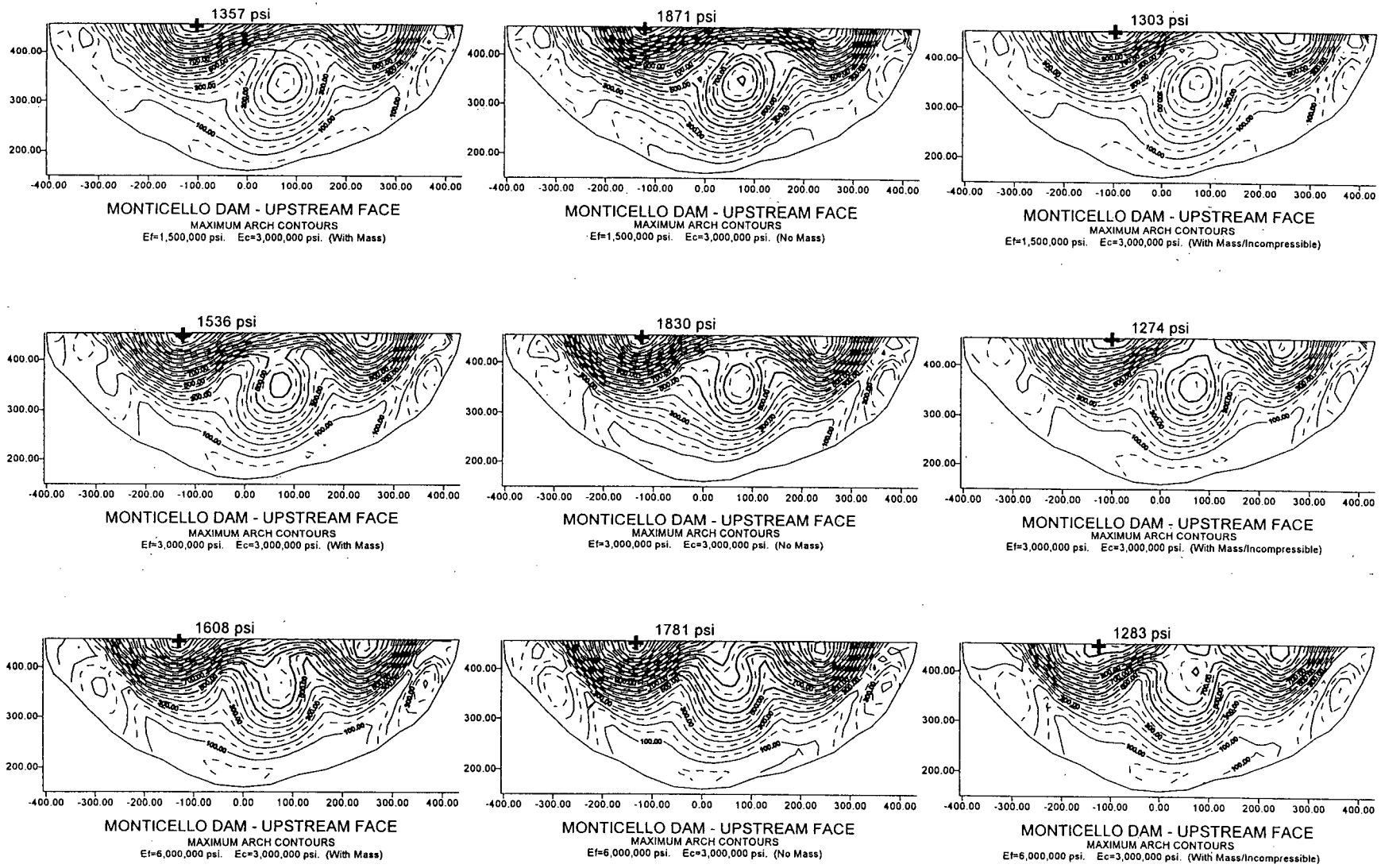
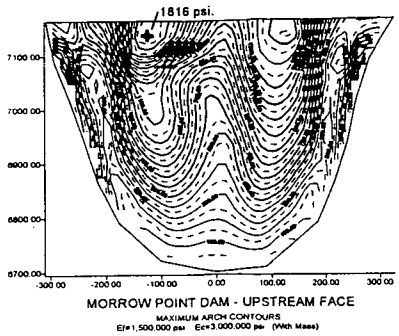
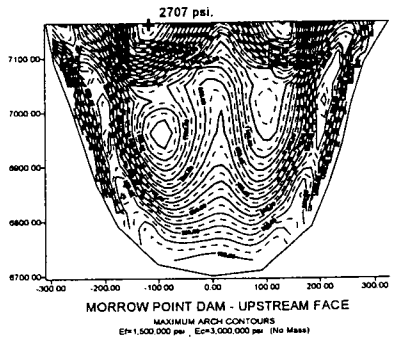
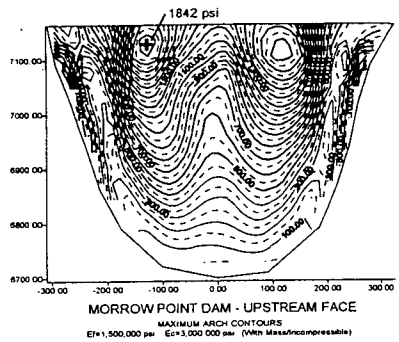
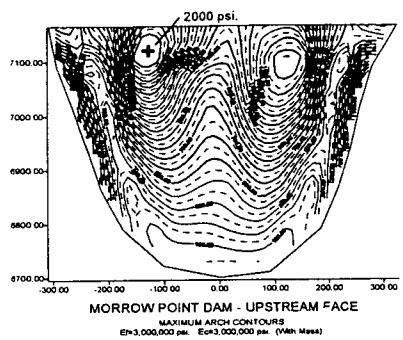

1357 psi
MONTICELLO DAM - UPSTREAM FACE
MAXIMUM ARCH CONTOURS
Ef=1,500,000 psi. Ec=3,000,000 psi. (With Mass)
1871 psi
MONTICELLO DAM - UPSTREAM FACE
MAXIMUM ARCH CONTOURS
Ef=1,500,000 psi. Ec=3,000,000 psi. (No Mass)
1303 psi
MONTICELLO DAM - UPSTREAM FACE
MAXIMUM ARCH CONTOURS
Ef=1,500,000 psi. Ec=3,000,000 psi. (With Mass/Incompressible)
1536 psi
MONTICELLO DAM - UPSTREAM FACE
MAXIMUM ARCH CONTOURS
Ef=3,000,000 psi. Ec=3,000,000 psi. (With Mass)
1830 psi
MONTICELLO DAM - UPSTREAM FACE
MAXIMUM ARCH CONTOURS
Ef=3,000,000 psi. Ec=3,000,000 psi. (No Mass)
1274 psi
MONTICELLO DAM - UPSTREAM FACE
MAXIMUM ARCH CONTOURS
Ef=3,000,000 psi. Ec=3,000,000 psi. (With Mass/Incompressible)
1608 psi
MONTICELLO DAM - UPSTREAM FACE
MAXIMUM ARCH CONTOURS
Ef=6,000,000 psi. Ec=3,000,000 psi. (With Mass)
1781 psi
MONTICELLO DAM - UPSTREAM FACE
MAXIMUM ARCH CONTOURS
Ef=6,000,000 psi. Ec=3,000,000 psi. (No Mass)
1283 psi
MONTICELLO DAM - UPSTREAM FACE
MAXIMUM ARCH CONTOURS
Ef=6,000,000 psi. Ec=3,000,000 psi. (With Mass/Incompressible)

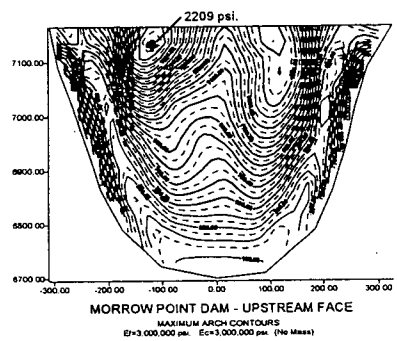
Figure 3

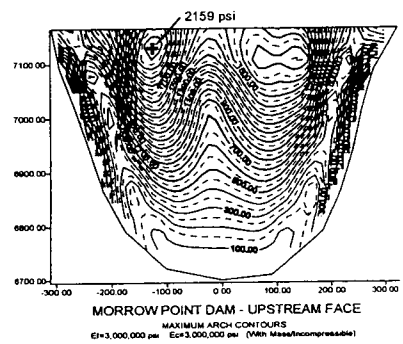

1816 psi.
MORROW POINT DAM - UPSTREAM FACE
MAXIMUM ARCH CONTOURS

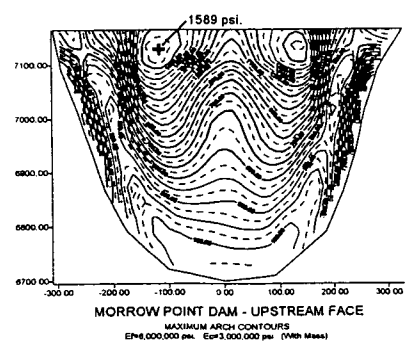

2707 psi.
MORROW POINT DAM - UPSTREAM FACE
MAXIMUM ARCH CONTOURS

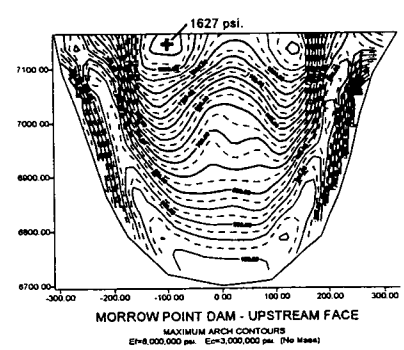

1842 psi
MORROW POINT DAM - UPSTREAM FACE
MAXIMUM ARCH CONTOURS


2000 psi.
MORROW POINT DAM - UPSTREAM FACE
MAXIMUM ARCH CONTOURS


2209 psi.
MORROW POINT DAM - UPSTREAM FACE
MAXIMUM ARCH CONTOURS


2159 psi
MORROW POINT DAM - UPSTREAM FACE
MAXIMUM ARCH CONTOURS


1589 psi.
MORROW POINT DAM - UPSTREAM FACE
MAXIMUM ARCH CONTOURS


1627 psi.
MORROW POINT DAM - UPSTREAM FACE
MAXIMUM ARCH CONTOURS

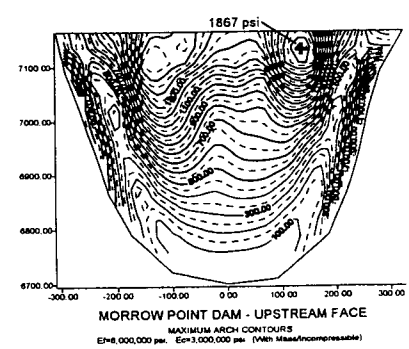

1867 psi
MORROW POINT DAM - UPSTREAM FACE
MAXIMUM ARCH CONTOURS

Figure 4

Technical Session 5

Embankment Dams (3)

Dynamic Centrifuge Tests on Flow Failure of Fills and Infinite Slopes

by

Osamu MATSUO[1], Yukiko SAITO[2], Tetsuya SASAKI[3] and Takashi SATO[4]

ABSTRACT

Conditions that yield earthquake-induced flow failures to earth fills and sloping soil layers with seepage water that are resting on stiff slopes were investigated by two series of dynamic centrifuge tests. The test parameters included soil density, slope angle, level of phreatic water and shaking intensity. The test results showed that downward deformation increased with decreasing soil density, increasing phreatic water elevation and shaking intensity, and that there existed a threshold soil density below which flow failures occurred. Monotonic and cyclic undrained torsional simple shear tests were also conducted. Conditions inducing very large deformation or flow failure that were obtained by the undrained shear tests were consistent with those as observed in the model tests.

Key Words: *Flow failure*
Earthquake
Centrifuge test
Seepage

1. INTRODUCTION

During past earthquakes, road embankments constructed on mountain/hill side have experienced catastrophic flow failures. In most of the cases, the fills were located at crossing slope dips (mildly concave topography in slopes), at which surface water or subsurface water are likely to accumulate. For example, **Fig. 1** shows a road fill that had been damaged by the 1993 Kushiro-oki earthquake (PWRI, 1994). As indicated by contour lines in Fig. 1(c), the damaged area was located at a concave topography. The fill material moved down a flat marshland as far as 40 m. According to the reconnaissance survey, the soil was volcanic ash sandy loam and was almost completely saturated, and draining of seepage water was observed at the bottom of the scarp.

Another example is given in **Fig. 2**. This road embankment was damaged by the 1968 Tokachi-oki earthquake (PWRI, 1971). The topography is similar to that of the above example. During the last week before the quake, there had been a precipitation of about 100 mm, suggesting that the fill was highly saturated. The fill material was volcanic ash silty sand, whose grain size distribution and density are given in Figs. 2(c) and (d). It is obvious from Fig. 2(d) that the soil density was very low. By the quake, the fill material flowed down a rice field as far as 40 m.

The third example is a fill that was damaged by the 1995 Hyogoken-nanbu earthquake (PWRI, 1997), which is shown in **Fig. 3.** The fill has been serving both as a road embankment and an irrigation dam. Although no exact historical document and soil exploration data are available for this earth structure, it is speculated that an earth dam of only three or four meters high was originally constructed for irrigation in very old time, at least several hundred years ago, and it was filled up in recent year, probably after the World War II , to serve as a road embankment. As shown in the figure, extensive slope failure took place in the upstream slope with a total length of 66 m and the sliding mass extending to the downstream side crest

1) Head, Soil Dynamics Division, Public Works Research Institute, Japan
2) Assistant Research Engineer, ditto
3) Research Engineer, ditto
4) Graduate Student, Tsukuba University, Japan

shoulder (see Fig. 3(b)) slid down to about 10 to 20 m beyond the slope toe. As illustrated in Fig. 3(c), the upstream side slope toes was submerged by the reservoir water and the bottom layer of the embankment should have been saturated by the seepage water. It is now suggested from the failure mode and the existence of saturated layer at the bottom of the fill, that liquefaction and the associated flow failure of saturated fill or subsurface soil resulted in such a devastating slope failure. Another remark regarding the damage caused by the earthquake is interesting, which follows: A survey conducted after the earthquake revealed that there were eleven sites of road embankments which were severely damaged by the earthquake; three of which were located at slope dips, six of which were partly submerged by pond water.

These examples demonstrated above strongly suggest that existence of seepage water in embankments is one of the causative factors of earthquake-induced flow failure. As a number of previous studies on flow failure of slopes have suggested (e.g. Robertson et al., 1997), the soil density also plays an important role in controlling the occurrence of flow failures. Most of the studies, however, seem to be limited to the case record studies and/or laboratory element tests. There are several model experimental studies on flow failure of slopes. For example, Dobry et al. (1997) conducted dynamic centrifuge tests on slightly inclined sand slopes by using a laminar shear box and investigated the effects of several factors on earthquake-induced permanent shear deformation. Pilgrim (1998) also conducted a series of dynamic centrifuge tests on sand slopes. However, in their model experiments, the observed permanent deformation was limited to continuous deformation with a shear strain level of at most 10 %, and no rupture failure was reproduced as observed in the fills during past earthquakes.

In this study, a comprehensive research consisting of soil element tests and dynamic centrifuge tests were conducted in order to reproduce the phenomena, thus to study the mechanism and to clarify the conditions for the flow failures to take place.

2. UNDRAINED BEHAVIOR OF TESTED SAND

(1) Testing Program

Prior to the dynamic centrifuge model tests, a series of undrained torsional shear tests was performed for the soil that was used in the model tests. The soil is relatively clean sand and is called Edosaki sand, the properties of which are presented in **Table 1**, together with the grain size distribution in **Fig. 4**. Also presented in **Fig. 5** is a laboratory compaction test data that was obtained in accordance with 'the Test Method for Soil Compaction Using a Rammer' (JSF T 711-1990) (JGF, 1990), in which soil is compacted in a cylindrical mold (ϕ = 100 mm) in three layers with a 25 times free drops of 2.5 kg rammer each. The test determines the relationship between the moisture content and density of soils. As the Edosaki sand has a fines content of 10 %, it is not considered appropriate to use a relative density as a density index. Thus, the degree of compaction, Dc, will be hereinafter used as a density index, defined as:

$$Dc = \rho_d / \rho_{dmax}$$

where ρ_d is the dry density of the soil, and ρ_{dmax} is the maximum dry density of the soil as determined to be 1.588 g/cm3 in Fig. 5.

To investigate the effects of density, initial confining stress, initial shear and cyclic shear stresses on undrained residual shear strength of the sand, an experimental program was developed. The testing conditions are summarized in **Table 2**. Two sets of tests were conducted. The first set is to investigate the residual shear strength under monotonic loading, while the second set is to see the effect of cyclic shear on the residual shear strength characteristics.

Torsional simple shear apparatus was used and the size of the specimens were 100 mm in outer diameter, 60 mm in innner

diameter and 200 mm in height. The specimens were prepared by carefully compacting the sand with an optimal water content of 19 % by using a wooden plate every two centimeters in thickness, to get a predetermined density. Fully saturated specimens were prepared by infiltrating CO_2 gas into the specimen, and then infiltrating deaired water under an inner pressure of about -90 kPa and an effective confining pressure of 20 kPa (total confining pressure = -70 kPa). Then the specimens were consolidated under an isotropic stress of 98 kPa with a back pressure of 196 kPa. B-values measured at this stage were over 0.95 for all specimens. For specimens with initial shear stress, torsional shear stress was applied monotonically under drained condition. Monotonic or cyclic torsional shear tests were performed under undrained condition. Both tests were of strain-control with a rate of 1 %/min. In cyclic shear tests, however, control of shear direction reversal was made manually while monitoring the shear stress.

(2) Monotonic Loading Test Results

Typical set of monotonic loading test data for specimens with different densities are presented in **Fig. 6**. Fig. 6a shows the stress-strain curves, and Fig. 6b shows the corresponding effective stress paths. The Dc = 80.2 % specimen is observed to experience a peak shear strength at very small strain and subsequently show a significant drop in shear stress over a wide range of shear strain. This may be called static liquefaction or steady state (Castro, 1969). The Dc = 88.0 % and 90.4 % specimens exhibit dilative behavior without peak shear stress throughout the shearing process. The Dc = 84.1 % specimen shows the transient behavior, i.e., after experiencing peak stress and subsequent modest stress drop, it is going to dilate with an increase in shear stress with increasing strain. This may be called "quasi-steady state" (Ishihara, 1993).

Fig. 7 shows a set of test results for specimens with initial static shear stresses of different magnitude. The specimens with initial shear stress ratio (τ_s / σ_{m0}') of 0.0, 0.05 and 0.15 exhibit identical stress-strain behavior. In contrast, the specimen with much larger stress ratio of 0.4 shows larger peak stress than the others, however at a strain level of 14 % it experiences an abrupt drop in stress and converges on the same stress as those of the other specimens. According to visual observation, when the abrupt stress drop occurred, localization of shear straining took place at interfaces between compaction layers in the specimen. If one accepts this test result as one of the normal element test results, it may be stated that the existence of initial shear stress does not affect the residual shear strength. If one does not accept the result, then vice versa.

Fig. 8 shows a set of test data for specimens with different confining stresses. The confining stresses of three test data range from 49 to 157 kPa. In Fig. 8, the shear stresses are normalized by initial effective confining stresses. For specimens with confining pressures of 98 and 157 kPa, density of which are almost the same as each other, the stress ratio-strain curves are identical. Although the specimen with a confining stress of 49 kPa shows smaller stress ratio, its density are lower than those of the other two specimens. Thus it may well be stated from the data set that the residual shear strength is proportional to initial effective confining stress.

(3) Conditions to Induce Flow Failure

An attempt was made from the limited number of undrained shear tests as shown in the above, to develop a chart to predict the occurrence of flow failure.

First, the residual or quasi steady state shear strength was read from the data in Fig. 7 with different initial static shear. Note that the residual shear strength was defined here as the minimum shear stress in large shear strain range of about 30 %, and the quasi steady state shear strength as the minimum shear stress over the peak point. These strength is hereinafter called as residual shear strength.

Fig. 9 plots the residual shear strength data in relation to initial shear stresses, for two densities. Both stresses are normalized by the initial effective confining pressures, which may be justified by the data in Fig. 8 indicating that the residual shear strength is proportional to the confining pressure at least within the stress range tested. In the figure, the data with Sus $> \tau$ s indicate that flow failure will not occur, while the data with Sus $< \tau$ s indicate that flow failure is possible to occur. Therefore, the minimum initial shear stress ratio over which flow failure can occur is read τ s/σ m0' = 0.3 for density of D = 83.0-84.4 %. Similarly, τ s/σ m0' = 0.1 for density of D = 80.2 %. Test results, not presented here, have shown that according to the data for the Edosaki sand up to 30 % shear strain, steady state appeared for Dc < 82 %, quasi steady state for 82 < Dc < 86 %, and no strain softening appeared for 86 % < Dc.

Now let us consider the conditions under which earthquake induced flow failure is possible to occur for an infinite slope as shown in **Fig. 10**. For this, the threshold initial shear stress ratio was plotted against the soil density Dc, so that the line A may be obtained as shown in **Fig. 11**. The stress-density state lying over the line A indicate that flow failure is possible to occur. In the figure, line B corresponds to the drained shear strength ratio over which no infinite slope can sustain itself even under static condition. Line C, Dc = 86 %, corresponds to the boundary distinguishing quasi steady state flow failure and no flow failure as stated above. Line D separates steady state flow failure and quasi steady state flow failure. Schematical stress-strain relations are inserted in the corresponding regions in the figure.

3. DYNAMIC CENTRIFUGE TESTS ON FLOW DEFORMATION OF FILLS RESTING ON SLOPES AND INFINITE SLOPES

In order to simulate the flow failure of fills that had been triggered by past earthquakes, two series of dynamic centrifuge model tests were performed.

(1) The Experimental Program

The tests were done by use of a dynamic centrifuge facility at PWRI, which has an effective radius of 6.6 m (Matsuo, et al., 1998). The tests included two series; one was to study the behavior of fills resting on slopes (Series A), the other was to study the behavior of infinite slopes (Series B). The testing programs are summarized in **Tables 3 and 4.** In both test series, it was aimed to see the effects of the parameters including soil density, slope inclination, shaking intensity, and elevation of seepage water on the occurrence of earthquake induced flow failures. The models are illustrated in **Figs. 12 and 13.**

Series A models were prepared in a rigid container, 0.8 m long, 0.2 m wide, and 0.3 m high. The stiff base layer of 20 mm thick and base slope with a slope inclination of 35 ° and a height of 200 mm were made from plaster. Sand paper was glued to the surface of base and slope surfaces to ensure mechanical friction at the plaster slope/sand interface. In order for use to provide and control the seepage water, a reservoir tank was constructed at the back side of the slope, and also a pipe at the bottom of the slope. To facilitate the fluid to proliferate over the entire slope surface, ditches were carved on the surface and they were covered with fine steel mesh. The fill was constructed by carefully compacting Edosaki sand, the optimal water content of 14 %, with a wooden plate. Filling and compaction was repeated in ten layers of 20 mm elevation each. During model construction, accelerometers, pore pressure transducers were embedded at prescribed locations and line markers of noodle were placed at the front side of the sand slope to enable visual observation of the model deformation through a transparent glass plate.

After model construction, the model was

spun up to a centrifugal acceleration of 50 g. A fluid, methyl-cellulose solution, 50 times as viscous as water, was then introduced into the reservoir tank through the rotary joint of the centrifuge, while the discharge rate was carefully controlled. Through the process of seepage, elevation of the phreatic line was indirectly monitored with measurements of pore pressure transducers embedded in the model. When it becomes likely that the pore pressures measurements had reached target values and in a steady state, the model was horizontally shaken by a sinusoidal base acceleration of 75 Hz and 20 cycles.

Series B models were prepared in a rigid container, 1.5 m long, 0.3 m wide, and 0.5 m high. The stiff base layer of 20 mm thick and stiff slope with a slope angle of 15 ° and 5 ° was made from plaster. Sand paper was glued to the surface of base and slope surfaces to ensure mechanical friction at the plaster slope/sand interface. In order for use to provide and control the seepage water, a reservoir tank was constructed at the top of the slope. The reservoir was filled with coarse sand (Pilgrim, 1998), confined by a steel mesh and steel plate with slit. The fill was constructed by carefully compacting Edosaki sand, the optimal water content of 14 %, with a wooden plate, while the container being tilted so that the base slope became horizontal. Filling and compaction was repeated for every 20 mm thickness in 6 layers. At the toe of the slope, a toe drain made from crush stone with an average grain size of 5 mm was placed to prevent surface erosion. During model construction, accelerometers, pore pressure transducers were embedded at prescribed locations, and line markers of colored sand were placed at the front side of the sand slope.

After model construction, the model was spun up to a centrifugal acceleration of 50 g. Silicon oil, 50 times as viscous as water, was then introduced into the reservoir tank through the rotary joint of the centrifuge, while the discharge rate was automatically controlled by using the float/electric valve system. Through the process of seepage, elevation of the phreatic line was indirectly monitored with measurements of pore pressure transducers embedded in the model. When it becomes likely that the pore pressures measurements had reached target values and in a steady state, the model was horizontally shaken by a sinusoidal base acceleration of 75 Hz and 10 cycles.

(2) Test Results and Discussions

a) Series A

Deformed configurations of models A1, A3 and A6 with different densities but identical level of phreatic line and shaking amplitude are given in **Fig. 14**. The following are observed from the figure: (1) Shear strain and associated distortion is larger in models with lower density. (2) Shear deformation concentrates below the phreatic lines and near the toes of fills. Note that some of the noodles did not exhibit the same distortion as the surrounding sand, in regions over the phreatic lines, due to adhesion to the glass wall of model container. Complete flow failure was not observed in all the models.

Fig. 15 illustrates the relationship between fill densities and crest settlements induced by 22 g shaking. The results clearly demonstrate that well compacted fills are very stable against such a severe earthquake, and, on the contrary, loosely compacted fills with higher seepage water level are susceptible to large deformation due to earthquakes.

Fig. 16 shows the relationship between shaking amplitudes and crest settlement for the test cases with a phreatic line of 10 cm high in model scale. For models of Dc = 76-78 %, the crest settlement increases significantly when magnitude of the input earthquake exceeds 5 g in model scale (0.1 g in prototype scale). The crest settlement of model A-6, Dc = 91 %, with 22.5 g shaking, is equivalent to that of Dc = 77 % model with 6 g shaking. This suggests that well compacted fill is invulnerable to earthquake induced damage.

b) Series B

Fig. 17 shows development of phreatic line, for selected models (models B2, B4 and B6), that was plotted from pore pressure measurements at the bottom of slopes. All the data indicate smooth development of seepage. The time required to attain targeted steady state seepage was longer for models with milder slope inclination (models B3 and B4) and with higher soil density (model B5).

Fig. 18 shows deformation of all models after shaking. In models B1, B2, and B6 with a slope inclination of 15 ° and low soil densities of Dc = 81 %, a discrete rupture zone of about 20 mm thickness is observed at the bottom of the slope, average shear strain of which seems to exceed 1000 %, while the remaining depth showing smaller shear strain. In model B7 of Dc = 85 %, the contrast of shear strain levels at the rupture zone and the remaining is more significant. In contrast, shear deformations of the slopes are small and no rupture apparent in models B3 and B4 with milder slope inclination of 5 ° and low soil density and in model B5 with higher soil density (Dc = 91 %). Possible reasons why the discrete ruptures occurred in models B1, B2, B6 and B7 might be explained as follows: As the cyclic shear stresses induced by base shaking are transmitted upwards from the bottom, the deepest soil experiences the stresses first. In addition, if the soil is more contractive under a larger confining stress condition (although this assumption is contradictive to the experimental results demonstrated in Fig. 8), the deepest soil would be most likely to get steady state. Once the deepest soil layer yielded the post-peak steady state, the shear stress larger than the strength could not be propagated to upward soil layer, thus the upward soil layer being in much smaller shear straining.

Fig. 19 shows time histories of selected pore pressure, acceleration and displacement measurements in model B7. The data are presented, and accelerations and lateral displacement are taken positive in downward direction. The following may be pointed out in the data:

1) The responses of both accelerations and pore pressures are not uniform along the direction of slope, although the model was an "infinite slope". This came from the fact that the model was not actually the infinite slope, i.e., the upside and downside boundary conditions would have affected the slope behavior. As can be seen in Fig. 18, a mound was formed by the flown down soil at the toe of the slope, as the region, part of which had been unsaturated, was more resistant against external force. Also, the pore pressure responses tended to be somewhat related to the lateral strain of the soil, i.e., the soil at which larger pore pressure accumulation was recorded yielded larger extentional strain in slope direction, and vice versa.

2) The acceleration records in the surface layer are asynmetrical; positive peaks are truncated and negative peaks are spiky. This behavior can be qualitatively explained by a stress-strain relationship of liquefied soil with initial shear stress, as will be given later in **Fig. 21**.

3) Slope displacement is increasing from the very beginning of the shaking. Attention should be paid to that the time rate and amount of displacement after the shaking has ceased is as large as or larger than those during shaking. This is the evidence of flow failure. Morover, the time rate of displacement is increasing during the time period 0.25 to 0.4 sec. This, in turn, suggests that the soil layer is flowing down with positive acceleration, which means that the external forces acting to the soil layer is not in equilibrium. Thus, one may conclude that the rupture zone at the bottom of the slope has reached in a steady state and the steady state strength could not sustain the downslope driving force of the soil layer due to gravity. This will be discussed again later by using effective stress paths.

Fig. 20 summarizes the relationship between the soil density and earthquake-induced permanent displacement of

the slope. Figures in parentheses indicate shaking amplitudes. The following are pointed out:

1) The effect of soil compaction density is evident as in the case of the tests on fills, the results of which were given in Fig. 15.

2) The tests B1, B2, B6 and B7 in which flow failure or discrete rupture plane was observed show large sliding displacements. Even among these, the magnitude of permanent displacement are dependent on soil density, probably due to the difference in the steady state shear strength.

3) Permanent displacements in Tests B3 and B4 with a slope angle of 5° are much smaller than those in the tests with a slope angle of 15°. These results were against the authors' expectation.

4) Effect of seepage water level on the magnitude of permanent displacement is negligible, which can be understood by comparing the data of Tests B2 and B6.

Fig. 21 shows the effective stress paths for all the tests. The shear stresses and normal effective stresses are those obtained at the bottom plane of the soil slopes. The shear stresses were obtained by integrating the inertial force acting on the overlying soil by using the following formula (Koga et al., 1989):

$$\tau(t) = \Sigma \{ \rho \cdot dz \cdot a_i(t) \}$$

where ρ: wet soil density, dz: thickness of soil layer represented by each accelerometer, and $a_i(t)$: measured accelerations in the soil slope.

The effective normal stresses were obtained by:

$$\sigma n' = \sigma n0' - u(t)$$

where $\sigma n0'$: initial effective normal stress, and $u(t)$: measured excess pore pressure. Note that the change of total normal stress induced by horizontal shaking was neglected.

In addition, as the measurements of pore pressure were not uniform along the bottom of slopes as demonstrated in Fig. 19, both the shear stresses and the effective normal stresses were averaged in the slope direction. The failure lines in the figure were drawn by using the peak $\tau / \sigma n'$ data obtained by the undrained shear tests, which values correspond to the line B in Fig. 11.

The following are pointed out from Fig. 21:

1) The initial factor of safety against sliding that are defined by the equation below is very close to unity, Fs = 1.2-1.5, for the models with slope inclination of 15° (B1, B2, B5, B6 and B7), while Fs = 3.6 for models B3 and B4 with slope inclination of 5°.

$$Fs = (\tau \max / \sigma n') / (\tau 0 / \sigma n0')$$

in which $(\tau \max / \sigma n')$: maximum effective shear stress ratio as measured in the drained simple shear tests, and $(\tau 0 / \sigma n0')$: initial effective shear stress ratio.

2) For the tests in which flow failures took place, the effective stress path traces hysteresis loops, moving towards the failure line, then crosses over the line, now showing decayed cyclic shear stress response. It should be noted here that, as discussed above in Fig. 19, the shear stress after the stress path crossed over the failure line does not mean the shear stress mobilized at the bottom layer of the soil slopes. Within this time, the soil is no longer in equilibrium, the shear stress mobilized in the discrete rupture zone should have been smaller than the driving shear stress due to gravitational body force. Thus, it is suggested that the 'true' effective stress path within the discrete rupture zone at the bottom of the soil slope would have moved down along the failure line after it approached the line.

3) Test B5 of Dc = 91 % indicates large amplification of response shear stress, which is obvious by comparing with Test B1 with same testing conditions except Dc = 81 %. This comes from the dilative behavior that is typical for dense sand.

4) In Tests B3 and B4, the stress paths are getting stationary in front of the failure lines. These results were against the authors' expectation, because the shaking magintude was considered large enough to render the stress points reaching the failure lines. The

reason is still questionable to the authors.

Fig. 22 summarizes the stress points just after the end of shaking for all the tests together with those at pre-shaking states. The data were read from Fig. 21. Figures in parentheses in Fig. 22 indicate the magnitude of permanent deformation of each soil slope. In the legend, 'flow failure' indicates that discrete rupture zone was observed and deformation proceeded even after the end of shaking, 'limited deformation' indicates that neither the rupture zone was observed nor displacement proceeded after the end of shaking. It clearly shows that 'the post-shaking stress points' (not necessarily indicating the real stress state in the rupture zones) of the tests in which flow failure took place are located beyond the failure line.

(3) Comparison With the Undrained Shear Tests

In an attempt to predict the occurrence of flow failure of infinite slopes from the results of undrained shear tests, the results of the model tests in Series B were compared with those of the undrained shear tests that were described in the previous section.

To do this, the soil density and initial stress ratio of each Series B model was plotted in Fig. 11 that was proposed to predict the flow failure occurrence. The result is given in **Fig. 23**. This demonstrates that Line A well separates 'flow failure' cases and 'no flow failure' cases. It would thus be concluded that the usefulness of the diagram in Fig. 11 was verified by a series of model shaking tests, at least to predict the occurrence and non-occurrence of flow failure to infinite slopes. Verification with respect to earth fills was left for a future task, which will appear elsewhere.

4. SUMMARY AND CONCLUSIONS

The results of undrained simple shear tests and two series of dynamic centrifuge model tests on infinite slopes and earth fills may be summarized and concluded as follows.

1) For Edosaki sand with fines content of 10 %, three types of shear behavior were observed in the undrained monotonic -loading simple shear tests; steady state shear, quasi-steady state shear and dilative behavior, depending on the density. This is consistent with the previous studies.
2) Within shear strain range up to 30 %, capable in the shear apparatus used, the steady state and quasi-steady state shear strength was proportional to the initial confining stress and was dependent on the initial shear stress. These results seems to contradict to the previous similar studies. The number of shear tests and the range of shear strain are limited in the study presented in this paper. Therefore, further tests are required to make the points clear.
3) A diagram was developed to predict the occurrence of earthquake-induced flow failure of infinite slope, as presented in Fig. 11, from results of the undrained shear tests.
4) A series of model tests on earth fills on stiff base slope demonstrated that the effects of soil compaction density and shaking intensity on the magnitude of earthquake-induced permanent deformation were significant. Elevation of seepage water also affected the magnitude of deformation. These results suggests that, in the practice of earth works of road fills in hilly areas, soil compaction and placement of surface/subsurface drainage systems are very important to prevent and mitigate earthquake-induced damage as well as to prevent landslide or erosion due to rainfall.
5) In a series of model tests on 'infinite slopes' , earthquake-induced flow failure was observed when the soil density was low and slope inclination was large (15 °). The downward displacement proceeded even after the end of shaking, and the magnitude of displacement during the period was larger than that developed during shaking.

6) For the models in which flow failure took place, discrete rupture zone was developed at the bottom of the soil slope. The forces acting on the soil layer over the rupture zone was found to be inequilibrium when the soil layer was moving downslope. This proved that the discrete rupture zone had attained a steady state shear strength.
7) Elevation of phreatic line did not affect the magnitude of displacement in the 'infinite slope' model tests, unlike in the earth fill model tests.
8) Effect of shaking magnitude on the slope displacement was insignificant when flow failure had taken place.
9) The diagram as presented in Fig. 11 well predicted the occurrence and non-occurrence of flow failure in the tests of infinite slopes.

Verification of the diagram in the case of earth fills on stiff slopes was left as a future work, which will be presented elsewhere.

REFERENCES

Aomori Prefecture (1969): *Report on the Tokachi-oki earthquake*, Department of Civil Engineering, Aomori Prefecture.

Castro, G. (1969): Liquefaction of sands, *Harvard Soil Mechanics Series No. 81*, Harvard University, Cambridge, MA.

Dobry, R., V. Taboada and L. Liu (1997): Centrifuge modeling of liquefaction effects during earthquakes, *Proc. IS-TOKYO'95/The 1st Intl. Conf. on E.q. Geotech. Engrg./Tokyo/14-16 November 1995*, A.A.Balkema, pp. 1291-1324.

Ishihara, K. (1993): Liquefaction and flow failure during earthquakes, The 33rd Rankine Lecture, *Geotechnique* 43, No. 3, pp. 351-415.

Japanese Geotechnical Society (1990): *Standard Soil Testing Methods*, pp. 201-214.

Koga, Y. and O.Matsuo (1990): Shaking table tests of embankments resting on liquefiable sandy ground, *Soils and Foundations*, Vol. 30, No. 4, pp. 162-174.

Matsuo, O., T.Tsutsumi, K.Kondoh and S.Tamoto (1998): The dynamic geotechnical centrifuge at PWRI, *Proc. Intl. Conf. CENTRIFUGE'98/Tokyo/Japan/23-25 September 1998*, A.A.Balkema, pp. 25-30.

Pilgrim, N.K. (1998): Earthquake-related deformation beneath gently inclined ground, *Geotechnique* 48, No. 2, pp.187-199.

Public Works Research Institute (1971): Survey on disaster caused by the Tokachi-oki Earthquake 1968, *Report of PWRI*, Vol. 141, pp. 67-77 (in Japanese).

Public Works Research Institute (1994): Report on the disaster caused by the Kushiro-oki Earthquake of 1993, *Report of PWRI*, Vol. 193, pp. 158-170 (in Japanese).

Public Works Research Institute (1997): Report on the disaster caused by the 1995 Hyogoken Nanbu Earthquake, *Journal of Research*, Vol. 33, pp. 257-299.

Robertson, P.K. and C.E. Fear (1997): Liquefaction of sands and its evaluation, *Proc. IS-TOKYO'95/The 1st Intl. Conf. on Earthquake Geotechnical Engineering./Tokyo/14-16 November 1995*, A.A.Balkema, pp. 1253-1289.

Table 1 Properties of Edosaki sand

Parameter	Value
G (specific gravity)	2.684
ρ_{dmax}* (g/cm^3)	1.567
F_c (%)	10.8
e_{max}**	1.526
e_{min}**	0.894

* determined from the standard compaction test

** determined from the maximum/minimum density test (out of application)

Table2. Summary of laboratory tests

(a)Monotonic shear test

Type of tests	Test No.	Dry density ρ_d (g/cm^3)	Void ratio e	Degree of compaction D_c(%)	Effective confining pressure $\sigma_a' = \sigma_r' = \sigma_{mo}'$ (kPa)	Initial shear stress ratio τ_s / σ_{mo}'	Back pressure (kPa)	B-value	Rate of shear strain (%/min)
No initial shear stress	1-1	1.274	1.11	80.2	98	0	196	0.97	1
	1-2	1.336	1.012	84.1				0.97	
	1-3	1.398	0.923	88.0				0.95	
	1-4	1.435	0.873	90.4				0.97	
	2-1	1.297	1.072	81.7	49			0.98	
	2-2	1.348	0.994	84.9	157			0.94	
With initial shear stress	3-1	1.327	1.026	83.6	98	0.05		0.96	
	3-2	1.317	1.041	83.0		0.15		1.00	
	3-3	1.340	1.006	84.4		0.40		0.97	

(b)Cyclic shear test

Initial shear stress ratio	Test No.	Dry density ρ_d (g/cm^3)	Void ratio e	Degree of compaction D_c(%)	Effective confining pressure $\sigma_a' = \sigma_r' = \sigma_{mo}'$ (kPa)	Cyclic shear stress ratio τ_d / σ_{mo}'	Back pressure (kPa)	B-value	Rate of shear strain (%/min)
0	4-1-1	1.321	1.035	83.2	98	0.075	196	0.97	1
	4-1-2	1.347	0.996	84.8		0.10		0.97	
	4-1-3	1.340	1.006	84.4		0.15		0.94	
	4-1-4	1.326	1.027	83.5		0.20		0.98	
0.05	4-2-1	1.326	1.027	83.5		0.10		0.96	
	4-2-2	1.319	1.038	83.1		0.125		0.97	
	4-2-3	1.332	1.018	83.9		0.15		0.96	
0.15	4-3-1	1.321	1.035	83.2		0.05		0.97	
	4-3-2	1.332	1.018	83.9		0.075		0.98	
	4-3-3	1.320	1.036	83.1		0.10		0.92	
0.4	4-4-1	1.337	1.010	84.2		0.05		0.97	
0	5-1	1.427	0.884	89.9		0.15		0.95	

Table 3 Testing program for Series A (Road fill models on slopes)

Test	Slope : degrees	Dry density : ρd (g/cm^3)	Degree of compaction : Dc (%)	Seepage water level** : mm	Shaking magnitude : g (% of g)*
A1	35	1.218	78	95	22 (0.44)
A2	35	1.221	78	39	22 (0.44)
A3	35	1.306	83	110	22 (0.44)
A4	35	1.236	79	104	1.2, 4.1, 10 (0.02, 0.08, 0.20)
A5	35	1.244	79	0	21.5 (0.43)
A6	35	1.443	92	102	22.5 (0.45)

* All tests were performed under a centrifugal acceleration of 50g, and input accelerations were of sinusoidal wave with 75Hz, 20cycles.

** measured by the pore pressure transducers at the base slope

Table 4 Testing program for Series B (Infinite slope models)

Test	Slope : degrees	Dry density : ρd (g/cm^3)	Degree of compaction : Dc (%)	Seepage water level** : mm	Shaking magnitude : g (% of g)*
B1	15	1.274	81	115	15 (0.30)
B2	15	1.262	81	110	8 (0.16)
B3	5	1.272	81	110	7.5 (0.15)
B4	5	1.264	81	104	16 (0.32)
B5	15	1.419	91	111	5,15 (0.10, 0.30)
B6	15	1.264	81	74	9 (0.30)
B7	15	1.325	85	116	8.5 (0.17)

* All tests were performed under a centrifugal acceleration of 50g, and input accelerations were of sinusoidal wave with 75Hz, 20cycles.

** measured by the pore pressure transducers at the base slope

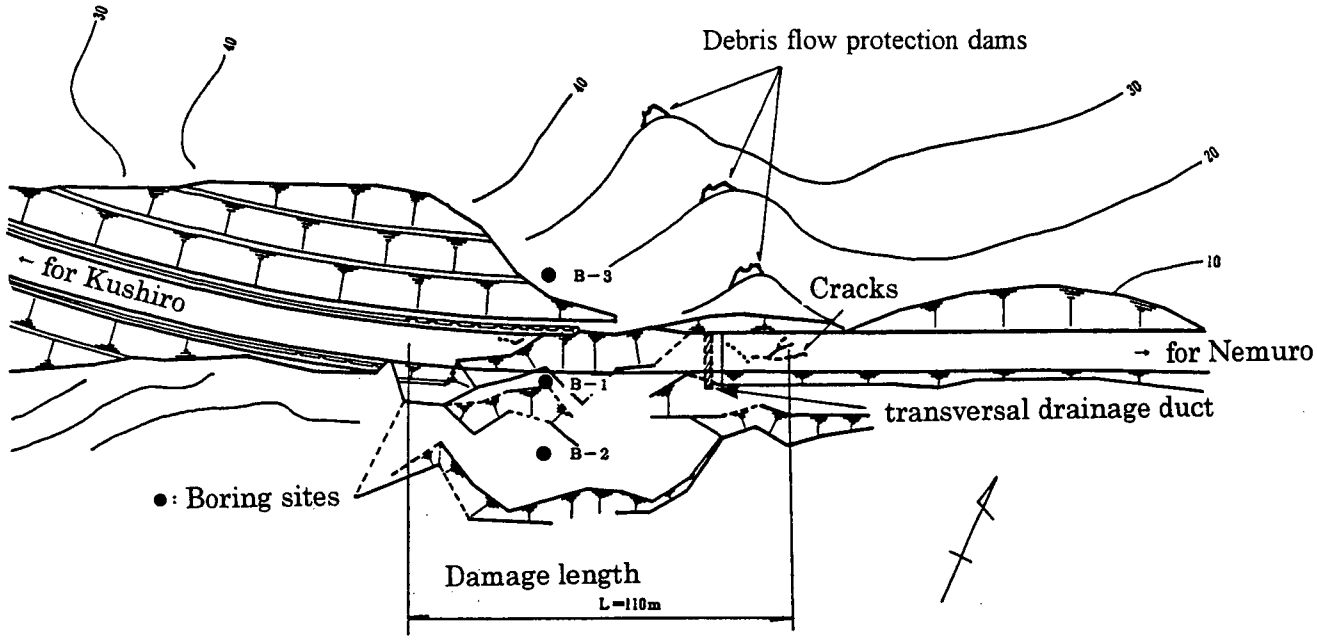


(a) aerial photograph after the earthquake

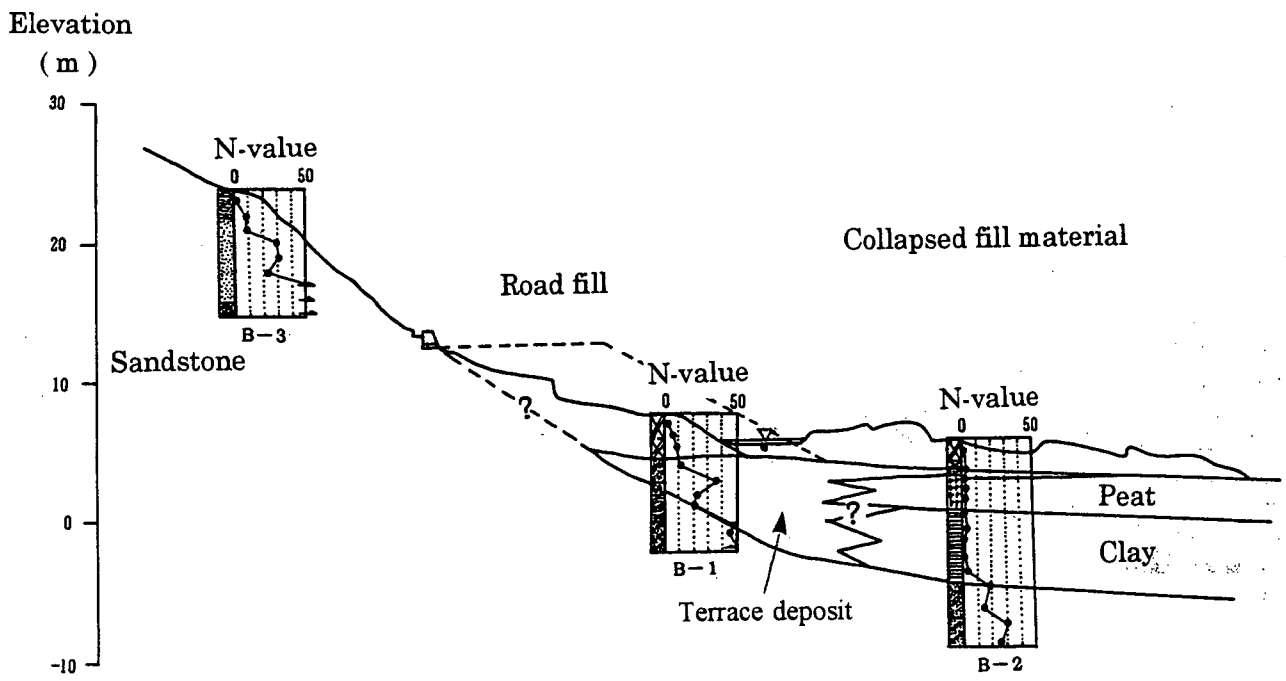


(b) photograph after the earthquake

Fig. 1 Damage of a road fill at Itoizawa, Kushiro, during the 1993 Kushiro-oki earthquake (PWRI, 1994)

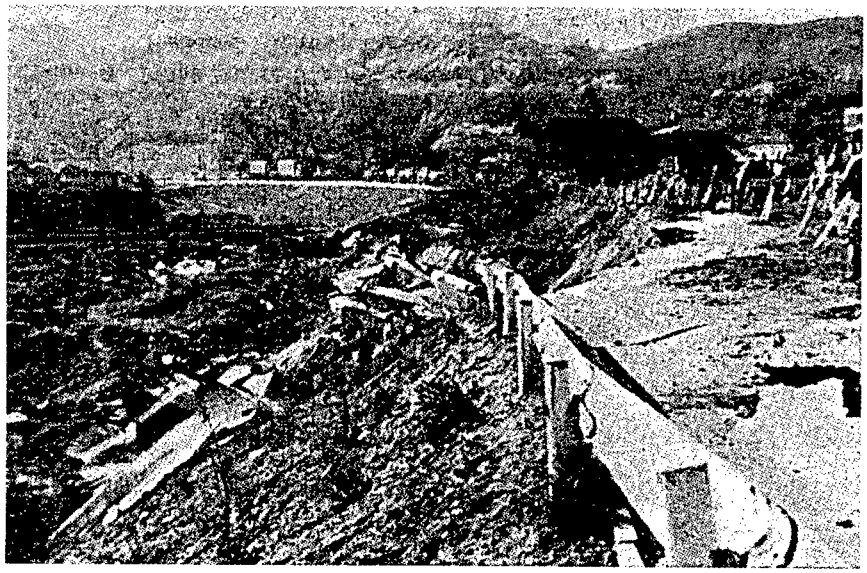


(c) plan view

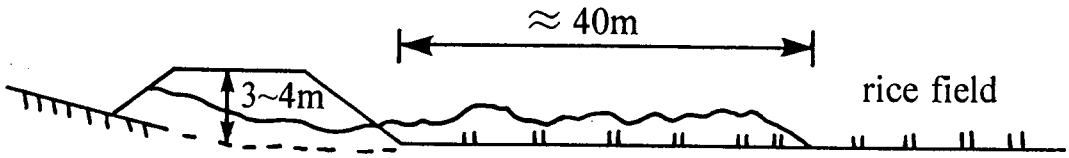


(d) cross sectional view

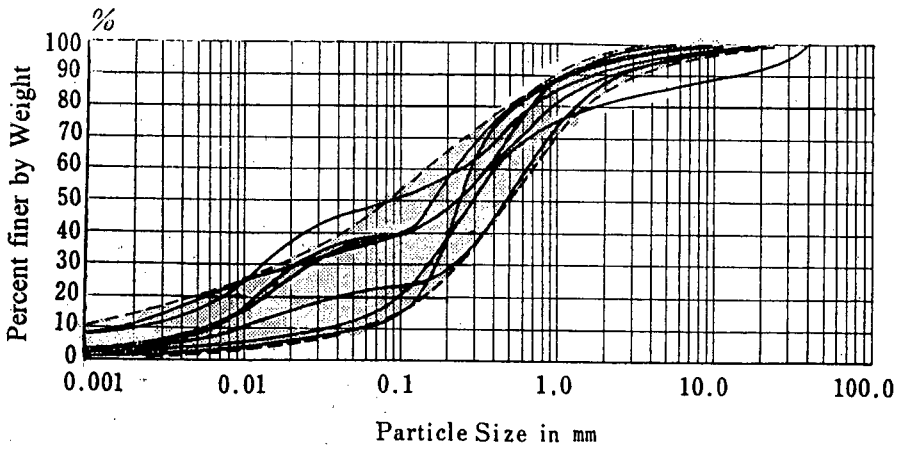
Fig. 1 Damage of a road fill at Itoizawa, Kushiro, during the 1993 Kushiro-oki earthquake (PWRI, 1994)



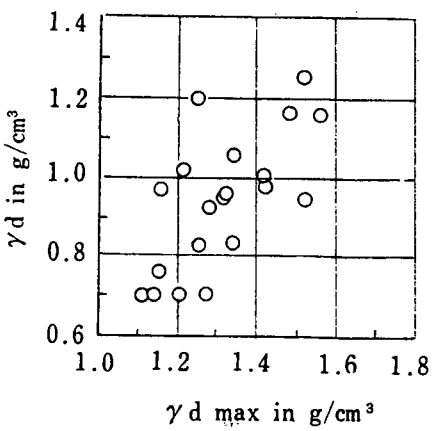
(a) photograph (Aomori Prefecture, 1969)



(b) cross sectional view (not scaled)

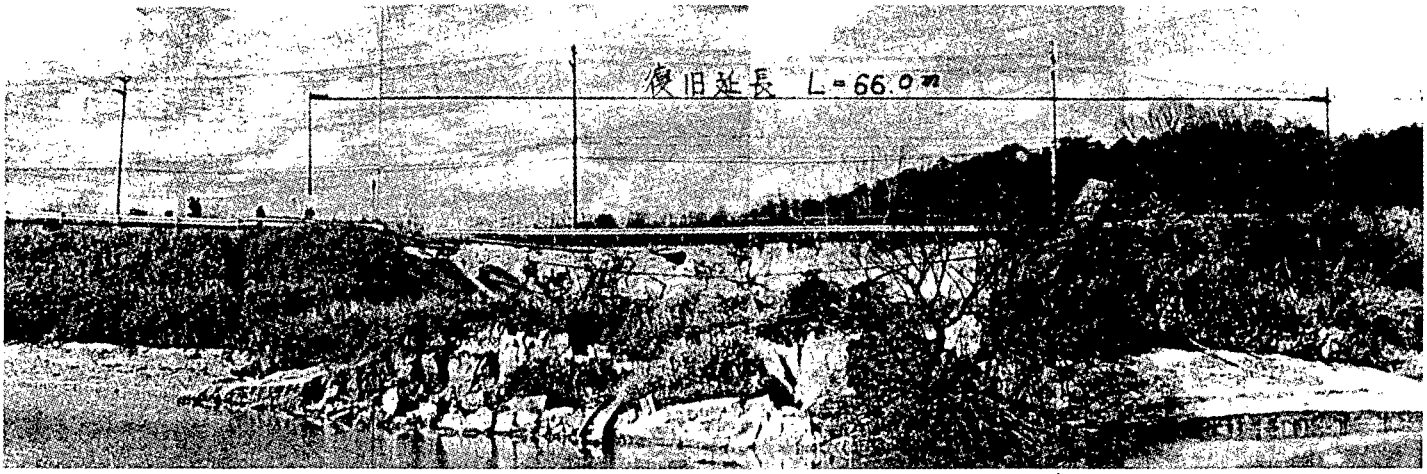


(c) grain size distribution of fill material

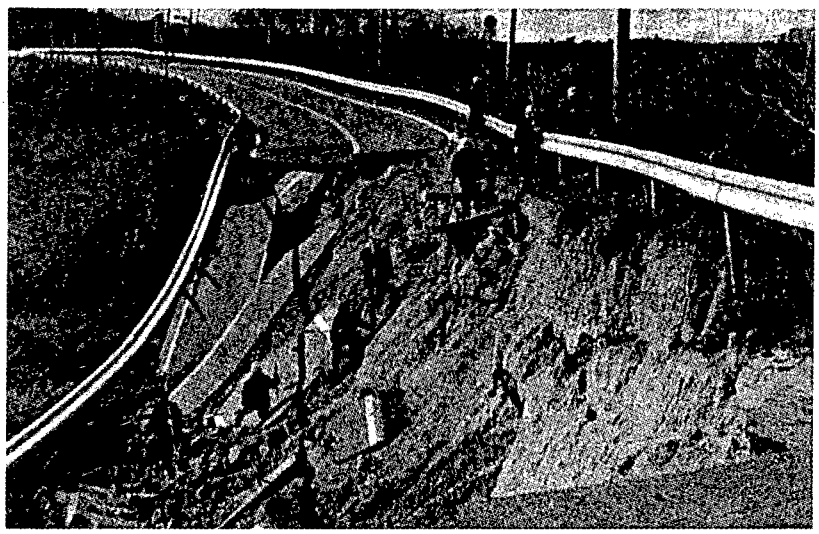


(d) density of fill material

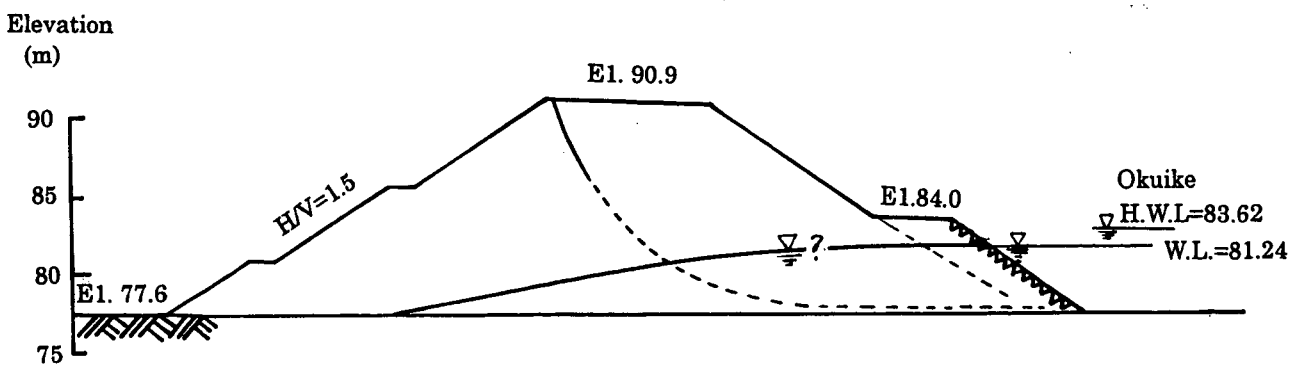
Fig. 2 Damage of a road fill at Metoki, Aomori Prefecture, during the 1968 Tokachi-oki earthquake



(a) photograph



(b) cross sectional view (not scaled)



(c) cross sectional view (in meter)

Fig. 3 Damage of a road fill at Miki City, near Kobe, during the 1995 Hyogoken-nanbu earthquake

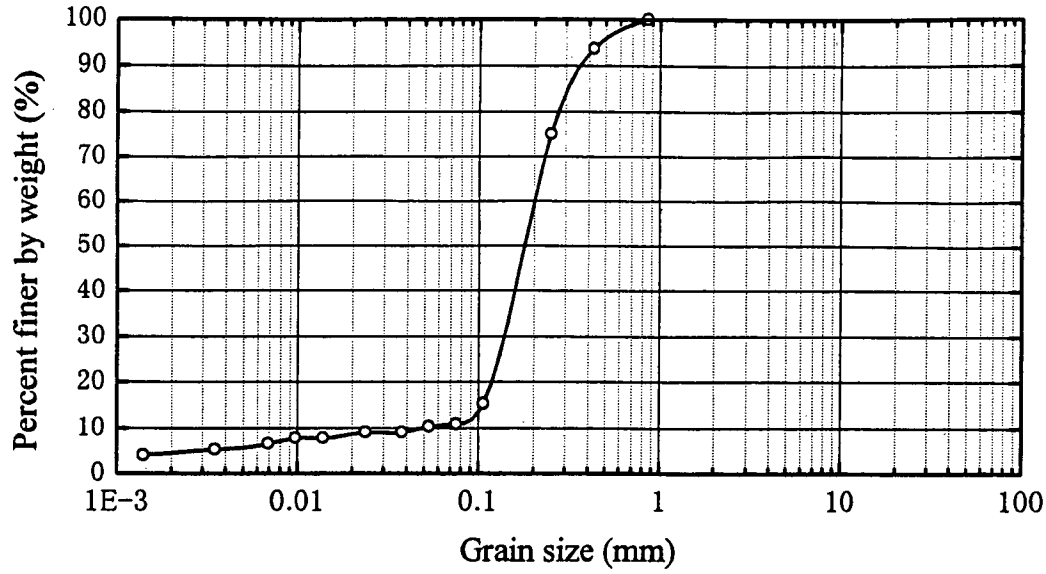


Fig.4 Grain size distribution of Edosaki sand

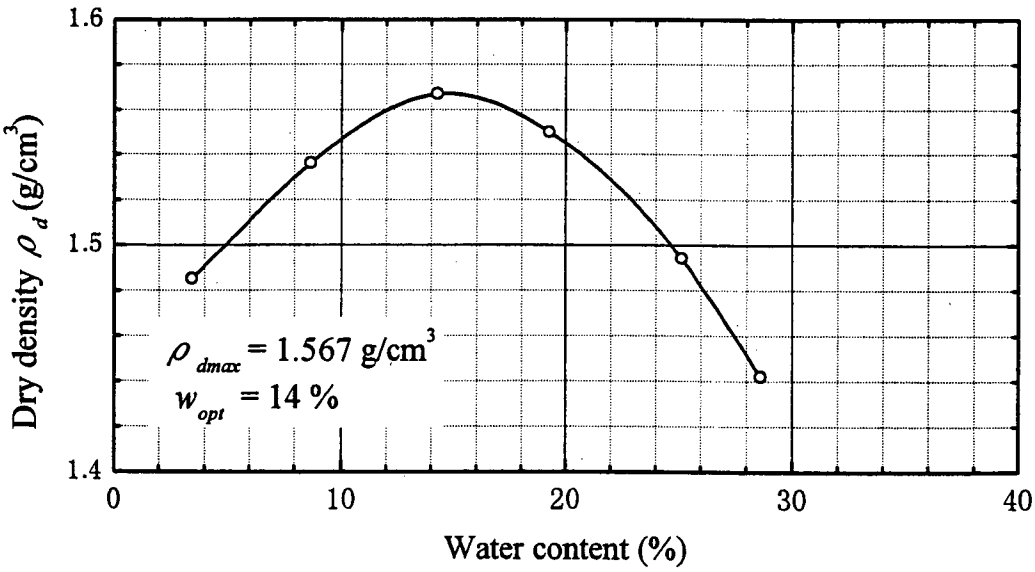
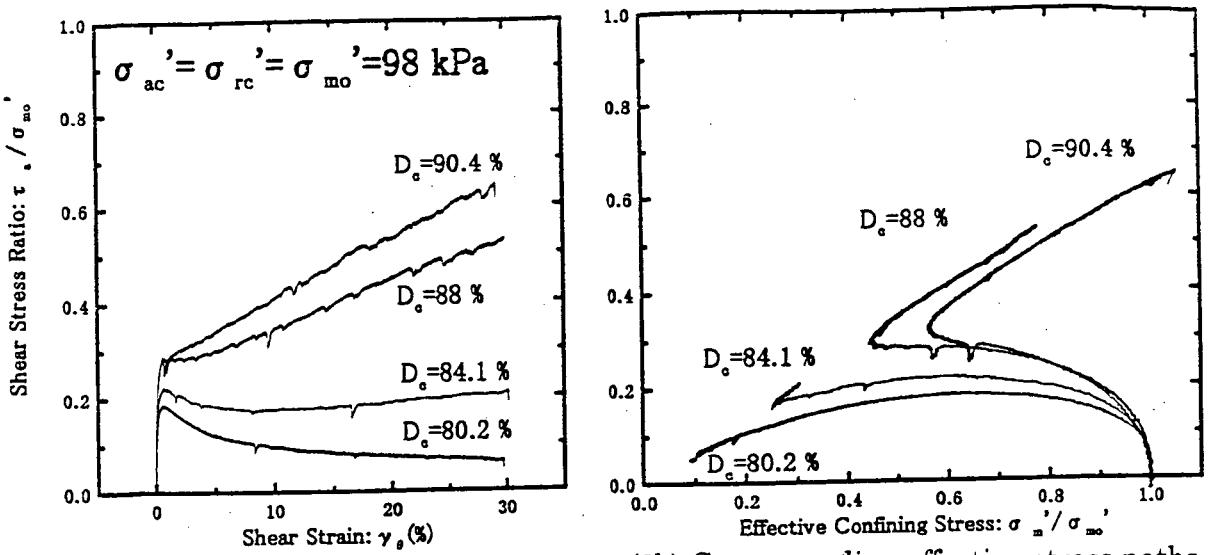
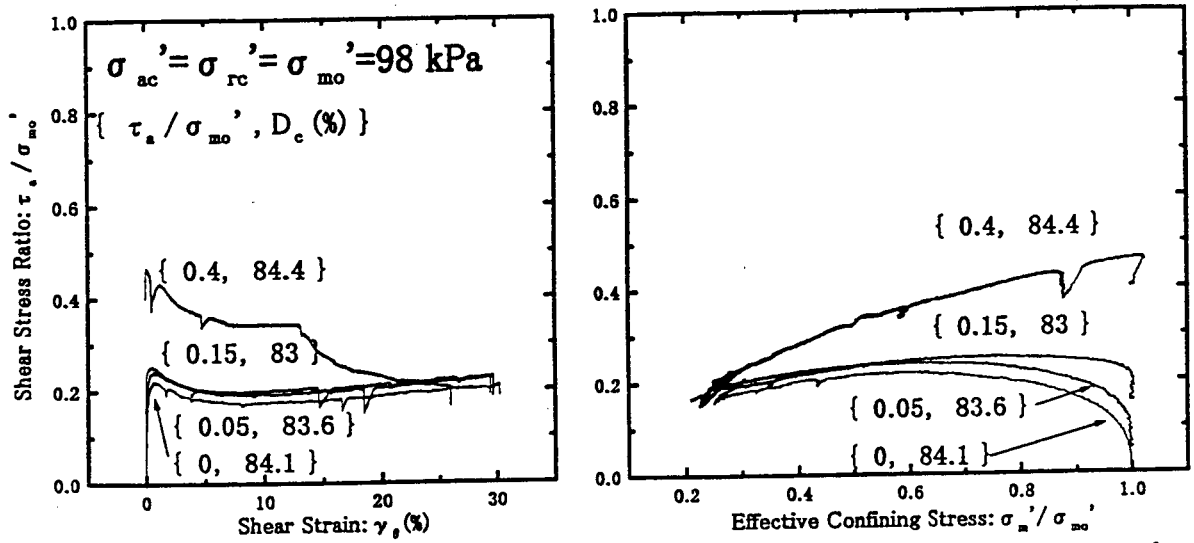


Fig. 5 Standard compaction test (JIS A 1210-1990)



(6a) Stress-strain curve (6b) Corresponding effective stress paths

Fig.6 Effect of density on monotonic shear behavior



(7a) Stress-strain curve (7b) Corresponding effective stress paths

Fig.7 Effect of initial shear stress on residual shear strength

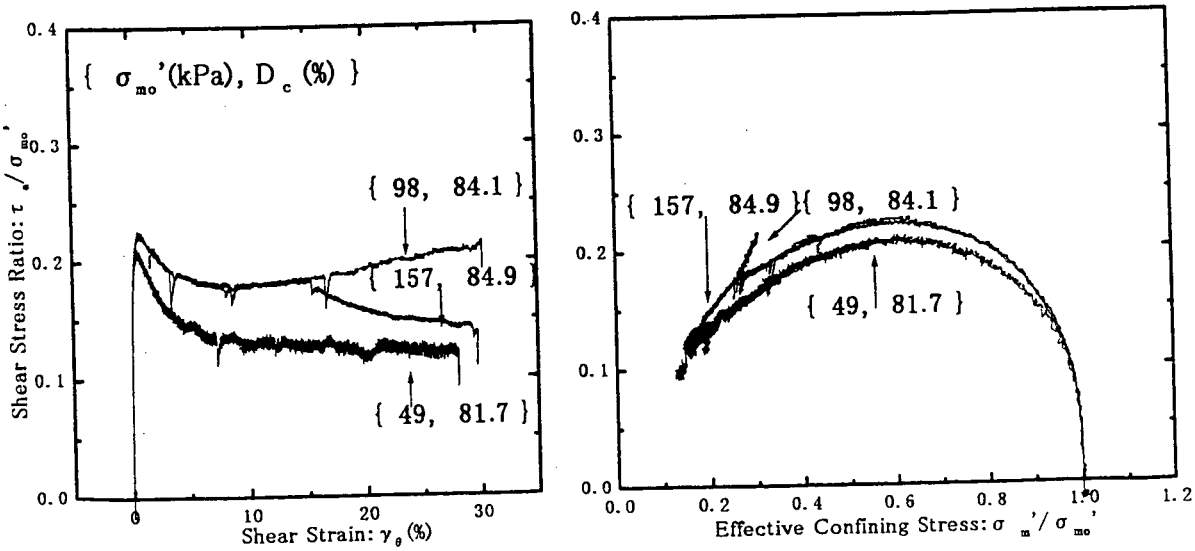


Fig.8 Effect of confining pressure on stress-strain relationship and effective stress path

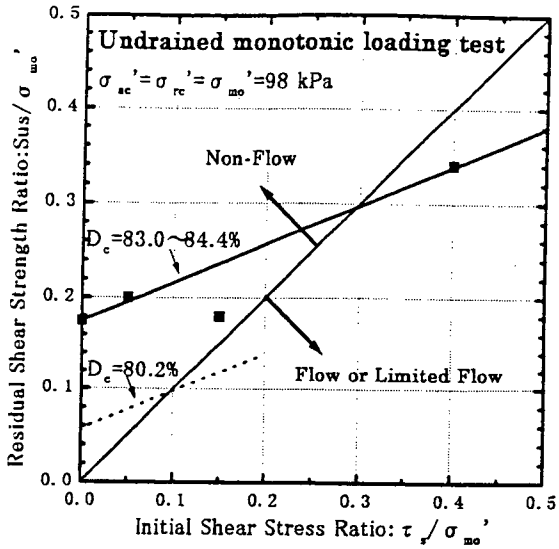


Fig.9 Residual shear strength ratio vs.initial shear stress ratio plots

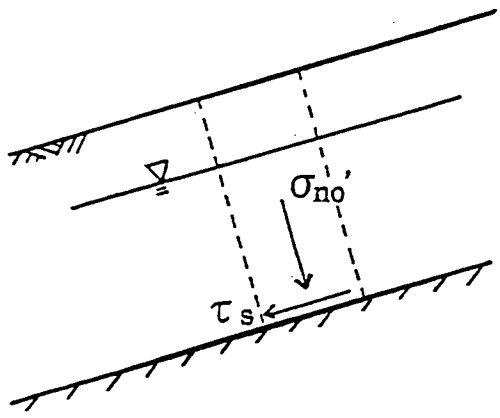


Fig.10 Infinite slope and corresponding stress state

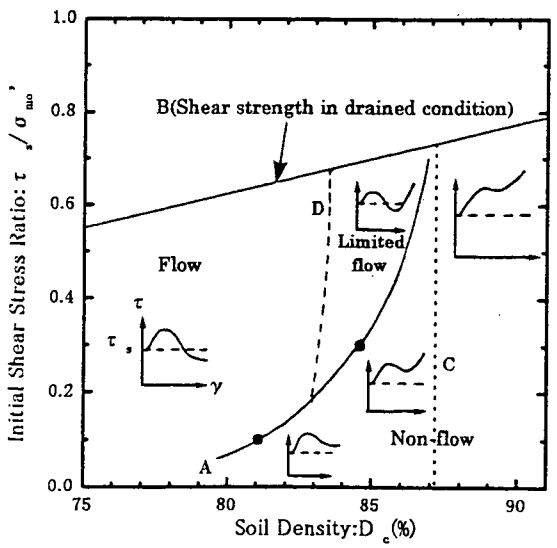


Fig.11 Soil density vs.initial shear stress ratio diagram distinguishing flow failure occurrence

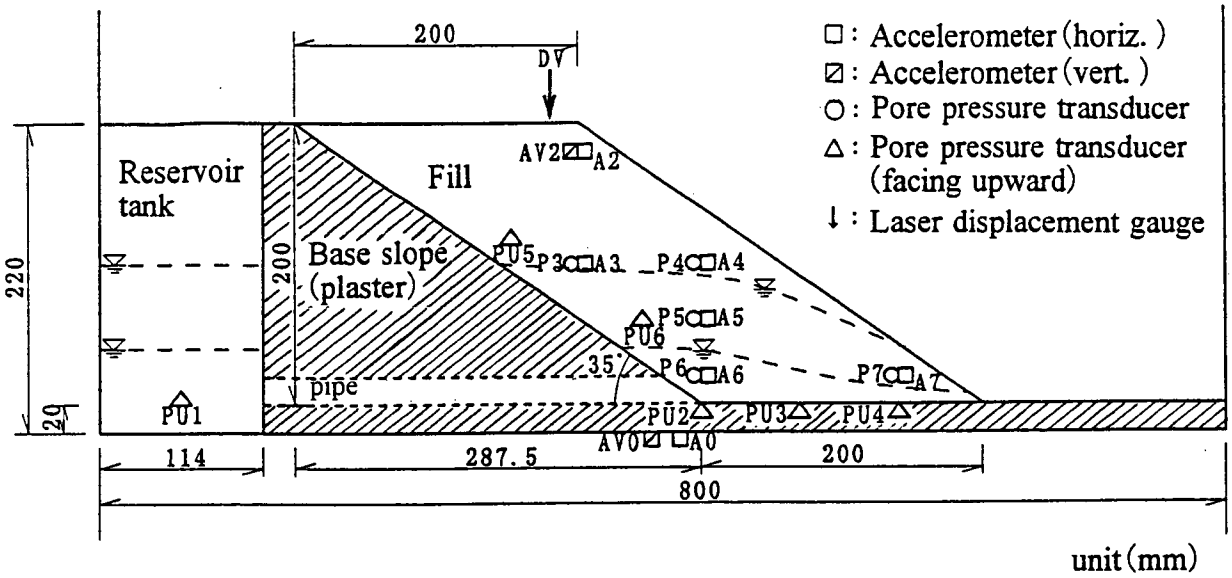


Fig. 12 Series A models

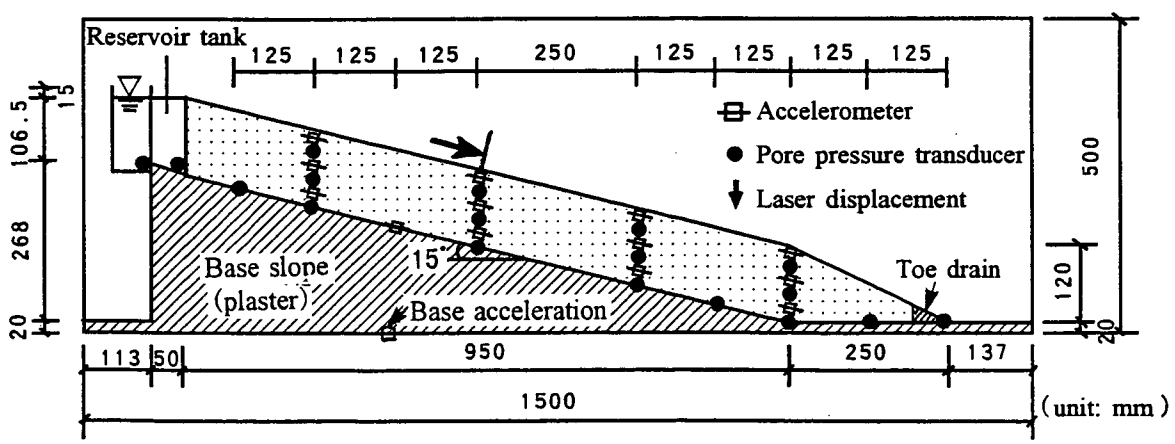
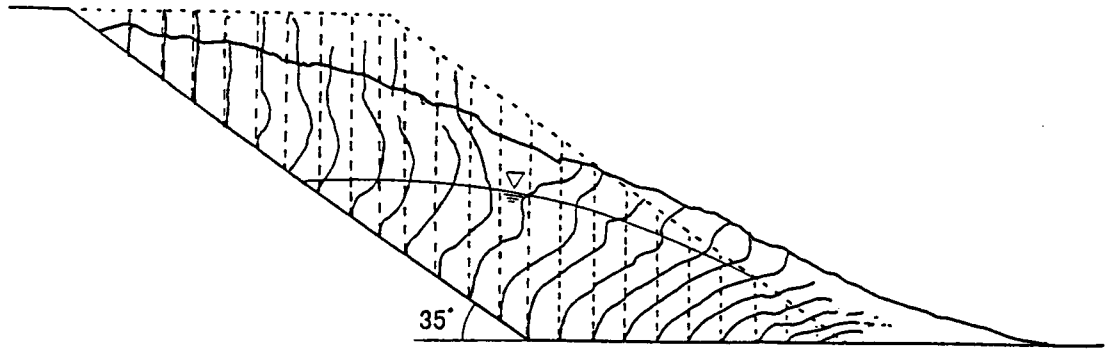
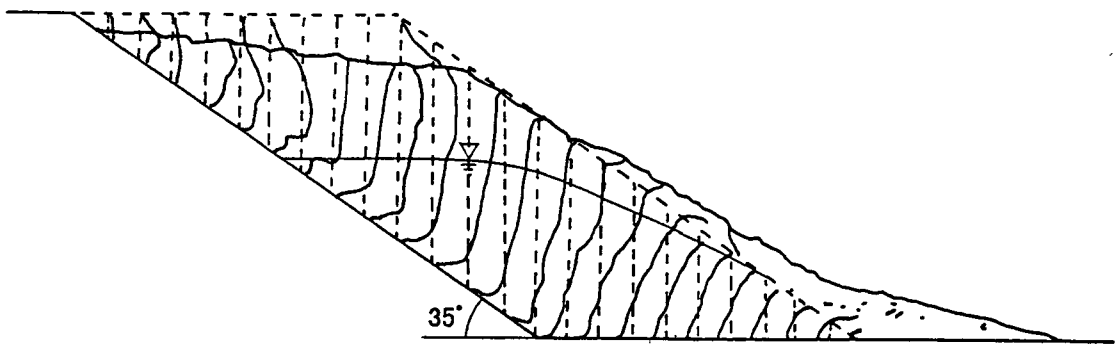


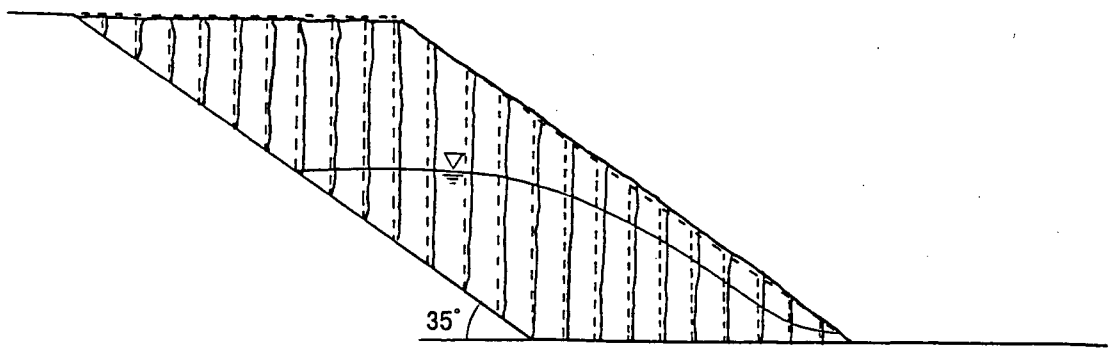
Fig. 13 Series B models



Test A1 (Dc=78%)



Test A3 (Dc=83%)



Test A6 (Dc=92%)

Fig. 14 Configurations of models A1, A3 and A6 after shaking, Series A

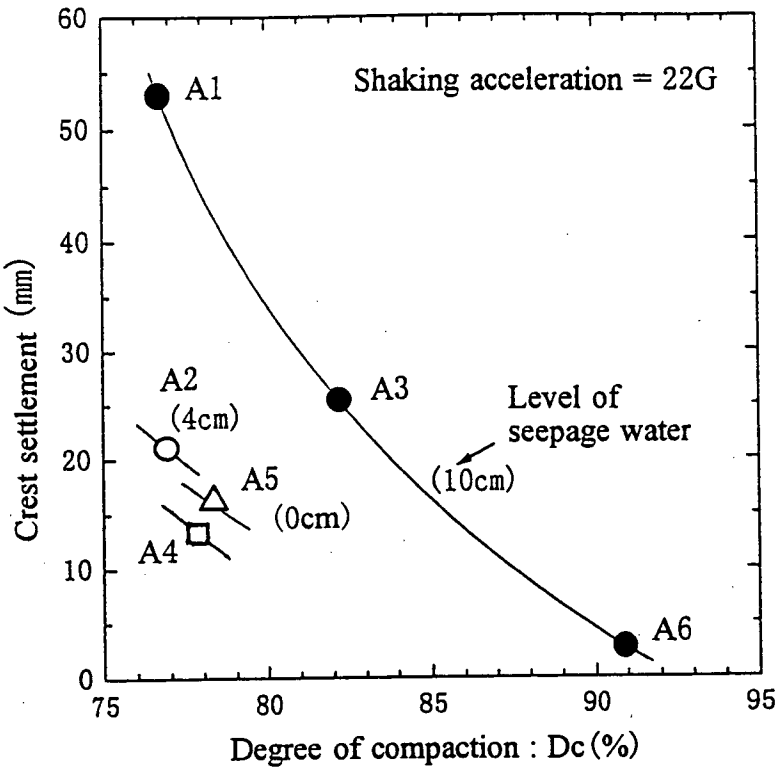


Fig. 15 Relationship between soil density and crest settlement, Series A

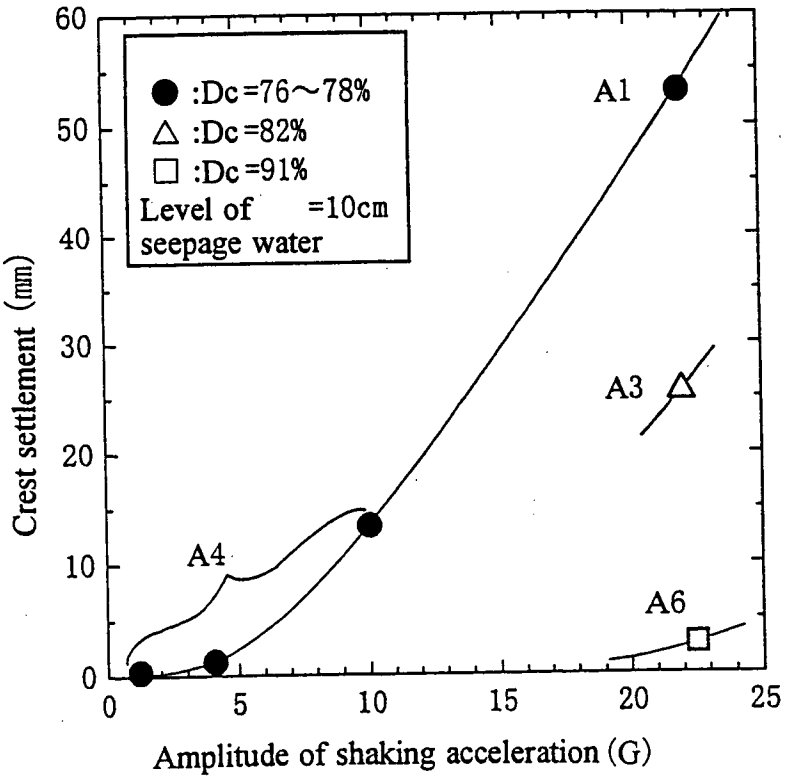
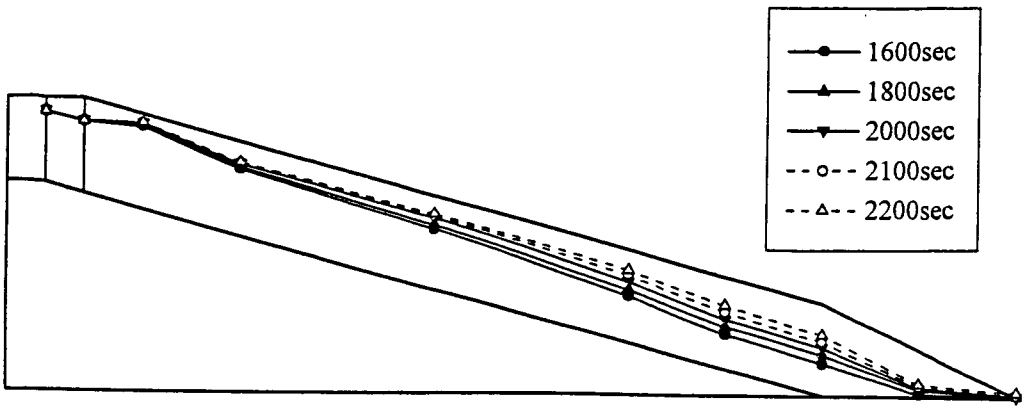
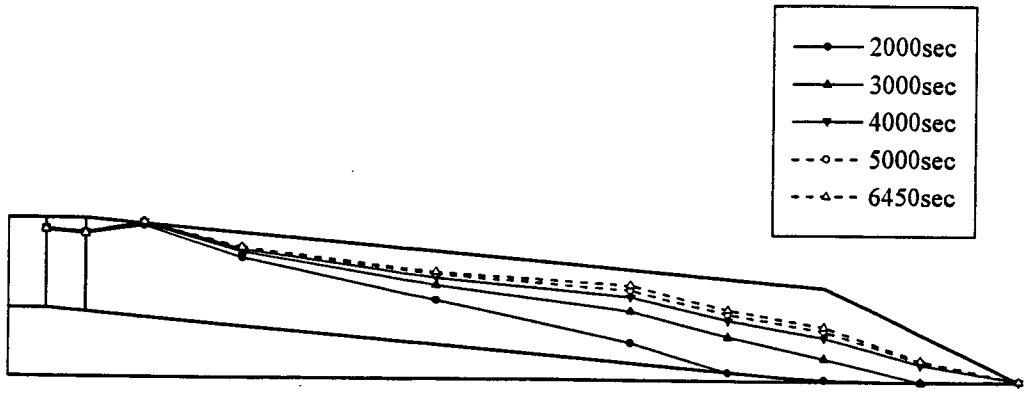


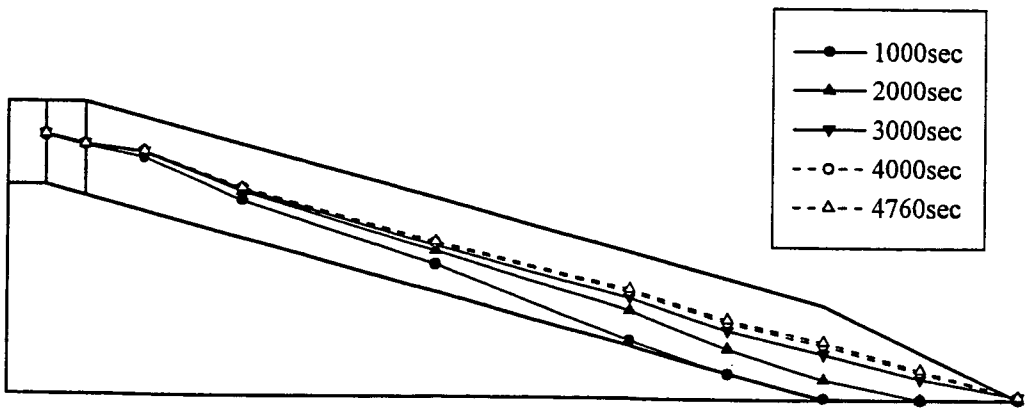
Fig. 16 Relationship between shaking amplitude and crest settlement, Series A



(a) Model B2

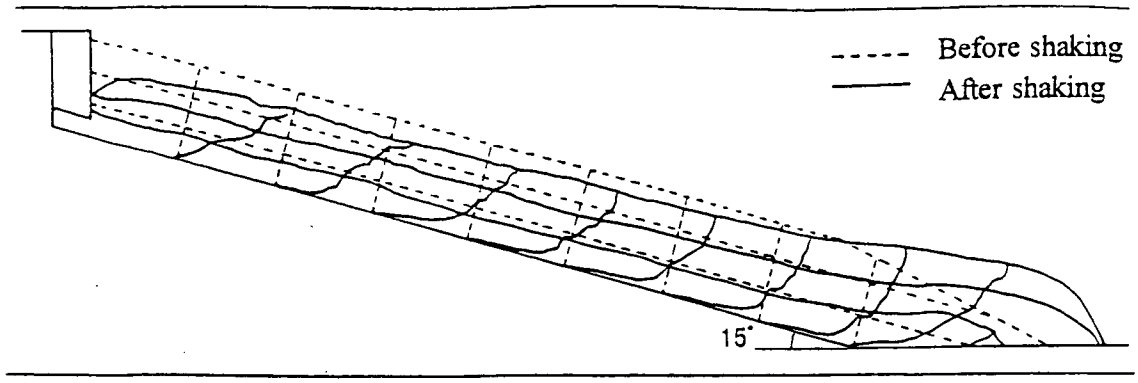


(b) Model B4

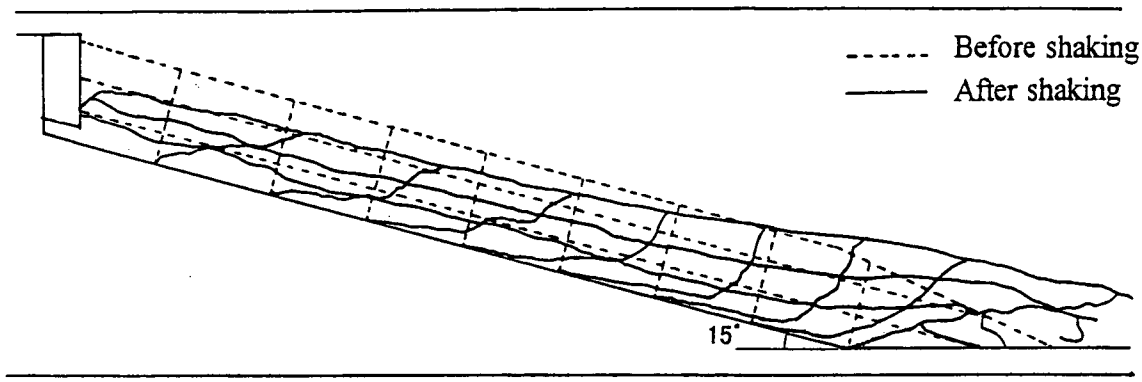


(c) Model B6

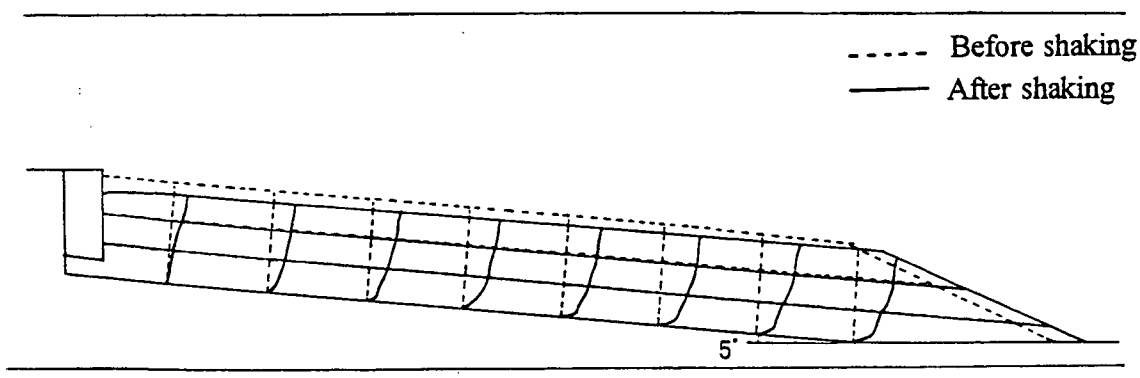
Fig. 17 Development of phreatic line due to seepage, models B2, B4 and B6 in Series B



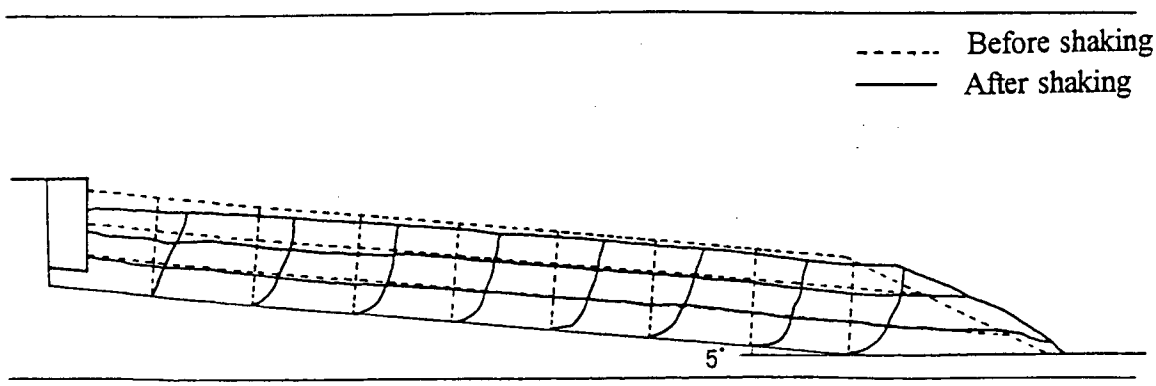
(a) Test B1 (Dc=81%)



(b) Test B2 (Dc=81%)

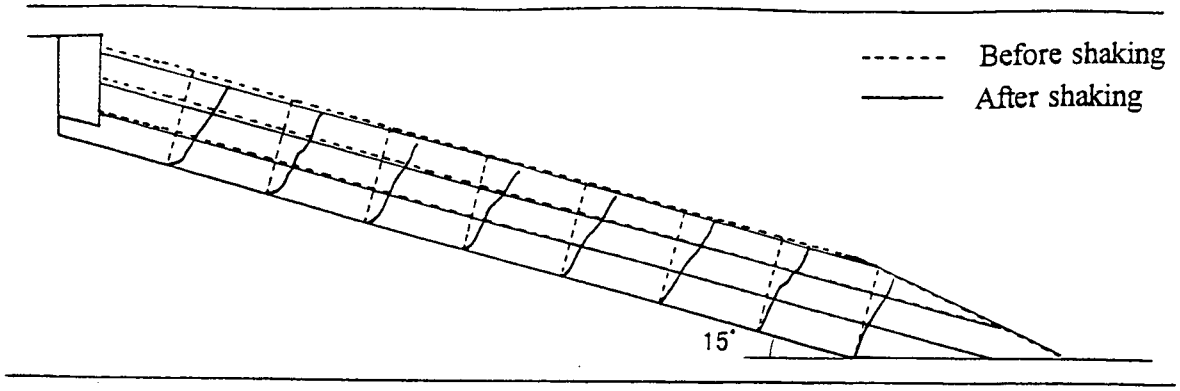


(c) Test B3 (Dc=81%)

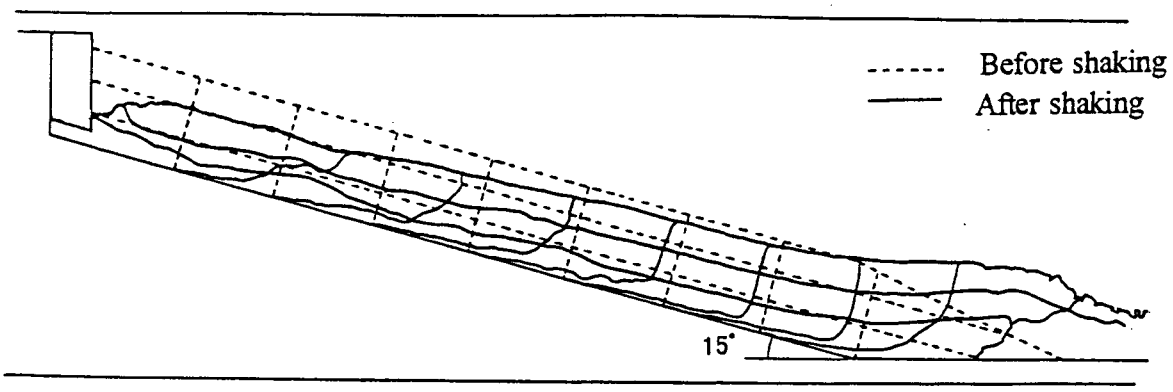


(d) Test B4 (Dc=81%)

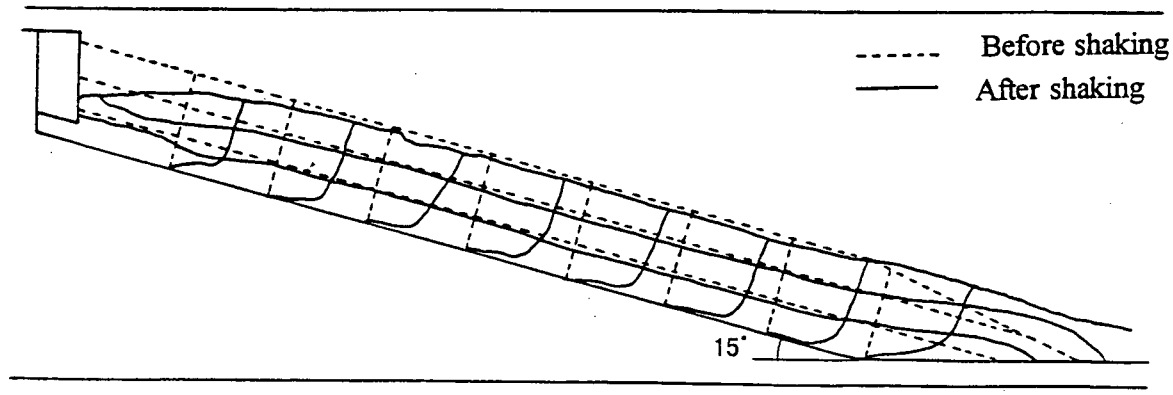
Fig. 18 Deformation of models due to shaking, Series B



(e) Test B5 (Dc=91%)



(f) Test B6 (Dc=81%)



(g) Test B7 (Dc=85%)

Fig. 18 Deformation of models due to shaking, Series B

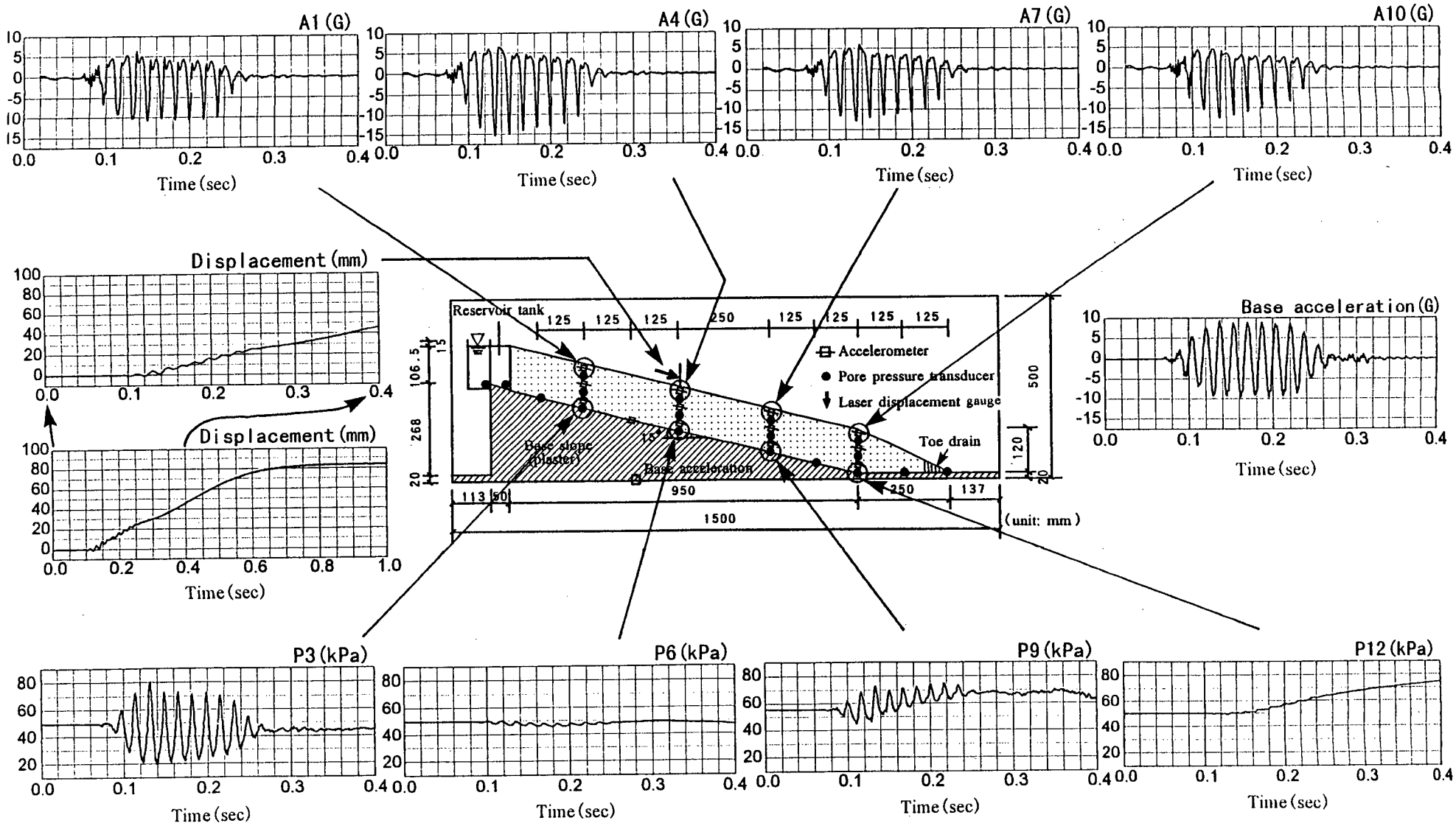


Fig. 19 Time history data of selected measurements, model B7 in Series B

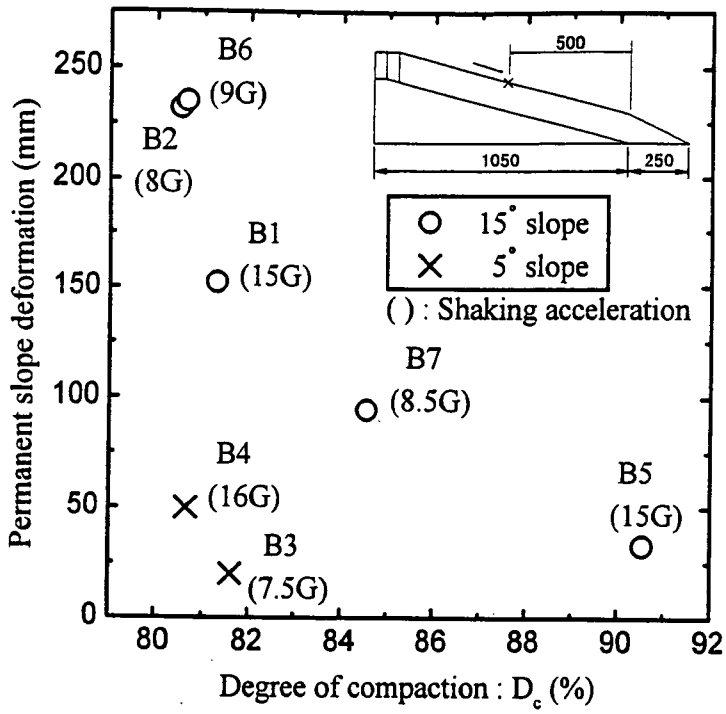


Fig. 20 Relationship between the soil density
and earthquake-induced permanent displacement of slopes, Series B

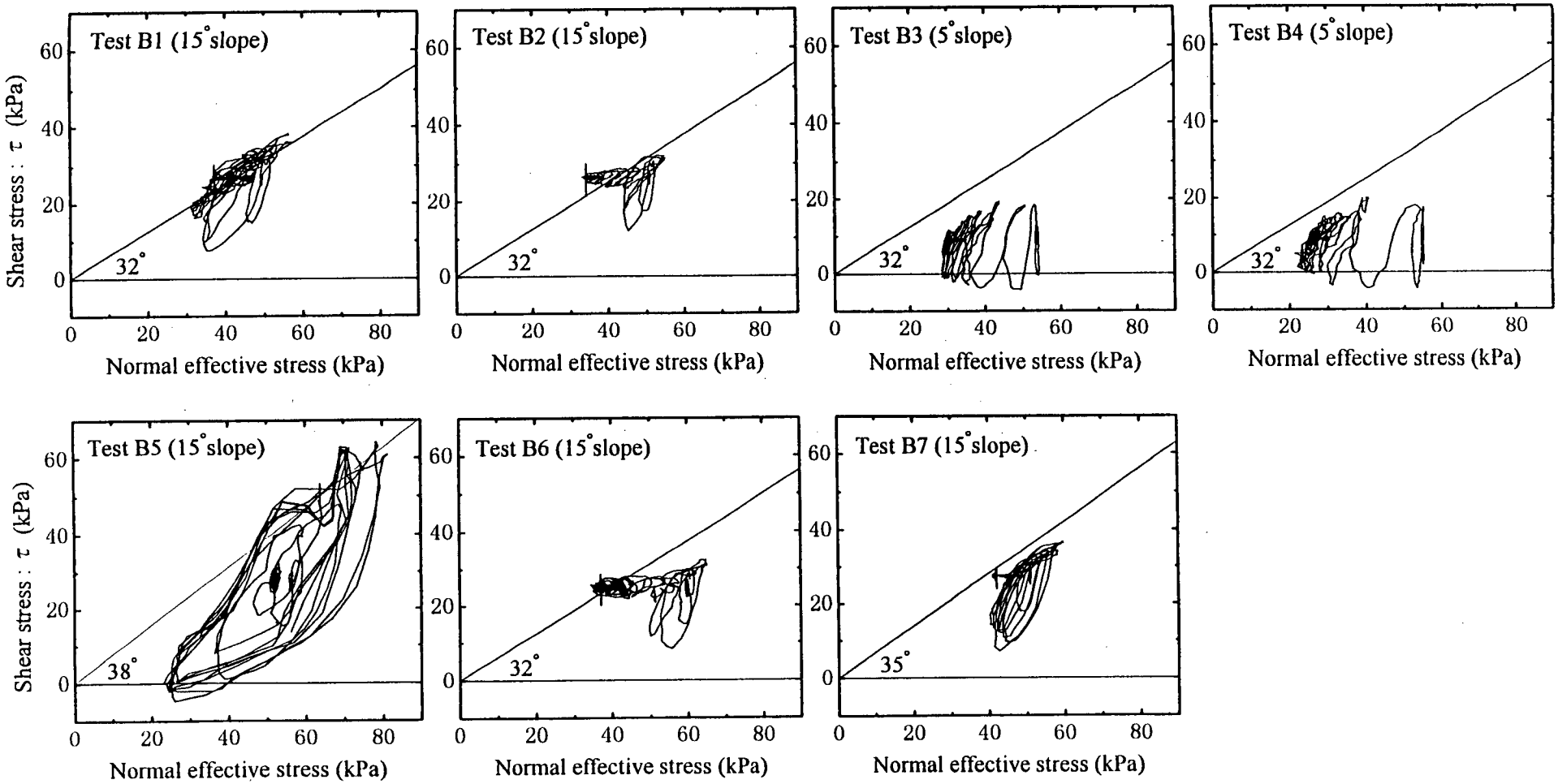


Fig. 21 Effective stress paths at the bottom of soil slope, Series B

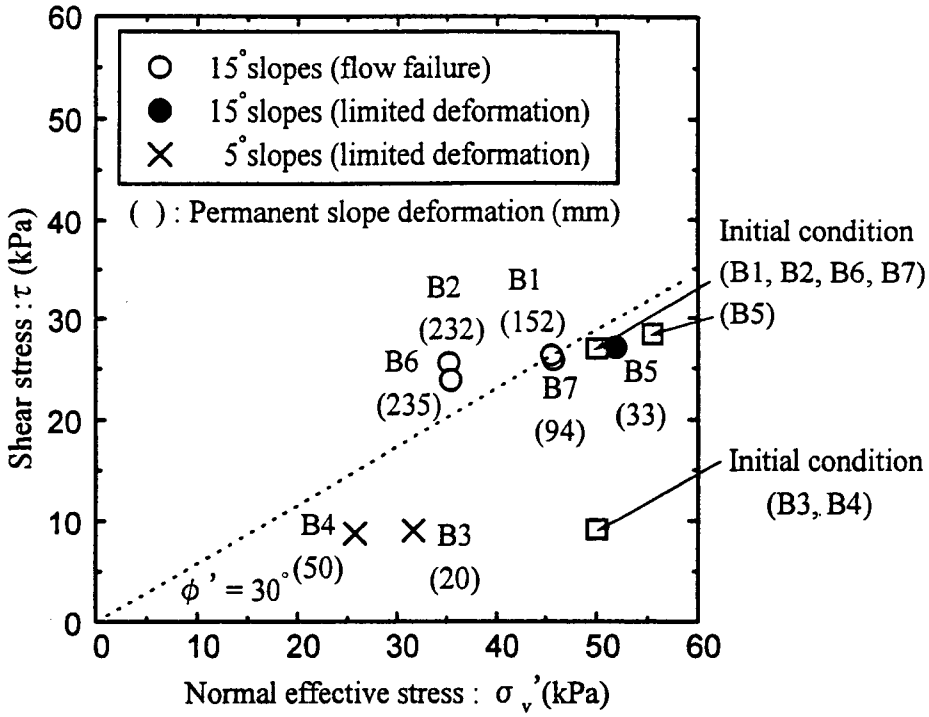


Fig. 22 Stress states at the bottom of slopes at the end of shaking, Series B

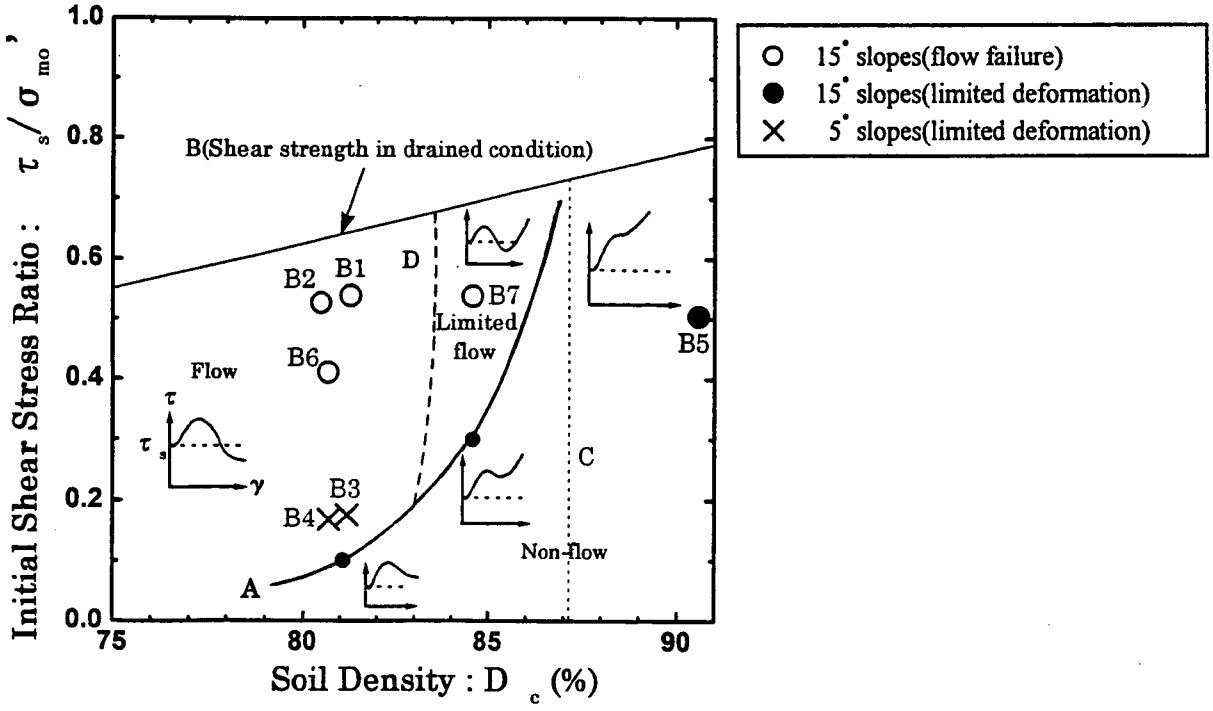


Fig. 23 Plots of the Series B test data on Fig. 11 that was proposed in differentiating conditions of flow and non-flow for infinite slopes

EVALUATION OF MOTIONS RECORDED AT AND WITHIN EMBANKMENT DAMS DURING EARTHQUAKES

I. M. Idriss

Department of Civil and Environmental Engineering
University of California at Davis
Davis, California 95616-5294 (USA)
E-mail: imidriss@aol.com

ABSTRACT

Accelerographs installed at various locations in embankment dams recorded the motions generated during several California earthquakes over the past 25 ± years. These included motions along the crest, along intermediate benches, at abutments, near the toe, and a few downstream of the dams. At San Justo Dam, the motions were recorded within the embankment below the crest of the dam during the 1989 Loma Prieta earthquake.

The purpose of this presentation is to present and examine these data. The motions recorded at two dams are then examined in greater detail and are compared to the results of various analyses to assess the accuracy of some of the current methods used to calculate the response of embankment dams during earthquakes.

These two dams are the San Justo and the San Luis dams. Shear waves had been measured in the embankment and in the underlying foundation layers at each dam. In addition, classification as well strength tests had been conducted on specimen of these materials.

Both two-dimensional and one-dimensional solutions are used to back-calculate the motions for each dam. The results are presented and are used to examine the current procedures used in the dynamic analyses for existing as well as for new embankment dams.

Seismic Analysis and Safety Evaluation of Embankment Dams

by

Gilles Bureau[1]

ABSTRACT

This paper discusses nonlinear embankment dam analysis techniques using an elastic-plastic Mohr-Coulomb constitutive relationship and a semi-coupled excess pore pressure model. The applicability and limitations of such analyses are discussed, using the examples of two existing dams (Los Leones, Chile and Los Angeles, CA) affected by historic earthquakes.

The seismic safety of embankment dams is governed by whether loss of strength will occur or not within the dam or its foundation, and whether earthquake-induced deformations will remain within acceptable limits. When sufficient information about the embankment and foundation materials is available, nonlinear evaluation procedures are reliable. Yet, as any other numerical method, nonlinear analysis has limitations in its applicability and ability to account for some phenomena of potential significance to the dam seismic response. Hence, the evaluation of the potential for earthquake-induced deformations or liquefaction with nonlinear techniques should be pondered by a critical assessment of any factors that may impact the reliability of such estimates.

1. INTRODUCTION

In the last twenty five years, engineers have witnessed significant advances in methods and analytical tools to evaluate the seismic performance of embankment dams. The simplest of these tools rely on empirical correlations derived from observed or calculated seismic response. For example, expectable deformations can be related to the severity of a postulated earthquake event, and field penetration data can be interpreted to assess the potential for liquefaction.

Numerical analysis techniques include: simplified procedures; equivalent-linear (EQL) solutions; and nonlinear (NL) discrete element, finite element, or finite difference formulations. First, this paper reviews current tools for dam analysis and safety evaluation. Next, it focuses on nonlinear analysis techniques. Required parameters, factors of significance to the evaluation, and the advantages and limitations of such techniques are reviewed. Examples are provided, using two major dams affected by historic earthquakes.

2. CONVENTIONAL DAM ANALYSIS PROCEDURES

Simplified procedures and EQL analysis have frequently been used for seismic safety evaluation of new or existing dams. A brief review of such procedures is provided in the following paragraphs.

Simplified Procedures

Commonly used simplified procedures include: Newmark's Method (1965); Makdisi-Seed's Procedure (1977); Romo-Resendiz's Procedure (1981); Bureau, et al.'s correlations (1985, 1987); Jansen's formula (1987); and Swaisgood's empirical approach (1995, 1998). These procedures have been compared by Bureau (1997). When liquefaction is a concern, the simplified method of Seed and Idriss (1970) is often implemented. It applies only to dams with flat slopes. Idriss (1999) updated the original Seed-Idriss procedure. Another way to assess the liquefaction potential, if field penetration tests have been performed (SPT, CPT or Becker Hammer), is to use

[1] Senior Consultant, URS Greiner Woodward Clyde, 500 12th Street, Suite 200, Oakland, CA 94607, USA

empirical correlations between cyclic stress ratios causing liquefaction and modified penetration resistance (Seed, et al., 1983, 1985; Idriss, 1999). Yet, multiple correction factors required to obtain the modified penetration resistance bring an uncertainty to the procedure. Simplified procedures are useful to obtain preliminary insight regarding the seismic performance of a dam, but should be applied cautiously and with full recognition of their implied assumptions and inherent limitations. They can be used to obtain crude estimates of seismic deformations, and assess the need for detailed investigations. They are not suitable when the consequences of liquefaction or large deformations must be quantified.

Equivalent-Linear Analysis

EQL analysis has been routinely used for embankment dams, worldwide, since 1971. It forms the basis of the Seed-Lee-Idriss procedure (Seed, et al., 1983). EQL response is obtained with well-known computer programs based on wave propagation or finite element techniques, such as SHAKE91 (one-dimensional), QUAD4M, FLUSH or SuperFLUSH (two-dimensional). These programs compute total dynamic stress and strain histories, using iterated shear moduli and damping coefficients compatible with the average induced strains. New versions of these programs include compliant base modeling and absorbing boundaries. Dams in narrow valleys may require three-dimensional EQL analysis, such as using TLUSH (Mejia and Seed, 1983).

Time histories of stress and strain elastic response are interpreted to assess the impact of dynamic loading on the embankment. The method does not predict deformations directly, and requires considerable judgment to estimate such deformations. Its reliability strongly decreases as calculated strain levels increase.

For materials not susceptible of liquefying, displacement estimates may be obtained through double integration of accelerations that exceed the yield acceleration, assuming that only downslope movement is possible. Attempts to convert EQL elastic strains into non-recoverable deformations have been made, e.g. using the concepts of stiffness softening (Lee, 1974) or strain potential (Serff et al., 1976), but have not led to well-accepted procedures to compute deformations.

Liquefaction potential is assessed as in the Seed-Idriss simplified procedure, except that stress response histories are calculated directly. Cyclic strength ratios are first defined for the applicable confinement and initial static shear stress. Then, for all elements of the model, average induced cyclic stress ratios are obtained from the maximum dynamic shear stresses by using a reduction factor (typically 0.65). Peak amplitudes between consecutive zero crossings (half cycles) of the stress response histories can be tracked and the contributions of all stress cycles summed up toward potentially reaching a cumulative state of liquefaction.

Following EQL analysis, one may require post-earthquake stability analyses of the dam slopes. Residual strength properties and pore pressure ratios, as obtained from calculated average dynamic stresses and estimated number of equivalent uniform cycles, can be assigned to zones within the embankment concluded to have experienced or approached liquefaction.

3. NONLINEAR ANALYSIS

Modern methods to assess seismic deformations of embankment dams rely upon NL analyses. These methods fall into two broad categories: elastic-plastic (EPNL) and direct nonlinear (DNL). They can simulate progressive embankment construction and reservoir filling to establish the initial state of stress. Excess dynamic pore pressures can be represented through semi-coupled or fully-coupled equations for the soil and water phases. In semi-coupled procedures, pore pressures are calculated at each time step through the use of empirical functions, and added to the stresses obtained from the dynamic solution. Fully-coupled dynamic solutions solve simultaneously the problems of wave propagation, material volume and excess pore pressure changes through coupled governing equations.

Analysis Tools

EPNL computer programs used in the U.S. include DYNAFLOW (Prevost, 1981; Elgamal, et al., 1984); DYNARD (Moriwaki, et al., 1988); DYSLAND (Salah-Mars, et al., 1989); DSAGE (Roth, et al., 1991); and FLAC (Itasca Consulting Group, 1992). DNL programs include TARA-3 and TARA-3L (Finn and Yogendrakumar, 1989) and GEFDYN (Coyne et Bellier et al., 1991). The United States Bureau of Reclamation (Harris, 1986) has also used ADINA/BM (Bathe, 1978).

FLAC

The author's experience is based on the computer program FLAC, available in two- or three-dimensional versions. FLAC solves the displacements due to static and dynamic external forces through finite difference equations (Cundall, 1976). At every calculation step, incremental strains are computed for each elementary zone, and the resulting stress increments are derived from the applicable constitutive relationship. Once stresses have been calculated for all zones, grid node displacements are updated, and new incremental strains are computed. The explicit formulation of FLAC allows large strains, material anisotropies, sliding interfaces and other nonlinearities.

A major feature in FLAC is the availability of a built-in macro-programming language, which allows the user to customize input and output, create new variables and, most impotantly, reproduce existing or develop new costitutive models. Hence, the user is not confined to a computational environment dictated by the software developer, but can create and compile new routines and tailor the use of the program to the specific needs of his project.

In addition to extensive checking by the developer, detailed verifications of FLAC at various deformation levels including liquefaction, have been performed for dam analysis purposes, (Roth, et al., 1986; Dames & Moore, 1991; Inel, Roth and De Rubertis, 1993; Bureau, et al., 1994, 1996).

Seismic Input

NL analysis requires input motion specified as time histories. Recent seismological studies and an increase of available strong motion records have improved our understanding of the characteristics of ground motion. Near-field characteristics are significant to NL response studies, and extreme care is required to select input acceleration histories.

NL response is stress-path dependent, and several sets of independent input histories must be considered. Successive use of different accelerations time histories matching a same response spectra may result in up to 25 percent variations in calculated displacements, or may even lead to reversals of the predicted direction of movement during the most severe shaking (Bureau, 1997). Failure criteria depend on both normal and shear stresses, and the vertical component of motion must be included, which differs from conventional EQL analysis. Omitting the vertical component has been found to result in up to 20 percent difference in the deformation response.

Elastic Material Properties

For NL analysis based on elastic-plastic constitutive models, the dynamic modulus and damping coefficient are less significant parameters than for EQL analysis. Strain-dependent modulus degradation and damping curves are not required. This is because stiffness degradation and loss of energy occur through stress-strain looping and plastic flow.

The low-strain modulus and damping control elastic displacements in FLAC. For embankment or foundation materials, it is convenient to represent such modulus as proposed in Janbu (1963) or Duncan's hyperbolic soil model (Wong and Duncan, 1974). In such formulations, the initial tangent static modulus Ei is related to the minor principal stress and atmospheric pressure through an exponent that defines the rate of modulus variation as a function of the confining stress. Mass- and stiffness-dependent Rayleigh damping is used for energy dissipation.

Plasticity Model

Numerous NL constitutive models and their derivatives, based on single or multiple-nested failure surfaces, have been developed in recent years, e.g.: hyperbolic, Cam-Clay, Drucker-Prager, Pyke, Weidlinger Cap, Mohr-Coulomb, etc.. For dam analysis purposes, the Mohr-Coulomb model performs satisfactorily, based on the author's and other experience (Roth, et al., 1986). The parameters required by the Mohr-Coulomb model can be routinely obtained in the laboratory. This model represents a failure concept which most engineers are familiar with.

Dynamic Strength Properties

Stress-controlled cyclic triaxial and cyclic simple-shear tests can be used to develop cyclic strength curves. For numerical analysis purposes, it is convenient to normalize cyclic strength data to simple shear condition and a confinement of 2,000 psf. The cyclic stress ratio (CSR) causing liquefaction (or 100 percent excess pore pressure) decreases as the overburden pressure increases. The CSR also depends on the initial static shear stress ratio (shear stress divided by normal stress).

The influence of the initial state of stress upon the CSR can be represented through the use of empirical functions relating static state of stress and cyclic loading resistance (Seed, 1983; Seed and Harder, 1990). These functions correct the CSR using two factors that depend on the applicable shear stress ratio and effective vertical stress.

For existing dams, a trend has been to use field penetration data for the purpose of assessing the potential for liquefaction. In-situ standard penetration tests (SPT) or cone penetration tests (CPT) are used in sands and fine-grained materials. Becker Hammer tests (BHT) may be used when coarse gradations are expected to be encountered. For silty materials, it is customary to correct blowcounts in terms of the modified penetration resistance, as would be measured in an equivalent clean sand. Empirical procedures can be used as a basis to estimate the cyclic shear strength of materials for which an average equivalent modified penetration resistance is available.

Pore Pressures

Also needed for dynamic NL effective-stress analysis is the rate at which excess pore pressures build up during earthquake loading. In FLAC, excess pore pressures can be fully coupled to computed material volume changes, or incrementally generated at each calculation step through user-specified, semi-coupled, empirical procedures.

Fully-coupled analyses continuously relate volume changes and excess pore pressure build-up through constitutive models derived from the results of triaxial laboratory tests that include measurements of volume and pore pressure changes.

One useful semi-coupled procedure is based on the concept of cumulative damage (Roth, et al., 1991). It relates excess pore pressures and cumulative damage, D, through an incremental form of the well-established liquefaction analysis method of Seed and Idriss (1982). Through real-time coupling of this scheme with the dynamic analysis, effective stresses are continuously updated and, as excess pore pressures increase during the shaking, liquefaction may occur in frictional materials. Shear stresses are continuously tracked throughout the entire analysis by finding consecutive peaks, zero crossings and reversals. D is updated in each saturated zone of the model for each completed stress cycle. The rate of pore pressure buildup is defined through relationships such as proposed by Martin and Seed (1978), where material-dependent excess pore pressure ratios are empirically related to effective overburden pressure, current number of cycles, and reference number of equivalent uniform cycles causing an excess pore pressure of 100 percent.

Post-Earthquake Stability

In NL analysis, post-earthquake stability can be evaluated by continuing the analysis in the time domain through a quiet period after the shaking. In that manner, one can check whether the dam rapidly reaches a stable configuration after the end of the shaking. Excess pore pressures generated during the shaking can be are allowed to dissipate or redistribute themselves within the dam section. The residual shear strength S_r, which can be

specified as a lower bound strength limit in the constitutive model, is needed for post-earthquake analyses.

4. APPLICATION EXAMPLES

Essential to NL analysis is verifying modeling concepts and numerical solutions. One can use case histories of several instrumented embankment dams that were shaken by significant earthquakes, and whose performance is described in the literature. Essential to such verifications are reliable material properties and performance being described with sufficient detail.

Worldwide, about a dozen dams meet the above requirement. Materials properties established in detailed pre- or post-earthquake investigations allow meaningful use of such experience to calibrate and verify numerical models. Recorded ground and crest motions were obtained at several of those dams, which include: Upper Van Norman and Lower Van Norman, CA (1971 San Fernando Earthquake, M 6.5); Cerro Negro and Los Leones, Chile (1985 Chile Earthquake, M 7.8); Cogswell, CA (1987 Whittier Narrows, M 6.0, and 1991 Sierra Madre, M 5.6, earthquakes); Lexington, CA (1984 Morgan Hill, M 6.2, and 1989 Loma Prieta, M 7.1, earthquakes); El Infiernillo and La Villita, Mexico (1985 Michoacan Earthquake, M 8.1); Matahina, New Zealand (1987 Edgecumbe Earthquake, M 6.3); Austrian, CA (1989 Loma Prieta Earthquake, M 7.1); Ambuklao, Philippines (1990 Philippines Earthquake, M 7.7); and Los Angeles and Upper Van Norman dams, CA (1994 Northridge Earthquake, M 6.7). Most of these case histories have been used in post-earthquake studies to explain observed performance and verify numerical analysis procedures. The following paragraphs present the examples of Los Leones and Los Angeles dams.

Los Leones Dam, Chile

Los Leones Dam, located in the Andes Mountains of Central Chile, is owned and operated by Codelco Chile, Division Andina. The embankment impounds copper tailings and was built in four stages as a rolled earthfill, with a final height of 650 feet above streambed and a volume of 16 millions cubic yards. A shallow (10-foot deep) clear water pond covers the top of tailings. The reservoir has a Stage IV capacity of 120,000 acre-feet and retains 222 million metric tons of tailings. The dam has an upstream core built of morainic deposits, an inclined chimney drain downstream of the core, and a downstream drainage blanket. The downstream shell is built of compacted earthfill. Near the toe, a secondary drainage system collects seepage from the underlying aquifer and paleostreams in the dam foundation. The dam section is shown on Figure 1.

Performance during the March 3, 1985 Chilean Earthquake

The March 3, 1985 earthquake (M_s 7.8) occurred offshore near the coast of Central Chile. Los Leones Stage II dam, located 144 km from the epicenter, had reached a height of 354 feet. The tailings pond surface was 98 feet below the dam crest. Strong motion records were obtained, with a horizontal peak ground acceleration (PGA) of 0.13g at the toe, and 0.21g at the crest of the dam (PCA). Shaking at the site exceeded 100 seconds. Figure 2 shows the significant phase of the recorded time histories. Spectral amplification approached five at the fundamental period of the dam. Los Leones Dam responded elastically to the 1985 event, as post-earthquake surveys indicated no measurable crest settlement or slope movements.

Numerical Model and Basis for Analysis

Laboratory testing, performed in Chile, included moisture, density, gradation, compaction, specific density, and drained and undrained triaxial compression tests on isotropically consolidated samples of the core and shell materials. The influence of confinement on the effective friction angle was expressed through empirical relationships developed from the laboratory test results.

The shell materials are remarkably similar in grain-size distribution and density to the gravels of Oroville Dam, CA, for which an extensive cyclic test program was conducted

in 1979 at the University of California, Berkeley. Hence, in the absence of large-scale cyclic tests applicable to the Los Leones materials, the same cyclic strength curves as developed for the Oroville materials were used. The cyclic strength of the copper tailings was also estimated from the literature.

The FLAC analyses used an effective-stress, Mohr-Coulomb, elastic-plastic model and the semi-coupled dynamic pore pressure generation scheme described earlier. A two-dimensional grid represented the largest section of the dam, see Figure 3. To include the effect of the staged construction on the initial static stresses, a nine-step incremental model building scheme was implemented.

As Los Leones Dam was built across a narrow valley, three-dimensional effects were expected. Such effects were approximated by using two approaches. The first used a two-fold increase in material stiffness to simulate three-dimensional effects and the resulting shift in frequency response of the maximum section of the dam ("full model"). The "geometric adjustment" proposed by Edwards (1990) in an earlier study of Los Leones Dam was also tested. That second method uses the actual modulus of elasticity, but a reduced model height represents the influence of the change in geometry of the dam across the width of the canyon.

Calibration Study

The 1985 records were used to calibrate the dam model. The zones representing Stages III and IV and the upper tailings were not activated. The base motion recorded in March 1985 was used as seismic input to the model of the Stage II dam. The exact phreatic level in the Stage II dam was uncertain. Successive analyses assumed the dam to be partially saturated or dry. The crest motion was used to compare calculated and recorded responses.

Calculated crest settlement was about 0.1 inch, which is acceptable compared with the observed performance (no settlement reported). The comparison between calculated and recorded response spectra, see Figure 4, is satisfactory and validates the numerical model. It suggests that only partial saturation due to clear fluid seepage prevailed at the time of the earthquake.

The calibration study was conducted in three phases. First, the influence of key parameters on the overall model response was assessed. Next, using the results of the sensitivity analysis, a detailed parametric "geometric adjustment" study was performed. Lastly, additional parametric analyses were conducted using the "full model".

The initial phase identified a combination of analysis parameters, within the range of values derived from the laboratory testing program, that led to a reasonable matching of the characteristics of the recorded response. Multiple indicators were used to compare calculated and recorded responses, including: peak crest acceleration (PCA), maximum crest spectral acceleration (PSA), Arias Intensity (a measure of the energy content of acceleration time histories), effective and bracketed durations, root-mean-square (RMS) acceleration, and the shape and peaks of the crest response spectrum. The response of the "full model" compared better with the recorded response than the "geometrically adjusted model". The results are given in Table 1.

Stage IV Dam Analysis

The finite difference model was expanded up to the top of Stage IV, using the optimized material properties. The specified Design Earthquake (DE) would produce more severe motion at the site than distant subduction earthquakes such as the 1985 event. The DE had a 30-second duration and a PGA of 0.50g, and represented a local event of magnitude 7.0 at 10 km distance from the dam.

The most critical condition exists when the clear water in the tailings pond has reached maximum level. The phreatic surface and distribution of steady-state pore pressures shown on Figure 5 were used. Unsaturated seepage emanating from the tailings also occurs in the upstream shell, but the chimney drain and drainage blanket provide sufficient drainage capacity to absorb such seepage. Computed crest settlements are shown on Figure 6. Most deformations occurred within the first 17 seconds of shaking, which include the largest pulses of the input motion.

Earthquake-induced settlements stabilized after about 20 seconds. Maximum settlement was 5 feet, or considerably less than the available freeboard (16 ft). Up to 10 feet of lateral spreading were also calculated near the top of the upstream slope, where the largest non-recoverable movements occur due to induced excess pore pressures that reduced the effective strength of the saturated part of the core.

Peak acceleration response was about 1.0g, or twice the PGA. To assess post-earthquake stability, the input excitation was lengthened by ten seconds of trailing zeroes. The dam continued to oscillate in free vibrations a few seconds after the end of the shaking. Figure 7 shows a typical excess pore pressure history along with the shear stresses that drive it. Excess pore pressures increased regularly during the first 15 seconds, with the fastest rate between 5 and 7 seconds, when the largest shear stress pulses occur. The maximum pore pressure coefficient (r_u) in the saturated portion of the embankment was less than one, which indicated that "initial liquefaction" had not occurred. A state of liquefaction would be reached, however, in the tailings.

Modest deformations of the Stage IV dam are expected under the Design Earthquake. As long as the chimney drain and pervious blanket keep most of the shell dry, satisfactory performance of the embankment will be expected, despite liquefaction of the impounded tailings.

Los Angeles Dam, CA

The Van Norman Complex (VNC) includes the decommissioned Upper Van Norman and Lower Van Norman dams and their replacement, Los Angeles Dam (LAD), built in 1979. The LAD reservoir has about 10,000 acre-feet capacity. LAD is a modern, well-instrumented embankment of maximum height 155 feet, founded on bedrock. It includes upstream and downstream shells of compacted silty sand, a central vertical chimney drain, a downstream, near-horizontal, drainage blanket and a clay core upstream of the chimney drain. The embankment was compacted to 93 percent relative compaction (33,750 ft.lbs/ft^3 energy). The maximum dam section and its model are shown on Figure 8.

Performance during the January 17, 1994 Northridge Earthquake

The January 17, 1994 Northridge Earthquake (M_w 6.7) was centered about 10 km away from LAD, at a focal depth of about 19 km, along a blind thrust segment of the Oakridge Fault. Strong motion instruments recorded free-field motion and the dam response. Corrected peak accelerations were 0.42g (transverse), 0.33g (longitudinal) and 0.32g (vertical) at the right abutment (Station 2) and 0.60g (transverse), 0.42g (longitudinal) and 0.38g (vertical) at the crest (Station 4).

A unique particularity is that ground motion was recorded underground, at the maximum section, at bedrock foundation level and a depth of about 155 feet (Station 3). Peak accelerations of 0.27g (transverse), 0.32g (longitudinal) and 0.12g (vertical) were recorded. Hence, bedrock abutment motions (free-field) were more severe than below the maximum section of the dam (within profile). Motions recorded at the dam are shown on Figure 9.

During the 1994 Earthquake, LAD experienced maximum crest settlement of about 3.5 inches and horizontal movement of 1.2 inches toward downstream. The downstream slope settled up to 0.8 inch, and moved laterally up to two inches toward downstream. The asphalt concrete facing along the upstream slope also experienced surficial cracking. Most cracks were of the shear type. Near the left abutment, compression cracks were associated with waving, bulgy surfaces. Trenching of the largest cracks indicated that they did not extend through the body of the dam. A few cracks pre-existed, but most were probably caused by transient stresses and deformations during the earthquake (Bardet and Davis, 1996). Seepage levels, piezometers and observation wells indicated increases in pore pressure in and around LAD that returned to normal within a short time after the earthquake.

Material Properties

Dames & Moore (1973) designed LAD.

Numerous static and cyclic triaxial, resonant column and cyclic simple-shear tests were performed on the core and shell materials. These extensive data were used to develop a representative numerical model of the dam and compare observed and calculated performances during the Northridge Earthquake (Bureau, et al., 1996).

Mohr-Coulomb strength envelopes for moist shell material indicated an effective cohesion of 720 psf and friction angle of 37 degrees. Saturated effective strength parameters were 350 psf and 39 degrees. The effective cohesion of the core material was 360 psf, and its effective friction angle 26 degrees; its undrained strength ranged from 2,000 to 4,000 psf at 1,000 to 8,000 psf confinement.

Strain-controlled and stress-controlled cyclic triaxial tests were performed on remolded shell samples compacted at 95 or 98 percent relative compaction (33,750 ft.lbs/ft3) and core samples compacted at 95 percent relative compaction. The functions describing the rates of pore pressure increase under cyclic loading were obtained from the laboratory data.

Nonlinear Analysis

The dam response was calculated using the 1973 design properties and the model shown on Figure 8. The grid included 26 columns and 11 rows of elements sized to transmit frequencies of 15 Hz or higher with little or no attenuation. Five zones represented the silty sand shells, the clayey core, the vertical chimney drain, the drainage blanket and a small cobble zone at the bottom of the chimney drain. The reservoir level at the time of the earthquake was used. Hydrostatic water pressures were applied along theupstream face and within the saturated embankment zones.

The model was first excited at bedrock level with the vertical and transverse horizontal foundation records (Station 3). Only about one inch of settlement was calculated, or less than the measured 3.5 inches. The computed peak crest acceleration of 0.58g agrees well with the 0.60g recorded. Figure 10 compares recorded and calculated crest accelerations histories and their five percent damping response spectra. Most significant pulses of the recorded crest motion were reproduced. Reasonable but imperfect spectral match was obtained.

The strong motion records indicated that ground motion along the dam bottom was not uniform. At the downstream toe, shaking was probably similar to that at the right abutment. Hence, abutment and foundation records should represent upper and lower bounds of bedrock motion along the bottom of the maximum section of LAD. A second analysis used the abutment motions as input. Computed cumulative crest settlement was exactly equal to the observed 3.5 inches, but peak horizontal crest movement was greater (5.9 inches) than surveyed (1.2 inches), and occurred toward upstream. Figure 11 shows the calculated crest settlements for the two analysis cases.

The analyses indicated development of excess pore pressures in the lower upstream shell, see Figure 12 (first analysis case). Excess pore pressure increases were related to large shear stress pulses. Pore pressures in the second analysis were slightly higher, but did not reach 100 percent.

Contrary to the fine-tuning of the model performed for Los Leones Dam, the Los Angeles Dam analyses used the input parameters developed in 1973, without any attempt to match the recorded response more closely. Hence, they truly test the ability of standard laboratory tests and interpretation procedures to define the material properties of a completed structure. Calculated and observed responses have strong similarities, which is encouraging, but also differences such as in the crest response spectra or direction of horizontal crest movements.

6. CONCLUSIONS

First and foremost, modern computerized analysis tools operate with an apparent accuracy that far exceeds the Engineer's ability to obtain in-situ material properties or assess their variability within the dam or foundation. Numerical analyses are simply "exact" solutions to poorly-defined and approximate problems. Hence, despite their sophistication, numerical analyses are limited by the quality of the data and understanding of the dam configuration and construction history.

NL analyses are reliable, but must be interpreted carefully. Models that do not take volume changes into account may underestimate vertical-to-horizontal deformation ratios or settlements. Fully-coupled, effective-stress procedures may best predict liquefaction-induced deformations, but are difficult to implement other than to reproduce controlled laboratory environments. In the author's opinion, and if supported through reliable field and laboratory data, realistic solutions can be obtained with simpler to understand and verify semi-coupled pore pressure models.

NL solutions should be validated through the "duplication" of static or cyclic triaxial test results or, preferably, through prediction or back-calculation of the response of full-size dams or physical models, for both small and large deformations. Then, consistent modeling techniques, analysis assumptions and checking procedures can be implemented. While this paper discusses examples involving small deformations, similar procedures have been successfully applied to cases of failure or large deformations (Roth, et al., 1986, 1993).

NL analysis methods can realistically evaluate shaking-induced permanent deformations and predict occurrence of liquefaction, but cannot account for all factors of significance to the complex problem of dam response. Judgment is required, therefore, to decide whether predicted behavior is acceptable from a safety point of view. Errors occur in the calculations, due to unknown, poorly understood or neglected physical phenomena, necessary simplifications in the representation of stress-strain relationships and, especially, uncertainties regarding the seismic input and its variations at foundation level.

Because of their stress path dependency, NL analyses are sensitive to the applied base motions and directions of application. Furthermore, 3-D effects influence dam response in the case of narrow valleys or irregular foundation profiles. Seismic input is normally assumed to be uniform along the dam footprint or at some depth within a deep foundation. In reality, phase characteristics and amplitudes vary both transversely and longitudinally along the dam bottom, as observed at LAD in 1994. At this time, an insufficient strong motion database for dams and lack of a solid theoretical basis prevent analysis using non-uniform base excitation, a shortcoming for any large embankment dam. Yet, the example of LAD suggests that uniform base shaking with free-field records, as is normally used, provides more conservative response than the use of motions recorded in depth.

Other limitations in model detailing, understanding of soil behavior, and ability to simulate pore-pressure effects must be taken into account. Frequently used 2-D models can approximate 3-D response, but cannot predict transverse cracking. Long-term seepage increases or internal erosion that could develop after earthquake loading cannot be investigated in 2-D or 3-D response analyses.

In the author's opinion, deformations calculated by well-verified NL computer programs, using quality input data, should be reliable up to calculated crest settlement to dam height ratios of about ten percent. Use of larger relative settlements as a basis to define a safe freeboard is speculative. The above ratio applies to wide dams, built on regular foundations and gently sloping abutments. Moderate seismic deformations are acceptable, as long as they do not cause significant longitudinal or transverse cracking, failure of the core or other seepage control systems, and excessive loss of freeboard. Deformation and liquefaction estimates should be pondered by a critical assessment of factors that may impact their reliability. Such factors include the method of dam construction, the degree of saturation, state of compaction, deformability and plasticity of the embankment materials, the dam zoning and geometry, the abutment and foundation profiles and, not to be forgotten, the practical experience and judgment of the analyst.

REFERENCES

Bardet, J.P.; Davis, C.A. (1996), "Performance of San Fernando Dams during the 1994 Northridge Earthquake", ASCE Journal of Geotechnical Engineering, Vol. 122, No. 7, July, pp. 544-564.

Bathe, K.J. (1978), "ADINA/BM - A General Computer Program for Nonlinear Analysis of Mines Structures", Final Report to Office of Assistant-Director Mining, U.S. Dept of the Interior, Contract No. 30255008.
Bureau, G. (1997), "Evaluation Methods and Acceptability of Seismic Deformations in Embankment Dams", XIXth International Congress on Large Dams (ICOLD), Q. 73, R. 11, Firenze, Italy, May, pp. 175-200.
Bureau, G.; Edwards, A.; Blumel, A.S. (1994), "Seismic Design of Stage IV Raising, Los Leones Dam, Chile", 11th ASDSO Conference, Boston, Sept., Proceedings, Supplement, pp. 77-86.
Bureau, G.; Inel, S.; Davis, C.A.; Roth, W.H. (1996), "Seismic Response of Los Angeles Dam, CA During the 1994 Northridge Earthquake", USCOLD Annual Meeting, Los Angeles, July 22-26, Proceeding, pp. 281-295.
Bureau, G.; Volpe, R.L.; Roth, W.R.; Udaka, T. (1985), "Seismic Analysis of Concrete Face Rockfill Dams", ASCE International Symposium on CFRD's, Detroit, Oct. 21, in "Concrete Face Rockfill Dams - Design, Construction and Performance", pp. 479-508.
Bureau, G.; Volpe, R.L.; Roth, W.R.; Udaka, T. (1987), "Seismic Analysis of Concrete Face Rockfill Dams", Closure, ASCE Journal of the Geotechnical Engineering Division, Vol. 113, No. 10, October, pp. 1255-1264.
Cundall, P.E. (1976), "Explicit Finite-Difference Methods in Geomechanics", 2nd International Conference on Numerical Methods in Geomechanics, Blackburg, VA, June.
Dames & Moore (1973), "Studies to Evaluate the Seismic Stability of the Proposed Los Angeles Dam", Report to City of Los Angeles, Dept. of Water & Power, September.
Dames & Moore (1991), "Stability Evaluation - South Haiwee Dam, Inyo County", Report to City of Los Angeles, Dept. of Water & Power, July.
Edwards, R. (1990), "Seismic Behavior - Los Leones Dam", ICOLD International Symposium on Safety and Rehabilitation of Tailings Dams, Sydney, Australia, May 23, Proceedings, pp. 63-81.
Elgamal, A. M.; Abdel-Ghaffar, A.M.; Prevost, J.H. (1984), "Nonlinear Earthquake-Response Analysis of Earth Dams", Princeton University, Report No. 84-SM-14, December, 384 pp.
Finn, W.D. Liam; Yogendrakumar, M. (1989), "TARA 3-FL Program for Analysis of Liquefaction-Induced Flow Liquefaction", University of British Columbia, Vancouver, Canada.
Harris, D.W. (1986), "Dynamic Effective Stress Finite Element Analysis of Dams Subjected to Liquefaction", Embankment Dams Branch, Division of Dam and Waterway Design, Engineering and Research Center, U.S. Dept. of the Interior, Bureau of Reclamation, Report REC-ERC-86-4, December, 42 pp.
Idriss, I.M. (1999), "An Update of the Seed-Idriss Simplified Procedure for Evaluating Liquefaction Potential", Presentation Notes, Transportation Research Board, 1999 Workshop, "New Approaches to Liquefaction Analysis", Washington, D.C., January 10.
Inel, S.; Roth, W.H.; De Rubertis, C. (1993), "Nonlinear Dynamic Effective-Stress Analysis of Two Case Histories", Session on "Geotechnical Aspects of Recent Earthquakes", 3rd International Conference on Case Histories in Geotechnical Engineering, St Louis, Missouri, June 1-6.
Itasca Consulting Group (1992), "FLAC - Fast Lagrangian Analysis of Continua - Volume I, User's Manual and Volume II, Verification Problems and Example Applications".
Janbu, N. (1963), "Soil Compressibility as Determined by Oedometer and Triaxial Tests", European Conf. on Soil Mech. and Found. Engineering, Weisbaden, Germany, Vol. 1, pp. 19-26.
Jansen, R.B. (1987), "The Concrete Face Rockfill Dam. Performance of Cogoti Dam under Seismic Loading", ASCE Journal of the Geotechnical Engineering Division, Vol. 113, No. 10, October.
Makdisi, F.; Seed, H.B. (1977), "A Simplified Procedure for Estimating Earthquake-Induced Deformations in Dams and Embankments", University of California, Berkeley, EERC Report No. UCB/EERC-77/19, 33 pp.
Martin, P.P.; Seed, H.B. (1978), "Apollo, A Computer Program for the Analysis of Pressure Generation and Dissipation in Horizontal Sand Layers During Cyclic or Earthquake Loading", U.C. Berkeley,

Earthquake Engineering Research Center, Report No. UCB/EERC 78-21, 53 pp.
Mejia, L.H.; Seed, H.B. (1983), "Comparison of 2-D and 3-D Dynamic Analysis of Earth Dams", ASCE Journal of Geotechnical Engineering, Vol. 109, No. GT11, pp. 1383-1398.
Newmark, N.M. (1965), "Effects of Earthquakes on Dams and Embankments", Rankine Lecture, Geotechnique 15, No. 2, pp. 139-160.
Prevost, J.H. (1981), "DYNAFLOW: A Nonlinear Transient Finite Element Analysis Program", Princeton University, New Jersey.
Romo, M.P.; Resendiz, D. (1981), "Computed and Observed Deformations of Two Embankment Dams Under Earthquake Loading", in "Dams and Earthquakes", ICE, London, pp. 267-274.
Roth, W.H.; Bureau, G.; Brodt, G. (1991), "Pleasant Valley Dam: An Approach to Quantifying the Effect of Foundation Liquefaction", 17th ICOLD, Vienna, June, Proceedings, pp. 1199-1223.
Roth, W.H; Scott, R.F.; Cundall, P.A (1986), "Nonlinear Dynamic Analysis of a Centrifuge Model Embankment", 3rd U.S. National Conference on Earthquake Engineering, Charleston, South Carolina, August 24-28, Proceedings, Volume I, pp. 506-516.
Roth, W.H.; Inel, S.; Davis, C.; Brodt, G. (1993), Upper San Fernando Dam 1971 Revisited", 10th Annual Conference of the Association of State Dam Safety Officials (ASDSO), Kansas City, MO, September 26-29, Proceedings.
Salah-Mars, S. et al. (1992), "Nonlinear Dynamic Response Analysis of Lexington Dam", SMIP92, Seminar on Seismological and Engineering Implications of Recent Strong Motion Data", May 21, Sacramento, CA, Proceedings, pp. 10.1-10.14.
Seed, H.B.; Idriss, I.M. (1970), "A Simplified Procedure for Evaluating Soil Liquefaction Potential", University of California, Berkeley, Earthquake Engineering Research Center, Report No. EERC 70-9, 38 pp.
Seed, H.B.; Idriss, I.M. (1982), "Ground Motions and Soil Liquefaction During Earthquakes", Earthquake Engineering Research Institute, Berkeley, CA, Monograph Series, Lib. of Congress Cat. Number 82-84224.
Seed, H.B.; Idriss, I.M.; Arango, I. (1983), "Evaluation of Liquefaction Potential Using Field Performance Data", ASCE Journal of the Geotechnical Engineering Division, Vol. 109, No. 3, March, pp. 458-482.
Seed, H.B.; Tokimatsu, K.; Harder, L.; Chung, R.M. (1985), "Influence of SPT Procedures in Soil Liquefaction Resistance Evaluations", ASCE Journal of the Geotechnical Eng. Div., Vol. 111, No. 12, December, pp. 1425-1445.
Seed, R.B.; Harder, L.F., Jr. (1990), "SPT-Based Analysis of Cyclic Pore Pressure Generation and Undrained Residual Strength", Presented at H. Bolton Seed Memorial Symposium, Proceedings, Volume 2, BiTech Publishers, Canada, May.
Serff, N.; Seed, H.B.; Makdisi, F.I.; Chang, C.K. (1976), "Earthquake-Induced Deformations of Earth Dams", U. of California, Berkeley, EERC Report No. EERC/76-4.
Swaisgood, J.R. (1995), "Estimating Deformation of Embankment Dams Caused by Earthquakes", ASDSO Western Regional Conference, Red Lodge, Montana, May 22-25.
Swaisgood, J.R. (1998), "Seismically-Induced Deformation of Embankment Dams", 6th U.S. National Conference on Earthquake Engineering, Seattle, June.
Wong, K.S.; Duncan, J.M. (1974), "Hyperbolic Stress-Strain Parameters for Nonlinear Finite Element Analyses of Stresses and Movements in Soil Masses", University of California, Berkeley, Report No. TE-74-3.

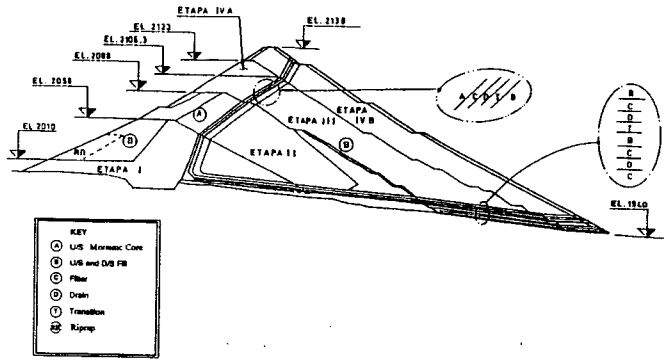


Figure 1. Maximum section of Los Leones Dam.

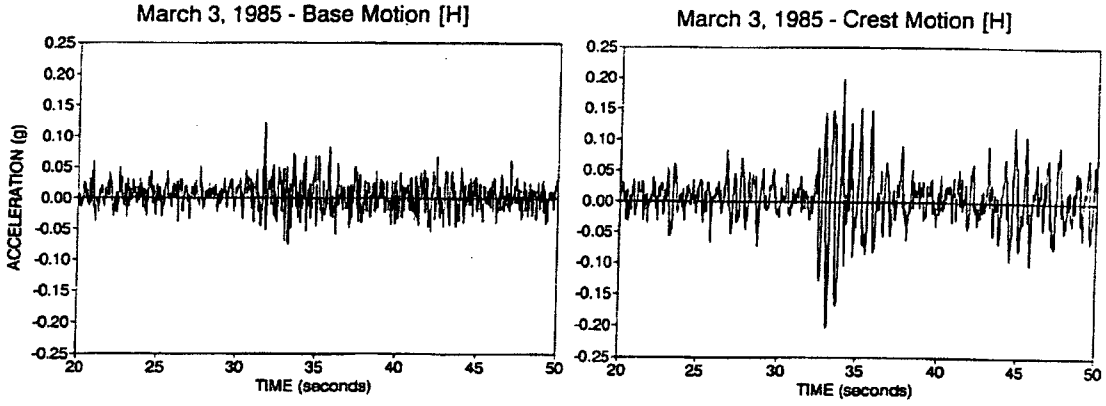


Figure 2. Recorded 1985 acceleration time histories.

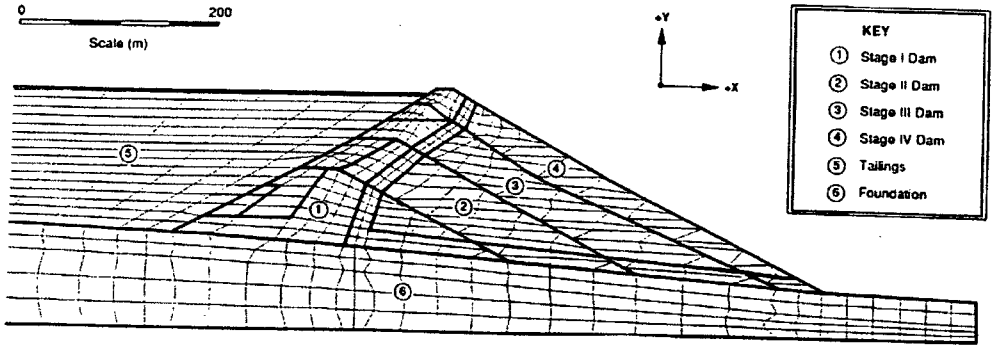


Figure 3. Finite-difference model of Los Leones Stage IV Dam.

Table 1. Comparison of computed and recorded responses.

Indicator	Computed	Recorded	Difference
Peak crest acceleration	0.199g	0.204g	2%
Peak spectral acceleration	0.800g	0.945g	15%
RMS acceleration	0.049g	0.048g	2%
Arias intensity (30s)	3.20	2.85	12%
Bracketed duration	26.60	26.90	1%

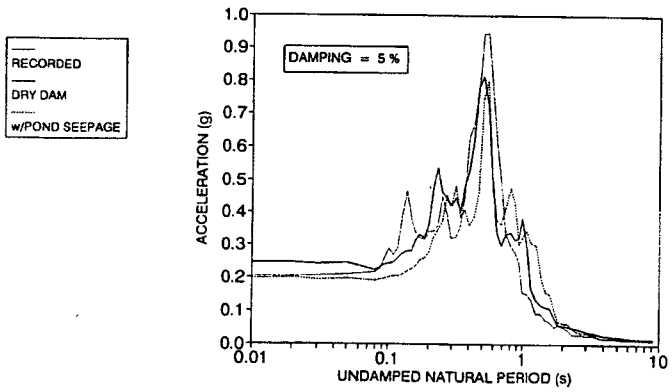


Figure 4. Spectral comparison between recorded and calculated crest motions.

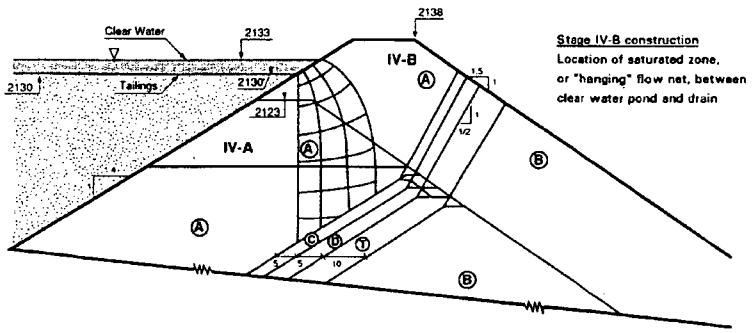


Figure 5. Saturated Zone Near Dam Crest

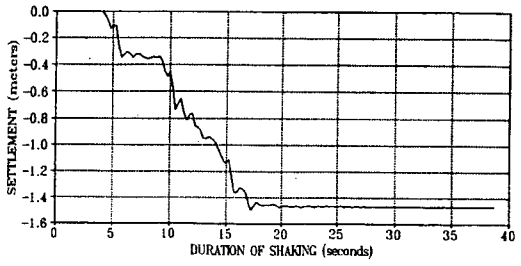


Figure 6. Calculated settlement at crest center.

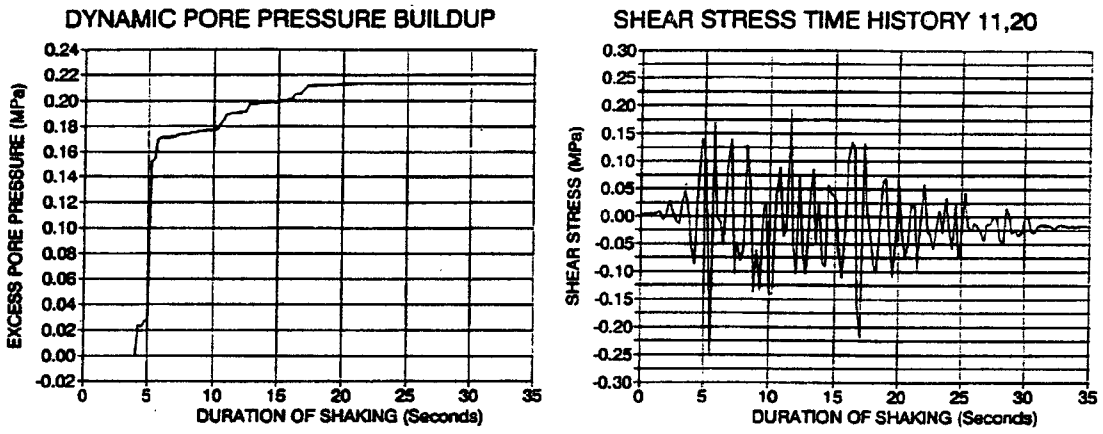


Figure 7. Shear stress and pore pressure response.

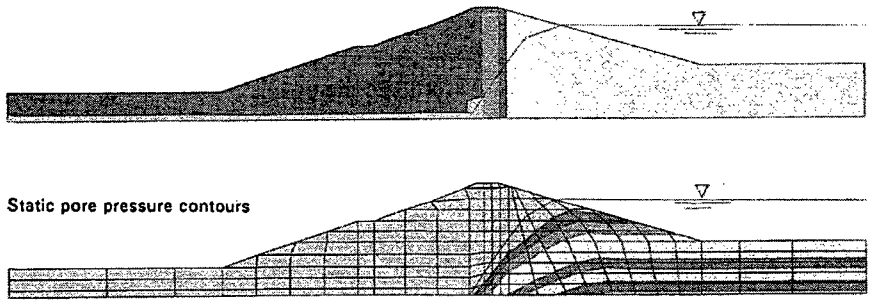


FIGURE 3: FINITE DIFFERENCE GRID AND MODEL ZONING

Figure 8. Los Angeles Dam zoning and numerical model.

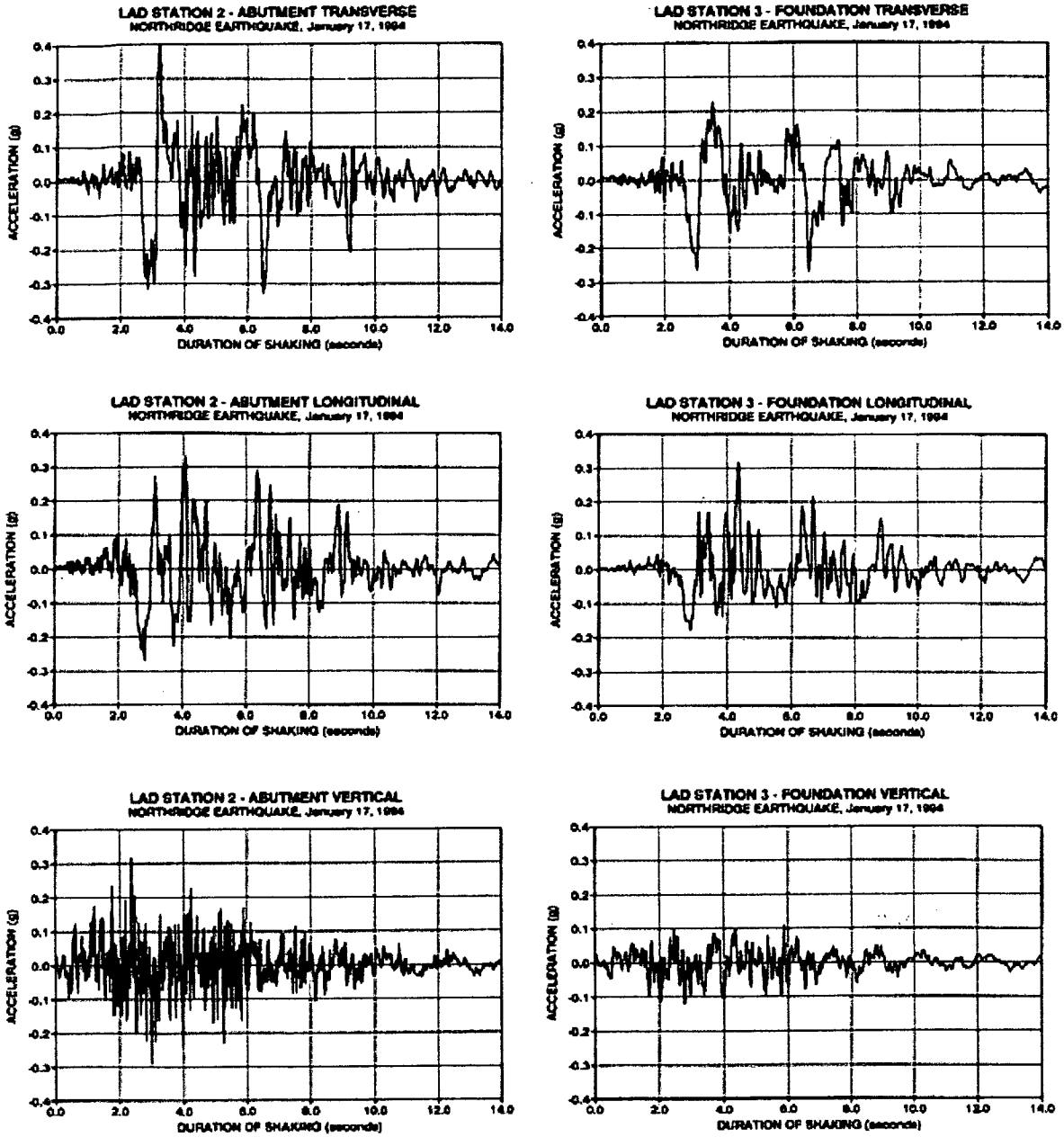


Figure 9. Recorded motions at Los Angeles Dam (Northridge 1994).

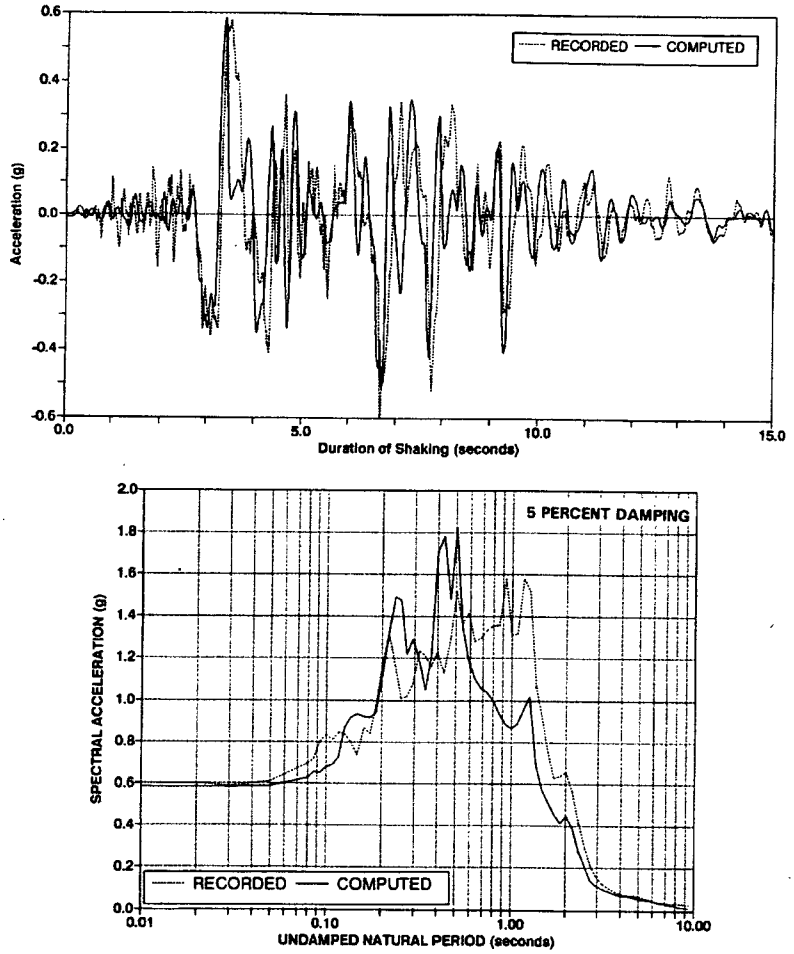


Figure 10. Crest response of Los Angeles Dam to 1994 Northridge Earthquake.

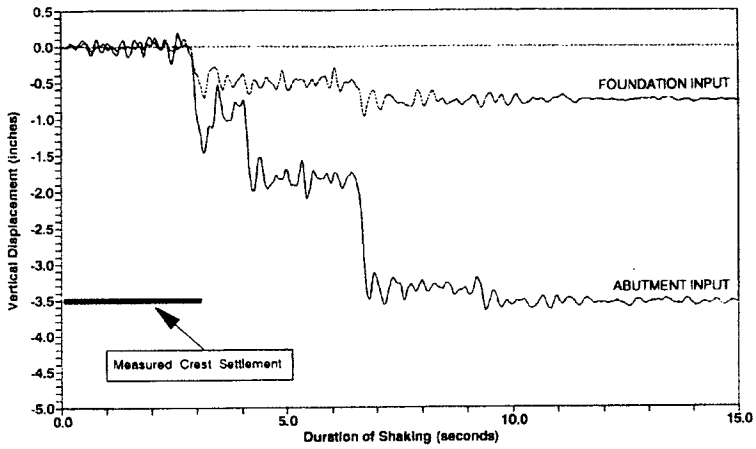


Figure 11. Calculated Crest Settlement.

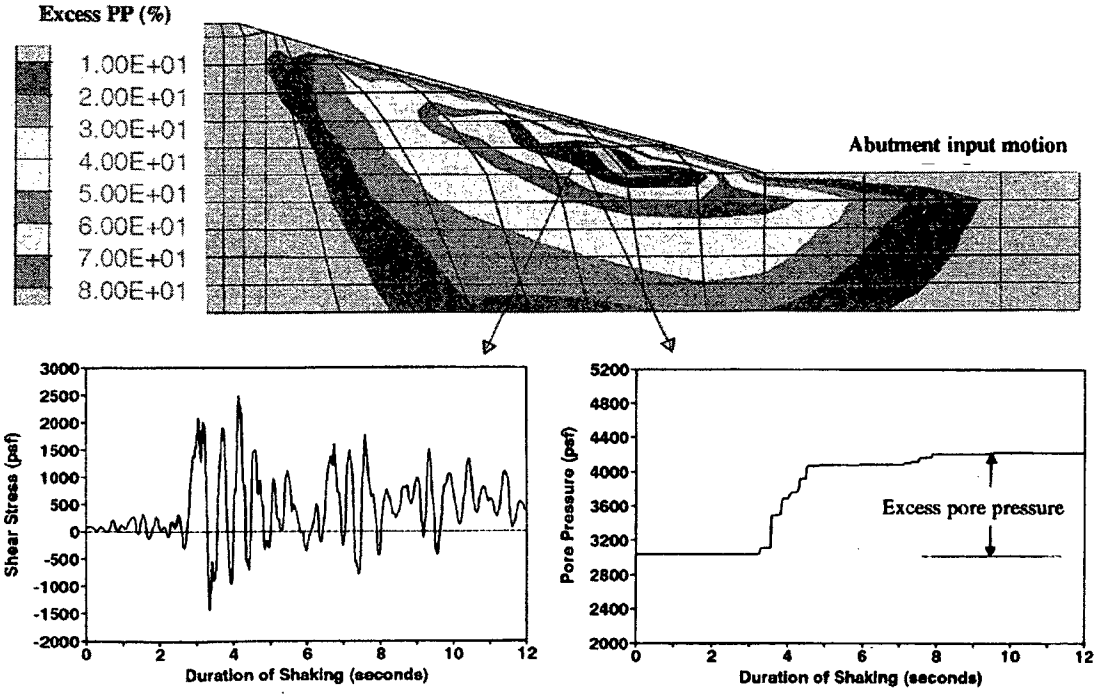


Figure 12. Excess pore pressure development.

Seismic Response of an Earth Dam with Liquefiable Foundation

Michael K. Sharp[1] and Sara J. Lacy[2]

INTRODUCTION

This report presents an analysis of the seismic response of a zoned earth dam overlying a foundation containing a horizontal stratum of liquefiable soil. The effect of the thickness of the liquefiable soil stratum on the response of the dam is investigated. The analysis includes both physical modeling using the large U.S. Army centrifuge at the Engineering Research and Development Center and finite element modeling with the program *Dynaflow* (Prevost 1987). This report describes the constitutive model used to assess stress-strain relations and describes the model parameters and their definition for this problem. The response of the dam to sinusoidal base accelerations is presented, including computed time histories of excess pore water pressure in the dam foundation. Contours of mean effective stress at time intervals during and after the application of base accelerations show zones of liquefaction in the dam. The time histories of displacement of the dam crest and toe show how the thickness of the liquefiable layer affects the magnitude of permanent deformations.

PROBLEM DESCRIPTION

The idealized dam investigated in this study, and shown in figure 1, is a zoned earth dam with a pervious shell over an impervious inner core. The dam is 150 feet tall with a 25 foot crest and rests on 48 feet of foundation material that in turn rests on bedrock. The reservoir is at height 673 feet. The foundation contains a horizontal stratum of loose soil. When the dam is excited by horizontal base accelerations, the loose foundation soil liquefies. This study investigates the effect of the thickness of the loose foundation material on the deformation of the dam during and immediately following the earthquake.

In this study four cases, each with a different thickness of loose foundation material, are analyzed. Figure 1 shows the idealized dam and the location of the loose foundation strata: layer 2 on the upstream side of the dam and layer 5 on the downstream side. Table 1 lists the location of the loose, liquefiable foundation soil. In Case IV, the entire foundation is dense and does not liquefy when excited by horizontal base accelerations. In Cases I, II, and III, a loose layer is overlaid by a twelve foot deep dense layer of soil. In each case the loose layer is progressively larger. In Case III this layer extends to bedrock. For each case the base of the dam is subjected to horizontal accelerations at 2 cycles per second for 8 seconds. The loose foundation soil is calibrated to liquefy in this time while the remaining soil in the dam does not.

	Foundation Soil			
Elevation (feet)	Case I	Case II	Case III	Case IV
553-656	Dense	Dense	Dense	Dense
541-553	Loose	Loose	Loose	Dense
529-541	Dense	Loose	Loose	Dense
517-529	Dense	Dense	Loose	Dense

Table 1. Foundation Soil

MODEL DESCRIPTION

The finite element computer code *Dynaflow* (Prevost 1987) is used to compute the seismic response of the idealized dam. *Dynaflow* can be used to compute dynamic response of structures and dry or saturated soil, in one, two or three dimensions. The nonlinear elasto-plastic behavior of the soil skeleton is modeled by multi-yield surface plasticity (Prevost 1985). Time integration of the semi-discrete finite element equations is performed by an implicit-explicit predictor-corrector algorithm (Hughes et al. 1979).

[1] Research Civil Engineer, Waterways Experiment Station, Vicksburg, MS, USA
[2] Research Civil Engineer, Boston, MA, USA

Dynaflow is a fully coupled finite element procedure using equations that simultaneously compute the response of a fluid phase and a solid phase in the saturated zone. Tensors relate increments of all stress components to all strain components, so the calculation of plastic volumetric strains and change in pore water pressure is coupled to the calculation of shear strains. Pore water pressures are computed along with soil stresses and deformations, and the interaction of the two is fully considered. The finite element computer program follows the stress path of the soil at each moment of time in each element of the finite element mesh and computes time histories of the stresses, pore water pressures, accelerations, and deformations simultaneously. *Dynaflow* includes a variety of plasticity models that use nested yield surfaces. The constitutive model that has been used for seismic analysis of the idealized dam is called the Multi-Yield Surface Elasto-Plastic stress model for pressure sensitive materials. Soil yielding depends on confining stress. Stress-strain behavior is nonlinear and hysteretic, resulting in permanent deformations. A nonassociative volumetric component of flow allows dilation and compaction under shear stress.

CALCULATED RESPONSE TO SINUSOIDAL LOADING

A two dimensional finite element mesh was made reflecting the dam's geometry and boundary conditions. Figure 2 shows the 368 node and 317 element mesh. The base of the mesh was constrained from moving in the vertical direction. The nodes on the right side of the foundation were constrained to have the same horizontal motion as the nodes at the same elevation on the left side of the foundation. The mesh is composed of six different element groups reflecting different zones of the dam shown in figure 1: saturated dense foundation material, saturated loose foundation material, saturated shell below the free surface and dry shell above the free surface on the upstream side and on the downstream side, saturated core below the free surface and dry core above the free surface. For each saturated element, four degrees of freedom are defined for each node: horizontal and vertical displacement of the solid phase and horizontal and vertical displacement of the fluid phase. For dry elements there are two degrees of freedom for each node: the horizontal and vertical soil displacement. The reservoir is at height 673 feet. The water load of the reservoir is simulated by forces applied to the nodes on the upstream face of the dam.

Computations were performed in three stages. First gravity was applied and initial stresses calculated. Initial pore water pressures were calculated. Figure 3 shows contours of initial pore water pressures. In the second computational stage, a ten second horizontal sinusoidal acceleration was applied to the base of the dam. The base acceleration consisted of eight seconds of shaking at two cycles per second. The base acceleration amplitude was set at 2 ft/sec^2 to induce a cyclic stress ratio above 0.15 but less than 0.25 in the foundation soils, so that the loose foundation material would liquefy, but the dense foundation material would not. The analysis included a third computational stage of consolidation for 24 hours following the earthquake.

Time histories of the soil displacements were computed at each node in the dam. Time histories of pore water pressures were calculated in each saturated element. In all four analyses the same material parameters, boundary conditions, time step and integration procedures were used, so that the differences in the four sets of results reflect only the effect of changing the depth of the loose foundation material.

Figures 4 through 14 show the results of the analysis for Case III. The most striking feature of these results is the failure of the dam in Case III. In this case, the bottom 36 feet of foundation soil is calibrated to liquefy in 15 cycles of loading. Once this large stratum of soil has liquefied, the dam moves rapidly in the downstream direction. In the five seconds after the base accelerations stop, pore water pressures in the foundation remain high, the downstream toe moves downstream and the crest of the dam

moves vertically downward as well as downstream as the dam fails. Calculations for Case III end when the dam fails. The dam in Case IV experiences no liquefaction and the deformations during shaking are very small. The dams in Case II and Case III, with 12 feet and 24 foot strata of loose soil surrounded on the top and bottom by dense soil which does not liquefy, have a more localized liquefied area. In these cases displacements are contained. Excess pore water pressures dissipate soon after the base acceleration ceases, the displacements do not continue, and damage is not large.

EXCESS PORE WATER PRESSURE

Figure 4 shows excess pore water pressure histories for Analysis Case III. In this case the bottom three layers of elements are loose, liquefiable material, and only the top layer is dense foundation material. For this case, the three layers liquefy progressively from top to bottom. The third layer liquefies at time 2 seconds, the second layer liquefies at time 5 seconds, and the bottom layer liquefies at time 6 seconds. The pore water pressure remains elevated through time 13 seconds. At this time, the downstream foundation material is undergoing large deformations causing the dam to collapse. Consequently there are no long term pore water pressure histories for Case III.

MEAN EFFECTIVE PRESSURE

Figure 5 and 6 show contours of mean effective pressure in the dam at times 2, 4, 6, 8, 10, and 12 seconds, at 3 minutes, and at 24 hours. Figure 5 contains a color contour scale showing values of effective pressure in pounds per square foot associated with each color. Values of mean effective pressure go up to 13000 psf and all values of mean effective pressure greater than 9000 psf are red. As shaking continues the pore water pressure tends to increase and the effective stress decreases. Elements of zero mean effective pressure, where liquefaction has occurred, are white.

Figure 5 and 6 show contours of mean effective pressure for Case III, with a 36 foot stratum of loose soil, represented by three rows of elements, under the top 12 feet of dense soil in the foundation. At time 0 seconds, geostatic effective stresses exist in the dam. At time 2, and 4 seconds, the number of white elements increases in the top layer of liquefiable elements, as nearly the entire row of elements liquefies. At time 6, 8 and 10 seconds, the bottom two rows of elements with loose soil liquefy. At time 13 seconds, the effective stresses approach zero throughout the foundation and the dam fails.

DISPLACEMENT

Table 2 shows the final displacements of the crest and downstream toe for Case I, II, III and IV. The numbers represent the permanent displacement, 24 hours after the shaking, when excess pore water pressures have dissipated for Cases I, II, and IV. The number for Case III show the displacements at time 13 seconds, five seconds after the end of shaking. The foundation is liquefied and the dam is experiencing large deformations at this time.

Figures 7 through 10 show time histories of displacement of the crest and downstream toe of the dam during the 8 seconds of shaking and the first five seconds thereafter. These figures show that there are only substantial movements in Case III, where the loose layer of soil extends 36 feet, to bedrock. In this case the rate of movement increases when the entire layer has liquefied, after 15 cycles of shaking. At that time the downstream toe begins to move horizontally in the downstream direction. Figure 7 shows that the downstream toe has moved 0.38 feet at time 8 seconds, 1.33 feet at time 10 seconds, and over 3 feet at time twelve seconds. The toe has moved horizontally 7.4 feet at time 13 seconds. Figure 8 shows that the downstream toe settles 0.4 feet and then moves upward after 11 seconds as the dam moves downstream, and the soil downstream of the dam toe bulges. The crest of the dam moves downstream (3.68 feet) and vertically downward (4.52 feet) as the dam fails. Figures 11 and 12

show long-term time histories of the horizontal displacement of the downstream toe and the vertical displacement of the dam crest. For Cases I, II, and IV, most of the displacement has occurred by time 10 seconds and it is complete by time 10 minutes.

	Toe Displacement (ft.)		Crest Displacement (ft.)	
	Horiz.	Vert.	Horiz.	Vert.
Case I	0.38	-0.05	0.28	-0.28
Case II	0.55	-.011	0.35	-0.36
Case III	7.43	0.37	3.68	-4.52
Case IV	0.10	0.01	0.23	-0.32

Table 2. Final Displacement of Toe and Crest

Figure 13 shows the deformed mesh for Case III at time 10 seconds. Figure 14 shows the deformed mesh at time 13 seconds. At 10 seconds, the liquefied foundation material on the downstream side of the dam has begun to move horizontally in the downstream direction. Some bulging occurs below the downstream toe. At 13 seconds, the second row of elements in the loose foundation material under the downstream side of the dam is experiencing large deformations in the downstream direction causing the dam above it to move substantially in both the downward and downstream directions.

CONCLUSIONS

A finite element analysis shows the seismic behavior of a zoned earth dam overlying a foundation containing a horizontal stratum of liquefiable soil. Four cases, each with a different thickness of loose foundation material, have been analyzed. The two-phase analysis includes a plasticity model for soil stress strain behavior and consequently the computational results show development of excess pore water pressure and soil liquefaction in the loose foundation soil stratum. All analyses show permanent settlement of the crest and horizontal downstream motion of the downstream toe. The results show that thickness of the loose foundation stratum controls the magnitude of the displacements in the dam during and after an earthquake.

When the loose foundation layer under the dam liquefies, the dam experiences horizontal displacements in the downstream direction. The thicker the loose stratum, the larger the downstream displacement. The dam in Case IV, with no loose foundation stratum, experiences no liquefaction and the deformations during shaking are small. The analysis in Case III of the dam with the thickest loose soil stratum, extending 36 feet to bedrock, is the only analysis which results in failure of the dam. Once this large stratum of soil has liquefied, the dense soil overlying the loose stratum also liquefies. Two seconds after the earthquake, the foundation material on the downstream side of the dam begins to move rapidly in the downstream direction. Some bulging occurs below the downstream toe. Five seconds after the earthquake, elements in the loose foundation material under the downstream side of the dam have experienced large deformations in the downstream direction causing the dam above it to fail by moving substantially in both the downward and downstream directions.

In the analyses of the dams in Case II and Case III, with 12 foot and 24 foot strata of loose soil surrounded on the top and bottom by dense soil, excess pore water pressures dissipate soon after the base acceleration ceases, the displacements do not continue, and damage is not large. The dam crests settle 0.28 feet and 0.36 feet respectively. The dam toes move 0.38 and 0.55 feet respectively in the downstream direction. In both these cases, computations show that as excess pore water pressure dissipates in the liquefied stratum, water seeps upward causing the overlying, dense, soil layer to liquefy after the end of the shaking.

The finite element method is a valuable tool for examining the affect of different geometry and soil properties on the seismic response of earth dams. Although this method cannot predict the presence of some phenomena that occur during earthquakes, such as sand boils

or pockets of water developing between soil strata, it can show deformations and pore water pressures which indicate the seismic stability of earth dams.

REFERENCES

Hughes, T.J.R., Pister, K.S., and Taylor, R.L. (1979) "Implicit-Explicit Finite Elements in Nonlinear Transient Analysis," *Comp. Method Appl. Mech. Engr.*, 17/18, pp. 159-182.

Prevost, J.H. (1985) "A simple plasticity theory for frictional cohesionless soils," *Soil Dynamics and Earthquake Engineering,* Vol. 4, No. 1.

Prevost, J.H. (1987) *DYNAFLOW: A Nonlinear Transient Finite Element Analysis Program*, Report 81-SM-1, Dept. of Civil Engineering, Princeton University, Princeton, N.J.

	Layer (dense) 1.4	Layer (loose) 2.5	Layer (dense) 3.6
Case	12 ft	12 ft	24 ft
Case	12 ft	24 ft	12 ft
Case	12 ft	36 ft	0 ft
Case	Laver 1.2.3 and 4.5.6 dense laver 48		

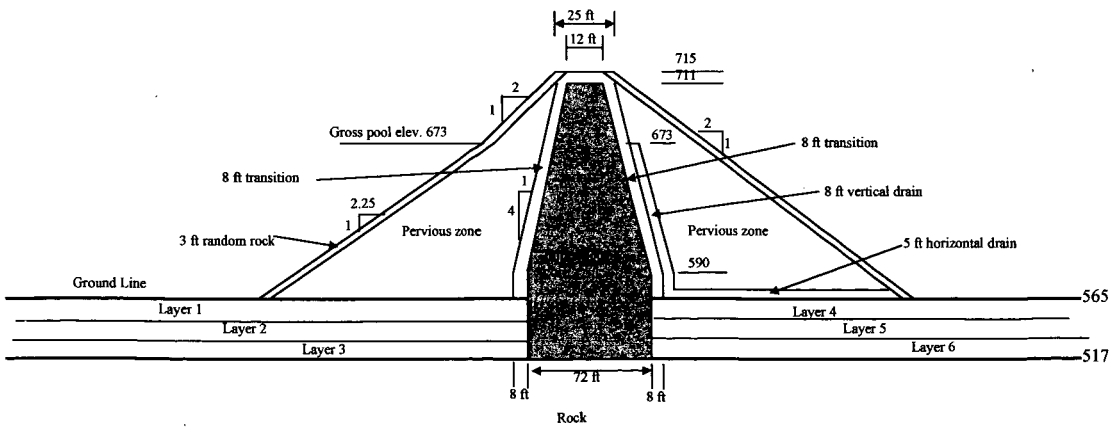


Figure 1. Idealized Dam

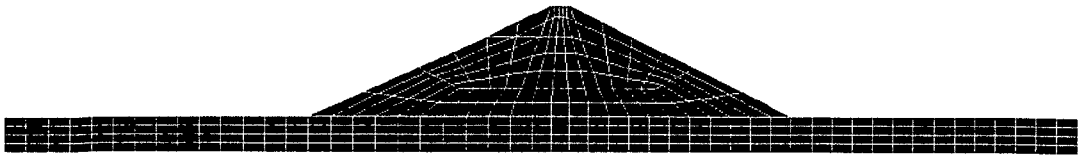


Figure 2. Finite Element Mesh

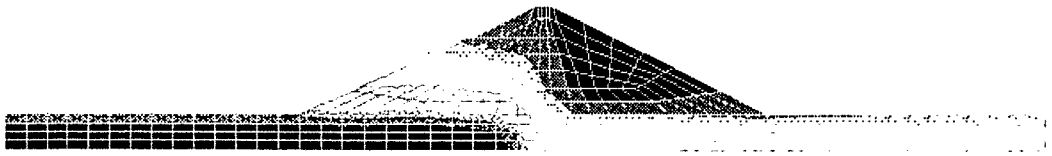


Figure 3. Initial Pore Water Pressure Distribution

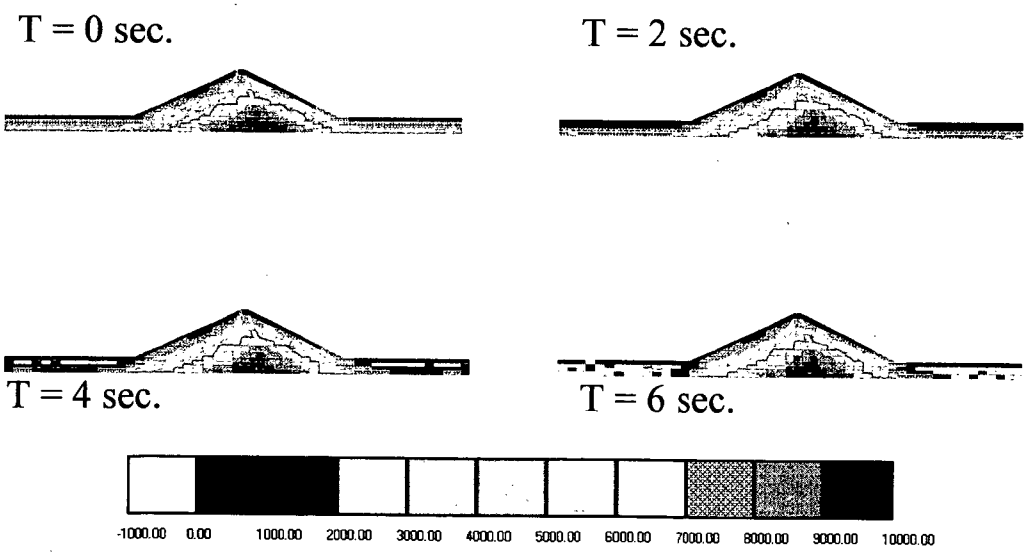


Figure 4. Contours of Mean Effective Pressure, Case III

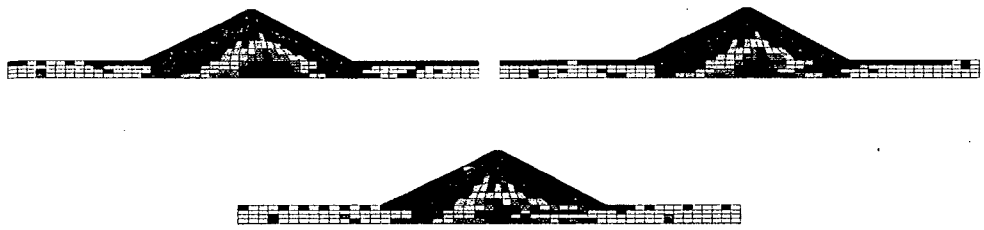


Figure 5. Contours of Mean Effective Pressure, Case III

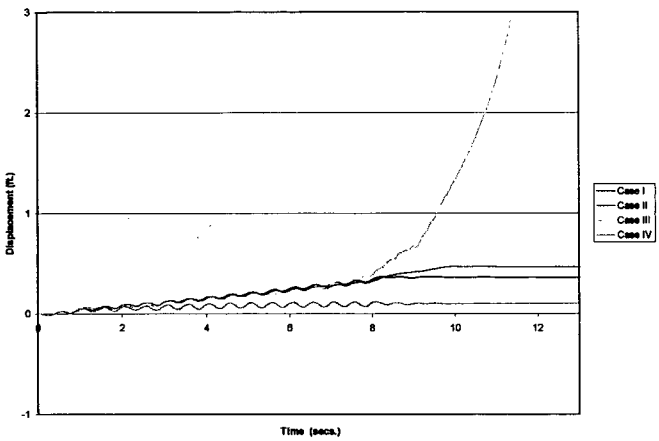


Figure 6. Horizontal Displacement of Downstream Toe

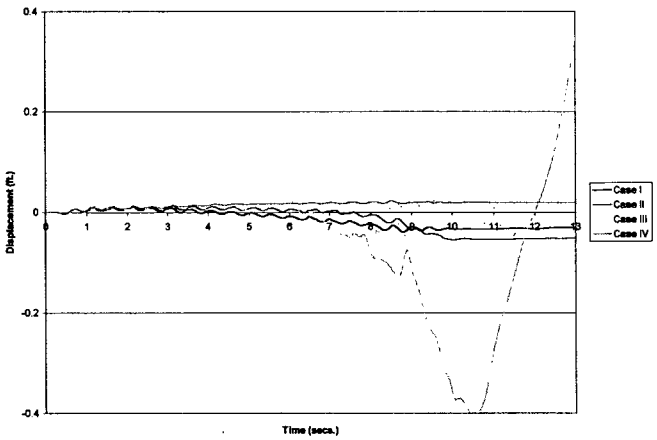


Figure 7. Vertical Displacement of Downstream Toe

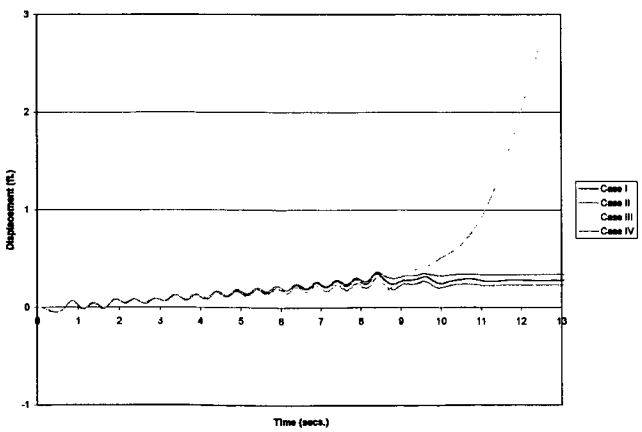


Figure 8. Horizontal Displacement of Crest

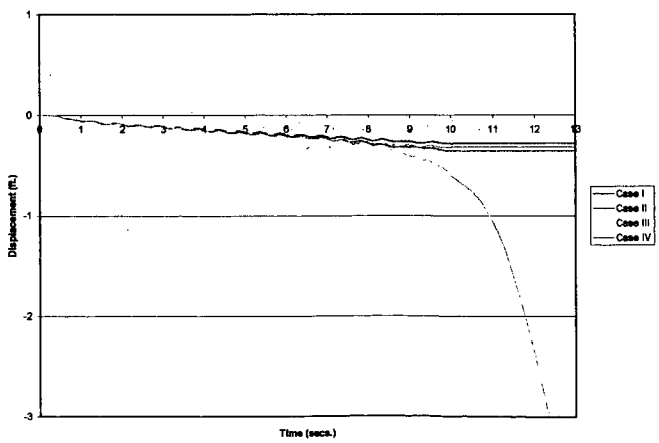


Figure 9. Vertical Displacement of Crest

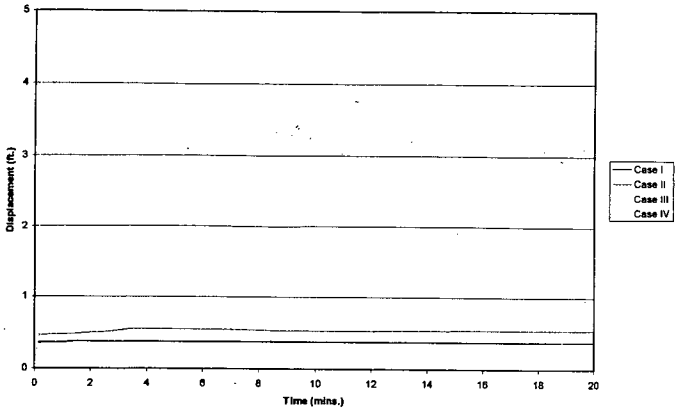


Figure 10. Long-term Horizontal Displacement of Downstream Toe

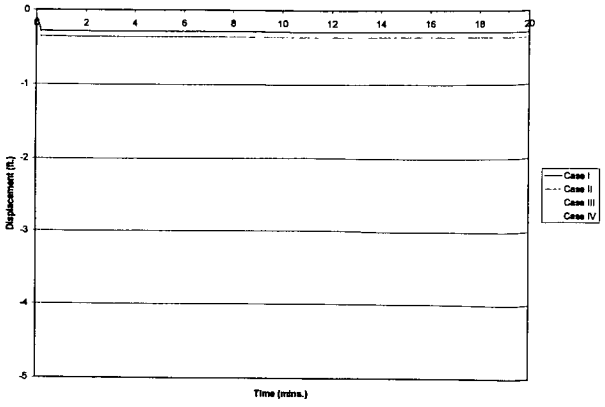


Figure 11. Long-term Vertical Displacement of Crest

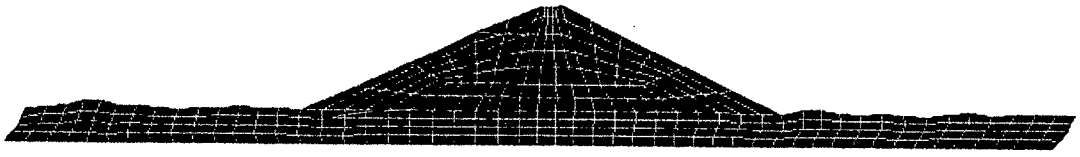


Figure 12. Deformed Mesh at Time 10 Seconds, Case III



Figure 13. Deformed Mesh at Time 13 Seconds, Case III

Technical Session 6

Concrete Dams (3)

An Investigation on the Radiation Damping of Dam–Foundation System

by

Yoshiaki ARIGA[1], Zengyan CAO[2], Masatoshi YOSHIDA[3] and Hiroyuki WATANABE[4]

ABSTRACT

The radiation damping of foundation in the dynamic analysis of dam - foundation system, have been investigated with a FE-FD hybrid analytic method which has a excellent energy absorbing function at the artificial FE boundaries. Examination of frequency response functions of acceleration shows that the energy embarrassed in the vibrating system, when radiation damping is not considered, decreases with the increment of foundation stiffness and increases with the increment of foundation density. An estimation method of the equivalent radiation damping factor has been given, with which the dynamic responses of dams could be predicated with considerable accuracy.

Key Words: *Radiation Damping, Dam Foundation System, 3-D Dynamic Analysis, Stiffness, Density Frequency Response Function*

1. INTRODUCTION

It is well known that in the dynamic analysis of finite element method, radiation damping has remarkable effects on the responses of dam – foundation system. In order to eliminate the effect of energy reflection at FE boundaries, radiation damping is usually taken into account by introducing a damping parameter as that of the material damping. However, it is not clear that how to determine such parameter, what relationship exist between this parameter and the material properties such as stiffness, density etc.

Recently, for solving the problem in the dynamic analysis of infinite media, viscous boundaries which absorbs energy at boundaries,[1][2] and boundary element method etc.[3] have been developed and applied in numerical analysis of the coupled dam – foundation system. It has been reported that with such methods reasonable solutions have been got. But for practice, especially in the phase of dam design, replacing the mentioned methods a simple and applicable way for taking the effect of the radiation damping into account is preferable.

Replying to such need, the behavior of the radiation damping in the dam – foundation system is investigated, and a simple predication method for evaluating the effect of radiation damping is presented in the study.

2. METHOD

A 3-D dynamic and static analytic program "UNIVERSE" [4] is used in the study. With this program, the energy radiating form the inner

1) Advisor, Engineering Research Institute, Electric Power Development Co., Ltd.
2) Ph.D., Senior research engineer, Scientific System Department, Kaihatsu Computing Service Center Ltd.
3) Assistant manager, Scientific System Department, Kaihatsu Computing Service Center Ltd.
4) Dr. Eng., Professor, Department of Civil and Environment Engineering., Saitama University.

part of the analyzed domain can be absorbed fully at the boundaries around the foundation and the effects of the free field vibration motion on the response of dam – foundation system can be taken into account at the same time. This coupled system is expressed in the following equation.

$$\begin{cases} \begin{bmatrix} M_d & M_{df} \\ M_{fd} & M_f \end{bmatrix} \begin{Bmatrix} \ddot{u}_d \\ \ddot{u}_f \end{Bmatrix} + \begin{bmatrix} C_d & C_{df} \\ C_{fd} & C_f^* \end{bmatrix} \begin{Bmatrix} \dot{u}_d \\ \dot{u}_f \end{Bmatrix} + \\ \qquad \begin{bmatrix} K_d & K_{df} \\ K_{fd} & K_f \end{bmatrix} \begin{Bmatrix} u_d \\ u_f \end{Bmatrix} = \begin{Bmatrix} F_w \\ T_f \end{Bmatrix} \quad (1.1) \\ \left[M_g\right]\left\{\ddot{u}_g\right\} + \left[C_g\right]\left\{\dot{u}_g\right\} + \left[K_g\right]\left\{u_g\right\} = \left\{T_b\right\} \quad (1.2) \end{cases}$$

Here, form (1.1) and (1.2) are the motion equation of the dam - foundation and that of the free field around the foundation. The variables of the equations are:

- Φ : Velocity potential function
- x, y, z : Cartesian coordinates
- t : Time
- C_0 : Sound velocity in water ($\fallingdotseq 1440\ m/s$)
- M, C, K : Mass, damping, stiffness matrix, and the footnotes d, df (fd), f and g mean that the matrix belongs to the dam, the junction of dam and foundation, foundation, and free field respectively.
- C_f^* : Damping matrix (including the components of the material damping and that of the viscous boundaries, please refer equation 2)
- $u,\ \dot{u},\ \ddot{u}$: Displacement, velocity and acceleration vectors
- F_w : Hydrodynamic pressure acting on the upstream surface of the dam
- T_f : Earthquake load and the inflow of energy resulted from the motion of the free field
- T_b : Earthquake input of the free field

The detail of the above matrices is explained in the reference [2][4].

The matrix C_f^* of equation (1.2) is of the following form

$$C_f^* = C_f + C_v \quad (2)$$

Here, C_f is the component of the material damping of foundation and C_v is the damping component of viscous boundaries around the foundation. The viscous boundary matrix C_v is derived based on the principle of virtual work.[2] It has been proved that at such boundaries energy propagating from the inner part of the foundation will be absorbed fully. At same time, the effect of the free field motion to the response of inner domain (dam–foundation) is taken into account with the vector of T_f. Therefore the energy giving and receiving between inner domain and outer domain (free field) is considered in such system.

In order to investigate the energy radiation behavior of the dam – foundation system, the energy confined in the system is examined by comparing the responses of the following two cases. One is that of the viscous boundary and the other is that of no such boundary (please refer Fig.1). In the two cases the energy inflow from the free field is considered, and the earthquake is inputted from the rock surface (bottom of foundation).

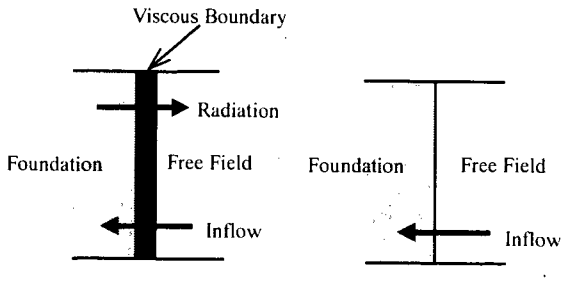


Fig.1 Model for evaluating radiation damping of dam – foundation system

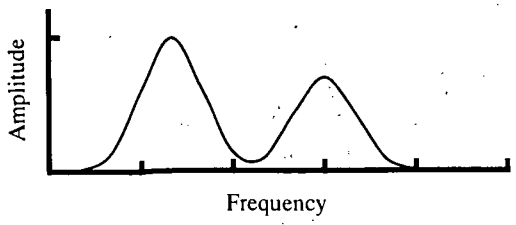


Fig.2 Radiation damping is evaluated by the examining the variation of frequency response functions

The following method is used for investigating the variation of the energy confined in the system.

As well known, frequency response function is an kind of expression of the energy existing in the vibrating system. Hence, the comparison of the area (please refer Fig.2) formed by the coordinate axes and the response curve is to be done between the two cases mentioned in the above paragraph. The area ratio μ expressed by the following equation (3) is taken as a measurement for the comparison. It is thought that a larger value of the μ means that, if radiation damping is not considered, the effect of the energy reflection problem on the response of dam – foundation system is larger.

$$\mu = \frac{S_0}{S_r} = \int_0^F A_0(f)df \Big/ \int_0^F A_r(f)df \qquad (3)$$

Here, A_r, A_0 is the frequency response function of the case where radiation damping is taken into account and that of the case without this consideration respectively. F is the maximum interested frequency.

It is also known that radiation damping is dependent on the natural vibration mode. But for the dynamic analysis of time domain, a problem, i.e., which mode should be selected as the representative one to give an estimation on the radiation damping, is difficult to determine. In the way proposed in the paper, since the evaluation on the radiation damping is based on the total dimension of frequency response functions, it could be thought that the evaluation result will be independent on any special frequency, and convenient to be applied in time domain analysis.

3. ANALYTIC MODEL

A concrete gravity dam coupled with foundation and reservoir is taken as the object model. Its maximum height is 60 m, and the maximum length of its top is 160 m. Since free field is enclosed in the analytic model, the foundation is modeled in a relatively small domain where the interaction between dam and foundation occurs (please refer Fig.3).

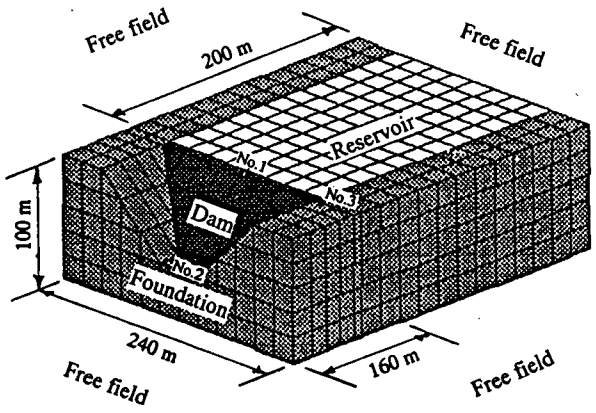


Fig.3 Analytic model of dam - foundation - reservoir system

In this model the free field in the stream direction is modeled in the same shape as the valley, and in the direction of dam axis is of the stratiform shape.

The reservoir is of a depth 60 m, and a length 200 m.

The dam - foundation system is dispersed into 406 elements with total 1132 nodes. The reservoir is dispersed with 312 FD grids.

It is supposed that the dam concrete and foundation rock are of linear elastic properties. The properties of the foundation are adjusted in order to investigate the effect of material properties on the radiation damping behavior. But for all of the cases, the material properties of the dam are fixed at the following values:

Yang's Modulus E=16000 N/mm^2
Density ρ =2.4 g/cm^3
Poison Ratio ν =0.167
Damping Factor h=5%

The material properties of foundation and free field are adjusted in the following way. When the density is fixed to be 2.4 g/cm^3, the Yang's modulus is adjusted with the values shown in Table-1. And when the Yang's modulus is fixed to be 24000 N/mm^2, the density is adjusted to be the values shown in Table-2. For all of the cases the Poison ratio is set to be 0.15. In order to eliminate the effect of the material damping on the response of the system the material damping factor of the foundation and free field is supposed to be 0.0%.

Table-1 Yang's Modulus of foundation & free field for investigating the relationship of stiffness - radiation damping (N/mm^2)

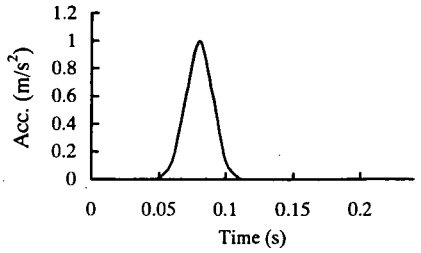
Case1	Case2	Case3	Case4
8000.0	16000.0	24000.0	32000.0

Case5	Case6	Case7	Case8
48000.0	64000.0	80000.0	160000.

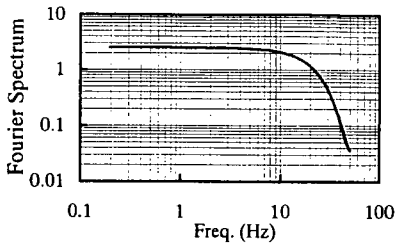
Table-2 Density of foundation & free field for investigating the relationship of density - radiation damping (g/cm^3)

Case 1	Case 2	Case 3	Case 4	Case 5	Case 6
0.0	1.0	2.0	2.4	3.0	4.0

Gauss Pulse of the maximum amplitude 1 m/s^2 is applied as the earthquake motion. As shown in Fig.4, in the frequency domain until 16 Hz (around the third natural frequency of the dam - foundation system), the Fourier spectrum of the wave is almost float. It is expected within this frequency domain the response of the system can be analyzed with high accuracy and the result will be independent on frequency. The length of the pulse is 5.12 sec., and the time interval for the time domain calculation is 0.01 sec.



(a) Gauss Pulse



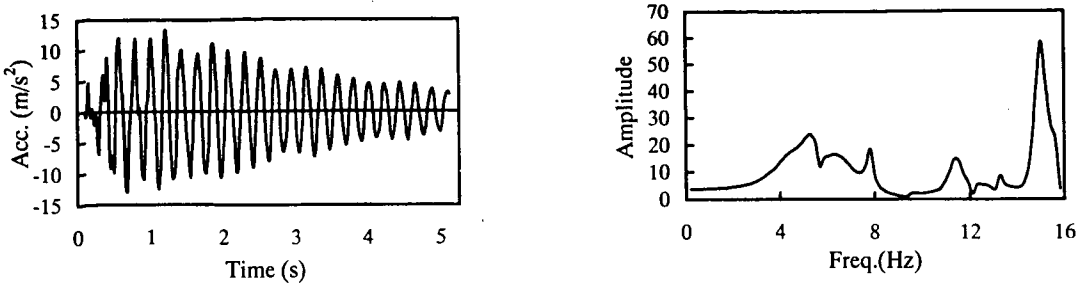
(b) Spectrum of Gauss Pulse

Fig.4 Input wave used for the investigation

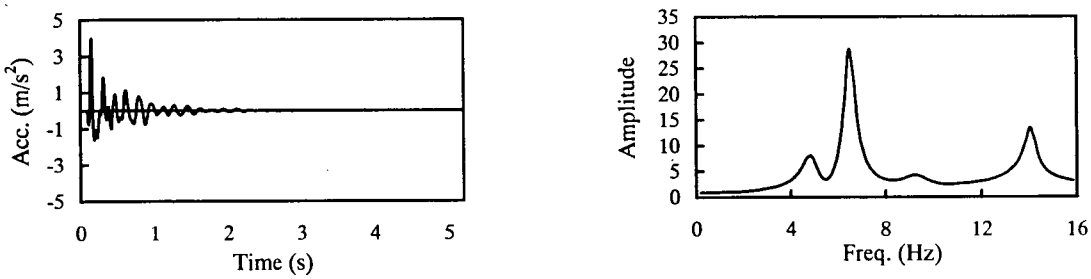
4. RELATIONSHIP BETWEEN STIFFNESS, DENSITY AND RADIATION DAMPING

The energy confined in the dam - foundation system will varies with the alteration of the stiffness and density of the foundation. This phenomenon is examined at some selected positions (shown in Fig.1).

The acceleration response and the acceleration transfer function from the dam toe to the top are examined. Fig.5 shows the comparison between the case where radiation damping is simulated by applying the viscous boundary condition and the case where the radiation damping is not considered.

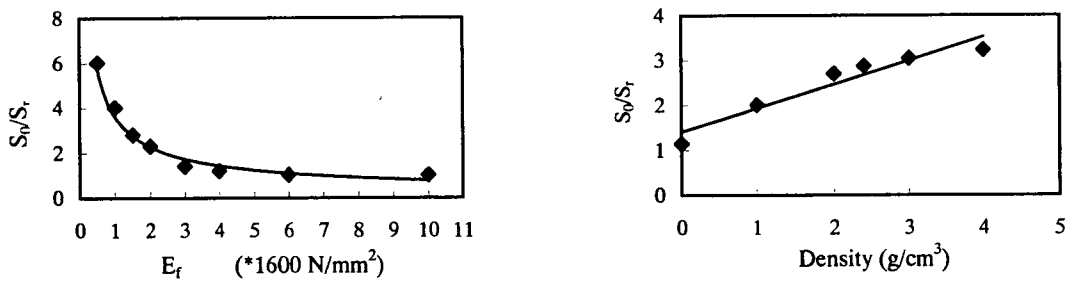


(a) Without viscous boundaries

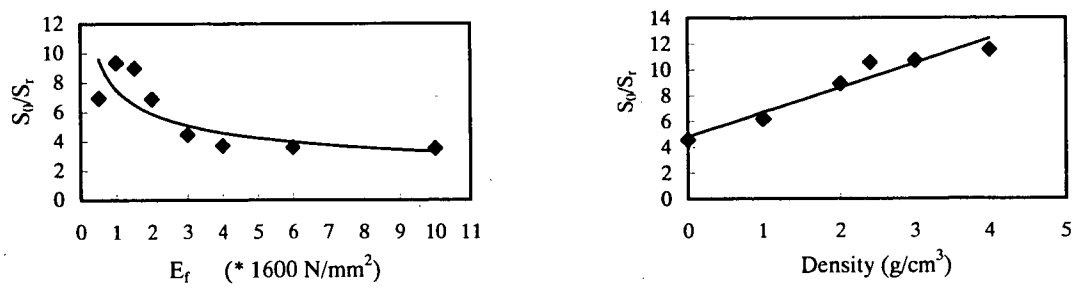


(b) With viscous boundaries

Fig.5 Comparison of the dam responses between the cases whether radiation damping is considered or not



(a) At Point No.2



(b) At Point No.3

Fig.6 Relationship of stiffness - S_0/S_r and that of density - S_0/S_r

E_f : Yang's modulus of foundation E_d : Yang's modulus of dam

S_0/S_r : (S_r and S_0 are the dimension of the frequency response function when radiation damping is considered and that when this is not considered respectively)

It is clear that the responses of the system are absolutely different whether the radiation damping is considered or not. Here, taking the point No.2 and No.3 of Fig.1 as example, the relationship between the ratio μ (S_0/S_r, S_r and S_0 are the area of the frequency response function when radiation damping is considered and that when this damping is not considered respectively) and the material properties shown in Table-1 and Table-2 is plotted in Fig.6.

From Fig.6 followings can be found.

1). With the stiffness of the foundation increases, the energy confined in the system gets less. Except the cases where the foundation stiffness is extremely low, the amount of the energy confined in the system (assumed to be Ω') can be expressed as a function of Yang's modulus as below.

$$\Omega' \propto C_1' \cdot e^{-C_2' \cdot E_f} \tag{4}$$

Here, C_1', C_2' are the unknown parameters which could been determined by experiment. Equation (4) means that the amount of energy which should be disembarrassed to the half infinite free field gets less exponentially with the increment of Yang's modulus of the foundation.

2). The larger the density of the foundation, the more the energy confined in the system. The relationship between the amount Ω'' and the foundation density ρ can be expressed approximately with a linear form.

$$\Omega'' \propto C_3'' \cdot \rho \tag{5}$$

Here C_3'' is an unknown parameter and which also could be determined by experiment .

Synthesizing equation (4) and equation (5), we can get a general expression on the relationship between the material properties of the foundation and the energy which should been disembarrassed to the half infinite free field in the following form.

$$\Omega \propto \left(C_1 \cdot e^{-C_2 \cdot E_f} + C_3 \cdot \rho \right) \tag{6}$$

5. ESTIMATION OF RADIATION DAMPING

In the ordinary dynamic FE analysis where no viscous boundary or other energy absorbing condition is applied, a radiation damping factor h_r can be introduced in order to disembarrass the energy Ω through the artificial boundaries. Therefore, h_r should directly proportionate to the Ω expressed in the equation (6).

It is thought that h_r should be, except the dependence on the material properties, a function of ground motion intensity, and have an uneven distribution along the direction of depth. But for conciseness, here it is assumed that h_r depends on material properties only, and has a linear relationship with Ω. Then h_r can be expressed as

$$h_r = \alpha_1 \cdot e^{-\alpha_2 \cdot E_f} + \alpha_3 \cdot \rho + \alpha_4 \tag{7}$$

Here, $\alpha_i \ (i = 1,\cdots,4)$ are the unknown parameters, and they could been determined by experiments.

With the material properties shown in Table-1 and Table-2, comparison analyses are done between the following two conditions. One is that where viscous boundaries are applied, and the other is that where replacing the viscous boundary, the radiation damping factor h_r is introduced and its value is adjusted in order to get equivalent result as that of the former condition. In this way, a series of data concerning the material properties and the factor h_r has been obtained. Based on such data the parameters $\alpha_i \ (i = 1,\cdots,4)$ of the equation (7) have been determined tentatively. Then the equation (7) can be rewritten as

$$h_r = 67.2e^{-12.0\times10^{-5} E_f} + 2.3\rho + 3.8 \tag{8}$$

Here the units of E_f and ρ are N/mm^2 and g/cm^3 respectively, and h_r is expressed in percentage.

It should be noticed that equation (8) is introduced from the analysis of concrete dams. And hence attention should be paid on its application.

6. APPLICATION ON THE EARTHQUAKE RESPONSE ANALYSIS OF A REAL DAM

In order to test the validity of the equation (8) introduced in the above paragraph, it is applied to the analysis of a real concrete gravity dam [6]. It is thought that if the equation (8) is adequate, the analytic result got with the radiation damping factor h_r should be consistent with that got with the viscous boundary conditions.

The maximum section and the upstream surface of the dam are shown in Fig.7. The dimensions of the foundation are as followings.

Length in stream direction = dam height
Depth = 0.5 dam height
Width in axial direction = 0.5 dam height

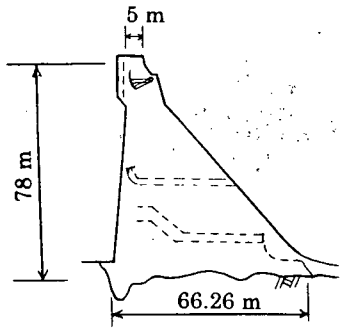
Table-4 Material properties of dam and foundation

	G N/mm^2	ρ g/cm^3	ν	h
Dam	28000	2.4	0.167	5%
Foundation Free Field	50000	2.6	0.2	3%

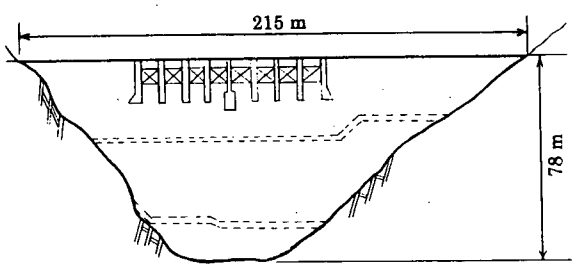
The material properties of the dam and foundation (shown in Table-4) are obtained from the dam site experiment.

The earthquake wave of EL-Centro NS is used as the ground motion, but its maximum amplitude is adjusted to be 1 m/s^2. The ground motion lasts 10.24 sec., and the time interval of the history data is 0.01 sec.

As mentioned above, two cases are analyzed. One is that of viscous boundary, and the other is that of no viscous boundary but the radiation damping factor determined from equation (8) is applied.



(a) Maximum section



(b) Upstream surface

Fig.7 The maximum section and upstream surface of a real dam

The acceleration response and the Fourier spectrum of the selected points (the middle of the dam top and the bottom of the dam) are shown in Fig.8.

Comparing the acceleration response histories, we can find that the maximum differences are no more than 10% and 5% at the middle of the dam top and the bottom of the dam respectively. But generally, the time histories got in the two ways are consistent with each other. On the other hand, the spectrum ratio between the middle of the dam top and the dam bottom, and that between the dam bottom and the rock surface are also generally similar to each other between the mentioned two cases.

From above test it has been known that equation (8) can give a good predication on the radiation damping factor, and with this factor

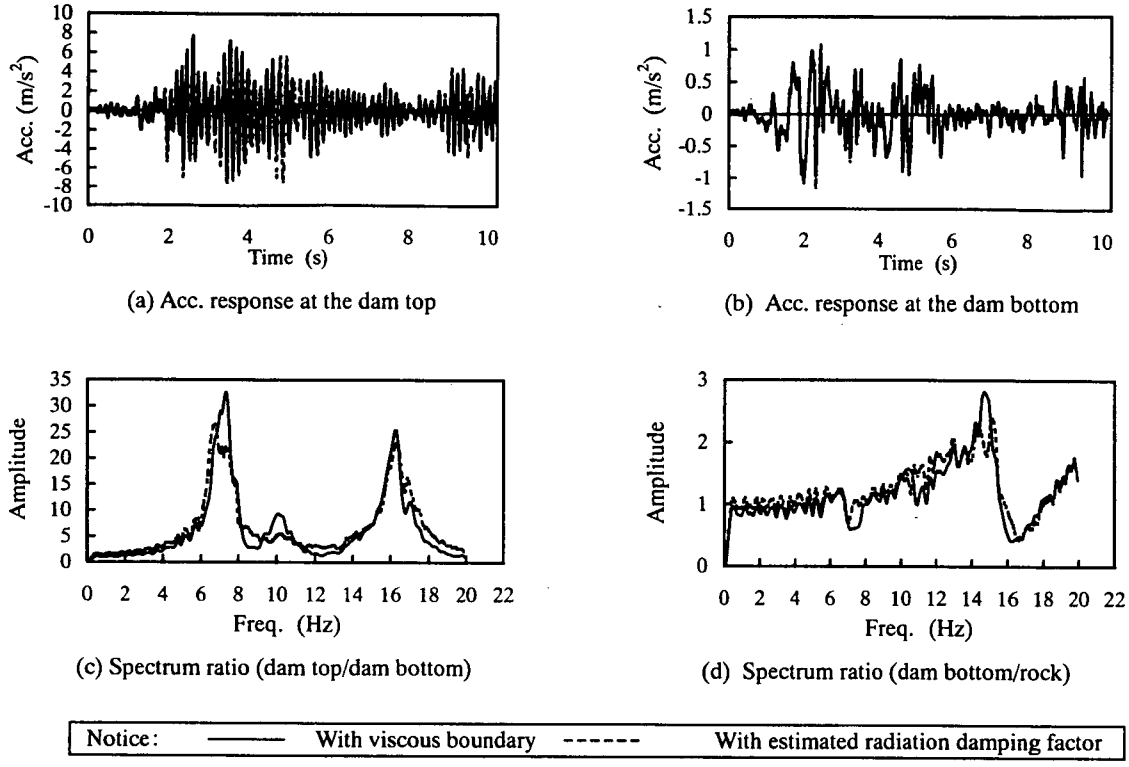


Fig.8 Comparison between the results got with viscous boundary and those got with radiation damping factor

the dynamic analysis can be done with an acceptable error even though viscous boundary is not applied.

As a further research topic, the validity of the presupposition for introducing equation (8) should be examined with more sampling analysis and dam site experiments. It is necessary to modify equation (8) by applying it to the analyses of more real dams in order to estimate the radiation damping factor, and further more for give a predication on the dam response with higher accuracy.

7. CONCLUSION

With the method proposed in the study, i.e., by examining the variation of the frequency response function, the radiation damping behavior of the concrete dam - foundation system has been generally understood. When radiation damping is not considered in a dynamic analysis, the energy confined in the system decreases as the foundation stiffness gets greater. And this amount increases as the density of the foundation gets larger.

By introducing a radiation damping factor determined with the proposed equation (8) in the study it is possible to get an accurate predication on the earthquake response of the dam - foundation system even in the case where no viscous boundary or other energy disembarrassing condition is available.

As a further research topic, the dependence of the radiation damping factor on the ground motion intensity, the radiation behavior in the soft foundation like that of fill dams should be investigated. And it is necessary to modify the

predication equation proposed in the study with more data of real dams.

REFERENCES

1) Hiroyuki Watanabe and Zengyan Cao: Upstream Boundary of Reservoir in Dynamic Analysis, Journal of Engineering Mechanics, ASCE, Vol.124, pg.468-470, April 1998
2) Fusanori Miura and Hiroshi Okinaka: Dynamic Analysis Method for 3-D Soil – Structure Interaction Systems With the Viscous Boundary Based on the Principle of Virtual Work, Journal of JSCE, Vol.404, April, 1989
3) John P. Wolf and Chongmin Song: Finite-Element Modelling of Unbounded Media, Proceedings 11th World Conference on Earthquake Engineering, Acapulco, Mexico, June, 1996
4) Electric Power Development Co., Ltd.: "UNIVERSE" - A Program for the 3-D Dynamic and Static Analysis of Dams, (Research report, February, 1999)
5) Tadashi Hatano and Tomoyasu Nakagawa: Seismic Analysis of Arch Dams, Journal of JSCE, Vol.207, November, 1972
6) Tadashi Hatano, Tadashi Takahashi and Hajime Tsutsumi: Vibration Tests and Their Studies on Tsukabaru Gravity Dam, Journal of JSCE, No.59, pg.133-140, Nov., 1958

A 3-D FE–BE Method for Dynamic Response Analysis of Dam–Foundation–Reservoir Systems

by

Shojiro KATAOKA[1)]

ABSTRACT

A simulation method is developed for dynamic response of 3-D dam–foundation–reservoir systems. The dam is modeled with finite elements; while the foundation and reservoir are modeled with boundary elements. Interaction effects and radiation conditions can be taken into account without any geometric restriction such as uniformity of the cross section of the canyon. Responses of a 3-D arch dam interacted with foundation to harmonic ground motions are simulated by the present method. The validity of the present method and effects of nonuniform seismic input are discussed based on the computed responses.

Keywords: *3-D FE–BE method, dam–foundation–reservoir system, dynamic response analysis, nonuniform seismic input.*

1. INTRODUCTION

Dynamic interaction may have significant effects on earthquake response of dam-foundation-reservoir systems (Ohmachi and Kataoka, 1996). Recent progress in computer technology and numerical analyses enables us to evaluate more precisely than ever the dynamic interaction effects by using FEM (Fok and Chopra, 1986), BEM (Dominguez and Maeso, 1993), or their hybrid method called FE-BE method (Touhei and Ohmachi, 1993; Tan and Chopra, 1995). Among other methods, the FE-BE method seems most effective in dynamic response analysis of a dam interacted with foundation and reservoir. The method is advantageous to taking into account all the effects not only of dam-foundation, dam-reservoir and reservoir-foundation interactions, but of radiation damping of both elastdynamic and hydrodynamic waves.

Touhei and Ohmachi (1993) formulated a 2-D FE–BE method in time domain and performed impulsive response analyses of a dam–foundation–reservoir system. The weighted residual procedure was employed to couple several equations of motion for solid and fluid in their formulation.

Tan and Chopra (1995) developed a 3-D FE–BE method under the assumption that the canyon is infinitely long with an arbitrary but uniform cross-section. They investigated the effects of dam–foundation interaction using a wide range of parameters characterizing the properties of the dam, foundation, impounded water and reservoir boundary materials. However, the earthquake input was assumed to be uniform over the dam–foundation interface in their study though it is expected to vary significantly (Nowak and Hall, 1990).

In this paper, a 3-D FE-BE method for dam–foundation–reservoir systems with arbitrary shape is formulated and applied to dynamic response analyses of an arch dam–foundation system subjected to harmonic ground motion. The computed responses are presented to show the effects of nonuniform seismic input on the response of the dam. Studies on the effects of shape of the canyon and impounded water are forthcoming.

1) Dr. Eng., Research Engineer, Ground Vibration Division, Public Works Research Institute, Tsukuba, Japan

2. FORMULATION

Let us consider a dam-foundation-reservoir system as shown in Fig. 1. Both the dam and semi-infinite foundation are assumed to be elastic bodies of isotropic homogeneity, and the reservoir water compressible and non-viscous. However, since the dam body is modeled with finite elements, its heterogeneity can be easily taken into account, if necessary. Further, the responses of the system are assumed to be linear and analyzed in frequency domain. In the following formulation, subscripts $_{\mathrm{d}}$, $_{\mathrm{f}}$ and $_{\mathrm{r}}$ of matrices and vectors denote the corresponding domains, dam, foundation and reservoir, respectively.

2.1 FEM for dam

If a steady-state wave propagation is assumed and body forces except inertia forces are negligible, equation of motion for 3-D wave field is specified by

$$(\lambda+\mu)u_{j,ij}+\mu u_{i,jj}+\rho\omega^2 u_i=0 \quad (1)$$

where u_i denotes x_i-component of the displacement in x_1-x_2-x_3 Cartesian coordinate, λ and μ are Lame's constants, ρ and ω are mass density and angular frequency. The subscripts with comma, such as $_{,j}$, denote partial differentiation: $u_{i,j}=\partial u_i/\partial x_j$, and the summation convention is used for brevity.

By discretizing the dam in Fig. 1 into a set of finite elements, Eq. (1) can be written in the following form:

$$[Z_{\mathrm{d}}]\{u_{\mathrm{d}}\}=\{f_{\mathrm{d}}\}, \quad (2)$$

where $\{u\}$ and $\{f\}$ are the nodal displacement and nodal force vectors, respectively. If internal damping in dam body is considered, the matrix $[Z]$ can be written as

$$[Z_{\mathrm{d}}]=-\omega^2[M_{\mathrm{d}}]+i\omega[C_{\mathrm{d}}]+[K_{\mathrm{d}}], \quad (3)$$

where $[M]$, $[C]$ and $[K]$ are the global mass, damping and stiffness matrices, respectively, and $i=\sqrt{-1}$.

2.2 BEM for foundation

The boundary integral equation on the boundary Γ_{f} of the foundation in Fig. 1 is expressed as follows:

$$\begin{aligned} &c_{ij}(\boldsymbol{x})u_j(\boldsymbol{x}) \\ &+\int_{\Gamma_{\mathrm{f}}} T_{ij}(\boldsymbol{x},\boldsymbol{y})u_j(\boldsymbol{y})d\Gamma(\boldsymbol{y}) \\ &-\int_{\Gamma_{\mathrm{f}}} U_{ij}(\boldsymbol{x},\boldsymbol{y})\tau_j(\boldsymbol{y})d\Gamma(\boldsymbol{y})=\bar{\psi}_i(\boldsymbol{x}), \end{aligned} \quad (4)$$

where τ_i denotes traction, U_{ij} the fundamental solution, T_{ij} its traction, $\boldsymbol{y}$ and $\boldsymbol{x}$ source and field points, c_{ij} free-term which depends on the boundary shape at $\boldsymbol{y}$, respectively, and $\bar{\psi}_i$ represents effects of the incident wave. The first integral on the left-hand side is to be interpreted in the sense of Cauchy principal value. The full-space Green's functions are employed as the fundamental solutions.

By discretizing the boundary Γ_{f} into a set of boundary elements, Eq. (4) can be written in a matrix form as:

$$[H_{\mathrm{f}}]\{u_{\mathrm{f}}\}-[G_{\mathrm{f}}]\{\tau_{\mathrm{f}}\}=\{\bar{\psi}\}. \quad (5)$$

2.3 BEM for reservoir

Similarly, if the impounded water in the reservoir is assumed compressible, the boundary integral equation on the boundary Γ_{r} can be written as:

$$\begin{aligned} &\frac{\chi(\boldsymbol{x})}{4\pi}p(\boldsymbol{x})-\int_{\Gamma_{\mathrm{r}}} Q(\boldsymbol{x},\boldsymbol{y})p(\boldsymbol{y})d\Gamma(\boldsymbol{y}) \\ &+\int_{\Gamma_{\mathrm{r}}} P(\boldsymbol{x},\boldsymbol{y})q(\boldsymbol{y})d\Gamma(\boldsymbol{y})=0, \end{aligned} \quad (6)$$

where χ denotes solid angle at $\boldsymbol{x}$, p water pressure, q gradient of p in the direction inward normal to Γ_{r}: $q=\partial p/\partial n$, respectively. P and Q are the fundamental solutions of water pressure and its gradient. The half-space fundamental solutions are employed to reduce computational task (Tsai and Lee, 1987).

By discretizing the boundary Γ_{r} into a

set of boundary elements, the following matrix equation can be obtained.

$$[H_r]\{p_r\} - [G_r]\{q_r\} = 0 \tag{7}$$

2.4 Boundary conditions

Continuity and equilibrium conditions along the boundary between the dam and foundation, Γ_B, require that

$$\begin{aligned} \{u_d\} &= \{u_f\}, \\ \{f_d\} &= -[D_f]\{\tau_f\}. \end{aligned} \tag{8}$$

The distribution matrix $[D_f]$ depends on the type of interpolation functions.

Similarly, the following boundary conditions must be satisfied along the boundary between the reservoir and the solid (dam and foundation) domains, Γ_I:

$$\begin{aligned} \{f\} &= -[\Lambda]\{p\}, \\ [D_r]\{q\} &= \omega^2 \rho_h E_v [\Lambda]^T \{u\}, \end{aligned} \tag{9}$$

where $[D_r]$ denotes distribution matrix for reservoir, ρ_h and E_v are water mass density and bulk modulus, respectively. $[\Lambda]$ is defined as:

$$[\Lambda] = \int_{\Gamma_I} [\Phi]^T \vec{n} [\Psi] d\Gamma, \tag{10}$$

where $[\Phi]$ and $[\Psi]$ are interpolation matrices for solid and reservoir, and $\vec{n}$ denotes a normal vector inward of reservoir domain, i.e., outward of solid domain.

2.5 Unified matrix equation

The dynamic response analysis of the dam-foundation-reservoir system by the 3-D FE-BE method can be carried out by solving Eq. (2), (5), (7), (8) and (9) simultaneously. The unified matrix equation is derived as follows:

$$\begin{bmatrix} Z_d + L_f & \Lambda \\ -\omega^2 \rho_h E_v \Lambda^T & L_r \end{bmatrix} \begin{Bmatrix} u \\ p \end{Bmatrix} = \begin{Bmatrix} \bar{\phi} \\ 0 \end{Bmatrix}, \tag{11}$$

where

$$\begin{aligned} [L_f] &= [D_f][G_f]^{-1}[H_f], \\ [L_r] &= [D_r][G_r]^{-1}[H_r], \\ \{\bar{\phi}\} &= [D_f][G_f]^{-1}\{\bar{\psi}\}. \end{aligned} \tag{12}$$

The matrix equation for systems without solid–fluid interaction can be obtained by assuming $[\Lambda] = [0]$:

$$\begin{aligned} [Z_d + L_f]\{u\} &= \{\bar{\phi}\}, \\ \{p\} &= \{0\}. \end{aligned} \tag{13}$$

3. EXAMPLE ANALYSIS OF AN ARCH DAM

3.1 Modeling the Morrow Point Dam

A series of dynamic response analyses has been carried out by the present method to demonstrate its validity and effects of nonuniform seismic input. A simple model of the Morrow Point Dam (142m high) is constructed referring to Tan and Chopra (1995), as shown in Fig. 2. Since the dam–foundation system is symmetric, only its half is shown in the figure.

The finite elements for the dam are solid ones with quadratic interpolation functions except its interface with the foundation, which is interpolated with linear functions because linear boundary elements are employed for the foundation. Grid spacings are about 15 m for both dam and foundation. The foundation model has almost uniform cross-section though the upstream and downstream cross-sections are slightly different from each other because the upstream face of the dam is wider than the downstream face.

Table 1 shows material properties assigned to each domain after Tan and Chopra (1995). Viscous damping of 5 % (damping ratio $h = 0.05$) is considered for both dam and foundation domains by using complex S wave velocity $\hat{v_S}$:

$$\hat{v_S} = \frac{v_S}{1 - ih}. \tag{14}$$

3.2 Comparison with a previous study

Results presented in Fig. 3 are radial acceleration responses of the dam to harmonic ground motions of unit amplitude (frequency response functions) in the upstream, vertical, and cross-stream directions. The uniform ground motions were given, i.e. phase difference over the dam–foundation interface due to the canyon shape was neglected. The top and middle figures show the responses at point A and the bottom figure at point B in Fig. 2.

These frequency response functions are plotted against the normalized excitation frequency ω/ω_1 where ω_1 is the fundamental natural frequency of the dam supported on the rigid foundation rock; $\omega_1 = \omega_1^s$ of the symmetric mode for responses to upstream and vertical ground motions, and $\omega_1 = \omega_1^a$ of the antisymmetric mode for responses to cross-stream ground motion. When the material properties of the dam shown in Table 1 are used, ω_1^s and ω_1^a are 26.8 rad/s and 24.4 rad/s, respectively.

The solid and broken lines are the results from Tan and Chopra (1995) using standard and refined boundary element meshes of the foundation at its interface with the dam (Fig. 4). The boundary element mesh of the foundation at its interface with the dam employed for the present method, which coincides with the finite element mesh of the dam at its interface with the foundation, is also shown in Fig. 4.

The open circles, result from the present method, agree with the broken line (refined mesh) rather than the solid line (standard mesh) though the number of nodes of the boundary element mesh at the interface for the present method, 26, is the same as the standard mesh and about 1/3 of the refined mesh, 75. Since Tan and Chopra (1995) assumed a uniform canyon, which introduces incompatibility between the dam and the foundation, the impedance matrix at the nodal points of the dam at its interface with the foundation was obtained by a linear transformation from the impedance matrix at the nodal points of the foundation. This could cause the deterioration of the accuracy.

3.3 Effects of nonuniform seismic input

Fig. 5 compares frequency response functions for two different seismic inputs. Fig. 5 (a) shows those at point A and (b) shows those at point B in Fig. 2. The solid lines show the responses due to vertically incident plane S waves whose amplitude are 0.5, which become unity at free-field. The broken lines show the responses due to uniform ground motion over the dam–foundation interface, which are the same as the open circles in Fig. 3.

For both upstream and cross-stream ground motions, the acceleration responses due to vertically incident wave input are reduced below those from uniform input, in agreement with Nowak and Hall (1990). However, further investigation is needed as Nowak and Hall (1990) also examined effects of angle of incidence and found the potential for a significant increase of the response due to nonuniform seismic input.

4. CONCLUSION

In this paper, a 3-D FE–BE method has been formulated and the results obtained by the method are presented to demonstrate its applicability to dynamic response analysis of a realistic dam. The Morrow Point Dam and the foundation in its vicinity were modeled with finite elements and boundary elements, respectively, as an arch dam–foundation system.

The computed responses of the system due to uniform input showed a good agreement with the results from Tan and Chopra (1995).

The effects of nonuniform seismic input on the response of the dam were also examined but further research is required to introduce the effects into the earthquake resistant design of dams.

REFERENCES

Dominguez, J. and Maeso, O. (1993): Earthquake analysis of arch dams. II : dam-water-foundation interaction. *J. Eng. Mech.*, ASCE, 119, 513-530.

Fok, K. and Chopra, A. K. (1986): Frequency response functions for arch dams: hydrodynamic and foundation flexibility effects. *Earthq. Eng. Struct. Dyn.*, 14, 769-795.

Nowak, P. S. and Hall, J. F. (1990): Arch dam response to nonuniform seismic input. *J. Eng. Mech.*, ASCE, 116, 125-139.

Ohmachi, T. and Kataoka, S. (1996): Earthquake response of 2-D concrete gravity dam interacted with foundation and reservoir. *Proceedings of the International Symposium on Seismic and Environmental Aspects of Dams Design*, 1, 327-336.

Tan, H. and Chopra, A. K. (1995): Earthquake analysis and response of concrete arch dams. *Report No. UCB/EERC-95/07*, EERC, UC Berkeley.

Touhei, T. and Ohmachi, T. (1993): A FE-BE method for dynamic analysis of dam-foundation-reservoir systems in the time domain. *Earthq. Eng. Struct. Dyn.*, 22, 195-209.

Tsai, C. -S. and Lee, G. C. (1987): Arch dam-fluid interactions: by FEM-BEM and substructure concept. *Int. J. Numer. Methods Eng.*, 24, 2367-2388.

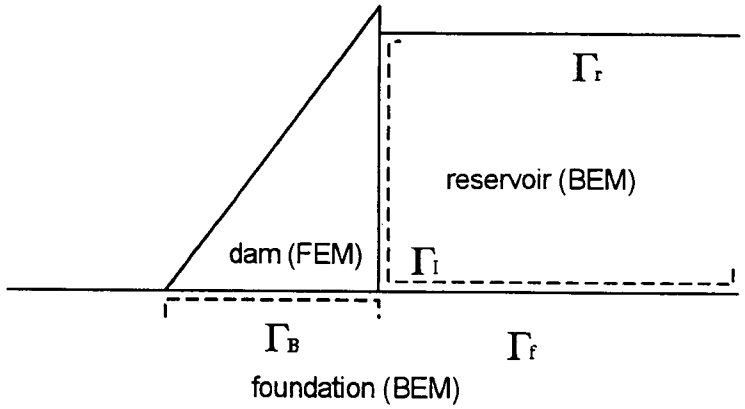


Figure 1: Outline of a dam–foundation–reservoir system.

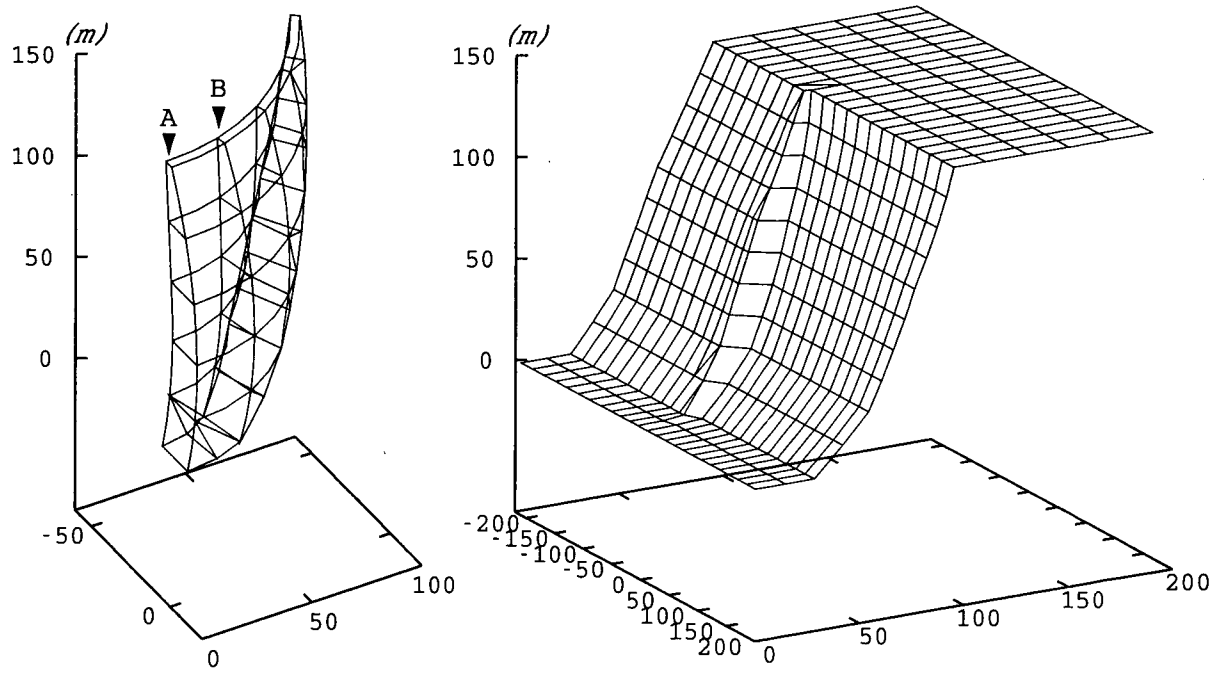


Figure 2: Finite element mesh of the Morrow Point Dam and boundary element mesh of the foundation in the vicinity.

Table 1: Material properties of the dam–foundation system.

Dam			Foundation		
ρ	ν	v_S	ρ	ν	v_S
2.48	0.200	2.15	2.64	0.200	2.08

ρ: density (t/m^3), ν: Poisson's ratio, v_S: S wave velocity(km/s)

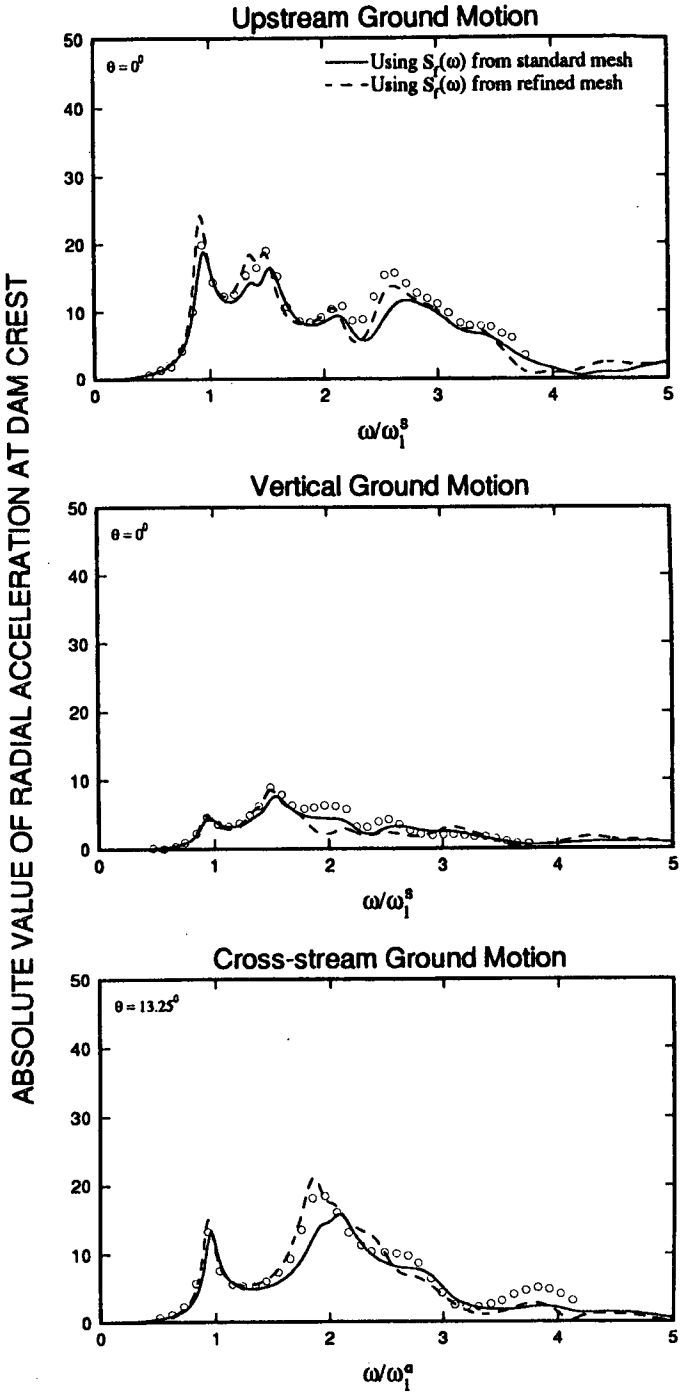


Figure 3: Comparison of frequency response functions for Morrow Point Dam. The solid and broken lines are the results from Tan and Chopra (1995) and the open circles are from the present method.

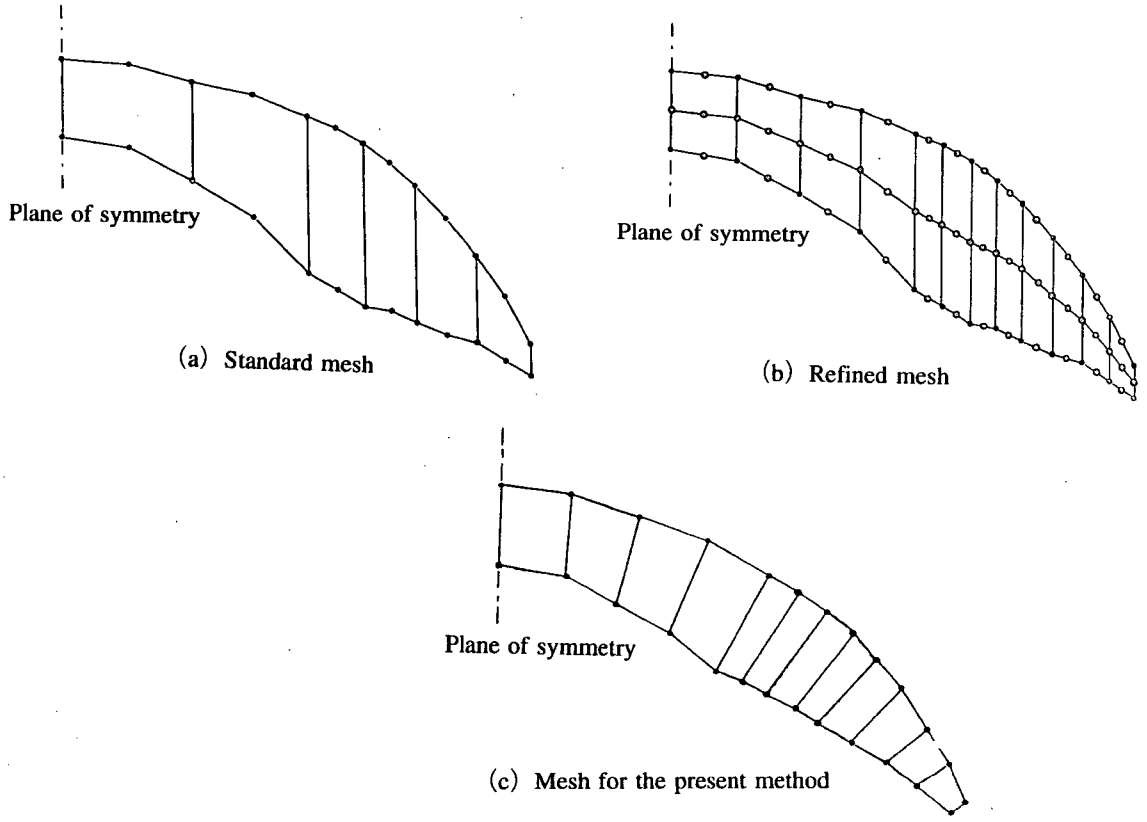
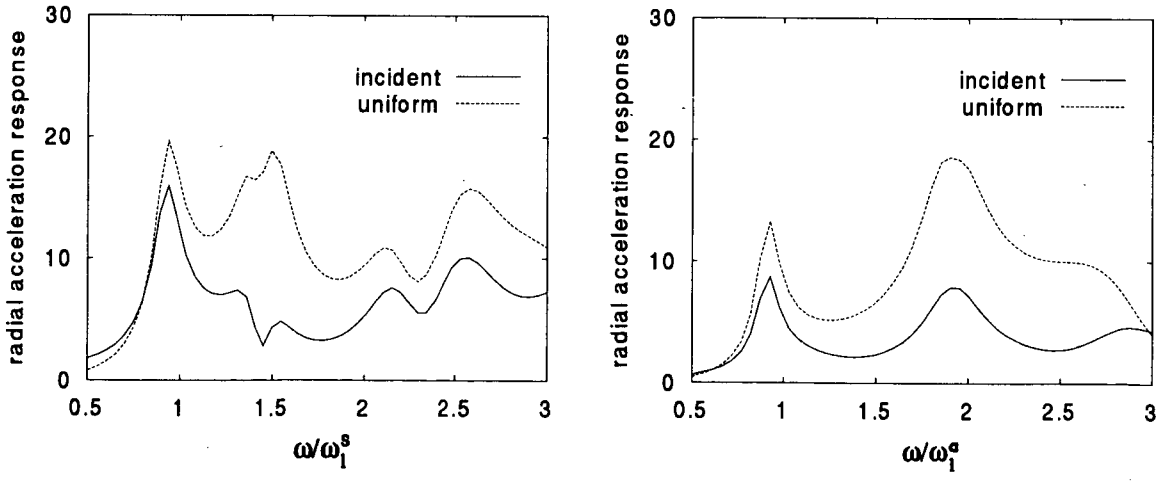


Figure 4: Boundary element meshes of one-half of the foundation at its interface with the dam. (a) and (b): standard and refined meshes (Tan and Chopra, 1995); (c): mesh for the present method coincides with the finite element mesh of the dam at its interface with the foundation.



(a) Upstream ground motion.

(b) Cross-stream ground motion.

Figure 5: Comparison of frequency response functions for Morrow Point Dam obtained using two different seismic inputs. (a) response at A due to upstream ground motion, and (b) response at B due to cross-stream ground motion.

Building a Database of Observational Evidence for Large Structures

by

Ziyad H. Duron[1] and Steven Alves[2]

ABSTRACT

A database is under construction aimed at supporting analytical and experimental investigations of large civil structures. Specifically, the database is geared toward the study of observational evidence of dynamic response behavior for structures such as dams, bridges, and buildings. The paper outlines the motivation, conceptual layout, and some applications for the database. Samples of an evaluation module for experimental results are presented. A proposed timetable for completion of the database to is also discussed.

1. INTRODUCTION

Advances in computer, instrumentation, and Internet technologies in recent years have enticed civil engineers to reconsider the benefits of field testing large structures. Civil engineering, long considered as one of the more conservative disciplines in engineering, has historically viewed field testing as a costly endeavor to be taken on only in the face of assured technical and economic benefits.

Modern analytical capabilities have significantly reduced the complexities of numerical analysis and have contributed to a shift in focus away from field investigations for validation purposes to an increased reliance on numerical computations. The irony, however, is that with this reliance on numerical solutions, the need for algorithm validation is only increased.

The following describes an attempt to construct a database of observational evidence for large civil structures. While the idea for this type of database is certainly not new, the construction of the database and its contents are significantly unlike present databases associated with earthquake engineering. Typical databases contain earthquake records that can be downloaded by the engineer, while others may contain photos and limited information on site conditions, or descriptions of failures that might have occurred. The database described herein strives to provide the engineer with a wide range of information suited primarily for the evaluation and investigation of the dynamic response characteristics associated with large structures.

2. DATABASE OBJECTIVES

The main objectives for this database are (1) to provide engineers with tools to enhance their understanding of large structural response characteristics, (2) to provide a focus on field test procedures and evaluation methodologies for health monitoring , and (3) to provide support of analytical investigations. Tools (referred to as evaluation modules below) offered in the database should facilitate enhanced understanding through comparisons of measured (experimental) and predicted (analytical) results for a particular structure.

3. DESCRIPTION OF DATABASE LAYOUT AND CONTENTS

The database will be internet based, with access granted to the user through a Web page easily found from keyword searches (e.g. dams, database, earthquake engineering). The Web page will contain descriptions of the database, its contents and format, along with information in the form of reports and photos. In addition, the Web page will provide guidelines for standardized approaches to data acquisition, instrumentation, and data processing of ambient, transient, and forced vibration data. Evaluation Modules (EM) for conducting limited analyses of experimental results and of analytical findings will also be available. The class and types of structures to be included in the database are listed in Table I.

[1] Professor of Engineering, Department of Engineering, Harvey Mudd College, Claremont, California, 91711 USA.
[2] DePietro Research Fellow, Department of Engineering, Harvey Mudd College, Claremont, California, 91711 USA.

While the original concept of this database focused only on dams, the scope has been expanded to include bridges and buildings. However, for the purposes of this discussion, capabilities will be described in the context of concrete dams only. The described capabilities will be made available for each class and type of structure listed in Table I. Available information for concrete dams will include descriptions of the dam (design and construction), foundation (inspections and reports), reservoir, and of any seismic investigations performed. This information will be accessed directly through the Web page, while the modules will provide access to seismic evaluation results – both analytical and experimental.

Table II lists the available dam sites and data types available from a number of investigations conducted since 1985 by the research group at Harvey Mudd College. The table indicates the name of the dam, its type (single arch, gravity, or multiple arch), and dimensions, and the method of excitation employed during the field investigations. Methods of excitation include (1) forced vibration using an eccentric mass vibrator capable of producing up to 20 kips over a 20 Hz range, (2) transient resulting from a calibrated device used to impact the dam or from the sudden release of compressed air in the reservoir, and (3) ambient conditions occurring naturally due to seismic micro-tremors, wind, wave action, or were flow induced through the dam's power intakes. Also indicated in the table are designations for the measured responses (accelerations and hydrodynamic pressures). Acceleration responses were typically acquired using sensitive (flat response from DC to beyond 300 Hz) force-balance accelerometers and hydrodynamic pressures were acquired using solid state hydrophone instrument arrays. The next column indicates whether reservoir dynamics were investigated at the dam site based on measurements of acceleration response along the height of the dam and hydrodynamic pressures at coincident elevations in the reservoir along the dam-reservoir interface. With these measurements, computation of a reservoir frequency response function is possible that can be associated with reservoir bottom geometry and boundary absorption characteristics. The last column in Table II indicates whether an analytical study of the dam site was completed

4. DESCRIPTION OF EVALUATION MODULES (EM)

Two evaluation modules are proposed for the database – one for reviewing analytical (numerical model) results, and one for reviewing experimental data. The modules are to be constructed using Visual Basic, run in Excel, and downloaded to the user's (PC) computer platform (modules are not planned for non-PC platforms at this time). Upon opening a module, the user will be required to login to the database server (to be housed at the U.S. Army Corps of Engineer Waterways Experiment Station in Mississippi, USA) in order to access the necessary datafiles. The evaluation module for experimental data is nearly complete and is described in some detail below.

The module, originally intended to provide viewing capabilities only, now provides data evaluation and analysis capabilities of the experimental data. Plots and corresponding data files will automatically appear in the user's Excel workbook. A unique feature of the module allows the user to conduct alternative spectral analyses. Applications to short and long term health monitoring techniques for large structures are described on the Web page to help the user evaluate the usefulness and relevance to a particular need or requirement.

Response measurements included in the database will be categorized according to the test procedure conducted. That is, responses will be classified as steady-state (from forced vibration testing), transient (from testing with impact devices or poppers), and random (from ambient testing). In this way, responses are characterized by signal type rather than by structure.

Capabilities associated with the random excitation or ambient test technique are nearly complete. All of the ambient data have been analyzed using Fast Fourier Transform (FFT) based techniques resulting in power spectral

density, frequency response, and coherence functions. In addition, the module contains relevant information pertaining to measurement uncertainties, information typically not provided in the reporting of full scale field testing of large structures (particularly dams). Descriptions of probable sources of measurement errors for each test will also be provided on the Web page along with guidelines for minimum ambient record lengths required to ensure satisfactory data quality.

An automated peak picking routine is available to help identify structural resonances based on peaks in power spectra and regions of high coherence. Time synchronized, animated modal response shapes measured during the ambient tests can also be viewed. Similar capabilities will be offered for forced vibration and transient test results

5. POSSIBLE APPLICATIONS OF THE DATABASE

Descriptions of possible database applications are presented here. The authors intend that the database may provide a platform where engineers can investigate new, alternative methods for analysis of real, measured response information. For instance, FFT based analyses may sometimes limit the engineer's ability to adequately characterize time records acquired from test procedures in which short duration, highly sampled, non-stationary responses are obtained. The analyst's inability to analyze such data should not, however, be taken to mean that the data somehow does not contain relevant and important information on the structure's dynamic response characteristics. Alternate analysis techniques may provide additional insights

6. ALTERNATIVE SPECTRAL ANALYSIS

Advantages of using alternate techniques are illustrated by the sample response measurement acquired on a small concrete arch dam (Big Creek Dam No. 4) shown in Figure 1. The measurement is hydrodynamic pressure acquired (using the solid-state hydrophone instrument array) over a two second interval originally sampled (digitized) at 1000 samples per second. Only the last second of the record is shown which clearly indicates the pre-event conditions to be ambient pressure response followed by the sudden appearance of the forced (pulsed) response, subsequent transient decay, and return to pre-event ambient conditions (evidenced by the small amplitude response levels consistent with those seen prior to the sudden disturbance). The second plot in the figure illustrates the comparison between spectra computed using a FFT based algorithm (dotted line) and a maximum entropy method (MEM) based approach (solid line). The FFT estimate demonstrates an abundance of spectral peaks, none of which can be identified readily as system resonances. The MEM estimate, however, obtained from the same time record, clearly shows a single strong resonance near 12 Hz and a bandwidth consistent with modal damping equal to 8% of critical. The peak frequency and width are consistent with actual dynamic characteristics of the dam derived from forced vibration. The effectiveness of the MEM estimate to capture the resonant behavior is almost predicted by the mathematical form (see Figure 1) of the estimate . The equation reflects the use of "poles" to represent spectral peaks in the response. The method is well suited for these short duration, non-stationary time records and does not rely on periodicity for accuracy. In fact, the resulting spectral resolution is unlimited since the spectrum is described by a polynomial in frequency

7. HEALTH MONITORING

The database may also provide engineers with capabilities for health monitoring of large structures. As an example, data acquired on a steel stringer bridge (located in Cincinnati, Ohio USA) during a program sponsored by the (USA) Federal Highway Administration (FHWA) and the Ohio Department of Transportation (ODOT) to develop damage detection methodologies are presented here. The bridge was of particular interest to FHWA since the design comprises a significant percentage of the national inventory

and improved evaluation techniques may lead to reduced or mitigated repair costs.

The research program was aimed at developing damage detection techniques for this class of bridge based on measurement of flexibility and estimated static deflection capability. In support of this objective, a wave speed based test approach for damage detection was developed.

In this approach, only two accelerometers and an impact device (calibrated hammer) are required to capture the first arrival of a known disturbance (force pulse) applied at a known location on the bridge. Only the end abutments require monitoring, and only the initial or first arrivals of the pulse at each end are required for analysis. The technique has advantages such as minimal instrumentation and data storage requirements, and uses simple procedures easily carried out either on the upper or lower bridge deck surfaces. More importantly, the technique does not require that the bridge be closed to traffic while still ensuring a high degree of safety during the conduct of the test.

For the bridge in Cincinnati, the photo in Figure 2 illustrates the type of damage induced in the bridge. It consisted of a cut lower flange and web (cut almost 70% of its height) and cut lateral members at the same location. The test layout is illustrated by the schematic in the figure and shows the locations of the accelerometers on each end abutment and the location of the impact on the upper bridge deck. The deck consisted of a concrete slab (6.5 in. thick) covered by an asphalt layer (2.5 in. thick). The signals shown in Figure 2 clearly indicate the arrival of the disturbance at each end of the bridge. Knowing the exact locations of both measurement and impact locations, the objective of the test is to obtain an accurate reading of the propagation times from the instant of impact to the first arrivals at each end. Estimates of wave speed (ratio of distance over time traveled) are indicated in the figure (bottom plot).

Wave speed estimates across each half of the girder tested revealed a 40% drop in wave speed associated with the damaged section of the girder. By contrast, the flexibility based approach for detecting the damage induced on the bridge resulted in a 10%-15% change in static deflected shape. The technique may prove particularly useful if periodic testing is carried out on these types of bridges across each of the main support girders. Estimates can be complied into the database and deviations in measured speeds may prove invaluable for the early identification of probable changes in structural condition

8. NUMERICAL MODEL VALIDATION

One of the more important applications of this database will be the ability of engineers to perform numerical model validation checks with actual measured response information. A current effort related to the analysis of a large, concrete multiple arch is described.

The owner of the dam must demonstrate the dam's ability to withstand the maximum credible earthquake defined for the site, and a combined analytical and experimental approach has been used to identify the dam's seismic deformation capacity. The study began with the development of a numerical model used to identify static and dynamic stress levels in the dam. However, prior to the acceptance of the model's characteristics, experimental field studies consisting of ambient surveys were conducted in order to obtain reliable information that could be used to validate the numerical model. Ambient surveys were conducted with both empty and full reservoir conditions. Validation of the model proceeded by using the empty reservoir response information to verify eigensolutions associated with the dam-foundation subsystem. Then, after attaching the reservoir, the resulting response behavior was compared against the full reservoir response measurements. A complete comparison of the resonances identified from both comparisons is shown in Figure 3, and a typical comparison of response shapes (model and measured) is also shown.

The significance of these comparison studies is highlighted by the fact that the numerical model

actually only modeled one-half of the river section of the dam. Whereas the river section of the actual dam consists of nine arches, a right abutment and a left thrust block, the numerical model included only three and one-half arches and a representative boundary used for both the abutment and thrust block. A peer panel asked to review the use of a symmetric model for the analysis of the dam expressed concern over this approach, however, the comparisons indicated here show that the majority of the measurable resonances in the dam system were actually found to be present in the model response

9. EVALUATION MODULE – SAMPLE EXPERIMENTAL ANALYSIS CAPABILITIES

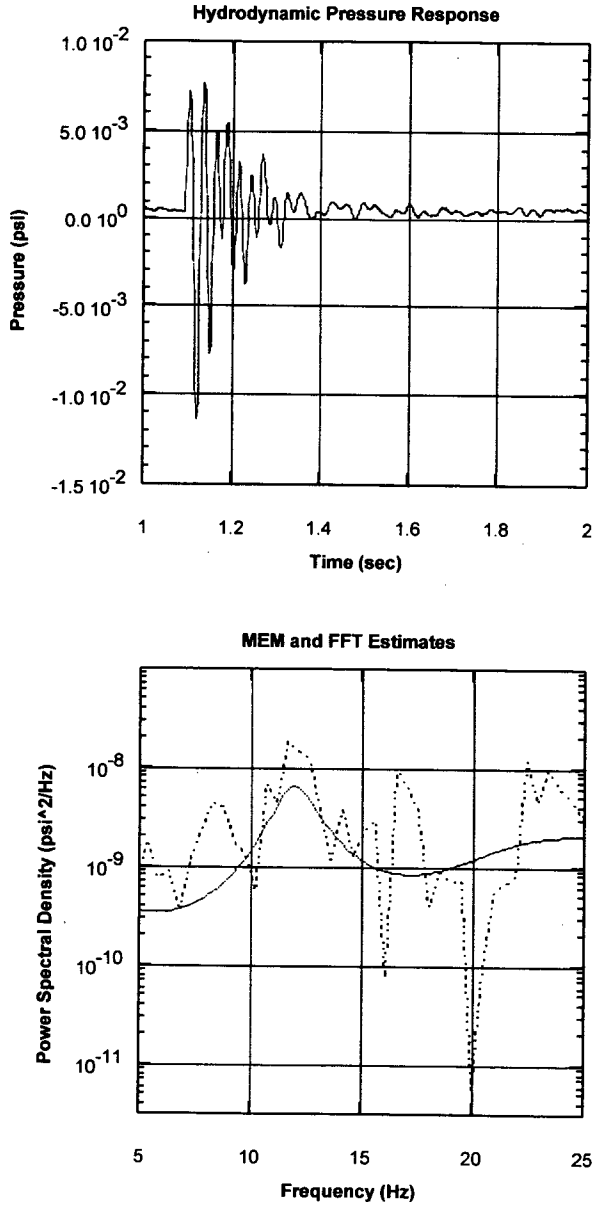
Figure 4 shows the type of presentation offered for the spectral estimates derived from ambient responses processed using FFT based algorithms. The particular data are taken from one of the ambient surveys conducted on the large multiple concrete arch dam (referred to above). The user accesses particular measurement locations (measurement layouts and other relevant information will be on the Web page) through the FTP utility provided in the module.

Added features include the ability to superimpose coherence results onto power spectral plots allowing the user to quickly identify regions of high coherence where data quality can be assumed to be high. In addition, automated peak picking helps identify resonances from the power spectra and a list of these peak frequencies and corresponding coherence values is returned.

Upon choosing the "Plot Mode Shapes" option, the user is prompted to select among the listed peak frequencies and full modal response shapes can be viewed. If the response at 3.076 Hz is selected as shown in Figure 4, the resulting screen will show the deformed (solid line) and undeformed (dashed line) shapes of the dam. The solid dots seen on the dark blue curve (deformed shape) are used to denote locations on the dam where coherence falls below 0.6 (a suggested threshold below which data quality may be questioned). Finally, the user will have the ability to view animations of the modal shapes.

10. FUTURE WORK

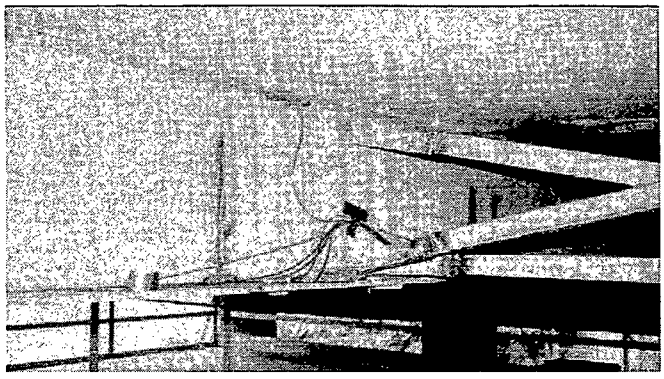
Table III summarizes the remaining work necessary to complete the first phase of the database project. In addition, the table presents a schedule for completing the development culminating with the database going on-line in September 2000. Maintenance and upgrade plans (to be developed) will be needed to ensure continued reliability and accuracy over the life of the database.

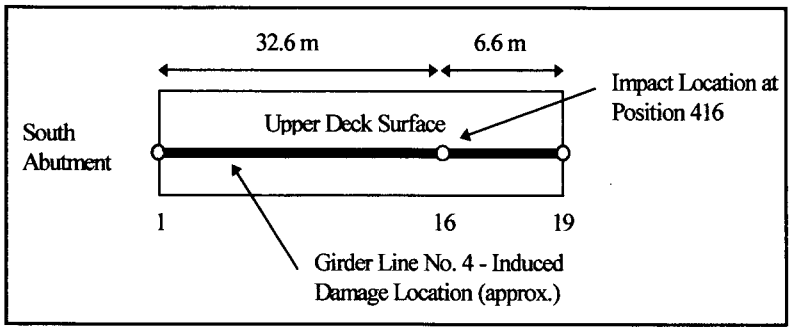


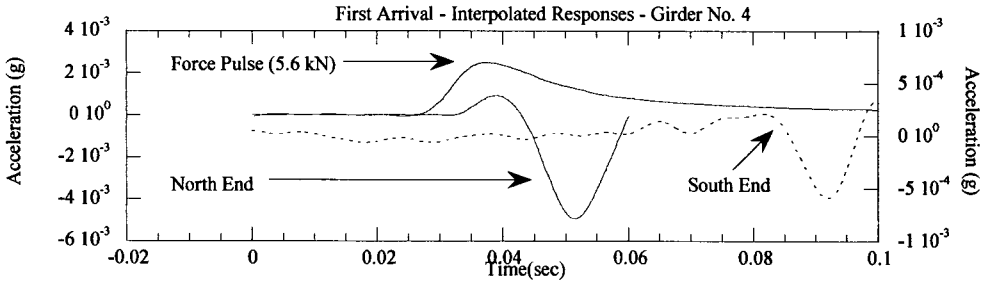
$$G_{xx}(f) \approx \frac{2}{N\Delta t} \frac{a_0}{\left|1 + \sum_{n=1}^{M} a_n z^n\right|^2}$$

$$z = e^{-j2\pi f \Delta t}$$

Figure 1 – Measured hydrodynamic pressure response (top trace) acquired at Big Creek Dam No. 4 due to a release of compressed air in the reservoir. The bottom traces compare associated power spectral density estimates from FFT (dashed line) and MEM (solid line) based analyses. The mathematical form of the MEM estimate is shown to the right of the power spectra comparison. The MEM estimate is modeled by a polynomial function of frequency, allowing any desired spectral resolution to be selected.







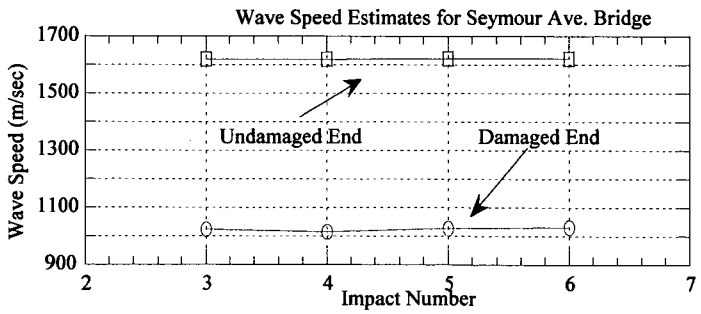


Figure 2 – Modal testing was conducted on a steel stringer bridge in which damage was induced as shown in the top photo. Using the measurement layout shown (2nd figure), first arrival of transient responses at each end of the bridge (3rd figure) was used to estimate wave speeds across the support girders. Results indicated in the bottom figure reveal a 40% reduction in wave speed associated with the damaged condition, relative to the undamaged state of the bridge.

Experimental (Hz) Ambient Empty Res	Eigenvalue (Hz) Dam-Fdn Only	Experimental (Hz) Ambient Full Res	Freq Analysis (Hz) Dam-Fdn-Res
3.0	3.3	3.5	3.5
3.4	3.6	6.3	6.4
5.5	5.9	6.8	7.3
6.2	6.5	9.9	9.5
6.6	6.8	11.7	11.8
7.3	7.5	14.3	14.0
7.7	7.9	16.8	16.8
8.1	8.2		
9.4	9.4		

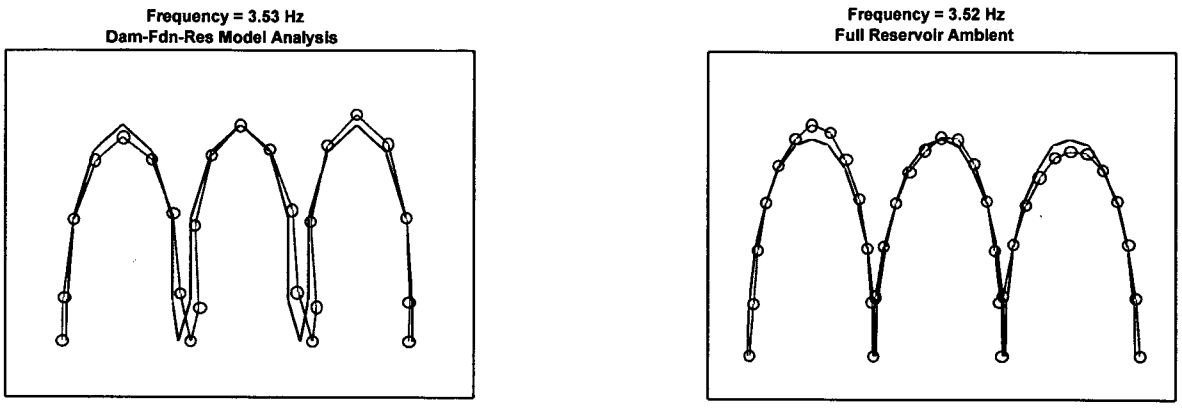


Figure 3 – Resonant frequencies associated with the numerical and experimental evaluation of a large concrete multiple arch dam. Ambient surveys were conducted on the dam under empty and full reservoir conditions and were used to validate model characteristics associated the dam-foundation and dam-foundation-reservoir response behavior. The response shape comparison indicated (a 180 degree phase shift is shown between model and experimental results) is typical of the quality observed in this evaluation.

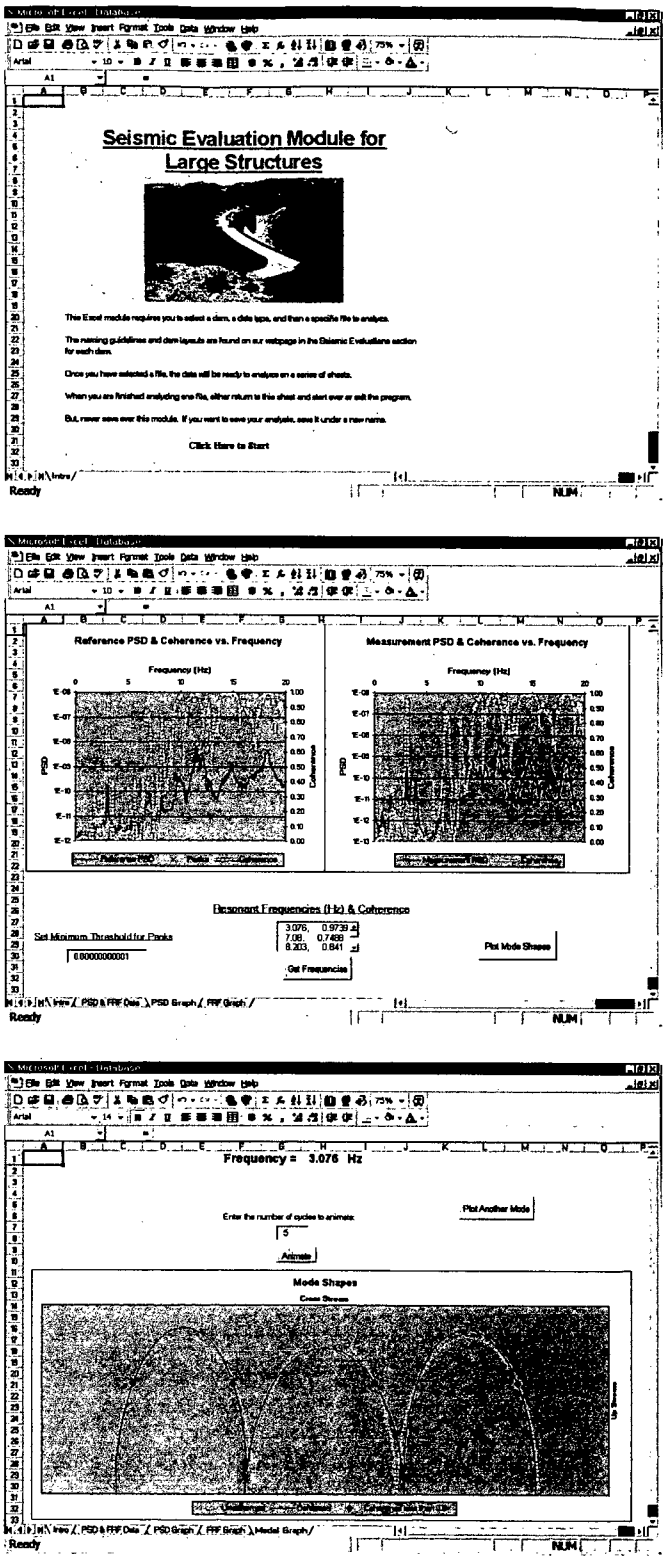


Figure 4 – Sample layouts of analysis capabilities found in the evaluation module for experimental data included in the database. An automated peak picking routine aids in the selection of candidate resonances and modal response shapes can be viewed and animated as indicated in the bottom layout.

Table I – Available class and type of structure to be included in the database

Structure Class	*Type*
Dams	Concrete arch(single and multiple)
	Concrete gravity
Bridges	Concrete(freeway interchanges)
	Steel (stringer, box girder)
	Railroad
Buildings	Reinforced concrete frame
	Steel frame

Table II – List of dam sites to be included in the database

Dam Site	*Type*	*Crest(ft)*	*Height(ft)*	*Excitation*	*Measured Responses*	*Reservoir Dynamics*	*Analytical Study*
Santa Anita	SA	612	225	FV	Acc, Press	Yes	Yes
Morrow Point	SA	724	500	FV	Acc, Press	Yes	Yes
Big Creek Dam No. 4	SA	287	75	FV, Ambient, Transient	Acc, Press	Yes	Yes
Seven Mile	G	1140	263	FV, Ambient	Acc, Press	Yes	Yes
Outardes 3	G	1150	230	FV	Acc, Press	Yes	Yes
Shaver Lake	G	2169	185	FV	Acc, Press	Yes	Yes
Big Dalton	MA (7)	140	75	FV	Acc	No	Yes
Florence Lake	MA (58)	3100	150	Ambient, Transient	Acc, Press	Yes	Yes
Gem Lake	MA (18)	688	80	Ambient	Acc	No	Yes
Agnew Lake	MA (7)	278	30	Ambient	Acc	No	Yes

Table III – Proposed timetable for release of the database

Task	*Description*	*Tentative Schedule*
Design Review at WES	Conduct in-depth review of Phase I effort and present a demonstration of module capabilities. Update schedule and deliverables. Discuss timing of distribution of Phase I Demo CD for outside peer review.	July 25-26 1999
Initiate Phase II	Define objectives for Phase II portion of project. Detail schedule and deliverables.	September 1999
Compile WES test and analysis data	Identify available information from WES for inclusion. Identify WES liaison and set tentative timetable for data transfer into database.	September 1999 – April 2000
Conduct 2nd Design Review at WES	Review Phase II results	June 2000
Place Database On-line		September 2000

The Estimation on Dynamic Behavior of Arch Dam Modeling Non-linear Properties of Contraction Joints During Earthquake

by

Tatsuo NISHIUCHI[1], Yukihiro TOYODA[1]

ABSTRACT

This paper describes a numerical study on the seismic response of a typical arch dam with the non-linear contraction joint behavior. The seismic-induced joint opening effects, along with seasonal changes in the joint opening behavior due to temperature loads, were investigated by using a newly developed analysis procedure based on 3D finite element method. The non-linear analysis procedure specifically addresses the redistribution of forces that occur in arch dams when the contraction joints open and close in response to earthquake ground motion. Compared with the results of standard linear analyses of the monolithic model, it is found that the opening of the dam's contraction joints in winter season has a significant effect on the transient response of the membrane stress and the maximum crest displacement in stream direction at crown cantilever.

Key Words: *Arch Dam,*
Non-linear Seismic Analysis,
Contraction Joints,
Shear-Slip Failuer Criterion.

1. INTRODUCTION

Arch dams are usually constructed as cantilever monoliths separated by contraction joints. From our numerical and experimental study [1], it is found that some of the contraction joints open near the surface of an existing arch dam. Therefore, it is expected that the contraction joints may open and close through several cycles of vibration during earthquake, affecting the transfer of internal forces between the arches and cantilevers. Despite the possibility of contraction joint opening, it is impossible to simulate the non-linear joint behavior by standard seismic analysis procedures, which assume that a dam is a monolithic structure and the behavior is linear elastic. This makes it indispensable to develop a newly analysis procedure for computing the earthquake response of arch dams including the non-linear effects of contraction joint opening. The non-linear analysis procedure specifically addresses the redistribution of forces that occur in arch dams, when the contraction joints open and close in response to earthquake ground motion.

The objectives of this study are as follows;

(1) To validate the applicability of the newly developed analysis procedure to this specific problem.

(2) To examine the effects of contraction joint opening on the seismic response of a typical arch dam.

---

1) Senior Researcher,
Structure Department, Central Research Institute of Electric Power Industry, Abiko, Japan

2. METHOD OF THE ANALYSIS PROCEDURE

(1) Finite element model of the arch dam

The finite element model of the existing arch dam has a 133m high and crest length of 276m, almost perfectly symmetric doubly curved arch. The dam consists of 20 monolith cantilevers separated by contraction joints.

Fig.1 shows the finite element mesh pattern. The region of dam-foundation rock was modeled by 8 node isoparametric solid elements. The fine mesh pattern through thickness in the stream direction was used near the surface of the dam body, while coarse mesh pattern was used in the internal portion of the dam body. The contraction joints were modeled by three dimensional non-linear elements. Opening of the contraction joints in the model was controlled by specifying appropriate properties for the joint elements. More details about the joint elements are given in the next section. The seismic-induced hydrodynamic effects of the reservoir water were represented by an added mass concepts proposed by Westergarrd, neglecting water compressibility.

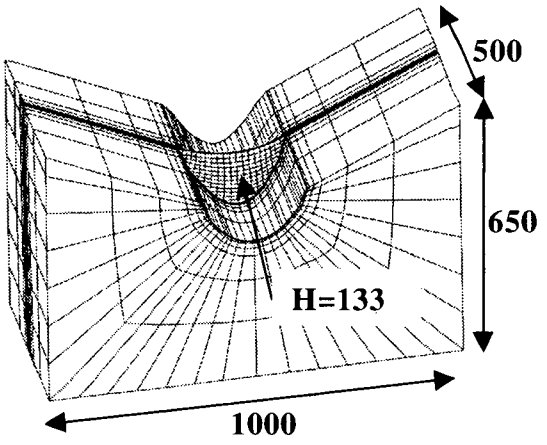


Fig.1 Calculation model of Arch

Based on the in-situ measurement results, energy dissipation in the finite element model was provided by Rayleigh damping. The damping was evaluated from the specified modal damping ratios, that is, approximately 2% of critical damping in the first and second vibrational modes[2].

The material properties for the seismic response analyses are shown in Table-1. For the analyses, concrete and rock elements were assumed to be elastic.

Table-1 Material Properties

	concrete	joint	rock
E(MPa)	30000	9000	7000
ν	0.2	0.2	0.2

(2) Modeling of contraction joint

Fig.2 illustrates the basic concept of contraction joint modeling in an arch dam.

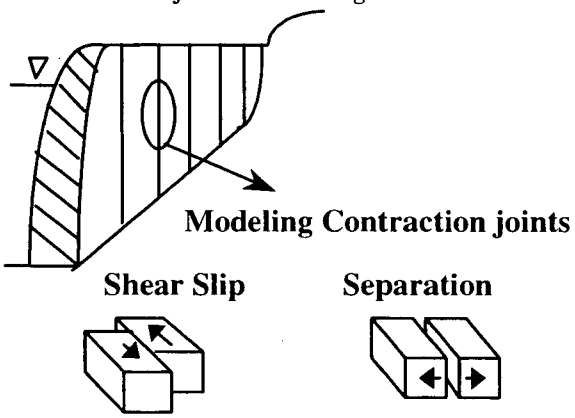


Fig.2 Characteristics of calculation method

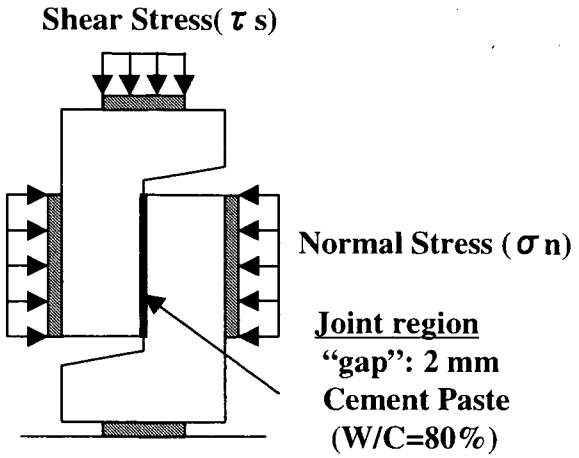


Fig.3 Static push off test

As shown in this figure, the joint elements develop resisting forces due to relative normal and tangential displacements between the two surfaces.

Coulomb type failure criterion, as shown in Fig. 4, was used as the failure condition of the joint elements. The parameters in the yield function were determined from the results of "Push-off test"(Fig.3), which was conducted in the previous study [3,4]. The stress-strain relationship at the joint surface is shown in Fig 5 and 6.

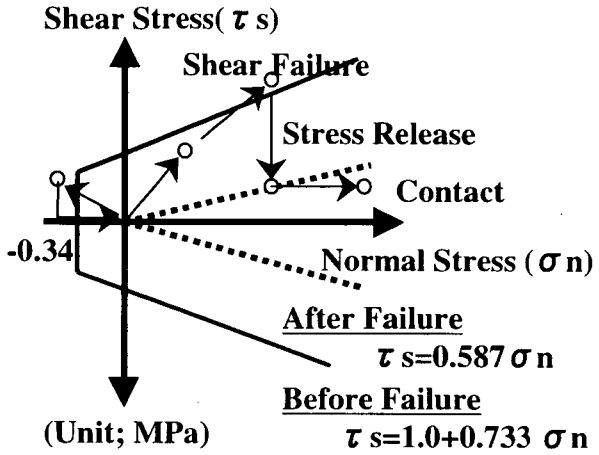


Fig.4 Failure criterion on joint elements

The normal stresses, σ n, in the joint are non-linear functions of the strain, (ε n). The joint has a specific tensile strength, σ n=0.34(MPa), in the normal direction, and once it is reached the joint unloads and the subsequent tensile strength is zero. The reduced stiffness is provides for the joint when the two joint surfaces contact again. On the other hand, shear failure is assumed to begin when the shear stress of the joint exceeds a specified value defined by τ =1.0+0.733 σ n. After the threshold value is reached, the shear stress is released and the subsequent shear strength is provided by τ =0.587 σ n for the remainder of the analysis. The tangential stiffness coefficients are reduced when the shear strain is reversed as shown in Fig. 6.

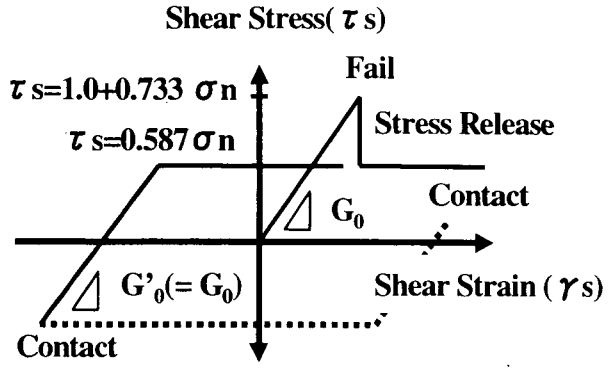


Fig.5 Shear stress - strain relationship

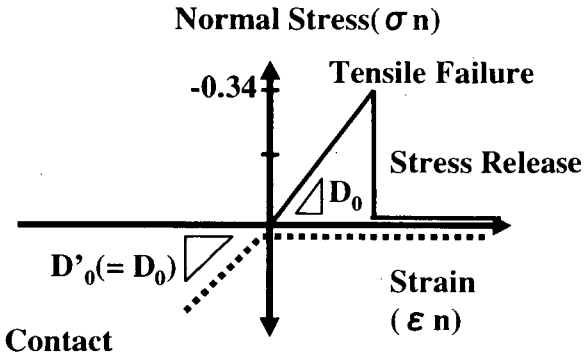


Fig.6 Normal stress - strain relationship

(3) Conditions of the numerical simulation

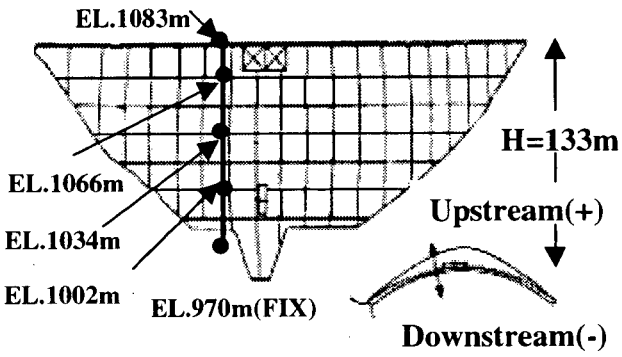
The actual earthquake response of arch dams includes the static effects of the dam weight, the hydrostatic pressure of the impounded water and temperature loads. Several kinds of analyses were carried out to these specific problems. The separate gravity analysis was performed in order to simulate the construction sequence of the dam. For cases with a full reservoir, the hydrostatic load was applied to the entire dam.

Heat-transfer analyses were performed in order to investigate thermal stress induced by the seasonal changes in the temperature condition. The results of the above mentioned static analyses were used as the initial conditions of the seismic response analyses of the arch dam.

3. STATIC BEHAVIOR OF THE DAM

(1) Outline of in-situ measurements of the dam

To verify the performance of joint model, we carried out several static tests and measurements[2], vibration test, static measurement of ordinary deformation at crown cantilever section and displacement of joint. In this paper, we showed one result of displacement of crown cantilever. The location of measurement instruments are showed in Fig.7.



(2) Comparison between measurement results and simulation results

The comparison between the test results and the analysis results are shown in Fig.8, in which the displacement data measured at the crown cantilever were plotted.

The static deformation at crown cantilever obtained from non-linear analysis is as same as that of linear analysis.

It is confirmed that the results of the simulation are consistent with the trend found in the tests, though the slight discrepancy between the measured displacements and the computed ones is recognized

The initial states of joint elements at time zero (starting seismic load) are showed in Fig.9. Most of the joints open and close repeatedly through the seasonal changes of the deformation. In particular, the closure of the joints in winter season plays an important role to transfer the internal forces between the arches and cantilevers. Usually, the transfer region of internal forces in the dam body is called "Secondary Arch","Inner Arch" and " Effective Arch"

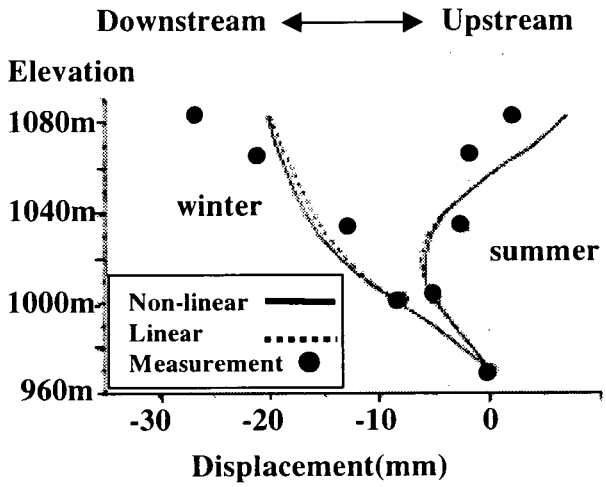


Fig.8 Comparison between tesr results and static analytical results (Crown cantilever)

4. RESUTTS OF EARTHQUAKE RESPONSE ANALYSES

(1) Analytical conditions

In this papers, we explains the typical 4-cases which showed in Table-2.

Table-2 Analytical conditions

		Contraction Joint	
		Modeling	No model
Thermal Load	In winter	C1	C3
	In summer	C2	C4

The following cases are considered:

C1. With joints, including thermal stresses in winter season (February)

C2: With joints, including thermal stresses in summer season (August)

C3: No joints, including thermal stresses in winter (February)

C4: With joints, including thermal stresses in summer season (August)

The seismic wave and fourier spectrum which used in analysis are showed in Fig.10. The earthquake ground motion was evaluated by "SHAKE" code, and the modified ground motion was applied in the stream direction at the artificial boundary of the foundation rock

(2) Displacement at crown cantilever

The largest displacement in stream direction at the crown cantilever is showed in Fig.11.

The maximum displacement of the crown cantilever occurred at the time of 12.26sec as the dam displaces in the upstream direction.

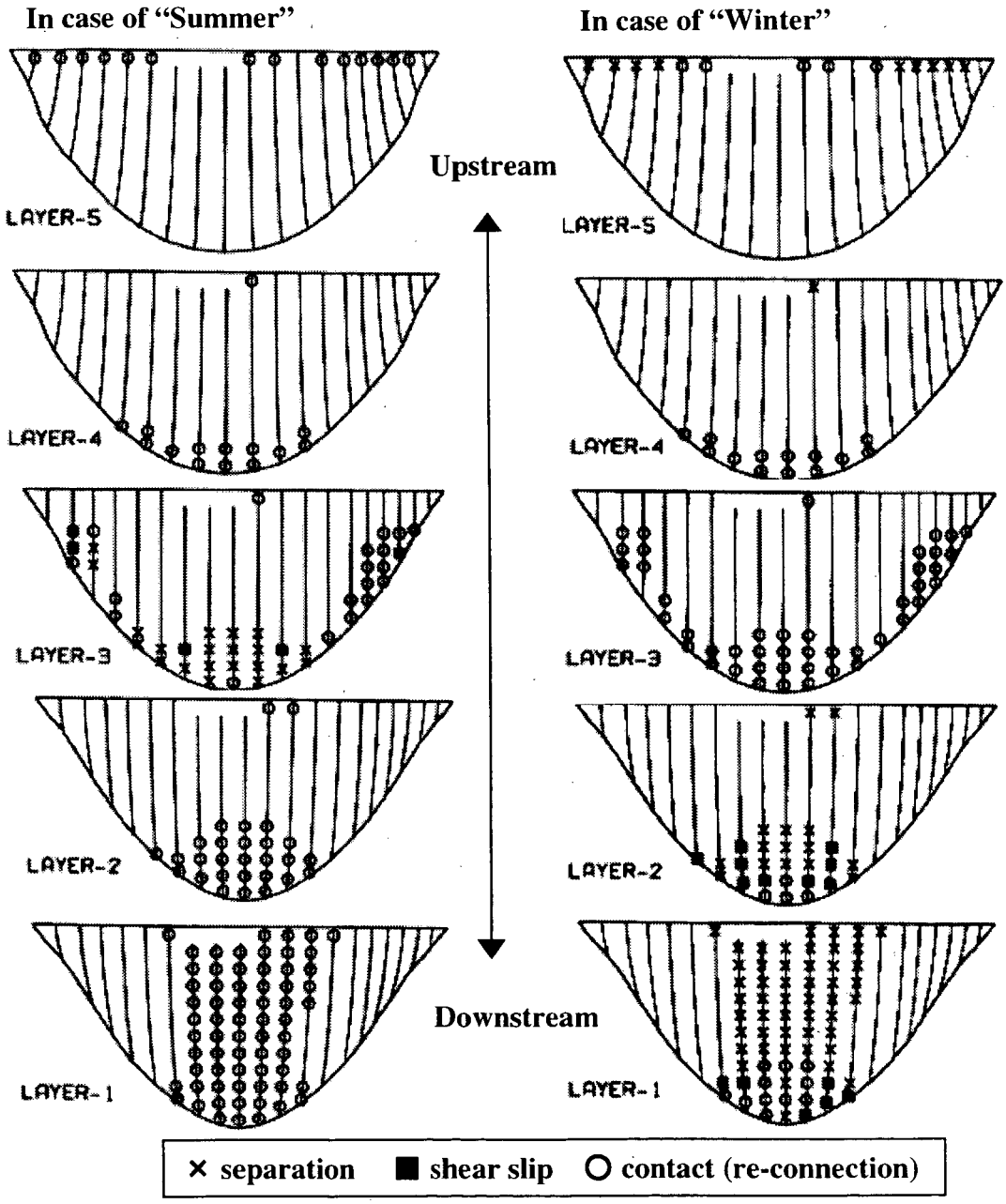


Fig.9 Initial states of joint elements at T=0.0sec

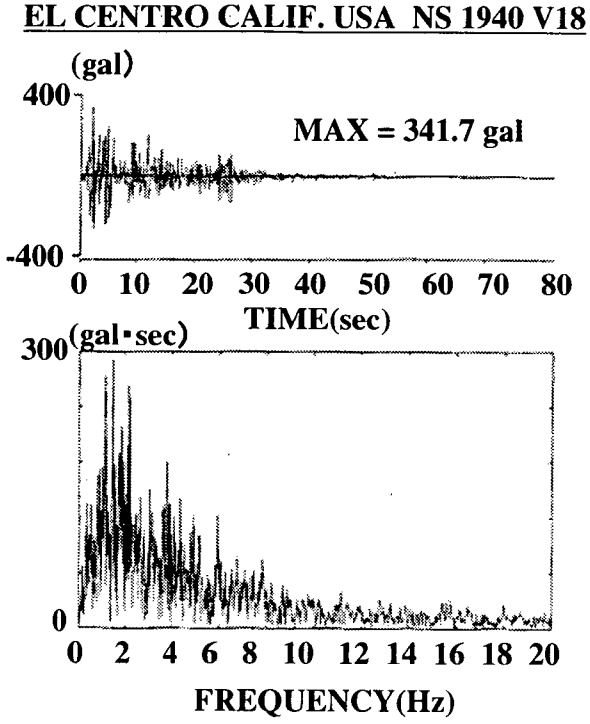


Fig.10 Seismic wave and fourier spectrum

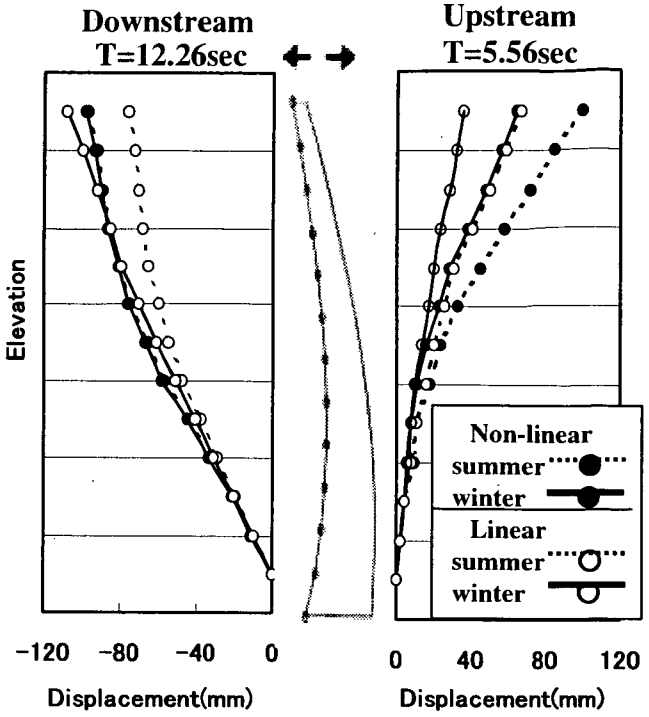


Fig.11 Deformation of Dam body at the crown cantilever

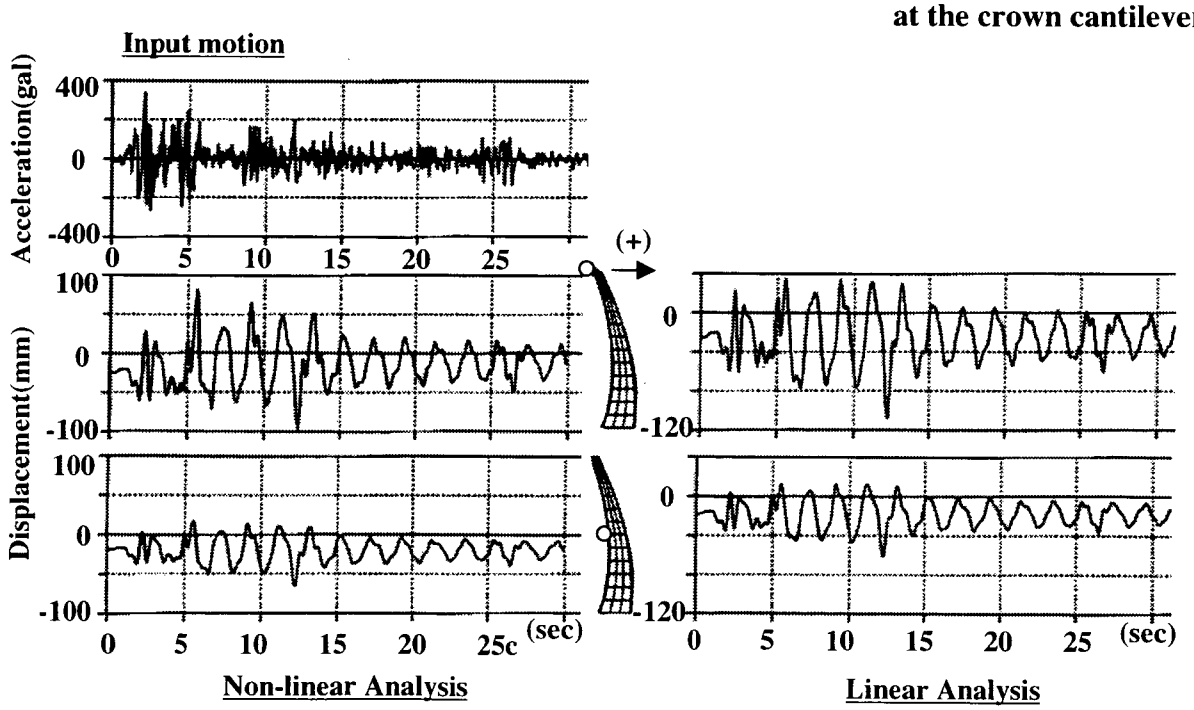


Fig.12 Numerical results (in case of "winter")
- Time histories of displacement in stream direction at crown cantilever

When the crown cantilever moves to upstream, the difference between displacement of non-linear analysis and that of linear analysis is bigger. But when the crown cantilever moves to downstream, the difference between displacement of

non-linear analysis and that of linear analysis is smaller. The reason which occurred this difference may be due to the restriction of dam-side rock. When the crown cantilever moves to upstream, there is no restriction and the crown cantilever is easy to move.

Time histories of displacement in stream direction at crown cantilever are showed in Fig.12. The maximum acceleration of seismic wave is occurred at the time of about 2.0 sec, the biggest displacement at crown cantilever occurs late for the time which occurred maximum acceleration. The difference between time history of displacement of non-linear analysis and that of linear analysis is smaller.

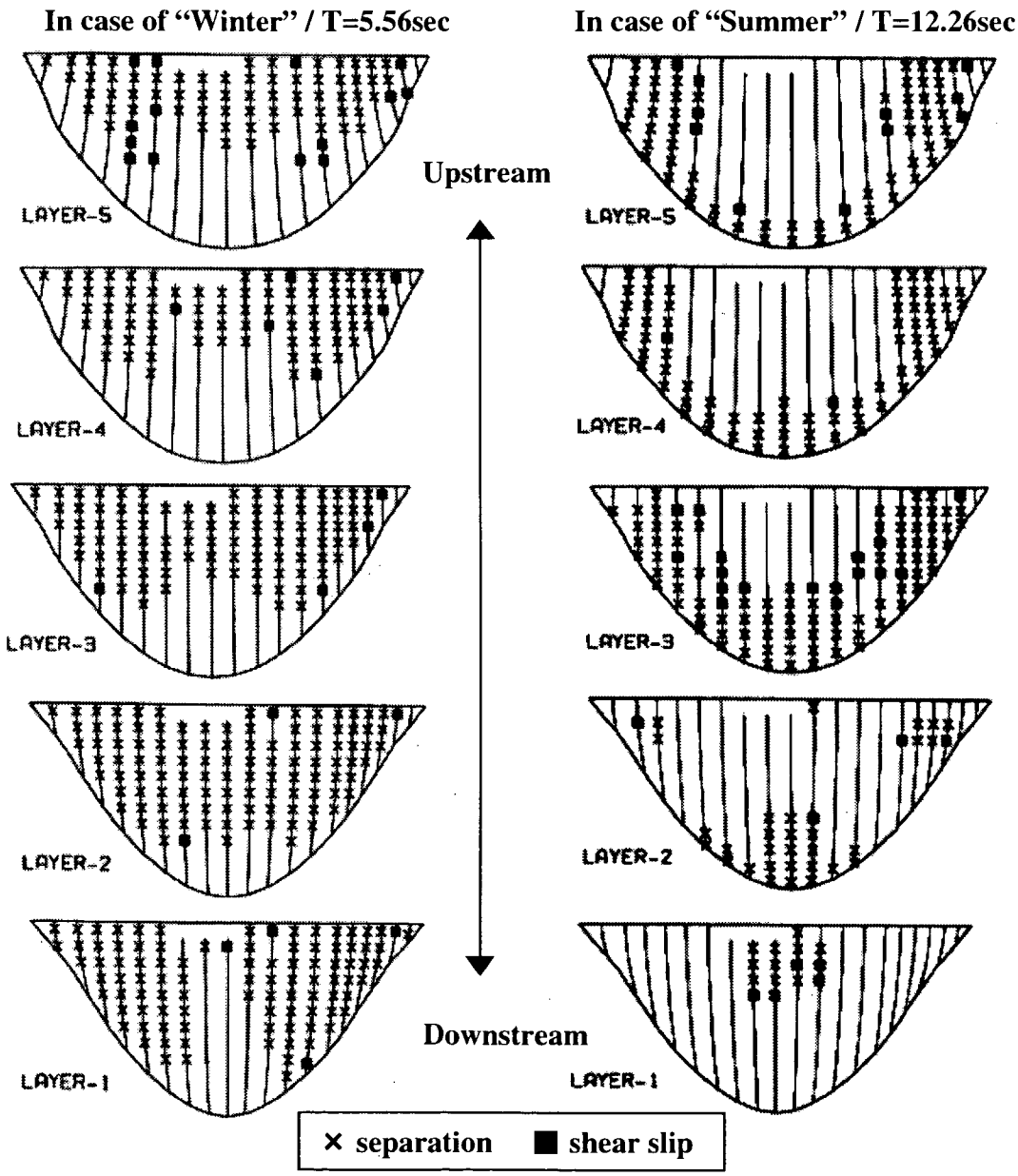


Fig.13 Numerical results
- Non-linear behavior of joints -

(3) Non-linear behaviors of joint

Allowing the contraction joints to open reduces the maximum arch tensile stresses at the crown section.

The results of non-linear behaviors of joints in the Case C1 and C2 are shown in Fig.13. In case of summer, at the time of 12.26 sec, crown cantilever moves to downstream and arch forces are strong at joints, therefore large area of joints transfer the arch forces and some area of joints slip caused by seismic load. In this condition, maximum vertical tensile stress occurs at concrete-rock interface at upstream heel. In case of winter, at the time of 5.56 sec, crown cantilever moves to upstream and arch forces are weak at joints, therefore large area of joints are separated and it becomes easy to move crown cantilever, because arch forces are weak at joints, therefore several cantilever blocks move independently. The maximum vertical tensile stress of concrete occurs at downstream surface.

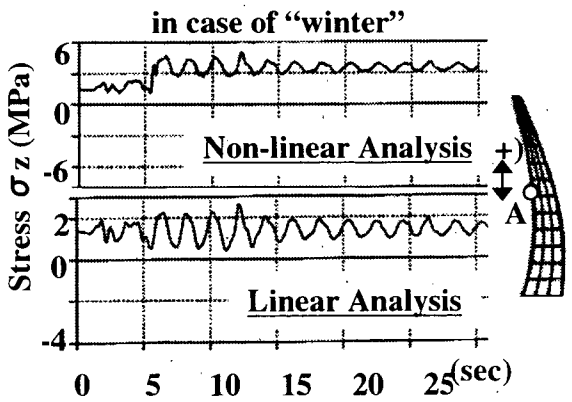


Fig.14 Time histories of the membrane stress at "point A" in the vertical direction(σ z) at crown section

(4) Time history and distribution of stress

The time histories of the membrane stress" σ z" in the vertical direction at point A are showed in Fig.14.

In the case of winter and in non-linear analysis, at the time of 5.56 sec, the stress level increases caused by the change of joints condition.

The membrane stress distribution at point A and B are showed in Fig.15.

In the case of winter, at the time of 5.56 sec, crown cantilever moves to upstream, the direction of static stress in non-linear analysis is as same as that in linear analysis, but the direction of dynamic stress in non-linear analysis is different from that in linear analysis.

In case of non-linear analysis, crown cantilever is easy to move compared to that in linear analysis, caused by this movement. So, tensile stress of concrete at downstream surface is much bigger than that in linear analysis. Oppositely, compressive stress of upstream surface is much bigger than that in linear analysis. In this results show the flexibility of crown cantilever caused by non-linear behaviors of joints.

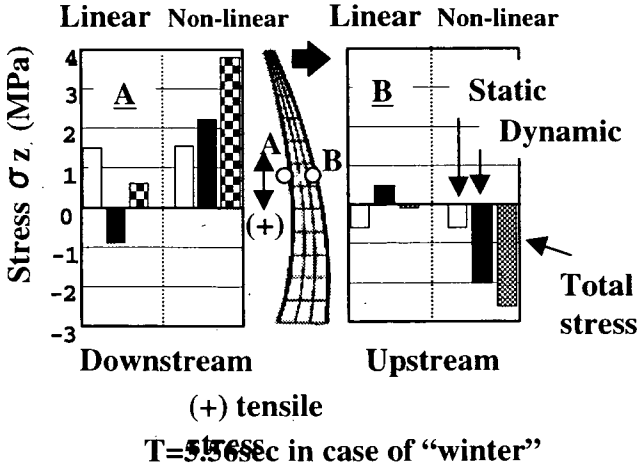


Fig.15 Membrane stress "σ z" distribution at point A and B

The opening of the joints and release of arch tensile stresses has an important effect on the maximum cantilever stresses in the dam. The large cantilever tensile stresses on the downstream surface occur

as the dam displaces in the stream direction, and the internal forces are redistributed from arch action to cantilever bending in the upstream direction.

In the case of winter, predicted crack patterns on the downstream surface is showed in Fig.16. In this analysis, material property of concrete is linear, therefore it can not estimate the concrete crack correctly. In this figure, crack area is the mark which occurred the tensile stress of concrete is over 2.45MPa and crack line's direction is calculating result from principle stress.

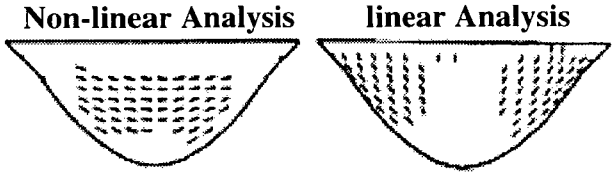


Fig.16 Crack patterns on the downstream Surface (" in case of winter ")

These cracks only occurred at downstream and upstream surface and there are no cracks in case of summer because of the strong arch forces.

5. CONCLUSION

The seismic behavior of the existing arch dam subjected to horizontal earthquake ground motion was investigated and the applicability of the newly developed analysis procedure to this specific problem was clarified. The conclusions obtained from this study are as follows.

(1) Compared with the results of standard linear analyses of the monolithic model, it is found that the opening of the dam's contraction joints in winter season has a significant effect on the transient response of the membrane stress and the maximum crest displacement in stream direction at crown cantilever.

(2) The earthquake analysis of the arch dam with contraction joint opening has shown that the arch tensile stresses predicted by a linear analysis are unrealistically large. The cantilever stresses from a linear analysis, however, are unrealistically low, and the problems associated with large downstream cantilever stresses induced by joint opening may be severe.

(3) The non-linear analysis procedure seems to be useful as a direct simulation tool for getting full understanding of the seismic behaviors of arch dams including joint opening effects.

To assess the generality of these findings, both additional numerical simulation and comparison with experiment data should be performed.

REFERENCES

[1]T.NISHIUCHI,Y.TOYODA,T.MATAUO, M.UEDA and K.MIZUNO;"Investigation on the Static Behavior of an Aged Arch Dam Using Non-Linear Finite Element Method", CRIEPI Report No.U97060, 1998.1

[2]Y.TOYODA,T.MATAUO,T.NISHIUCHI, M.UEDA and K.MIZUNO;"Study on the Dynamic Response Properties of an Existing Arch Dam Based on Dynamic In-situ Test Results", CRIEPI Report No.U97031, 1997.9

[3]T.NISHIUCHI,T.KANAZUand M.Xu;"A Study on Shear-Slip Failure Criterion of Concrete Blocks Joints", CRIEPI Report No.U94051, 1995.3

[4]T.NISHIUCHI,T.KANAZUand M.Xu;"A Study on the Effect of Shear Key Blocks on the Behavior of Vertical Joints in Arch Dams", CRIEPI Report No.U94052, 1995.3